Physics Lib.
Faxon

THE JOURNAL
OF
CHEMICAL PHYSICS

VOLUME 21, NUMBER 7 JULY, 1953

Space-Charge Layer and Distribution of Lattice Defects at the Surface of Ionic Crystals

KURT LEHOVEC
Sprague Electric Company, North Adams, Massachusetts
(Received December 17, 1952)

It is shown that an electric potential exists between the surface and the bulk of ionic crystals. The potential is expressed in terms of the energies necessary for formation of lattice defects. The distribution of the potential and of lattice defects near the surface is calculated. The difference between the concentration of lattice defects near the surface and that in the bulk leads to a "surface conduction." The magnitude of the potential, the thickness of the space-charge layer near the surface and the "surface conduction" are calculated for NaCl crystals using numerical values, calculated by Mott and Littleton [N. F. Mott and M. J. Littleton, Trans. Faraday Soc. 34, 485 (1938)] for the energies of formation of lattice defects. The effect of charged impurities in the crystals on the surface potential is discussed. The importance of the surface potential on diffusion, photoelectric effect, and photographic effect is mentioned.

I. INTRODUCTION

IN pure ionic crystals lattice defects of atomic dimension may consist of interstitial cations (symbol A_1), interstitial anions (symbol A_2), vacancies of cations (symbol A_3), and vacancies of anions (symbol A_4).[1] Assuming that the energies associated with the creation of lattice defects are known, the concentrations of the lattice defects have been calculated for the bulk of ionic crystals, making use of the condition of zero space charge.[2] As we shall prove in what follows, this condition is not fulfilled in general for a surface zone of the crystal, comprising many atomic layers. The space charge in the surface zone causes an electrostatic potential between the bulk and the surface of the crystal. In what follows we shall calculate the magnitude of this potential and the distribution of potential and of lattice defects in the space-charge layer.

II. GENERAL APPROACH FOR THE CALCULATION OF EQUILIBRIUM CONCENTRATION OF LATTICE DEFECTS

In thermal equilibrium the change in Gibbs' potential is zero for any "reaction" involving the creation or annihilation of lattice defects. Any such reaction may be written in the form

$$\sum_i \nu_i A_i = 0, \tag{1}$$

where A_i refers to the type of defect or particle participating in the reaction, ν_i are integers, which are positive if particles are created, and negative if particles are annihilated. The condition of zero change of Gibbs' potential for the reaction (1) may be written

$$\sum \nu_i (\delta G_i/\delta N_i) = 0. \tag{2}$$

At a sufficiently small concentration of lattice defects, Gibbs' potential of lattice defects is a logarithmic function of their concentration

$$(\delta G_i/\delta N_i) = E_i + kT \ln(N_i/Z_i) \tag{3}$$

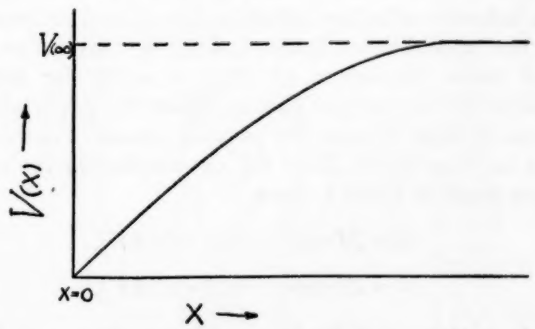

FIG. 1. Potential distribution $V(x)$ perpendicular to the surface ($x=0$) of an ionic crystal.

[1] We shall not discuss defects arising from the substitution of an anion by a cation, and vice versa, since this type of defect will normally not occur in ionic crystals because of the large energy required.

[2] W. Schottky, Z. physik. Chem. **B29**, 335 (1935).

(k Boltzman constant, T absolute temperature, Z_i number of possible positions per unit volume available for the particles of type i, N_i concentration of the particles of type i). With the aid of the relation (3), Eq. (2) can be transformed into the "mass action law"

$$\Pi \equiv (N_i/Z_i)^{\nu_i} = \exp(-\sum \nu_i E_i/kT), \tag{4}$$

where $\sum \nu_i E_i$ is the heat of the reaction. The four most simple reactions, by which a lattice defect of either of the four types may be created in an ionic crystal, are listed in Table I, column 1. Each of the reactions implies the transport of a charged particle between surface and the position x, where the lattice defect is located. Suppose there is an electrostatic potential $V(x)$ between the surface and the position x (Fig. 1). Then the "heat of reaction" (listed in Table I, column 2) will contain a term $\pm eV(x)$. When inserting the heat of reaction into Eq. (4), it is found that the concentration of lattice defects depends on $V(x)$.

TABLE I. The four simplest reactions creating a lattice defect.

Reaction	Heat of reaction $\sum_i \nu_i E_i$	u value for NaCl in electron volts[a]
Transport of a positive ion from the surface into an interstitial position	u_1+eV[b]	2.26
Transport of a negative ion from the surface into an interstitial position	u_2-eV	>2.26
Transport of a positive ion from the bulk to the surface	u_3-eV	0.65
Transport of a negative ion from the bulk to the surface	u_4+eV	1.21

[a] Calculated by Mott and Littleton, reference 8 (the pressure × volume terms by which Gibbs' potential differs from the free energy is negligible for purposes of this paper).
[b] V is the electric potential between the position of creation of the defect and the surface.

III. CONCENTRATION OF LATTICE DEFECTS IN A NaCl TYPE OF LATTICE AS FUNCTION OF THE LOCAL POTENTIAL

We shall now proceed to an explicit calculation of the concentration of lattice defects as a function of the local potential. For simplicity, we shall consider a NaCl type of lattice, and we shall assume that interstitial ions may occur only in the center of the cube of side length $a/2$ (a lattice constant). Also we shall neglect the influence of lattice defects on the vibrational energy of the crystal.[3] For lattice points we have $N_i \approx Z_i$,[4] and hence the factor $(N_i/Z_i)^{\nu_i}$ is unity for lattice points. For interstitial ions we have $Z_i = 2Z$, where Z is the number of molecules per unit volume. For vacancies we have $Z_i = Z$. Thus Eq. (4) written for the reactions listed in Table I, gives

$$N_1 = 2Z \exp[(-u_1 - eV)/kT], \tag{5}$$

$$N_2 = 2Z \exp[(-u_2 + eV)/kT], \tag{6}$$

$$N_3 = Z \exp[(-u_3 + eV)/kT], \tag{7}$$

$$N_4 = Z \exp[(-u_4 - eV)/kT]. \tag{8}$$

The indices $1 \cdots 4$ refer to interstitial cations, interstitial anions, cation vacancies, and anion vacancies, respectively. From the concentrations of lattice defects, a space charge

$$\rho = e(N_1 - N_2 - N_3 + N_4) \tag{9}$$

results. When introducing the values of Eq. (5) to (8), the space charge becomes a function of $V(x)$. In the region close to the surface we have by definition $V(0) = 0$. It is evident that the corresponding value of ρ differs in general from zero. A space charge differing from zero implies a space-dependent potential. Hence it is necessary to consider a space-dependent function $V(x)$.

The magnitude of the space-charge density close to the surface is $\ll Ze$ if $u_1 \cdots u_4 \gg kT (\approx 1/40\ eV$ at room temperature). This condition is always fulfilled in cases of practical interest (see u values of Table I). Hence we do not expect that the concentration of defects in the space charge layer is so large that the u values near the surface deviate appreciably from those in the bulk because of interaction of impurities.

The origin of the potential between surface and bulk of the crystal is easily understood from the following considerations: Imagine a perfect crystal without any lattice defects. Permit now the formation of lattice defects,[5] starting from the surface. If the energy of formation of interstitial cations is less than the energy of formation of interstitial anions, initially more interstitial cations will form and migrate into the interior than interstitial anions. This will lead to a positive space-charge layer and leave a corresponding negative charge at the surface of the crystal. The corresponding potential will obstruct migration of cations from the surface into the interior but enhance migration of anions, which is necessary to obtain a stationary state.

IV. CALCULATION OF THE POTENTIAL DISTRIBUTION

It may be concluded already for reasons of symmetry that in thermal equilibrium the bulk of a macrocrystal must be at a constant potential. Hence the space charge is zero for the bulk of the crystal and the potential difference $V(\infty)$ between the bulk of the crystal and the surface can be calculated from the zero space-charge condition, using Eq. (9) with Eqs. (5) to (8). Values of $V(\infty)$ and of the corresponding concentrations of lattice defects in the bulk of the crystal are listed in Table II for the four standard cases of disorder in ionic crystals.

The distribution of the potential between the surface and the bulk of the crystal can be calculated from Poisson's equation

$$(d^2V/dx^2) = -\rho/\epsilon\epsilon_0 \tag{10}$$

[3] N. F. Mott and R. W. Gurney, *Electronic Processes in Ionic Crystals* (Clarendon Press, Oxford, 1940).
[4] Assuming a very small degree of disorder.
[5] For simplicity, we shall discuss interstitial ions only.

(ϵ dielectric constant, $\epsilon_0=8.84\times10^{-14}$ amp sec/volt cm, ρ in amp sec/cm^3, x in cm, V in volts), using the boundary conditions $(dV/dx)=0$, $x=\infty$, and $V=0$ for $x=0$. With the aid of Eqs. (5)–(8), Eq. (9) can be transformed into

$$\rho(V)=-e[N_1(\infty)+N_4(\infty)]\times\{\exp[-e\langle V(x)-V(\infty)\rangle/kT]-\exp[e\langle V(x)-V(\infty)\rangle/kT]\}. \quad (11)$$

In writing down the equation above, use has been made of the zero space-charge condition for the bulk of the crystal: $N_1(\infty)+N_4(\infty)=N_2(\infty)+N_3(\infty)$. Introducing the dimensionless coordinates

$$p=e[V(x)-V(\infty)]/kT, \quad (12a)$$

$$\mathfrak{L}=x/\lambda, \quad (12b)$$

where

$$\lambda=(\epsilon\epsilon_0\cdot kT/e^2[N_1(\infty)+N_4(\infty)])^{\frac{1}{2}}, \quad (13)$$

Poisson's equation becomes

$$(d^2p/d\mathfrak{L}^2)=+2\sinh(+p) \quad (14)$$

with the boundary condition $p=0$ and $(dp/d\mathfrak{L})=0$ for $x=\infty$. First integration gives[6]

$$dp/d\mathfrak{L}=-\sqrt{8}\sinh p/2. \quad (15)$$

Second integration gives

$$\ln\cdot\frac{\exp(-p/2)+1}{\exp(-p/2)-1}=\sqrt{2}\mathfrak{L}+\ln\frac{\exp(-p_0/2)+1}{\exp(-p_0/2)-1}, \quad (16)$$

where $p_0=-eV(\infty)/kT$ corresponds to the position $\mathfrak{L}=0$. The potential distribution given by Eq. (16) in conjunction with Eqs. (5) to (8) determines the concentration of lattice defects as function of distance from the surface.

V. SPACE-CHARGE LAYER AND IONIC CONDUCTION

The ionic conductivity resulting from the migration of lattice defects is

$$\sigma=\sum_i (N_i b_i)\cdot e, \quad (17)$$

where b_i is the mobility of the ith type of the lattice defects. Since the concentrations of lattice defects near the surface of the crystal differ from those in the bulk, the conductivity near the surface differs from that in the bulk also.

Let us consider a cube-shaped crystal of side length A with two area-electrodes on opposite faces. The conduction of such a cube is

$$\sigma_\infty A+4\cdot e\sum_i\int_0^\infty[N_i(x)-N_i(\infty)]b_i dx=\sigma_\infty A\cdot(1+4B/A), \quad (18)$$

[6] One obtains first $(dp/d\mathfrak{L})^2=+4(\cosh p \text{ const})$. The boundary condition shows that the constant is $+1$. In taking the square root, the minus sign must be used.

TABLE II. Bulk concentration of lattice defects and surface potential (the important terms in the columns 6–9 are underlined)

1	2		3	4	5	6	7	8	9
Type of disorder	Majority defects positive	negative	Condition for presence of type of disorder indicated in column 1	Zero space-charge condition	$eV(\infty)$	$N_1(\infty)/Z$	$N_2(\infty)/Z$	$N_3(\infty)/Z$	$N_4(\infty)/Z$
Frenkel disorder of cations[a]	Interstitial cations	Cation vacancies	$N_1\gg N_4$, $N_2\gg N_3$ $u_4\gg u_1$[b] $u_2\gg u_3$	$N_1\approx N_3$	$(kT/2)\ln 2+(u_3-u_1)/2$	$2^{\frac{1}{2}}\cdot\exp[-(u_1+u_3)/2kT]$	$2^{\frac{1}{2}}\cdot\exp[-(u_1+2u_3-u_2)/2kT]$	$2^{\frac{1}{2}}\cdot\exp[-(u_1+u_3)/2kT]$	$2^{-\frac{1}{2}}\cdot\exp[-(-u_1+u_3+2u_4)/2kT]$
Frenkel disorder of anions	Anion vacancies	Interstitial anions	$N_2\gg N_3$, $N_4\gg N_1$ $u_3\gg u_2$ $u_1\gg u_4$	$N_2\approx N_4$	$(-kT/2)\ln 2-(u_4-u_2)/2$	$2^{\frac{1}{2}}\cdot\exp[-(2u_1+u_3-u_4)/2kT]$	$2^{\frac{1}{2}}\cdot\exp[-(u_3+u_4)/2kT]$	$2^{-\frac{1}{2}}\cdot\exp[-(-u_2+2u_3+u_4)/2kT]$	$2^{\frac{1}{2}}\cdot\exp[-(u_2+u_4)/2kT]$
Schottky disorder[c]	Anion vacancies	Cation vacancies	$N_4\gg N_1$, $N_2\gg N_3$ $u_1\gg u_4$ $u_2\gg u_3$	$N_2\approx N_4$	$(u_4-u_1)/2$	$2\cdot\exp[-(2u_1+u_3-u_4)/2kT]$	$2\cdot\exp[-(2u_3-u_3+u_4)/2kT]$	$\exp[-(u_3+u_4)/2kT]$	$\exp-[(u_3+u_4)/2kT]$
	Interstitial cations	Interstitial anions	$N_1\gg N_4$, $N_2\gg N_3$ $u_4\gg u_1$ $u_3\gg u_2$	$N_1\approx N_3$	$(-u_1+u_3)/2$	$2\cdot\exp[-(u_1+u_3)/2kT]$	$2\cdot\exp[-(u_1+u_3)/2kT]$	$\exp[-(u_1-u_3+2u_3)/2kT]$	$\exp[-(-u_1+u_3+2u_4)/2kT]$

[a] J. Frenkel, Z. Physik **35**, 652 (1926); applied to AgCl.
[b] $u_4\gg u_1$ means that $u_4-u_1\gg kT$ (kT is of the order of 1/40 ev at room temperature).
[c] W. Schottky, Z. physik. Chem. **B29**, 335 (1935); applied to alkali halides.

where

$$B=\left[\sum_i \int_0^\infty \langle N_i(x)-N_i(\infty)\rangle b_i dx\right]\Big/ \left[\sum_i N_i(\infty)\cdot b_i\right]. \quad (19)$$

The parameter B has the dimension of a length and may be interpreted as the width of a layer of bulk conductivity σ_∞ with a conduction equal to the extra conduction introduced by the space-charge layer near the surface. If we introduce the Eqs. (5) to (8) into Eq. (19), we are led to integrals of the type

$$\beta_i=\int_0^\infty \{\exp(-p)-1\}dx \quad (20a)$$

($i=1, 4$), and

$$\beta_i'=\int_0^\infty \{\exp(p)-1\}dx \quad (20b)$$

($i=2, 3$), where the parameter p is defined by Eq. (12a). Considering Eqs. (12b) and (15), we obtain

$$\beta_i=\int_0^{p_0} \lambda\cdot\frac{\{\exp(-p)-1\}}{8^{\frac{1}{2}}\sinh(p/2)}\cdot dp = \lambda\sqrt{2}\{\exp(-p_0/2)-1\}, \quad (21a)$$

and

$$\beta_i'=\int_0^{p_0} \lambda\cdot\frac{\exp(p)-1}{8^{\frac{1}{2}}\sinh(p/2)}\cdot dp = \lambda\sqrt{2}\{\exp(p_0/2)-1\}. \quad (21b)$$

Hence[7]

$$B=\sqrt{2}\lambda\cdot\{[N_1b_1+N_4b_4]\cdot[\exp(eV/2kT)-1] +[N_2b_2+N_3b_3]\cdot[\exp(-eV/2kT)-1]\}/\sigma_\infty. \quad (22)$$

Equation (22) applied to Schottky disorder [$N_1=N_2=0$; $N_3(\infty)=N_4(\infty)$] becomes

$$B=\sqrt{2}\lambda\cdot\exp(eV/2kT)/(1+b_3/b_4) \quad (23a)$$

if $eV(\infty)\gg 2kT$, and

$$B=\sqrt{2}\lambda\cdot\exp(-eV/2kT)/(1+b_4/b_3), \quad (23b)$$

if $eV(\infty)\ll -2kT$.

TABLE III. Thickness of space charge layer λ and "equivalent length" B of its ionic conduction, calculated for NaCl crystals using Eq. (13), Table II, and Eq. (23b), and the energy values calculated by Mott and Littleton (reference 8) (our Table I, column 5).

T	λ	B
600°K	2.2×10^{-5} cm	4.7×10^{-4} cm
900°K	1.3×10^{-6} cm	1.1×10^{-5} cm

[7] In Eqs. (22) to (23b), the argument ∞ is omitted for the N's and V.

VI. APPLICATION TO NaCl CRYSTALS

The u_i values of lattice defects of NaCl crystals have been calculated by Mott and Littleton,[8] (Table I, column 3). We shall use these values to calculate the parameters V_∞, λ, and B. Since $u_1-u_4\gg kT$, and $u_2\gg u_3$, we are dealing with Schottky defects (see Table II). The potential between surface and bulk is

$$V_\infty=(u_3-u_4)/2e=-0.28 \text{ volts}.$$

In the surface region there will be an excess of vacancies of positive ions, corresponding to a negative space charge. The corresponding excess of positive lattice ions forms a positive surface charge on the crystal. The value λ, which characterizes the order of magnitude of the penetration of the space-charge layer into the crystal, is [see Eq. (13) and Table II]

$$\lambda \text{ (in cm)}=(\epsilon\epsilon_0kT/Ze^2)^{\frac{1}{2}}\cdot\exp[(u_3+u_4)/4kT] =1.1\times10^{-10}\sqrt{T}\cdot\exp(5400/T)$$

(T in degrees Kelvin). The value of B, which characterizes the equivalent thickness for additional conduction resulting from the space-charge layer, is [Eqs. (22b), (13), and Table II]

$$B=(2\epsilon\epsilon_0kT/Ze^2)^{\frac{1}{2}}\cdot\exp(u_4/2kT)/(1+b_4/b_3) =1.55\times10^{-10}\sqrt{T}\exp(7000/\mathrm{T})/(1+b_4/b_3).$$

Numerical values of λ and B are compiled in Table III for two temperatures, $T=600$°K, and $T=900$°K. In calculating the values of B, the term b_4/b_3 was neglected. This should not introduce any error in the order of magnitude of the values obtained since it is known from the transport measurements that in NaCl $b_4/b_3\lesssim 1$.

The numerical values of Table III indicate that there will be no effect of the space-charge conduction on the conductivity of NaCl macrocrystals in the temperature range $\gtrsim 300$°C. There should be some effect of the space-charge conduction on the conduction of microcrystalline samples of grain size $\lesssim 10^{-4}$ cm. Notice that the additional conductivity due to the space charge layer $B\sigma$ increases much less with temperature than the bulk conductivity σ, because B decreases with increasing temperature.

The magnitude of the charge per unit area of the surface is [using Eq. (15), (12a), and (12b)]

$$Q=+\epsilon\epsilon_0(dV/dx)_{x=0} =(\epsilon\epsilon_0\cdot kT/\lambda)\cdot 8^{\frac{1}{2}}\cdot\sinh(eV_\infty/2kT). \quad (24)$$

When inserting the values calculated for NaCl for $T=600$°K, we obtain $Q\approx 1.6\times10^{11}$ electronic charges/cm^2. Now there are about 10^{15} ions per 1-cm^2 surface. Hence it is sufficient that only about 0.01 percent of the negative ions on the surface is missing to yield the needed surface charge. A discussion of the effect of the surface charge on the relative stability of various crystal faces is outside of the scope of this paper.

[8] N. F. Mott and M. J. Littleton, Trans. Faraday Soc. **34**, 485 (1938).

VII. INFLUENCE OF THE PRESENCE OF IMPURITIES

So far we have dealt with pure crystals. Let us now assume that impurities carrying an extra charge are present in the crystal. The contribution of these impurities must be included in the space-charge Eq. (9). The calculations of Secs. 4–6 can be repeated by using the modified space-charge equation. For the general case, these calculations are not difficult, but cumbersome. Therefore, we shall confine ourselves to a few remarks on special cases only.

If the impurities are not mobile, and if they have a space-independent concentration, and if they do not associate with mobile lattice defects into neutral clusters, then the contribution of the impurities to the space-charge equation consist in a constant term De.

At a sufficiently high impurity concentration D, namely if $D \gg 2Z\exp(-u_1)/kT$; $2Z\exp(-u_2/kT)$; $Z\exp(-u_3/kT)$; $Z\exp(-u_4/kT)$, the space charge near the surface will be

$$\rho \approx De. \tag{25}$$

Then the thickness of the space-charge layer d will be given approximately by the relation[9]

$$V_\infty = Ded^2/(2\epsilon\epsilon_0). \tag{26}$$

If one type of defect is present, say cation vacancies, and if the concentration of the impurities is sufficiently high, the zero space-charge equation becomes

$$D = N_3(\infty) \tag{27}$$

(D is the space-independent concentration of the impurities, which are assumed to be bivalent cations, substituted for lattice cations, e.g., Cd for Na in NaCl). Using Eq. (7), we obtain

$$V_\infty = -u_3/e + kT/e \ln D/Z. \tag{28}$$

Notice that the potential between surface and bulk is a function of the impurity concentration.

VIII. METAL-SALT INTERFACE

We have considered so far the case that the surface of the ionic crystal is free, i.e., is in contact with its equilibrium vapor. Another interesting case is the contact of the surface with a solid phase, e.g., a metal. The energies appearing in Table I will then contain an additional term, resulting from the bond energy of the surface ions of the salt with the metal. If the metal electrode consists of the same element which is present in the salt, the concentration of metal vacancies in the salt near the boundary of the electrode will be smaller (relative to the bulk of the salt) and the concentration of metalloid vacancies will be larger. Again there will be a space-charge layer and a space-charge potential; the surface charge will be an electronic charge located at the electrode surface. The space-charge layer at the metal-salt interface should show up in conductance measurements, if the conductivity in the space-charge layer is smaller than in the bulk layer.

IX. DISCUSSION

(a) Ionic Conduction

In Sec. 5, we have calculated the implications of the surface space-charge layer on the ionic conduction of a pure crystal. These equations could be tested by measuring the conductivity of samples of varying ratio surface to volume. In such experiments care must be taken to avoid adsorption of foreign ions at the surface, which would modify the space charge layer in the crystal. In the interpretation of the measurements, the space-charge conduction must be distinguished from any possible conduction along the very surface of the crystal, which may arise from the fact that the energy required for moving ions along the very surface of a crystal can be much smaller than that for movement through the bulk of the crystal.[10] Obviously, this type of surface conduction has nothing in common with the space-charge layer conduction discussed in this paper: the space-charge layer conduction extends to a depth *large* compared to interatomic spacings and is based on activation energies and mobilities which are space independent. Measurements of the conductivity of AgBr pressed pellets were made by Shapiro and Kolthoff.[11] The decrease of the low temperature conduction of pressed AgBr pellets with aging was attributed to a decrease in the internal free surface, assuming that the low temperature conduction arises from the presence of internal surfaces. The activation energy of the low temperature conduction was found to be identical with that of the mobility of Ag ions derived by Wagner and Koch.[12] This would indicate that the concentration of carriers causing the surface conduction does not depend on temperature. This conduction cannot be attributed to a surface space-charge layer, because the concentration of carriers in the surface space-charge layer depends on temperature.

(b) Diffusion

The distribution of potential and of lattice defect concentration near the surface of an ionic crystal may have some bearing on the diffusion of ions from the surface into the bulk of an ionic crystal. A possible effect of the space-charge layer should be considered in diffusion experiments, in which the particles diffuse over distances which are not much larger than λ. Distances of diffusion of the order of magnitude of 10^{-3} cm or

[9] Compare the calculations of W. Schottky [Z. Physik **118**, 539 (1942)] regarding the exhaustion space-charge layer in electronic semiconductors.

[10] A. Smekal, *Handbuch der Physik* **24/2**, 88 (1933).

[11] I. Shapiro and I. M. Kolthoff, J. Chem. Phys. **15**, 41 (1947); J. Phys. and Colloid Chem. **52**, 1319 (1948).

[12] C. Wagner and E. Koch, Z. physik. Chem. **B38**, 295 (1937).

smaller are not uncommon in experiments using radioactive isotopes.[13]

(c) Photovoltaic Effect

We like to mention briefly some implications of the surface space-charge layer for electronic processes in ionic crystals. Suppose electrons and holes are generated within the space-charge layer, say by light absorption or by nucleon bombardment. The electrons and holes will be driven in opposite direction by the existing field. This will lead to a decrease in the surface potential. After the light is switched off, the original surface potential will be reestablished with time.

If the crystal is placed between two condenser plates, the change of potential between surface and bulk of the crystal by illumination should be reflected in a voltage between the condenser plates. This arrangement may be used to measure $V(\infty)$. Measurements of this sort were made by Bergmann and Hänsler[14] on many crystals, including some ionic compounds in form of microcrystalline powder. The measurements were made at room temperature, where ionic conduction is likely to result from impurities. It would be interesting to measure the surface potential of thin slices of ionic crystals at elevated temperatures by using the technique of Bergmann and Hänsler.[14] Both the change in potential and the time needed for restoring the original state after switching off the light should be studied. The restitution of the original potential may occur by either one of the two following processes: (1) Lattice defects migrate from the surface into the bulk of the crystal. (2) The electrons and (or) the holes overcome the surface potential and recombine. It is likely that both the electrons and holes are trapped very soon at lattice defects of opposite sign. Hence the first-mentioned process is the more likely one.

(d) Photographic Effect

Photoelectric processes of the type just mentioned may play an important role in the formation of the latent image in silver bromide and silver chloride. It is known[4] that the primary process in the latent image formation consists in the photoelectric release of an electron. The electron soon is trapped and attracts a silver ion. The silver ion is neutralized by the trapped electron. The neutral silver atom may trap a further electron, etc., until a silver speck consisting of many atoms is formed. For the subsequent chemical development it is favorable, if not necessary, that the silver speck forms at the surface of the silver bromide grain. This will be the case if the first electron, which caused the formation of the silver speck, was released in the space-charge layer near the surface and if the surface field is such as to draw electrons toward the surface. In practice, the surface field is likely to be determined by impurities, both adsorbed at the crystal and included in the crystal, rather than by the intrinsic properties of the pure crystal. It would be very interesting to study the photographic process on thin sheets of single crystals as a function of the thickness of the sheet and of impurities.

(e) Surface Potential and Lattice Theory

From an analysis of conductivity of ionic crystals as function of impurity content and of temperature, it is possible[12] to derive values of the energy of formation of a *pair* of lattice defects (e.g., in the case of Schottky defects u_3+u_4).[15] If the surface potential $V(\infty)$ were known from experiment, the energies of formation of the individual lattice defect could be derived.

I like to express my appreciation to Dr. P. Robinson for his support of this work and to Dr. E. Belmont for reading the manuscript and presenting the topic for me at the American Physical Society Meeting,[16] which I was unable to attend because of an illness.

Note added in Proof:—Mr. R. J. Friauf has brought to my attention a previous discussion of the surface space-charge layer in pure ionic crystals by J. Frenkel [*Kinetic Theory of Liquids* (Oxford University Press, New York, 1946)]. The application of the surface space-charge layer to surface conduction and the role of impurities are not discussed in Frenkel's book.

[13] H. W. Etzel and R. J. Maurer, J. Chem. Phys. **18**, 1003 (1950); R. W. Redington, Phys. Rev. **87**, 1066 (1952).
[14] L. Bergmann and J. Hänsler, Z. Physik **100**, 50 (1936).
[15] Strictly the temperature independent part of u_3+u_4.
[16] K. Lehovec, Bull. Am. Phys. Soc. **28**, No. 1, 21 (1953).

The Infrared Spectrum of CF_3D

SANTIAGO R. POLO* AND M. KENT WILSON
Mallinckrodt Chemical Laboratory, Harvard University, Cambridge, Massachusetts
(Received October 24, 1952)

CF_3D was prepared in high purity and its infrared spectrum investigated. The fundamental frequencies are

$$\nu_1(a_1)=2257\ \text{cm}^{-1},\quad \nu_2(a_1)=1111\ \text{cm}^{-1},\quad \nu_3(a_1)=693\ \text{cm}^{-1},$$
$$\nu_4(e)=1210\ \text{cm}^{-1},\quad \nu_5(e)=977\ \text{cm}^{-1},\quad \nu_6(e)=502\ \text{cm}^{-1}.$$

Thermodynamic functions have been calculated with the usual assumptions.

INTRODUCTION

IN relation to an investigation of the absolute intensities of the infrared bands in compounds of the type CX_3H and CX_3D, the compound CF_3D has been prepared and its infrared spectrum studied.

Approximate values of the fundamental frequencies have been calculated,[1] but no reference to the preparation of this substance in isotopic purity nor to any experimental work concerning the vibrational spectrum was found in the literature. Recently the results of a microwave study have been reported.[2]

EXPERIMENTAL

To obtain reliable intensity data it is desirable to have products of high purity. The preparative method described below proved to be completely satisfactory in this respect.

About 4 g of CF_3I from a sample used in a previous investigation[3] was distilled in vacuum and condensed at -80°C into a stainless steel bomb containing 3 g of yellow phosphorus. The bomb was then heated at 250°C for 36 hours.[4] The reaction products were vacuum fractionated into a volatile portion consisting of unreacted CF_3I, a middle fraction consisting in the main of $P(CF_3)_3$ to be used for other purposes, and a final portion consisting of a mixture of $PI(CF_3)_2$ and PI_2CF_3. The final portion was hydrolyzed with a 50 percent solution of sodium deuteroxide in heavy water (99.8 percent D_2O) to yield CF_3D. Traces of unreacted phosphines were easily separated from the product by bulb-to-bulb distillation in vacuum.

The purity of the CF_3D obtained is believed to be very high, as deduced from its infrared spectrum. The strongest band of CF_3H, 1152 cm^{-1}, did not appear at pressures low enough for its observation. At high pressures of CF_3D the strong bands of the deutero compound at 1111 and 1210 cm^{-1} completely obscure the 1150-cm^{-1} region. The second strong band of CF_3H lies at 1372 cm^{-1}. A very weak absorption was observed at 1380 cm^{-1} in the sample of CF_3D, but as the first overtone of the CF_3D fundamental at 693 cm^{-1} might also appear in this region, it is difficult to say whether the sample of CF_3D contained any CF_3H. However, because of the low intensity of the absorption near 1380 cm^{-1} and the characterisitcs of the preparative method, we believe that the ratio of D to H in the product must correspond closely to that of the heavy water used.

Measurements of the infrared spectrum were obtained by means of a Baird Associates spectrophotometer equipped with NaCl optics and a Perkin-Elmer 12 C spectrograph equipped with CaF_2, NaCl, and KBr prisms. Gas cells 5 and 10 cm in length with KBr windows were used.

EXPERIMENTAL RESULTS

The observed frequencies and band assignments are listed in Table I. The observed spectrum replotted on a linear frequency scale is shown in Fig. 1. Since the

TABLE I. Observed frequencies and band assignments for gaseous CF_3D.

ν(cm^{-1})	Assignment	Δ(cm^{-1})[a]
502	$\nu_6(e)$	
693	$\nu_3(a_1)$	
973, 981	$\nu_5(e)$, $2\nu_6(A_1+E)$	27
1111	$\nu_2(a_1)$	
1193	$\nu_6+\nu_3(E)$	2
1210	$\nu_4(e)$	
1378	($2\nu_3$, CF_3H)?	8
1612	$\nu_2+\nu_6(E)$	1
1671	$\nu_3+\nu_5(E)$	-1
1896	$\nu_3+\nu_4(E)$	7
1948	$2\nu_5(A_1+E)$	6
2078, 2090	$\nu_2+\nu_5(E)$	4
2150, 2156	$\nu_4+\nu_5(A_1+E)$	36
2257	$\nu_1(a_1)$	
2311	$\nu_2+\nu_4(E)$	10
2412, 2429	$2\nu_4(A_1+E)$	0
3256	$\nu_1+\nu_5(E)$	-23
~3360	$\nu_1+\nu_2(A_1)$	~10
~3530	$\nu_2+2\nu_4(A_1+E)$	~0
~3620	$3\nu_4(A_1+E)$	~10

[a] Δ = calc frequency − obs frequency.

* Research Fellow of the Spanish National Council for Scientific Research.

[1] Decker, Meister, and Cleveland, J. Chem. Phys. **19**, 784 (1951).

[2] Ghosh, Trambarulo, and Gordy, J. Chem. Phys. **20**, 605 (1952).

[3] S. R. Polo and M. K. Wilson, J. Chem. Phys. **20**, 1183 (1952).

[4] Bennet, Brandt, Emeleus, and Haszeldine, Nature **166**, 225 (1950).

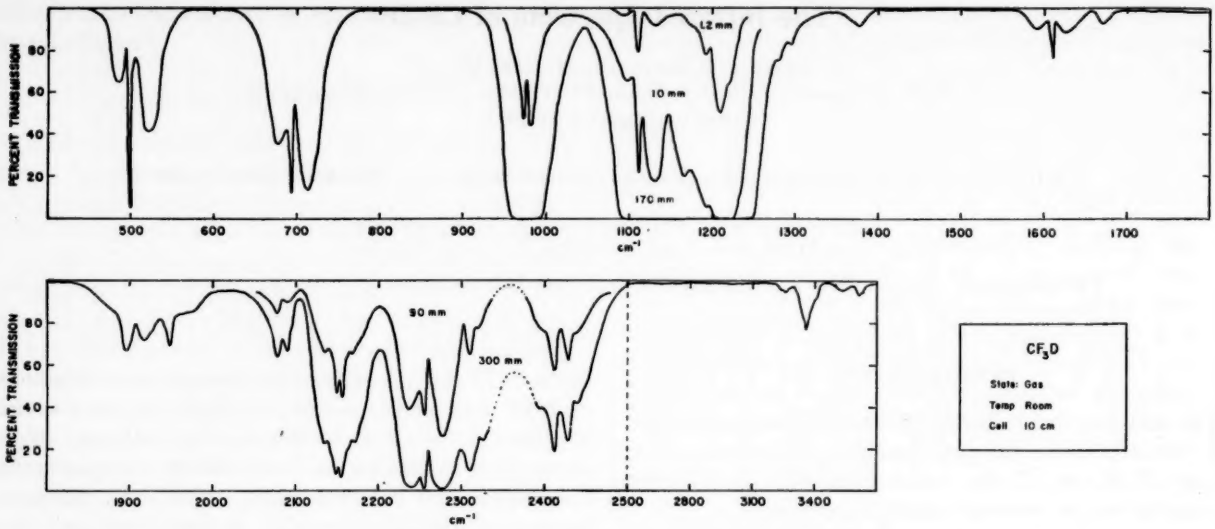

FIG. 1. The infrared spectrum of gaseous CF_3D.

spectra were taken at various pressures and path lengths, the equivalent pressure for a 10-cm path length is indicated in the figure.

DISCUSSION

The assignment of the fundamentals has been made on the basis of the structures and intensities of the bands and by comparison with the assignments previously given for CF_3H,[5,6] which the present investigation supports. There is also good agreement with the predicted frequencies.[1]

The three a_1 fundamental bands have the *PQR* structure characteristic of parallel bands of a symmetric top. The *e*-type fundamental ν_6, at 502 cm^{-1}, also has a *PQR* structure similar to that of a parallel band, indicating that the ζ value is close to $1-I_z/I_x$. The corresponding band in several other symmetric top molecules, for example, CF_3H,[6] NF_3 and PF_3,[7] and BF_3,[8] has this same shape.

The structures of the other two *e*-type bands ν_5 and ν_4 are somewhat more particular. The first, ν_5, shows two clearly resolved peaks of almost the same intensity at 973 and 981 cm^{-1}. Its shape clearly does not correspond to any of the normal band shapes expected for symmetric top molecules.† It is suggested that the observed band shape is the result of Fermi resonance of ν_5 with $2\nu_6(A_1+E)$ whose calculated frequency is 1004 cm^{-1}. Because of the nearly equal intensity of the two peaks of the observed doublet, the two unperturbed levels must be almost coincident. This leads to an anharmonicity for the overtone of about 25 cm^{-1}, which is unexpected in view of the fact that the $2\nu_6$ in CF_3H occurs at exactly twice the frequency of the fundamental.[6] It should be noted that for other overtones and combination bands there is not always correspondence between the two isotopic molecules.

The strong absorption in the 1200-cm^{-1} region may be interpreted as the superposition of $\nu_4(e)$, to which the strong peak at 1210 cm^{-1} may be assigned, and the combination band $\nu_3+\nu_6(E)$. In CF_3H this combination appears as a strong band with a well-defined *PQR* structure. Accordingly, in CF_3D the peak at 1193 cm^{-1} may be ascribed to the *Q* branch of $\nu_3+\nu_6$; the calculated value is 1195 cm^{-1}. This combination band is rather intense in both molecules, perhaps caused in part by Fermi resonance with the neighboring fundamentals.

In agreement with what has been said about ν_4 and

TABLE II. The fundamental frequencies of gaseous CF_3H and CF_3D.

Assignment	$\nu(cm^{-1})$ CF_3H	CF_3D
$\nu_1(a_1)$	3031	2257
$\nu_2(a_1)$	(1152)[a]	1111
$\nu_3(a_1)$	700	693
$\nu_4(e)$	1372	1210
$\nu_5(e)$	(1152)[a]	977
$\nu_6(e)$	507	502

[a] The frequencies ν_3 and ν_2 of CF_3H are somewhat uncertain as these two bands are unresolved.

[5] Rank, Shull, and Pace, J. Chem. Phys. **18**, 885 (1950).
[6] E. K. Plyler and W. S. Benedict, J. Research Natl. Bur. Standards **47**, 202 (1951).
[7] M. K. Wilson and S. R. Polo, J. Chem. Phys. **20**, 1716, (1952).
[8] D. M. Gage and E. F. Barker, J. Chem. Phys. **7**, 455 (1939).

† A similar structure has been observed in the *e*-type fundamental at 970 cm^{-1} of CF_3CH_3 as well as in a number of combination bands involving this fundamental. [Cowan, Herzberg, and Sinha, J. Chem. Phys. **18**, 1538 (1950); Smith, Brown, Nielsen, Smith, and Liang, J. Chem. Phys. **20**, 473 (1952); Nielsen, Claasen, and Smith, J. Chem. Phys. **18**, 1471 (1950)]. The explanation suggested by Cowan, Herzberg, and Sinha is that the doubling results from a splitting of the degeneracy associated with the three potential minima of the torsional mode.

An alternative explanation that can be given is that of a Fermi resonance interaction with the combination of the two low frequency bands, $367+603=970$ cm^{-1}. This combination band possesses the required symmetry.

ν_5 the combination bands involving these fundamentals also show a splitting as can be observed in Fig. 1.

A check on the consistency of the assignments is given by the fulfillment of the isotopic relations among the frequencies of CF_3H and CF_3D. From the observed frequencies one obtains

$$\frac{(\nu_1\nu_2\nu_3)_H}{(\nu_1\nu_2\nu_3)_D}=1.407, \quad \text{and} \quad \frac{(\nu_4\nu_5\nu_6)_H}{(\nu_4\nu_5\nu_6)_D}=1.350.$$

The calculated values are 1.404 and 1.375, respectively. The values of the frequencies used in these calculations are those listed in Table II. The moments of inertia I_x are those obtained from microwave data.[2]

Calculation of potential constants are in progress and will be reported in connection with further work on related molecules.

THERMODYNAMIC FUNCTIONS

Thermodynamic functions for CF_3D within a convenient temperature range are listed in Table III.

TABLE III. Thermodynamic functions for CF_3D.[a]

T(°K)	$C_p°$	S°	$\frac{H-H_0}{T}$	$\frac{-(F-H_0)}{T}$
200	10.04	57.82	8.45	49.37
273.15	12.06	61.24	9.14	52.10
298.15	12.76	62.33	9.42	52.91
400	15.40	66.46	10.61	55.84
600	19.08	73.46	12.88	60.59
800	21.25	79.28	14.72	64.56
1000	22.56	84.17	16.17	68.00
1200	23.41	88.37	17.31	71.06
1500	24.18	93.68	18.61	75.06

[a] The units are cal/deg mole.

These values have been calculated for an ideal gas at 1-atmos pressure with a rigid-rotor, harmonic oscillator approximation.

We wish to thank Professor Geoffrey Wilkinson for help with the phosphine preparation and Professor Richard C. Lord, Jr., for helpful discussions. It is also a pleasure to acknowledge a grant-in-aid from the American Academy of Arts and Sciences.

THE JOURNAL OF CHEMICAL PHYSICS VOLUME 21, NUMBER 7 JULY, 1953

An Application of Perturbation Theory to the *F* and *G* Matrix Method of Calculating Molecular Vibration Frequencies

P. W. HIGGS
Wheatstone Physics Laboratory, King's College, Strand, London, W.C. 2., England.

(Received February 17, 1953)

The *F* and *G* matrix form of the secular equation for molecular vibrations may be split into two approximate equations, of which one has as its roots the high frequencies (corresponding to relatively rigid bonds, etc.), the other the low frequencies (corresponding to relatively weak bonds, etc.). With the aid of the eigenvectors of these two equations, the exact equation is transformed into a form which yields the corrections to the approximate frequencies by a straightforward application of perturbation theory. The use of the correction terms so derived and the convergence of the perturbation series are illustrated by a discussion of the totally symmetric modes of ethylene.

INTRODUCTION

THE *F* and *G* matrix method introduced by Wilson[1,2] is often useful in the calculation of the vibration frequencies of polyatomic molecules: its chief virtue is that it reduces the order of the secular equation for a molecule containing N atoms from $3N$ to $3N-6$ by eliminating the zero roots which correspond to translation and rotation. In this method the frequencies are obtained from the matrix equation,

$$\mathbf{GF}\mathbf{y}_i=\lambda_i\mathbf{y}_i. \tag{1}$$

In this equation

$$\lambda_i=4\pi^2c^2\tilde{\nu}_i^2,$$

where $\tilde{\nu}_i$ is a vibration frequency measured in wave numbers, $\mathbf{y}_i$ is the column vector of internal displacements (extensions of bonds, angular deformations, etc.) in the corresponding normal mode, and **F** and **G** are known symmetric matrices. **F** is the potential energy matrix defined by

$$V=\tfrac{1}{2}\mathbf{y}'\mathbf{F}\mathbf{y},$$

where **y** is a general internal displacement; **G** is the inverse kinetic-energy matrix, such that the kinetic energy of vibration is

$$T=\tfrac{1}{2}\dot{\mathbf{y}}'\mathbf{G}\dot{\mathbf{y}}^{-1}.$$

λ_i is then the ith root of the determinantal equation,

$$|\mathbf{GF}-\lambda\mathbf{I}|=0, \tag{2}$$

where **I** is the unit matrix of order $3N-6$.

(In matrix equations boldface lettering is used to denote matrices, square and rectangular matrices being printed in capitals and row and column vectors in

[1] E. B. Wilson, Jr., J. Chem. Phys. 7, 1047 (1939).
[2] E. B. Wilson, Jr., J. Chem. Phys. 9, 76 (1941).

lower case. A prime is used to denote the transpose of a matrix.)

Frequently it is possible and convenient to effect a further simplification by an approximate procedure. We partition the complete set of frequencies into two classes, high frequencies (A) and low frequencies (B). We may consider that these classes are related to a corresponding partition of $\mathbf{F}$ into large and small force-constants, that is, we assume that $\mathbf{F}$ may be written in the form,

$$\mathbf{F}=\begin{pmatrix}\mathbf{F}_A, & \mathbf{0}\\ \mathbf{0}, & \mathbf{F}_B\end{pmatrix},$$

where $\mathbf{F}_A$, $\mathbf{F}_B$ are of orders n_A, n_B, respectively ($n_A+n_B=3N-6$), and the latent roots of $\mathbf{F}_A$ are large compared with those of $\mathbf{F}_B$. Let the corresponding partitions of $\mathbf{y}$ and $\mathbf{G}$ be

$$\mathbf{y}=\begin{pmatrix}\mathbf{y}_A\\ \mathbf{y}_B\end{pmatrix} \quad \text{and} \quad \mathbf{G}=\begin{pmatrix}\mathbf{G}_{AA}, & \mathbf{G}_{AB}\\ \mathbf{G}_{BA}, & \mathbf{G}_{BB}\end{pmatrix},$$

where $\mathbf{G}_{BA}=\mathbf{G}'_{BA}$. The secular Eq. (2) becomes

$$\begin{vmatrix}\mathbf{G}_{AA}\mathbf{F}_A-\lambda\mathbf{I}_A, & \mathbf{G}_{AB}\mathbf{F}_B\\ \mathbf{G}_{BA}\mathbf{F}_A, & \mathbf{G}_{BB}\mathbf{F}_B-\lambda\mathbf{I}_B\end{vmatrix}=0,$$

where $\mathbf{I}_A$, $\mathbf{I}_B$ are the unit matrices of orders n_A, n_B, respectively. Obviously if we neglect $\mathbf{F}_B$ in comparison with $\mathbf{F}_A$, the high frequencies are the n_A roots of the equation,

$$|\mathbf{G}_{AA}\mathbf{F}_A-\lambda_A\mathbf{I}_A|=0. \tag{3a}$$

Wilson[2] showed that when $\mathbf{F}_A$ is large compared with $\mathbf{F}_B$ (so that the bonds of class A are effectively rigid during normal vibrations of class B), the low frequencies are the n_B roots of the equation,

$$|\mathbf{G}^*_{BB}\mathbf{F}_B-\lambda_B\mathbf{I}_B|=0, \tag{3b}$$

where

$$\mathbf{G}^*_{BB}=\mathbf{G}_{BB}-\mathbf{G}_{BA}\mathbf{G}_{AA}^{-1}\mathbf{G}_{AB}. \tag{4}$$

This replacement of one secular equation of order $3N-6$ by two approximate ones of orders n_A and n_B often simplifies the computation considerably.

There are several instances in which the approximation is adequate: for example, the CH stretching frequency (about 3000 cm^{-1}) is high compared with most of the other frequencies of organic molecules and is therefore nearly constant in all molecules, since it may be calculated from Eq. (3a) without reference to the dynamical properties of the rest of the molecule. Conversely, one may usually treat a CH bond as rigid in calculating the remaining frequencies from Eq. (3b). However, it is sometimes desirable to apply corrections to this first approximation: in this paper the necessary correction terms are derived by an application of matrix perturbation theory. The remarkable constancy throughout a large number of molecules of the spectral frequencies associated with certain bonds or groups of bonds (the CH frequency already mentioned is a notable example) indicates that the series of correction terms so derived may be expected to converge rapidly in many cases of importance.

TRANSFORMATION OF THE SECULAR EQUATION

The exact secular equation which we wish to solve is Eq. (2), in which

$$\mathbf{GF}=\begin{pmatrix}\mathbf{G}_{AA}\mathbf{F}_A, & \mathbf{G}_{AB}\mathbf{F}_B\\ \mathbf{G}_{BA}\mathbf{F}_A, & \mathbf{G}_{BB}\mathbf{F}_B\end{pmatrix}.$$

Let us suppose that we have already solved the approximate Eqs. (3a) and (3b) to obtain approximate eigenvalues which we shall denote by λ^0_{Ai} ($i=1$ to n_A) and λ^1_{Bj} ($j=1$ to n_B), respectively: for simplicity we assume that these are nondegenerate. We now calculate the corresponding row eigenvectors $\mathbf{x}_{Ai}$ and $\mathbf{x}_{Bj}$ from the matrix equations,

$$\mathbf{x}_{Ai}\mathbf{G}_{AA}\mathbf{F}_A=\lambda^0_{Ai}\mathbf{x}_{Ai}, \tag{5a}$$

$$\mathbf{x}_{Bj}\mathbf{G}^*_{BB}\mathbf{F}_B=\lambda^1_{Bj}\mathbf{x}_{Bj}. \tag{5b}$$

These eigenvectors contain an arbitrary scalar factor and so may be normalized by imposing the conditions,

$$\mathbf{x}_{Ai}\mathbf{G}_{AA}\mathbf{x}'_{Ai}=1, \tag{6a}$$

$$\mathbf{x}_{Bj}\mathbf{G}^*_{BB}\mathbf{x}'_{Bj}=1. \tag{6b}$$

By postmultiplying Eq. (5a) by $\mathbf{G}_{AA}\mathbf{x}'_{Ah}$, premultiplying the transpose of the corresponding equation in λ^0_{Ah} by $\mathbf{x}_{Ai}\mathbf{G}_{AA}$, and subtracting one from the other, we prove the eigenvectors to be orthogonal in the sense,

$$\mathbf{x}_{Ai}\mathbf{G}_{AA}\mathbf{x}'_{Ah}=0 \quad (i\neq h). \tag{7a}$$

Similarly we may prove that

$$\mathbf{x}_{Bj}\mathbf{G}^*_{BB}\mathbf{x}'_{Bk}=0 \quad (j\neq k). \tag{7b}$$

Let us construct square matrices $\mathbf{X}_A$ and $\mathbf{X}_B$ from rows $\mathbf{x}_{Ai}$ ($i=1$ to n_A) and $\mathbf{x}_{Bj}$ ($j=1$ to n_B), respectively: since a complete set of eigenvectors is a linearly independent set, $\mathbf{X}_A$ and $\mathbf{X}_B$ are regular. The Eqs. (5) may now be written

$$\mathbf{X}_A\mathbf{G}_{AA}\mathbf{F}_A=\mathbf{\Lambda}^0{}_A\mathbf{X}_A, \tag{8a}$$

$$\mathbf{X}_B\mathbf{G}^*_{BB}\mathbf{F}_B=\mathbf{\Lambda}^1{}_B\mathbf{X}_B, \tag{8b}$$

where

$$\mathbf{\Lambda}^0{}_A=\text{diag}\ (\lambda^0_{Ai}), \quad \mathbf{\Lambda}^1{}_B=\text{diag}\ (\lambda^1_{Bj}).$$

Equations (6) and (7) may be combined into

$$\mathbf{X}_A\mathbf{G}_{AA}\mathbf{X}'_A=\mathbf{I}_A, \tag{9a}$$

$$\mathbf{X}_B\mathbf{G}^*_{BB}\mathbf{X}'_B=\mathbf{I}_B. \tag{9b}$$

We next construct the matrices

$$\mathbf{P}=\begin{pmatrix}\mathbf{X}_A, & \mathbf{0}\\ -\mathbf{X}_B\mathbf{G}_{BA}\mathbf{G}_{AA}^{-1}, & \mathbf{X}_B\end{pmatrix}$$

and

$$\mathbf{Q}=\begin{pmatrix}\mathbf{G}_{AA}\mathbf{X}'_A, & \mathbf{0}\\ \mathbf{G}_{BA}\mathbf{X}'_A, & \mathbf{G}^*_{BB}\mathbf{X}'_B\end{pmatrix},$$

which are easily seen from Eqs. (9) to be reciprocals ($\mathbf{PQ}=\mathbf{I}$). Pre- and postmultiplication of $\mathbf{GF}$ by $\mathbf{P}$ and $\mathbf{Q}$ respectively yields the symmetric matrix,

$$\mathbf{H}=\mathbf{PGFQ}=\begin{pmatrix}\mathbf{X}_A\mathbf{G}_{AA}\mathbf{F}_A\mathbf{G}_{AA}\mathbf{X}'_A & \\ +\mathbf{X}_A\mathbf{G}_{AB}\mathbf{F}_B\mathbf{G}_{BA}\mathbf{X}'_A, & \mathbf{X}_A\mathbf{G}_{AB}\mathbf{F}_B\mathbf{G}^*_{BB}\mathbf{X}'_B\\ \mathbf{X}_B\mathbf{G}^*_{BB}\mathbf{F}_B\mathbf{G}_{BA}\mathbf{X}'_A, & \mathbf{X}_B\mathbf{G}^*_{BB}\mathbf{F}_B\mathbf{G}^*_{BB}\mathbf{X}'_B\end{pmatrix}.$$

This formula may be simplified by defining the new matrices,

$$\begin{aligned}\mathbf{\Gamma}_{AB}&=\mathbf{X}_A\mathbf{G}_{AB}\mathbf{X}'_B, \qquad (10)\\ \mathbf{\Gamma}_{BA}&=\mathbf{\Gamma}'_{AB},\end{aligned}$$

and using Eqs. (8) and (9),

$$\mathbf{H}=\begin{pmatrix}\mathbf{\Lambda}^0{}_A+\mathbf{\Gamma}_{AB}\mathbf{\Lambda}^1{}_B\mathbf{\Gamma}_{BA}, & \mathbf{\Gamma}_{AB}\mathbf{\Lambda}^1{}_B\\ \mathbf{\Lambda}^1{}_B\mathbf{\Gamma}_{BA}, & \mathbf{\Lambda}^1{}_B\end{pmatrix}. \qquad (11)$$

Thus pre- and postmultiplication of the secular Eq. (2) by $|\mathbf{P}|$ and $|\mathbf{Q}|$, respectively, transforms it to the new form,

$$|\mathbf{H}-\lambda\mathbf{I}|=0, \qquad (12)$$

where $\mathbf{H}$ is defined by Eq. (11).

APPLICATION OF PERTURBATION THEORY

So far, in the derivation of Eq. (12) from the original secular equation, the theory has been exact. Now let us suppose that the frequencies of class B are low compared with those of class A, that is, that all the ratios $\lambda^1{}_{Bj}/\lambda^0{}_{Ai}$ are small. Then $\mathbf{\Lambda}^1{}_B$ may be considered as of the first order of smallness relative to $\mathbf{\Lambda}^0{}_A$, and $\mathbf{H}$ may be expanded as a series,

$$\mathbf{H}=\mathbf{H}^0+\mathbf{H}^1,$$

where, from Eq. (11), the zeroth- and first-order terms are, respectively,

$$\mathbf{H}^0=\begin{pmatrix}\mathbf{\Lambda}^0{}_A, & \mathbf{0}\\ \mathbf{0}, & \mathbf{0}\end{pmatrix},$$

$$\mathbf{H}^1=\begin{pmatrix}\mathbf{\Gamma}_{AB}\mathbf{\Lambda}^1{}_B\mathbf{\Gamma}_{BA}, & \mathbf{\Gamma}_{AB}\mathbf{\Lambda}^1{}_B\\ \mathbf{\Lambda}^1{}_B\mathbf{\Gamma}_{BA}, & \mathbf{\Lambda}^1{}_B\end{pmatrix}.$$

Let the corresponding series for the eigenvalues be

$$\begin{aligned}\lambda_{Ai}&=\lambda^0{}_{Ai}+\lambda^1{}_{Ai}+\lambda^2{}_{Ai}+\cdots\text{etc.},\\ \lambda_{Bj}&=\qquad\lambda^1{}_{Bj}+\lambda^2{}_{Bj}+\lambda^3{}_{Bj}+\cdots\text{etc.}\end{aligned}$$

A straightforward application of perturbation theory leads to the following formulas for the successive corrections to $\lambda^\circ{}_{Ai}$ and $\lambda^1{}_{Bj}$.

First correction:

$$\lambda^1{}_{Ai}=H^1{}_{Ai,Ai}=\sum_{j=1}^{n_B}(\Gamma_{Ai,Bj})^2\lambda^1{}_{Bj}.$$

$$\lambda^2{}_{Bj}=\sum_i H^1{}_{Bj,Ai}H^1{}_{Ai,Bj}/(\lambda^0{}_{Bj}-\lambda^0{}_{Ai})=-(\lambda^1{}_{Bj})^2\sum_{i=1}^{n_A}(\Gamma_{Bj,Ai})^2/\lambda^0{}_{Ai}.$$

Second correction:

$$\begin{aligned}\lambda^2{}_{Ai}&=\sum_h{}' H^1{}_{Ai,Ah}H^1{}_{Ah,Ai}/(\lambda^0{}_{Ai}-\lambda^0{}_{Ah})\\ &\quad+\sum_j H^1{}_{Ai,Bj}H^1{}_{Bj,Ai}/(\lambda^0{}_{Ai}-\lambda^0{}_{Bj})\\ &=\sum_{h=1}^{n_A}{}'\{\sum_{j=1}^{n_B}\Gamma_{Ai,Bj}\lambda^1{}_{Bj}\Gamma_{Bj,Ah}\}^2/(\lambda^0{}_{Ai}-\lambda^0{}_{Ah})\\ &\quad+(\lambda^0{}_{Ai})^{-1}\sum_{j=1}^{n_B}(\Gamma_{Ai,Bj}\lambda^1{}_{Bj})^2.\end{aligned}$$

$$\begin{aligned}\lambda^3{}_{Bj}&=\sum_{i,h}H^1{}_{Bj,Ai}H^1{}_{Ai,Ah}H^1{}_{Ah,Bj}/(\lambda^0{}_{Bj}-\lambda^0{}_{Ai})(\lambda^0{}_{Bj}-\lambda^0{}_{Ah})\\ &\quad-\sum_i H^1{}_{Bj,Bj}H^1{}_{Bj,Ai}H^1{}_{Ai,Bj}/(\lambda^0{}_{Bj}-\lambda^0{}_{Ai})^2\\ &\quad+\sum_k{}'\{\sum_i H^1{}_{Bj,Ai}H^1{}_{Ai,Bk}/(\lambda^0{}_{Bj}-\lambda^0{}_{Ai})\}^2/(\lambda^1{}_{Bj}-\lambda^1{}_{Bk})\\ &=(\lambda^1{}_{Bj})^3[\sum_{k=1}^{n_B}{}'\{\sum_{i=1}^{n_A}\Gamma_{Bj,Ai}(\lambda^0{}_{Ai})^{-1}\Gamma_{Ai,Bk}\}^2\times\lambda^1{}_{Bk}/(\lambda^1{}_{Bj}-\lambda^1{}_{Bk})\\ &\quad+\{\sum_{i=1}^{n_A}(\Gamma_{Bj,Ai})^2/\lambda^0{}_{Ai}\}^2-\sum_{i=1}^{n_A}(\Gamma_{Bj,Ai}/\lambda^0{}_{Ai})^2].\end{aligned}$$

(In the formulas for $\lambda^2{}_{Ai}$ and $\lambda^3{}_{Bj}$ the primed summation signs indicate that the terms $h=i$ and $k=j$ are to be omitted from the respective summations.)

EXAMPLE: THE A_g MODES OF ETHYLENE

As a simple example of the application of the formulas derived above and to illustrate the convergence (or otherwise) of the perturbation series, let us consider the totally symmetric (A_g) modes of ethylene. There are three such modes, which may be specified roughly as follows: deformation of the HCH angles ($\tilde{\nu}_1$), stretching of the CC double bond ($\tilde{\nu}_2$) and stretching of the CH single bonds ($\tilde{\nu}_3$). The observed frequencies listed by Herzberg[3] are 1342, 1623, and 3019 cm^{-1}, respectively.

[3] G. Herzberg, *Infrared and Raman Spectra of Polyatomic Molecules* (D. Van Nostrand Company, Inc., New York, 1945), p. 184.

Three of the six possible classifications of the frequencies into sets A (high) and B (low) are set out in Table I: of these, (1) is obviously the most sensible, since $\tilde{\nu}_3$ is much higher than $\tilde{\nu}_1$ and $\tilde{\nu}_2$. (2) is more risky, for $\tilde{\nu}_1$ is not much smaller than $\tilde{\nu}_2$; (3) reverses the order of $\tilde{\nu}_1$ and $\tilde{\nu}_2$ and may therefore be expected to yield poor approximations.

In Table II are tabulated the approximate frequencies calculated according to each of the schemes (1), (2), and (3): the first entry (denoted by 0) in each section is the solution of the approximate secular equations; the other entries (labeled 1 and 2) are the same frequencies after the application of the first and second corrections, respectively. In addition, the exact solution of the cubic secular equation is given for purposes of comparison. The force-constants used in the computations are those listed by Herzberg:[3] these are chosen to fit the whole of the ethylene spectrum (six force-constants are chosen to fit a total of twelve frequencies), so the exactly calculated A_g frequencies do not agree very closely with the observed lines. This discrepancy is irrelevant to the present comparison between exact and approximate theoretical frequencies.

TABLE I. Methods of classifying the ethylene A_g modes.

	$\tilde{\nu}_1$	$\tilde{\nu}_2$	$\tilde{\nu}_3$
(1)	B	B	A
(2)	B	A	A
(3)	A	B	A

DISCUSSION

Inspection of the values of $\tilde{\nu}_1$ and $\tilde{\nu}_2$ in Table II shows that, as was to be expected, the successive approximations of calculation (1) converge quite rapidly, those of (2) converge rather more slowly, whereas those of (3) appear to be divergent. One may conclude from this that when [as in (2)] the classification into low and high frequencies is a poor one, several corrections may be necessary before reasonably accurate values are obtained for frequencies near the borderline of the classification; and that when [as in (3)] the classification actually reverses the proper order of some of the frequencies, the crude approximate solution of the secular equations is the one which lies closest to the exact solution for the reversed frequencies. On the other hand, the highest frequency ($\tilde{\nu}_3$) is obtained with good accuracy even by method (3); method (2), in which the influence of the middle frequency ($\tilde{\nu}_2$) is taken into account from the outset by including it in class A, leads to the best results. One may conclude that in the calculation of the more remote frequencies of a spectrum the method of classifying the middle frequencies is of little importance.

TABLE II. A_g frequencies of ethylene.

Type of calculation		$\tilde{\nu}_1$ (cm^{-1})	Error (%)	$\tilde{\nu}_2$ (cm^{-1})	Error (%)	$\tilde{\nu}_3$ (cm^{-1})	Error (%)
Exact		1237	—	1758	—	3013	—
(1)	0	1238	0.1	1774	0.9	2983	−1.0
	1	1237	0.0	1763	0.3	3003	−0.3
	2	1237	0.0	1759	0.1	3009	−0.1
(2)	0	1363	10.2	1598	−9.1	3009	−0.1
	1	1303	5.3	1664	−5.3	3012	−0.03
	2	1263	2.1	1710	−2.7	3012	−0.03
(3)	0	1442	16.6	1522	−13.4	2985	−0.9
	1	1534	24.0	1408	−19.9	3005	−0.3
	2	1629	31.7	1297	−26.2	3010	−0.1

The amount of labor involved in applying the corrections is quite small, when once the approximate secular equations have been solved for the eigenvalues λ^0_{Ai}, λ^1_{Bj} and the corresponding eigenvectors $\mathbf{x}_{Ai}$, $\mathbf{x}_{Bj}$. The construction of the matrix $\mathbf{\Gamma}_{AB}$ and the calculation of the successive correction terms consist merely of straightforward algebraic manipulations which can be performed rapidly on a desk calculating machine. The apparent disadvantage of the procedure is that it involves finding eigenvectors as well as eigenvalues, but for large secular equations the extra labor which this entails is small compared with that needed for the solution of the complete secular equation. For example, it is easier to compute eigenvalues and eigenvectors for two quartics than to obtain the eigenvalues of one eighth-order equation.

Finally, one comment must be made concerning the nature of the approximation used in the derivation of the approximate secular equations. In the introduction it was stated (following the usual derivation of these equations) that the classification of the frequencies corresponds to a partition of the force constants into low and high classes, that is, to a classification of the bonds, etc., into weak and strong classes. But the transformed exact secular Eq. (12) shows that it is the approximate frequencies whose relative magnitudes are important: More precisely, the convergence of the perturbation series depends on the ratios $\lambda^1_{Bj}/\lambda^0_{Ai}$. Thus the effective rigidity of a bond, in the sense which is important for the calculation of frequencies, depends not only on its having a relatively large force constant, but also on its being attached to a relatively light atom. For example, the effective rigidity of a CH bond relative to a CC single bond is a consequence of the relatively small mass of the H atom: the force constants are not very different in magnitude.

I wish to thank Professor H. C. Longuet-Higgins for reading the manuscript of this paper and for suggesting several improvements.

Free Radicals by Mass Spectrometry. IV. The Rate of Combination of Methyl Radicals*

K. U. INGOLD† AND F. P. LOSSING
Division of Pure Chemistry, National Research Council, Ottawa, Canada
(Received February 17, 1953)

The rate of combination of methyl radicals produced by the thermal decomposition of mercury dimethyl has been studied with a free radical mass spectrometer over a large range of temperature (161° to 814°C) and at one temperature (735°C) over a range of total pressure from 4.8 mm to 18.5 mm. The combination was found to be complex, consisting of a second-order homogeneous reaction and a first-order, presumably heterogeneous reaction. Only the second-order reaction was studied in any detail. The rate constant or collision efficiency of this reaction was found to increase with decreasing temperature but showed no dependence on the carrier gas pressure. A negative temperature coefficient was found for the combination which, if expressed as an activation energy, was -2.2 ± 0.5 kcal. It seems, however, more reasonable to regard this effect as a change in the effective collision diameter of the methyl radicals with temperature, the change being due to the van der Waals energy of attraction between the radicals.

INTRODUCTION

THE absolute rate of any elementary reaction in the gas phase is rarely known with any certainty; the relative rates of two reactions can, however, often be found with some accuracy. For this reason a knowledge of the rate constant ($2k_1$) for the combination of methyl radicals

$$CH_3+CH_3\rightarrow C_2H_6 \qquad (1)$$

is of considerable importance, since the ratio of this rate and the rates of a number of other elementary reactions involving methyl radicals have been measured.[1]

Quantitative work on the rate and collision efficiency of reaction (1) at a variety of temperatures and pressures is now quite extensive. The earliest work is that of Allen and Bawn,[2] who used the Polanyi flame technique to prepare the radicals and then detected them with antimony mirrors. At 621°K and at a radical pressure of 2×10^{-3} mm (total pressure 4.1 mm) they found the methyl concentration had not decreased at a distance where about 10 collisions between the radicals had occurred. Thus an upper limit of 0.1 can be given to the collision efficiency of reaction (1) at this temperature.

By the photolysis of mercury dimethyl in the presence of nitric oxide, Marcus and Steacie[3] and Miller and Steacie[4] have examined the ratio of the rate constants at room temperature for the combination of methyl radicals and the reaction of methyl radicals with nitric oxide:

$$CH_3+NO\rightarrow ?. \qquad (2)$$

The value used in both cases for the rate constant of reaction (2) was that given by Forsyth.[5]

Some work has also been done on the rate constant of the chain terminating reaction in the photolysis of acetaldehyde.[6-8] This step is generally considered to be reaction (1). Gomer and Kistiakowsky[9] have determined the rate constant of methyl combination by applying the rotating sector technique to the photolysis of acetone and mercury dimethyl. The methyl steady-state concentration was obtained from the small but accurately measurable rate of methane formation.

Values have also been reported from this laboratory[10,11] for the collision efficiency of reaction (1). However, a more elementary experimental technique and method of calculation was employed than that used in the present work, and we do not consider the results so obtained to be as accurate as those reported in this paper.

The values for the rate constant and collision efficiency of reaction (1) which have been found by the workers mentioned above, have been collected together into Table IV in the Discussion.

Experimental evidence for the magnitude of any third-body restriction on reaction (1) is rather sketchy. Davis[12] finds no significant variation in $k_n/k_1^{\frac{1}{2}}$ from 95 to 233 mm of acetone at 120° to 138°C, where k_n is the rate constant of the general reaction,

$$CH_3+RH\xrightarrow{k_n}CH_4+R, \qquad (3)$$

RH in this case being acetone. $k_n/k_1^{\frac{1}{2}}$ is also apparently invariant from 5 mm to 100 mm in the case of ethylene

* National Research Council Contribution No. 3013.
† National Research Council Postdoctorate Fellow.
[1] See, for example, A. F. Trotman-Dickenson and E. W. R. Steacie, J. Am. Chem. Soc. **72**, 2310 (1950).
[2] A. O. Allen and C. E. H. Bawn, Trans. Faraday Soc. **34**, 463 (1938).
[3] R. A. Marcus and E. W. R. Steacie, Z. Naturforsch **4a**, 332 (1949).
[4] D. M. Miller and E. W. R. Steacie, J. Chem. Phys. **19**, 73 (1951).
[5] J. S. A. Forsyth, Trans. Faraday Soc. **37**, 312 (1941).
[6] W. L. Haden and O. K. Rice, J. Chem. Phys. **10**, 445 (1942).
[7] R. E. Dodd, J. Chem. Phys. **18**, 234 (1950); Trans. Faraday Soc. **47**, 56 (1951).
[8] V. E. Lucas and O. K. Rice, J. Chem. Phys. **18**, 993 (1950).
[9] R. Gomer and G. B. Kistiakowsky, J. Chem. Phys. **19**, 85 (1951).
[10] F. P. Lossing and A. W. Tickner, J. Chem. Phys. **20**, 907 (1952).
[11] Lossing, Ingold, and Tickner, Disc. Faraday Soc. **14**, 34 (1953).
[12] W. Davis, Jr., J. Am. Chem. Soc. **70**, 1867 (1948).

oxide and mercury dimethyl at 175°C.[13] On the other hand, Trotman-Dickenson and Steacie[1,14] found some variation in this ratio during the photolysis of acetone at 150°C over a pressure range from 3.7 to 100 mm. Although the change in the ratio was not large, it was in the direction to be expected if reaction (1) is subject to a third-body restriction. A further examination of the acetone photolysis by Linnel and Noyes[15] has confirmed this variation. However, the effect is not very large; for instance, a ninefold change of acetone pressure at 120°C from 55.9 to 6.3 mm only changed $k_n/k_1^{\frac{1}{2}}$ from 4.0 to 5.2.

There have also been a number of theoretical calculations on the rate of reaction (1). Kimball[16] has calculated on classical grounds a mean life of 2.4×10^{-12} sec for the collision complex $(CH_3)_2^*$, from which it might be concluded that this reaction would occur only at the wall or in three-body collisions. Kassel[17] has, however, criticized these calculations for quantum-mechanical reasons; he concludes that they are fundamentally unsound.

Bawn[18] has calculated the steric factor of reaction (1) by the transition state method. When the activation energy of this reaction was assumed to be zero, the steric factor lay between 2×10^{-4} and 8×10^{-6} depending on the value taken for the activation energy of the reverse reaction.

From an expression obtained by Gorin[19] for the absolute rate of combination of free radicals, Gorin *et al.*[20] have deduced a value for the rate of combination of two methyl radicals at 873°K of 2.54×10^{-11} (molecules/cc)$^{-1}$ sec^{-1}, i.e., 1.53×10^{13} (moles/cc)$^{-1}$ sec^{-1}, if the transmission coefficient is unity. It is pointed out that this figure is a maximum and may have to be lowered by a factor of 2 or 3; moreover, at low pressures the rate will fall off as a result of redissociation before stabilization.

Hill[21] has recently calculated the steric factor of reaction (1) to be 1.39κ at 120°C, where κ is the transmission coefficient. κ is pressure-dependent since the three-body restriction has been accepted in this calculation; it will become unity when every molecule of ethane formed is deactivated before redissociation can occur. Hill found that at this temperature and at an acetone pressure of 117.4 mm, $\kappa=8.0\times10^{-4}$, assuming every collision to be effective in deactivation. However, this value is probably too low and can be considered to be only a lower limit for κ.

Marcus[22] has calculated the regions in which the rate of reaction (1) would be expected to show a pressure dependence. These pressure ranges were found to depend on the type of activated complex which is used in the calculations.

EXPERIMENTAL

Description of Apparatus

A description of the free-radical mass spectrometer used in this work has been given previously.[10] For the experiments described in this paper, some modifications and additions were made to the design of the reactor, a schematic diagram of which is given in Fig. 1. The outer heating element, although cut in the way previously described, was made from tantalum sheet 0.005 in. in thickness. It was not open to the atmosphere as before, the electrical leads running out from the vacuum system through two Kovar-glass seals. The quartz reactor, which had an internal diameter of 7 mm, contained a platinum—platinum 10 percent rhodium thermocouple in a quartz capillary sheath. Also inside the reactor was a small tubular furnace about 3 cm long consisting of two concentric quartz tubes sealed together top and bottom. Enclosed in the annular space so formed was a heating element of 0.010-in. tungsten wire wound noninductively. The furnace could be raised and lowered in the reactor by means of two lengths of rack which carried the heating current. The upper ends of the two lengths of rack engaged two pinions which were on a common axis but were insulated from each other by a disk of Bakelite of larger diameter. Two similar disks of Bakelite, one on the outside of each pinion, prevented the racks from slipping sideways. The axis carrying the disks and pinions was supported at one end by a sleeve, and at the other end was connected to a greased standard-taper joint, the rotation of which raised or lowered the small furnace in the reactor. Electrical contact to the racks was made through two springs, which pressed the racks against the pinions and ensured a positive engagement of the teeth. The heating currents for the two furnaces was supplied from adjustable autotransformers operated from a Sorenson voltage regulator. The rest of the reactor and its associated pumping system have been described previously.[10]

Method of Operation

The method of measuring the partial pressures of methyl radicals, ethane, and methane produced by the pyrolysis of mercury dimethyl was the same as described in Part I of this series,[10] i.e., by the subtraction of spectra obtained with electrons of 50-volts energy. Measurement of the temperature coefficients of sensi-

[13] L. M. Dorfman and R. Gomer, Chem. Revs. **46**, 499 (1950).
[14] A. F. Trotman-Dickenson and E. W. R. Steacie, J. Chem. Phys. **18**, 1097 (1950).
[15] R. H. Linnel and W. A. Noyes, Jr., J. Am. Chem. Soc. **73**, 3986 (1951).
[16] G. E. Kimball, J. Chem. Phys. **5**, 310 (1937).
[17] L. S. Kassel, J. Chem. Phys. **5**, 922 (1937).
[18] C. E. H. Bawn, Trans. Faraday Soc. **31**, 1542 (1935).
[19] E. Gorin, Acta Phisicochemica U.R.S.S. **9**, 691 (1938).
[20] Gorin, Kauzmann, Walter, and Eyring, J. Chem. Phys. **7**, 633 (1939). See also Glasstone, Laidler, and Eyring, *Theory of Rate Processes* (McGraw-Hill Book Company, Inc., New York, 1941), pp. 131 and 260.
[21] T. L. Hill, J. Chem. Phys. **17**, 503 (1949).
[22] R. A. Marcus, J. Chem. Phys. **20**, 352, 355, 359, 364 (1952).

tivity and the changes (with temperature) in the cracking patterns have also been described previously.

In order to obtain more accurate values for the combination rate of methyl radicals than were presented in Parts I[10] and II[11] of this series, it is necessary to use a method in which the contact time can be more precisely measured. As pointed out for the previous method, the progressive decomposition of mercury dimethyl down the heated tube results in unknown concentration gradients of methyl and ethane, giving large uncertainty in the contact time and collision frequency. To avoid this difficulty the new reactor described above and shown in Fig. 1 was designed. Mercury dimethyl at a few microns pressure was carried in a stream of helium through the reactor. The outer furnace was turned off and the movable furnace was heated to about 935°C, at which temperature some 85 to 90 percent of the mercury dimethyl was decomposed. The products were analyzed starting with the movable furnace at the bottom of the reactor, just above the leak. The furnace was then retracted 0.5 cm, and a new analysis of the products was made. Figure 1 shows the withdrawal over the next 0.5-cm interval. These retractions were repeated in 0.5-cm steps until most of the methyl radicals had combined. The amount of reaction occurring in the zone of unknown contact time immediately surrounding the movable furnace is, of course, the same in any position. The difference in the partial pressures before and after any 0.5-cm retraction can therefore be attributed to reactions occurring in each new 0.5-cm zone which appears just above the leak.

However, the temperature of the gas stream falls quite rapidly below the movable furnace, with a consequent increase in the contact time over each 0.5 cm zone of reaction. The difficulty which immediately arises, therefore, is to determine the temperature to be assigned to each zone. There is considerable difficulty in measuring the temperature of a gas in such a small volume close to a radiating body, owing in part to conduction of heat along the thermocouple wires. It was found, however, that the temperature coefficients of sensitivity of methane and ethane could be quite

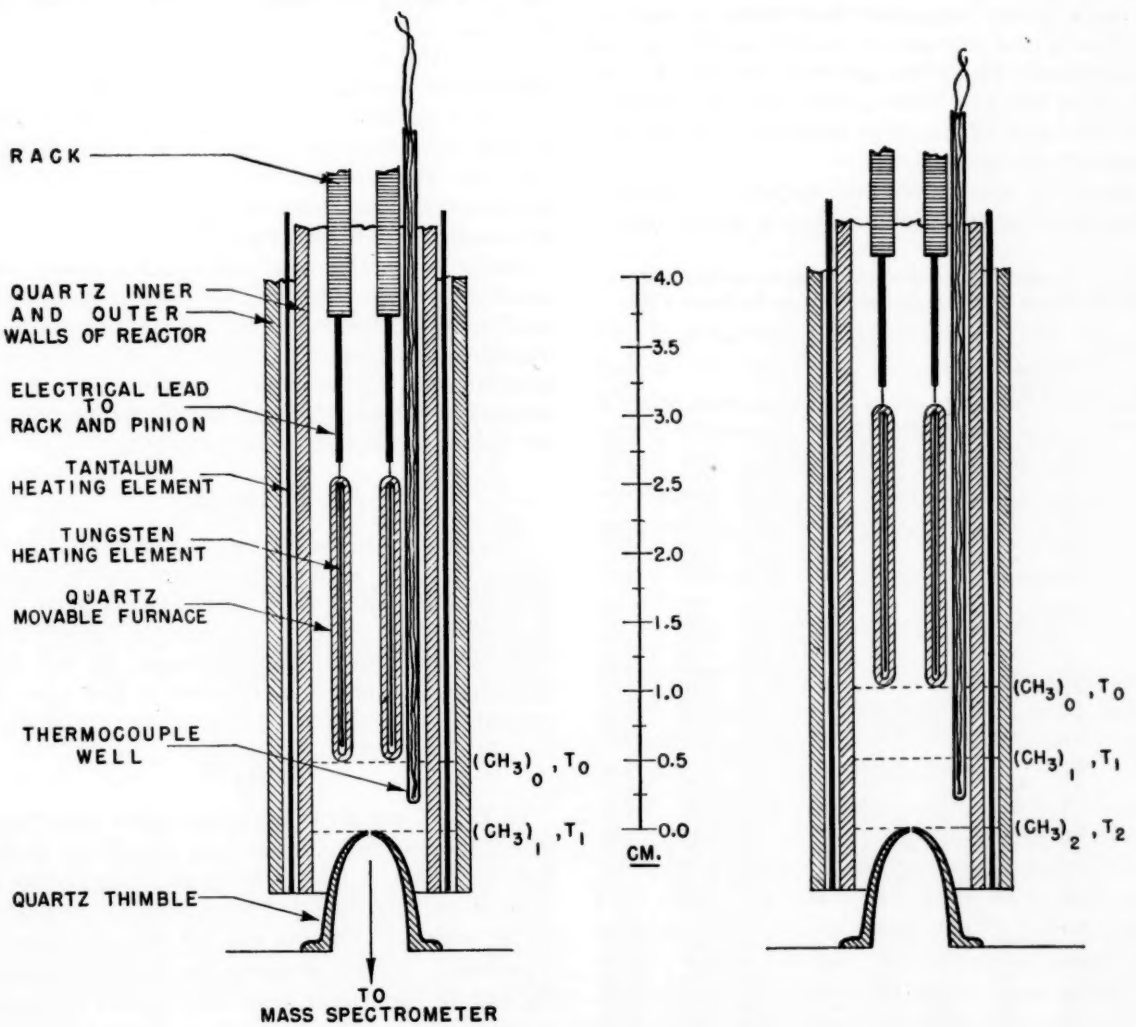

FIG. 1. Schematic diagram of the reactor.

accurately determined and were reproducible under constant helium flow conditions. These coefficients were first determined using the outer furnace with a mixture of ethane and methane in helium passing through the reactor. The outer furnace was then turned off and the relation between the peak heights and the position of the heated movable furnace was obtained. By comparing this relation with the curve for the temperature coefficient of sensitivity obtained with the outer furnace, it was possible to measure the gas temperature at different positions of the movable furnace. These temperatures were generally several degrees below the temperature indicated by the thermocouple for the corresponding positions, but the values obtained in this way from the methane and ethane temperature coefficients agreed with each other within a few degrees. The temperature assigned to each new 0.5-cm zone of reaction formed by withdrawing the movable furnace was the arithmetic mean of the temperatures found at the two end positions. The contact time for each zone was that calculated from the measured flow rate using the mean temperature of the zone. As a result of the retraction, each newly formed reaction zone was at successively lower temperatures and had successively longer contact times. Withdrawal experiments of this kind were carried out using different partial pressures of mercury dimethyl and different pressures of helium.

It might be noted that this method of operation avoids some of the errors inherent in flow systems which were pointed out by Gomer[23] since the "mirror," in this case the leak, is not moved relative to the pumping geometry. It might also be noted that the partial pressure of any component in the stream is not dependent on the temperature since the gas expands at constant pressure as the temperature is raised. However, the concentration of the component for a given partial pressure must be calculated using the actual gas temperature.

TABLE I. Composition of products from mercury dimethyl (He pressure = 9.0 mm). Partial pressures in microns Hg.

Initial $Hg(CH_3)_2$	Position of furnace (cm)	Mean temp. (°K)	CH_3	CH_4	C_2H_6	ΔCH_3	$2\Delta C_2H_6$	$\Sigma CH_3 + CH_4 + 2C_2H_6$
2.2	0.2	···	1.69	0.065	0.0222	···	···	1.80
	0.5	1087	1.53	0.065	0.0423	0.16	0.04	1.68
	1.0	872	1.43	0.065	0.0971	0.10	0.11	1.69
	1.5	713	1.27	0.065	0.190	0.16	0.19	1.69
	2.0	617	1.10	0.065	0.312	0.17	0.24	1.79
	2.5	551	0.882	0.065	0.457	0.21	0.29	1.86
	3.0	502	0.732	0.065	0.571	0.15	0.23	1.94
	3.5	466	0.580	0.065	0.682	0.15	0.22	2.01
	4.0	434	0.480	0.065	0.747	0.10	0.13	2.04
3.6	0.2	···	2.75	0.10	0.113	···	···	3.08
	0.5	1087	2.68	0.10	0.156	0.07	0.086	3.09
	1.0	872	2.36	0.10	0.269	0.32	0.23	3.00
	1.5	713	1.94	0.10	0.511	0.42	0.48	3.06
	2.0	617	1.53	0.10	0.726	0.41	0.43	3.09
	2.5	551	1.16	0.10	0.894	0.37	0.34	3.05
	3.0	502	0.903	0.10	1.05	0.26	0.31	3.10
	3.5	466	0.703	0.10	1.18	0.20	0.26	3.16
	4.0	434	0.539	0.10	1.25	0.16	0.14	3.14
7.5	0.2	···	5.69	0.275	0.306	···	···	6.57
	0.5	1087	5.30	0.275	0.430	0.39	0.25	6.43
	1.0	872	4.34	0.275	0.847	0.96	0.83	6.31
	1.5	713	3.32	0.275	1.49	1.02	1.28	6.57
	2.0	617	2.34	0.275	2.01	0.98	1.04	6.64
	2.5	551	1.66	0.275	2.33	0.68	0.64	6.59
	3.0	502	1.22	0.275	2.58	0.44	0.50	6.65
	3.5	466	0.904	0.275	2.75	0.32	0.26	6.68
	4.0	434	0.656	0.275	2.93	0.25	0.36	6.79
25.3	0.2	···	17.07	1.12	2.33	···	···	22.85
	0.5	1087	14.41	1.12	3.36	2.66	2.06	22.25
	1.0	872	9.29	1.12	5.41	5.12	4.10	21.23
	1.5	713	5.76	1.12	7.13	3.53	3.44	21.14
	2.0	617	3.38	1.12	8.55	2.38	2.84	21.60
	2.5	551	1.90	1.12	9.12	1.48	1.14	21.26
	3.0	502	1.22	1.12	9.80	0.68	1.36	21.94

Correction for Reaction in the Ion Source

With a given partial pressure of mercury dimethyl entering the reactor, it was found that the amount of methane formed decreased with the methyl concentration as the movable furnace was retracted from the leak. If the methane concentration was plotted against the methyl concentration for such experiments, straight lines were obtained with a positive slope of 0.2 which was independent of the amount of mercury dimethyl. The intercepts of the lines at $[CH_3]=0$, however, were found to be proportional to the amount of mercury dimethyl entering the furnace and indicated that about 4 percent of the mercury dimethyl decomposed had formed methane. If the remaining fraction of the methane were formed in the reactor by abstraction reactions of methyl, the methane concentration should increase with the total contact time as the furnace is retracted. The fact that it decreases proportionally to the methyl radical concentration shows that it is formed from methyl radicals after the passage through the leak, probably by reaction with compounds adsorbed on the metal walls of the ion chamber. Since this amount of methane left the reactor as methyl radicals, the amount of methyl measured from the peak heights was increased by a factor of 0.2. In order to preserve the validity of the carbon balance, the amounts of methane shown in the Tables correspond to the intercepts.

Materials

The mercury dimethyl was prepared by Dr. L. C. Leitch and was purified by several distillations in a good column. The helium was of 99.8 percent purity and was further purified by passing it through a charcoal trap immersed in liquid nitrogen. By this means, the oxygen content was reduced to less than 0.005 percent.

RESULTS

In Table I are given the results of an experiment in which the movable furnace was withdrawn from the leak in successive 0.5-cm intervals. Four partial pressures of mercury dimethyl were used, and the pressure of the helium carrier gas was 9.0 mm throughout the experiment. Partial pressures are given in microns of Hg and all corrections have been applied as described

[23] R. Gomer, J. Chem. Phys. 19, 284 (1951).

above. The last column represents a carbon balance for the mercury dimethyl which has been decomposed, the difference between this value and the partial pressure of mercury dimethyl entering the furnace representing the amount of undecomposed mercury dimethyl. The contact time per 0.5 cm was 1.39×10^{-4} sec at 1000°K.

The constancy of the carbon balance, that is, the equality between the amount of methyl disappearing and the amount of ethane being formed, shows that no appreciable amount of ethane is being formed by the reaction

$$CH_3+Hg(CH_3)_2\rightarrow C_2H_6+Hg+CH_3, \qquad (4)$$

which has been reported by Gomer and Noyes in the photolysis of mercury dimethyl.[24] In addition, if the ethane concentration is plotted against the time of reaction, the lines obtained at each of the four concentrations of mercury dimethyl pass through the origin ($t=0$, $[C_2H_6]=0$) within the accuracy of the measurements, showing that no ethane is formed directly from mercury dimethyl by the following reaction:

$$Hg(CH_3)_2\rightarrow C_2H_6+Hg. \qquad (5)$$

It was shown in the previous section that only about 4 percent of the mercury dimethyl decomposed forms methane. This small and constant amount of methane is shown in Table I. It is presumably formed from mercury dimethyl adsorbed on the walls of the movable furnace and not by hydrogen abstraction in the gas phase.

In view of these facts, it is safe to assume that the only reaction occurring to any appreciable extent is the combination of methyl radicals to give ethane, either by a first-order wall reaction or by a second-order homogeneous reaction. The formation of ethane may then be expressed in the form

$$\frac{d}{dt}[C_2H_6]=-\frac{1}{2}\frac{d}{dt}[CH_3]=k'[CH_3][M]+k_1[CH_3]^2,$$

where k' and k_1 are the rate constants for the first-order wall reaction and the second-order homogeneous reaction, respectively. The first- and second-order rates may be separated by plotting either

$$\frac{d}{dt}[C_2H_6]\Big/[CH_3] \quad \text{or} \quad \frac{d}{dt}[CH_3]\Big/[CH_3]$$

against $[CH_3]$. This is shown in Fig. 2. The partial pressures of the products given in Table I were corrected to concentrations at the appropriate temperature and then expressed as $\Delta CH_3/\bar{C}\bar{H}_3$ per second. This function has been plotted against $\bar{C}\bar{H}_3$ in moles/cc (ΔCH_3 is the change, and $\bar{C}\bar{H}_3$ the arithmetic mean of

[24] R. Gomer and W. A. Noyes, Jr., J. Am. Chem. Soc. **71**, 3390 (1950).

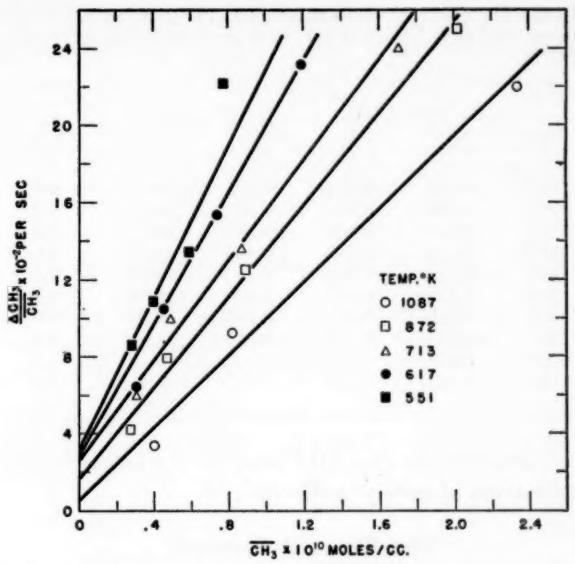

FIG. 2. The slopes of the lines in this graph are proportional to the rates of the second-order combination of methyl radicals at the temperatures indicated. The intercepts are proportional to the rate of the first-order combination.

the methyl radical concentration at either end of the 0.5-cm intervals). The contact time over each 0.5 cm was found by measuring the time required for the flow of a known volume of helium down the reactor; this was then corrected to any required reactor temperature.

The straight lines in Fig. 2 have been drawn through values of $\Delta CH_3/\bar{C}\bar{H}_3$ sec^{-1} which were measured at corresponding positions of the movable furnace and which therefore represent "isothermal" values in which $\bar{C}\bar{H}_3$ was varied by changing the partial pressure of the mercury dimethyl entering the furnace. The slopes of these lines are equal to $2k_1$ in (moles/cc)$^{-1}$ sec^{-1} for each temperature. Similar lines obtained by plotting $\Delta C_2H_6/\bar{C}\bar{H}_3$ sec^{-1} against CH_3 give k_1 directly from their slopes. The collision efficiency (C_E) of the second-order process is defined as the ratio,

$$\frac{\text{number of collisions leading to reaction}}{\text{total number of collisions}},$$

and is given by k_1/NZ, where N is Avogadro's number and Z is the collision number at the appropriate temperature. The collision diameter of the methyl radical was taken to be 3.5×10^{-8} cm.[21]

The magnitude of the variation of $k_1T^{-\frac{1}{2}}$ and the collision efficiency with temperature can be seen from the data in Table II, in which values calculated from both ΔCH_3 and ΔC_2H_6 are given. A plot of $\log(C_E)$ against $1/T$(°K) is given in Fig. 3 and is approximately linear. The line was drawn with reference to the collision efficiencies calculated from ΔCH_3 which were considered more reliable than those obtained from ΔC_2H_6. The slope of this line corresponds to a tempera-

TABLE II. Effect of temperature and pressure on $k_1T^{-\frac{1}{2}}$ and collision efficiency. Values of $k_1T^{-\frac{1}{2}}$ are given in $(\text{moles/cc})^{-1}\ \text{sec}^{-1}\ (°\text{K})^{-\frac{1}{2}}$.

Temp (°K)	From ΔCH_3 $k_1T^{-\frac{1}{2}}$ $\times 10^{-12}$	From ΔCH_3 C_E	From ΔC_2H_6 $k_1T^{-\frac{1}{2}}$ $\times 10^{-12}$	From ΔC_2H_6 C_E	He pressure (mm)
1087	0.144	0.024	0.107	0.018	9.0
872	0.200	0.033	0.165	0.027	9.0
713	0.242	0.039	0.253	0.041	9.0
617	0.344	0.055	0.348	0.055	9.0
551	0.414	0.066	0.432	0.070	9.0
502	0.520	0.085	0.600	0.100	9.0
466	0.540	0.090	0.690	0.110	9.0
434	0.655	0.105	0.655	0.105	9.0
1008	0.176	0.029	...	...	4.8
1008	0.163	0.027	...	...	18.5

ture coefficient of -2.2 ± 0.5 kcal, for the homogeneous combination of methyl radicals.

The Effect of Pressure

The effect of total pressure on the rate of combination of the methyl radicals at 1008°K in a given 0.5-cm interval was studied by varying the mercury dimethyl pressure in two experiments similar to the one described above, but at helium pressures of 4.8 and 18.5 mm. The resulting data are shown graphically in Fig. 4. Neither the first-order nor the second-order reaction show any significant change over this range of pressure. The values for the two collision efficiencies obtained from least mean square lines are given in Table II and are the same within the error of measurement. It can be seen from Fig. 3 that these two points agree with the value at 9-mm pressure at the corresponding temperature. It was not possible to extend the pressure range studied without changing the size of leak used in the mass spectrometer.

Low Electron Energy Experiments

In order to confirm that the effect of temperature on the rate of combination was not in part due to some systematic error in the method of measuring the concentrations, two experiments were carried out in which the methyl and ethane peaks were measured at low electron energies. As described in Part I of this series,[10] relative partial pressures of methyl radicals can be measured directly in this way without the necessity of correcting the peak heights for contributions from other compounds, although the absolute concentrations are not known. With the movable furnace withdrawn to the 3.0-cm mark, and with sufficient heating current to decompose all the mercury dimethyl, the peak heights of methyl (mass 15) and ethane (mass 30) were measured with an electron energy of about 13 volts. Under these conditions the thermocouple temperature was 874°K. Using the outer furnace the temperature of the 3.0-cm zone below the movable furnace was raised to 1048°K. Although the mercury dimethyl was all decomposed on the movable furnace, the methyl peak increased and the ethane peak decreased as shown in Table III. A repeat of this experiment at about 12 electron volts led to the same result. The ratio of the ethane peak heights may be used to calculate the ratio of the collision efficiencies at the two temperatures, after making allowance for the change in concentration, collision number, and contact time with temperature. The ratio of the collision efficiencies obtained in this way is given in Table III for comparison with the ratio over the same temperature intervals calculated from the line in Fig. 3. It can be seen that the agreement between the values obtained by the two methods is satisfactory, when allowance is made for the approximate nature of the low electron energy experiment. It should be noted that, in this experiment, the pressure of mercury dimethyl was large enough that the first-order combination was of minor importance.

DISCUSSION

In a previous section it was noted that for each withdrawal experiment a plot of the methane concentration *versus* the methyl concentration gave a straight line which intercepted the methane axis. If these intercepts (i.e., the methane in Table I) are plotted against the concentration of mercury dimethyl, a straight line is obtained at concentrations of $Hg(CH_3)_2$ above 10^{-10} mole/cc, that is, the methane is being formed in the region of the movable furnace by some first-order process. Below this concentration, the order of reaction increases slowly as the concentration is diminished. The direct formation of methane from mercury dimethyl,

$$Hg(CH_3)_2 \rightarrow CH_4 + HgCH_2, \qquad (6)$$

would seem to be less probable than hydrogen abstrac-

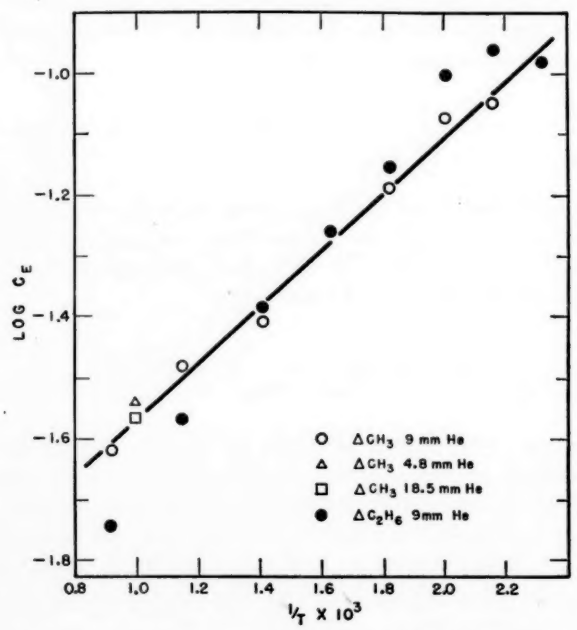

FIG. 3. The temperature coefficient of the rate of the second-order combination of methyl radicals.

tion from mercury dimethyl by a methyl radical on the surface of the movable furnace:

$$CH_3+Hg(CH_3)_2 \xrightarrow[\text{surface}]{\text{hot}} CH_4+CH_3HgCH_2. \quad (7)$$

At this temperature (*ca* 930°C) and concentrations of $Hg(CH_3)_2$ above 10^{-10} mole/cc it is possible that the adsorbed reactant saturates the surface and the reaction is first order, but below this concentration the amount adsorbed depends on the concentration in the gas phase, and the reaction tends to become second order. Over the concentration range studied, methane formed in this way made up about 4 percent of the products.

The extent of the first-order heterogeneous combination of methyl radicals (given by the intercepts on the $\Delta CH_3/\bar{C}\bar{H}_3$ axis in Fig. 2) may depend on both the nature and the temperature of the surface. Since the proportion of methyl radicals which combine on the surface will depend not only on these two factors but also on the diameter of the reactor, this reaction was not studied further.

The situation applying in the case of the second-order homogeneous part of the methyl combination is most easily understood in terms of the Lindemann collision mechanism,

$$CH_3+CH_3 \underset{k_2}{\overset{k_1}{\rightleftarrows}} C_2H_6^*,$$

$$C_2H_6^*+M \xrightarrow[k_3]{} C_2H_6+M^*.$$

The activated complex $C_2H_6^*$ can either redissociate to two methyl radicals or be stabilized to an ethane molecule by collision with M, in this case a helium atom. According to this scheme,

$$\frac{d[C_2H_6^*]}{dt}=k_1[CH_3]^2-k_2[C_2H_6^*]-k_3[C_2H_6^*][M].$$

For a steady state,

$$\frac{d(C_2H_6^*)}{dt}=0$$

and

$$[C_2H_6^*]=\frac{k_1[CH_3]^2}{k_2+k_3[M]}.$$

The over-all rate of formation of ethane is given by

$$\frac{d}{dt}[C_2H_6]=-\frac{1}{2}\frac{d}{dt}[CH_3]=k_3[C_2H_6^*][M]$$

$$=\frac{k_1k_3[M][CH_3]^2}{k_2+k_3[M]}.$$

When the lifetime of the complex is short compared with the time between collisions $k_3[M] \ll k_2$ and

$$-\frac{1}{2}\frac{d}{dt}[CH_3]=\frac{k_1k_3[M][CH_3]^2}{k_2}.$$

The rate is then dependent on the concentration of the third body and would show a dependence on the pressure of helium. If the life of the complex is long compared with the rate of collisional deactivation, $k_3[M] \gg k_2$ and

$$-\frac{1}{2}\frac{d[CH_3]}{dt}=k_1[CH_3]^2.$$

Under these conditions, the rate is independent of the pressure.

As described above, a change in the helium pressure from 4.8 to 18.5 mm at 1008°K was found to have no effect on the rate. Therefore, the life of the complex must be longer than the time between deactivating collisions, and the rate is given by the last equation. Benson[25] has recently suggested that the combination

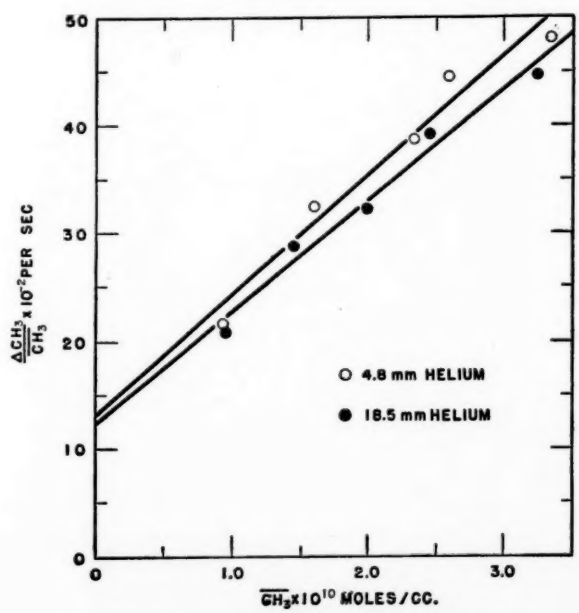

FIG. 4. The effect of helium pressure on the rate of combination of methyl radicals.

TABLE III. Low electron energy experiments.

Electron energy (volts)	Temp (°K)	Mass 15 peak (cm)	Mass 30 peak (cm)	Ratio of C_g low electron energies	Ratio of C_g 50-volt electron energy
~13.0	874	3.4	8.7		
~13.0	1048	6.4	5.4	1.22	1.23
~12.0	878	2.5	3.7		
~12.0	1161	6.2	1.7	1.43	1.35

[25] S. W. Benson, J. Chem. Phys. **20**, 1064 (1952).

of methyl radicals might be expected to have a negative temperature coefficient in the region of pressure dependence. He assigns the negative temperature coefficient to the rate of dissociation of the activated complex (k_2). However, under conditions where no pressure dependence is found, a further decrease in k_2 brought about by lower temperatures cannot introduce a temperature coefficient into the rate of combination. One is, in fact, forced to ascribe the temperature coefficient to k_1. This coefficient can be regarded as an effect of velocity on the interaction between two approaching methyl radicals. That is, the collision cross section varies with the temperature, probably on account of the van der Waals energy of attraction between the two radicals (i.e., the same factor that brings in the Sutherland or Reinganum correction for the effect of temperature on gas viscosity). The magnitude of the temperature coefficient of the collision efficiency found in the present work (-2.2 ± 0.5 kcal) does not seem to be too large to be accounted for by these attractive forces. Over the temperature range studied, the negative temperature coefficient can be accounted for by a change in the effective collision cross section by a factor of two.

A similar change in the effective collision diameter of atoms has been detected in studies of their scattering by gases.[26] A related effect in which a particular species has a different collision cross section for different reactions has been suggested by Szwarc.[27]

The experimental results given in Fig. 3 were calculated on the assumption that the collision diameter of the methyl radical is 3.5A at all temperatures.[21] To obtain a temperature coefficient, a straight line was drawn through these results. It will be noticed that at the higher temperatures the collision efficiencies obtained from the formation of ethane (i.e., the ΔC_2H_6 values) tend to drop below this line. This is probably the result of the instability of ethane at these temperatures, some of the ethane formed being again decomposed, probably to ethylene and hydrogen. Rates and collision efficiencies measured by $(d/dt)[C_2H_6]$ will therefore diminish more rapidly than is predicted by extrapolation from lower temperatures, but rates measured by $-\frac{1}{2}(d/dt)[CH_3]$ will remain unaffected.

It is interesting to compare the results obtained in the present work with those obtained by other workers using different experimental methods. Table IV gives the experimental conditions used by these workers, together with the values found for $k_1T^{-\frac{1}{2}}$ in (moles/cc)$^{-1}$ sec^{-1} (°K)$^{-\frac{1}{2}}$, the collision efficiency calculated on the assumption $\sigma_{CH_3}=3.5$A, and the activation energy. For purposes of comparison, the values for $k_1T^{-\frac{1}{2}}$ and the collision efficiencies found in the present work at corresponding temperatures have also been given. The experimental methods used have been described in the Introduction, but a few additional points might be noted here.

In connection with the results of Marcus and Steacie[3] and Miller and Steacie,[4] a careful redetermination of the rate constant for the reaction

$$CH_3+NO\rightarrow? \qquad (2)$$

has been made recently.[28] The two values of $k_1T^{-\frac{1}{2}}$ given in Table IV have been recalculated using this new value and therefore differ from the values given in the two papers which were based on the results of Forsyth.[5] Miller and Steacie's value for $k_1T^{-\frac{1}{2}}$ should be the more accurate since the other work was only exploratory in nature, no attempt being made to replenish the nitric

TABLE IV. Values of rate constants for ethane formation as reported in literature. $k_1T^{-\frac{1}{2}}$ is given in (moles/cc)$^{-1}$ sec^{-1} (°K)$^{-\frac{1}{2}}$.

Authors	Temp (°K)	Total pressure (mm)	$k_1T^{-\frac{1}{2}}\times10^{-12}$	C_E	E (kcal)	$k_1T^{-\frac{1}{2}}\times10^{-12}$ present work	C_E present work
Allen and Bawn	621	4.1	...	$\leq$0.1	...	0.32	0.052
Haden and Rice	473	100	4.6	0.75	2.6	0.55	0.089
Lucas and Rice	473	100	2.8	0.45	small	0.55	0.089
Dodd	473	200 to 400	$\geq$2.9	$\geq$0.47	0.8±0.8	0.55	0.089
Marcus and Steacie	298	40	8.1	$\sim$1.0	...	2.2[a]	0.35[a]
Miller and Steacie	298	4.5 to 10	0.06	0.01	...	2.2[a]	0.35[a]
Gomer and Kistiakowsky							
Acetone	398	50	2.3	0.37		0.85[a]	0.14[a]
	448	15	2.0	0.32	0±0.7	0.65	0.105
$Hg(CH_3)_2$	448	21	2.2	0.35		0.65	0.105
	493	10	3.0	0.49		0.50	0.081
Lossing and Tickner							
$Hg(CH_3)_2$	1123	15.5	0.09	0.015	...	0.15[a]	0.024[a]
Di-*t*-butyl peroxide	669	12.5	0.26	0.042	...	0.29	0.046
	726	12.5	0.28	0.046	...	0.25	0.041
	779	12.5	0.27	0.043	...	0.23	0.037
Lossing, Ingold, and Tickner	1198	15	0.09	0.015	...	0.14[a]	0.023[a]
$(CH_2)_2O$	1248	15	0.07	0.011	...	0.14[a]	0.022[a]

[a] Obtained by extrapolation.

[26] Amdur, Kells, and Davenport, J. Chem. Phys. **18**, 1676 (1950).
[27] M. Szwarc, Disc. Faraday Soc. **10**, 143 (1951).
[28] R. W. Durham and E. W. R. Steacie, J. Chem. Phys. **20**, 582 (1952).

oxide as it was consumed. However, the pressure used by Durham and Steacie[28] was only about 5 percent of that used by Miller and Steacie, so that some fall-off in the rate of reaction (2) may be expected owing to third-body effects. This means that $k_1T^{-\frac{1}{2}}$ and the collision efficiency calculated from it are actually lower limits.

Rice[6,8] considers the chain terminating step in the photolysis of acetaldehyde to be a combination of methyl radicals; on the other hand, Dodd[7] has suggested that it may be a combination of methyl and formyl radicals. From the general agreement of the data with that obtained by Gomer and Kistiakowsky[9] (see below) the former suggestion is probably true; the results obtained in all three papers are therefore quoted in Table IV. It should be noted that the value for $k_1T^{-\frac{1}{2}}$ given under Haden and Rice[6] has been corrected as suggested by Lucas and Rice.[8] The close agreement between Lucas and Rice, and Dodd is largely fortuitous since the latter value is a minimum, and moreover, different values were assumed in the two papers for the efficiency of production of radicals by light absorption.

Gomer and Kistiakowsky's values for $k_1T^{-\frac{1}{2}}$ and the collision efficiency at three temperatures are given in Table IV. There appears to be some doubt whether or not the homogeneous combination of methyl radicals is free from third-body restrictions, but over the pressure changes involved in these experiments it is probably permissible to compare the rate constants obtained at different temperatures, even though they were obtained at different pressures. Since they were able to measure the rate of combination directly, their determination of $k_1T^{-\frac{1}{2}}$ is probably more accurate than the values obtained by earlier workers. Although the results of the present work show a fair degree of internal consistency, the error in the absolute values of k_1 may be fairly large. This error is, however, not likely to be large enough to account completely for the discrepancy between the present results and those of Gomer and Kistiakowsky.

Table IV also shows the data obtained in this laboratory and quoted in Parts I[10] and II[11] of this series, for the collision efficiency of reaction (1). As originally quoted, they contain an error of a factor of two owing to a wrong assumption made about the collision number. Although this is within the experimental error, it has been corrected in the data given in Table IV. As was mentioned in the Introduction, we do not consider these corrected data to be as accurate as those reported here, but there is, nevertheless, fair agreement with the present work. The data given in Table VIIa, Part I, for the decomposition of di-*t*-butyl peroxide have also been evaluated. The collision efficiencies obtained from these data where decomposition is complete are in excellent agreement with the present work, but for incomplete decomposition where abstraction reactions are likely to occur, agreement was not quite as close. It was considered necessary only to compare the results obtained under similar conditions, i.e., complete decomposition, with the results of the present work, and therefore only these values are given in Table IV.

In Part I the discrepancy between the amounts of ethane formed for a given concentration of methyl from mercury dimethyl at 850°C, and from di-*t*-butyl peroxide at 400–500°C was attributed to a possible abstraction of a methyl group from acetone or di-*t*-butyl peroxide. This discrepancy can, however, be almost completely accounted for by the negative temperature coefficient found in the present work.

Schultz and Taylor[29] have photolyzed methyl iodide and investigated the rate of methane and ethane formation under varying conditions. They concluded that ethane was formed by the combination of cold methyl radicals, as opposed to the "hot" radicals produced in the primary reaction. The interesting point to note in connection with the present work is that the rate of ethane formation decreases with rise of temperature, thus in two runs (14 and 15) they found the rate decreased from 8.4 to 5.1 mm/hour as the temperature was increased from 40° to 100°C. This was attributed to a positive activation energy of 1 kcal for the reaction

$$CH_3+I_2\rightarrow CH_3I+I, \qquad (8)$$

which, with increase of temperature, would cause a decrease in the methyl concentration and a consequent decrease in the rate of ethane formation. In view of the results reported in this paper, we would suggest that the effect found by these workers may be due to the negative temperature coefficient of reaction (1). The two rates given above yield a temperature coefficient of -1.9 kcal, which is in excellent agreement with our own value of -2.2 ± 0.5 kcal.

It is interesting to note that the value obtained theoretically by Gorin *et al.*[20] for the rate of combination of methyl radicals at 873°K, i.e., 1.53×10^{13} (moles/cc)$^{-1}$ sec^{-1}, is in remarkably close agreement with the value for $2k_1$ obtained at this temperature in the present work (1.13×10^{13} (moles/cc)$^{-1}$ sec^{-1}).

The collision efficiencies obtained at 1008°K using 4.8 and 18.5 mm of helium (*viz.*, 0.029 and 0.027, respectively) are shown in Fig. 3. Although these two values are the same within the limit of the experimental error, the experiment at the lower pressure gave the larger value for the collision efficiency, and therefore the rate constant of reaction (1). However, if the rate were pressure dependent, a lower collision efficiency would be expected at the lower pressure. It may be concluded that within the limits of the experimental method, the rate is not pressure-dependent over the range studied. This result is in general agreement with the findings of other workers.[1,12–15,24] It would appear, therefore, that the energy of combination can become distributed among some of the internal degrees of free-

[29] R. D. Schultz and H. A. Taylor, J. Chem. Phys. 18, 194, 760 (1950).

dom of the ethane molecule, thus increasing the lifetime of the excited state and making reaction (1) independent of third-body requirements at these pressures. Using a classical model, Benson[25] has calculated that the rate will show a pressure dependence at around 0.01 mm.

At the lowest pressure used in this work, i.e., 4.8 mm, an excited ethane molecule will have about 5×10^7 collisions per sec; its lifetime before redissociation must therefore be not less than 10^{-7} sec. As was pointed out by Gomer and Kistiakowsky,[9] the combination of this long lifetime with a high collision efficiency is interesting as the former calls for precise orientation of the activated ethane molecule on dissociation, while the latter suggests that orientation of the methyl radicals is not important in combination.

THE JOURNAL OF CHEMICAL PHYSICS VOLUME 21, NUMBER 7 JULY, 1953

The Specific Heat of Crystalline Selenium at Low Temperatures*†

WARREN DESORBO
General Electric Research Laboratory, The Knolls, Schenectady, New York

(Received January 12, 1953)

Studies on the low temperature specific heat of crystalline selenium have been extended down to 15°K. The data are compared with a calculation based on a one-dimensional-continuum model with which good agreement is shown to exist down to about 37°K. Below this temperature, deviations are described in terms of an anisotropic continuum which considers the "interaction" between atom chains.

The values of the thermodynamic functions, entropy, enthalpy, and free energy have been evaluated and tabulated at regular integral values of temperature up to 300°K. The entropy of crystalline selenium at 298.16°K is 10.15 ± 0.05 cal/g-atom/deg, of which 0.22 was obtained by extrapolating below 15°K. For this extrapolation, the anisotropic-continuum model was used.

INTRODUCTION

RECENTLY, the T^2 dependence of the specific heat graphite at low temperatures has attracted considerable attention. This seemingly anomalous specific heat variation has been attributed to the highly anisotropic nature of the graphite lattice. Tarassov[1] and Gurney,[2] independently, have pointed out a two-dimensional frequency-distribution function that predicts a T^2 dependence of the specific heat of graphite at the low temperatures. Recently, Komatsu and Nagamiya[3] and Krumhansl and Brooks[4] have developed more elaborate theories on this unique property. This T^2 dependence of the specific heat of graphite has been verified by Estermann and Kirkland[5] and by DeSorbo and Tyler.[6] More recently, DeSorbo[7] has pointed out a T^2 dependence of the low temperature specific heat of "layer-structure" gallium.

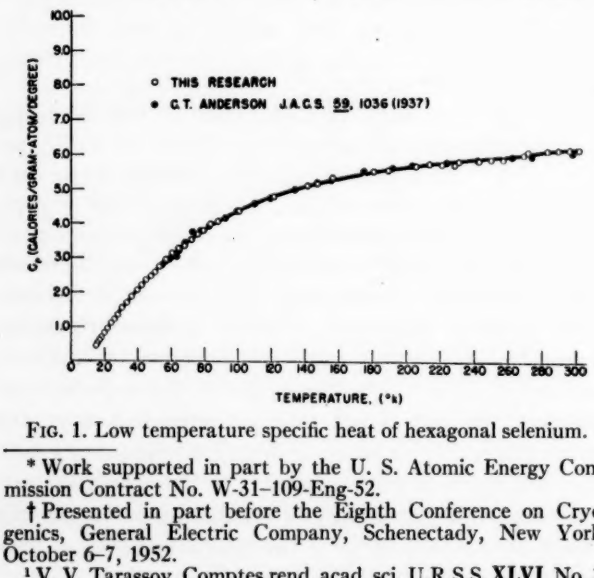

FIG. 1. Low temperature specific heat of hexagonal selenium.

It would be of great interest to find a substance that is so highly anisotropic in its elastic behavior that its specific heat has a linear temperature dependence at low temperatures. If approximations similar to the Debye type of approximation are considered for a "one-dimensional lattice," the specific heat should follow a T^1 dependence at the low temperatures.

In the absence of dispersion and in the presence of a sufficiently large number, $3N$, of vibrational degrees of freedom, the vibrating linear chains of atoms may be replaced by an elastic rod or a one-dimensional continuum. The number of characteristic vibrations in the interval ν to $\nu+d\nu$ is taken to be the following:

$$n(\nu)d\nu=\frac{2L}{C}d\nu, \tag{1a}$$

* Work supported in part by the U. S. Atomic Energy Commission Contract No. W-31-109-Eng-52.

† Presented in part before the Eighth Conference on Cryogenics, General Electric Company, Schenectady, New York, October 6–7, 1952.

[1] V. V. Tarassov, Comptes rend. acad. sci. U.R.S.S. **XLVI**, No. 3, (1945).

[2] R. W. Gurney, Phys. Rev. **88**, 465–466 (1952).

[3] K. Komatsu and T. Nagamiya, J. Phys. Soc. Japan **6**, 438–444 (1951).

[4] J. A. Krumhansl and H. Brooks, "Lattice Vibration Specific Heat in Graphite," J. Chem. Phys. (to be published).

[5] Estermann and Kirkland (unpublished) (25°–60°K; see reference 2).

[6] W. DeSorbo and W. W. Tyler, Phys. Rev. **83**, 878 (1951).

[7] W. DeSorbo, J. Chem. Phys. **21**, 168 (1953).

where C is the velocity of propagation and L the length of the vibrating rod.

The total number of vibrational degrees of freedom will be assumed equal to $3N$; then the distribution function can be written

$$n(\nu)d\nu = 3N\nu_{\max}^{-1}d\nu. \quad (1b)$$

The log of the partition function can be expressed in the following manner:

$$\log z = -\frac{E_0}{kT} - 3N\left(\frac{T}{\theta_1}\right)^1 \int_0^{\theta_1/T} \log(1-e^{-x})dx - \tfrac{3}{4}N\left(\frac{\theta_1}{T}\right) + \log G_0, \quad (2)$$

where

$$\theta_1 = \frac{h\nu_{\max}}{k} \quad \text{and} \quad x = \frac{h\nu}{kT}.$$

For low temperatures, or $T \ll \theta_1$, the specific heat is given by the following simple linear equation:

$$C_v = \pi^2 R(T/\theta_1)^1. \quad (3)$$

Tarassov,[8] using some specific-heat data of Anderson's,[9] which extended down to liquid nitrogen temperature only, showed that the specific heat of crystalline selenium followed the "law of direct proportionality," based on a one-dimensional-continuum integral. Turnbull[10] suggested, independently and from structural considerations only, that the specific heat of crystalline selenium might have a first-power temperature dependence at the low temperatures. Crystalline selenium is an example of a monatomic linear high polymer. This modification can be considered to have a chain or "fiber" structure where the "interaction" between these units is weak. The atoms in the crystal lattice, having only two nearest neighbors, are bound into continuous chains by forces of main valences. These chains lie at the corners of the unit cell. The distance between the centers of any two neighboring chains is 4.34A. The Se—Se bond length is 2.32A. The nearest approach of two selenium atoms in adjacent chains is 3.46A.[11] It is, therefore, of interest to determine whether the specific heat of the selenium lattice would be in agreement, at the low temperatures, with the partition function cited. The main purpose of this investigation has been to extend the specific-heat data of crystalline selenium to the lower temperatures in order to study the temperature dependence of this property of a "chain" or "fiber" structure of a monatomic solid. Also, new measurements over a wide range of temperatures were thought desirable, inasmuch as the sample available was of very high purity.

[8] V. V. Tarassov, Zhur. Fiz. Khim. **XXIV 1**, 111–128 (1950).
[9] C. T. Anderson, J. Am. Chem. Soc. **59**, 1036 (1937).
[10] D. Turnbull (private communication).
[11] R. W. G. Wyckoff, *Crystal Structure* (Interscience Publishers, Inc., New York), Vol. I, Chapter II, illus. p. 8.

TABLE I. Specific heat of crystalline selenium. Atomic wt. = 78.96; 1.9701 gram-atoms.

Mean temp, °K	ΔT	C_p cal/g-atom/°K	Mean temp, °K	ΔT	C_p cal/g-atom/°K
14.97	0.320	0.449	172.77	4.165	5.367
15.73	1.024	0.520	180.50	4.749	5.473
16.87	1.181	0.607	189.05	4.645	5.515
18.17	1.390	0.689	205.28	4.369	5.622
19.87	1.866	0.813	213.10	4.276	5.674
21.76	1.884	0.945	220.36	3.366	5.657
23.82	1.827	1.105	227.73	3.329	5.641
25.72	1.919	1.214	235.10	3.253	5.730
27.81	2.248	1.340	242.04	2.737	5.752
30.38	2.809	1.541	249.10	2.693	5.783
33.21	2.865	1.687	256.09	2.661	5.781
36.06	2.838	1.871	268.19	3.214	5.906
39.38	2.890	2.060	275.27	3.154	5.979
42.11	2.680	2.200	281.82	3.111	6.018
44.86	2.828	2.357	288.25	3.074	6.031
47.62	2.672	2.460	294.85	3.032	6.051
50.21	2.529	2.588	300.30	3.005	6.035
52.82	2.724	2.743			
56.74	2.519	2.948			
60.63	2.365	3.137			
64.34	2.260	3.269			
67.99	2.172	3.345			
72.30	2.351	3.538			
76.00	2.610	3.683			
79.46	2.529	3.791			
83.63	4.817	3.980			
87.97	3.972	4.050			
100.64	4.180	4.360			
121.34	4.459	4.775			
141.53	4.808	5.079			
147.21	3.764	5.143			
156.19	3.952	5.303			

EXPERIMENTAL

The crystalline selenium used in this investigation was obtained by transforming a sample of amorphous selenium. A supply of the amorphous phase had been obtained from the Canadian Copper Refiners Ltd., Montreal, Canada.‡ The specimen consisted of granules having an average "diameter" of about 2 to 3 mm. The purity of the sample reported by the suppliers is approximately 99.999 percent. The manufacturers report the presence of the following impurities, all in parts per million; 0.4 Cu, 0.1 Pb, 0.9 Fe, and 0.1 Te. The amorphous phase was transformed into the hexagonal form by heating in vacuum to a temperature of about 130°C. The material was kept at this temperature for a period of one week. An x-ray photograph of this transformed material showed a pattern that corresponded to crystalline or hexagonal selenium.§ Approximately two gram-atoms of selenium were used in the experiment.

The copper calorimeter, cryostat, and accessory apparatus employed in this investigation have been used previously and are described elsewhere.[12] The accuracy of the measurements is comparable to that cited earlier; namely, 0.1 percent down to about 40°K, de-

‡ Loaned to the writer by Dr. P. E. Pashler.
§ This analysis was performed by Mrs. B. F. Decker.
[12] W. DeSorbo, J. Am. Chem. Soc. **75**, 1825 (1953).

creasing to approximately 2 percent at the lowest attainable temperature.

RESULTS

The specific-heat measurements, extending from 15° to 300°K, are presented graphically in Fig. 1. The data of C. T. Anderson are also included. The experimental results are summarized in Table I.

Table II lists the values of the thermodynamic functions obtained from a smooth curve of large graphs of specific heats *vs* T and of specific heats *vs* $\log T$. Simpson's rule was used to evaluate entropy and enthalpy functions. The entropy of crystalline selenium at 298.16°K is 10.15±0.05 cal/g-atom/deg. The extrapolated portion below 15°K amounts to 0.22.

DISCUSSION

A direct analysis of the data in terms of Eq. (3) can readily be made by a graphical presentation as shown in Fig. 2, where the $\log C_v$ is plotted as a function of $\log T$. At $T \ll \theta_1$—or at T less than approximately 30°K, where one might expect the Debye type of approximations to be more valid—it is clearly seen that Eq. (3), which expresses the "law of direct proportionality," is not obeyed. The exponential n has a value greater than 1 and is increasing with decreasing temperature.

Another illustration of the nonvalidity of this "law" at these lower temperatures is presented in Fig. 3. Graphically shown are the characteristic temperatures, θ_1 and θ_3, plotted as a function of temperature. The characteristic temperature, θ_1, has been computed by graphical interpolation of the specific-heat integral for a one-dimensional continuum. The characteristic temperature, θ_3, has been computed from the three-dimensional Debye integrals. The conversion from

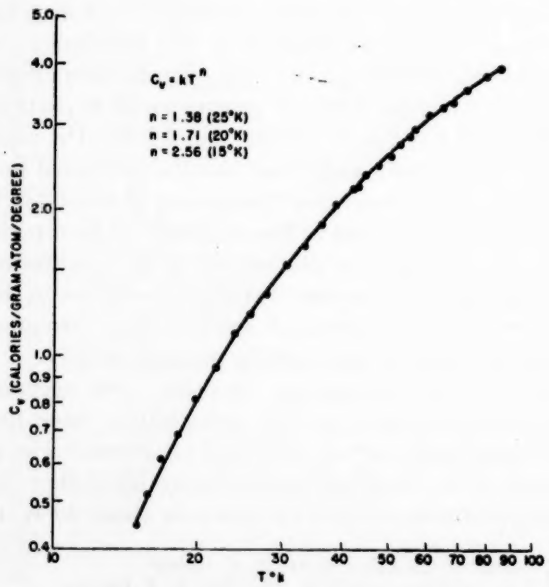

FIG. 2. LogC_v as a function of log$T$ for hexagonal selenium.

C_p to C_v values has been accomplished by the use of the Nernst-Lindemann formula.[13] The specific heat C_p data had been taken from a smooth curve.

In this type of graphical representation, where the characteristic temperature is plotted as a function of the absolute temperature, any deviation that the characteristic temperature shows from a constant value reflects the deviation of the distribution function assumed in the continuum spectrum. The data verify the good agreement with the predictions of the one-dimensional integral function in the temperature region 43°K to 150°K. Tarassov[8] had earlier shown that the constancy with temperature of these characteristic temperatures, θ_1, existed from 50°K to 150°K. His analysis was based on Anderson's data. The results of this investigation below 40°K show a sharp rise in the θ_1 as the temperature decreases. On the other hand, at these low temperatures θ_3 is decreasing with decreasing temperature. Similar results have also been shown by the author for tellurium and sulfur.[14] The values of either characteristic tempera-

TABLE II. Thermodynamic functions of selenium based on the smooth curve of specific heat.

T°K	C_p cal/g-atom/deg	$H^0-H_0^0$ cal/g-atom	$\frac{H^0-H_0^0}{T}$ cal/g-atom/deg	S^0 cal/g-atom/deg	$-\frac{F^0-H_0^0}{T}$ cal/g-atom/deg
25	1.170	8.2578	0.3303	0.6245	0.2942
50	2.620	56.460	1.1292	1.748	0.6188
75	3.661	135.83	1.8110	3.174	1.3630
100	4.344	236.38	2.3637	4.326	1.962
125	4.820	351.23	2.8099	5.350	2.5401
150	5.184	476.52	3.1767	6.264	3.0873
175	5.427	609.44	3.4828	7.083	3.6002
200	5.583	747.18	3.7359	7.821	4.0851
225	5.700	888.30	3.9480	8.489	4.541
250	5.804	1032.1	4.1284	9.100	4.9716
275	5.970	1179.2	4.2879	9.662	5.3741
298.16	6.062	1319.2	4.4245	10.144	5.7195
300	6.067	1329.8	4.4326	10.181	5.7484

ture, θ_1 or θ_3, are almost constant with temperature above the liquid nitrogen temperatures. In this temperature region, it appears that either the one-dimensional-continuum integral or the Debye theory could describe the specific heat to a rather good degree of approximation. However, it would be difficult to use these continuum ideas at these temperatures to distinguish between a "chain" structure or a three-dimensional structure. This lack of sensitivity at the higher temperatures results from the fact that the specific heat is proportional only to the total integral of the distribution function. The distinction between these continuum models is more apparent at low temperatures where the exact form of the distribution function is important.

One possible explanation of the increase in θ_1 and decrease in θ_3 at the low temperatures may be that the

[13] W. Nernst and F. Lindemann, Z. Elektrochem. **17**, 817 (1911).
[14] W. DeSorbo, Eighth Conference on Cryogenics, General Electric Company, Schenectady, New York, October 6–7, 1952.

frequency-distribution function following initially a one-dimensional form is going over into a three-dimensional form with decreasing temperature. That is to say, as lower temperatures are attained, the higher frequencies become less highly excited and leave waves of longer and longer wavelengths. At a sufficiently low temperature, the remaining waves present are of sufficient length that they are no longer influenced by the individual atoms in the lattice. For these waves, the isotropic-three-dimensional continuum model is more nearly correct. Therefore, it seems appropriate at the present time to apply to an anisotropic monatomic lattice a continuum model that postulates the "interaction" between the chains.

A simplified "interaction" model based on the Debye approximations has recently been proposed by Tarassov[8] but, as yet, has not been applied to "interacting" chains of monatomic lattices. In case of "interacting" chains, the assumption is made that there exist for a

TABLE III. Specific heats calculated from one-dimensional and "interaction" continuum models.

T°K	C_p(Expt'l) cal/g-atom/°K	C_v cal/g-atom/°K	$C_{1(3)}$, calc cal/g-atom/°K	C_1 calc cal/g-atom/°K
15	0.468	0.468	(0.544)[a]	(0.830)[a]
18	0.687	0.687	0.715	0.963
20	0.835	0.834	0.840	1.065
25	1.170	1.169	1.114	1.290
30	1.490	1.487	1.440	1.570
35	1.797	1.792	1.740	1.840
40	2.092	2.084	2.013	2.100
50	2.615	2.600	2.546	2.600
60	3.082	3.057	3.034	3.075
70	3.480	3.443	3.537	3.565
80	3.820	3.769	3.785	3.805
100	4.342	4.260	4.356	4.370
150	5.182	5.008	5.103	5.108
200	5.580	5.310	5.440	5.442
250	5.802	5.437	5.540	5.542
300	6.065	5.587	5.710	5.712

[a] Extrapolated from Tarassov's table.

gram-atom of a solid $3N$ vibrational degrees of freedom. In a chain structure, not all of the $3N$ frequencies, ranging from 0 to ν_{max}, are distributed according to a linear continuum [see Eq. (1b)]. It is supposed that only some number, $3N_1$, of the frequencies fall between the limits ν_1 and ν_{max}. The frequency-distribution function, them, can be written in the form

$$n(\nu)d\nu = 3N_1(\nu_{max}-\nu_1)^{-1}d\nu. \tag{4}$$

Therefore,

$$\int_{\nu_1}^{\nu_{max}} 3N_1(\nu_{max}-\nu_1)^{-1}d\nu = 3N_1. \tag{5}$$

It is further postulated that all the frequencies lower than ν_1—that is, those whose frequencies lie in the range 0 to ν_1—are distributed by the Debye three-dimensional continuum instead of by the "law of the linear continuum." The frequency-distribution function for these

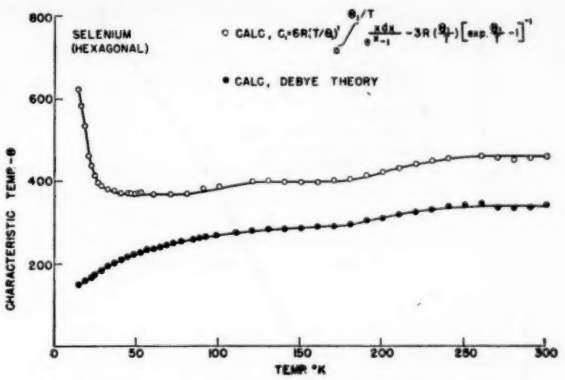

FIG. 3. Characteristic temperatures as a function of temperature for hexagonal selenium calculated from one- and three-dimensional continuum models.

waves can be written

$$n(\nu)d\nu = 9N_2\nu_1^{-3}\nu^2 d\nu. \tag{6}$$

Therefore,

$$\int_0^{\nu_1} 9N_2\nu_1^{-3}\nu^2 d\nu = 3N_2,$$
$$3N_1+3N_2=3N. \tag{7}$$

The internal energy of the "interacting" chains can be readily derived from the two distribution functions, Eqs. (4) and (6), and has the following form:

$$U_{1(3)} = 3N_1(\nu_{max}-\nu_1)^{-1}\int_{\nu_1}^{\nu_{max}} \frac{h\nu}{e^{h\nu/kT}-1}d\nu + 9N_2\nu_1^{-3}\int_0^{\nu_1}\frac{h\nu^3}{e^{h\nu/kT}-1}d\nu. \tag{8}$$

Introducing the notations, $h\nu/kT=x$, $\theta_1=h\nu_m/k$, and $\theta_3=h\nu_1/k$, one can deduce the following expressions for the specific heat of "interacting" chains:

$$C_{1(3)} = \frac{\partial U_{1(3)}}{\partial T} = 3R\left(\frac{T}{\theta_1}\right)\int_0^{\theta_1/T}\frac{x^2e^x}{(e^x-1)^2}dx - \left(\frac{\theta_3}{\theta_1}\right)\left[\frac{3RT}{\theta_3}\int_0^{\theta_3/T}\frac{x^2e^x}{(e^x-1)^2}dx - \frac{9RT^3}{\theta_3^3}\int_0^{\theta_3/T}\frac{x^4e^x}{(e^x-1)^2}dx\right]. \tag{9}$$

If one uses the symbol D_1 to denote the integral function for the heat capacity of the linear continuum and the symbol D_3 to denote the usual Debye function, Eq. (9) then becomes

$$C_{1(3)} = D_1(\theta_1/T) - (\theta_3/\theta_1)[D_1(\theta_3/T) - D_3(\theta_3/T)]. \tag{10}$$

At sufficiently low temperatures, as $T\to 0$, Eq. (10)

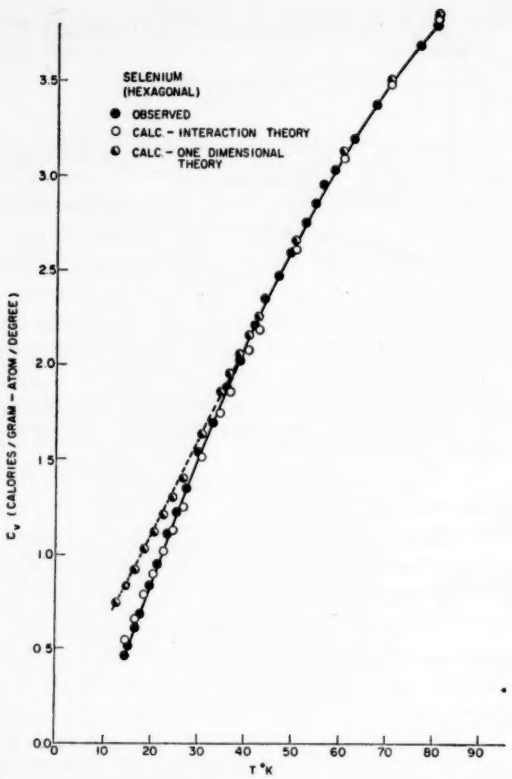

FIG. 4. Specific heat calculated from a one-dimensional and "interaction" continuum models compared with experimental data.

reduces to the T^3 law, i.e.,

$$C_v=\frac{12}{5}\pi^4R\frac{T^3}{\theta_1\bar{\theta}_3^2}. \tag{11}$$

The results of the application of this continuum specific-heat model to the data of crystalline selenium are tabulated in Table III. The experimental C_p values taken from a smooth curve are listed, as well as the C_v values calculated from the Nernst-Lindemann formula.[13] The values of the specific heat calculated by using Eq. (9) are listed in the third column. In this calculation, θ_1 has been assigned a value of 370 degrees and θ_3 has been given a value of 75 degrees. The fourth column is a tabulation of the specific heats calculated from the one-dimensional integral, where again θ_1 has the value of 370 degrees. A graphical representation of this comparison is shown in Fig. 4. Below approximately 37°K, values of the specific heat calculated from the "interaction" continuum model give better agreement than those calculated from the one-dimensional-continuum.

From Eq. (11), it follows that the formula for calculating entropy in the region where the T^3 law is valid is given by

$$S_0{}^T=\frac{4}{5}\pi^4\frac{RT^3}{\theta_1\bar{\theta}_3^2}. \tag{12}$$

At 15°K, the lowest temperature studied, the T^3 region has not been reached (Fig. 2; $n_{15°K}=2.56$). For the purpose of extrapolating to 0°K to evaluate entropy, an estimate for the temperature at which $n=3$ has been made and found equal to approximately 12°K. The entropy at 15°K may then be expressed in the following manner:

$$S_0{}^{15}=\int_0^{12}\frac{12}{5}\frac{\pi^4RT^2}{\theta_1\bar{\theta}_3^2}dT+\int_{12}^{15}\frac{C_{1(3)}}{T}dT. \tag{13}$$

The first integral has been evaluated for $\theta_1=370°$ and $\theta_3=75°$. The second integral has been evaluated graphically. The values $C_{1(3)}$ have been calculated at regular integrals of temperatures from 12° to 15°K. This has been done by using Eq. (9), where the characteristic temperatures, θ_1 and θ_3, have the values cited previously. The entropy increment $S_0{}^{15}=0.22$ cal/g-atom/deg.

ACKNOWLEDGMENTS

The author wishes to acknowledge the assistance rendered by Mrs. E. L. Fontanella in the experimental work and in the data computation. For the latter the author also thanks Mrs. M. V. Doyle and the calculating group of the Metallurgy Research Department. Criticisms of the manuscript by Dr. R. W. Schmitt and Dr. R. H. Pry are also gratefully acknowledged.

The Intermolecular Force Constants of Fluorine*

DAVID WHITE, JIH-HENG HU, AND HERRICK L. JOHNSTON
Cryogenic Laboratory and Department of Chemistry, Ohio State University, Columbus, Ohio

(Received February 3, 1953)

The intermolecular force constants of gaseous fluorine have been determined from measurements of the second virial coefficients in the region 80–300°K. On the assumption that gas imperfection results only from binary collisions of spherical nonpolar molecules whose potential is of the form given by Eq. (1), the force constants obtained were $r_0=3.61\pm0.04$A and $\epsilon_0/k=121\pm3$°K. These force constants yield viscosities in good agreement with the experimental data of Kanda if the high temperature point is discarded.

INTRODUCTION

THE intermolecular force constants of gaseous fluorine have remained uncertain, due to the lack of experimental data on the gaseous density, and the peculiar temperature dependence of the viscosity.[1] From the existing information on the physical properties of liquid and gaseous fluorine, it is reasonable to expect fluorine to behave like nitrogen or oxygen. Since it is nonpolar and, if like nitrogen and oxygen, can be assumed spherically symmetrical, one should expect the potential energy at a binary collision to be

$$V(r)=4\epsilon_0\left[\left(\frac{r_0}{r}\right)^{12}-\left(\frac{r_0}{r}\right)^{6}\right], \qquad (1)$$

the Lennard-Jones expression, with constants in the neighborhood of those of oxygen or nitrogen. This, however, would still leave unresolved the temperature dependence of the viscosity.

An attempt has been made here to determine the intermolecular force constants from measurements of the second virial coefficients to shed some additional light on the nature of gas imperfection in fluorine.

APPARATUS AND PROCEDURE

The experimental apparatus, shown schematically in Fig. 1, consisted of the condensed gas silver calorimeter A used in the determinations of the heat capacity of the corrosive materials hydrogen fluoride[2] and fluorine.[3] The calorimeter was attached to one side of an oil manometer C by means of Monel capillary B. This manometer was filled with Fluorolube S (Hooker Electrochemical Company) which had previously been pumped down to 1×10^{-5} mm Hg to remove any of its volatile components.† The other side of the oil manometer was connected to a mercury manometer D. Both manometers were read with cathetometers and compared with a standard meter bar. The uncertainty in each of the readings amounted to ±0.03 mm Hg. The temperature of the calorimeter was read by means of a thermocouple which had been intercompared with a helium gas thermometer.[4]

The experimental procedure consisted of the introduction of a sample of gas into the calorimeter at 300°K and at a pressure of approximately 1 atmosphere by opening valve E. The system was then isolated from the gas storage cylinder and the calorimeter cooled down to approximately 80°K. The measurements were then identical to those of gas thermometry, for a system of constant volume (corrected for the variation with temperature) and constant number of moles; pressures and temperatures were read at various intervals in the region 80–300°K. During the experiments the oil level in the arm of the oil manometer in contact with the calorimeter was always kept at a fixed point by means of valve F which permitted air to be introduced or removed. Also, the temperature gradient along the capillary B leading from the calorimeter to the manometer was kept as linear as possible by means of a set of heater blocks (see description of condensed gas calorimeter[2]). Since nearly all the dead space was in contact with the room, the room tempertture was held constant to within ±0.5°C.

Assuming that (1) the equation of state for 1 mole

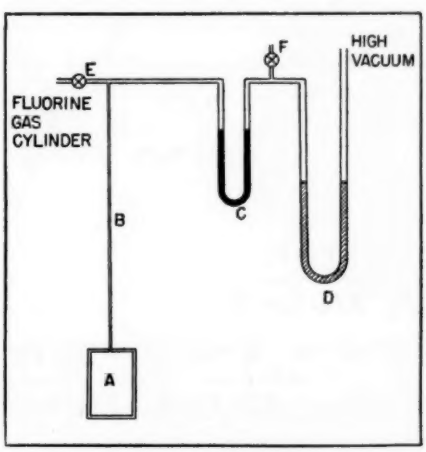

FIG. 1. Experimental apparatus.

* This work was supported in part by the U. S. Office of Naval Research under contract with the Ohio State University Research Foundation.

[1] E. Kanda, Bull. Chem. Soc. Japan **12**, 463–468 (1937).

[2] Hu, White, and Johnston, J. Am. Chem. Soc. **75**, 1232 (1953).

[3] Hu, White, and Johnston, "On the heat capacity, heat of transition, fusion and vaporization and vapor pressure of fluorine" (submitted for publication to J. Am. Chem. Soc.).

† Before using the fluorolube, experimental tests showed that it neither reacted nor dissolved fluorine to any appreciable extent.

[4] Rubin, Altman, and Johnston, J. Am. Chem. Soc. **73**, 3401 (1951).

of gas at all temperatures can be represented by

$$PV=RT+BP,$$

where B is the second virial coefficient at temperature T, and that (2) the system can be split into two parts characterized by the calorimeter temperature T_1 and room tempertture T_0, with corresponding volumes V_1^1 and V_2^0, for a fixed number of moles at two different

TABLE I. Second virial coefficients of nitrogen, oxygen and fluorine.

Temp °K	B_{nitrogen} (cc) this experiment	B_{nitrogen} (cc) from gas densities[a]	B_{oxygen} (cc) this experiment	B_{oxygen} (cc) from gas density and velocity of sound[b]	$(B-B_0)_{\text{fluorine}}$ (cc)
80	−265	−251	−339	−278	−375
					−358
85	−247	−223	—	—	−298
					−285
90	−213	−199	−237	−222	−247
					−228
95	−174	−178	—	—	−201
					−208
100	−158	−161	−170	−186	−180
					−185
110	−142	−134	—	—	−155
					−157
125	− 90	−105	−112	−130	−115
					−120
150	− 56	− 71	− 94	− 90	− 73
					− 84
175	− 29	− 50	− 62	− 56	− 46
					− 49
200	− 34	− 35	− 42	− 48	− 33
					− 26
250	− 23	− 16	− 35	− 27	− 8
					− 6

[a] See reference 6.
[b] G. P. Nijhoff and W. H. Keesom, Leiden Comm. **179(b)** (1926); H. K. Onnes and H. A. Kuypers, Leiden Comm. **169(a)** (1924); J. A. van Lammeren, Leiden Comm. Suppl. **77(b)** (1935).

calorimeter temperatures, we have the relation,

$$\frac{P_1V_1^1}{RT_1+B_1P_1}+\frac{P_1V_2^0}{RT_0+B_0P_1}=\frac{P_0V_1^0}{RT_0+B_0P_0}+\frac{P_0V_2^0}{RT_0+B_0P_0},$$

or (2)

$$\frac{1}{RT_1/P_1+B_1}+\frac{V_2^0/V_1^1}{RT_0/P_1+B_0}=\frac{V_1^0/V_1^1}{RT_0/P_0+B_0}+\frac{V_2^0/V_1^1}{RT_0/P_0+B_0}.$$

$$V_1^0/V_1^1=\mu_1$$
$$V_2^0/V_1^0=\beta$$
$$RT/P=\lambda,$$

and substitute into Eq. (2). Thus

$$\frac{1}{\mu_1\lambda_1+\mu_1B_1}-\frac{1}{\lambda_0+B_0}=\beta\left[\frac{1}{RT_0/P_0+B_0}-\frac{1}{RT_0/P_1+B_0}\right]=\beta\alpha, \quad (3)$$

where

$$\alpha=\frac{1}{RT_0/P_0+B_0}-\frac{1}{RT_0/P_1+B_0}.$$

Rearranging, Eq. (3) becomes

$$(B_1-B_0)+B_0\left[1-\frac{1-\beta\alpha\mu_1\lambda_1}{\mu_1[1+\beta\alpha\lambda_0]}\right]+\frac{\beta\alpha B_0B_1}{1+\beta\alpha\lambda_0}=\frac{(\lambda_0-\mu_1\lambda_1)-\beta\alpha\lambda_0\mu_1\lambda_1}{\mu_1[1+\beta\alpha\lambda_0]}. \quad (4)$$

In practice it is found that the second and third terms on the left-hand side of Eq. (4) are very small compared to (B_1-B_0). Neglecting these terms, Eq. (4) becomes

$$B_1-B_0=\frac{(\lambda_0-\mu_1\lambda_1)-\beta\alpha\lambda_0\mu_1\lambda_1}{\mu_1[1+\beta\alpha\lambda_0]}. \quad (5)$$

Since the quantities λ and α are directly determined experimentally and μ_1 can be calculated from the coefficient of thermal expansion of silver,[5] the only quantity that needs to be determined before a value of B_1-B_0 can be obtained is β. It is evident from the definition of β that it cannot be directly determined in this case from the dimensions of the apparatus because of the hypothetically chosen boundary separating V_1^0 and V_2^0. Thus calibration experiments were performed with gaseous nitrogen whose virial coefficients are accurately known.[6] The value of β obtained was 0.0381 ± 0.0003. At temperatures in the vicinity of the boiling point of nitrogen there was a considerable deviation from this value. However, this is to be expected since the simple equation of state used in the calculations is probably not valid.

MATERIALS USED

The fluorine gas used in the experiments was prepared electrolytically. Purification was effected by passing it over a sodium fluoride train to remove hydrogen fluoride and then triply distilling it to remove any traces of impurities. From freezing point determina-

[5] F. C. Nix and D. MacNair, Phys. Rev. **61**, 74–78 (1942).
[6] Friedman, White, and Johnston, "On the vapor-volume-temperature relationships of nitrogen from its boiling point to room temperature and from 0 to 200 atmospheres" (unpublished results). David White, Engr. Exp. Station News (The Ohio State University) **24**, No. 3, pp. 12–15 (1952).

TABLE II. Calculated and experimental values for the second virial coefficients and the viscosity of fluorine.

Temp (°K)	B_{exp} (av) (cc)	B_{calc} (cc)	$\eta_{exp}\times10^7$ (poise) smoothed	$\eta_{calc}\times10^7$ (poise)
80	−385	−310	...	...
85	−310	−278	...	...
90	−256	−252	592	651
95	−224	−230	...	...
100	−202	−210	691	720
110	−175	−178	782	795
125	−137	−143	906	903
150	− 98	−103	1088	1082
175	− 67	− 77	1260	1257
200	− 49	− 58	1422	1420
250	− 26	− 34	1732	1725
273.2	...	...	2093	1858

tions, the resulting fluorine was found to have a purity of 99.97 percent.[3] The materials of construction were of either silver, Monel, or glass, to reduce to a minimum the contamination of the fluorine during the experiments. All valves were constructed of Monel and packed with Teflon.

EXPERIMENTAL RESULTS

The second virial coefficients of nitrogen, oxygen, and fluorine are shown in Table I. Measurements on the former two gases were carried out so that consistency of the measurements resulting from a gas thermometry technique could be determined by comparison with results obtained from determinations of the gas density and velocity of sound. The accurate virial coefficients determined from measurements of the gas densities of nitrogen[6] and from gas densities and the velocity of sound of oxygen are given in columns 3 and 5, respectively. The results on fluorine are shown in the last column under the heading $B-B_0$, where B is the virial coefficient at the temperature given, and B_0 the virial coefficient at 300°K. The data from two different experiments are tabulated in the last column.

DISCUSSION OF RESULTS

From a comparison of the results of nitrogen and oxygen with those from the density measurements, the uncertainties arising from this experimental technique can be seen. The low results at the lowest temperatures probably arise from the fact that higher virial coefficients have been neglected in the calculations. The equation of state used in the calculations was assumed to be simply $PV=RT+BP$. Thus any contribution from the third and higher virial coefficients would appear in the B's. However, above 90°K the differences arise from uncertainties in pressure readings, variations in dead space due to different temperature gradients along the capillary leading to the calorimeter, and uncertainties in the temperature scale. In general the results are sufficiently good to evaluate force constants, since it is the temperature dependence which is more important than the absolute value.

On the assumption that the fluorine molecule is spherically symmetrical the data for fluorine were fitted to a Lennard-Jones potential function with the aid of the tables published by Benedict,[7] using a value for B_0, as a first approximation, equal to that of oxygen. After obtaining a set of force constants a new value of B_0 was calculated and the data again fitted to the potential function. The value of B_0 and the force constants thus obtained are

$$B_0=-19 \text{ cc},$$

$$r_0=3.61\pm0.04\text{A},$$

$$\epsilon_0/k=121\pm3\text{°K}.$$

It is evident from the results given above that the limits of uncertainty for the intermolecular force constands are considerable. This is mainly a result of the uncertainty of the second virial coefficients at the lowest temperatures (owing to contributions from higher virial coefficients which are not corrected for in the calculations), making it difficult to determine how much emphasis must be placed on them. A comparison of the second virial coefficients, calculated from the above force constants, with the experimental values are given in Table II and shown graphically in Fig. 2.

A comparison is also made in Table II of the smoothed experimental results of Kanda[1] on the viscosity of fluorine with those calculated from the force constants.[8] Figure 3 shows graphically a comparison of the actual experimental results with the calculated ones. The deviations at lowest temperatures have been found for other gases; however, there is fairly good agreement

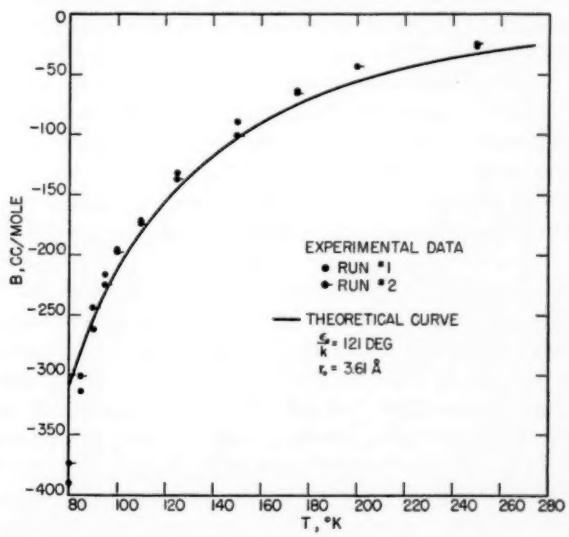

FIG. 2. Second virial coefficient of fluorine.

[7] W. S. Benedict, Natl. Bur. Standards (U. S.) Tech News Bull., January 31, 1950, "Tables of corrections to thermodynamic properties for gas imperfections, using the Lennard-Jones 6-12 potential."

[8] Hirschfelder, Bird, and Spotz, J. Chem. Phys. 16, 968 (1948).

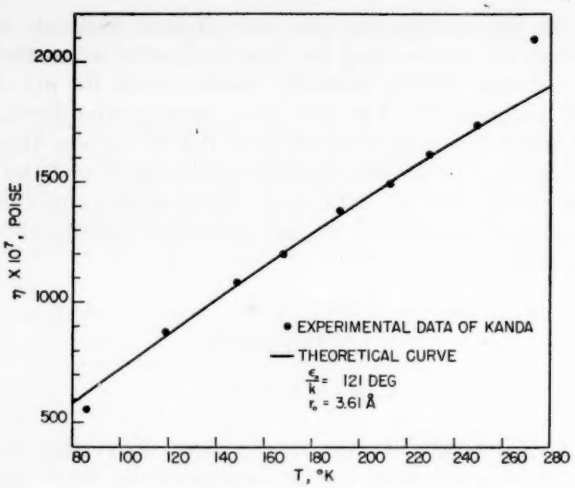

FIG. 3. Viscosity of fluorine.

above 90°K. At 273.2°K the experimental viscosity is much larger than the calculated one. We believe that this is a result of impurities of high molecular weight which are vaporized into the gas phase at this temperature, resulting in the anomalous viscosity. At lower temperatures these impurities remained condensed and thus do not affect the experimental results. A very similar effect was observed in the experiments on the second virial coefficients. After the introduction of the first quantity of fluorine gas to the system, the pressure continued to rise very slowly, and only after successive flushing and evacuation was the effect practically eliminated. The resulting products of the reaction could be condensed out at lower temperatures.

A slightly better fit to the experimental viscosity data can be obtained (neglecting the point at 273.2°K) using the force constants $r_0=3.59$A and $\epsilon_0/k=124$°K. This is, however, within the uncertainty given.

As estimate of the critical temperature, T_c, of fluorine can be made from the value of ϵ_0/k, on the assumption that the Lennard-Jones and Devonshire[9] dense gas theory is applicable. For such a model R. H. Wentorf *et al.*[10] have found $T_c=1.30\epsilon_0/k$, and therefore, for fluorine, $T_c=157\pm4$°K.

---

[9] J. E. Lennard-Jones and A. F. Devonshire, Proc. Roy. Soc. (London) **163A**, 53 (1937); **165A**, 1 (1938).

[10] Wentorf, Buehler, Hirschfelder, and Curtiss, J. Chem. Phys. **18**, 1484 (1950).

A Study of the Formation of Iron Percarbide

JOHN J. MITCHELL
Beacon Laboratories of The Texas Company, Beacon, New York
(Received April 2, 1952)

Carbon 14-labeled CO was used in a study of the carbiding of reduced iron in the temperature range 170–231°C. It was shown that the percarbide forms around nuclei scattered throughout the iron, that carbon in percarbide volumes is held firmly in place, and that a substantial fraction of the surface of partially carbided iron is occupied by percarbide.

I. INTRODUCTION

THE role of the carbide formed from an iron catalyst during the Fischer-Tropsch synthesis of hydrocarbons from carbon monoxide and hydrogen has been the subject of much investigation and speculation. Some have held that the carbide is an intermediate step in the process;[1–3] others that the carbide is simply a by-product;[4–6] and still others have stated that, while not an intermediate, the carbide is the active catalyst in the process.[7] This uncertainty as to the role of the catalyst carbide led Kummer, DeWitt, and Emmett[8] to perform an experiment with radioactive carbon to find if iron percarbide Fe_2C was an intermediate in the hydrogenation of carbon monoxide over an iron catalyst. While their work appeared to show that at most 10–15 percent of the synthesis went via the carbide, they also uncovered a complication with regard to the formation of the carbide. They showed that it was formed neither in layers nor uniformly throughout the iron and suggested that perhaps it grew at nuclei throughout the iron.

The experiments to be described in this paper were designed to determine if a nucleation process was that followed. In these experiments, completely reduced iron was first carbided partially with radioactive carbon monoxide. Then carbiding was continued at the same temperature and pressure with ordinary carbon monoxide. Since the carbide carbon laid down in the first portion of the experiment was radioactive, its fate could be determined during the second portion. It was expected that, since many chemical processes are equilibrium processes, radioactive carbon would be found in the off-gas during the later portion. One possible set of equilibria would be

$$\mathrm{CO(gas)}\rightleftharpoons\mathrm{CO(ads)}\rightleftharpoons\mathrm{C(ads)}+\mathrm{O(ads)},$$
$$\mathrm{CO(ads)}+\mathrm{O(ads)}\rightleftharpoons\mathrm{CO_2(ads)}\rightleftharpoons\mathrm{CO_2(gas)},$$
$$\mathrm{C(ads)}\rightleftharpoons\mathrm{C(dissolved)}\rightleftharpoons\mathrm{C(carbide)}.$$

If the carbide were laid down in successive layers with the outermost layer displacing the others inward, one would expect the off-gas to become free of radioactive carbon promptly. If, on the other hand, carbon could diffuse readily through iron and through carbide, one would expect the amount of radioactive carbon in the off-gas to decrease exponentially with time. If carbon did not diffuse as readily through carbide as through iron, a nucleation process would be expected to give rise to an intermediate behavior.

The experiments were conducted over a temperature range of 170 to 230°C and with initial radioactive carbide concentrations ranging from 3 to 30 mole percent to determine if the mechanism were the same over a wide range of conditions.

II. EXPERIMENTAL PROCEDURE

Catalysts

Two catalysts[9] were used in their reduced state in this work. The first, called "pure iron," was shown by x-ray analysis[10] to be, before reduction, goethite, or $\alpha-Fe_2O_3\cdot H_2O$. In its preparation a solution of 3258-g cp $Fe(NO_3)_3\cdot 9H_2O$ in 10 liters of water was completely precipitated by the slow addition with agitation of 3.5 liters of dilute NH_4OH (14 percent NH_3). The precipitate was filtered and washed ten times by slurrying in 5 liters of water containing 25-cc concentrated NH_4OH. This was followed by a wash with pure water. The washed gel was dried at 120°C, crushed, pelleted in a $\frac{1}{8}$-in. die, and the pellets were heated for six hours at 315°C.

The second catalyst, called "copper-promoted iron," was likewise shown by x-ray analysis to consist, before reduction, principally of goethite. In its preparation a solution of 21 400 g of cp $Fe(NO_3)_3\cdot 9H_2O$ and 114 g of cp $Cu(NO_3)_2\cdot 3H_2O$ in 40 liters of water was poured as rapidly as possible with good agitation into 72 liters of 10 percent NaOH. The precipitate was washed six times with 20 gallons of water. It was dried at 150°C and then pelleted in $\frac{1}{2}$-in. dies with 30 percent water. These pellets were then broken up into 10–20 mesh granules. Chemical analysis showed that the completely reduced

[1] F. Fischer and H. Koch, Brennstoff-Chem. **13**, 428–34 (1932).
[2] S. R. Craxford, Trans. Faraday Soc. **42**, 576–9, 580–5 (1946).
[3] S. R. Craxford and E. K. Rideal, J. Chem. Soc. **1939**, 1604–14.
[4] W. Brötz, Z. Elektrochem. **53**, 301–306 (1949).
[5] S. Hamai, Bull. Chem. Soc. Japan **16**, 213–228 (1941).
[6] Anderson, Friedel, and Storch, J. Chem. Phys. **19**, 313–319 (1951).
[7] H. Pichler and H. Merkel, U. S. Dept. of Interior, Bureau of Mines, Technical Paper 718, pp. 108 (1949).
[8] Kummer, DeWitt, and Emmett, J. Am. Chem. Soc. **70**, 3632–3643 (1948).

[9] These catalysts were prepared under the direction of Leon W. Cook of this laboratory.
[10] All of the x-ray analyses reported in this paper were carried out by J. W. Fitzwilliam of this laboratory.

catalyst would contain one part of Cu to 91.5 parts of Fe.

Gases

The hydrogen used was commercial, high purity H_2; the CO was prepared in this laboratory in large quantities by dehydration of formic acid for large scale studies on the hydrogenation of CO.

The radioactive carbon monoxide, called C*O, was made up by mixing ordinary CO with a portion of carbon monoxide[11] containing $C^{14}O$. Whenever C* is used in this paper, it will mean carbon containing the same percentage of C^{14} as this carbon monoxide does of $C^{14}O$.

Apparatus

The reaction system is shown schematically in Figs. 1 and 2. It was arranged so that the catalyst could be reduced with hydrogen, carbided with C*O in a closed circuit to conserve C*O, or carbided with ordinary CO without recirculation. Traps IV and V in Fig. 2 were arranged in parallel so that, while the off-gas was flowing into one trap, the contents of the other trap could be assayed.

During operation of the system as a closed circuit, the Maass[12] pump removed carbon monoxide from the collecting trap which was chilled with liquid N_2, compressed it to atmospheric pressure, and delivered it through the gasometer and flowmeter[13] to the reactor at the desired flow rate. The bellows-type gasometer acted as a reservoir for C*O, as a surge tank for decreasing pressure fluctuations due to the pump, and, by slowly collapsing, as a means of keeping the pressure in the reactor atmospheric as the C*O was consumed. The center member of the reactor was packed with glass-wool so that the gas, entering downflow, was thoroughly preheated before encountering the catalyst packed in the outer annular space. The check-valve,[14] which con-

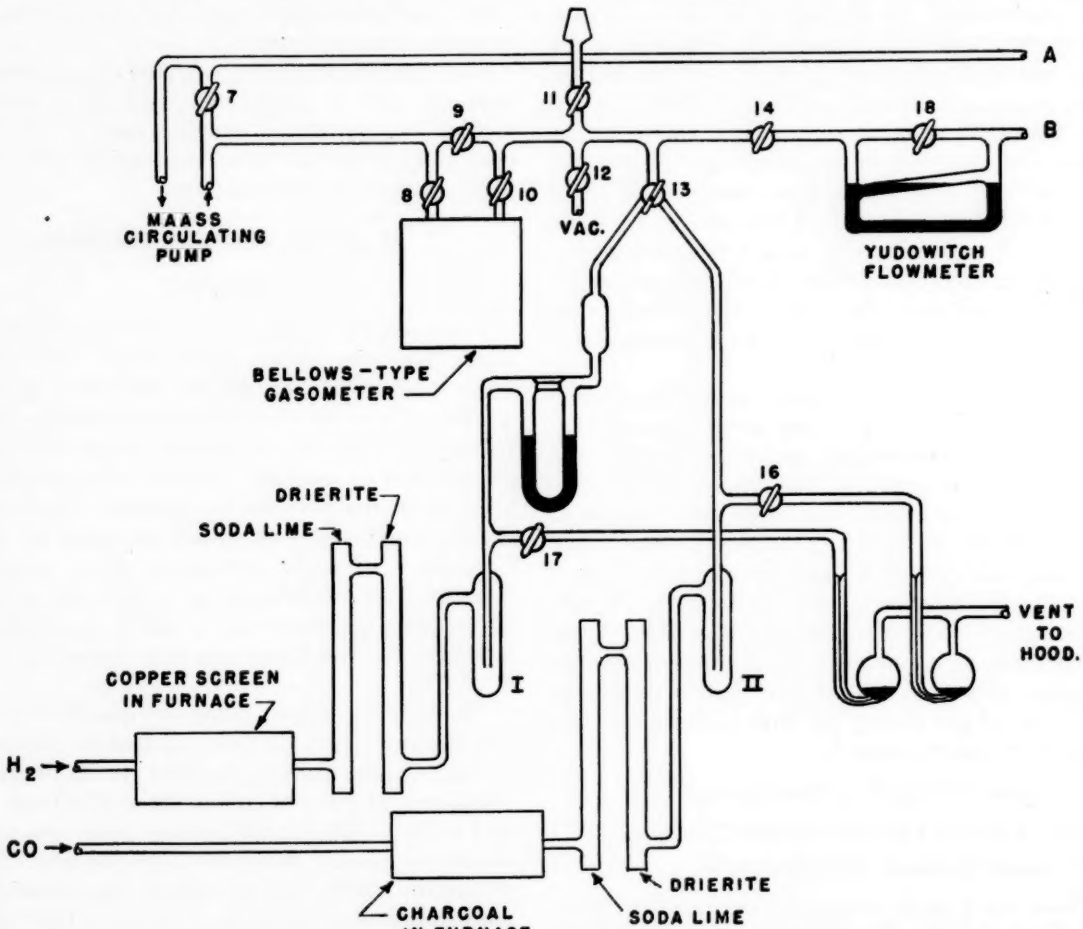

FIG. 1. Schematic diagram of the gas supply system. The ground-glass joint above stopcock 11 was the point of attachment of the bulb containing C*O.

[11] The radioactive carbon monoxide was made by R. P. Eischens of this laboratory from barium carbonate purchased from the U. S. Atomic Energy Commission. The procedure used was that of R. B. Bernstein and T. I. Taylor, Science **106**, 498–499 (1947).

[12] O. Maass, J. Am. Chem. Soc. **41**, 53–59 (1919).

[13] K. L. Yudowitch, Anal. Chem. **20**, 86 (1948).

[14] This valve was adapted from one due to W. B. Leslie and illustrated in O. K. Neville, AECD-2075 (September 8, 1948), U. S. Atomic Energy Commission.

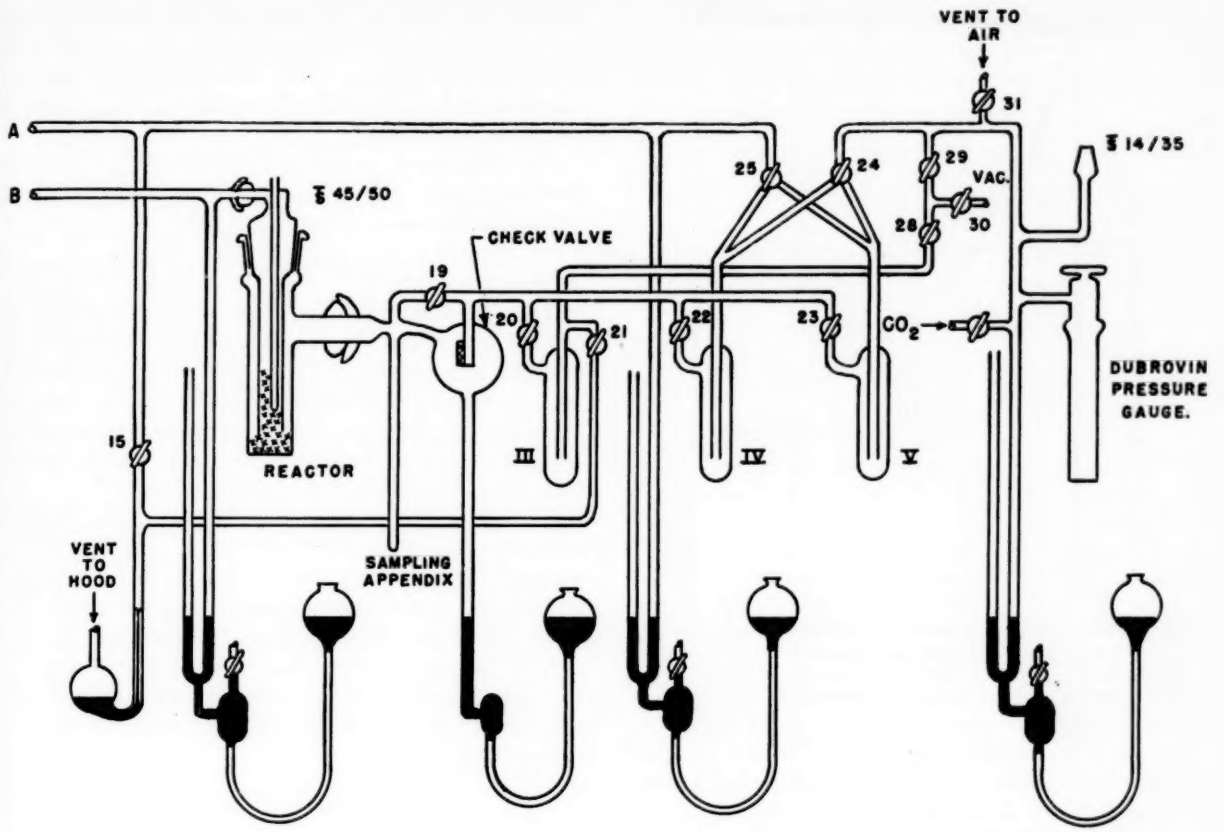

FIG. 2. Schematic diagram of the reactor and sampling system. This is connected with the apparatus in Fig. 1 at A and B. The ground-glass joint above the Dubrovin pressure gauge was the point of attachment of the ionization chambers.

sisted of a sintered-glass disk which could be covered wholly or partially by mercury, maintained atmospheric pressure in the reactor and yet allowed gas to flow at the desired rate into the chilled collecting trap.

When the system was operated with ordinary CO, the gas simply flowed through flowmeter, reactor, and check-valve into an evacuated and chilled trap. This collected CO as liquid and CO_2 as solid.

Radioactive Carbon Assay

The radioactivity of the gases collected was measured by means of ionization chambers.[15] A chamber was attached to the reaction system at the ground-glass joint shown in Fig. 2. It and the connecting tubing were evacuated. The liquid-N_2-chilled trap (either IV or V) which was isolated from the reaction system was then opened to the evacuated portion. This allowed any carbon monoxide present to be shared between trap and chamber. Its pressure was measured; the chamber and trap were closed; the intervening tubing was evacuated and finally ordinary CO_2 was run into the chamber to bring the total pressure to atmospheric. A second chamber was attached, and this time the chilled trap was also evacuated, thus removing all carbon monoxide (vapor pressure 456 mm Hg at liquid N_2 temperature). The trap was then allowed to warm; the pressure of the released carbon dioxide was measured; and then the carbon dioxide was condensed into the chamber by chilling an appendage on the chamber with liquid N_2. Once again the pressure in the chamber was made up to atmospheric by adding ordinary CO_2.

The ion current from a chamber, which is directly proportional to the radioactivity contained in the chamber, was measured by a vibrating-reed electrometer[16] in terms of charging rate as millivolts per chart division on a Leeds and Northrup Speedomax recorder.

TABLE I. Activities of carbon dioxide samples from a typical run.

Activity mv/div	Amount of CO_2 condensed into chamber mM	Specific activity (mv/div)/mM	Amount of C^*O_2 mM
22 000	5.34	4120	...
13 800	3.41	4050	...
567	4.88	115	0.137
109	4.15	24.3	0.0244
166	6.34	25.0	0.0386
141	5.52	24.1	0.0325
70.0	2.62	23.7	0.0152

[15] The guard-ring, insulation assembly of these chambers, is adapted from that given by C. J. Borkowski, MDDC-1099, (June 12, 1947), U. S. Atomic Energy Commission, while the guard-ring shielding, and vacuum-seal were adapted from those given by C. D. Janney and B. J. Moyer, Rev. Sci. Instr. **19**, 667–74 (1948).

[16] Model 30, Serial No. 95, Applied Physics Corporation.

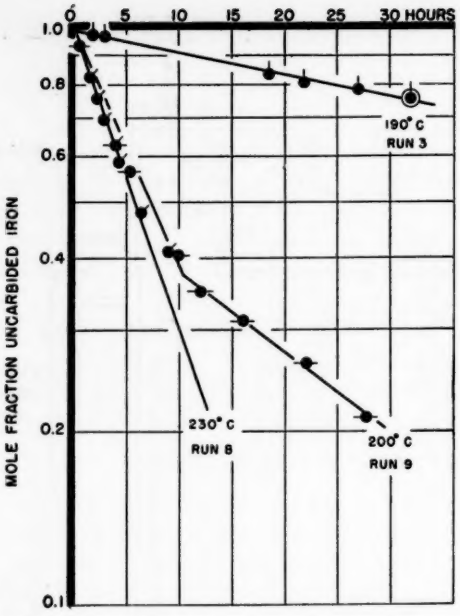

FIG. 3. Plots of extent of carbiding against carbiding time for three copper-promoted iron samples. The encircled point in Run 3 was determined after an interruption during which the evacuated catalyst was held 16 hr at reaction temperature.

Some idea of the activities involved is given in Table I, which shows the activities of the carbon dioxide samples obtained during Run 8. The specific activity was obtained by dividing the amount of CO_2 into the net activity obtained by subtracting chamber background, 8 mv/div in this case, from the measured activity. The first two samples were taken while carbiding with C*O; the remainder while carbiding with ordinary CO. The amount of C^*O_2, given in millimoles, in each of the latter samples was found by dividing the net activity of the sample by the average specific activity of the first two samples.

Carbiding Procedure

In each run, a weighed sample of catalyst, of approximately 10-cc volume, was reduced with H_2 at atmospheric pressure, 260–270°C and 1000 volumes per catalyst volume per hour for six days. During the last three days, the glass-bead-packed trap (Trap I in Fig. 1) in the H_2 line was chilled with liquid N_2 to remove any last traces of water.[17] The reactor was then evacuated, and its temperature adjusted to the desired carbiding temperature (170–230°C).[18] The carbiding was started by admitting C*O at atmospheric pressure with a flow rate of 100 volumes per catalyst volume per hour. This carbiding was interrupted by evacuation of the heated reactor. Then carbiding was resumed at the same temperature by admitting ordinary CO under the same conditions.

The progress of carbiding was followed by measuring manometrically the CO_2 evolved as described under "radioactive carbon assay." Assuming

$$2Fe+2CO\rightarrow Fe_2C+CO_2$$

to hold, the carbide content was calculated on the basis of CO_2 production. The validity of this assumption was checked in every run by removing samples of catalyst with a magnet from the reactor to a sampling appendage shown in Fig. 2. X-ray analysis of these samples showed for all of the runs presented here good checks between CO_2 production and Fe_2C concentration.

At the lower temperatures, the percarbide found by x-rays was the Merkel-Pichler[19] form. At higher temperatures, although the initial percarbide was Merkel-Pichler carbide, a larger and larger proportion was found to be Hägg[19] carbide as carbiding proceeded. However, there was no corresponding difference in the results of the experiments reported here. For that reason, all of the percarbide produced was assumed to have the formula Fe_2C.

III. RESULTS AND DISCUSSION

The carbon monoxide which was collected after resumption of carbiding with ordinary CO was found

TABLE II. Data with regard to production of C^*O_2.

Run	Reaction temp. °C.	Initial amount of iron (gms)	Initial Fe_2C^* mole percent	Carbiding rate constant k[a] (hours^{-1})	Constants of straight-line portion of C^*O_2 removal curve: I_{C^*}, Ordinate intercept (mMC^*O_2)	Slope (mMC^*O_2/ mMFe_2C)
Over pure iron						
1BA	180	10.43	15.3	0.019	0.077	0.0065
2BA	185	8.71	19.5	0.030	0.117	0.0132
3BA	190	8.58	4.7	0.073	0.020	0.0012
4BA	170	5.47	5.2	0.025	0.012	0.0011
Over copper-promoted iron						
2	170	7.05	3.5	0.0078	0.300	0.0118
3	190	6.24	2.8	0.0088	0.180	0.0073
5	210	6.88	12.0	0.061	0.117	0.0132
7	210	5.64	29.0	0.073	0.443	0.0093
8	230	6.12	17.5	0.12	0.110	0.0060
9	200	7.58	6.1	0.10	0.167	0.0048

[a] Because several of the carbiding curves show two straight-line portions on a semilog plot, this "carbiding rate constant k," taken in these cases from the portion with the most data, indicates only approximately the relative rates of carbiding.

[17] This reduction procedure was shown by R. P. Eischens of this laboratory to convert the "pure iron" catalyst to a reduced condition in which the CO chemisorption area was equivalent to the N_2 physical adsorption B.E.T. area.

[18] The reactor was heated by an electric furnace, the temperature of which was controlled manually. The temperature was measured by an iron-constantan thermocouple in a thermowell in contact with the inner wall of the reactor at the level of the catalyst bed. This temperature was recorded by a Leeds and Northrup Micromax recorder and usually stayed constant to ±3°C.

[19] The Merkel-Pichler carbide is hexagonal Fe_2C. (H. Pichler and H. Merkel, "Chemical and Thermomagnetic Studies on Iron Catalysts for the Synthesis of Hydrocarbons," translation by R. Brinkley, Report No. 3141-Q:88, Research and Development Branch, Bureau of Mines, U. S. Dept. of Interior, May 3, 1948). The constitution of the Hägg carbide is not known definitely, although $Fe_{20}C_9$ has been suggested as a formula.

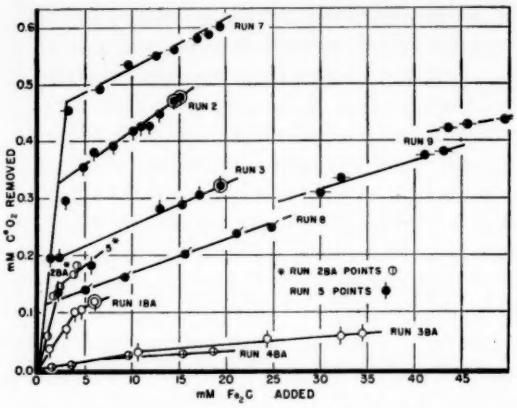

FIG. 4. A plot of amount of C* removed against the amount of unlabeled carbide produced after the carbiding gas was changed from C*O to CO. It should be noted that the encircled points, determined after heat treatment, are consistent with previous points in the same run.

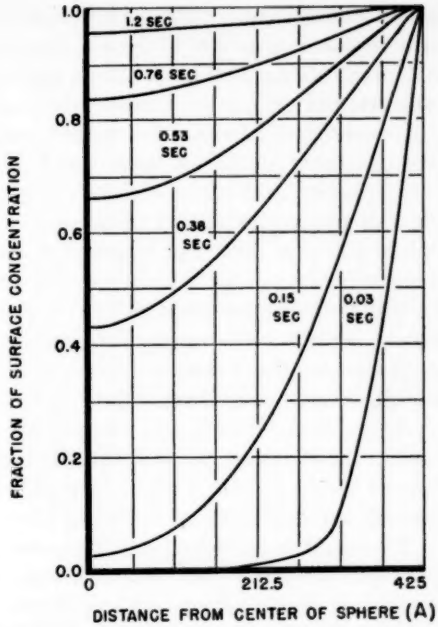

FIG. 5. Concentrations of dissolved carbon in an 850A diameter iron sphere at various times after the imaginary act of an instantaneous formation of an infinitesimally thick surface layer of iron containing a constant concentration of carbon. These curves are computed from the first 5 terms of

$$c(r)/c(a)=1-(2a/\pi r)\sum_n n^{-1}(-1)^n.\ \sin(n\pi r/a)\cdot\exp(-Dn\pi^2t/a^2),$$

where $c(r)$ is the concentration at radius r, a is the radius of the sphere, and t is the time. This equation differs by a necessary factor of $1/r$ from that of R. M. Barrer, *Diffusion In and Through Solids* (Cambridge University Press, Cambridge 1950).

within experimental error to contain no C*O. However, the level of radioactivity used, coupled with the possibility of 99-fold dilution with ordinary CO arising from the fact that only one percent of the CO passed over the catalyst was converted to carbide and CO_2, prevents one from saying that there was no C*O in the off-gas. Thus, one does not know from these data if CO is desorbed under these conditions of constant CO pressure and prompt CO_2 removal. The appearance of C^*O_2 in the off-gas, however, indicates definitely that the reaction

$$CO(ads)\rightleftharpoons C(ads)+O(ads),$$

must run in both directions.

The amount of CO_2 produced, and hence of Fe_2C formed, was followed as a function of time as shown in Fig. 3. Two types of curves were found, those following $dP/dt=k(100-P)$ where P is mole percent Fe_2C, t is time in hours, and k is an empirical constant, and those showing two straight-line portions on a semilog plot. Of the runs presented in Table II, Runs 1BA, 2BA, 3BA, 5 and 9 showed two portions. The other runs gave single lines. This behavior and lack of precise temperature control make it impossible to draw any conclusions as to the kinetics of the reaction from these data.[20] However, the constant k, given in Table II for the part of the carbiding curve representing the most data, does give an approximate idea of the relative rates of carbiding.

One further result evident from the data in Fig. 3 is the fact that the encircled point in Run 3, which was determined after carbiding had been interrupted by evacuation and the partially carbided catalyst held evacuated for 16 hours at reaction temperature, fell on the carbiding curve. The same behavior was found for a five-hour interruption in Run 2 and a 3.5-hour interruption in Run 1BA. This is evidence that the factors governing rate of carbiding were not changing with time. Such a possible factor might have been increase in size of large carbide nuclei at the expense of small, with a consequent withdrawal of carbide from the catalyst surface resulting in an increase in surface reactivity.

Uncertainty as to the rate of the reaction does not affect the results determined by measurement of the C^*O_2 produced after resumption of carbiding with ordinary CO. These are shown in Fig. 4 where the millimoles of C^*O_2 produced are plotted against the millimoles of normal Fe_2C produced. The encircled points represent the C^*O_2 removal after the interruptions just described. These points all fall on the second, or low slope, portion of these curves and show that there was no change in C* availability due to prolonged heating at reaction temperature in vacuum after five millimoles of Fe_2C had been formed. This result allows one to conclude (1) that C* is not lost from the catalyst surface by reaction with oxygen[21] and (2) that C* is not gained by the surface by equilibration with C* already present as carbide carbon.

This latter conclusion is of interest in view of the mobility of carbon in alpha iron at these temperatures.

[20] It had been hoped that establishment of simple kinetics for this complex reaction would allow the identification of some simple process as the slow step in the reaction.

[21] Kummer, DeWitt, and Emmett (reference 8) have found that carbiding with CO always led to the formation of oxide corresponding to about 0.3 weight percent oxygen.

If one uses an average value[22] for the diffusion constant of carbon in alpha iron at 200°C, he can calculate the isochronal curves shown in Fig. 5. These curves show the concentration of carbon at various locations inside an 850A diameter iron sphere if the surface concentration is kept constant. A catalyst made up of spheres of this size would have a surface area of 8.9 m^2/g which is consistent with areas of reduced iron catalysts.[23]

The high mobility of carbon in iron and the presence on the catalyst surface of C* which does not exchange with carbide carbon suggests that this C* is present on the surface as carbide carbon and that carbide carbon does not equilibrate with dissolved carbon.

It should be noted on Fig. 4 that these considerations apply only to the second or straight-line portions of the curves shown. These curves are made up of two portions with a distinct break. It would appear that C* is more easily removed during the initial carbiding after changing from C*O to CO as carbiding gas. Since the surface C* removed in the second portion was identified with carbide carbon, it seems natural to identify the easily removed C* with surface carbon existing as atoms on the iron surface. The percarbide is an interstitial compound in which the iron lattice has been shifted so as to accommodate the carbon atoms. Thus one would expect that on the carbide portion of the catalyst surface the iron atoms would be located so that surface C atoms would be held more strongly than they would be by the iron atoms in the regular iron lattice of the iron portion of the catalyst surface.

If this identification is made, then the ordinate intercept I_{C^*} of the straight-line portion can be taken to give the C* removed from the iron portion of the catalyst surface. This in turn allows a speculation as to the extent of surface underlaid by carbide. The specific surface area A_s of the reduced catalyst in Runs 8 and 9 was found to be, respectively, $A_s = 9.1 \pm 1.2$ m^2/gm and $A_s = 8.7$ m^2/gm[24]. On the assumption that there is no copper on the surface of the catalyst, the number of surface Fe atoms is $N_{Fe} = A_s W / A_{Fe}$ where W is the weight of the catalyst in grams and $A_{Fe} = 8.1 \times 10^{-20}$ m^2 is the area one Fe atom is assumed to occupy on the iron surface.[25] If each surface C* required two surface Fe atoms, then 0.6 mM of C* would cover the surface in the first case and 0.7 mM of C* in the second. The ordinate intercepts are $I_{C^*} = 0.110$ mM C^*O_2 for Run 8 and $I_{C^*} = 0.167$ mM C^*O_2 for Run 9. Now, if one had initially a surface covered with C*, this C* could be removed either as C^*O_2 or as C* dissolved into the iron to form carbide. If one assumes that the reaction,

$$CO(ads) \rightleftharpoons C(ads) + O(ads),$$

reaches equilibrium very rapidly, then it follows that for each C^*O_2 removed there will be one C* converted into Fe_2C^*. Thus, in Run 8 approximately one-third of the surface is underlaid by pure iron and two-thirds by carbide. In Run 9 the corresponding fractions are 3/7 and 4/7.

Another fact evident from Fig. 4 and Table II is that the slopes of the straight-line portions of the C* re-

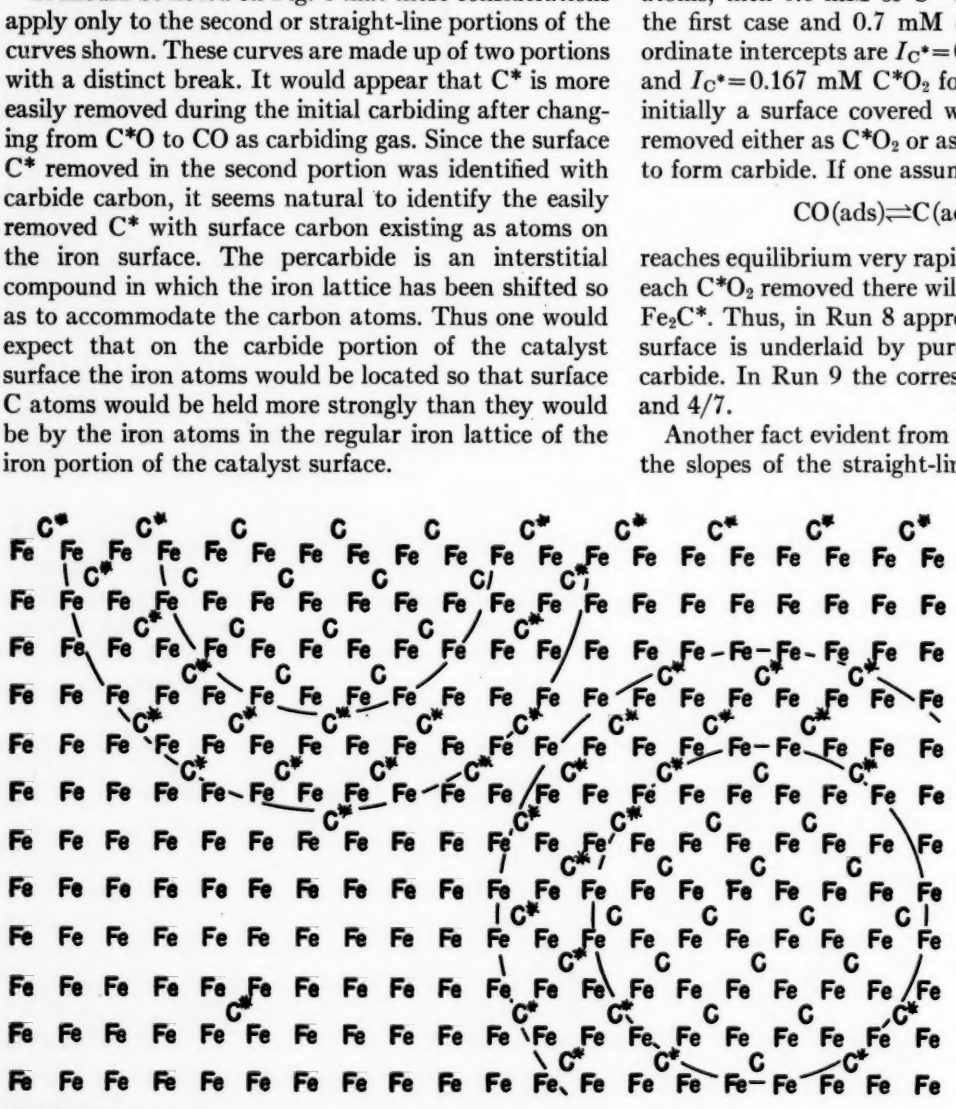

FIG. 6. A schematic cross-section diagram of a portion of an iron particle which has been carbided first with CO and then with C*O. This is not intended to represent the actual structure of the iron or of iron percarbide. It is simply a means of visualizing the relative locations of C* and C after such treatment.

[22] This average, $D = 6.0 \times 10^{-12}$ cm^2 sec^{-1}, was derived from values taken from: (a) D. Polder, Phillips Research Rept. **1**, 5 (1945); (b) C. Wert and C. Zener, Phys. Rev. **76**, 1169–75 (1949); and (c) C. A. Wert, Phys. Rev. **79**, 601–5 (1950).

[23] Hall, Tarn, and Anderson, J. Am. Chem. Soc. **72**, 5436–43 (1950).

[24] These areas were measured by H. M. Allred of this laboratory using a krypton adsorption procedure similar to that of Beebe, Beckwith, and Honig, J. Am. Chem. Soc. **67**, 1554 (1945). Unfortunately the apparatus was not available until the last two carbiding runs were made.

[25] This Fe atom area is on the basis that the iron is crystalline and the (100) crystal faces are exposed. Some of the other possible values are 5.8×10^{-20} m^2 for (110) faces or 5.4×10^{-20} m^2 which is the $\frac{2}{3}$ power of the volume occupied by an iron atom in the unit cell.

moval curves are remarkably similar in spite of differences in reaction temperature or initial mole percent Fe_2C^*. The effect of copper-promotion seems to have been mainly an increase in easily removed C*. One can speculate that this is due to a greater ease of formation of percarbide at nuclei deeper within the catalyst particle than is the case for pure iron. This greater ease might be due to distortions induced in the iron lattice by the copper and would lead to fewer percarbide volumes starting at nuclei near enough to the surface so that the catalyst surface shortly would become one boundary of the percarbide volume.

The similarity of slopes is what one would expect if the mechanism of C^*O_2 removal were the same as that for production of CO_2 during carbiding but that some factor acting in a manner such as the collision frequency factor in gaseous reactions was making the removal of C* less probable. From the average slope of the second portions of the copper-promoted catalyst family of curves, one finds that this reduction in probability corresponds to one C^*O_2 produced for each 115 Fe_2C molecules produced.

The results quoted by Kummer, DeWitt, and Emmett[8] are consistent with those just presented. They carbided a fused synthetic ammonia catalyst[26] to approximately 63 weight percent percarbide with ordinary CO. Carbiding was then continued with C*O to an extent roughly five times that necessary to form one surface layer. The nucleation mechanism would result in the situation, sketched roughly in Fig. 6, where there there would be volumes of Fe_2C surrounded by skins of Fe_2C^* inside the catalyst, much smaller volumes of Fe_2C^* inside the catalyst, surface C atoms where Fe_2C was exposed at the catalyst surface, and surface C* atoms where only iron lay underneath. These authors then reduced the catalyst until CH_4 corresponding to one-quarter of a surface layer of C atoms had been removed. Radio-assay of the CH_4 showed it to be only one-quarter as radioactive as the C*O used in carbiding. If one assumes with the authors that reduction removes all kinds of surface carbon indifferently, he finds that this corresponds to three-quarters of the surface being underlaid by carbide.

These authors also showed that heat treatment did not make C* more available to reduction. Finally, they showed that exhaustive reduction recovered C* in diminishing, but not exponentially decreasing, amount until the last carbon had been removed from the catalyst. This is consistent with the reasonable assumption that surface carbon is most easily reduced, that percarbide volumes in contact with the catalyst surface are next most easily reduced, and that iron percarbide volumes wholly within the catalyst are reduced last.

The results obtained in this work and those presented by Kummer, DeWitt, and Emmett are consistent with a carbiding mechanism which pictures percarbide growing around nuclei scattered throughout the internal volume of the reduced iron. (See Fig. 6.) It appears further that some of these nuclei lie near enough to the iron surface so that the latter becomes one boundary of several percarbide volumes and, hence, is made up of patches of percarbide and uncarbided iron, with carbon atoms on the surface of the uncarbided iron. One further feature of the mechanism is that once carbon becomes situated as percarbide, it no longer is free to return to solution in the iron, that is, percarbide volumes will not grow at the expense of others.

The author wishes to thank A. K. Blom for carrying out many of the carbiding runs and radioactivity assays and L. C. Roess, F. J. Moore, and R. P. Eischens for many stimulating discussions.

[26] Catalyst B: 2.26 percent Al_2O_3, 0.62 percent SiO_2, and 0.21 percent zirconia; surface 35 percent iron and 65 percent promotor.

Dependence of Joshi Effect on Electronic Part of the Discharge Current

N. A. RAMAIAH,* M. G. BHATAWDEKAR, AND N. SUBRAHMANYAM
Department of Chemistry, Hindu University, Benares, India

(Received August 20, 1951)

Association of Joshi effect Δi with electronic part i_e of the discharge current i was investigated by elimination principle. i_e was suppressed under transverse magnetic field H. In agreement with Joshi's theory, negative effect ($-$percent Δi) in water and iodine vapor was maximum in i and negligible in $i-i_e$; comparatively, positive effect was unaffected by H.

I. THE PHENOMENON

PROFESSOR Joshi's discovery of the phenomenon, called Joshi effect,[1,2] is a landmark in the domain of the science of the behavior of electrically excited media and the influence thereon of irradiation. The classical photoelectric effect requires that the action of light on matter should enhance its electrical conductivity i. That this last of a gas or vapor can be inhibited by light, is the essence of negative Joshi effect, $-\Delta i$. The resulting current suppression and its complete restoration on shutting off the light are almost instantaneous. This (as also the positive effect $+\Delta i$, *viz.*, a current increase by light under definite experimental conditions,[3,4] see below) is observed in numerous gases and vapors when exposed to discharge and is apparently a general property of discharge phenomenon.

It has been pointed out by Joshi[1,5] that the effect Δi is distinct from the well-known photoelectric effect; while the latter increases linearly with a million-fold increase of light intensity I, Δi attains saturation at large I.[5] Unlike the Budde effect which is restricted to *unexcited* halogens, Δi occurs under all frequency ranges from extreme red (7070A) to x-rays.[5] Further, $-\Delta i$ is not analogous to the Penning effect which involves a rise in the sparking potential (followed by a decrease in the discharge current) of a mixture of gases particularly helium and neon due to photodestruction of their metastables.[4] This new effect $-\Delta i$ evoked much interest in view of the work done by Thompson,[6] Townsend,[7] Loeb,[8] and others, which reveals that external irradiation is an indespensable factor for the inception of discharge.

II. A THEORY OF THE PHENOMENON

For the occurrence of Δi, Joshi[9] postulates that (*a*) an adsorption-like electrode layer consisting of excited particles, ions, and electrons is formed under discharge; (*b*) light releases electrons from this layer; (*c*) negative ion formation due to capture of the photoelectrons by excited nuetral particles reduces the current to give $-\Delta i$ mainly as a *space-charge effect* (see below); and (*d*) uncaptured photoelectrons and their secondaries, produced under applied fields, give $+\Delta i$.

The observed favorable influence on Δi of "aging" and coating materials which enhance sorption of gases, supports the postulate (*a*);[3] furthermore, the marked increase of Δi with the deposition of photosensitive substances on the electrode surface, follows from (*b*).[10] A direct consequence of (*c*) is that the magnitude of Δi depends upon the electron affinity E of the excited media: Suggestively enough, $-\Delta i$ is marked in electronegative gases and vapors,[3,4] like I_2 and H_2O; in this last case, the observed appreciable Δi is attributed[3] to the large electron affinity of the dissociation products of H_2O, chiefly of OH; $E_{OH}=88$[11] and $E_I=76$ kcal.[12]

III. PRESENT INVESTIGATION AND ITS PRINCIPLE

In the above postulate (*c*), it is contemplated that $-\Delta i$ originates from formation of negative ions. The influence of the latter is twofold: first, because of their low mobility and consequently low ionizing power, the resulting avalanches are few; and second, as space-charge effect, the negative ions repel the electrons released from the cathode or arriving at the anode. Removal of electrons before the ionizing region results in equal loss of both electronic (i_e) and ionic parts of the discharge current. On the other hand, if the repulsion of electrons in the neighborhood of the positive electrode by negative ions is assumed, Δi originates from the suppression of the electronic part i_e. This is now investigated by elimination principle. The method is to compare the magnitude of Δi in the total i as against that observed in the *residual* current obtained after

* Present address: Chemistry Department, University of Delhi, Delhi, India.

[1] S. S. Joshi, Proc. Indian Sci. Congr. Presidential Address, Chem. Sec. (1943).

[2] S. S. Joshi, Nature, **151**, 561 (1943).

[3] N. A. Ramaiah, J. Phys. Chem. **56**, 218 (1952).

[4] N. A. Ramaiah, J. Sci. Ind. Research (India) **10A**, 182 (1951).

[5] N. A. Ramaiah, J. Sci. Research, Benares Hindu Univ. **1**, 91 (1950–51); **2**, 1 (1951–52).

[6] J. J. Thompson, *Conduction of Electricity through Gases* (Cambridge University Press, Cambridge, 1933).

[7] J. S. Townsend, *Electrons in Gases* (Huchinson's Scientific and Technical Publications, London, 1947).

[8] L. B. Loeb, *Fundamental Processes in Electrical Discharge in Gases* (John Wiley and Sons, Inc., New York, 1939).

[9] S. S. Joshi, Proc. Indian Sci. Congr., Phys. Sec. **A26**, (1946); *ibid.* **A25**, (1947); Current Sci. (India) **16**, 19 (1947).

[10] B. M. Shukla, Proc. Indian Sci. Congr., Chem. Sec. (1950, 51).

[11] J. Wiess, Trans. Faraday Soc. **36**, 1856 (1940); C. D. West, J. Phys. Chem. **39**, 503 (1935); E. Laderle, Z. physik. Chem. **17B**, 368 (1932); A. and L. Farkas, Trans. Faraday Soc. **34**, 111 (1938).

[12] P. P. Suttan and J. E. Mayer, J. Chem. Phys. **3**, 20 (1935).

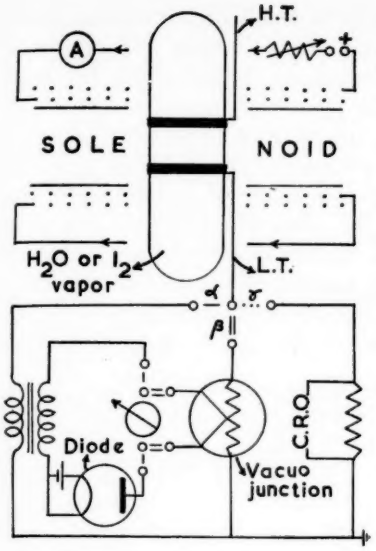

FIG. 1. Experimental set-up for the study of the influence of magnetic field on Joshi effect.

suppression, in part, of i_e. For this purpose, the familiar principle of magnetron set-up due to transverse magnetic field, is used.

IV. EXPERIMENTAL

Ordinary cylindrical discharge tubes fitted with external sleeve electrodes were employed (see Fig. 1). They were filled with pure water vapor at 0.01 and 13.5 mm Hg; this last pressure was found optimum for Δi in water vapor.[3,5] Similar vessels were also filled with iodine vapor at 0.04 mm Hg. They were excited by alternating potentials of 50~ in the range of 1–8 kV. The current was measured by a galvanometer connected to either a diode (α) or a vacuum junction (β, Fig. 1), when the discharge tube was screened from light from a 200-watt 200-volt incandescent bulb (i_D), and exposed to it momentarily ($<\frac{1}{2}$ min) till the current attained a stationary value (i_L). The net ($\Delta i = i_L - i_D$) and relative (percent $\Delta i = 100\Delta i/i_D$) Joshi effect were calculated. The current structure under different experimental conditions was observed by a cathode-ray oscillograph, Du Mont type 274 (γ, Fig. 1).

Magnetic fields (H) of desired strength ($H<400$ gauss) were obtained by passing suitable current through a few windings of a solenoid consisting of 17 turns of enamelled copper wire (B.S.G. 24) per cm of a uniform glass tubing (diameter 4.8 cm). The solenoid was branched into two parts and kept on either side of the discharge tube (see Fig. 1) such that the produced H was at right angles to the *normal* electronic and ionic paths under electric fields and that the inhomogeneity from end effects was minimum.

$H>400$ gauss was obtained by an electromagnet and calibrated by means of a "search" coil.

V. RESULTS

Figure 2 gives a typical group of results on potential variation of discharge current i and Joshi effect (percent Δi) in water vapor ($p=13.5$ mm Hg, 28°C) at different H. Curve 1 refers to the data with $H=0$, the solenoid current being off. Below the "threshold" potential V_m, at which, because of dielectric breakdown of the gas, the conductivity i increased rapidly with applied kV, and which was found by extrapolation of $kV-i$ curves to the potential axis (see Fig. 2), no negative Joshi effect could be detected despite the use of intense and even short-wave radiations.[4] Above V_m, $-\Delta i$ increased numerically with rise of kV over a limited range. The relative effect $-$percent Δi was maximum near V_m and decreased thereafter. Thus, for example, it was 63 and 17 at 1.35 and 2.67 kV, respectively. When the current structure was observed with cro, $-\Delta i$ was associated with the decrease of the amplitude of hf pulses (see oscillograms a, Fig. 3). At $kV \gg V_m$, the action of light was to give $+\Delta i$ (Fig. 2), represented by preferential

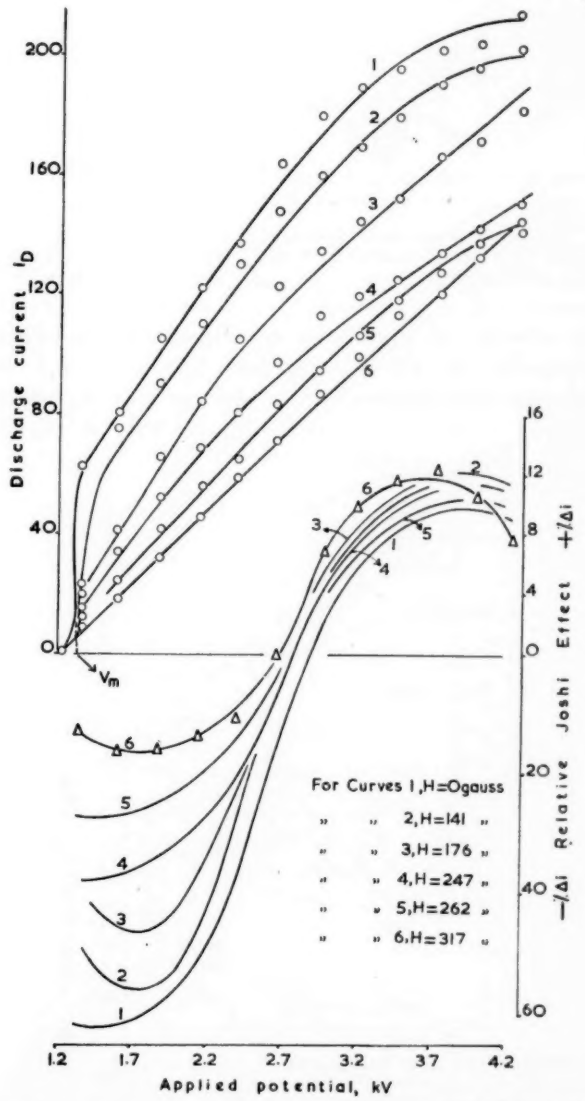

FIG. 2. Influence of magnetic field on potential variation of the discharge current and Joshi effect in water vapor (13.5 mm Hg, 28°C).

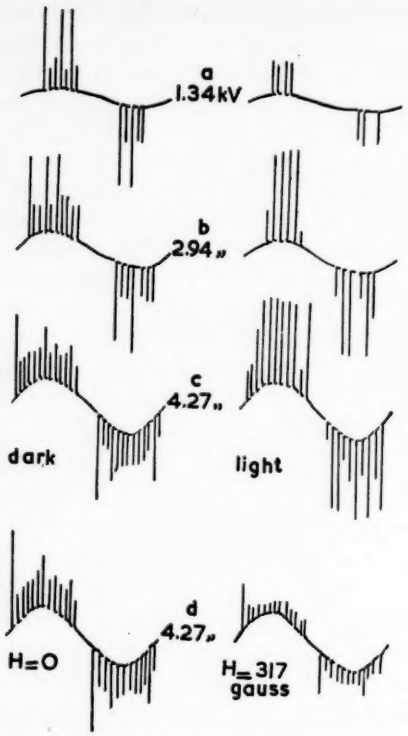

FIG. 3. Oscillograms in dark and under light for the potential range 1.3 to 4.3 kV, and at $H=0$ and 317 gauss. (p $H_2O=13.5$ mm Hg, 28°C.)

increase of hf amplitudes (*c*, Fig. 3). At a critical potential (*viz.* 2.8 kV, for curve 1, Fig. 2) or in its neighborhood, while the observations with the galvanometer showed negligibly small Δi, numerous oscillograms revealed a simultaneous decrease and increase of hf's (*b*, Fig. 3). This suggested that under favorable conditions, $\mp\Delta i$ might co-occur.[3,5]

Curves 2–6, Fig. 2, give data for Δi obtained when the magnetic field H was on. Low values of $H<80$ gauss did not affect i. When H was increased, i diminished progressively (see Fig. 4). This decrease of i due to a constant H was more marked at low exciting potentials near V_m than at large applied kV. Thus, i decreased by about 87 percent at 1.34 kV and 31 percent at 4.5 kV due to $H=317$ gauss. Further, hf's also decreased in respect of their amplitudes under H (*d*, Fig. 3); the action of light was similar. Increase of H beyond 3000 gauss could not cause any enhancement of i at large pressures such as used in the present investigation (see below the data at low pressures). It was instructive to observe that negative Joshi effect was maximum in total i ($H=0$) and appreciably small in that observed when $H>100$ gauss; at 1.34 kV, it corresponded to 63 percent when $H=0$ and about 12 percent current diminution under light was observed when $H=317$ gauss.

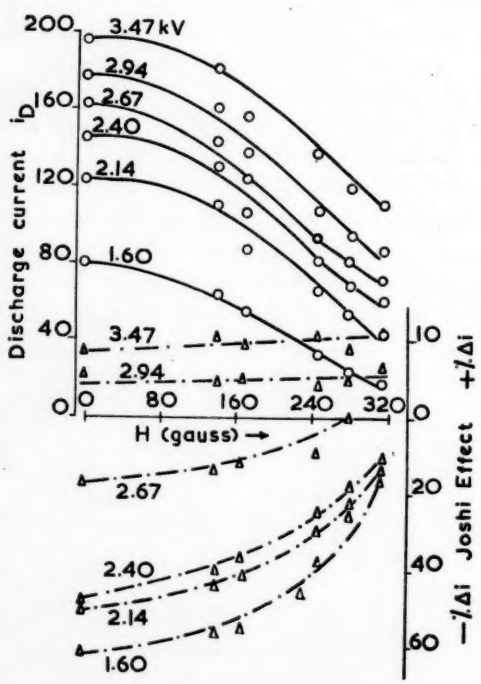

FIG. 4. Variation of the discharge current and Joshi effect in H_2O vapor with magnetic field.

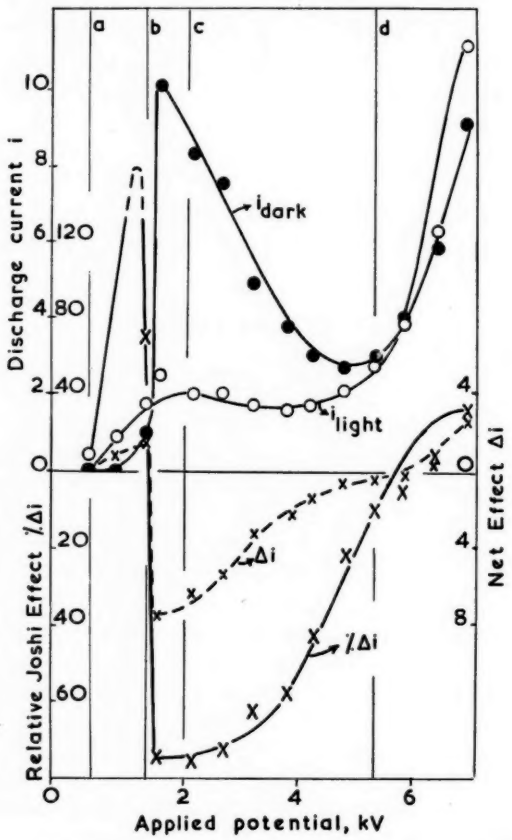

FIG. 5. Joshi effect in a low pressure iodine vapor discharge. (p $I_2=0.03$ mm Hg, 28°C; detector—vacuum junction.)

The data in Fig. 4 show further that the positive effect observed at large kV, represented by increase of hf pulses, was sensibly unaltered with the magnetic field.

B. At Low Pressures †

The data in Fig. 5 show the variation with applied potential of discharge conductivity i and the associated Joshi effect in iodine vapor ($p=0.03$ mm Hg, 28°C). Below the "threshold" potential, the discharge was little as evidenced by negligible current and the absence of hf pulses on the current trace. In the potential range $a-b$ (Fig. 5), the action of light was to enhance i, i.e., to give positive effect $+\Delta i$; this was accompanied by initiation of hf pulses on otherwise smooth sinusoidal trace (see *a*, Fig. 6). These existed so long as the external radiation was in operation. Further, the pulses produced were characteristically of the same height as in the so-called Geiger or non-self-maintained region.[13] After the potential *b* (i.e., V_m, Fig. 5), the applied field was sufficient to maintain the discharge and give pulses of sustained character. These results suggested that V_m marked the change of discharge from non-self-maintained to self-maintained nature.[5] Above V_m, over a small potential range ($b-c$, Fig. 5) the rate of increase of i with applied kV was appreciably rapid. In this region, the negative Joshi effect $-\Delta i$ represented by the suppression of hf pulses (*b*, Fig. 6), attained invariably its maximum. After *c* (Fig. 5), the current i, curiously enough, decreased to a minimum, followed by a further increase, with continuous rise of kV; this variation of i as shown by the curve marked i_{dark} in Fig. 5 appeared to be characteristic of low pressure discharge and was observed also in H_2O vapor at 0.01 mm Hg (30°C); at large pressures, however, it could not be noticed (see curve 1, Fig. 2). The negative effect $-\Delta i$ was appreciable only in potential region $b-d$ (Fig. 5). These data were essentially similar to those obtained with fields due to rf potentials; visual studies of the type of glow and other characteristics of the discharge with these last, suggested that the discharge in the potential range corresponding to *bc* (Fig. 5) was chiefly electrostatic and beyond *c*, electromagnetic in nature.[14] This aspect will be discussed elsewhere in detail. Above *d* (Fig. 5), the action of light was to give $+\Delta i$, followed by increase in hf pulses.

The variation of the discharge current in I_2 vapor with transverse magnetic field is represented in Fig. 7. In agreement with the results obtained at large pressures, V_m for I_2 vapor ($p=0.03$ mm Hg, 28°C), was unaffected by $H<400$ gauss; $H>1000$ gauss, however, decreased V_m. Thus, for example V_m was 1.4 and 0.8 kV at $H=200$ and 2700 gauss, respectively. In the potential range corresponding to *bc* (Fig. 5), the current i was inhibited by H; this was followed by suppression of a few hf pulses (*d*, Fig. 6). Large values of H, however, increased the conductivity. Thus, e.g., at 1.60 kV, i was 10.4, 7.0, and 11.8 with $H=0$, 200, and 2700 gauss, respectively. These results are in agreement with the observations of Bhiday, Bhide, and Asolkar.[15] At large

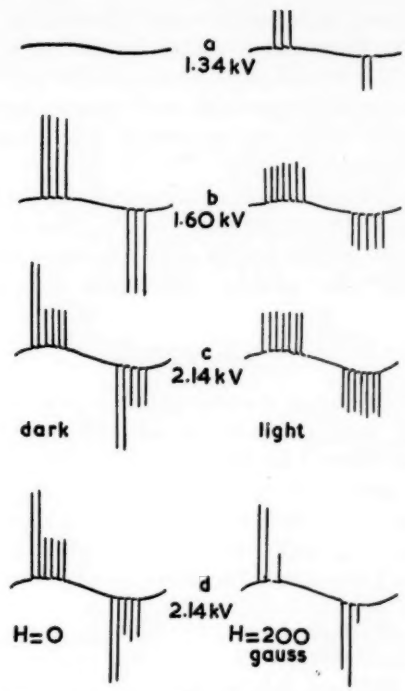

FIG. 6. Oscillograms representing the current structure in iodine vapor discharge.

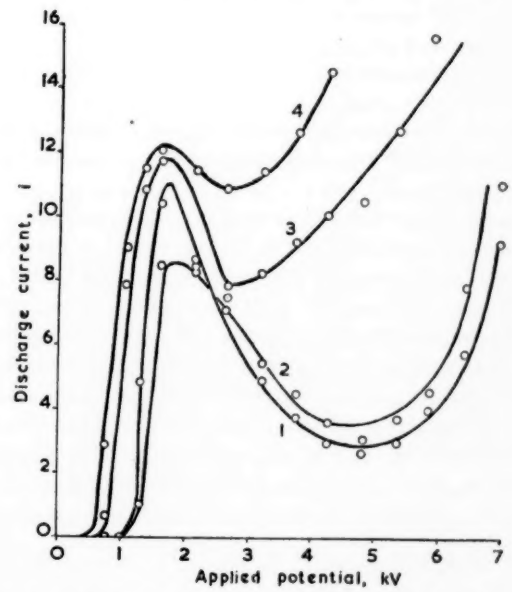

FIG. 7. Influence of magnetic field on potential variation of discharge current in iodine vapor (0.03 mm Hg, 28°C). For curve 1, $H=0$; 2, $H=200$; 3, $H=2700$; and 4, $H=3743$ gauss.

† Results in iodine vapor alone were returned here. The variation of the discharge current i in H_2O vapor ($p=0.01$ mm Hg, 30°C) with applied kV and magnetic field H was similar to that in iodine vapor. There was, however, one difference: in H_2O vapor at low $p<0.1$ mm Hg, no Joshi effect could be noticed,[2,5] while in iodine vapor, it was appreciable. To substantiate the inhibitory action of H on Δi observed at large p (Sec. V, A), the studies were extended to iodine vapor.

[13] S. A. Korff, *Electron and Nuclear Counters* (D. van Nostrand and Company, New York, 1948).

[14] N. Subrahmanyam and N. A. Ramaiah, Proc. Indian Sci. Congr., Chem. Sec. **A105** (1953).

[15] Bhiday, Bhide, and Asolkar, Proc. Indian Sci. Congr., Phys. Sec. **A38** (1951).

$H>800$ gauss, increase of i was followed by enhancement in the heights of hf pulses. At $kV>c$ (Fig. 7) the action of H was always to increase i. It may be mentioned that at large pressures, this type of augmentation of i under H could not be noticed despite the use of $H=3500$ gauss.

Similar to the data obtained at large pressures (Sec. VA), $-\Delta i$ was inhibited by H. Thus at 2.14 kV, $-$percent Δi was 76 and 38 with $H=0$ and 3743 gauss, respectively; the positive effect $+\Delta i$ was unaltered by H.

VI. DISCUSSION

When a stream of charged particles is subjected to a transverse magnetic field H, electrons are deflected more than heavy ions. In a uniform H, the path of a deflected particle is cycloidal.[6,7] Under simple enough conditions, i.e., when the applied field between two electrodes is not sufficient to cause ionization by collision, it has been possible to isolate the electronic part i_e

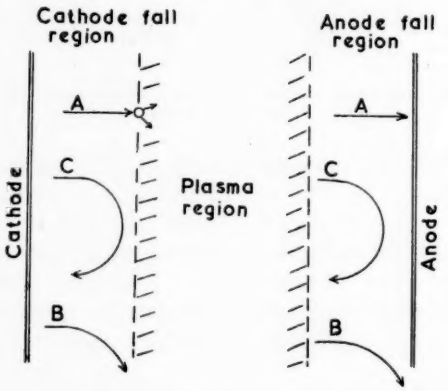

FIG. 8. Influence of magnetic field on electron "trajectories" near the cathode in a low pressure discharge tube.

from the total current and lead to the determination by Mayer *et al.*[12,16,17,18] of electron affinity of atoms like Cl, Br, I, and O.

Under fields causing ionization, the conditions are, however, complicated. It is known that a transverse H applied to the whole or part of the discharge tube decreases i.[19] The effect of H on electrical conductivity can be followed by considering Fig. 8 which represents the processes occurring at the cathode and anode. In Fig. 8, A refers to the path of an electron in the absence of H. Electrons produced at or in the neighborhood of the cathode by any of the allowed secondary mechanisms[8] are energized under fields and start ionization by inelastic collisions from as ensibly fixed point. The electrons initially increase nearly exponentially in number with distance from the electrode. The process of ionization or avalanche production continues till the electrons recede to region where the field is too weak to cause ionization. While positive ions reach the cathode, electrons and negative ions go to the anode to contribute the current i. An electron can be deflected by H only when its velocity is small. This can occur either in the cathode or anode drop region where the kinetic energy of an electron is relatively small. In Fig. 8, B refers to the trajectory of a deflected electron, the path of which is determined by electric and magnetic fields; under constant conditions of the former, low values of H will cause some of the electrons to move away from the region of the electric field (see B, Fig. 8). This leads to the enhanced diffusion coefficient[7] and consequently to reduced current under H. The electrons deflected by large H in the cathode fall region will return to the cathode, while those in the anode fall region enter the ionization zone (C, Fig. 8); the latter will again contribute to the ion production, to yield enhanced current (Sec. VB). The circumstances produced by H in the anode fall region appear to be primarily important for the observed changes. While investigating the suppression of plasma oscillations under H, Cobine and Gallagher[20] observed that the oscillations could not be eliminated in systems in which the electrons could reach the anode directly despite H.

At large pressures, no enhancement of i under the available H could be noticed; it, however, decreased under H. This observation, *viz.*, a reduction of i under H even at such large pressures as 13.5 mm Hg, appears to be the first of its own type. At large p, the plasma region is much wider and the collision processes occur much closer to the cathode than at low p. At large p, the electron moves very short distance in the trajectory; the possibility of an electron entering the ionization zone from the anode fall region on account of H, is little.

To summarize, that the observed decrease of i under H is assumed to be due to removal of electrons (diffusion) in the anode fall region and that the increase of i (noticed at low p only) is on account of the entry of electrons with long cycloidal paths, from the anode fall region to the plasma region.

It is of interest to observe that the negative Joshi effect $-\Delta i$ decreases markedly with H, i.e., $-\Delta i$ is negligible in the current in which the electronic part i_e is, to some extent, eliminated. This suggests the dependence of $-\Delta i$ on i_e, as anticipated from Joshi's theory (see Sec. II). The action of light is assumed to produce enhanced number of negative ions.[21] The present studies point out that in Joshi's theory, $-\Delta i$ is

[16] K. J. McCallum and J. E. Mayer, J. Chem. Phys. **11**, 56 (1943).
[17] P. M. Dotty, and J. E. Mayer, J. Chem. Phys. **12**, 223 (1944).
[18] M. Metlay and G. E. Kimball, J. Chem. Phys. **16**, 774 (1945); D. T. Vier and J. E. Mayer, J. Chem. Phys. **12**, 28 (1944).
[19] M. Palzow and F. Neeson, Ann. Phys. **63**, 209 (1897); J. E. Ives, Phys. Rev. **9**, 353 (1915); **12**, 298 (1918); A. E. Brown, Phil. Mag. **29**, 302 (1940).
[20] J. D. Cobine and C. G. Gallagher, Phys. Rev. **70**, 113 (1946); J. Appl. Phys. **18**, 110 (1947); see also S. Rutherberg, Phys. Rev. **70**, 112 (1946).
[21] The assumption that under light enhanced number of negative ions are produced was taken for granted. The discussion of its validity is beyond the scope of the present communication.

due to the repulsion by negative ions of *slow* moving electrons primarily in the anode fall region. It may be added that this low field region is chiefly favorable, as pointed out by Trichel,[22] for the accumulation of negative ions to build up strong negative space charges.

That $+\Delta i$ occurs at large kV follows from the postulate (d) of Joshi's theory; on account of their enhanced velocities at increased kV, photoelectrons and their secondaries are less susceptible to be captured to form negative ions. This is illustrated by the general finding that, comparatively, the currents i and $+\Delta i$ observed at large kV are unaffected by magnetic field.

[22] G. W. Trichel, Phys. Rev. **54**, 1078 (1938).

ACKNOWLEDGMENT

Grateful thanks are due Professor Joshi for his kind interest in our work and L. R. Ganesan, K. S. Iyyangar, K. A. Raju, and K. N. Tantry for their assistance.

THE JOURNAL OF CHEMICAL PHYSICS VOLUME 21, NUMBER 7 JULY, 1953

Effects of Self-Absorption on Rotational "Temperatures" of OH in Flames*

HERBERT P. BROIDA
National Bureau of Standards, Washington, D. C.

(Received November 4, 1952)

Penner's method of calculating effects of absorption on measured OH($^2\Sigma^+$) rotational distributions has been applied to the R_2 branch and the results compared with intensity measurements of acetylene-oxygen flames at atmospheric pressure. It is shown that distributions in the hot gases above the reaction zone are in agreement with calculated distributions and that for isothermal regions the method can give both emissivity and rotational "temperature," even when there is appreciable self-absorption. Measured intensities in the reaction zone indicate that there is a rotational "temperature" several hundred degrees in excess of the adiabatic temperature and that the "temperature" of the emitters is greater than that of the absorbers.

1. INTRODUCTION

RECENTLY the evidence[1–7] leading to the interpretation of nonthermal "temperatures" of OH($^2\Sigma^+$) in flames has been questioned by Penner[8–11] in view of his calculations on the effects of self-absorption on the intensity distributions. Shuler[12] has defended the viewpoint of nonthermal distributions and has pointed out that the various workers in the field of kinetic spectroscopy are aware that self-absorption can affect the intensity distributions.

Rather than attempt to evaluate the past literature, we shall apply the method of analysis developed by Penner to selected flame conditions with the aim of (1) determining the validity and applicability of such methods to the analysis of intensity distributions in flames and (2) finding a set of experimental flame conditions giving apparent nonthermal distributions of OH which are not explained by calculated effects of self-absorption. Penner's methods of calculation on the P branches of OH have been applied to the R_2 branch. This branch has a much smaller frequency spread than the previously considered P branches and, in addition, is less intense. Both factors tend to reduce the effect of self-absorption on observed intensity distributions. This paper presents additional evidence for nonthermal distributions of excited OH. However, lacking detailed calculations on the effect of pressure broadening, the results do not give a rigorous proof of a departure from equilibrium.

The calculated distributions are compared with experimental measurements in both the inner cone (reaction zone) and the hot gases above the inner cone of an acetylene-oxygen flame. In the latter case, theory and experiment are in agreement. The possibility of obtaining both the rotational "temperature" and the emissivity of OH from the emission data also is shown. After correcting for self-absorption, the observed distribution of rotational intensities in the reaction zone indicates a "temperature" several hundred degrees in excess of the adiabatic temperature.

2. CALCULATION

Rotational distributions of OH have been determined previously from the R_2 branch, because lines of this

* Supported in part by the U. S. Office of Ordnance Research.
[1] A. G. Gaydon and H. G. Wolfhard, Proc. Roy. Soc. (London) **A194**, 169 (1948).
[2] A. G. Gaydon and H. G. Wolfhard, Proc. Roy. Soc. (London) **A208**, 63 (1951).
[3] A. G. Gaydon and H. G. Wolfhard, *Third Symposium on Combustion Flame and Explosion Phenomena* (Williams & Wilkins, Baltimore, 1949), p. 504.
[4] H. P. Broida, J. Chem. Phys. **19**, 1385 (1951).
[5] H. P. Broida and K. E. Shuler, J. Chem. Phys. **20**, 168 (1952).
[6] H. P. Broida and G. Lalos, J. Chem. Phys. **20**, 1466 (1952).
[7] W. R. Kane and H. P. Broida, J. Chem. Phys. **21**, 347 (1953).
[8] S. S. Penner, J. Chem. Phys. **20**, 507 (1952).
[9] S. S. Penner, J. Chem. Phys. **20**, 1175 (1952).
[10] S. S. Penner, J. Chem. Phys. **20**, 1334 (1952).
[11] S. S. Penner, Technical Report No. 5, Contract Nonr-220(03), April 1952.
[12] K. E. Shuler, J. Chem. Phys. **20**, 1176 (1952).

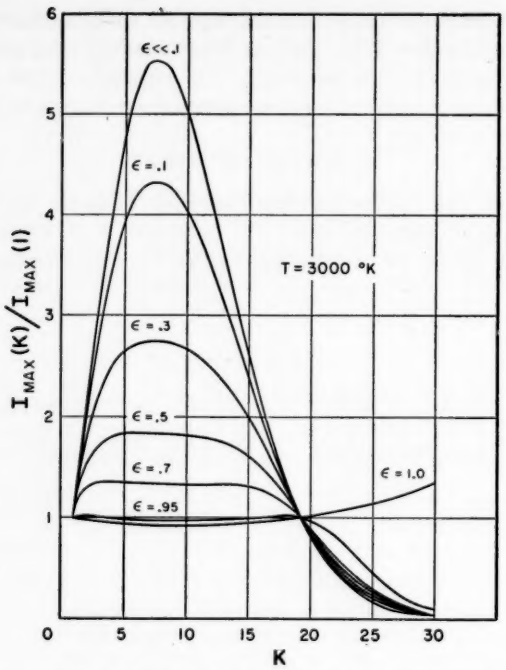

FIG. 1. Calculated intensity ratios of line peaks at 3000°K for the R_2 branch of OH($^2\Sigma^+$) for various emissivities of the first line.

branch have no satellites and the first 19 lines fall in a wavelength region of 17A. The method outlined by Penner[11] determines the effects of self-absorption by calculating the intensity distributions for selected values of emissivity of the first line of a branch. It is helpful to recast his equations in a different form, more easily derived from blackbody laws. The ratio of the maximum observable intensity in emission of the Kth line $(I_{\max})_K$ to the intensity of the first line $(I_{\max})_1$ can be equated to factors dependent only upon the emissivities ϵ_K, the frequencies ν_K, and the temperature T.

$$\frac{(I_{\max})_K}{(I_{\max})_1}=\frac{\epsilon_K}{\epsilon_1}\left(\frac{\nu_K}{\nu_1}\right)^3 e^{(\nu_1-\nu_K)/kT}, \qquad (1)$$

where k is the Boltzman constant in units of cm^{-1} deg^{-1}. The emissivity, ϵ_K, is given by

$$\epsilon_K=1-e^{-(P_{\max}X)_K}, \qquad (2)$$

where $P_{\max}$ is the spectral absorption coefficient and X is the optical density of the emitting molecules. For Doppler broadened lines

$$(P_{\max}X)_K=(P_{\max}X)_1(A_K/A_1) \exp[-(E_K''-E_1'')/kT]. \qquad (3)$$

A_K is the transition probability including the statistical weight and E_K'' is the energy of the lower state of the Kth transition. It is to be emphasized that these equations hold strictly only for emission from an isothermal region with no temperature gradients and for lines with negligible pressure broadening. [Also there can be no instrumental distortion.]

Since values of A_K, E_K'', and ν_K are known, for a selected T and ϵ_1, the ratio $(I_{\max})_K/(I_{\max})_1$ can be found from Eqs. (1), (2), and (3). Values of this ratio for the R_2 branch at 3000°K and for emissivities $\epsilon_1 \ll 1$ to $\epsilon_1=1.0$ have been calculated and the resulting distributions are plotted in Fig. 1. Table I lists for a representive emissivity $\epsilon_1=0.5$ the calculated values of the several factors contributing to the intensity ratio. The effect of each factor upon the resultant distribution can be seen from the table. For example, at large emissivities the ratio ϵ_K/ϵ_1 is nearly constant over the more populated states and the frequency factors mainly determine the intensity distribution. At low emissivity the frequency factors have a negligible effect upon the distribution except for high K lines. Intensity distributions for several emissivities at 2000°K also have been calculated and are shown in Fig. 2. While the calculated results are applicable in a strict sense only to emission of Doppler broadened spectral lines in an isothermal region, comparison with distributions of pressure broadened lines from regions with small temperature gradients indicate that the method is qualitatively applicable under such conditions, for example, see Fig. 5.

Penner[11] has shown that the iso-intensity method of temperature determination is not reliable for the P_1 branch. This might be expected since the iso-intensity method includes the restriction that lines must have the same frequency as well as the same intensity.[13]

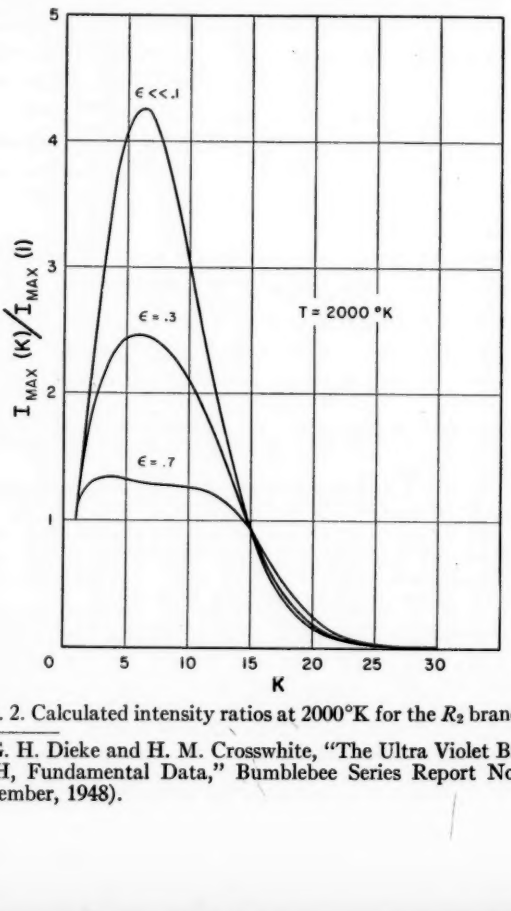

FIG. 2. Calculated intensity ratios at 2000°K for the R_2 branch.

[13] G. H. Dieke and H. M. Crosswhite, "The Ultra Violet Bands of OH, Fundamental Data," Bumblebee Series Report No. 87 (November, 1948).

Since in the R_2 branch of the 0, 0 transition there is an increase in frequency from the $K=1$ to the $K=10$ line and then a decrease, lines of equal intensity are also close to equal frequency. The possibility of using the iso-intensity temperatures from the R_2 branch can be seen from Figs. 3 and 4, in which Shuler's[14] method of plotting is used for the intensity distributions in Fig. 1 and 2. Straight lines are drawn with slopes corresponding to 3000°K and 2000°K, respectively, and the points are determined form the iso-intensity pairs at several selected emissivities. K' refers to the K value of a line having the same intensity as a line of lower K. It will be observed that for very low emissivity there is excellent agreement between the temperatures obtained by this method and the temperature of the calculated isothermal region. Within the accuracy of the experimental measurements, the measured temperatures would be fairly good even with emissivities of the $R_2(1)$ line approaching 0.7. The reason for the large

TABLE I. Effect of several factors on the intensity distribution in an isothermal region at a temperature of 3000°K and an emissivity of 0.5 of the first line of the R_2 branch of OH.

K	$(\nu_K/\nu_1)^3$	$\exp(\nu_1-\nu_K)/kT$	$(P_{\max}X)_K$	ϵ_K	$(I_{\max})_K/(I_{\max})_1$
1	1.000	1.000	0.69315	0.500	1.00
3	1.006	0.965	2.113	0.879	1.707
5	1.011	0.942	3.404	0.967	1.843
7	1.015	0.927	4.036	0.982	1.849
9	1.016	0.921	3.988	0.982	1.837
11	1.016	0.922	3.455	0.968	1.815
13	1.014	0.930	2.698	0.933	1.759
15	1.010	0.945	1.920	0.853	1.628
17	1.006	0.970	1.259	0.716	1.398
19	0.999	1.004	0.767	0.535	1.073
21	0.990	1.048	0.437	0.354	0.735
23	0.980	1.110	0.234	0.209	0.455
25	0.968	1.180	0.118	0.112	0.256
27	0.954	1.272	0.0568	0.057	0.138
29	0.938	1.386	0.0256	0.026	0.068
00	0.000	0.000	0.00000	0.000	0.000

deviation at small $\log(A_{K'}/A_K)$ for $\epsilon_1=0.7$ is due to the flat maximum in the intensity distribution as shown in Fig. 1. It should be pointed out that the effect of emissivity on this method is temperature dependent and that it is fortuitous that there is so little difference between the "true" and "measured" temperatures at 3000°K. This is due to the very small frequency differences between the iso-intensity pairs. However, even at 2000°K the method is good for emissivities less than 0.5 to within the experimental precision presently available. It is clear that this method can not be applied blindly. However, a plot such as Fig. 1 of the measured points will show when the emissivity is too large to be used for a temperature determination. For temperatures below 2900°K self-absorption can only lower the measured temperature determined from iso-intensity pairs in the R_2 branch.

Total line intensities I_{total} are calculated by dividing

[14] K. E. Shuler, J. Chem. Phys. 18, 1466 (1950).

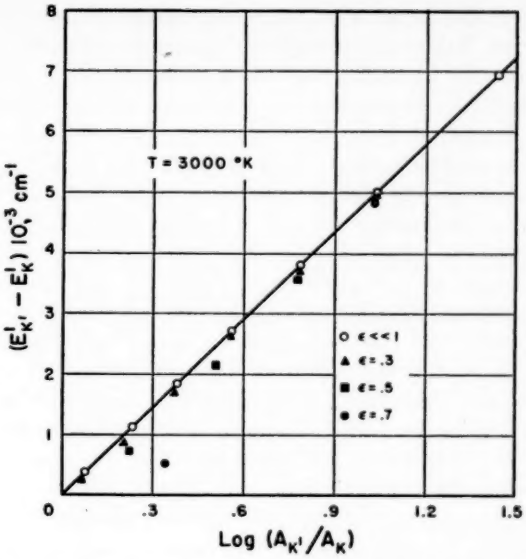

FIG. 3. Iso-intensity plot for several emissivities obtained from distributions in Fig. 1. The solid line corresponds to a temperature of 3000°K.

the maximum observable intensity $I_{\max}$ by a factor ξ which slowly decreases with increasing $P_{\max}X$.

$$\frac{(I_{\text{total}})_K}{(I_{\text{total}})}=\frac{(I_{\max})_K}{(I_{\max})_1}\frac{\nu_K\xi_1}{\nu_1\xi_K}. \tag{4}$$

Values of ξ are given graphically by Penner[11] for $P_{\max}X$ from zero to one hundred. Effects of self-absorption on temperature determinations are not as large for measurements of total line intensity as for measurements of peak line intensity.

3. EXPERIMENTAL RESULTS

Measured OH rotational distributions[5,6] in the hot gases above the reaction zone of flames have indicated that the gases are in thermal equilibrium and that the observed "temperatures" are about 10 percent less than the adiabatic temperature. For this reason the region

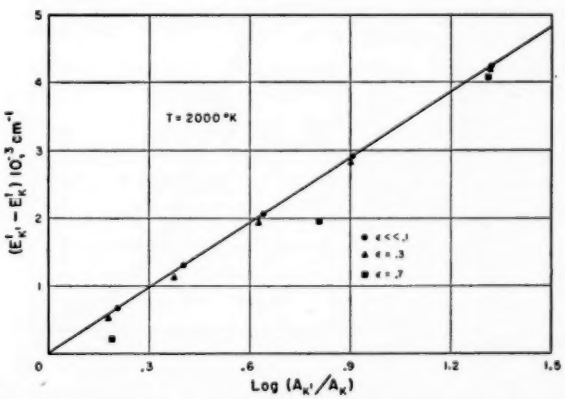

FIG. 4. Iso-intensity plot for several emissivities obtained from distributions in Fig. 2. The solid line corresponds to a temperature of 2000°K.

above the inner cone of a stoichiometric acetylene-oxygen flame at atmospheric pressure was used as a source for checking the calculated effects of various emissivities on the intensity distributions. It was recognized that, at best, this experimental check could only be an approximation, since the observed region is not isothermal and the lines are pressure broadened as well as Doppler broadened. By using sufficiently thick regions the effect of cooler outer layers was minimized. Although no calculations are available for the effect of pressure broadening on relative distributions, it is unlikely that lines of equal intensity and frequency would be different affected. The comparison of measured and calculated distributions shows that this assumption is reasonable. The total observed intensity of a wide line would be less affected by self-absorption than would a narrow line.

The acetylene-oxygen flame was selected for two reasons: (1) the measured rotational "temperature" of the inner cone exceeds the adiabatic temperature[1,6] and (2) the "temperature" of the hot gases above the inner cone is about 3000°K.

The burners used for these experiments consisted of an ordinary welding torch of 1.5-mm diameter and a slot burner with a width of 0.076 mm and a total length of 50 mm. It was possible to use any length of the slot up to the full length. However, the shape of the flames for lengths less than 3 or 4 mm made smaller lengths unusable. Gas flow was controlled by needle valves and was measured by flowmeters of the floating ball type calibrated to an accuracy of ±5 percent.

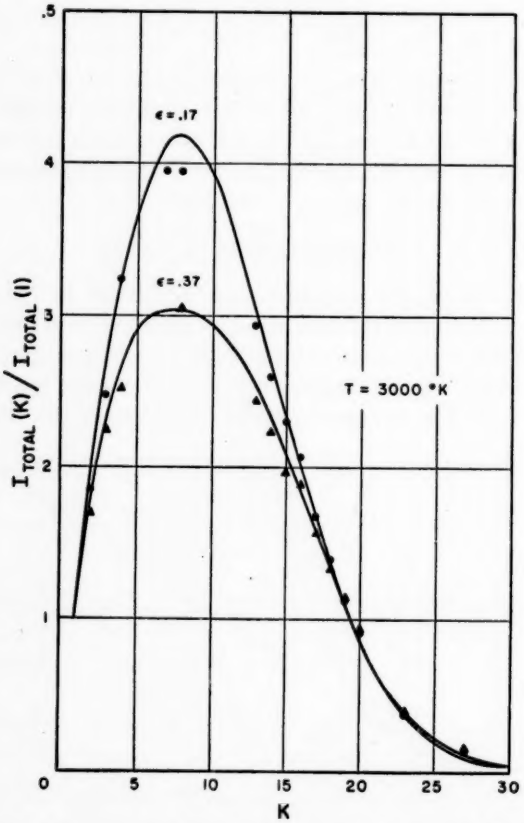

FIG. 5. Measured intensity distributions of OH($^2\Sigma^+$) for two thicknesses of hot gases above the reaction zone of a stoichiometric acetylene-oxygen flame. The solid lines are calculated using emissivities of 0.17 and 0.37 at a temperature of 3000°K.

A high resolution grating monochromator,[15] having a usable resolving power of 55 000, was used for obtaining the spectra. A slit width corresponding to 0.15A was used so that peak measured intensities corresponded to total line intensities of OH which have a half-width of the order of 0.05A.

In Fig. 5 experimentally determined total intensities of the R_2 branch of the 0, 0 band of OH near 3070A are shown for two thicknesses, 5.1 and 10.2 mm, of the hot gases above the inner cone. The curves are those calculated for total intensities with the emissivities indicated. A change of emissivity by more than 10 percent would give a markedly inferior fit to the experimental points. A slightly increased temperature and increased emissivities would give a better fit to the points. However, in the present example no such precision is desired.

Figure 6 presents the experimentally measured intensities at the base of the inner cone of a round burner and from flame lengths of 6, 12, and 50 mm in the slot burner. The curves are the visual best fit to the points. The shift of the maximum intensity to higher K with increasing path length is markedly different from the calculated distributions and from those measured in the hot gases outside the reaction zone. This strongly suggests that the effect is not caused by self-absorption in an isothermal region. Calculations of the distributions to be expected when the emitted radiation is absorbed by a region at lower temperature shows that the distributions of Fig. 6 might be caused by the rotational distribution of the emitting radicals being at a higher temperature than the absorbing radicals. Unfortunately calculations corresponding to the real situation with emission and absorption distributed over the whole region is much more complicated and has not been carried out. The rotational "temperature" of the excited state is probably close to the iso-intensity "temperature" of 4200°K as measured from the smallest thickness.

4. CONCLUSIONS

It has been shown that by applying Penner's method of calculating effects of emissivity on rotational intensity distributions it is possible to obtain values both for the rotational temperature and for the emissivity of OH in an isothermal region. Using the R_2 branch, the iso-intensity "temperature" is determined. This "temperature" together with the ratio of the maximum intensity to the intensity of the first line gives a value

[15] This instrument was constructed by the Research Department of Leeds and Northrup Company and loaned to the Heat and Power Division of the National Bureau of Standards on a field trial arrangement.

for the emissivity. Then the emissivity can be used to determine a better "temperature". The procedure can be repeated to the extent justified by the assumptions and by the experimental accuracy.

Since these measurements were made under conditions in which the spectral line width is determined by pressure as well as Doppler broadening, it is to be expected that the measured emissivities are somewhat low. Until calculations on the effect of pressure broadening can be made, accurate emissivities cannot be measured at atmospheric pressure. However, when the line shapes are well enough known so that pressure broadening effects can be included, a correction to the emissivities determined with the present assumptions probably can be made. Moreover, in a low pressure flame where Doppler broadening is the dominant factor in the line shape, this method would be directly applicable.

For lines with Doppler broadening, Penner[8] has derived equations for calculating the spectral absorption coefficient P_{max} at the center of a line from the measured oscillator strengths f[16] of OH. With these equations[17] and the calculated OH concentration in the burned gases from an acetylene-oxygen flame at 3000°K, $P_{max}X$ and the emissivity can be computed. For the $R_2 1$ line and a gas thickness of 5.1 mm the calculated emissivity is 0.96. This is greatly in excess of the value of 0.17 measured (Fig. 5) in the atmospheric pressure flame. However, until the effect of pressure broadening is calculated, it is not possible to know the actual magnitude of this difference. Pressure broadening included in the computations will have the effect of increasing the measured and decreasing the calculated peak emissivity. Since the total intensity of a wide line is less affected by absorption at the center, the measured emissivity is greater than that given by calculations using only Doppler broadening. The calculated P_{max} is inversely proportional to the line width[18] and, therefore, is reduced for a wider line.

The calculations of the effects of self-absorption on intensity distributions have made it possible to show that in the reaction zone of an acetylene-oxygen flame the rotational "temperature" is probably greater

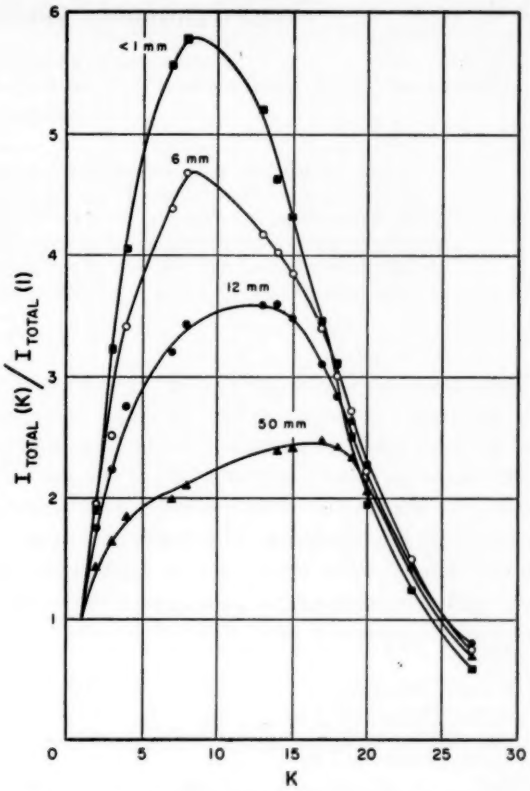

FIG. 6. Measured intensity distributions for several thicknesses of the reaction zone of a stoichiometric acetylene-oxygen flame.

than adiabatic. This calculation method of Penner, if correctly applied, makes it possible to sort out the contribution of self-absorption to an observed intensity distribution. It has been shown that in the R_2 branch self-absorption in an isothermal region does not cause a shift of the position of the maximum intensity to higher K. Therefore, the observed shift in Fig. 6 with increasing path length cannot be caused by self-absorption in a single temperature region. However, the shape of the measured distribution peaking abnormally at $K=16$ in the 50-mm slot burner (Fig. 6) is consistent with a rotational "temperature" of greater than 4000°K in the excited state and a rotational "temperature" near 3000°K in the ground state. The adiabatic temperature is 3320°K.[1] These results substantiate the conclusion that nonthermal distributions of rotational line intensities do occur in the reaction zones of flames.

The author is grateful to Dr. R. D. Arnold for several helpful discussions. He also acknowledges the assistance of Mr. N. Kiess in doing many of the calculations.

[16] O. Oldenberg and F. F. Rieke, J. Chem. Phys. **6**, 439 (1938). R. J. Dwyer and O. Oldenberg, J. Chem. Phys. **12**, 351 (1944).

[17] Unfortunately, reference 8 changes the meaning of the symbol X without notice. For calculating the spectral absorption coefficient from the f numbers, X is the concentration of radicals in the lower energy state of the transition.

[18] R. D. Cowan and G. H. Dieke, Revs. Modern Phys. **20**, 418 (1948).

The Vibrational Spectra of Pyridine and Pyridine-d_5*

LESTER CORRSIN,† B. J. FAX,‡ AND R. C. LORD
Spectroscopy Laboratory and Department of Chemistry, Massachusetts Institute of Technology, Cambridge 39, Massachusetts
(Received February 23, 1953)

Pyridine-d_5 has been prepared by exchange between pyridine vapor and heavy water in the presence of a palladium catalyst. Infrared and Raman spectra are reported for pyridine and pyridine-d_5 over the spectral range 300–4000 cm^{-1}. Interpretation of the spectra with the help of the product rule and by analogy with the fundamental frequencies of benzene and benzene-d_6 leads to complete sets of frequencies for the 27 vibrational degrees of freedom of pyridine and of pyridine-d_5. The frequency assignment for pyridine does not differ greatly from previous ones, but is believed to be more reliable because of the additional spectroscopic data.

THE extensive investigations of the Raman[1,2] and infrared[2,3] spectra of the partially deuterated benzenes were undertaken mainly in the hope that controlled alteration of the D_{6h} symmetry of benzene would render the silent D_{6h} frequencies spectroscopically active and easily identifiable. This hope was not entirely realized. The reasons why certain vibrations, even though formally allowed, do not appear plainly in the spectra of the partially deuterated compounds can be understood in a rough way. The electronic structure of the ring still has D_{6h} symmetry in these compounds, and if in certain ring vibrations the carbon amplitudes are not much affected by deuterium substitution, the polarizability and dipole-moment changes may still approximate zero.

Another way of changing the symmetry of the benzene ring without drastic effect on force constants and without large-mass effects is to replace CH groups by the iso-electronic and nearly isobaric nitrogen atom. It has been realized for some years that pyridine and benzene have a remarkably similar set of fundamental frequencies. Since pyridine can at most have C_{2v} symmetry, one might go still further by placing more than one nitrogen atom in the ring. The three diazines and symmetrical triazine have a set of structures of different symmetry, and their spectroscopic investigation might be expected to furnish additional information bearing on the benzene problem. In a succeeding paper[4] the spectra of the diazines will be reported. The present one is devoted to an interpretation of the pyridine spectrum with the help of the spectra of pyridine-d_5 and the deuterated benzenes.

TABLE I. Raman spectra of pyridine[a] and pyridine-d_5.

Pyridine	Pyridine-d_5	Pyridine	Pyridine-d_5
374 (0)	329 (1)	1596 (2)	1301 (0)
404 (1)	371 (1)	2368 (0?)	1339 (1) p
605 (2)	530 (1)	2451 (0)	1375 (0b)
652 (5)	582 (3)	2868 (1)	1537 (6)
710 (0)	625 (6)	2911 (1)	1552 (4)
749 (0)	690 (5)	2952 (1)	1587 (1)
812 (0)	713 (0)	2988 (1)	1633 (0)
886 (1) p?	768 (4)	3023 (1)	1676 (0)
942 (0)	798 (0)	3031 (0)	1954 (1)
981 (1)			
992 (10) p	824 (5)	3054 (5b) p	2083 (0)
1029 (10) p	837 (5)	3069 (0)	2117 (1)
1043 (0)	887 (5) p	3090 (0)	2160 (1)
1069 (1)	908 (5)	3143 (2) p	2222 (0)
1144 (0) p	962 (10) p	3175 (1)	2251 (6)
1218 (5) p	1006 (7b) p		2272 (2)
1438 (1)	1046 (0)		2293 (10) p
1480 (3) p?	1059 (1)		2370 (1)
1570 (5)	1228 (1)		2450 (1)
1580 (5)	1270 (0)		3076 (0)

Visually estimated intensities enclosed in parentheses; b = broad, p = polarized, ? = uncertain.

[a] See reference 6.

EXPERIMENTAL PROCEDURES AND RESULTS

Preparation and Purification of Pyridine and Pyridine-d_5

Refined pyridine from the Barrett Company was further purified by fractionation through an eight-foot column (60 theoretical plates, reflux ratio of 20–1) and only the part that came over on the temperature "flat" (115°C) was used. In the purified material there was no infrared absorption indicative of impurities (e.g., picoline) except for small amounts of water. The latter probably came in when the pyridine was placed in the infrared absorption cell, and since its presence did not interfere with the infrared or Raman spectrum, it was not regarded as of sufficient importance to bother with.

The pyridine-d_5 was prepared by catalytic exchange between pyridine and deuterium oxide, inasmuch as synthetic methods gave little promise of a straightforward preparation. The harmful effect of the pyridinium-ion formation on acid-catalyzed exchange in

* This paper was prepared mainly from data in the thesis submitted by Lester Corrsin to the Massachusetts Institute of Technology in partial fulfillment of the requirements for the degree of Doctor of Philosophy, June, 1948. Acknowledgment is made of financial support by the U. S. Office of Naval Research under Contract N5ori-07810, and of allocation of heavy water by the U. S. Atomic Energy Commission.

† Present address: 731 Highwood Drive, Baltimore, Maryland.
‡ Present address: Department of Psychiatry, School of Medicine, University of Maryland, Baltimore, Maryland.

[1] A. Langseth and R. C. Lord, Kgl. Danske Videnskab. Selskab, Mat.-fys. Medd. **16**, No. 6 (1938).

[2] C. K. Ingold and co-workers, J. Chem. Soc. (London) **1946**, 222 ff.

[3] F. A. Miller and B. L. Crawford, Jr., J. Chem. Phys. **14**, 292 (1946).

[4] Lord, Marston, and Miller (to be published).

aqueous solution eliminates this approach, and base-catalyzed exchange would presumably attack only the alpha and gamma positions. Therefore vapor-phase exchange between pyridine and D_2O over metallic catalysts was investigated. The catalyst finally used was palladium-on-asbestos, although nickel and platinum catalysts also were effective.§

The palladium catalyst was first activated *in situ* with D_2 gas at atmospheric pressure and 240° for 4 hr. The exchange vessel's temperature was then reduced to 225° and a mixture of pyridine and D_2O vapor from a boiler containing about 5 g of pyridine and 6 g of D_2O (2:1 molar excess of deuterium) was passed over the catalyst. After the vapors had passed through the exchange vessel, they were condensed and returned to the boiler for recycling over the catalyst. The cycling process was usually carried on for 12 hr, although in the later stages this time was raised to as much as 36 hr. After deuterium-hydrogen equilibrium was established, the mixture was removed from the boiler and most of the water (79 percent) separated from the pyridine with anhydrous potassium carbonate. A new batch of catalyst was placed in the exchange vessel and activated, a fresh supply of D_2O added and a new cycle of exchange carried out. After nine such steps, the C—H stretching band in the infrared spectrum of the pyridine-d_5 was so weak as to indicate an upper limit of about one atom-percent of hydrogen. The density of the spent D_2O after the eighth exchange showed 98 atom-percent deuterium.

The final sample (3.5 cm^3) of pyridine-d_5 represents about a 55 percent yield based on the starting amount of pyridine. It was dried at elevated temperatures over Baker's cp barium oxide and distilled twice through a micro-fractionating column. The infrared spectrum was used as the main evidence of purity. Because of the small size of the final sample and the effects that small amounts of water might have on the physical properties usually employed as criteria of isotopic purity, no precise measurements of molar volume, boiling and freezing points, and index of refraction of pyridine-d_5 were attempted. The infrared spectrum showed evidence of the presence of small amounts of H_2O but not D_2O. This means that the drying of the sample after the last exchange was effective, but that the pyridine-d_5 picked up atmospheric moisture on storage or on being transferred to the infrared absorption cell. Since no uncatalyzed exchange occurs between water and pyridine, and since the only water band found (at 3400 cm^{-1}) does not interfere with the pyridine-d_5 spectrum, no further attempt to remove the water was made.

No evidence was found for aliphatic C—D in the infrared spectrum, from which it was concluded that any piperidine-d_{11} or intermediate compounds that might have been formed by reduction over the D_2-activated catalyst were removed by the distillations. The sample showed some evidence of fluorescence in the first Raman spectrum taken, but several vacuum distillations and a final distillation into the Raman tube under diffusion-pump vacuum eliminated this difficulty.

§ Details of the exchange investigations can be found in the Ph.D. thesis of L. Corrsin.

TABLE II. Infrared spectra of liquid pyridine and pyridine-d_5.

Pyridine	Pyridine-d_5	Pyridine	Pyridine-d_5
	329 vvw	1482 s	1364 m
405 s	371 m	1572 m	1414 w
604 s	530 vs	1583 vs	1450 w
653 w	567 m	1599 s	1530 vs
675 w	582 s	1633 w	1542 s
703 vvs	625 w	1682 w	1550 m
749	762 m	1872 m	1581 vw
810 vw	798 w	1923 m	1645 m
883 vw	823 s	1987 m	1806 vw
938 vvw	833 m	2293 vw	1850 vw
981 w	886 m	2454 vw	1863 vw
991 vs	908 w	2908 w	1918 vw
1030 vs	963 s	2960 m	2042 vw
1068 s	1011 m	3004 s	2117 w
1148 s	1043 w	3036 vs	2254 vs
1217 s	1143 vw	3055 s	2270 s
1296 vw	1228 m	3083 vs	2285 s
1357 w	1302 s		2389 w
1375 m	1322 m		2460 w
1441 vs	1340 w		2566 w

(The qualitative intensities are based on a sample 0.05 mm thick; v = very, w = weak, m = medium, s = strong.)

Raman Spectra

The Raman spectra were photographed with equipment and techniques described elsewhere,[5] the exposure times being 1–2 hr. Polarization spectra were taken by a method[5b] yielding semiquantitative results. Measurement of Raman frequencies was carried out both by direct reading of the plates with a comparator microscope and by photographic enlargement (14×). The two methods agreed satisfactorily, and it is estimated that the frequencies of sharp Raman lines are accurate to 2 cm^{-1} or better, and of weak or fuzzy lines to 5 cm^{-1} or better, depending on the line shape.

Table I reports the results for pyridine by Kohlrausch and co-workers,[6] with whose values a large number of other workers as well as ourselves are in good agreement. Also reported in Table I are our results for pyridine-d_5. Lines found definitely to be polarized are marked "p"; other lines are either too weak to measure or have depolarization factors above about 0.75.

Infrared Spectra

The infrared spectra of pyridine and pyridine-d_5 were measured in the liquid phase over the spectral range 250–3500 cm^{-1}. A Perkin-Elmer 12B instrument so modified[7] that the carbon dioxide and water vapor

[5] a. Harrison, Lord, and Loofbourow, *Practical Spectroscopy* (Prentice-Hall, Inc., New York, 1948), pp. 513 ff.; b. R. C. Lord and E. Nielsen, J. Chem. Phys. **19**, 1 (1951).

[6] Herz, Kahovec, and Kohlrausch, Z. physik. Chem. **B53**, 124 (1943) and references there cited.

[7] Lord, McDonald, and Miller, J. Opt. Soc. Am. **42**, 149 (1952).

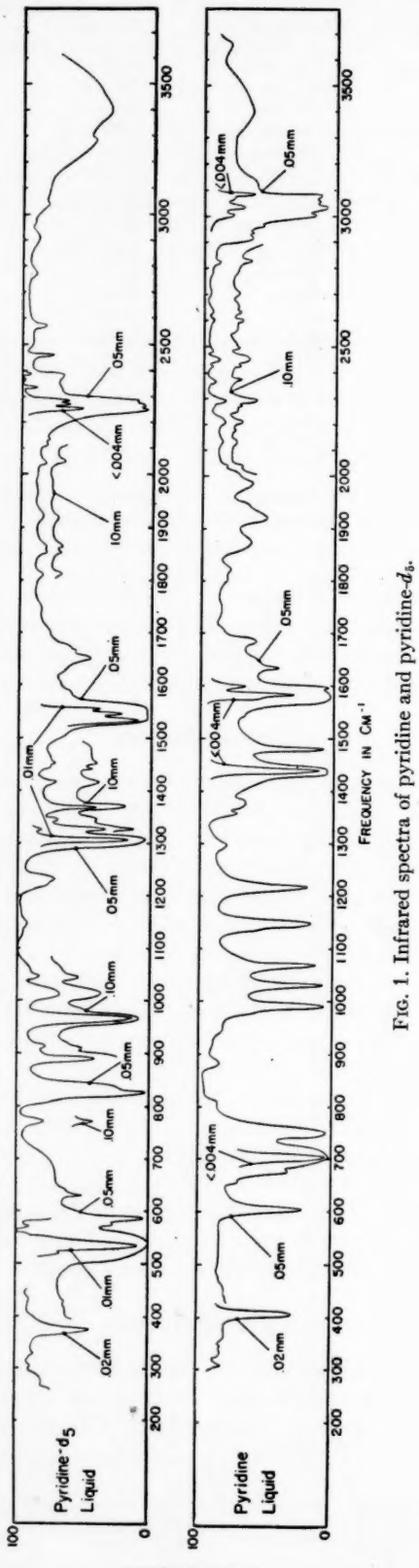

FIG. 1. Infrared spectra of pyridine and pyridine-d_5.

bands could be removed from the spectrum by flushing with dry nitrogen was used. The wave-number precision with which band minima are measured is 2 cm^{-1} or better except above 1700 cm^{-1}, where the precision slowly rises to about 5 cm^{-1} at 3500 cm^{-1}.

The infrared results are reported in Table II and plotted in Fig. 1. No attempt is made to summarize earlier work, since such a summary can be found in Table I of the paper of Kline and Turkevich.[8] Several differences of our results from those given in their table need comment. We list three new bands below 1600 cm^{-1}. One of these occurs at 405 cm^{-1} near the low frequency edge of the KBr region and the other two are found at 675 and 1357 as shoulders on stronger bands. The latter two may have been found because of improved resolution over that of earlier workers on the liquid spectrum. On the other hand we have failed to find in the liquid spectrum various bands in the range 600–1600 cm^{-1} that have been reported by Turkevich and Stevenson[9] in their vapor-phase study. One or two of these discrepancies perhaps may be ascribed to frequency differences between the liquid and vapor phases, and others to the larger band widths and $P-Q-R$ maxima in the vapor spectra. Table II does not list bands at 630, 669, 763, 795, 833, 847, 907, and 1263 that have been reported by Kline and Turkevich.[8]

Two of these bands need special comment. The band at 669 is reported "strong" as compared to the 710 vapor band, which is called "medium." In the liquid no band is found at 669, a weak band occurs at 675 and the band at 703 is extremely intense. We have reinvestigated the vapor spectrum in this region and have found no indication of a band with a Q branch at 669. In view of the strong carbon dioxide absorption at 667 (removed from our instrument by flushing with nitrogen) and the possibility of contamination with benzene (used by Turkevich and Stevenson for calibration), which has its most intense absorption at 667, we believe it justifiable to reject the 669 vapor band, at least as a fundamental.

The band at 630, reported to be of the same intensity as that at 610, does not appear in the liquid although it should have been easily detected unless its liquid phase intensity and frequency differ markedly from those in the vapor. The band shown in Table II as 938 (vvw) is presumably to be identified with that reported in the vapor at 936 (m). This intensity change is remarkable and we have no explanation for it. Certainly the liquid band at 938 is many times weaker than the one at 749, whereas in the vapor the latter is called weak and the former medium. It is to be noted that in a presumably 99.85 percent pure sample of pyridine, no liquid band of medium intensity could be found at this point.[10]

The remainder of the bands mentioned above were

[8] C. H. Kline and J. Turkevich, J. Chem. Phys. **12**, 300 (1944).
[9] J. Turkevich and P. C. Stevenson, J. Chem. Phys. **11**, 328 (1943). Table I of reference 8 gives several bands for the vapor that are not reported in the paper of Turkevich and Stevenson.
[10] E. F. G. Herington, Disc. Faraday Soc. **9**, 26 (1950).

explained as combination tones by Kline and Turkevich.[8] In view of the fact that combination tones are generally stronger rather than weaker in the liquid, it is our conclusion that these bands are spurious, and we will not include them in the set of infrared frequencies for assignment.

The liquid-state infrared band frequencies of pyridine-d_5 also are listed in Table II.

DISCUSSION OF SPECTRA

The vibrational spectra of benzene and its deuterium derivatives of various symmetries have been thoroughly discussed in the literature.[11] Pyridine has also been considered in detail by Kohlrausch and co-workers[6] and by Kline and Turkevich,[8] who have interpreted the main features of the spectrum in a satisfactory way. The present discussion will therefore consider only those aspects of the interpretation that require extension or revision as a result of the new data furnished by the infrared and Raman spectra of pyridine-d_5.

The numbering of the vibrational degrees of freedom for pyridine will be made by analogy with the usage established by Wilson[12] for benzene and extended by Langseth and Lord[1] to derivatives lacking degenerate vibrations.

Choice of axes and definition of vibrational species for a pyridine molecule of C_{2v} symmetry will be that of Langseth and Lord for benzene-d_1, a choice also followed by Kline and Turkevich.‖ Since pyridine has three fewer degrees of vibrational freedom, there are three benzene vibrations without analog in pyridine. These fall respectively in the vibrational species A_1, B_1, and B_2, and are arbitrarily taken to be vibrations $7a$, $9b$, and $17b$, as was done by Kline and Turkevich.

The assignment of frequencies to the totally symmetrical species A_1 is made first. These can be assigned fairly well on the basis of analogy with the corresponding benzene vibrations, all of which have been precisely located. There is need for caution in drawing such analogies, for in addition to the altered force system, the lower symmetry of pyridine permits mechanical interactions between vibrations that belong to different species in benzene. However, the combined spectra of pyridine and pyridine-d_5 enable the assignment of a reasonable set of frequencies that agree with the product rule for the A_1 species and show approximately the expected frequency shifts from pyridine to pyridine-d_5. The assignments are listed in Table III, where the values for the product-rule ratios[13,14] calculated with the help of the dimensions of the pyridine molecule reported by Schomaker and Pauling[15] also are given; τ_{calc} refers to the value of the ratio calculated from molecular masses and dimensions and τ_{obs} to the value given by the assignments of Table III. As is usual, the observed values are smaller than the calculated by the one or two percent expected from anharmonicity.[14]

The assignment for species A_1 agrees with that of Kline and Turkevich[8] except for vibrations numbered $9a$ and $18a$, to which those authors assigned the values 1139 and 884 cm^{-1}, respectively. There seems to be no compelling reason for their choice of 1139 over the frequency 1218, which is equally strong in the infrared and much more intense in the Raman spectrum. Both lines are reported as so slightly polarized that this characteristic is useless for the decision. The 1218 line can be traced readily to the polarized line at 887 in the Raman spectrum of pyridine-d_5, however, and on this basis the assignment of 1218 to vibration $9a$ is made.

Data from the ultraviolet spectrum of pyridine were used to justify the assignment of the Raman line at 884 cm^{-1} to vibration $18a$ by Kline and Turkevich. However, study of the ultraviolet spectrum of pyridine-d_5

TABLE III. Frequency assignments and product-rule values for pyridine and pyridine-d_5.

Species and τ-values	Vibration number	Frequency in cm^{-1} Pyridine	Pyridine-d_5
	1	992	962
	2	3054	2293
	$6a$	605	582
	$8a$	1580	1530
A_1	$9a$	1218	887
	12	1029	1006
	13	(3054)	2270
$\tau_{calc}=5.49$	$18a$	1068	823
	$19a$	1482	1340
$\tau_{obs}=5.38$	$20a$	3036	2254
B_1	3	(1217)	908
	$6b$	652	625
	$7b$	(3054)	2285
$\tau_{calc}=5.07$	$8b$	1572	1542
	14	1375	1322
$\tau_{obs}=4.95$	15	1148	(887)
	$18b$	(1068)	833
	$19b$	1439	1301
	$20b$	3083	(2293)
A_2			
	$10a$	886	690
$\tau_{calc}=1.84$	$16a$	374	329
	$17a$	981	798
$\tau_{obs}=1.80$			
B_2	4	675	(625)
	5	942	762
$\tau_{calc}=2.56$	$10b$	749	567
	11	703	530
$\tau_{obs}=2.55$	$16b$	405	371

( ) indicates a frequency assigned to two vibrations.

Data from the ultraviolet spectrum of pyridine were used to justify the assignment of the Raman line at 884 cm^{-1} to vibration $18a$ by Kline and Turkevich. However, study of the ultraviolet spectrum of pyridine-d_5

[11] See, for example, references 1–3.
[12] E. B. Wilson, Jr., Phys. Rev. **45**, 706 (1934).
‖ In Fig. 2b of Langseth and Lord, the a's and b's of split degenerate vibrations have been erroneously interchanged for derivatives of symmetry C_{2v}, C_{2v}*, and V_h.
[13] G. Herzberg, *Infrared and Raman Spectra* (D. Van Nostrand, Company, Inc., New York, 1945), p. 232.
[14] F. Halverson, Revs. Modern Phys. **19**, 87 (1947).
[15] V. Schomaker and L. C. Pauling, J. Am. Chem. Soc. **61**, 1769 (1939).

under high dispersion[16] shows that this is not a valid basis for the assignment. Moreover the value 884 is very low for a planar hydrogen bending frequency. A much more probable value is 1068, which is not far from the location of the corresponding vibration in benzene. To be sure, this line is not found to be polarized in the Raman effect, but the same objection can be raised about other A_1 assignments, since fewer polarized lines are observed than the number of A_1 vibrations. An analogous frequency is observed in pyridine-d_5 at 823 cm^{-1}.

In completing the assignment for the other planar species (B_1), one finds an insufficient number of distinct frequencies for the hydrogen bending and stretching vibrations, and therefore in Table III two bending modes (3 and 18*b*) and one stretching (7*b*) are assigned the same frequency values as those used for analogous vibrations in species A_1. These values are enclosed in parentheses in the table. In pyridine-d_5 the number of distinct frequencies is larger by one, and therefore one bending and one stretching frequency are assigned twice.

There are two significant departures from previous assignments for species B_1. One concerns the ring distortion vibration 6*b*, which is doubly degenerate in benzene. It has previously been assumed[8] that this vibration does not split in pyridine, since the position of one component at 605 cm^{-1} is so nearly that of the doubly degenerate vibration 6 in benzene. Neither Kline and Turkevich[8] nor Herz, Kahovec, and Kohlrausch[6] assigned the strong Raman line at 652 to vibration 6*b* on the respective grounds that vibration 6 is not split in the deuterated benzenes and that any splitting should give rise to one polarized and one depolarized line, the line at 605 being at best only slightly polarized. However, the *ring* symmetry in pyridine is different from that in benzene, so that a splitting might well occur in pyridine but not in deuterated benzenes. The splitting of vibration 6 need not produce a strongly polarized line, and the deficiency of polarized lines in both light and heavy pyridine shows that vibrations that have depolarized lines in benzene are likely to have little polarization in pyridine even though they become formally totally symmetrical in this molecule.

The 652 line was assigned to the ring puckering vibration 4 by Kline and Turkevich and to the nonplanar hydrogen vibration 17 by Herz, Kahovec, and Kohlrausch, though the latter workers commented on the unusual intensity. The spectrum of pyridine-d_5 contains a similar Raman line of high intensity at 625 cm^{-1}, the frequency shift being very nearly the same as that of the pair 605–582. There is no other Raman line below 582 of comparable intensity in pyridine-d_5 that could be associated with 652 in pyridine. Hence the 652 line must be ascribed to a ring vibration. The only possible choices are vibrations 4 and 6, since 16 can be definitely placed near 400 cm^{-1}. The arguments in favor of 6 over 4 are the Raman intensity, the size of the frequency shift (vibration 4 shifts from about 690 in benzene to 600 in benzene-d_6[2,3]) and the similar splittings observed in the spectra of the diazines.[4]

The other new assignment in species B_1 is that of the infrared bands of medium intensity in light and heavy pyridine at 1375 and 1322 to the ring vibration 14. This assignment was first suggested by the vibrational spectra of the diazines,[4] in each of which a frequency was found in the 1250–1400 region with an intensity to be expected of a fundamental rather than an overtone. In any event this pair of bands needs satisfactory explanation, whether as fundamentals of as overtones. The possibilities for the latter are few (if only binary combinations are included) and unsatisfactory in the sense that rather large (and usually negative) anharmonicities are needed to match the observed frequencies.

The traditional location for vibration 14 in benzene and pyridine has been in the 1600 region,[2,6,8] but it was pointed out by Langseth and Lord[17] that the Raman spectra of the deuterated benzenes showed no evidence suggestive of such a location. These authors, in fact, placed the frequency outside the range 1560–1640 in benzene and 1520–1600 in benzene-d_6. Recently Mair and Hornig[18] also have departed from the 1600 assignment, and have placed the frequency at 1310 and 1285 in benzene and benzene-d_6, respectively, on the basis of the infrared spectrum of crystalline benzene. These values are somewhat different from those we have assigned for pyridine and pyridine-d_5, but not unreasonably so.

The remaining B_1 assignments for pyridine are essentially the same as earlier ones[6,8] and the product-rule agreement is satisfactory.

The foregoing assignments account for all planar vibrations, and the remaining fundamental frequencies, being those of out-of-plane modes, are expected to fall below 1100 cm^{-1} in pyridine and 900 cm^{-1} in pyridine-d_5. The unassigned Raman and infrared frequencies in this range are 374, 405, 675, 703, 749, 812, 886, 942, 981, and 1043 in pyridine and 329, 371, 530, 567, 690, 713, 768, 798 in pyridine-d_5. These are the prospective values of the fundamentals of the A_2 and B_2 species, though of course the possibility exists that one of the strong A_1 or B_1 bands may obscure an A_2 or B_2 fundamental.

Species A_2 contains vibrations 10*a*, 16*a*, and 17*a*, and is forbidden in the infrared spectrum of the vapor. The bands may be missing or present with very low intensity in the liquid-phase spectrum. By analogy with benzene, vibration 16*a* should occur near 400 cm^{-1}. It is found at 374 in the Raman effect of pyridine and has not been reported in the infrared. The pyridine-d_5 frequency lies at 329 in the Raman effect and also is found as a very, very weak band in the infrared.

[16] B. J. Fax and R. C. Lord (to be published).

[17] Reference 1, p. 60.

[18] R. L. Mair and D. F. Hornig, J. Chem. Phys. **17**, 1236 (1949)

TABLE IV. Possible assignments for overtones.

Pyridine			Pyridine-d_5					
Obs. freq.	Assignment	Calc. freq.	Obs. freq.	Assignment	Calc. freq.	Obs. freq.	Assignment	Calc. freq.
710 RS	11; 2×16a	708	713 RS	16a+16b	700		8b+16a	1866
812 RS	2×16b	810	1046 RI	10a+16b	1061	1863 IR	1+3	1870
1043 RS	4+16a	1049	1059 RS	2×11	1060		11+19a	1870
1296 IR	2×6b	1306	1143 IR	5+16b	1139		3+2	1914
	6a+11	1307	1228 RI	10a+11	1220	1918 IR	6a+19a	1922
1357 IR	6a+10b	1354		3+16a	1237		2×1	1924
1599 RI	1+6a	1597	1270 RS	6a+10a	1272		6b+19b	1926
1633 IR	6a+12	1634	1364 IR	11+18a	1354	1954 RS	6b+19a	1965
	1+6b	1644		10b+17a	1365		1+12	1968
1682 IR	6b+12	1681	1375 RS	2×10a	1380	2042 IR	8a+11	2067
1872 IR	3+6b	1870	1414 IR	6a+18b	1415	2083 RS	17a+19b	2099
	2×5	1884		9a+11	1417	2117 RI	6a+8a	2112
1923 IR	9a+11	1921	1450 IR	6b+18a	1448		18a+19b	2124
1987 IR	2×1	1984		9a+10b	1454	2160 RS	18a+19a	2163
2293 IR	2×15	2296	1550 RI	1+6a	1545		6b+8b	2167
2368 RS	9a+15	2366	1585 RI	1+6b	1587	2222 RS	8a+10a	2220
2454 RI	8b+10a	2458		6a+12	1592		9a+19a	2227
2868 RS	2×19b	2878	1633 RS	6b+12	1631	2370 RS	8a+18b	2363
2908 RI	19a+19b	2921		17a+18b	1631	2389 IR	8b+18b	2375
2952 RI	8a+14	2955	1645 IR	2×18a	1648	2450 RI	3+8b	2450
	2×19a	2964		2×18b	1666	2460 RI	3×18a	2469
2988 RS	3×1?	2976		16a+19a	1669	2566 IR	8b+12	2548
3004 IR	8b+19b	3011	1676 RS	3+5	1670		7b+16a	2614
3023 RS	8a+19b	3019		16b+19b	1672	3076 RS	2×8b	3084
3143 RS	2×8b	3144		9a+17a	1685			
3175 RS	2×8a	3160		1+18b	1795			
			1806 IR	12+17a	1804			
				2×3	1816			
			1850 IR	1+9a	1849			

RS = observed only in Raman spectrum.
IR = observed only in infrared spectrum.
RI = observed in both.
Calculated frequencies based on Table II.

The frequency of vibration 10a should appear near 850 cm^{-1}, its position in benzene, because the moment of inertia of pyridine about the twofold axis is very nearly that of benzene. However, no Raman line is found there, nor in pyridine-d_5 at 664, the corresponding position in benzene-d_6. This means that the force constants for this vibration are different from the analogous ones in benzene, since the frequency in benzene-d_1, where vibrations 10a, 16a, and 17a also fall together in the A_2 symmetry species occurs unchanged at 850. The two nearest frequencies in pyridine lie at 810 and 886, both being very weak in the infrared and the latter somewhat stronger in the Raman effect. In pyridine-d_5 the nearest frequencies to 664 are at 625 and 690, both of which are of medium intensity in the Raman spectrum, the latter being absent in the infrared. This suggests that 690 is the choice in pyridine-d_5, from which the choice of 886 in pyridine follows. The rather considerable intensity increase in pyridine-d_5 is analogous to the increase observed in benzene-d_6, which has been quantitatively explained by Lord and Teller.[19] The line at 812 can be explained as the first overtone of the fundamental at 405.

The remaining A_2 vibration, 17a, should have a frequency somewhat above that of vibration 10a. A weak Raman line at 981 is one possible assignment, although it is found in the infrared, and the Raman line at 1043 is another. If 981 is chosen, only the weak line in pyridine-d_5 at 798 gives satisfactory agreement with the product rule. The counterpart of 1043 in pyridine-d_5 should lie at about 840 and might be concealed by the relatively strong line at 837. The choice here is 981, based chiefly on analogy with benzene, in which the frequency lies in this region. The 1043 line is then ascribed to an overtone, for example, 374 (A_2)+675 (B_2) = 1049 (B_1).

The other species of out-of-plane vibrations, B_2, contains two ring vibrations, 4 and 16b, and three hydrogen bending modes, 5, 10b, and 11. Interaction among the latter three might be expected to result in considerable displacement of the frequencies with respect to their benzene values and in a redistribution of the infrared and Raman intensities of vibrations 11 and 10b, respectively. This expectation is only partly realized. On the grounds of infrared intensity and isotopic frequency shift, vibration 11 is placed at 703 in pyridine and at 530 in pyridine-d_5. The companion bands at 749 and 567 are clearly out-of-plane hydrogen modes, and must be one of the two remaining B_2 hydrogen vibrations, 5 or 10b. Somewhat arbitrarily the latter is chosen, chiefly because the frequency of 10b is lower than that of 5 in benzene. The Raman line at 942 in pyridine is then selected as 5, which drops to 762 in pyridine-d_5.

[19] R. C. Lord and E. Teller, J. Chem. Soc. (London) **1937**, p. 1728.

One of the two B_2 ring vibrations, 16*b*, is located readily by its infrared activity at 404 in pyridine and at 371 in pyridine-d_5. The other, vibration 4, is not so readily found. All pyridine-d_5 frequencies below 1000 cm^{-1} have been assigned except the weak Raman line at 713. This frequency is higher than expected for the ring vibration, does not appear in the infrared and can be explained as an overtone (329 (A_2)+371 (B_2) =700 (B_1)). There is, moreover, no unassigned line in pyridine which would correspond to it. Therefore it is concluded that in pyridine-d_5 the vibration is either too weak to be observed or it is obscured by a stronger frequency of another symmetry species. In pyridine the only unassigned frequency is an infrared band at 675, which is a reasonable location for vibration 4. If this value is substituted along with the above B_2 assignments into the product rule expression, the value obtained for the missing frequency in pyridine-d_5 is approximately 625. At this point there is a strong Raman line and weak infrared band that might well be vibrations 4 and 6 superimposed.

TABLE V. Assignment of frequencies for benzene, pyridine, pyridine-d_5, and benzene-d_6.

Freq. No.	Species D_{6h}	Species C_{2v}	Frequencies in cm^{-1} Benzene	Pyridine	Pyridine-d_5	Benzene-d_6
1	A_{1g}	A_1	992	992	962	945
2	A_{1g}	A_1	3062	3054	2293	2293
3	A_{2g}	B_1	1326	1218	908	1037
4	B_{2g}	B_2	703	675	625	601
5	B_{2g}	B_2	993	942	762	827
6*a*, *b*	E_g^+	A_1, B_1	606	605, 652	582, 625	579
7*a*, *b*	E_g^+	A_1, B_1	3048	3054	2285	2266
8*a*, *b*	E_g^+	A_1, B_1	1595	1580, 1572	1530, 1542	1553
9*a*, *b*	E_g^+	A_1, B_1	1178	1218	887	869
10*a*, *b*	E_u^-	A_2, B_2	850	886, 749	690, 567	664
11	A_{2u}	B_2	671	703	530	497
12	B_{1u}	A_1	1010	1029	1006	962
13	B_{1u}	A_1	3060	3054	2270	2290
14	B_{2u}	B_1	?	1375	1322	?
15	B_{2u}	B_1	1160	1148	887	830
16*a*, *b*	E_u^+	A_2, B_2	405	374, 405	329, 371	350
17*a*, *b*	E_u^+	A_2, B_2	970	981	798	790
18*a*, *b*	E_u^-	A_1, B_1	1035	1068, 1068	823, 833	813
19*a*, *b*	E_u^-	A_1, B_1	1485	1482, 1439	1340, 1301	1333
20*a*, *b*	E_u^-	A_1, B_1	3080	3036, 3083	2254, 2293	2294

The above set of assignments, listed in Table III, completes the identification of the fundamentals. In many respects the present set differs from that of Kline and Turkevich,[8] the differences for the most part being indicated by the spectra of pyridine-d_5 and the product-rule. Interestingly enough, the differences lie only in the way in which the observed frequencies are assigned and not in the values of the frequencies themselves. The two collections of frequencies are essentially identical except for a replacement of one 605 frequency by 981 and 1723 by 1375. Since all vibrations are nondegenerate, this means that the thermodynamic functions calculated by Kline and Turkevich would not be changed much if recalculated with the present set of frequencies. The statistical entropy of pyridine vapor at 298.1°K and one atmosphere was calculated by them as 68.17 entropy units per mole, compared with an experimental value of 68.6. The frequency changes indicated above would increase this discrepancy, but in view of the limits of error (±1 percent) ascribed to the experimental value, this is perhaps not of great significance.

ASSIGNMENT OF OVERTONES

The nonrestrictive nature of the selection rules for the C_{2v} structure, together with the large number of fundamental frequencies and uncertainty about the amount of anharmonicity, makes it possible to explain the observed overtones without difficulty. Conversely, the interpretation of overtones is less meaningful for confirmation of the assignment of the fundamentals. In Table IV a set of overtone assignments is given. Finally in Table V the present assignment of frequencies in pyridine is compared with the generally accepted values of the fundamental frequencies in benzene and benzene-d_6.

Investigation of the Surface Reaction of Oxygen with Carbon on Tungsten with the Field Emission Microscope*

RALPH KLEIN
Explosives and Physical Sciences Division, Kinetics Section, Bureau of Mines, Pittsburgh, Pennsylvania
(Received February 9, 1953)

The adsorption of oxygen and carbon on tungsten and the surface reaction between carbon and oxygen on tungsten have been studied by means of the field emission microscope. Emission patterns for oxygen on tungsten, carbon on tungsten, and oxygen and carbon together on tungsten under a variety of temperature pretreatment conditions have been obtained. Average work functions over all exposed crystallographic planes, calculated from measured voltages and emission currents on the basis of the Fowler-Nordheim equation, give a measure of surface coverage in the case of oxygen on tungsten. The similarity of the emission-pattern changes in the evaporation of oxygen from tungsten with those found in the reaction between carbon and oxygen on tungsten suggests that the rate-controlling step in the reaction is desorption of oxygen from the tungsten surface. Diffusion of carbon into the tungsten lattice plays no role in the pattern changes since, in the absence of oxygen, the carbon-on-tungsten surface is found to be very stable.

SURFACE reactions represent a complex of phenomena, such as adsorption, surface mobility, and geometrical and electronic configuration effects. Detailed observations are required for elucidation of these factors, but the techniques available have been limited. One important method yields data on differences of catalytic activity of different crystal faces from observations on single crystals on which surface reactions occur. In this way Gwathmey and co-workers[1,2] have studied the oxidation of copper and the catalytic reaction of hydrogen and oxygen on copper. For example, the 100 and the 111 faces of copper exhibited appreciable differences in rates of the hydrogen-oxygen reaction. Regular rearrangements of the surface layers, showing symmetrical patterns on a polished single-crystal sphere, were also observed. In another experiment, carbon deposited selectively on the 111 face of a nickel crystal in the catalytic decomposition of carbon monoxide.

The method of investigating surface reactions on single crystals can be refined through the use of the field emission microscope[3] to give details of the order of molecular dimensions. The apparatus consists of an evacuated tube containing a wire etched to a point of about 1μ radius opposite a phosphorescent screen several cm distant. Application of a potential of the order of 10^4 v between the point and an anode ring, the latter being located between the point and the screen, results in a high local field of the order of 10^8 v/cm. Electron emission from the point occurs approximately radially, producing a pattern on the screen. That of clean tungsten, for example, consists of dark spots about the 011, 121, and 001 poles surrounded by bright areas. Surface impurities on the single-crystal point alter the pattern by changing the work function and hence the emission characteristics of the surfaces. Local enhancement of the field by clustering, crystallite formation, or even single large molecules, causes bright spots. In so far as surface reactions change the work function nonuniformly over the crystal surface, their progress may be observed by changes in the emission pattern. Ashworth[4] has obtained some field emission patterns representing the copper-oxygen reaction on tungsten using this method. The present paper describes some interesting results of a preliminary study of the reaction between carbon and oxygen on tungsten, using the field emission microscope technique. This study is facilitated by the fact that the reaction products are gases which do not remain on the surface in the temperature range of interest.

EXPERIMENTAL

To avoid extraneous surface contamination, ultra high-vacuum techniques are essential. In this work the vacuum system consisted of a three-stage, Hickman-type, water-cooled, oil-diffusion pump in conjunction with a Bayard-Alpert ionization gauge.[5] Special high-vacuum valves[6] were used to isolate the system from the pumps after the metal components of the emission tube were baked out and outgassed. A pressure of the order of 10^{-10} mm Hg could be attained in the system by the well-known pumping action of the ionization gauge, which also served as a pressure indicator.

The point itself was made, following Müller,[3] by etching a 0.01-cm-diam tungsten wire with sodium nitrite. Evaporation from an electrically heated graphite filament supplied carbon to the tungsten surface. Pure oxygen was supplied by diffusion through a silver thimble. The emitting surface was at the end of a 1-mm length of tungsten wire attached to a tungsten loop. A diagrammatic sketch is shown in Fig. 1. The

* This research is a part of the work being done at the Bureau of Mines on Contract AF 18(600)-156, supported by the U. S. Flight Research Laboratory, Wright Air Development Center, Wright-Patterson Air Force Base, Ohio.
[1] A. T. Gwathmey and A. F. Benton, J. Chem. Phys. **8**, 431 (1940).
[2] H. Leidheiser, Jr. and A. T. Gwathmey, J. Am. Chem. Soc. **70**, 1200 (1948).
[3] E. W. Müller, Physik Z. **37**, 838 (1936).
[4] F. Ashworth, Advances in Electronics, **3**, 32 (1951).
[5] R. T. Bayard and D. Alpert, Rev. Sci. Instr. **21**, 571 (1950).
[6] D. Alpert, Rev. Sci. Instr. **22**, 536 (1951).

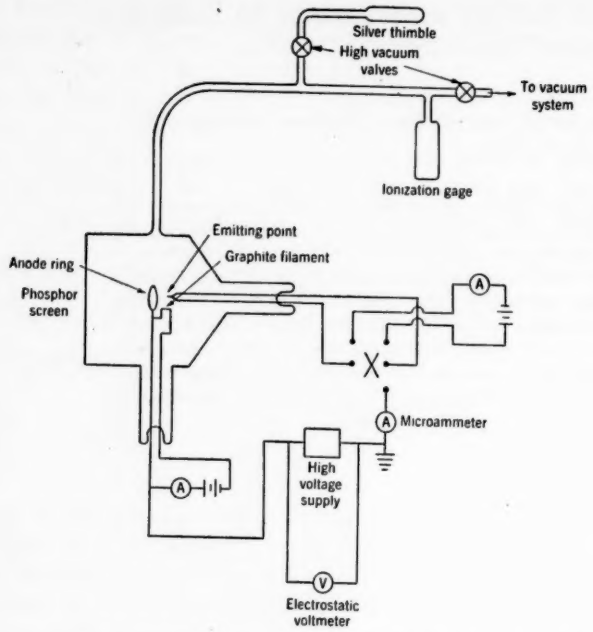

FIG. 1. Field emission microscope assembly for the oxygen-carbon reaction on tungsten.

temperature of the surface as a function of the heating current was determined by a micro-optical pyrometer focused $\frac{1}{2}$ mm from the tip. Measured temperatures were corrected for the emissivity of tungsten. The calculated difference in temperature between the measured and emitting surface due to radiation losses was small.[7]

The following procedure was used to study the reaction. After establishing a vacuum of the order of 10^{-10} mm Hg, carbon was deposited on the point. Oxygen was supplied to a pressure of 10^{-5} mm. After one minute the system was re-evacuated to the lowest pressure obtainable without subsequently baking out ($\sim 10^{-9}$ mm). With the ionization gauge pumping continuously, the point was heated to various temperatures for different time intervals, after each of which the point was brought to room temperature at which the emission pattern was photographed and the voltage required for a 5-microampere emission current was recorded.

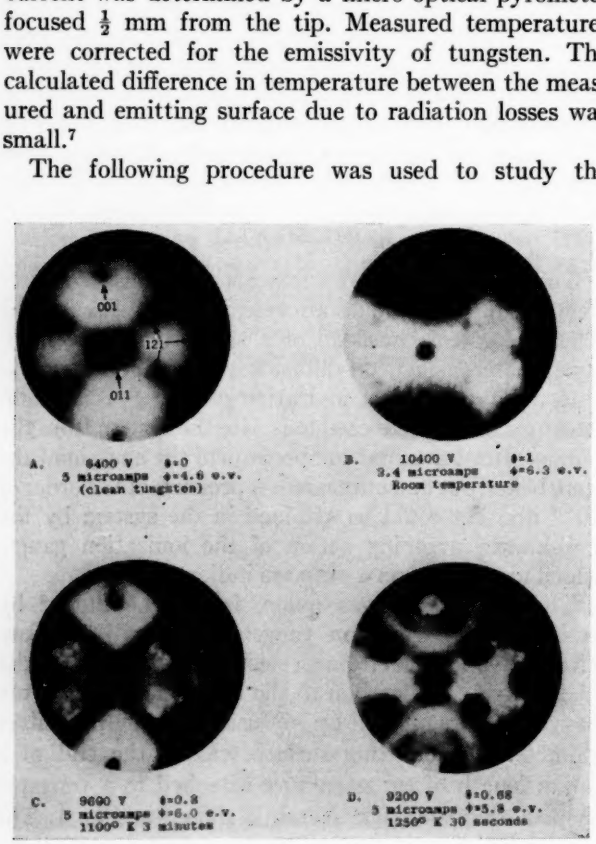

FIG. 2. Oxygen on tungsten.

RESULTS

Interpretation of the results requires data on the emission patterns and work functions of the reactant species individually. The system oxygen-on-tungsten has been extensively investigated.[8–10] Field emission patterns were first observed by Müller.[11] We have repeated this work and obtained patterns shown in Figs. 2 and 3. Oxygen initially was admitted to a pressure of 10^{-5} mm and then pumped off. The point was heated for specified time intervals and temperatures in the absence of a field and emission patterns were taken with the point at room temperature. The legends for each pattern in Figs. 2 through 5 show the voltage for a 5-microampere emission current (except that in Fig. 2(B) the emission current was reduced to 2.4 microamperes because of limitations of the voltage supply used); the temperature and time of heat treatment; the

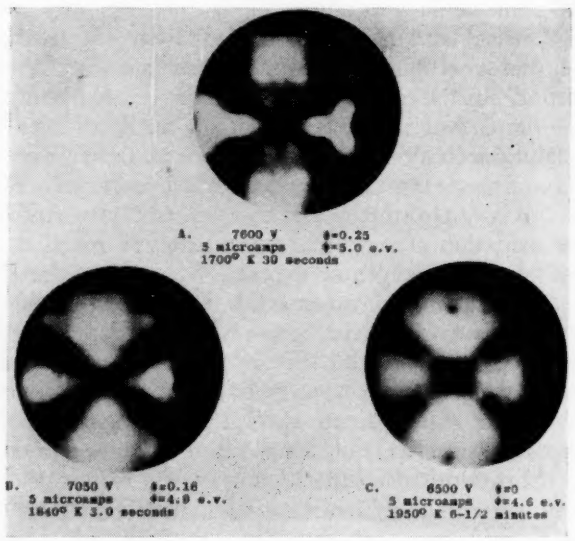
A. 7600 V φ=0.25
5 microamps φ=5.0 e.v.
1700° K 30 seconds
B. 7050 V φ=0.16
5 microamps φ=4.9 e.v.
1840° K 3.0 seconds
C. 6500 V φ=0
5 microamps φ=4.6 e.v.
1950° K 6-1/2 minutes

FIG. 3. Oxygen on tungsten (continued from Fig. 2).

[7] E. W. Müller, Z. Physik **126**, 642 (1949).

[8] I. Langmuir and D. S. Villars, J. Am. Chem. Soc. **53**, 486 (1931).

[9] J. K. Roberts, Proc. Roy. Soc. (London) **152A**, 464 (1935).

[10] R. C. L. Bosworth, J. Proc. Roy. Soc. (New South Wales) **79**, 53 (1946).

[11] E. W. Müller, Physik **106**, 541 (1937).

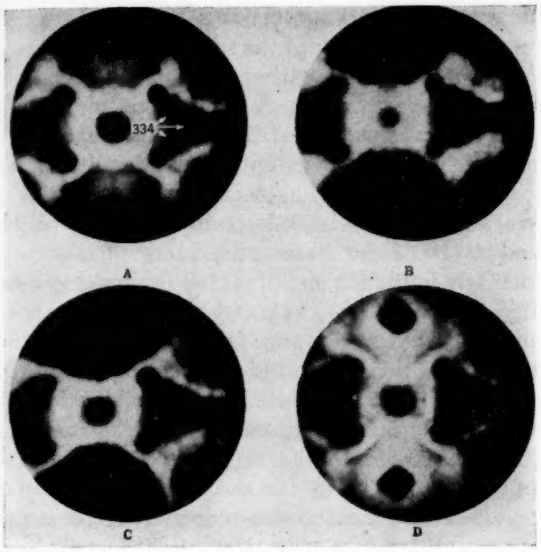

FIG. 4. Surface reaction of carbon with oxygen on tungsten. (A) 5800 v 5 microamperes. (Carbon alone. For this point when clean, 5600 v were required for a 5-microampere emission current.) (B) 9800 v 5-microamperes room temperature. (C) 8980 v 1000°K 110 minutes 5 microamperes. (D) 7800 v 1100°K 30 seconds 5 microamperes.

fractional surface coverage θ; and the work function φ. The latter has been calculated, assuming a linear relationship between surface coverage and the difference in work function between the oxygen-tungsten surface and tungsten. This is justified by Bosworth's[10] measurements of contact potentials, which showed that the dipole moment of the adsorbed oxygen varied but little with surface concentration. Since the work function difference, or its equivalent the contact potential, equals $1885\mu\sigma$ volts, where μ is the dipole moment and σ the number of adsorbed atoms per unit area of surface, the independence of μ with surface concentration requires linear dependence of work-function difference with surface coverage. The average work function was calculated on the basis of the modified Fowler-Nordheim equation[12]

$$J=\frac{1.5\times10^{-6}}{\varphi}F^2\exp\left(-\frac{6.85\times10^7\varphi^{\frac{3}{2}}}{F}\right)f(F,\varphi),$$

where J is the current density, φ the work function, F the field in v/cm, and $f(F,\varphi)$ an elliptical function. It must be emphasized that the surfaces concerned consist of patches of different work functions. A kind of an average work function is obtained to represent the surface such that

$$J(F,\bar{\varphi})=\frac{1}{S}\int J_S(F,\varphi_s)dS,$$

where φ is the average work function, S represents the emitting area, and J_S is the current density for the patch dS. For the same point giving the same emission current for different values of V and φ,

$$\frac{F_1^2}{\varphi_1}\exp\left(\frac{-6.85\times10^7\varphi_1^{\frac{3}{2}}}{F_1}\right)f(F_1,\varphi_1)$$

$$=\frac{F_2^2}{\varphi_2}\exp\left(\frac{-6.85\times10^7\varphi_2^{\frac{3}{2}}}{F_2}\right)f(F_2,\varphi_2).$$

Since

$$f(F_1,\varphi_1)\cong f(F_2,\varphi_2)$$

and

$$F\cong4\times10^3\,\mathrm{V},^{13}$$

where V is the applied voltage, one obtains

$$\frac{\ln\frac{\varphi_2}{\varphi_1}+2\ln\frac{V_1}{V_2}}{1.7\times10^4}=\left(\frac{\varphi_1^{\frac{1}{2}}}{V_1}-\frac{\varphi_2^{\frac{1}{2}}}{V_2}\right).$$

The term on the left is small, so that in general

$$\varphi_2=\varphi_1\left(\frac{V_2}{V_1}\right)^{\frac{3}{2}}.$$

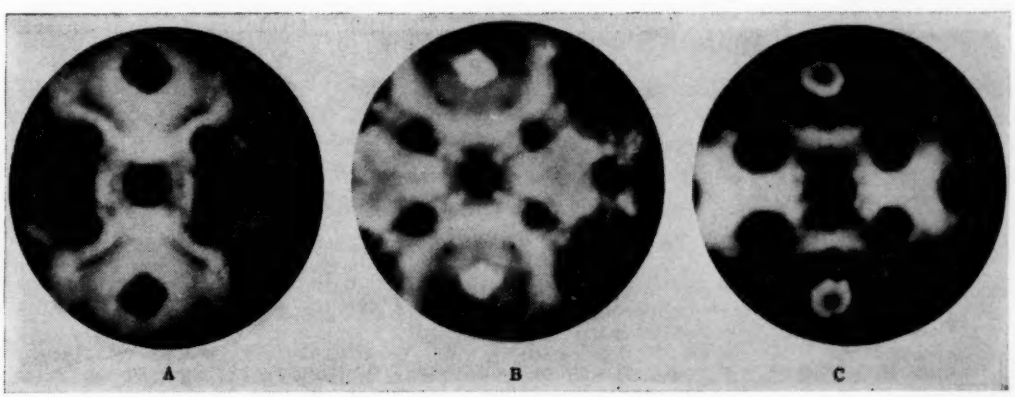

FIG. 5. Surface reaction of carbon with oxygen on tungsten (continued). (A) 7700 v 1100°K 45 seconds 5 microamperes. (B) 8000 v 1100°K 11 minutes 5 microamperes. (C) 7500 v 1150°K 30 minutes 5 microamperes.

[12] A. Sommerfeld and H. Bethe, *Handbuch der Physik* XXIV/2, 2nd ed. (1933), p. 441.
[13] W. P. Dyke and J. K. Trolan, U. S. Office of Naval Research Report N8-ONR-72401 (September 30, 1951).

Several assumptions are inherent in this formula such as the constancy of emission area with adsorption, and, as noted, the use of a single average work function to describe a patchy surface. The values of surface coverage derived from the average work-function values serve, nevertheless, as a useful basis of comparison of the emission patterns. Clean tungsten serves as a reference, the work function being taken as 4.56 ev. The surface of Fig. 2(B), calculated to have a work function of 6.3 ev, corresponds to a monolayer of oxygen. Bosworth determined a contact potential of a monolayer of oxygen on tungsten with respect to tungsten to be -1.78 v. This gives a value for the work function of $4.56+1.78=6.34$ ev, in agreement with the value found with the field emission microscope. Figures 2(C) and 2(D) and 3(A) through 3(C) represent a surface of progressively increased temperature treatment. The observations agree with those of Müller, except that in the present experiments the temperature scale is somewhat lower.

Carbon on tungsten is shown in Fig. 4(A). Carbon was condensed on the tip at room temperature and heated to 1250°K for 5 minutes before the photograph was taken. In addition to the usual spots of low emission present in the clean tungsten pattern, there are those caused by the 334 planes. With greater surface coverage, a pattern was found in which the 111 and 122 planes are also manifested as low emission regions. The work function of a carbon-on-tungsten surface was found to differ little from that of clean tungsten, regardless of the amount of carbon present. Carbon is not expected to exist as a surface dipole layer on tungsten, and this is confirmed by these observations.

The reaction between carbon and oxygen on tungsten may be followed by preparing the composite surface and observing the pattern changes as the surface treatment temperature is increased. Oxygen admitted to the system to a pressure of 10^{-5} mm and pumped off to a pressure of 10^{-9} mm is adsorbed by the carbon-on-tungsten point. The emission pattern is shown in Fig. 4(B), which has the appearance of a superposition of the oxygen-on-tungsten on the carbon-on-tungsten pattern. Figures 4(C) and (D) and Figs. 5(A), (B), and (C) represent the course of the surface reaction between adsorbed oxygen and carbon-on-tungsten through a sequence of temperatures. A comparison of Fig. 2(B) with 2(C) reveals that at 1000°K the reaction has occurred to only a small extent if at all, for although the over-all work function has decreased, pattern changes are very slight. In Fig. 4(D), where the tip has been heated to 1100°K for 30 seconds, reaction has occurred, particularly in the region 001. It has occurred to a more limited extent on 334, 111 and the surround of 011. Figure 5(A) shows no change from 4(D), but Fig. 5(B) indicates that the reaction is almost complete, for this pattern, as well as 5(C), is characteristic of an oxygen-on-tungsten surface [compare Figs. 5(C) with 2(D)]. Carbon diffusion into the tungsten lattice is not an alternative explanation for the disappearance of the carbon because the carbon-on-tungsten surface is stable even at temperatures several hundred degrees higher. The rather large surface coverage of oxygen remaining after the reaction is complete suggests that the initial carbon-on-tungsten surface was one of low surface coverage.

The oxidation of graphite occurs at a measurable rate[14] at temperatures several hundred degrees lower than the 1100–1200°K region in which the reaction, as revealed by the emission pattern changes, occurs on tungsten. This, in addition to the similarity of the emission pattern, changes as a function of the temperature for the system oxygen-on-tungsten with the system carbon-and-oxygen-on-tungsten, suggests that the rate-controlling step in the carbon oxidation is breaking of the W—O bonds of the chemisorbed oxygen. The effects attributable to surface migration of both oxygen and carbon on the tungsten surface remain to be evaluated. Application of methods similar to those used by Becker[15] in studies of surface migration of barium on tungsten should resolve these problems.

[14] E. A. Gulbransen and K. F. Andrew, Westinghouse Research Laboratories Scientific Paper 1595 (April 5, 1951).

[15] J. A. Becker, Bell System Tech. J. XXX, No. 4, 907 (1951).

Ultraviolet Absorption Spectra of Derivatives of Symmetric Triazine. I. Amino Triazines*

ROBERT C. HIRT AND D. J. SALLEY
Stamford Research Laboratories, American Cyanamid Company, Stamford, Connecticut
(Received January 12, 1953)

The near ultraviolet solution spectra of twenty one mono-, di-, and triamino derivatives of symmetric triazine are reported. The addition of amino groups to the *s*-triazine ring introduces electrons which can interact with those of the ring, with resultant changes in the intensity and position of the absorption bands. The spectra of mono-, di-, triamino-*s*-triazine may be arranged in a Platt sequence along with that of trichloro-*s*-triazine and that expected for *s*-triazine.

ULTRAVIOLET absorption spectra have been reported for only a few derivatives of symmetric triazine (a molecule isoelectronic with benzene, pyridine, and the diazines).

s-Triazine nucleus

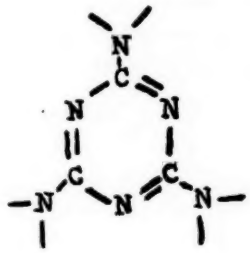

Melamine nucleus

These include melamine,[1-3] cyanuric acid,[2] cyanuric chloride,[2,3] and 2,4-diamino-6-phenyl-*s*-triazine (benzoguanamine),[4] with mention (but not full spectra) of some methylol melamines.[1,3] Certain expected features of the spectrum of *s*-triazine have been discussed from a valence-bond point of view.[5] Since *s*-triazine has never been prepared, it is necessary to study the spectra of its derivatives to extend the knowledge of nitrogen heterocyclic spectra. This paper reports studies made on amino derivatives.

EXPERIMENTAL PROCEDURE

Most of the data presented were obtained by use of a Beckman spectrophotometer, Model DUV, equipped with a water-cooled Nester hydrogen lamp. A Cary automatic recording spectrophotometer, Model 11, No. 67, was used to extend some of the spectra to shorter wavelengths, and to search for bands not resolvable by the Beckman instrument. Fused quartz cells of 5, 10, 20, and 50 mm light path length were used, as well as micrometer Baly cells which were adjustable from 5.00 to 0.01 mm in length.[6] Variations in cell length rather than concentration were made whenever possible, in order to avoid any changes in *pH* on dilution. Distilled water was used as the solvent.[7]

The spectrum of melamine was extended below 2080 A by use of a small Hilger spectrograph.[8] The spectrograph casing and the spaces between the Nester hydrogen lamp, absorption cell, and slit were continuously flushed with nitrogen to remove oxygen; this made measurements possible down to about 1900A (52 500 cm^{-1}). A 5-mm quartz cell and a 2-mm fluorite-window cell were used. Eastman Kodak 103-O UV-sensitized plates were used; these were microphotometered and the data corrected for blank cell absorption and the change of intensity of the light source with wavelength by the usual procedures.

The data are presented as plots of the log of the molar absorptivity (molar extinction) *versus* wave number ($\log\epsilon$ *vs* cm^{-1}). Beer's law was used in the form $A=(\epsilon/M)\cdot b\cdot c$, where A is the absorbance (optical density), ϵ is the molar absorptivity (molar extinction), M is the formula weight, b is the cell length in mm, and c is the concentration in grams per 100 ml.

All of the compounds here mentioned were prepared by various members of these Laboratories and recrystallized or resublimed to obtain a high degree of purity. Even so, some of the samples may have contained small amounts of closely related compounds formed during their preparation. Most of the samples were identical with those reported in other contributions from these Laboratories.[1,3,9,10]

RESULTS

The feature common to the spectra of all the amino derivatives of *s*-triazine which were examined is the presence of two major absorption systems, sometimes overlapped, in the 35 000- to 50 000-cm^{-1} region. The intensity of each system is appreciable ($\epsilon>1000$), with the higher wave-number system much the stronger.

* Presented in part by R. C. Hirt at the Symposium on Molecular Structure and Spectroscopy, The Ohio State University, Columbus, Ohio, June, 1950.

[1] Dixon, Woodberry, and Costa, J. Am. Chem. Soc. **69**, 599 (1947).

[2] I. M. Klotz and T. Askounis, J. Am. Chem. Soc. **69**, 801 (1947).

[3] Costa, Hirt, and Salley, J. Chem. Phys. **18**, 434 (1950).

[4] F. A. Nachod and E. A. Steck, J. Am. Chem. Soc. **70**, 2818 (1948).

[5] F. Halverson and R. C. Hirt, J. Chem. Phys. **19**, 711 (1951).

[6] R. C. Hirt and F. T. King, Anal. Chem. **24**, 1545 (1952).

[7] It was necessary to use 95 percent ethyl alcohol or cellosolve for two of the diamino derivatives which were insoluble in water. These are so marked in the table.

[8] We are grateful to W. W. Watson and M. Setlow of the Physics Department of Yale University for the loan of this instrument during the summer of 1950.

[9] Thurston, Dudley, Kaiser, Hechenbleikner, Schaefer, and Holm-Hansen, J. Am. Chem. Soc. **73**, 2981 2984 (1951).

[10] J. R. Dudley, J. Am. Chem. Soc. **73**, 3007 (1951).

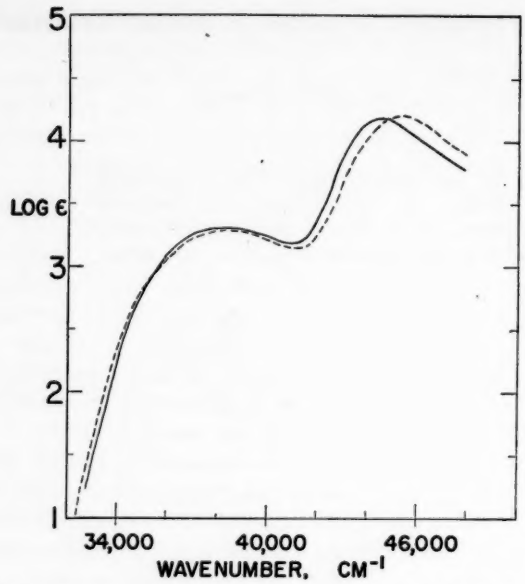

FIG. 1. Mono-amino-*s*-triazines. - - - - - 2-amino-*s*-triazine. ——— 2-amino-4,6-dichloro-*s*-triazine.

TABLE I. Absorption bands of mono- and diamino-*s*-triazines.

Substituted-*s*-triazine	Wave number cm^{-1}	ϵ	Wave number cm^{-1}	ϵ
2-amino	38 300	1960	45 440	16 230
2-amino-4,6-dichloro	38 170	1990	44 630	15 250
2,4-diamino (formoguanamine)	38 760	3620	>48 780	>34 500
2,4-diamino-6-methyl (acetoguanamine)	39 370	3435	>48 780	>38 400
2,4-diamino-6-chloro[a]	39 080	3250	>47 600	>35 000
2,4-diamino-6-heptadecyl[b] (stearoguanamine)	39 080	3600	>47 200	>26 000

[a] In cellosolve.
[b] In 95 percent ethyl alcohol.

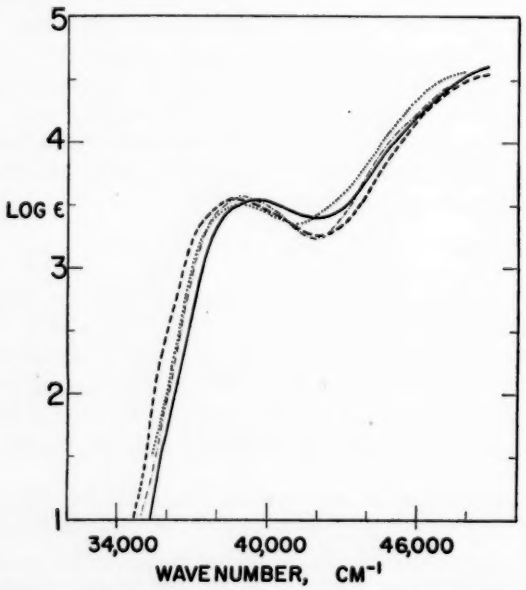

FIG. 2. Diamino-*s*-triazines. - - - - - 2,4-diamino-(formoguanamine). ····· 2,4-diamino-6-chloro-. —·—·—·—·— 2,4-diamino-6-heptadecyl-(stearoguanamine). ——— 2,4-diamino-6-methyl-(acetoguanamine).

Both are several factors of 10 more intense than the very weak band which was earlier attributed to a singlet-triplet transition.[3]

The spectra of mono-amino derivatives (Fig. 1 and Table I) show two clearly resolved bands, the lower near 38 200 cm.$^{-1}$ and the upper near 45 000 cm^{-1}. The presence of two Cl atoms on the triazine ring produces a bathochromic shift of both bands.

The spectra of the diamino derivatives (Fig. 2 and Table I) also show two absorption systems, with the lower near 39 000 cm^{-1} and the upper above the range investigated, that is, above 48 000 cm^{-1}. The intensities of both bands are greater than those of the corresponding bands in the mono-amino derivatives.

The clear-cut separation of the two bands is largely lost in the triamino derivatives (melamines). The complete spectrum of melamine (triamino-*s*-triazine) from 26 300 to 52 600 cm^{-1} (3800 to 1900A) is shown in Fig. 3. The region below 47 500 cm^{-1} is that presented

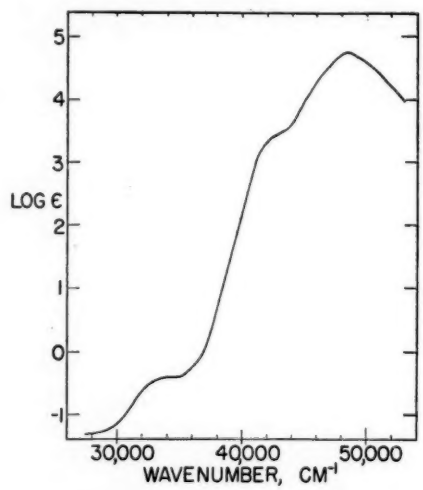

FIG. 3. 2,4,6-triamino-*s*-triazine (melamine).

previously,[3] while that up to 52 600 cm^{-1} is that obtained by use of the Cary and Hilger instruments as already described.

The symmetrically substituted (tri- or hexa-) melamines show shoulder-type spectra quite similar to that of the parent unsubstituted melamine, as shown in Fig. 4. The intensity of this lower band does not increase markedly with increased substitution. A pronounced bathochromic shift of both bands is the most prominent feature of these spectra. The contour of the spectral curve is quite well preserved, as shown by Fig. 4. The intensity of this overlapped band is difficult to estimate. However, an attempt was made in the case of melamine to compensate for the contribution of the overlapping stronger band. The slope of the upper band, taken above the "shoulder," was extrapolated to lower wave numbers to obtain a "background correction." This gave a "corrected" ϵ value of 1100 for the overlapped band at 42 500 cm^{-1}. A value not far from this

would hold for the other symmetrical melamines, judging from the appearance of the curves of Fig. 4.

For the unsymmetrical alkyl melamines, shown in Fig. 5, the two bands are not resolved. By comparison to the unsubstituted melamine, there are an increased intensity and possibly a small bathochromic shift of the lower band. The unsymmetrical alkylol melamines show a partially resolved or shoulder-type band, as shown in Fig. 6. Here also substitution leads to an increased intensity and a slight bathochromic shift of the lower band.

DISCUSSION

The substitution of an amino group for an H atom in *s*-triazine introduces new electrons which can interact (or conjugate) with those of the ring, with resultant

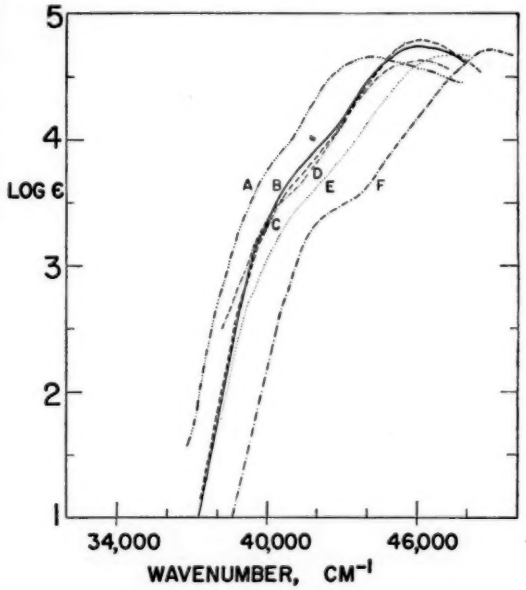

FIG. 4. Symmetrically substituted melamines. A —·—·—·— Hexamethyl. B ——— Triethylol. C – – – – Hexamethoxymethyl. D – – ·– ·– Hexamethylol. E ····· Trimethylol. F —·—·— unsubstituted.

changes in the intensity and position of the absorption bands. The triazines having 0, 1, 2, and 3 N atoms, attached to the ring, form a sequence of the type presented by Platt.[11] this is shown in Fig. 7. The length of the bars representing band systems is roughly proportional to logϵ.

In a previous report,[5] a reasonable spectrum for *s*-triazine was obtained from data on the diazines and cyanuric chloride, giving a π-electron band near 42 000 cm^{-1} and a *n*-electron band near 39 000 cm^{-1}. These are shown in Fig. 7 along with the data for cyanuric chloride.[3]

The trigonal symmetry of *s*-triazine would make the lowest singlet π transition symmetry-forbidden, and hence weak in intensity. The removal of this symmetry

[11] J. R. Platt, J. Chem. Phys. **19**, 101 (1951).

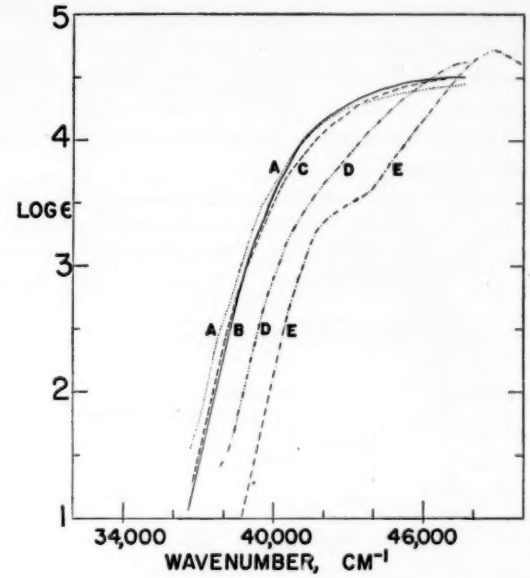

FIG. 5. Unsymmetrical alkyl melamines. A ····· *N*,*N*-diethyl-. B ——— *N*,*N*-diallyyl. C – – – – *N*,*N*-dimethyl. D —·—·· *N*-monoethyl. E —·—·—· unsubstituted.

by addition of one amino group would be expected to result in a considerable increase in intensity for this band. Furthermore, the amino group would be expected to cause a bathochromic shift of π bands and a slight hypsochromic shift of the *n* band. The effect of changing solvents from cyclohexane to water would further intensify these effects.[12] Thus it seems reasonable that the lower π band has shifted about 2800 cm^{-1} to the red and has increased in intensity from an estimated[5]

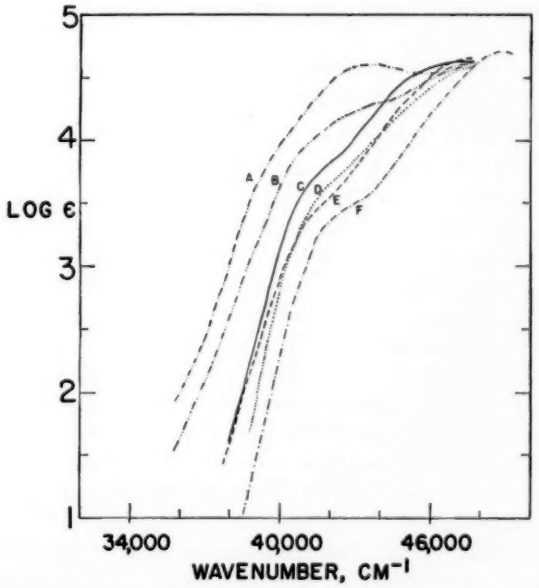

FIG. 6. Unsymmetrical alkylol melamines. A ··—·—·— *N*,*N*,*N*′,*N*′tetraethylol. B —·—·—·— *N*,*N*,diethylol. C ——— *N*,*N*-diethylol. D ····· *N*-monoethylol. E – – – *N*,*N*′-dimethylol. F —·—·— unsubstituted.

[12] H. McConnell, J. Chem. Phys. **20**, 700 (1952).

ϵ value of 250 to 1960, that the next higher π band has shifted from some unknown position down to 45 440 cm^{-1}, and that the n band has been masked by the stronger π bands. Except for the presence of the n band the hydrocarbon analogy would be the familiar benzene-to-aniline change.

The addition of a second amino group to *s*-triazine would not be expected to make such great changes as the first. An increased intensity of both upper and lower bands may be expected and are observed. Little change

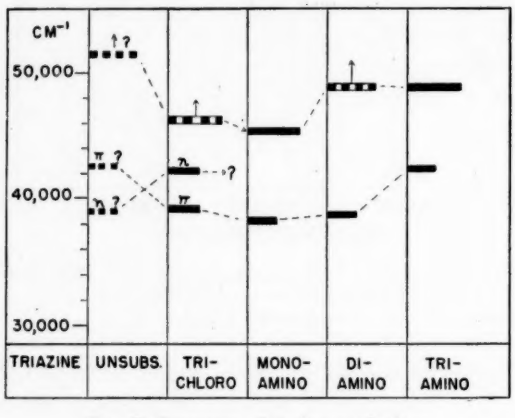

FIG. 7. Sequence of amino-*s*-triazines.

in band position might be expected, though some blue-shift of both bands is observed, particularly for the upper band. For both mono- and diamino triazines, the substitution of Cl or C atoms on the C atoms of the ring would be expected to have but a secondary effect on the band intensities and positions, since these bring no strongly interacting electrons into the system. Only such a secondary effect is observed.

The addition of a third amino group to the triazine ring restores the threefold symmetry axis of the unsubstituted *s*-triazine, and thus the lower band (at about 42 000 cm^{-1}) is assigned to a symmetry-forbidden π-electron transition. This would account for the diminished intensity of 1100 for the overlapped band of melamine. There is little to indicate what other changes should occur, except possibly a continuation of the blue-shift observed in going from one to two amino groups.

The substitution of alkyl or alkylol groups for the H atoms of the amino groups of melamine will preserve the trigonal symmetry if the substitution is symmetrical tri- or hexa-, and will destroy it if otherwise arranged. That the intensity of the weak, shoulder-type band in the 38 000–42 000-cm^{-1} region is little changed by tri- or hexa-substitution on melamine is evident from Fig. 4. The unsymmetrically substituted alkyl and alkylol melamines show an increased intensity and slight bathochromic shift of this band, with considerable change in the appearance of the spectrum (Figs. 5 and 6). Thus the presence or absence of trigonal symmetry explains the appearance of the substituted melamine spectra.[13]

All of the amino triazines here discussed have had H, N, C, or Cl atoms attached to the C atoms of the ring. Triazines having only Cl atoms so attached and amino triazines having O or S atoms or exocyclic double bonds and ionic forms are being investigated and will be reported later.

The authors wish to express their appreciation to various members of the Stamford Laboratories who prepared and purified the compounds used, to Mrs. D. M. Sousa and Mrs. E. S. Davis for aid with the experimental work and in the preparation of the figures, and expecially to F. Halverson for many helpful suggestions and discussions during this investigation.

[13] In an earlier investigation[1] on methylol melamines, a plot of this lower band *vs* molecular weight showed several points to fall well below the curve (see Fig. 5 of reference 1). Examination of their data shows the low points to be those of trigonally symmetric melamines. This lowered intensity is explainable in terms of a symmetry-forbidden transition, as above.

Some Observations on the Chemical Behavior of Iodine at Low Concentrations

MILTON KAHN* AND ARTHUR C. WAHL
Department of Chemistry, Washington University, St. Louis, Missouri
(Received March 6, 1953)

An investigation has been made of the chemical forms assumed by I^{131} initially in the form of iodide ion at low concentration (the order of $10^{-7}M$) when it is oxidized under various conditions. Oxidation at room temperature in $1f$ sulfuric acid solution by dichromate ion or cerium(IV) results in the formation of I_2 and three additional, unidentified, chemical fractions which are not readily exchangeable with I^-, I_2, or IO_3^-. Two of the unidentified fractions are extracted from aqueous sulfuric acid solution by organic solvents, one fraction being converted by aqueous sodium hydroxide to water-soluble forms exchangeable with I_2. At least some of the unidentified fractions probably are the products of reactions between trace impurities, molecular or colloidal, and iodine in an oxidized reactive form such as HIO. These unidentified fractions are quite inert toward oxidation and reduction.

When iodide ion at low concentration is treated with a hot sulfuric acid solution of cerium(IV), the principal product is IO_3^-, or a species readily exchangeable with IO_3^-. The IO_3^- formed in this way is readily reduced at room temperature to I^- by a sulfuric acid solution of iron(II).

INTRODUCTION

A KNOWLEDGE of the chemical behavior of iodine at very low concentrations is intrinsically of fundamental interest and would also be an aid in interpreting the low concentration behavior of astatine, which can be studied only at low concentrations.[1] That the behavior of very small amounts of iodine differs significantly from the known behavior of macro amounts of iodine is suggested by the difficulty of achieving complete exchange between the minute amounts of radioactive iodine isotopes formed in fission, and by beta decay, with macro-amounts of the stable inorganic forms of iodine (I^-, I_2, IO_3^-, and IO_4^-) added as carrier.[2] Differences in the behaviors of micro- and macro-amounts of iodine need not be too surprising since the stabilities of normally unstable intermediates such as HIO and HIO_2 may be much greater at low concentrations. Molecular iodine becomes increasingly easier to oxidize as its concentration is decreased, and kinetically, an intermediate whose rate of disappearance obeys a rate law involving its concentration to a power greater than one will be more stable at the lower concentrations.[3]

The experimental work reported in this paper was done concurrently with and independently of the detailed study of the chemical properties of astatine made by Johnson, Leininger, and Segrè.[1] Consequently, although some similarities and differences in the chemical behavior of astatine and iodine at low concentration are apparent, experiments parallel to those performed with astatine have not been made with iodine to expressly reveal such similarities and differences.

We have studied some oxidation and reduction reactions of iodine at very low concentrations using "carrier-free" 8.0-day I^{131}. It is estimated that the concentration of iodine in the so-called "carrier-free" solutions was about $10^{-7}M$. Several radioactive fractions were isolated, some of which do not correspond to any of the known stable oxidation states of iodine. Separation of the various iodine species was possible because of their different solubilities in aqueous solutions and benzene. In addition, the species were differentiated by their ability to exchange with I_2, I^-, and IO_3^- and by their acidic and basic properties.

EXPERIMENTAL

Preparation of Materials

The 8.0-day I^{131} used as tracer for iodine was supplied by the Clinton Laboratories and obtained on allocation from the United States Atomic Energy Commission. The iodine activity was received in a sodium acid sulfite solution buffered at a *p*H ranging from 8 to 9. One to two milliliters of the active iodine solution, containing of the order of 1 millicurie of I^{131}, were mixed with 2 ml of a solution $0.1f$ in iron(II) sulfate and $0.1f$ in iron(III) sulfate, and enough concentrated sulfuric acid was added to make the final solution $9f$ in sulfuric acid. This solution was distilled until fumes of sulfur trioxide appeared in the boiler, the distillate being trapped in water. About 3 ml of water was then added to the boiler and the distillation repeated. In this manner about 30 ml of active distillate was obtained, which contained approximately 85 percent of the total activity. The active distillate was made slightly alkaline with sodium hydroxide and then evaporated to approximately 1 ml. This final active solution was the source of the I^{131} activity used and will be referred to as "active solution" in the discussion.

* This paper is abstracted from the Ph.D. thesis of Milton Kahn, Washington University, February, 1950. Present address of Dr. Kahn is Department of Chemistry, University of New Mexico, Albuquerque, New Mexico.

[1] Johnson, Leininger, and Segrè, J. Chem. Phys. **17**, 1 (1948).

[2] C. D. Coryell and N. Sugarman, Editors, *Radiochemical Studies: The Fission Products* (McGraw-Hill Book Company, Inc., New York, 1951), National Nuclear Energy Series—IV 9, L. E. Glendenin and R. P. Metcalf, paper 140, p. 997; Katcoff, Dillard, Finston, Finkel, Seiler, and Sugarman, paper 141, p. 1007; Glendenin, Metcalf, Novey, and Coryell, paper 297, p. 1629.

[3] A. C. Wahl and N. A. Bonner, editors *Radioactivity Applied to Chemistry* (John Wiley and Sons, Inc., New York, 1951), Chap. 6 by N. A. Bonner and M. Kahn, p. 161.

Presumably all of the iodine in this "active solution" was in the form of iodide ion. As a check, tests were made to prove the absence of I_2 and to prove the activity was exchangeable with I_2. These tests, which are described below, did not eliminate the unlikely possibility that hypo-iodite ion could exist in a sulfite solution. In one test approximately 0.1 ml of the active solution was diluted to 1 ml with water and shaken, first with 5 ml of benzene, then with 5 ml of benzene containing iodine ($0.066M$ I_2), and finally with several portions of pure benzene to remove completely the iodine from the aqueous phase. The "active solution" was considered satisfactory if less than 1 percent of the total activity was found in the original 5 ml of benzene and less than 0.5 percent in the final water layer. In a second test some of the "active solution" was shaken with a benzene solution of I_2 at ordinary concentrations, and the specific activity of each phase measured by counting and by titrating with sodium thiosulfate. The equality of the specific activities showed the absence of radioactive impurities as well as chemical forms of I^{131} not exchangeable with I_2.

TABLE I. Oxidation of "carrier-free" I^- in $0.5f$ H_2SO_4 by Ce^{IV} at ~25°C. (8 ml; $0.015f$ Ce^{IV}, $0.015f$ Ce^{III}; 30 min).

Benzene extract, 5 ml	Aqueous extract of benzene, 5 ml	Activity, percent		Chemical fraction
A	H_2O-A	33	40	I_2
	H_2O-B	3		
	$0.2f$ KI	4		
	$0.1f$ NaOH	9		X
	Left in benzene	11		Y
B	...	4		
C (I_2 carrier)	...	8		I^-
Extracted aqueous reaction solution		14		Z
Not recovered		14		

The I^{131} obtained from Oak Ridge was "carrier-free"; that is, no other iodine isotope was purposely added to the I^{131}. However, I^{127} and I^{129} are also formed in the neutron bombardment of tellurium in yields about equal to I^{131}.[4] Therefore, an upper limit on the specific activity (S=fraction of total iodine atoms that are I^{131}) must be set at 0.3. Since the activity was probably contaminated with stable I^{127} from impure reagents used in the purification both at Oak Ridge and in this laboratory, the specific activity was probably less than 0.3. On the basis of such considerations as the lack of color in benzene solutions of carrier-free iodine ($S>5\times10^{-4}$) and the distribution of "carrier-free" iodine between benzene and acid solutions of iron(II) and iron(III), it is estimated that the specific activity of the solutions was about 10^{-3}, which corresponds to a concentration of about $10^{-7}M$.

The water used was obtained by distillation of ordinary distilled water from an alkaline permanganate solution.

Baker cp and Mallinckrodt A.R. grade chemicals were used without further purification. Reagents were prepared by solution of sodium or potassium salts of desired anions and sulfates of desired cations.

Detection of Radioactivity

A thick-walled, argon-alcohol filled, copper Geiger tube was used to detect the energetic gamma radiation associated with the decay of I^{131}. Liquid samples were counted throughout. Ordinary six-inch Pyrex test tubes served as sample holders. These tubes were selected so that when filled to a given height with a given active solution, the spread in counting rate was not greater than 1 percent.

The densities of the active solutions counted varied from that of pure benzene to that of $1f$ sulfuric acid. The variation in counting rate with density was less than the statistical error (*ca* 1 percent). The coincidence correction amounted to 1 percent per 1000 counts per minute.

Extraction

The distribution of iodine activity between benzene and various aqueous solutions was determined by measurement of the activity in a known volume of each phase. The activity was distributed between the two phases by vigorous shaking over a period of three minutes. The benzene layer was separated from the aqueous layer by centrifugation at 1000 rpm in a clinical centrifuge for approximately five minutes.

Two types of extraction vessels were used in these experiments. One type was designed so that 1 ml of an aqueous solution could be repeatedly extracted with 10-ml portions of benzene. It consisted of a bulb of 1-ml capacity sealed to a larger bulb via a short length of capillary tubing. A 12/18 standard taper joint was sealed to the other end of the larger bulb. The meniscus of the aqueous phase reached into the capillary tube, and consequently it was possible to withdraw at least 99 percent of the benzene layer free from the water phase. The other type of vessel was designed so that 5 ml of benzene could be repeatedly washed with 5-ml portions of aqueous solutions. It consisted of a bulb sealed to a 12/18 standard taper joint. The bottom of the bulb was drawn out slightly so that a small tip resulted. Withdrawal of the aqueous layer eventually caused the boundary between the two layers to reside in this small tip. It was possible to remove all of the aqueous layer accompanied by less than 1 percent of the benzene phase.

EXPERIMENTAL RESULTS

Separation of Chemical Fractions

When "carrier-free" iodide ion ("active solution") is oxidized in acid solution by cerium(IV) or dichromate

[4] D. S. Ballantine and W. E. Cohn, "The preparation of carrier-free I^{131}," United States Atomic Energy Commission Report-MDDC-1600.

ion, there are formed several different chemical species of iodine which may be separated by solvent extraction techniques. A typical procedure, which gave the results listed in Table I, is the following. Eight milliliters of reaction solution was extracted successively with two 5-ml portions of benzene (A and B) and one portion of benzene $0.007M$ in I_2(C). The first benzene extract (A) was then back-extracted successively with two 5-ml portions of water (H_2O—A and H_2O—B), a 5-ml portion of $0.2f$ potassium iodide, and a 5-ml portion of $0.1f$ sodium hydroxide.

We identify the following chemical fractions.

I_2: The behavior of the activity extracted into benzene from acid solution and back-extracted into water or aqueous potassium iodide is that expected for I_2 at low concentrations where the hydrolysis equilibrium

$$I_2+H_2O=I^-+H^++HIO$$

is shifted to the right. Aqueous iodide ion, through rapid exchange[5] with I_2, should complete the back-extraction.

X: The activity in this fraction is extracted from acid solution by benzene, is not back-extracted by water, or by aqueous solutions of KI, KIO_3, Fe^{II}, or H_2SO_3, but is back-extracted by aqueous sodium hydroxide.

Y: Same behavior as X except that it is not back-extracted by aqueous sodium hydroxide.

I^-: The behavior of the activity not extracted from acid solution by benzene but extracted by a benzene solution of I_2 is that expected for I^-. Iodide ion exchanges rapidly with I_2[5] and is not soluble in benzene.

Z: The behavior of the activity that is not extracted into benzene and does not exchange with I_2 is that expected for IO_3^-. However, it will be shown later that, except under drastic oxidation conditions, little of the activity in this fraction is exchangeable with iodate ion.

Rates of Oxidation and Reduction

Studies were made of the rates of formation and disappearance of the various chemical fractions formed by the action of several oxidizing agents on carrier-free iodide ion in sulfuric acid solution. The procedures used to separate the fractions were similar to those described in the previous section. The data are summarized in Table II. The activities found in the second benzene extract (B) are not recorded.

Studies were also made of the rates at which the various chemical fractions formed by oxidation could be destroyed or interconverted by several reducing agents. The results are summarized in Table III.

The following conclusions are drawn from the data.

(1) In hot cerium(IV) solution essentially all of the I^- is converted to fraction Z, which when formed under these conditions will be shown to be IO_3^-, or a substance readily exchangeable with IO_3^-.

(2) Carrier-free IO_3^- formed as above is readily reduced at room temperature by iron(II), mostly to I^-.

[5] Hull, Shiftlet, and Lind, J. Am. Chem. Soc. **58**, 535 (1936); Juliusberger, Topley, and Weiss, J. Chem. Phys. **3**, 437 (1935).

TABLE II. Oxidation of "carrier-free" I^- in $0.5f$ H_2SO_4.

Oxidizing couple	Temp., °C	Time, hr	Chemical fractions, percent[a] I_2	X	Y	I^-	Z	Not recovered[b]
$0.015f$ Ce^{IV}, $0.015f$ Ce^{III}	~25	0.5	40	9	11	8	14	15
		5.5	24	10	5	4	41	13
		19.0	17	9	4	2	53	12
		41.5	12	5	2	2	61	15
$0.015f$ Ce^{IV}, $0.015f$ Ce^{III}	105	0.25	2	1	2	0	86[c]	9
		1.17	..	..	..	0	86[c]	..
$0.005f$ $K_2Cr_2O_7$, $0.005f$ Cr^{III}	~25	0.08	63	10	7	16		1
		1.3	43	14	8	25		5
		3.7	29	15	10	25		15
		28	26	13	7	26		22
		95	25	9	5	28	7	21
$0.005f$ $K_2Cr_2O_7$, $0.005f$ Cr^{III}	105	0.55	28	13	9	7	22	13
		5	38	9	7	9	25	21
		19	30	3	16	3	34	8
		92	8	1	22	1	53	15
$0.05f$ Fe^{III}, $0.05f$ Fe^{II}	~25	0.5	3	0	0	96	1	[d]
None added	~25	0.17	33	2	2	65	1	[d]

[a] Based on activity used.
[b] Much of the activity that was lost in the normal procedure could be recovered from the walls of the reaction vessel.
[c] Probably IO_3^- as shown later.
[d] Percentages based on activity recovered.

(3) Iron(III) oxidizes essentially none of the I^-. This observation is consistent with the expectation that at low iodine concentrations the equilibrium

$$2Fe^{+++}+2I^-=2Fe^{++}+I_2$$

will lie to the left. From quantitative considerations of this equilibrium, we estimate that the specific activity of our iodine tracer was about 10^{-3} (i.e., ~0.1 percent of the iodine atoms were I^{131}), corresponding to an iodine atom concentration of the order of $10^{-7}f$.

TABLE III. Reduction of the various oxidized chemical fractions of "carrier-free" iodine in $0.5f$ H_2SO_4.

Reducing couple	Temp., °C	Time, hr[b]	Chemical fraction, percent[a] I_2	X	Y	I^-	Z	Oxidation conditions
$0.034f$ Fe^{II}, $0.046f$ Fe^{III}	~25	0	2	1	2	0	95[c]	$0.015f$ Ce^{IV}, 105°C, 1.25 hr
		0.5	11	2	2	83	3	
$0.034f$ Fe^{II}, $0.046f$ Fe^{III}	~25	0	47	11	13	9	16	$0.015f$ Ce^{IV}, 25°C, 0.25 hr
		0.5	13	17	24	32	14	
$0.026f$ Fe^{II}, $0.024f$ Fe^{III}	~25	0	55	12	8	20		$0.008f$ $K_2Cr_2O_7$, 25°C, ~0.5 hr
		0.17	25	8	5	26	26	
		4.3	21	10	6	25	29	
		19.5	22	10	7	36	15	
		47.5	20	11	8	33	14	
$0.026f$ Fe^{II} $0.024f$ Fe^{III}	105	1.6	10	4	2	75	6	$0.008f$ $K_2Cr_2O_7$, 25°C, ~0.5 hr
		21.5	8	6	1	83	2	
$0.045f$ H_2SO_3, $0.5f$ H_2SO_4	~25	0.25	3	7	3	85		$0.008f$ $K_2Cr_2O_7$, 25°C, ~0.5 hr
		1.0	3	5	6	86		
		11	2	8	7	81		
$0.004M$ I^-, $0.026M$ I_3^-	~25	0.17	..	16	11	..	9	$0.008f$ $K_2Cr_2O_7$, 25°C, ~0.5 hr

[a] Percent based on activity recovered.
[b] Time for reduction. Zero-time numbers give estimate, based on results in Table II, of distribution of activity before reduction occurred.
[c] Probably IO_3^- as shown later.

(4) When I^- is oxidized by $Cr_2O_7^=$ or Ce^{IV} at room temperature, appreciable amounts of all of the various chemical fractions are rapidly formed. Once formed, fractions X, Y, and Z are destroyed very slowly if at all by prolonged oxidation or by reduction. The I_2 initially formed is slowly converted to fraction Z or to a form adsorbed on the surfaces of the reaction vessels (not recovered).

(5) When no oxidizing agent is added some I^- is oxidized to I_2 probably by atmospheric oxygen.

(6) Essentially none of the activity is lost by adsorption when it is mainly in the form of I^- or I_2. When in other forms 10 to 20 percent is lost.

Concentration Studies

Experiments were carried out to determine how low the concentration of iodine had to be in order that the unidentified fractions X, Y, and Z would form. The results are summarized in Table IV. In these experiments 0.2 ml of an active "carrier-free" iodide ion solution and 0.3 ml of an inactive potassium iodide solution of known concentration were mixed. Then, 0.5 ml of an acid dichromate solution (1*f* H_2SO_4, 0.01*f* Cr^{III}, 0.01*f* $K_2Cr_2O_7$) was added. The reaction mixture was allowed to stand at room temperature for ten minutes and was then extracted with benzene.

The fractions X, Y, and Z definitely appeared at concentrations of iodine as high as 6×10^{-5} molar. Either the behavior of iodine was the same at concentrations less than $10^{-6}M$ or the "active solution" contained enough inactive iodine to maintain the concentration in the reaction mixture at $\sim10^{-6}M$, the addition of small quantities of inactive iodine having little effect on the total iodine concentration. Similar results were obtained on oxidation of iodine with acid solutions of cerium(IV) sulfate.

Further Investigations of the Chemical Behavior of the Chemical Fractions

X: A 0.1*f* sodium hydroxide solution containing fraction X was prepared in the usual manner. A 2-ml portion of this solution was mixed with 2 ml of 1*f* sulfuric acid and then extracted with 5 ml of benzene; only 7 percent of the activity was extracted into the benzene. Another portion of the 0.1*f* sodium hydroxide solution containing fraction X was acidified and extracted with a 0.06*f* solution of iodine in benzene; essentially all of the activity was found in the benzene phase. The results of these experiments indicate that fraction X decomposed rapidly and irreversibly in 0.1*f* sodium hydroxide and that the decomposition products exchanged rapidly with molecular iodine.

Y: Our first thought as to the identity of fraction Y was that it was the product of a reaction between benzene and an oxidized, reactive form of iodine, such as HIO, to form phenyl iodide or some other organic-iodine compound. It is interesting to note in this connection that Derbyshire and Waters[6] have observed that HBrO in aqueous acid solution reacts rapidly with benzene to form phenyl bromide.

In an attempt to determine whether fraction Y was phenyl iodide, a solution of fraction Y and inactive phenyl iodide in benzene was fractionally distilled. Practically all of the benzene was recovered free of activity. Some activity distilled over with the phenyl iodide, the successive fractions becoming increasingly richer in activity. The results indicated that not all (less than 70 percent) of fraction Y was phenyl iodide and that at least a part of fraction Y had a higher boiling point than phenyl iodide. It is possible under the conditions of the distillation (185°C), that exchange between fraction Y and phenyl iodide resulted in the appearance of activity in the phenyl iodide fractions.

The extraction of activity from acid dichromate solutions by carbon tetrachloride and toluene was investigated in order to determine whether fraction Y was formed through reaction of an iodine species with the organic solvent or impurities in the solvent. In these experiments 9 percent of the total activity was recovered as fraction Y in toluene and 5 percent in carbon tetrachloride. Since fraction Y appeared in the two solvents, it is unlikely that a simple iodine species reacted with a given organic species contained in the organic phase (solvent or impurity) since the solvent molecules and very probably the impurities were different in each instance. However, if the composition of fraction Y was different in each of the solvents, it is still possible that a simple inorganic species reacted with a solvent molecule or an impurity. In this connection, it is interesting to note that Zeltmann and Kahn[7] obtained results similar to those summarized in Table I, using benzene which was prepared in the laboratory from sodium benzoate and sodium hydroxide. The "carrier-free" iodine was extracted from neutron-irradiated tellurium metal according to the procedure of Kenney and Spragg.[8]

A $6.6\times10^{-5}M$ iodine (inactive) in benzene solution which had stood at room temperature for three months was used to extract an active acid dichromate solution; 6 percent of the total activity was recovered as fraction Y (7 percent as fraction X, 16 percent as fraction Z). If fraction Y (or fraction X or fraction Z) is to be attributed to an impurity in the benzene, this impurity must not have reacted with molecular iodine over a period of three months. (It is assumed that a radioactive iodine species did not exchange with an inactive organic compound of iodine that might have formed.)

In one experiment 0.5 ml of an active acid dichromate solution (0.007*f* $Cr_2O_7^=$, 0.7*f* H_2SO_4) was mixed with 5 ml of 1 *f* sodium hydroxide and the resulting solution

[6] D. H. Derbyshire and W. A. Waters, J. Chem. Soc. **1950**, 573.
[7] A. H. Zeltmann and M. Kahn (private communication), University of New Mexico.
[8] A. W. Kenney and W. T. Spragg, J. Chem. Soc. **1949**, Supplements and Index, 323.

extracted with two 5-ml portions of benzene; 7 percent of the total activity appeared in the first benzene layer; less than 0.1 percent appeared in the second benzene phase. These results suggest that at least part of fraction Y resulted from a reaction between an iodine species and some organic impurity in the aqueous solution.

Z: Experiments were carried out to determine whether fraction Z was iodate or some oxidation state readily exchangeable with iodate. A known amount of potassium iodate was added to a solution containing fraction Z and successive precipitations of silver iodate were carried out. The fraction of total iodate precipitated was determined in each case as well as the percent of total activity carried. These experiments revealed that oxidation in acid cerium(IV) solution, at 105°C, over a seventy-five-minute interval, yielded a fraction Z which was either iodate or some intermediate completely exchangeable with iodate; at room temperature, over a period of one-half hour, less than 20 percent of fraction Z formed was iodate. A similar experiment indicated that less than 10 percent of fraction Z formed by oxidation with acid dichromate at room temperature, over a ten-hour period, was iodate.

I_2: Further experiments were made to test the assumption that the chemical fraction called I_2 was actually molecular iodine. If fraction I_2 was extracted from benzene into water because of the hydrolysis of iodine, then acidification of the water should reverse the equilibrium and fraction I_2 should reappear in the benzene. It was found upon acidification of a 0.5-ml portion of water, containing fraction I_2, with 5 ml of $1f$ sulfuric acid that about 50 percent of the activity was extracted into two 5-ml portions of benzene; a subsequent extraction with a solution of iodine in benzene ($0.02f$ I_2) removed 96 percent of the remaining activity. These results suggest that (1) fraction I_2 was a mixture of molecular iodine and some other species or (2) that one of the hydrolysis products was partly destroyed in the water or in the acidified water (e.g. iodide might have been oxidized by oxygen in acid, or hypo-iodous acid might have been reduced or decomposed), so that iodine could not be quantitatively reformed.

Similar experiments were conducted using water instead of $1f$ sulfuric acid to dilute the water solution of fraction I_2. Only from 5 percent to 10 percent of the activity was extracted into benzene; these results are consistent with the calculated degree of hydrolysis of iodine in dilute solutions.[9]

[9] W. C. Bray and E. L. Connolly, J. Am. Chem. Soc. **33**, 1485 (1911).

DISCUSSION

We believe the most probable explanation of our observations on the oxidation of iodide ion at low concentration in acid solution is the following. During the oxidation in addition to molecular iodine, a reactive form of iodine such as HIO is formed which reacts with trace impurities (molecules or colloids) present in the aqueous solution. At least some of these impurities are organic in nature, and their reaction products with iodine are extracted into organic solvents forming fraction X (products decomposed by hydroxide ion) and fraction Y (products not decomposed by hydroxide ion). Part, but probably not all, of fraction Y may result from a reaction between benzene and a reactive form of iodine such as HIO, similar to the reaction between

TABLE IV. Oxidation of I^- at various concentrations in $0.5f$ H_2SO_4 by $Cr_2O_7^=$ at ~25°C. ($0.005f$ Cr^{III}, $0.005f$ $K_2Cr_2O_7$, 10 min).

Benzene extract, 5 ml	Aqueous extract of benzene, 5 ml	Chemical fraction	Percent of activity,[a] concentration of I^-, $f \times 10^6$ 600	60	6	0.6	0.06	Carrier-free
A	H_2O-A		3	10	31	44	40	37
	H_2O-B		3	8	19	4	4	11
	$0.2f$ KI		90	70	22	2	3	2
		I_2	96	88	72	50	47	50
	$0.1f$ NaOH	X	1	4	6	15	15	13
	Left in benzene	Y	1	3	7	9	9	10
B	...		1	1	3	4	4	3
C (I_2 carrier)		I^-	0.5	2	6	9	11	12
Extracted aqueous phase		Z	0.5	2	6	13	14	12

[a] Based on activity recovered.

HBrO and benzene.[6] Fraction Z may be either a product of a reaction between a reactive iodine species and an inorganic-type trace impurity, or a simple inorganic molecule or ion containing iodine in an oxidation state intermediate between $+1$ and $+5$ (e.g., HIO_2) which exists only at low concentration. Drastic oxidizing conditions [hot acid solution of cerium(IV)] are required to break up the iodine-impurity compounds or colloids and complete the oxidation to the $+5$ state.

It is interesting to note that Johnson, Leininger, and Segrè[1] observed incomplete extraction of astatine from organic solvents by aqueous sodium hydroxide. They also were troubled by loss of astatine activity to the walls of glass vessels during centrifugation, and they attributed this to the reaction of astatine with impurities in solution.

Molecular Size Distribution in the Copolymerization of N-Carboxyamino Acid Anhydrides

LOUIS GOLD
Lincoln Laboratory, Massachusetts Institute of Technology, Cambridge, Massachusetts
(Received November 25, 1952)

The theory of molecular size distributions which are intrinsically Poisson in character is extended to cover two complementary aspects of copolymerization which are specifically adapted to polypeptide synthesis via the N-carboxyamino acid anhydride (Leuchs monomer). The statistical aspects for (1) discrete monomer reacting with a Poisson ensemble of initiators and (2) the circumstance of an array of monomers copolymerized by a discrete initiator are delineated. Explicit relations for the number and weight average molecular weights are derived.

IT is generally recognized that the molecular size distribution arising from the polymerization of an N-caboxyamino acid anhydride is described by the very relations derived by Flory[1] for the polymerization of ethylene oxide.[2] Indeed, Waley and Watson have succeeded in demonstrating that the kinetics of the polymerization of sarcosine carbonic anhydride accord with the type of polymerization where only monomer can react with polymer, but interaction between polymer molecules does not occur.[3] This latter work is representative of current interest in polypeptide synthesis for which no explicit theory is available to predict the molecular size distribution originating in variations of the polymerization process; the Flory relations cannot be directly applied, for example, to the theoretical deduction of the molecular size distribution for a copolymer.

The present communication is in fact a generalization of the Flory analysis, with provision made for the simultaneous reaction of any number of discrete monomer species with diverse assortments of initiator. Two particular cases have already found their way into actual practice:[4] First, there is the copolymer prepared by reacting a mixture of equimolar quantities of two N-carboxyamino acid anhydrides with the same catalyst; second, Waley, has effected a copolymer of glycine and sarcosine by initiating the polymerization of N-carboxyglycine anhydride by a sarcosine polymer. The findings of this report not only elucidate the molecular size distribution and the associated statistical molecular weights for such preparations but also afford a basis for arriving at patterns of protein synthesis in the procurement of desired properties. The relative value of procedural arrangements as to order and concentration of monomer and initiator may be guided by the deductions to follow.

Before embarking into the main body of this report, it should be pointed out that the foundations of the theory of molecular size distribution provided in the researches of Schulz[5] and Dostal and Mark[6] are sufficiently well known to make a completely detailed development somewhat needless. Also, a wealth of background material covering copolymerization of vinyl polymers[7] renders a proper setting for the chief contents of this writing; however, the fact that there exists a distinct difference in the mechanism for the growth of macromolecules for the polymers in this class and those derived from Leuchs monomers is the *raison d'être* for this writing.

STATISTICAL ASPECTS OF A DISCRETE LEUCHS MONOMER REACTING WITH AN ENSEMBLE OF INITIATORS

The type of copolymerization we are considering here may be symbolically represented by the kinetic equation

$$\frac{dN_R}{dt}=-f(N_{01}+N_{02}+\cdots N_{0n})=-f\sum_{j=1}^{n}N_{0j}, \quad (1)$$

where N_R denotes the number of Leuchs molecules supplying the R groups to the array of initiators N_{0j}; the form of (1) implies equal reactivities of the various catalysts.

An especially meaningful ramification of this sort of polymerization is associated with the situation where N_{0j} concentrations are defined by a Poisson distribution, i.e.,

$$\frac{N_{0j}}{N_0}=\frac{e^{-\nu_0}\nu_0^{j-1}}{(j-1)!} \quad (2)$$

with N_0 properly the original number of a single type initiator employed in the preparation of this polymer, which in turn serves as initiator in the subsequent polymerization. The index of the distribution ν_0 is given by

$$\nu_0=N_{R0}/N_0, \quad (3)$$

where N_{R0} represents the number of monomer mole-

[1] P. J. Flory, J. Am. Chem. Soc. **62**, 1561 (1940).
[2] E. Katchalski, *Advances in Protein Chemistry* (Academic Press, Inc., New York, 1951), Vol. VI, pp. 145–152.
[3] S. G. Waley and J. Watson, Proc. Roy. Soc. (London) **A199**, 499 (1949).
[4] See reference 2, pp. 152–153.
[5] G. V. Schulz, Z. Physik. Chem. **B30**, 379 (1935).
[6] H. Dostal and H. Mark, Z. Physik. Chem. **B29**, 299 (1935).
[7] H. Mark and A. V. Tobolsky, *Physical Chemistry of High Polymeric Systems* (Interscience Publishers, New York, 1950), Chapter XII.

cules participating in the initial polymerization. Consequently Eq. (1) reduces simply to

$$\frac{dN_R}{dt} = -fN_0, \tag{4}$$

whereby the subsequent polymerization generates the mole fraction distribution still Poisson in character, *viz.*,

$$\frac{N_{xt}}{N_0} = \frac{e^{-\nu_t}\nu_t^{x-1}}{(x-1)!}, \quad \nu_t = \frac{N_R}{N_0}, \tag{5}$$

where N_{xt} represents the total number of x-mer species summed over all j units.

Accordingly the resultant molecular weight for each combination of $(x-1)$ units of M_R and $(j-1)$ of M_{R_0} is taken to be

$$M_{xj} = (x-1)M_R + (j-1)M_{R_0} + M_0, \tag{6}$$

where M_0 is the contribution from the initiator associated with the distribution (2). Thus each x-mer in the new distribution (5) has an expected or weighted molecular weight,

$$M_{xt} = (x-1)M_R + (\bar{j}_w - 1)M_{R_0} + M_0, \tag{7}$$

with $\bar{j}_w$ the weighted average of j deduced in the usual manner from (2) to be

$$\bar{j}_w = \frac{\nu_0^2 + 3\nu_0 + 1}{\nu_0 + 1}. \tag{8}$$

Hence the number average molecular weight we find is

$$M\bar{x}_{nt} = \nu_t M_R + (\bar{j}_w - 1)M_{R_0} + M_0, \tag{9}$$

where we have made use of the number-average x-mer relation

$$\bar{x}_{nt} = \nu_t + 1 \tag{10}$$

readily derived from (5).

The companion weight-average molecular weight is found from the associated weight distribution function of (5),

$$w_{xt} = \frac{(x-1)M_R + (\bar{j}_w - 1)M_{R_0} + M_0}{\nu t M_R + (\bar{j}_w - 1)M_{R_0} + M_0} \cdot \frac{N_{xt}}{N_0}, \tag{11}$$

from whence the weight-average x-mer result calculates as

$$\bar{x}_{wt} = \frac{\nu_t(\nu_t+2)M_R + (\nu_t+1)[(\bar{j}_w - 1)M_{R_0} + M_0]}{\nu_t M_R + (\bar{j}_w - 1)M_{R_0} + M_0} \tag{12}$$

and

$$M\bar{x}_{wt} = \frac{\nu_t(\nu_t+1)M_R + \nu_t\nu_0\left(\frac{\nu_0+2}{\nu_0+1}\right)M_{R_0} + \nu_t M_0}{\nu_t M_R + \nu_0\left(\frac{\nu_0+2}{\nu_0+1}\right)M_{R_0} + M_0} M_R + \nu_0\left(\frac{\nu_0+2}{\nu_0+1}\right)M_{R_0} + M_0. \tag{13}$$

Thus we have characterized the statistical nature of the copolymer synthesized by the addition of monomer to a previously prepared batch of Leuchs type polymer. It should be pointed out that, whereas there is no definite information as to the relative reactivities of individual Leuchs monomers, the work of Waley and Watson (referred to earlier) does support the assumption of equal reactivity of polymer molecules, regardless of chain length. Presumably then, relation (1) is likely valid for the interaction of a polymerized Leuchs compound with a Leuchs monomer. Furthermore, we observe that where the various initiators differ chemically, it may be necessary to modify (1); but where the initiator molecule is of low molecular weight and the mean polymer molecular weight reasonably high, *ca* 100 or more monomer units, this is a consideration of no great consequence.

STATISTICAL ASPECTS FOR A MIXTURE OF LEUCHS MONOMERS OF VARIABLE REACTIVITY INITIATED BY A DISCRETE SPECIES

We turn now to an alternate scheme of copolymerization more closely allied to the prevailing state of affairs in vinyl copolymerization. For simplicity we consider a binary system and deduce results which can readily be extended to any number of participating monomers.

Thus, for the copolymerization of two N-carboxyamino acid anhydrides whose initial concentrations are $N_{R_a}{}^0$ and $N_{R_b}{}^0$ molecules, the Poisson distribution index is

$$\nu_t = (N_{R_a}' + N_{R_b}')/N_0, \tag{14}$$

where N_{R_a}' and N_{R_b}' are evidently the instantaneous concentrations of monomer that have reacted with N_0 molecules of catalyst. Clearly, the problem of characterizing the molecular size distribution centers about interrelating N_{R_a}' and N_{R_b}' in terms of their initial concentrations and relative reaction rates with the initiator.

The over-all kinetic equation

$$\frac{d(N_{R_a} + N_{R_b})}{dt} = -fN_0 \tag{15}$$

obviously entails the separate equations for the individual components, *viz.*,

$$\begin{cases} \dfrac{dN_{R_a}}{dt} = -f_a \cdot \dfrac{N_{R_a}}{N_{R_a} + N_{R_b}} \cdot N_0 \\ \dfrac{dN_{R_b}}{dt} = -f_b \cdot \dfrac{N_{R_b}}{N_{R_a} + N_{R_b}} \cdot N_0, \end{cases} \tag{16}$$

where f_a and f_b are the rate constants for the two species related to f as prescribed by

$$f = f_a \cdot \frac{N_{R_a}}{N_{R_a} + N_{R_b}} + f_b \cdot \frac{N_{R_b}}{N_{R_a} + N_{R_b}}. \tag{17}$$

The N_{R_a} and N_{R_b} quantities are the unreacted concentrations of the monomers.

Elimination of the time variable enables us to write for (16)

$$\frac{dN_{R_a}}{dN_{R_b}}=\frac{f_a}{f_b}\cdot\frac{N_{R_a}}{N_{R_b}}, \tag{18}$$

which integrated from $N_{R_a}^0$ to N_{R_a} and $N_{R_b}^0$ to N_{R_b}, followed by elimination of logarithmic form, yields the familiar Rayleigh[8]-type relation

$$N_{R_a}/N_{R_a}^0=(N_{R_b}/N_{R_b}^0)^r \tag{19}$$

with

$$f_a/f_b=r. \tag{20}$$

This result closely parallels that derived for the earlier versions of vinyl copolymerization theory;[9] however, it is also analogous to findings originating from the effusion fractionation of isotopes and the related field of fractional distillation.[10]

Now making use of the conservation conditions

$$\begin{cases} N_{R_a}'+N_{R_a}=N_{R_a}^0 \\ N_{R_b}'+N_{R_b}=N_{R_b}^0 \end{cases} \tag{21}$$

we transform (19) to the more useful result

$$N_{R_a}'/N_{R_a}^0=1-(1-N_{R_b}'/N_{R_b}^0)^r \tag{22}$$

so that replacement of N_{R_a}' in (14) can be carried out, giving

$$\nu_t=\frac{1}{N_0}\{N_{R_a}^0[1-(1-N_{R_b}'/N_{R_b}^0)^r]+N_{R_b}'\}. \tag{23}$$

It is evident that $r\to 0$, i.e., $f_a\ll f_b$, reduces this to

$$\nu_t=N_{R_b}'/N_0, \quad r\to 0, \tag{24}$$

while the other limiting circumstance $r\to\infty$, i.e., $f_a\ll f_b$, may be readily analyzed by writing (23) in an alternate form in terms of N_{R_a}',

$$\nu_t=\frac{1}{N_0}\{N_{R_a}'+N_{R_b}[1-(1-N_{R_a}'/N_{R_a}^0)^{1/r}]\}, \tag{25}$$

whereby it is immediately manifest that

$$\nu_t=N_{R_a}'/N_0, \quad r\to\infty. \tag{26}$$

Next the molecular weight of x-mer in the Poisson distribution is given by

$$M_{x,\,a+b}=(x-1)M_t+M_0, \tag{27}$$

where

$$M_t=\frac{N_{R_a}'}{N_{R_a}'+N_{R_b}}\cdot M_{R_a}+\frac{N_{R_b}'}{N_{R_a}'+N_{R_b}'}\cdot M_{R_b}. \tag{28}$$

M_{R_a} and M_{R_b} denote the molecular weights of the polypeptide groups R_a and R_b. Elimination of either N_{R_a}' or N_{R_b}', whichever is more convenient, alters (28) to

$$M_t=\frac{N_{R_a}^0[1-(1-N_{R_b}'/N_{R_b}^0)^r]M_{R_a}+N_{R_b}'M_{R_b}}{N_{R_a}^0[1-(1-N_{R_b}'/N_{R_b}^0)^r]+N_{R_b}'} \tag{29}$$

or

$$M_t=\frac{N_{R_b}^0[1-(1-N_{R_a}'/N_{R_a}^0)^{1/r}]M_{R_b}+N_{R_a}'M_{R_a}}{N_{R_b}^0[1-(1-N_{R_a}'/N_{R_a}^0)^{1/r}]+N_{R_a}'}. \tag{29a}$$

Now with ν_t and M_t delineated in terms of the basic parameters for the copolymer synthesis we can describe the weight distribution via

$$w_{x,\,t}=\frac{(x-1)M_t+M_0}{\nu_t M_t+M_0}\cdot\frac{e^{-\nu_t}\nu_t^{x-1}}{(x-1)!}. \tag{30}$$

Then from the relations

$$M\bar{x}_{n,\,t}=\nu_t M_t+M_0 \tag{31}$$

and

$$M\bar{x}_{w,\,t}=\frac{\nu_t(\nu_t+1)M_t^2+M_tM_0\nu_t}{\nu_tM_t+M_0}+M_0 \tag{32}$$

we can write explicit results for the number-average and weight-average molecular weights, respectively. Equations (30), (31), and (32) follow directly from the same considerations encountered in the previous section.

The foregoing argument can next be generalized to cover the circumstance of unlimited numbers of Leuchs monomers reacting with sundry rates. Thus, if we represent our reference or standard monomer group by R_s and let R_1, $R_2\cdots R_n$ be the other monomer groups, then for ν_t we can show

$$\nu_t=\frac{1}{N_0}\left\{\sum_{j=1}^{n}N_{R_j}^0\left[1-\left(1-\frac{N_{R_s}'}{N_{R_s}^0}\right)^{r_j}\right]+N_{R_s}'\right\}, \tag{33}$$

where

$$r_j=f_j/f_s, \quad j=1,\,2,\,\cdots n. \tag{34}$$

The task is completed by deducing for M_t

$$M_t=\frac{\sum_{j=1}^{n}N_{R_j}^0M_{R_j}[1-(1-N_{R_s}'/N_{R_s}^0)^{r_j}]+N_{R_s}'M_{R_s}}{\sum_{j=1}^{n}N_{R_j}^0[1-(1-N_{R_s}'/N_{R_s}^0)^{r_j}]+N_{R_s}'}, \tag{35}$$

where the M_{R_j} are the molecular weights of the R_j groups for the diverse species.

[8] Lord Rayleigh, Phil. Mag. **III**, 493 (1896).
[9] F. T. Wall, J. Am. Chem. Soc. **63**, 1862 (1941).
[10] K. Cohen, *The Theory of Isotope Separation* (McGraw-Hill Book Company, Inc., New York, 1951), p. 150.

The Polarizability and Configuration of *n*-Paraffins*

RICHARD S. STEIN
Department of Chemistry, University of Massachusetts, Amherst, Massachusetts
(Received February 23, 1953)

The principal polarizabilities of a flexible paraffin hydrocarbon molecule may be calculated from the bond polarizabilities. The result will depend upon the average configuration of the molecule. The light scattering depolarization which is calculated from these polarizabilities may be compared with measured values. The comparison favors a configuration requiring preferential *trans*-arrangements about carbon-carbon single bonds.

INTRODUCTION

THE average shape of a *n*-paraffin molecule larger than propane depends on such factors as the degree of freedom of rotation about the C—C bonds and the attractive and repulsive forces between portions of the chain. A measurement of the shape provides information about the nature of these interactions. Ubbelohde *et al.* have recently published[1] the results of some measurements of the viscosities of gaseous hydrocarbons from which they conclude that these molecules are considerably more compact than would be expected from statistical considerations.[2] In view of this somewhat surprising conclusion, the present work was undertaken in an effort to establish the configuration by an independent method.

THE ANISOTROPY OF POLARIZABILITY

In general, a molecule has three principal polarizabilities, P_1, P_2, and P_3 which are unequal except in the case of isotropic molecules. A highly extended molecule will have one of its principal polarizabilities considerably greater than the others, while a compact or more tightly coiled molecule will be more nearly isotropic and the polarizabilities will be more nearly equal.

The depolarization of scattered light for molecules in the gas phase having their greatest dimension small compared with the wavelength of the light is given by the theory of Gans,[3] where ρ_v is the ratio of the horizontally,

$$\rho_v=\frac{6\delta}{5+7\delta}, \tag{1}$$

polarized to vertically polarized components of the scattered light for unpolarized incident light:

$$\delta=\frac{P_1^2+P_2^2+P_3^2-P_1P_2-P_1P_3-P_2P_3}{(P_1+P_2+P_3)^2}. \tag{2}$$

If one can calculate P_1, P_2, and P_3 for an assumed configuration of the molecule one may check this assumption by comparing the measured depolarization with the calculated value.

THE CALCULATION OF PRINCIPAL POLARIZABILITIES

The calculation of principal polarizabilities is dependent upon the additivity of bond polarizabilities. The values of principal bond polarizabilities given by Denbigh[4] are used in this work. These are given in Table I for the C—C and C—H bonds. b_1 is the polarizability along the axis of the bond and b_2 that perpendicular to the bond axis. If a bond i makes an angle θ_i with one of the principal axes, its contribution to the polarizability along this axis will be[5]

$$\begin{aligned}(P_1)_i&=b_{1i}\cos^2\theta_i+b_{2i}\sin^2\theta_i\\&=(b_{1i}-b_{2i})\cos^2\theta_i+b_{2i}.\end{aligned} \tag{3}$$

The total polarizability along this axis is found by summing the contribution of all of the bonds,

$$\begin{aligned}P_1=(b_{1CC}-b_{2CC})\sum_i\cos^2\theta_i+n_{CC}b_{2CC}\\+(b_{1CH}-b_{2CH})\sum_j\cos^2\theta_j+n_{CH}b_{2CH}.\end{aligned} \tag{4}$$

b_{1CC} is the polarizability along the axis of the C—C bond, etc. The summation over i is over all C—C bonds, and that over j is over all C—H bonds; n_{CC} and n_{CH} are the numbers of C—C and C—H bonds, respectively.

If $\boldsymbol{\sigma}_i$ is a vector in the direction of the ith bond and $\mathbf{M}$ a vector along the axis of P_1, then from the definition of the scalar product of two vectors,

$$\cos^2\theta_i=\frac{(\boldsymbol{\sigma}_i\cdot\mathbf{M})^2}{|\boldsymbol{\sigma}_i|^2|\mathbf{M}|^2} \tag{5}$$

TABLE I. The polarizabilities of some bonds.

Bond	$b_1\times10^{25}$ cm³	$b_2\times10^{25}$ cm³
C—C	18.8	0.2
C—H	7.9	5.8

* Presented in part before the National meeting of the American Chemical Society in Atlantic City, New Jersey, September, 1952. The work was supported in part by the U. S. Office of Naval Research.

[1] McCoubrey, McCrea, and Ubbelohde, J. Chem. Soc. **439**, 1961 (1951).
[2] W. J. Taylor, J. Chem. Phys. **16**, 257 (1948).
[3] R. Gans, Ann. Physik (4) **37**, 881 (1912).
[4] K. G. Denbigh, Trans. Faraday Soc. **36**, 936 (1940).
[5] W. Kuhn and F. Grün, Kolloid-Z. **101**, 248 (1942).

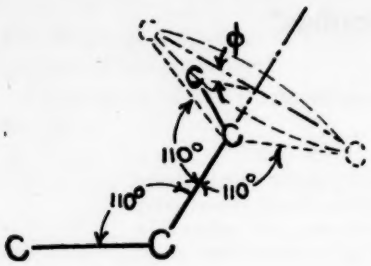

FIG. 1. The angle of internal rotation about the C−C bond.

and

$$Q_{CC}=\sum_i \cos^2\theta_i=\sum_i \frac{(\boldsymbol{\sigma}_i\cdot\mathbf{M})^2}{|\boldsymbol{\sigma}_i|^2|\mathbf{M}|^2}; \quad (6)$$

similarly

$$Q_{CH}=\sum_j \cos^2\theta_j=\sum_j \frac{(\boldsymbol{\sigma}_j\cdot\mathbf{M})^2}{|\boldsymbol{\sigma}_j|^2|\mathbf{M}|^2}. \quad (7)$$

Then

$$P_1=(b_{1CC}-b_{2CC})Q_{CC}+(b_{1CH}-b_{2CH})Q_{CH}+n_{CC}b_{2CC}+n_{CH}b_{2CH}. \quad (8)$$

The C−C bonds make tetrahedral angles with each other. The potential energy of a set of three C−C bonds depends upon the angle of internal rotation, ϕ, (see Fig. 1) in a manner which was described by Pitzer[6] and others[7] and is plotted in Fig. 2. There are 3 potential energy minima which are lower in energy by about 3000 cal/mole than the maxima. At room temperature, it is approximately 150 times more probable that the bonds will be in a configuration corresponding to an energy minimum than one corresponding to a maximum. Thus, it is most probable that the molecules will have all their C−C bonds in arrangements corresponding to these energy minima. Since the molecules will spend most of the time in these equilibrium configurations, they will be the only ones which we shall consider. That is, the hydrocarbon will be considered to consist of a mixture of rotational isomers.

It has been shown[8] that if the molecule is in such an equilibrium configuration, all of the carbon atoms will have their centers at the lattice points of a diamond lattice. In this case, the bond vectors bear a simple relationship to each other. If the vector $\boldsymbol{\sigma}_1$ associated with the first C−C bond is taken with the coordinates (111) (with arbitrary length of $\sqrt{3}$ lattice units), $\boldsymbol{\sigma}_2$ the lattice vector for the second C−C bond must have the coordinates $(\bar{1}11)$, $(1\bar{1}1)$, or $(11\bar{1})$. If $\boldsymbol{\sigma}_2$ has coordinates $(11\bar{1})$, then $\boldsymbol{\sigma}_3$ must be $(\bar{1}1\bar{1})$, $(1\bar{1}\bar{1})$, or (111). The coordinates of any lattice vector may be obtained from the previous one by changing the sign of any *one* of the three components. Since the orientation of two of the bonds determines the position of the molecule as a whole in space, and since there are three possible orientations for each additional bond, the number of different equilibrium internal configurations for a chain consisting of n bonds is 3^{n-2}. The $\boldsymbol{\sigma}_i$'s of the four C−C bonds for the nine configurations of n-pentane are listed in Table II. The components of the vector R connecting the first and last carbon atoms may be found by adding together the four bond vectors,

$$\mathbf{R}=\sum_{i=j}^{4}\boldsymbol{\sigma}_i. \quad (9)$$

The square of the length of this vector is found by adding together the squares of the three components of R and is given in the column labeled R^2.

Configuration No. 1 corresponds to the completely stretched out planar zig-zag configuration in which two sets of three C−C bonds are in the *trans*-configuration ($n_{trans}=2$) while the other configurations are more coiled in which one or no sets of C−C bonds are *trans*.

The coordinates, $\boldsymbol{\sigma}_j$, of the C−H bonds may be designated in a similar manner. While the C−H and C−C bonds are not of the same length, and the hydrogen atoms do not lie directly on the lattice points of a diamond lattice, one may still represent the C−H bonds by vectors in this lattice, since only the directions of the bond vectors are important. The method for designating these bonds for n-pentane is indicated in Fig. 3. The coordinates of these vectors are then the remaining possible vectors in the diamond lattice after the (C−C) bond vectors have been placed in the lattice. These vectors are listed in Table III for n-

TABLE II. The configurations of n-pentane.

Config. No.	$\boldsymbol{\sigma}_1$	$\boldsymbol{\sigma}_2$	$\boldsymbol{\sigma}_3$	$\boldsymbol{\sigma}_4$	R	R^2	n_{trans}
1	111	$11\bar{1}$	111	$11\bar{1}$	440	32	2
2	111	$11\bar{1}$	111	$1\bar{1}1$	422	24	1
3	111	$11\bar{1}$	111	$\bar{1}11$	242	24	1
4	111	$11\bar{1}$	$1\bar{1}\bar{1}$	$1\bar{1}1$	400	16	0
5	111	$11\bar{1}$	$1\bar{1}\bar{1}$	$11\bar{1}$	$42\bar{2}$	24	1
6	111	$11\bar{1}$	$1\bar{1}\bar{1}$	$\bar{1}\bar{1}\bar{1}$	$20\bar{2}$	8	0
7	111	$11\bar{1}$	$\bar{1}1\bar{1}$	$\bar{1}11$	040	16	0
8	111	$11\bar{1}$	$\bar{1}1\bar{1}$	$\bar{1}\bar{1}\bar{1}$	$02\bar{2}$	8	0
9	111	$11\bar{1}$	$\bar{1}1\bar{1}$	$11\bar{1}$	$24\bar{2}$	24	1

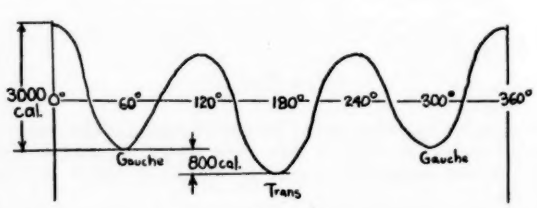

FIG. 2. The molar potential energy of a C−C bond as a function of the angle of internal rotation. The "equilibrium configurations" correspond to the *trans*- and the two *gauche*-positions.

[6] J. D. Kemp and K. S. Pitzer, J. Am. Chem. Soc. **59**, 276 (1937); K. S. Pitzer and J. D. Kemp, J. Am. Chem. Soc. **60**, 1515 (1938), K. S. Pitzer, J. Chem. Phys. **12**, 310 (1944). Beckett, Pitzer, and Spitzer, J. Am. Chem. Soc. **69**, 2488 (1947).

[7] Kistiakowsky, Lacher, and Stitt, J. Chem. Phys. **7**, 289 (1934).

[8] Tobolsky, Powell, and Eyring. "Elastic Viscous Properties of Matter" in Burke and Grummit, *The Chemistry of Large Molecules* (Interscience Publishers, Inc., New York, 1943), p. 156.

pentane. In order to calculate the Q's in Eqs. (6) and (7), it is necessary to know the coordinates of the vector **M** in the direction of a principal polarizability axis. This direction is characterized by the polarizability P_1 having its maximum value in this direction. In practice, **M** is assigned the arbitrary coordinates $(1, y, z)$ where y and z are variable.† Then the Q's are expressed in terms of these variables.

For example, for configuration No. 2 for pentane,

$$Q_{CC}=\frac{4}{3}\left(1+\frac{y+z}{1+y^2+z^2}\right) \tag{10}$$

and

$$Q_{CH}=4\left(1-\frac{2}{3}\frac{y+z}{1+y^2+z^2}\right). \tag{11}$$

Then from Eqs. (4) through (7)

$$P_1=\frac{4}{3}(b_{1CC}-b_{2CC})+4(b_{1CH}-b_{2CH})+4b_{2CC}+12b_{2CH}$$
$$+\left[\frac{4}{3}(b_{1CC}-b_{2CC})-\frac{8}{3}(b_{1CH}-b_{2CH})\right]\frac{y+z}{1+y^2+z^2}. \tag{12}$$

To find the values of y and z corresponding to a maximum P_1, the partial derivatives $(\partial P_1/\partial y)$ and $(\partial P_1/\partial z)$ are equated to zero. This gives the two equations

$$\left[\frac{4}{3}(b_{1CC}-b_{2CC})-\frac{8}{3}(b_{1CH}-b_{2CH})\right]$$
$$\times\frac{(1+y^2+z^2)-(y+z)(2y)}{1+y^2+z^2}=0 \tag{13}$$

and

$$\left[\frac{4}{3}(b_{1CC}-b_{2CC})-\frac{8}{3}(b_{1CH}-b_{2CH})\right]$$
$$\times\frac{(1+y^2+z^2)-(y+z)(2z)}{1+y^2+z^2}=0. \tag{14}$$

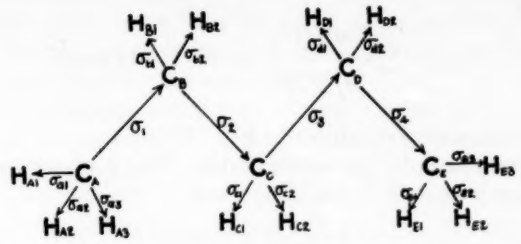

FIG. 3. The designation of the bonds and atoms in n-pentane.

Since $(1+y^2+z^2)$ is finite, these equations reduce to

$$1-y^2+z^2-2yz=0,$$
$$1+y^2-z^2-2yz=0.$$

The solutions of these equations are $x=y=\sqrt{2}/2$, and the coordinates of one of the principal polarizabilities for this configuration are $(1, \sqrt{2}/2, \sqrt{2}/2)$.

The coordinates of the principal polarizability axis, the values of Q_{CC} and Q_{CH} and the polarizabilities along this axis for each of the nine configurations of n-pentane are listed in Table IV.

In a somewhat similar manner one may determine the coordinates of a vector **N** lying in the direction of a second principal axis. The polarizability in this direction is a maximum (or minimum) subject to the constraint that this axis be perpendicular to the first one. That is, the scalar product $(\mathbf{M}\cdot\mathbf{N})$ must be zero. If **N** has the components $(1, u, v)$ and **M** is $(1, y, z)$, then

$$\mathbf{M}\cdot\mathbf{N}=1+uy+vz=0. \tag{15}$$

The polarizability P_2 in the direction of the vector **N** is given by an equation analogous to Eq. (8)

$$P_2=(b_{1CC}-b_{2CC})G_{CC}+(b_{1CH}-b_{2CH})G_{CH}$$
$$+n_{CC}b_{2CC}+n_{CH}b_{2CH}, \tag{16}$$

where

$$G_{CC}=\sum_i\frac{(\boldsymbol{\sigma}_i\cdot\mathbf{N})^2}{|\boldsymbol{\sigma}_i|^2|\mathbf{N}|^2}\quad\text{for all C}-\text{C bonds} \tag{17}$$

TABLE III. The coordinates of the CH bond vectors.

Config. No.	σ_{a_1}	σ_{a_2}	σ_{a_3}	σ_{b_1}	σ_{b_2}	σ_{c_1}	σ_{c_2}	σ_{d_1}	σ_{d_2}	σ_{e_1}	σ_{e_2}	σ_{e_3}
1	$11\bar{1}$	$\bar{1}11$	$1\bar{1}1$	$\bar{1}11$	$1\bar{1}1$	$\bar{1}1\bar{1}$	$\bar{1}\bar{1}\bar{1}$	$\bar{1}11$	$1\bar{1}1$	$\bar{1}1\bar{1}$	$1\bar{1}\bar{1}$	111
2	$11\bar{1}$	$\bar{1}11$	$1\bar{1}1$	$\bar{1}11$	$1\bar{1}1$	$\bar{1}1\bar{1}$	$\bar{1}\bar{1}\bar{1}$	$\bar{1}11$	$11\bar{1}$	$\bar{1}\bar{1}1$	111	$1\bar{1}\bar{1}$
3	$11\bar{1}$	$\bar{1}11$	$1\bar{1}1$	$\bar{1}11$	$1\bar{1}1$	$\bar{1}1\bar{1}$	$\bar{1}\bar{1}\bar{1}$	$1\bar{1}1$	$11\bar{1}$	111	$\bar{1}\bar{1}1$	$\bar{1}1\bar{1}$
4	$11\bar{1}$	$\bar{1}11$	$1\bar{1}1$	$\bar{1}11$	$1\bar{1}1$	$\bar{1}1\bar{1}$	111	$\bar{1}\bar{1}\bar{1}$	$11\bar{1}$	$\bar{1}\bar{1}1$	111	$1\bar{1}\bar{1}$
5	$11\bar{1}$	$\bar{1}11$	$1\bar{1}1$	$\bar{1}11$	$1\bar{1}1$	$\bar{1}1\bar{1}$	111	$\bar{1}\bar{1}\bar{1}$	$1\bar{1}1$	$1\bar{1}\bar{1}$	$1\bar{1}\bar{1}$	111
6	$11\bar{1}$	$\bar{1}11$	$1\bar{1}1$	$\bar{1}11$	$1\bar{1}1$	$\bar{1}1\bar{1}$	111	$11\bar{1}$	$1\bar{1}1$	$1\bar{1}\bar{1}$	$\bar{1}1\bar{1}$	$\bar{1}\bar{1}1$
7	$11\bar{1}$	$\bar{1}11$	$1\bar{1}1$	$\bar{1}11$	$1\bar{1}1$	$1\bar{1}\bar{1}$	111	$11\bar{1}$	$\bar{1}\bar{1}\bar{1}$	111	$\bar{1}\bar{1}1$	$\bar{1}1\bar{1}$
8	$11\bar{1}$	$\bar{1}11$	$1\bar{1}1$	$\bar{1}11$	$1\bar{1}1$	$1\bar{1}\bar{1}$	111	$11\bar{1}$	$\bar{1}11$	$1\bar{1}\bar{1}$	$\bar{1}1\bar{1}$	$\bar{1}\bar{1}1$
9	$11\bar{1}$	$\bar{1}11$	$1\bar{1}1$	$\bar{1}11$	$1\bar{1}1$	$1\bar{1}\bar{1}$	111	$\bar{1}\bar{1}\bar{1}$	$\bar{1}11$	$\bar{1}1\bar{1}$	$\bar{1}1\bar{1}$	111

† The x coordinate of M may be arbitrarily taken as 1 since its magnitude is arbitrary and only two coordinates are necessary to establish its direction.

and

$$G_{CH}=\sum_i \frac{(\boldsymbol{\sigma}_j\cdot\mathbf{N})^2}{|\boldsymbol{\sigma}_j|^2|\mathbf{N}|^2} \text{ for all C}-\text{H bonds.}$$

P_2 is maximized subject to Eq. (15).

For example, for configuration No. 2 of *n*-pentane where $y=z=\sqrt{2}/2$, Eq. (15) gives

$$1+\sqrt{2}/2(u+v)=0$$

so

$$v=-(u+\sqrt{2}) \tag{18}$$

and $\mathbf{N}$ has components $(1, u, -(u+\sqrt{2}))$.

Then

$$G_{CC}=\frac{4}{3}\left(1-\frac{\sqrt{2}}{2u^2+2\sqrt{2}u+3}\right) \tag{19}$$

and

$$G_{CH}=4\left(1+\frac{2}{3}\frac{\sqrt{2}}{2u^2+2\sqrt{2}u+3}\right). \tag{20}$$

On substituting (19) and (20) into Eq. (16) and setting the derivative of P_2 with respect to u equal to zero, one gets on simplifying that

$$u=-\sqrt{2}/2. \tag{21}$$

From Eq. (18),

$$v=-\sqrt{2}/2. \tag{22}$$

These correspond to $G_{CC}=0.390$, $G_{CH}=5.89$, and P_2 9.01×10^{-24} cm³.

These data are recorded for all nine configurations of *n*-pentane in Table V. The values of P_3, the polarizability along the third principal axis, are obtained by subtracting P_1+P_2 from three times the average polarizability of *n*-pentane, which is 31.08×10^{-24} cm³. Values of δ and ρ are calculated using Eqs. (1) and (2).

THE AVERAGE DEPOLARIZATION

If all of the configurations are equally probable, the average depolarization of *n*-pentane is found from the simple average of all the ρ's of Table V. This value, 0.0054, is compared in Table VI, in the column labeled Free rotation, with experimental values of ρ reported by Bhagavantam[9] and Cabannes[10] for gaseous *n*-paraffins. The values for some of the other *n*-paraffins were calculated in a similar manner and are also reported here. One finds, especially with the larger paraffins, that the calculated value is lower than the experimental. This is to be expected, since all of the configurations are not equally probable. Statistical theory (2) indicates that the more extended configurations are the more probable.

TABLE IV. The principal polarizabilities for the configurations of pentane.

Config. No.	Coordinates of M	Q_{CC}	Q_{CH}	$P_1\times10^{24}$ cm³
1	(1, 1, 0)	2.66	1.33	12.31
2	(1, √2/2, √2/2)	2.27	2.12	11.71
3	(1, √2, 1)	2.27	2.12	11.71
4	isotropic[a]	1.33	4.00	10.36
5	(1, √2/2, −√2/2)	2.27	2.12	11.71
6	(1, √2, 1)	2.27	2.12	11.71
7	isotropic[a]	1.33	4.00	10.36
8	(1, √2/2, √2/2)	2.27	2.12	11.71
9	(1, √2, −1)	2.27	2.12	11.71

[a] For the isotropic configurations, the equations of the type of Eq. (14) are independent of y and z, since the polarizability is the same in all directions.

One sees from the potential energy diagram in Fig. 2 that a *trans*-arrangement of three carbon bonds is lower in energy by about 800 cal/mole than the other two (*gauche*) equilibrium arrangements of the bonds. It was pointed out that more of the bonds are in the *trans*-arrangement in the more extended configurations. Consequently, these configurations would have lower energy and be more probable and should be weighted more heavily in averaging the ρ's.

THE WEIGHTING OF *TRANS*-CONFIGURATIONS

If a *trans*-arrangement of three bonds has an energy E_t given by Fig. 2 and a *gauche*-arrangement has an energy E_g, then each configuration may be assigned an energy

$$E=n_tE_t+n_gE_g$$
$$=n_t(E_t-E_g)+nE_g, \tag{23}$$

where n_t, n_g are the numbers of *trans*- and *gauche*-arrangements of three bonds and n is the total number of

TABLE V. The depolarizations for the configurations of pentane.

Config. No.	Coordinates of $\mathbf{N}$	G_{CC}	G_{CH}	$P_2\times10^{24}$ cm³	$P_3\times10^{24}$ cm³	δ	ρ
1	(1, −1, 0)	0	6.67	8.44	10.33	0.0125	0.0133
2	(1, −√2/2, −√2/2)	0.390	5.89	9.01	10.36	0.0050	0.0059
3	(1, −√2/2, 1)	0.390	5.89	9.01	10.36	0.0050	0.0059
4	isotropic	1.33	4.00	10.36	10.36	0	0
5	(1, √2/2, −√2/2)	0.390	5.89	9.01	10.36	0.0050	0.0059
6	(1, −√2, 1)	0.390	5.89	9.01	10.36	0.0050	0.0059
7	isotropic	1.33	4.00	10.36	10.36	0	0
8	(1, −√2/2, −√2/2)	0.390	5.89	9.01	10.36	0.0050	0.0059
9	(1, −√2, −1)	0.390	5.89	9.01	10.36	0.0050	0.0059

[9] S. Bhagavantam, *Scattering of Light and the Raman Effect* (Chemical Publishing Company, Brooklyn, New York, 1942), p. 54.
[10] J. Cabannes, *La diffusion moléculaire de la Lumière* (Presses University France, Paris, 1929).

TABLE VI. A comparison of experimental and calculated depolarizations.

	$\rho \times 10^2$				
	Experimental		Theory		
Substance	Bhagavantam	Cabannes	Free rot.	Rest. rot.	Interact.
Ethane	0.5	1.6	1.35	1.35	1.35
Propane	0.7	1.6	1.03	1.03	1.03
Butane	0.9	1.7	0.88	1.24	1.21
Pentane	1.3	1.3	0.54	0.93	0.86
Hexane	1.5	1.5	...	...	...
Heptane	1.6	1.6	...	...	...
Octane	1.8	1.8	...	...	...

groups of three successive bonds. This is $(N-3)$ where N is the number of carbon atoms in the chain. The average ρ is then found from

$$\rho=\frac{\sum_i \rho_i \exp(-E_i/RT)}{\sum_i \exp(-E_i/RT)} \tag{24}$$

$$=\frac{\sum_i \rho_i [\exp(E_g-E_t/RT)]^{n_{ti}}}{\sum_i [\exp(E_g-E_t/RT)]^{n_{ti}}}, \tag{25}$$

where ρ_i and n_{ti} are the depolarization and the number of *trans*-arrangements in the ith configuration. For $(E_g-E_t)=800$ cal and $T=25°C$, this becomes

$$\rho=\frac{\sum_i \rho_i (3.8)^{n_{ti}}}{\sum_i (3.8)^{n_{ti}}}. \tag{26}$$

This average is listed in Table VI in the column labeled rest. rot. One notes that the values listed are still below the experimental values.

A DETAILED CONSIDERATION OF INTERACTIONS

A third method for averaging the ρ's for the various configurations is to consider in detail the interaction between the various parts of the chain. The origin of the energy difference between the *trans*- and *gauche*-configuration largely originates from the difference in attractive and repulsive energy between the hydrogen atoms. The above treatment neglects two factors: (a) excluded configurations in which two different atoms would have to occupy the same position, and (b) interaction between hydrogens and carbons which are more than three atoms apart.

The approach which will be used is to determine the distances between all pairs of hydrogens in each configuration, calculate the van der Waals energy corresponding to each pair of hydrogens, and sum these for each configuration to obtain the total configurational energy and use this in Eq. (24) to average the ρ's.

If the difference between the C−C and C−H bond lengths is neglected,‡ the hydrogen atoms as well as the carbon atoms will be on the points of a diamond lattice. The lattice coordinate of any hydrogen atom may be obtained by summing the coordinates of all the bond vectors leading from the first carbon atom (at the origin) to the atom in question. The coordinates of all of the atoms in the nine configurations of n-pentane is given in Table VII. The coordinates of the vector connecting any pair of hydrogen atoms may then be found by subtracting the coordinates of these atoms. The square of the distance between these atoms, R^2, may be found by adding together the squares of the three coordinates. In this manner, a table of values of R^2's may be obtained for each configuration.

On carrying out this process for n-pentane, one finds that the nine configurations fall into four classes according to the values of R^2:

Class (a)—Config. No. 1
Class (b)—Configs. No. 2, 3, 5, and 9
Class (c)—Configs. No. 4 and 7
Class (d)—Configs. No. 6 and 8.

All configurations within a given class have the same set of R^2's and the same interaction energy. Class (d) is that of the excluded configurations in which two different hydrogen atoms are in the same place. In Table VIII the number of times that a given value of R^2 appears in each configuration is listed. R^2's are listed in lattice units in which a C−C bond has a length of $\sqrt{3}$. Its value in square angstroms may be obtained by multiplying by $(1.54)^2/3$.

TABLE VII. The coordinates of the atoms in pentane.

Config. No.	C_A	H_{A1}	H_{A2}	H_{A3}	C_B	H_{B1}	H_{B2}	C_C	H_{C1}	H_{C2}	C_D	H_{D1}	H_{D2}	C_E	H_{E1}	H_{E2}	H_{E3}
1	000	$\bar{1}\bar{1}1$	$1\bar{1}\bar{1}$	$\bar{1}1\bar{1}$	111	022	202	220	$13\bar{1}$	$31\bar{1}$	331	242	422	440	$35\bar{1}$	$53\bar{1}$	551
2	000	$\bar{1}\bar{1}1$	$1\bar{1}\bar{1}$	$\bar{1}1\bar{1}$	111	022	202	220	$13\bar{1}$	$31\bar{1}$	331	242	440	422	313	533	511
3	000	$\bar{1}\bar{1}1$	$1\bar{1}\bar{1}$	$\bar{1}1\bar{1}$	111	022	202	220	$13\bar{1}$	$31\bar{1}$	331	422	440	242	353	133	151
4	000	$\bar{1}\bar{1}1$	$1\bar{1}\bar{1}$	$\bar{1}1\bar{1}$	111	022	202	220	$13\bar{1}$	331	$31\bar{1}$	$20\bar{2}$	$42\bar{2}$	400	$3\bar{1}1$	511	$5\bar{1}\bar{1}$
5	000	$\bar{1}\bar{1}1$	$1\bar{1}\bar{1}$	$\bar{1}1\bar{1}$	111	022	202	220	$13\bar{1}$	331	$31\bar{1}$	$20\bar{2}$	400	$42\bar{2}$	$33\bar{3}$	$51\bar{3}$	$53\bar{1}$
6	000	$\bar{1}\bar{1}1$	$1\bar{1}\bar{1}$	$\bar{1}1\bar{1}$	111	022	202	220	$13\bar{1}$	331	$31\bar{1}$	$42\bar{2}$	400	$20\bar{2}$	$31\bar{3}$	$11\bar{3}$	$1\bar{1}\bar{1}$
7	000	$\bar{1}\bar{1}1$	$1\bar{1}\bar{1}$	$\bar{1}1\bar{1}$	111	022	202	220	$31\bar{1}$	331	$13\bar{1}$	$24\bar{2}$	$02\bar{2}$	040	151	$\bar{1}31$	$\bar{1}5\bar{1}$
8	000	$\bar{1}\bar{1}1$	$1\bar{1}\bar{1}$	$\bar{1}1\bar{1}$	111	022	202	220	$31\bar{1}$	331	$13\bar{1}$	$24\bar{2}$	040	$02\bar{2}$	$11\bar{3}$	$\bar{1}3\bar{3}$	$\bar{1}1\bar{1}$
9	000	$\bar{1}\bar{1}1$	$1\bar{1}\bar{1}$	$\bar{1}1\bar{1}$	111	022	202	220	$31\bar{1}$	331	$13\bar{1}$	$02\bar{2}$	040	$24\bar{2}$	$15\bar{3}$	$33\bar{3}$	$35\bar{1}$

‡ The error resulting from this assumption is corrected at a later time.

TABLE VIII. The contributions to the potential energy of interaction in pentane.

	Configuration Nos.					
	1		2		4	
R^2	No. values	Contrib. to $V\times10^{14}$	No. values	Contrib. to $V\times10^{14}$	No. values	Contrib. to $V\times10^{14}$
3	0	0	1	+4.5	2	+9.0
8	6	−5.16	4	−3.44	3	−2.58
11	4	−2.32	7	−4.06	8	−4.64
16	6	−1.26	4	−0.84	5	−1.05
19	4	−0.52	4	−0.52	6	−0.78
24	4	−0.24	10	−0.60	10	−0.60
27	4	−0.16	3	−0.12	2	−0.08
32	2	−0.04	2	−0.04	3	−0.06
35	8	−0.16	4	−0.08	0	0
40	2	−0.02	3	−0.03	4	−0.04
43	0	0	0	0	2	−0.02
51	0	0	1	−0.00	0	0
56	4	0	2	−0.00	0	0
76	1	0	0	0	0	0
Total		−9.88		−5.2		−0.9

The van der Waals energy corresponding to a given R^2 may be calculated using an equation employed by Müller[11] for the calculation of the lattice energy of crystals of the *n*-paraffins,

$$V=\frac{-4.31\times10^{-12}}{r^6}+7.7\times10^{-10}e^{-4.58r},$$

where V is the energy in ergs per molecule and r is the distance between the centers of hydrogen atoms in angstrom units.

A plot of V against R^2 (in lattice units) is given in Fig. 4. The value for the steric energy for each configuration is obtained by adding together all of the V's corresponding to the R^2's for that configuration. For the $R^2=3$ interaction, it is necessary to correct for the assumed identity of the C−C and C−H bond lengths, because of the rapid variation of V with R^2 in this region. Upon doing this, one finds that this R^2 is really 4.5 instead of 3, for which the energy is 4.5×10^{-17} erg. The correction is not important for other values of R^2.

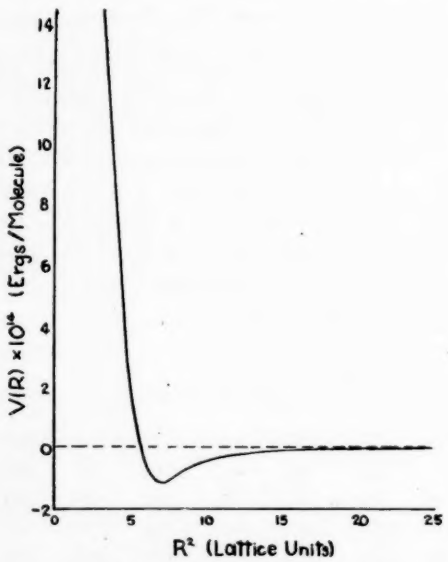

FIG. 4. The variation of the van der Waals interaction energy as a function of the distance between the centers of a pair of hydrogen atoms. The distance is measured in lattice units where the C−C bond has a length of 1.73.

[11] A. Müller, Proc. Roy. Soc. (London) **A154**, 624 (1936); **A178**, 227 (1941).

The total configuration energy for each class configuration for pentane is listed in Table IX. The weighting factor, $\exp(-V/RT)$ used in averaging the P's is listed in the last column of this table. The average ρ's calculated in this manner are listed in the last column of Table VI. These values are not very much different in these cases from the values calculated by simply weighting the trans configurations. The detailed consideration of interaction will, however, be increasingly more important for larger molecules, where interactions between more distant portions of the chain and steric exclusion of configurations become more important.

TABLE IX. The steric energy of the pentane configurations.

Configuration No.	Steric energy Ergs/molecule $\times10^{14}$	Cal/mole	$\exp(-V/RT)$ $T=25°C$
1	−9.9	−1430	11.2
2, 3, 5, 9	−5.2	−750	3.5
4, 7	−0.9	−130	1.2
6, 8	∞	∞	0

CONCLUSION

In all of the cases considered, the calculated value of depolarization is below the experimental. This discrepancy may arise from one or more of the following causes: (a) the experimental values for depolarization may be too high, (b) the values of bond polarizabilities given by Denbigh may be in error, (c) the molecules may be even more extended than statistical theory indicates.

It would seem difficult to reconcile these results with Ubbelohde's conclusion that the molecules are more compact than indicated by statistical theory.

In view of these developments, a reconsideration of the experimental depolarization values seems indicated. A measurement of the temperature dependency of depolarization would be valuable, since the Boltzman weighting factor is temperature dependent. The probability of the various configurations of a molecule should become more nearly equal as the temperature is raised, so the depolarization should increase or decrease with increasing temperature depending on whether the molecule is less or more extended than predicted by the free rotation model.

The Separation of the Rotational Coordinates from the N-Particle Schroedinger Equation. II*

C. F. CURTISS
University of Wisconsin, Naval Research Laboratory, Department of Chemistry, Madison, Wisconsin
(Received January 19, 1953)

Group theoretical methods are used to separate the rotational coordinates from the N-particle Schroedinger equation and obtain a set of equations which are particularly applicable to the study of collisions involving two sets of particles or two molecules. The coordinates used to describe the configuration of the N particles in a center of gravity coordinate system are those describing the orientation of the system as a whole, the relative orientation and separation of the two molecules, and the internal configuration of each of the molecules. Coupled differential equations involving only the coordinates describing the internal configuration and separation of the molecules are obtained. As a special case the equations are applied to a system consisting of two diatomic molecules.

THE separation of the rotational coordinates from the N-particle Schroedinger equation has been discussed in a previous paper.[1] In a succeeding paper,[2] the results were applied to the study of the scattering of atoms by diatomic molecules. Although the extension of these results to the study of collisions between more complex molecules is straightforward, the applications are difficult because of the formidable algebra required in carrying out the necessary changes of variables. It is the purpose of the present paper to apply group theoretical methods to circumvent these difficulties. That is, in the present paper we separate the rotational coordinates from the N-particle Schroedinger equation and obtain a set of equations which are particularly applicable to the study of collisions involving two sets of particles or two molecules.

The group theoretical methods used to accomplish the separation of variables are quite similar to those used in the previous paper.[1] However, in the present paper, as the coordinates describing the configuration of the N particles in the center of gravity coordinate system we use coordinates describing the orientation of the system as a whole, the relative orientation and separation of the two molecules, and the internal configuration of each of the molecules. Coupled differential equations involving only the coordinates describing the internal configuration of the two molecules and the separation of the molecules are obtained. In the equations applying to two diatomic molecules the coupling occurs only because of the potential of interaction between the two molecules. In the treatment of more complicated molecules further coupling occurs. Some of the results given in the present treatment are generalizations of those obtained earlier. These results usually appear somewhat different because of the use of more conventional definitions of the Eulerian angles and the spherical harmonics.

* This work was carried out under Contract DA-11-022-ORD-944 with the Office of Ordnance Research, U. S. Army.
[1] Curtiss, Hirschfelder, and Adler, J. Chem. Phys. **18**, 1638 (1950).
[2] C. F. Curtiss and F. T. Adler, J. Chem. Phys. **20**, 249 (1952).

I. THE SEPARATION OF THE TRANSLATIONAL COORDINATES

Let us consider a set of N particles of masses m_n. The kth coordinate of the nth particle in a space fixed coordinate system is designated x_{nk}. The Schroedinger equation of the set of particles in the space fixed coordinate system is then

$$-\frac{\hbar^2}{2}\sum_{n=1}^{N}\sum_{k=1}^{3}\frac{1}{m_n}\frac{\partial^2\Psi}{\partial x_{nk}^2}+V\Psi=E_T\Psi, \tag{1}$$

where V is the potential energy of the system and E_T is the total energy including that associated with the overall translational motion.

In the present treatment we assume that the set of N particles is made up of particles belonging to each of two molecules. The a particles belonging to the first molecule, molecule a, are numbered 1 to a; the $N-a$ particles belonging to the second molecule, molecule b, are numbered $a+1$ to N. In order to separate the coordinates representing a translation of the system as a whole, we change variables from the $3N$ coordinates x_{nk} to the following sets of variables: (a) $3a-3$ coordinates describing the configuration and orientation of molecule a. For these variables we choose the coordinates of the first $a-1$ particles with respect to the center of mass of molecule a,

$$y_{nk}=x_{nk}-\frac{1}{M_a}\sum_{n'=1}^{a}m_{n'}x_{n'k};\quad n=1,2,\cdots,a-1, \tag{2}$$

where

$$M_a=\sum_{n=1}^{a}m_n \tag{3}$$

is the total mass of molecule a. (b) A similar set of $3N-3a-3$ coordinates describing the configuration and orientation of molecule b,

$$y_{nk}=x_{nk}-\frac{1}{M_b}\sum_{n'=a+1}^{N}m_{n'}x_{n'k};\ n=a+1,a+2,\cdots N, \tag{4}$$

where

$$M_b=\sum_{n=a+1}^{N} m_n \tag{5}$$

is the total mass of molecule b. (c) The three coordinates describing the center of mass of molecule a with respect to that of molecule b,

$$x_k=\frac{1}{M_a}\sum_{n=1}^{a} m_n x_{nk}-\frac{1}{M_b}\sum_{n=a+1}^{N} m_n x_{nk}. \tag{6}$$

(d) The three coordinates of the center of mass of the system of N particles,

$$X_k=\frac{1}{M}\sum_{n=1}^{N} m_n x_{nk}, \tag{7}$$

where

$$M=M_a+M_b=\sum_{n=1}^{N} m_n \tag{8}$$

is the mass of the system as a whole.

The change of variables is straightforward. In terms of the new variables the Schroedinger equation, Eq. (1), is

$$\mathcal{K}_a\Psi+\mathcal{K}_b\Psi-\frac{\hbar^2}{2\mu}\sum_k\frac{\partial^2}{\partial x_k}\Psi \cdot -\frac{\hbar^2}{2M}\sum_k\frac{\partial^2}{\partial X_k^2}\Psi_k+V\Psi=E_T\Psi, \tag{9}$$

where

$$\mu=M_aM_b/M \tag{10}$$

is the reduced mass of the pair of molecules and

$$\mathcal{K}_a=-\frac{\hbar^2}{2}\sum_{n=1}^{a-1}\sum_{n'=1}^{a-1}\sum_{k=1}^{3}\frac{1}{m_n}\left(\delta_{nn'}-\frac{m_n}{M_a}\right)\frac{\partial^2}{\partial y_{nk}\partial y_{n'k}} \tag{11}$$

and

$$\mathcal{K}_b=-\frac{\hbar^2}{2}\sum_{n=a+1}^{N-1}\sum_{n'=a+1}^{N-1}\sum_{k=1}^{3}\frac{1}{m_n}\left(\delta_{nn'}-\frac{m_n}{M_b}\right)\frac{\partial^2}{\partial y_{nk}\partial y_{n'k}} \tag{12}$$

are the operators representing the energy associated with the rotational and internal degrees of freedom of the molecules a and b, respectively.

We assume that the N particles are moving in free space, that is, that the potential energy V does not depend on the coordinates of the center of mass X_k. Then if the total wave function Ψ is written as the product of a function of the coordinates of the center of mass and a function of the remaining coordinates

$$\Psi=f(X_k)\psi(y_{nk}, x_k), \tag{13}$$

it is easy to separate the Schroedinger equation, Eq. (9), into two equations. The equation for $f(X_k)$ is clearly the equation for a free particle of mass M,

$$-\frac{\hbar^2}{2M}\sum_k\frac{\partial^2}{\partial X_k^2}f=E_tf. \tag{14}$$

The ψ equation is

$$\mathcal{K}_a\psi+\mathcal{K}_b\psi-\frac{\hbar^2}{2\mu}\sum_k\frac{\partial^2}{\partial x_k^2}\psi+V\psi=E\psi, \tag{15}$$

where $E=E_T-E_t$ is the energy associated with the rotation and internal motion of the system of N particles.

II. THE SEPARATION OF THE ROTATIONAL COORDINATES

Since the system of N particles is assumed to move in free space the potential energy V is not only invariant under a translation of the coordinate system, it is also invariant under a rotation of the coordinate system. Hence the eigenfunctions of Eq. (I-15) may be chosen in such a manner that they form bases of irreducible representations of the rotation group. Thus,

$$P_R\psi_s{}^J=\sum_\mu D^J(R)_{\mu s}\psi_\mu{}^J, \tag{1}$$

where P_R is the operator which rotates the coordinate system by the rotation R and $\psi_\mu{}^J$ is an eigenfunction with the total angular momentum quantum number J and the quantum number corresponding to the z component of the angular momentum equal to μ.

Now, as in a previous paper,[1] let us choose a "standard configuration" corresponding to each configuration of the N particles in such a way that all configurations which differ only by a pure rotation correspond to the same standard configuration. Let R be the rotation of the coordinate system which brings the set of particles into a standard configuration, so that R indicates the orientation of the system in space. Then

$$P_R\psi_s{}^J(y_{nk}', x_k')=\psi_s{}^J(y_{nk}, x_k), \tag{2}$$

where the primes indicate the values of the coordinates in the rotated coordinate system. Hence, because of the definition of the rotation R the function

$$\chi_s{}^J=\psi_s{}^J(y_{nk}', x_k')=P_{R^{-1}}\psi_s{}^J(y_{nk}, x_k) \tag{3}$$

depends only on the relative configuration and is independent of a rotation of the system as a whole. It follows from Eq. (1) and the last equation that

$$\chi_s{}^J=\sum_\mu D^J(R^{-1})_{\mu s}\psi_\mu{}^J \tag{4}$$

or

$$\chi_s{}^J=\sum_\mu D^J(R)^*{}_{s\mu}\psi_\mu{}^J. \tag{5}$$

Then, since the representation coefficients are orthogonal in the sense that

$$\sum_s D^J(R)_{s\mu'}D^J(R)^*{}_{s\mu}=\delta_{\mu\mu'}, \tag{6}$$

it follows that

$$\psi_\mu{}^J=\sum_s D^J(R)_{s\mu}\chi_s{}^J. \tag{7}$$

This expression is a factorization of the wave function

into a sum of products of functions of the rotational coordinates and the internal coordinates.

The standard configuration may, of course, be chosen in any arbitrary manner. In the present applications it is convenient to choose as the standard configuration of the set of N particles that configuration in which the center of mass of molecule a lies on the positive z axis (the center of mass of molecule b then, of course, lies on the negative z axis) and particle 1 lies on the positive portion of the xz plane. The coordinates in the rotated coordinate system are

$$x_k'=\sum_j R_{kj}x_j, \tag{8}$$

$$y_{nk}'=\sum_j R_{kj}y_{nj}. \tag{9}$$

Then from the definition of the standard configuration the rotation R is defined by the equations

$$\sum_j R_{1j}x_j=0, \tag{10}$$

$$\sum_j R_{2j}x_j=0, \tag{11}$$

$$\sum_j R_{2j}y_{1j}=0. \tag{12}$$

The functions χ_s^J depend only on the internal configuration of the set of N particles. In particular, the χ_s^J may be taken to be functions of the distance between the centers of mass of the two molecules, $x_3'\equiv\rho$ the relative orientation of the two molecules and coordinates describing the internal configurations of each of the molecules. In order to define the relative orientation of the two molecules we introduce the concept of "standard configuration" by a method completely analogous with that used above in discussing the orientation of the complete system in space. The rotations $S^{(a)}$ and $S^{(b)}$ are defined as those rotations of the coordinate system (after the original rotation by R) which bring molecules a and b, respectively, into their standard configurations. Because the orientation of molecule a is partially specified by the original rotation R the rotations $S^{(a)}$ and $S^{(b)}$ depend only on five Eulerian angles. These five coordinates, along with $x_3'\equiv\rho$ and the $(3a-6)+(3N-3a-6)$ coordinates specifying the internal configurations of two molecules, are used as the $3N-6$ coordinates specifying the internal configuration of the system of N particles.

The standard configuration of molecule a is chosen as that configuration in which particle 1 lies on the positive z axis and particle 2 lies on the positive xz plane. The standard configuration of molecule b is defined in a similar manner with particles $a+1$ and $a+2$ playing the special roles. Because of these definitions and the definition of the standard configuration of the system the first Eulerian angle (α) associated with the rotation $S^{(a)}$ is zero.

We denote the coordinates in the final coordinate system by z_{nk}. Then, according to Eq. (9),

$$z_{nk}=\sum_j S_{kj}^{(a)}y_{nj}'=\sum_{j,j'} S_{kj}^{(a)}R_{jj'}y_{nj'} \qquad n=1, 2, \cdots, a-1, \tag{13}$$

$$z_{nk}=\sum_j S_{kj}^{(b)}y_{nj}'=\sum_{j,j'} S_{kj}^{(b)}R_{jj'}y_{nj'} \qquad n=a+1, a+2, \cdots N-1. \tag{14}$$

Thus, if we define

$$R^{(a)}=S^{(a)}R, \tag{15}$$

$$R^{(b)}=S^{(b)}R \tag{16}$$

as the over-all rotations of the coordinate systems, the z_{nk} are

$$z_{nk}=\sum_j R_{kj}^{(a)}y_{nj} \quad n=1, 2, \cdots a-1, \tag{17}$$

$$z_{nk}=\sum_j R_{kj}^{(b)}y_{nj} \quad n=a+1, a+2, \cdots N-1. \tag{18}$$

Because of the definition of the standard configuration of molecule a the rotation $R^{(a)}$ is defined by the following equations:

$$\sum_j R_{1j}^{(a)}y_{1j}=0, \tag{19}$$

$$\sum_j R_{2j}^{(a)}y_{1j}=0, \tag{20}$$

$$\sum_j R_{2j}^{(a)}y_{2j}=0. \tag{21}$$

A similar set of equations define the rotation $R^{(b)}$.

As mentioned above, the χ_s^J may be considered to be functions of the five Eulerian angles defining $S^{(a)}$ and $S^{(b)}$, the distance between the centers of mass of the two molecules ρ, and the set of z_{nk} which define the internal configurations of the two molecules. The set of representation coefficients $D^l(S)_{m\nu}$ form a complete set of functions in the space of all rotations, and the set of coefficients with a specified value of the second subscript form a complete set in the space of all rotations in which the Eulerian angle α is zero. Hence the χ_s^J may be expanded in the form

$$\chi_s^J=\sum_{\substack{l_1m_1\\ l_2m_2\nu}} D^{l_1}(S^{(a)})^*_{m_1,-s-\nu}D^{l_2}(S^{(b)})^*_{m_2\nu}G(Jsl_1m_1l_2m_2\nu|z_{nk}\rho). \tag{23}$$

The expansion coefficients are functions of ρ and the z_{nk}. We will obtain a set of coupled differential equations for functions closely related to the $G(Jsl_1m_1l_2m_2\nu)$.

If the form of $\chi_s{}^J$ as given by the last equation is used in Eq. (7), it follows that

$$\psi_\mu{}^J=\sum_{\substack{l_1m_1s\\l_2m_2\nu}} D^J(R)_{s\mu}D^{l_1}(S^{(a)})^*_{m_1,-s-\nu}D^{l_2}(S^{(b)})^*_{m_2\nu}G(Jsl_1m_1l_2m_2\nu|z_{nk}\rho). \tag{24}$$

It is convenient to write this equation in terms of the rotations $R^{(a)}$ and $R^{(b)}$ defined by Eqs. (15) and (16). Since $S^{(a)}=R^{(a)}R^{-1}$ and $S^{(b)}=R^{(b)}R^{-1}$, it follows that

$$\begin{aligned}D^{l_1}(S^{(a)})^*_{m_1,-s-\nu}&=\sum_{\nu_1} D^{l_1}(R^{(a)})^*_{m_1\nu_1}D^{l_1}(R^{-1})^*_{\nu_1,-s-\nu}\\&=\sum_{\nu_1} D^{l_1}(R^{(a)})^*_{m_1\nu_1}D^{l_1}(R)_{-s-\nu,\nu_1},\end{aligned} \tag{25}$$

$$\begin{aligned}D^{l_2}(S^{(b)})^*_{m_2\nu}&=\sum_{\nu_2} D^{l_2}(R^{(b)})^*_{m_2\nu_2}D^{l_2}(R^{-1})^*_{\nu_2\nu}\\&=\sum_{\nu_2} D^{l_2}(R^{(b)})^*_{m_2\nu_2}D^{l_2}(R)_{\nu\nu_2}.\end{aligned} \tag{26}$$

Thus in terms of R, $R^{(a)}$, and $R^{(b)}$ the wave function is

$$\psi_\mu{}^J=\sum_{\substack{l_1m_1s\\l_2m_2\nu\\\nu_1\nu_2}} D^J(R)_{s\mu}D^{l_1}(R)_{-s-\nu,\nu_1}D^{l_2}(R)_{\nu\nu_2}D^{l_1}(R^{(a)})^*_{m_1\nu_1}D^{l_2}(R^{(b)})^*_{m_2\nu_2}G(Jsl_1m_1l_2m_2\nu|z_{nk}\rho). \tag{27}$$

Wigner[3] has shown that the product of two representation coefficients may be expanded in the form

$$D^{l_1}(R)_{m_1\nu_1}D^{l_2}(R)_{m_2\nu_2}=\sum_{L=|l_1-l_2|}^{l_1+l_2} {}^{l_1l_2}S_{Lm_1m_2}{}^{l_1l_2}S_{L\nu_1\nu_2}D^L(R)_{m_1+m_2,\nu_1+\nu_2}. \tag{28}$$

He has also obtained explicit expressions for the coefficients ${}^{l_1l_2}S_{Lm_1m_2}$, and shown that they satisfy certain orthogonality conditions. If one uses Eq. (28), it follows from Eq. (27) that

$$\psi_\mu{}^J=\sum_{\substack{l_1m_1s\\l_2m_2\nu\\\nu_1\nu_2L_1L_2}} {}^{l_1l_2}S_{L_1,-s-\nu,\nu}{}^{l_1l_2}S_{L_1\nu_1\nu_2}{}^{JL_1}S_{L_2s-s}{}^{JL_1}S_{L_2,\mu,\nu_1+\nu_2}D^{L_2}(R)_{0,\mu+\nu_1+\nu_2}D^{l_1}(R^{(a)})^*_{m_1\nu_1}D^{l_2}(R^{(b)})^*_{m_2\nu_2}G(Jsl_1m_1l_2m_2\nu|z_{nk}\rho). \tag{29}$$

It is convenient to use in place of the functions $G(Jsl_1m_1l_2m_2\nu|z_{nk}\rho)$ a set of functions $F(JL_1L_2l_1m_1l_2m_2|z_{nk}\rho)$ which are defined as linear combinations of the $G(Jsl_1m_1l_2m_2\nu|z_{nk}\rho)$ in the following manner:

$$F(JL_1L_2l_1m_1l_2m_2|z_{nk}\rho)=\sum_{\nu s} {}^{l_1l_2}S_{L_1,-s-\nu,\nu}{}^{JL_1}S_{L_2s-s}G(Jsl_1m_1l_2m_2\nu|z_{nk}\rho). \tag{30}$$

This set of equations may be solved for the $G(Jsl_1m_1l_2m_2\nu|z_{nk}\rho)$ by using an orthogonality property of the ${}^{l_1l_2}S_{Lm_1m_2}$. Wigner[3] has shown that

$$\sum_L {}^{l_1l_2}S_{L,\mu,m-\mu}{}^{l_1l_2}S_{L,\mu',m-\mu'}=\delta\mu\mu'. \tag{31}$$

Equation (30) is multiplied by ${}^{JL_1}S_{L_2s'-s'}$ and summed over L_2. After making use of the orthogonality, Eq. (31), we multiply the resulting equation by ${}^{l_1l_2}S_{L_1,-s-\nu',\nu'}$ and sum over L_1. After making use of the orthogonality, Eq. (31), a second time we obtain the required solution,

$$G(Jsl_1m_1l_2m_2\nu|z_{nk}\rho)=\sum_{L_1L_2} {}^{l_1l_2}S_{L_1,-s-\nu,\nu}{}^{JL_1}S_{L_2s-s}F(JL_1L_2l_1m_1l_2m_2|z_{nk}\rho). \tag{32}$$

In terms of the functions $F(JL_1L_2l_1m_1l_2m_2|z_{nk}\rho)$ defined by Eq. (30), the expression for the wave function $\psi_\mu{}^J$ as given by Eq. (29) is

$$\psi_\mu{}^J=\sum_{\substack{l_1m_1l_2m_2\\\nu_1\nu_2L_1L_2}} {}^{l_1l_2}S_{L_1\nu_1\nu_2}{}^{JL_1}S_{L_2,\mu,\nu_1+\nu_2}D^{L_2}(R)_{0,\mu+\nu_1+\nu_2}D^{l_1}(R^{(a)})^*_{m_1\nu_1}D^{l_2}(R^{(b)})^*_{m_2\nu_2}F(JL_1L_2l_1m_1l_2m_2|z_{nk}\rho). \tag{33}$$

[3] E. P. Wigner, *Gruppentheorie und ihre Anwendung auf die Quanenmechanik der Atomspektren* (J. W. Edwards, Ann Arbor, 1944), p. 204. See also E. U. Condon and G. H. Shortley, *The Theory of Atomic Spectra* (MacMillan Company, New York, 1935).

We now consider the operation of the Hamiltonian operator as given by Eq. (I-15) on the wave function as given by Eq. (33). First, we note that in the form of the wave function as given by Eq. (33) the first subscript on the $D^{L_2}(R)_{0,\mu+\nu_1+\nu_2}$ is zero. These coefficients are independent of the third Eulerian angle γ. Thus, in considering the operation of the Hamiltonian operator of Eq. (I-15), one may take as independent coordinates specifying the orientation and the internal configuration of the system of N particles the two angles specifying the direction of the line between the centers of mass of the two molecules (that is, the Eulerian angles α and β of the rotation R), the six Eulerian angles defining the rotations $R^{(a)}$ and $R^{(b)}$, the distance ρ and the z_{nk}.

Let us consider the third term in Eq. (I-15), that is, the term

$$-\frac{\hbar^2}{2\mu}\sum_k \frac{\partial^2}{\partial x_k{}^2}\psi_\mu{}^J. \tag{34}$$

In this term we change variables from the x_k to the coordinates ρ, β, and α, where ρ is the distance between the centers of mass of the two molecules and β and α are the polar angles of the direction of the line between them (or two of the Eulerian angles of the rotation R). This transformation is the usual transformation to polar coordinates and the result is

$$-\frac{\hbar^2}{2\mu\rho^2}\left[\frac{\partial}{\partial\rho}\left(\rho^2\frac{\partial}{\partial\rho}\right)+\frac{1}{\sin\beta}\frac{\partial}{\partial\beta}\left(\sin\beta\frac{\partial}{\partial\beta}\right)+\frac{1}{\sin^2\beta}\frac{\partial^2}{\partial\alpha^2}\right]\psi_\mu{}^J. \tag{35}$$

It may be shown that

$$D^l(R)_{0m}=(4\pi/2l+1)^{\frac{1}{2}}Y_l{}^m(\beta,\alpha), \tag{36}$$

that is, the representation coefficients in which one subscript is zero are proportional to the spherical harmonics. Hence, these coefficients are eigenfunctions of the operator of Eq. (35) and the term of Eq. (I-15) given by Eq. (35) is

$$-\frac{\hbar^2}{2}\sum_{\substack{l_1m_1l_2m_2\\ \nu_1\nu_2L_1L_2}} S_{L_1\nu_1\nu_2}^{\ \ l_1l_2\ \ JL_1} S_{L_2,\mu,\nu_1+\nu_2} D^{L_2}(R)_{0,\mu+\nu_1+\nu_2} D^{l_1}(R^{(a)})^*_{m_1\nu_1} D^{l_2}(R^{(b)})^*_{m_2\nu_2}\left[\frac{1}{\mu\rho^2}\frac{\partial}{\partial\rho}\left(\rho^2\frac{\partial}{\partial\rho}\right)-\frac{L_2(L_2+1)}{\mu\rho^2}\right]\times F(JL_1L_2l_1m_1l_2m_2|z_{nk}\rho). \tag{37}$$

In order to evaluate the first term of Eq. (I-15), that is, $\mathcal{K}_a\psi_\mu{}^J$, we write the expression for $\psi_\mu{}^J$ as given by Eq. (33) in the form

$$\psi_\mu{}^J=\sum_{l_1m_1\nu_1} D^{l_1}(R^{(a)})^*_{m_1\nu_1}T^J(l_1\nu_1\mu)_{m_1}, \tag{38}$$

where

$$T^J(l_1\nu_1\mu)_{m_1}=\sum_{\substack{l_2m_2\nu_2\\ L_1L_2}} S_{L_1\nu_1\nu_2}^{\ \ l_1l_2\ \ JL_1} S_{L_2,\mu,\nu_1+\nu_2} D^{L_2}(R)_{0,\mu+\nu_1+\nu_2} D^{l_2}(R^{(b)})^*_{m_2\nu_2} F(JL_1L_2l_1m_1l_2m_2|z_{nk}\rho). \tag{39}$$

The evaluation of $\mathcal{K}_a\psi_\mu{}^J$ requires that we first evaluate $\partial\psi_\mu{}^J/\partial y_{nk}$, and this in turn requires that we differentiate the representation coefficients with respect to the y_{nk}. This differentiation was first carried out by Hirschfelder and Wigner.[4] However, because of differences in the definitions of the sperical harmonics the expression given here is somewhat different.

The rotation $R^{(a)}$ is defined as the rotation of the coordinate system required to bring molecule a into a standard configuration and hence depends upon the set of coordinates y_{nk}. If one coordinate y_{nk} is changed by an infinitesimal amount, the rotation of the coordinate system necessary to bring the system into a standard configuration is changed by an infinitesimal rotation S^{nk}. Thus, by definition the derivative of the rotation matrix with respect to y_{nk} is

$$\frac{\partial R_{ij}{}^{(a)}}{\partial y_{nk}}=\lim_{\delta y_{nk}\to 0}\left[(S^{nk}R^{(a)})_{ij}-R_{ij}{}^{(a)}\right]/\delta y_{nk}, \tag{40}$$

where S^{nk} is an infinitesimal rotation matrix. The infinitesimal rotation matrix S^{nk} may be written in the form

$$S_{ii}{}^{nk}=0, \tag{41}$$

$$S_{ij}{}^{nk}=\epsilon_{ij}{}^{nk}\delta y_{nk}\quad i\neq j, \tag{42}$$

where the $\epsilon_{ij}{}^{nk}$ are functions of y_{nk} which depend on the choice of the standard configuration. In terms of the $\epsilon_{ij}{}^{nk}$, it follows from Eq. (40) that

$$\frac{\partial R_{ij}{}^{(a)}}{\partial y_{nk}}=\sum_{l\neq i}\epsilon_{il}{}^{nk}R_{li}{}^{(a)}. \tag{43}$$

It can be shown that the derivatives of the representation coefficients may be written in terms of $\epsilon_{ij}{}^{nk}$. The explicit expression is

$$\begin{aligned}\frac{\partial D^J(R^{(a)})_{m\nu}}{\partial y_{nk}}=&-im\epsilon_{21}{}^{nk}D^J(R^{(a)})_{m\nu}\\ &+\tfrac{1}{2}[J(J+1)-m(m-1)]^{\frac{1}{2}}\\ &\times(\epsilon_{13}{}^{nk}+i\epsilon_{32}{}^{nk})D^J(R^{(a)})_{m-1,\nu}\\ &-\tfrac{1}{2}[J(J+1)-m(m+1)]^{\frac{1}{2}}\\ &\times(\epsilon_{13}{}^{nk}-i\epsilon_{32}{}^{nk})D^J(R^{(a)})_{m+1,\nu}.\end{aligned} \tag{44}$$

[4] J. O. Hirschfelder and E. P. Wigner, Proc. Natl. Acad. Sci. U. S. 21, 113 (1935). See also reference 1.

The functional form of the $\epsilon_{lj}{}^{nk}$ may be obtained by using the equations which define the rotation $R^{(a)}$, Eqs. (19)–(21). If one differentiates Eq. (19) with respect to y_{nk}, uses Eq. (43) for the derivative of the $R_{ij}{}^{(a)}$ and Eq. (17) for z_{nk}, one finds that

$$\epsilon_{13}{}^{nk}=-\delta_{1n}R_{1k}{}^{(a)}/z_{13}. \tag{45}$$

In a similar manner one finds from Eqs. (20) and (21) that

$$\epsilon_{32}{}^{nk}=\delta_{1n}R_{2k}{}^{(a)}/z_{13}, \tag{46}$$

$$\epsilon_{21}{}^{nk}=-\left[\delta_{2n}-\delta_{1n}\frac{z_{23}}{z_{13}}\right]\frac{R_{2k}{}^{(a)}}{z_{21}}. \tag{47}$$

The derivatives of the internal coordinates z_{nk} with respect to the y_{nk} are obtained in a straightforward manner from Eq. (17). In general, (where z_{11}, z_{12}, and z_{13} are defined to be zero)

$$\frac{\partial z_{n'k'}}{\partial y_{nk}}=\delta_{n'n}R_{k'k}{}^{(a)}+\sum_{l\neq k'} z_{n'l}\epsilon_{k'l}{}^{nk} \qquad n'=1, 2, \cdots, a-1. \tag{48}$$

We may now evaluate the $\partial\psi_\mu{}^J/\partial y_{nk}$ where $\psi_\mu{}^J$ is given by Eq. (38). Since $T^J(l_1\nu_1\mu)_{m_1}$ is independent of $R^{(a)}$ and $R^{(b)}$ is independent of the y_{nk} with $n=1, 2, \cdots a-1$,

$$\frac{\partial T^J(l_1\nu_1\mu)_{m_1}}{\partial y_{nk}}=\sum_{n'=1}^{a-1}\sum_{k'=1}^{3}\frac{\partial z_{n'k'}}{\partial y_{nk}}\frac{\partial T^J(l_1\nu_1\mu)_{m_1}}{\partial z_{n'k'}} \qquad n=1, 2, \cdots, a-1 \tag{49}$$

$$=\sum_{k'=1}^{3}R_{k'k}{}^{(a)}\frac{\partial T^J(l_1\nu_1\mu)_{m_1}}{\partial z_{nk'}}+\sum_{n'=1}^{a-1}\sum_{k'=1}^{3}\sum_{l\neq k'} z_{n'l}\epsilon_{k'l}{}^{nk}\frac{\partial T^J(l_1\nu_1\mu)_{m_1}}{\partial z_{n'k'}} \qquad n=1, 2, \cdots, a-1. \tag{50}$$

If we use this result and Eq. (44), it follows from Eq. (38) that

$$\frac{\partial\psi_\mu{}^J}{\partial y_{nk}}=\sum_{\substack{l_1m_1\nu\\ j}} D^{l_1}(R^{(a)})^*{}_{m_1\nu_1}R_{jk}\Lambda_{nj}T^J(l_1\nu_1\mu)_{m_1} \qquad n=1, 2, \cdots, a-1. \tag{51}$$

The Λ_{nj} are the operators defined by the following equations:

$$\Lambda_{n1}=\frac{\partial}{\partial z_{n1}}+\frac{\delta_{1n}}{z_{13}}\sum_{n'=2}^{a-1}\left[z_{n'1}\frac{\partial}{\partial z_{n'3}}-z_{n'3}\frac{\partial}{\partial z_{n'1}}\right]-\frac{\delta_{1n}}{2z_{13}}[\lambda_+(l_1m_1)\sigma_+-\lambda_-(l_1m_1)\sigma_-], \tag{52}$$

$$\Lambda_{n2}=\frac{\partial}{\partial z_{n2}}+\frac{1}{z_{21}}\left(\delta_{2n}-\delta_{1n}\frac{z_{23}}{z_{13}}\right)\times\sum_{n'=3}^{a-1}\left[z_{n'2}\frac{\partial}{\partial z_{n'1}}-z_{n'1}\frac{\partial}{\partial z_{n'2}}\right]-\frac{\delta_{1n}}{z_{13}}\sum_{n'=3}^{a-1}\left[z_{n'3}\frac{\partial}{\partial z_{n'2}}-z_{n'2}\frac{\partial}{\partial z_{n'3}}\right]-\frac{im_1}{z_{21}}\left(\delta_{2n}-\delta_{1n}\frac{z_{23}}{z_{13}}\right)-i\frac{\delta_{1n}}{2z_{13}}(\lambda_+(l_1m_1)\sigma_+-\lambda_-(l_1m_1)\sigma_-), \tag{53}$$

$$\Lambda_{n3}=\frac{\partial}{\partial z_{n3}}, \tag{54}$$

where σ_+ and σ_- are the operators defined by

$$\sigma_+T^J(l_1\nu_1\mu)_{m_1}=T^J(l_1\nu_1\mu)_{m_1+1},$$
$$\sigma_-T^J(l_1\nu_1\mu)_{m_1}=T^J(l_1\nu_1\mu)_{m_1-1}, \tag{55}$$

and $\lambda_+(lm)$ and $\lambda_-(lm)$ are the numbers defined by

$$\lambda_+(lm)=[l(l+1)-m(m+1)]^{\frac{1}{2}},$$
$$\lambda_-(lm)=[l(l+1)-m(m-1)]^{\frac{1}{2}}. \tag{56}$$

If one differentiates Eq. (51) once again, one obtains

$$\frac{\partial^2\psi_\mu{}^J}{\partial y_{n'k}\partial y_{nk}}=\sum_j\frac{\partial R_{jk}}{\partial y_{n'k}}\sum_{l_1m_1\nu_1}D^{l_1}(R^{(a)})^*{}_{m_1\nu_1}\Lambda_{nj}T^J(l_1\nu_1\mu)_{m_1}+\sum_j R_{jk}\frac{\partial}{\partial y_{n'k}}\sum_{l_1m_1\nu_1}D^{l_1}(R^{(a)})^*{}_{m_1\nu_1}\Lambda_{nj}T^J(l_1\nu_1\mu)_{m_1}. \tag{57}$$

In the differentiation of $\psi_\mu{}^J$, $T^J(l_1\nu_1\mu)_{m_1}$ was considered to be an arbitrary function of the z_{nk}. In the second term of the last equation $\Lambda_{nj}T^J(l_1\nu_1\mu)_{m_1}$ can be treated as another function of the z_{nk} and the differentiation carried out in the same manner. Thus,

$$\frac{\partial^2\psi_\mu{}^J}{\partial y_{n'k}\partial y_{nk}}=\sum_j\frac{\partial R_{jk}}{\partial y_{n'k}}\times\sum_{l_1m_1\nu_1}D^{l_1}(R^{(a)})^*{}_{m_1\nu_1}\Lambda_{nj}T^J(l_1\nu_1\mu)_{m_1}+\sum_j R_{jk}\sum_{\substack{l_1m_1\nu_1\\ j'}}D^{l_1}(R^{(a)})^*{}_{m_1\nu_1}R_{j'k}\Lambda_{n'j'}\Lambda_{nj}T^J(l_1\nu_1\mu)_{m_1}. \tag{58}$$

Now, if one uses the expression for the derivative of R_{ij}, Eq. (43), the expressions for the $\epsilon_{lj}{}^{nk}$, Eqs. (45)–(47), and the orthogonality of the R_{ij}, one obtains for the

sum of the second derivatives

$$\sum_k \frac{\partial^2 \psi_\mu{}^J}{\partial y_{n'k}\partial y_{nk}} = \sum_{l_1 m_1 \nu_1} D^{l_1}(R^{(a)})^*_{m_1\nu_1} \times \begin{bmatrix} \frac{1}{z_{21}}\left(\delta_{2n'} - \delta_{1n'}\frac{z_{23}}{z_{13}}\right)\Lambda_{n1} \\ +2\frac{\delta_{1n'}}{z_{13}}\Lambda_{n3} \\ +\sum_j \Lambda_{n'j}\Lambda_{nj} \end{bmatrix} T^J(l_1\nu_1\mu)_{m_1}. \quad (59)$$

The operator representing the energy associated with the rotational and internal degrees of freedom of molecule a is defined by Eq. (11). Using this expression and the last equation one finds that

$$\mathcal{K}_a\psi_\mu{}^J = -\frac{\hbar^2}{2}\sum_{l_1 m_1 \nu_1} D^{l_1}(R^{(a)})^*_{m_1\nu_1}\Lambda^{(a)}T^J(l_1\nu_1\mu)_{m_1}, \quad (60)$$

where $\Lambda^{(a)}$ is the operator

$$\Lambda^{(a)} = \sum_{n'=1}^{a-1}\sum_{n=1}^{a-1}\frac{1}{m_n}\left(\delta_{nn'} - \frac{m_n}{M_a}\right) \times \begin{bmatrix} \frac{1}{z_{21}}\left(\delta_{2n'} - \delta_{1n'}\frac{z_{23}}{z_{13}}\right)\Lambda_{n1} \\ +2\frac{\delta_{1n'}}{z_{13}}\Lambda_{n3} \\ +\sum_j \Lambda_{n'j}\Lambda_{nj} \end{bmatrix}. \quad (61)$$

The evaluation of $\mathcal{K}_b\psi_\mu{}^J$ may be carried out in a completely analogous manner and the result written in terms of an operator $\Lambda^{(b)}$ defined in a manner similar to that used to define $\Lambda^{(a)}$. If one uses these results along with Eq. (37), one finds that if the wave function is of the form of Eq. (33) then Eq. (I-15) is

$$\sum_{\substack{l_1 m_1 l_2 m_2 \\ \nu_1\nu_2 L_1 L_2}} S_{L_1\nu_1\nu_2}^{l_1 l_2 JL_1} S_{L_2,\mu,\nu_1+\nu_2}^{JL_1} D^{L_2}(R)_{0,\mu+\nu_1+\nu_2} D^{l_1}(R^{(a)})^*_{m_1\nu_1} D^{l_2}(R^{(b)})^*_{m_2\nu_2}\left[\Lambda - \frac{2}{\hbar^2}V + \frac{2}{\hbar^2}E\right]F(JL_1L_2l_1m_1l_2m_2|z_{nk}\rho) = 0, \quad (62)$$

where Λ is the operator defined by

$$\Lambda = \frac{1}{\mu\rho^2}\frac{\partial}{\partial\rho}\left(\rho^2\frac{\partial}{\partial\rho}\right) - \frac{L_2(L_2+1)}{\mu\rho^2} + \Lambda^{(a)} + \Lambda^{(b)}. \quad (63)$$

The representation coefficients are orthogonal in the sense that

$$\int D^{J'}(R)^*_{\mu'\nu'} D^J(R)_{\mu\nu} dR = \frac{\delta_{JJ'}\delta_{\mu\mu'}\delta_{\nu\nu'}}{2J+1}\int dR. \quad (64)$$

Thus if we multiply Eq. (62) by $D^{L_2'}(R)^*_{0,\mu+\nu_1'+\nu_2'} D^{l_1'}(R^{(a)})_{m_1'\nu_1'} D^{l_2'}(R^{(b)})_{m_2'\nu_2'}$ integrate over the rotations R, $R^{(a)}$, and $R^{(b)}$ and make use of this orthogonality we find that

$$\sum_{L_1} S_{L_1\nu_1\nu_2}^{l_1 l_2} S_{L_2,\mu,\nu_1+\nu_2}^{JL_1}\left[\Lambda + \frac{2}{\hbar^2}E\right]F(JL_1L_2l_1m_1l_2m_2|z_{nk}\rho) = \frac{2}{\hbar^2}(2L_2+1)(2l_1+1)(2l_2+1) \times \sum_{\substack{l_1'm_1'l_2'm_2' \\ \nu_1'\nu_2'L_2'L_1'}} S_{L_1'\nu_1'\nu_2'}^{l_1'l_2'} S_{L_2',\mu,\nu_1'+\nu_2'}^{JL_1'} V(L_2l_1'm_1'\nu_1'l_2'm_2'\nu_2'|L_2'l_1m_1\nu_1l_2m_2\nu_2)_\mu F(JL_1'L_2'l_1'm_1'l_2'm_2'|z_{nk}\rho), \quad (65)$$

where we have defined the matrix components

$$V(L_2l_1'm_1'\nu_1'l_2'm_2'\nu_2'|L_2'l_1m_1\nu_1l_2m_2\nu_2)\mu = \frac{1}{\int\int\int dR dR^{(a)} dR^{(b)}}\int\int\int D^{L_2}(R)^*_{0,\mu+\nu_1+\nu_2} D^{l_1'}(R^{(a)})^*_{m_1'\nu_1'} \times D^{l_2'}(R^{(b)})^*_{m_2'\nu_2'} V D^{L_2'}(R)_{0,\mu+\nu_1'+\nu_2'} D^{l_1}(R^{(a)})_{m_1\nu_1} D^{l_2}(R^{(b)})_{m_2\nu_2} dR dR^{(a)} dR^{(b)}. \quad (66)$$

In the evaluation of the matrix component of the potential energy defined by the last equation it is convenient to change coordinates back to those describing the rotations R, $S^{(a)}$, and $S^{(b)}$. Clearly the Jacobian of the transformation is unity. The actual transformation is conveniently carried out in the following manner: We first reintroduce

the functions $G(Jsl_1m_1l_2m_2\nu|z_{nk}\rho)$ related to the $F(JL_1L_2l_1m_1l_2m_2|z_{nk}\rho)$ by Eq. (30). Then we make use of the relations among the representation coefficients, Eqs. (25) and (26), which depend upon the defining relations $R^{(a)}=S^{(a)}R$ and $R^{(b)}=S^{(b)}R$ and the product rule of the coefficients, Eq. (28). The right side of Eq. (65) thus becomes

$$\frac{2}{\hbar^2}(2L_2+1)(2l_1+1)(2l_2+1)\sum_{\substack{l_1'm_1'l_2'm_2'\\ \nu s}} G(Jsl_1'm_1'l_2'm_2'\nu|z_{nk}\rho)$$

$$\times\frac{1}{\int\int\int dRdS^{(a)}dS^{(b)}}\int\int\int D^{L_2}(R)^*_{0,\mu+\nu_1+\nu_2}D^{l_1}(R^{(a)})_{m_1\nu_1}D^{l_2}(R^{(b)})_{m_2\nu_2}$$

$$\times D^{J}(R)_{s\mu}D^{l_1'}(S^{(a)})^*_{m_1',-s-\nu}D^{l_2'}(S^{(b)})^*_{m_2'\nu}VdRdS^{(a)}dS^{(b)}. \quad (67)$$

It follows from the definitions of $R^{(a)}$ and $R^{(b)}$ and the properties of the representation coefficients that

$$D^{l_1}(R^{(a)})_{m_1\nu_1}=\sum_{\mu_1} D^{l_1}(S^{(a)})_{m_1\mu_1}D^{l_1}(R)_{\mu_1\nu_1}, \quad (68)$$

$$D^{l_2}(R^{(b)})_{m_2\nu_2}=\sum_{\mu_2} D^{l_2}(S^{(b)})_{m_2\mu_2}D^{l_2}(R)_{\mu_2\nu_2}. \quad (69)$$

If we use these relations and the product rule of the representation coefficients, Eq. (28), the expressions in Eq. (67) becomes

$$\frac{2}{\hbar^2}(2L_2+1)(2l_1+1)(2l_2+1)\sum_{\substack{l_1'm_1'l_2'm_2'\\ \nu s\mu_1\mu_2\\ J'}} S^{l_1l_2}_{J'\mu_1\mu_2}S^{l_1l_2}_{J'\nu_1\nu_2}G(Jsl_1'm_1'l_2'm_2'\nu|z_{nk}\rho)$$

$$\times\frac{1}{\int\int\int dRdS^{(a)}dS^{(b)}}\int\int\int D^{L_2}(R)^*_{0,\mu+\nu_1+\nu_2}D^{J}(R)_{s\mu}D^{J'}(R)_{\mu_1+\mu_2,\nu_1+\nu_2}$$

$$\times D^{l_1'}(S^{(a)})^*_{m_1',-s-\nu}D^{l_2'}(S^{(b)})^*_{m_2'\nu}VD^{l_1}(S^{(a)})_{m_1\mu_1}D^{l_2}(S^{(b)})_{m_2\mu_2}dRdS^{(a)}dS^{(b)}. \quad (70)$$

Since the system of N particles or two molecules is assumed to be in free space, the potential energy is independent of the rotation R of the entire system. Hence, the integration over R may be carried out. If we use the product rule of the coefficients, Eq. (28), and the orthogonality, Eq. (64), we find upon integration of the last result that Eq. (65) becomes

$$\sum_{L_1} S^{l_1l_2}_{L_1\nu_1\nu_2}S^{JL_1}_{L_2,\mu,\nu_1+\nu_2}\left[\Lambda+\frac{2}{\hbar^2}E\right]F(JL_1L_2l_1m_1l_2m_2|z_{nk}\rho)=\frac{2}{\hbar^2}(2l_1+1)(2l_2+1)$$

$$\times\sum_{\substack{l_1'm_1'l_2'm_2'\\ \nu\nu' sL_1}} S^{l_1l_2}_{L_1,-s-\nu,\nu}S^{l_1l_2}_{L_1\nu_1\nu_2}S^{JL_1}_{L_2s-s}S^{JL_1}_{L_2,\mu,\nu_1+\nu_2}W(l_1'm_1'l_2'm_2'\nu'|l_1m_1l_2m_2\nu)_sG(Jsl_1'm_1'l_2'm_2'\nu'|z_{nk}\rho), \quad (71)$$

where we have defined the matrix component

$$W(l_1'm_1'l_2'm_2'\nu'|l_1m_1l_2m_2\nu)_s$$

$$=\frac{1}{\int\int dS^{(a)}dS^{(b)}}\int\int D^{l_1'}(S^{(a)})^*_{m_1',-s-\nu'}D^{l_2'}(S^{(b)})^*_{m_2'\nu'}VD^{l_1}(S^{(a)})_{m_1,-s-\nu}D^{l_2}(S^{(b)})_{m_2\nu}dS^{(a)}dS^{(b)}. \quad (72)$$

Wigner[3] has shown that the $S^{l_1l_2}_{L\mu\nu}$ are orthogonal in the sense that

$$\sum_{\mu} S^{l_1l_2}_{L,\mu,m-\mu}S^{l_1l_2}_{L',\mu,m-\mu}=\delta_{LL'} \quad (73)$$

and that

$$S^{l_1 l_2}_{L\mu\nu} = (-1)^{l_1+l_2+L} S^{l_2 l_1}_{L\nu\mu}. \tag{74}$$

Furthermore it has been shown that[2]

$$S^{l_1 l_2}_{L\mu\nu} = (-1)^{L+l_1+\nu}\left(\frac{2L+1}{2l_1+1}\right)^{\frac{1}{2}} S^{L l_2}_{l_1,\mu+\nu,-\nu}. \tag{75}$$

Hence, the $S^{l_1 l_2}_{L\mu\nu}$ also satisfy the orthogonality condition

$$\sum_{\mu} S^{JL_1' \; JL_1}_{L_2\mu\nu} S_{L_2\mu\nu} = \delta_{L_1 L_1'}\left(\frac{2L_2+1}{2L_1+1}\right). \tag{76}$$

Now if Eq. (71) is multiplied by $S^{JL_1'}_{L_2,\mu,\nu_1+\nu_2}$ and the equation summed over μ it follows on using the last result that

$$\left[\Lambda+\frac{2}{\hbar^2}E\right]F(JL_1L_2l_1m_1l_2m_2|z_{nk}\rho)=\frac{2}{\hbar^2}(2l_1+1)(2l_2+1)$$

$$\times \sum_{\substack{l_1'm_1'l_2'm_2' \\ \nu\nu' s}} S^{l_1 l_2}_{L_1,-s-\nu,\nu} S^{JL_1}_{L_2 s-s} W(l_1'm_1'l_2'm_2'\nu'|l_1m_1l_2m_2\nu)_s G(Jsl_1'm_1'l_2'm_2'\nu'|z_{nk}\rho). \tag{77}$$

If the G functions on the right are written in terms of the F functions using Eq. (32) and if Eq. (63) is used for the operator Λ, we find that

$$\left\{\frac{\hbar^2}{2}\left[\frac{1}{\mu\rho^2}\frac{\partial}{\partial\rho}\left(\rho^2\frac{\partial}{\partial\rho}\right)-\frac{L_2(L_2+1)}{\mu\rho^2}+\Lambda^{(a)}+\Lambda^{(b)}\right]+E\right\}F(JL_1L_2l_1m_1l_2m_2|z_{nk}\rho)=(2l_1+1)(2l_2+1)$$

$$\times \sum_{\substack{L_1'L_2'l_1'm_1' \\ l_2'm_2'}} F(JL_1'L_2'l_1'm_1'l_2'm_2'|z_{nk}\rho) \sum_{\nu\nu' s} S^{l_1 l_2}_{L_1,-s-\nu,\nu} S^{l_1' l_2'}_{L_1',-s-\nu',\nu'} S^{JL_1}_{L_2 s-s} S^{JL_1'}_{L_2' s-s} W(l_1'm_1'l_2'm_2'\nu'|l_1m_1l_2m_2\nu)_s, \tag{78}$$

where $\Lambda^{(a)}$ and $\Lambda^{(b)}$ are the operators defined by Eq. (61) and the W's are the matrix components defined by Eq. (72). This is the set of coupled equations for the F functions. The coupling occurs in the terms on the right as a result of the potential of interaction between the two molecules. There is further coupling caused by the σ_+ and σ_- operators which appear in the $\Lambda^{(a)}$ and $\Lambda^{(b)}$. Once the F functions are obtained as solutions of these equations, the complete wave function (in the center of gravity coordinate system) is given by Eqs. (24) and (32).

III. THE FOUR-PARTICLE SYSTEM

As an application of the equations derived in the preceding sections, let us consider a system made up of two diatomic molecules, that is, four particles. Particles one and two are associated with molecule a, and particles three and four are associated with molecule b. This system provides a particularly simple application of the results derived above. However, the results are somewhat special since only two (and not three) angles are required to specify the orientations of a diatomic molecule in space. Hence, it is necessary to re-examine some of the points of the derivation.

In this particular case the rotation $S^{(a)}$ is specified by a single angle representing the inclination of molecule a to the line between the centers of mass; the rotation $S^{(b)}$ is specified by two angles, the inclination of molecule b to the line between the centers of mass and the angle between the planes containing this line and molecule a and molecule b, respectively. Hence the expansion of $\chi_s{}^J$, Eq. (II-23) is of the form

$$\chi_s{}^J = \sum_{l_1 l_2 \nu} D^{l_1}(S^{(a)})^*_{0,-s-\nu} D^{l_2}(S^{(b)})^*_{0\nu} G(Jsl_1l_2\nu|z_{nk}\rho). \tag{1}$$

Since according to Eq. (II-36) the representation coefficients with one index zero are proportional to the $Y_l{}^m$, this expansion is an expansion in spherical harmonics.

The operator $\Lambda^{(a)}$ is given in terms of the Λ_{nj} by Eq. (II-61), and the Λ_{nj} are given by Eqs. (II-52)–(II-54). In this special case,

$$\Lambda_{11} = -\frac{1}{2z_{13}}[\lambda_+(l_1m_1)\sigma_+ - \lambda_-(l_1m_1)\sigma_-], \tag{2}$$

$$\Lambda_{12} = -\frac{i}{2z_{13}}[\lambda_+(l_1m_1)\sigma_+ + \lambda_-(l_1m_1)\sigma_-], \tag{3}$$

$$\Lambda_{13} = \frac{\partial}{\partial z_{13}}. \tag{4}$$

Hence, from Eq. (II-61)

$$\Lambda^{(a)}=\frac{m_2}{m_1M_a}\left[\frac{\partial^2}{\partial z_{13}^2}+\frac{2}{z_{13}}\frac{\partial}{\partial z_{13}}-\frac{l_1(l_1+1)}{z_{13}^2}\right]. \quad (5)$$

It is convenient to change from the coordinate z_{13} to the distance

$$\xi_a=M_az_{13}/m_2 \quad (6)$$

between particles one and two in molecule a, i.e., ξ_a is the interatomic distance. In terms of ξ_a, Eq. (5) becomes

$$\Lambda^{(a)}=\frac{1}{\mu_a\xi_a^2}\frac{\partial}{\partial\xi_a}\left(\xi_a^2\frac{\partial}{\partial\xi_a}\right)-\frac{l_1(l_1+1)}{\mu_a\xi_a^2}, \quad (7)$$

where

$$\mu_a=m_1m_2/M_a \quad (8)$$

is the reduced mass of the pair of particles one and two. The operator $\Lambda^{(b)}$ is given by a similar expression.

Using these results one finds that the equations for the F functions, Eqs. (II-68), are

$$\left[\begin{aligned}&\frac{\hbar^2}{2}\left[\frac{1}{\mu\rho^2}\frac{\partial}{\partial\rho}\left(\rho^2\frac{\partial}{\partial\rho}\right)-\frac{L_2(L_2+1)}{\mu\rho^2}\right]\\&+\frac{\hbar^2}{2}\left[\frac{1}{\mu_a\xi_a^2}\frac{\partial}{\partial\xi_a}\left(\xi_a^2\frac{\partial}{\partial\xi_a}\right)-\frac{l_1(l_1+1)}{\mu_a\xi_a^2}\right]\\&+\frac{\hbar^2}{2}\left[\frac{1}{\mu_b\xi_b^2}\frac{\partial}{\partial\xi_b}\left(\xi_b^2\frac{\partial}{\partial\xi_b}\right)-\frac{l_2(l_2+1)}{\mu_b\xi_b^2}\right]+E\end{aligned}\right]F(JL_1L_2l_1l_2|\xi_a\xi_b\rho)=(2l_1+1)(2l_2+1)$$

$$\times\sum_{L_1'L_2'l_1'l_2'}F(JL_1'L_2'l_1'l_2'|\xi_a\xi_b\rho)\sum_{\nu\nu's}{}^{l_1l_2}S_{L_1,-s-\nu,\nu}{}^{l_1'l_2'}S_{L_1',-s-\nu',\nu'}{}^{JL_1}S_{L_2s-s}{}^{JL_1'}S_{L_2's-s}W(l_1'l_2'\nu'|l_1l_2\nu)_s, \quad (9)$$

where the potential energy matrix components are given by Eq. (II-72) as

$$W(l_1'l_2'\nu'|l_1l_2\nu)_s=\frac{1}{\int\int dS^{(a)}dS^{(b)}}\int\int D^{l_1'}(S^{(a)})^*{}_{0,-s-\nu'}D^{l_2'}(S^{(b)})^*{}_{0\nu'}VD^{l_1}(S^{(a)})_{0,-s-\nu}D^{l_2}(S^{(b)})_{0\nu}dS^{(a)}dS^{(b)}. \quad (10)$$

In terms of the F functions, which are solutions of this set of equations, the complete wave function is given by Eqs. (II-24) and (II-32) as

$$\psi_\mu{}^J=\sum_{\substack{L_1L_2l_1l_2\\\nu s}}{}^{l_1l_2}S_{L_1,-s-\nu,\nu}{}^{JL_1}S_{L_2s-s}D^J(R)_{s\mu}D^{l_1}(S^{(a)})^*{}_{0,-s-\nu}D^{l_2}(S^{(b)})^*{}_{0\nu}F(JL_1L_2l_1l_2|\xi_a\xi_b\rho). \quad (11)$$

It is interesting to note that the expression on the left of Eq. (9) representing the kinetic energy of the system consists of the sum terms representing the kinetic energy associated with the "orbital motion" of one molecule about the other and that associated with vibrational motion of each molecule separately. The coupling terms on the right of the equation represent the interaction between the two molecules. If the potential energy V is independent of the relative orientation of the two molecules, i.e., if the molecules are virtually spherical, then the sum on the right reduces to a single term and the equations are uncoupled. In this limit, of course, transitions in the rotational states of the molecules do not occur. The application of this equation to the study of angular transition probabilities in the collisions of diatomic molecules will be discussed in a subsequent paper.

Chemical Effects Due to the Ionization of Impurities in Semiconductors

HOWARD REISS
Bell Telephone Laboratories, Murray Hill, New Jersey
(Received December 22, 1952)

This paper contains a theoretical account of the possible effects which the ionization of donor and acceptor impurities can induce in the thermodynamic phase relations involving their solutions with semiconductors. These effects reflect the energy band structure of the semiconductor. Furthermore, the phenomenon has an interest of its own, for within a certain range of experimental conditions the effects can be attributed to a chemical-like, mass action behavior of the electrons which play the roles of negative ions.

Section V is a brief discussion of a fine point concerning the Fermi level. It is shown that although the Fermi level is certainly the electronic electrochemical potential, it is not the Gibbs free energy per electron unless the density of electron energy levels is linear in the volume of the system.

I. INTRODUCTION

THE phenomenon of ionization of donor and acceptor impurities in semiconductors[1] has been studied extensively, yet little effort has been spent in investigating the possible consequences which the dissociative process may induce in the distribution of the impurity between the semiconductor and some other phase. It is tempting, and seemingly reasonable, to regard the impurity very much as a weak electrolyte[2] dissolved in an ionizing medium. One might compare its situation with that of acetic acid in aqueous solution. In the latter case, because of incomplete dissociation, the partial pressure of acetic acid fails to obey Henry's law,[3] even at very high dilutions, and the anomalous behavior of the distribution coefficient can be used[4] to study the ionization equilibrium. Similar effects with impurities in semiconductors might provide information on energy band structures.

In terms of the band picture of solids one might measure the concentration of undissociated donor atoms by the concentration of electrons in donor states.[5] In view of the high dilutions concerned, this concentration can be substituted into Henry's law for the determination of the pressure of the donor impurity. By formulating the relation between undissociated and dissociated donor, Henry's law can then be written for the total concentration of donor with a suitable activity coefficient. The latter is intimately related to the band structure, and its measurement should be capable of yielding valuable information. As an *equilibrium* quantity it would be free of the difficulties which attend the need (found in electrical measurements) for data on dissipative quantities such as electron and hole mobilities.[6]

There are several points in the above scheme which demand thoughtful consideration. In particular, the distinction between dissociated and undissociated donor atoms is not as clear from the chemical point of view as it is from the physical. A donor atom whose donor state is occupied (undissociated) nevertheless has its donor electron smeared over several lattice parameters of crystal.[7] When the electron escapes to the conduction band the resulting ion finds itself imbedded in a sea of conduction electrons and tends to develop a negative environment. Therefore, in both the undissociated and dissociated forms, the ion is surrounded by an electron atmosphere, which is more attenuated in the last case, so that the distinction between ionized and unionized donors rests mostly on the condition of attenuation of an atmosphere, and it is hard to regard the electron smear as a dissociable particle, to which the law of mass action[8] is applicable.

As long as one is concerned with the internal state of the semiconductor, and especially with physical properties such as conductivity, the mass action particle approach can be very fruitful.[9] But as soon as the necessity arises for considering the transfer of an atom from the semiconductor phase to another, care must be exercised.

The activity coefficient mentioned above can be derived by the methods of statistical mechanics in a manner, independent of the mechanism of transfer of the atom between two phases. This derivation is free, therefore, of the need for determining the nature of the undissociated species in the semiconductor. Subject to certain mild assumptions, it turns out that the statistical mechanical and the "weak electrolyte" mass action approach yield the same results, so that the latter is justified over a certain range of circumstances.

In the next two sections we shall derive some useful formulas by the "weak electrolyte" approach, and calculate the magnitudes of the effects which they predict. The later sections will be devoted to the statistical mechanical justification of these results.

[1] W. Shockley, *Electrons and Holes in Semiconductors* (D. Van Nostrand Company, Inc., New York, 1950).
[2] F. H. Getman and F. Daniels, *Outlines of Physical Chemistry* (John Wiley and Sons, Inc., New York, 1945), seventh edition.
[3] H. A. Taylor and H. S. Taylor, *Elementary Physical Chemistry* (D. Van Nostrand Company, Inc., New York, 1939), p. 328.
[4] See reference 3, pp. 375, 377.
[5] H. C. Torrey and C. A. Whitmer, *Crystal Rectifiers* (McGraw-Hill Book Company, Inc., New York, 1948), p. 47.
[6] See reference 1, Chapter 8.
[7] See reference 5, p. 65.
[8] See reference 3, p. 343.
[9] A. H. Wilson, Proc. Roy. Soc. (London) **A133**, 458 (1931); **A134**, 277 (1932).

II. USEFUL FORMULAS VIA THE "WEAK ELECTROLYTE" APPROACH

It is convenient to begin by considering a very dilute solution of donor in a semiconductor, such that ϵ_v represents the energy of the highest state in the valence band, ϵ_D the energy of the donor level, and ϵ_c the energy of the lowest state in the conduction band. Denote the Fermi level by μ, and, for simplicity, assume that the effective masses[10] of holes and electrons are identical scalar quantities. The middle of the forbidden band may be used as a zero to which all energetic quantities may be referred.

The concentration n_D of electrons in the donor level can be expressed, using Fermi-Dirac statistics,* as

$$n_D=[1/1+\tfrac{1}{2}\exp[(\epsilon_D-\mu)/kT]]N_D, \tag{2.1}$$

where N_D is the total concentration of donor atoms (dissociated and undissociated), k is the Boltzmann constant, and T is the absolute temperature. Application of Henry's law to n_D gives for p_D, the donor pressure,

$$p_D=K_D'[1/1+\tfrac{1}{2}\exp[(\epsilon_D-\mu)/kT]]N_D, \tag{2.2}$$

where K_D' is a constant, dependent upon temperature. If K_D' is written as

$$K_D'=K_D[1/1+\tfrac{1}{2}\exp(\epsilon_D/kT)], \tag{2.3}$$

where K_D is another constant, (2.2) becomes

$$p_D=K_D\left[\frac{1+\tfrac{1}{2}\exp(\epsilon_D/kT)}{1+\tfrac{1}{2}\exp[(\epsilon_D-\mu)/kT]}\right]N_D=K_D\gamma_D N_D, \tag{2.4}$$

where

$$\gamma_D=\left[\frac{1+\tfrac{1}{2}\exp(\epsilon_D/kT)}{1+\tfrac{1}{2}\exp[(\epsilon_D-\mu)/kT]}\right] \tag{2.5}$$

is an activity coefficient which passes to unity at infinite dilution when μ goes to zero as the semiconductor becomes intrinsic. The measurement of γ_D in its dependence upon N_D (through μ) thus furnishes information on the variation of μ with N_D, and hence on band structure.

Similar considerations may be applied to acceptors which dissociate to form negative ions and positive holes. This time it is the concentration of holes in the acceptor level which represents the concentration of undissociated atoms. In place of (2.4) and (2.5) we obtain

$$p_A=K_A\gamma_A N_A, \tag{2.6}$$

where

$$\gamma_A=\left[\frac{1+\tfrac{1}{2}\exp(-\epsilon_A/kT)}{1+\tfrac{1}{2}\exp[-(\epsilon_A-\mu)/kT]}\right] \tag{2.7}$$

the subscript A referring to acceptors.

[10] See reference 1, p. 397.

* The factor of $\frac{1}{2}$ appearing in (2.1) represents a departure from the usual Fermi-Dirac distribution function and demonstrates a peculiarity of the donor level based on the fact that one electron can occupy a donor state with either of two values of spin, but that two electrons cannot occupy such a state even with opposite spins.

The utility of (2.5) and (2.7) depends on the possibility of relating μ to N_D or N_A or both. The necessary relationship is achieved by invoking the principle of electrical neutrality which, when translated into the language we wish to use here, becomes[11]

$$N_D-N_A=n_c+n_D-h_v-h_A, \tag{2.8}$$

where n_c is the density of electrons in the conduction band, h_v the number of holes in the valence band, and, h_A the number of holes in the acceptor level. If it is assumed that the populations of holes and electrons in the valence and conduction bands, respectively, are sufficiently low so that classical statistics may be applied

$$n_c=\Gamma\exp[-(\epsilon_c-\mu)/kT], \tag{2.9}$$

$$h_v=\Gamma\exp[-(\epsilon_c+\mu)/kT], \tag{2.10}$$

where

$$\Gamma=2(2\pi mkT)^{\frac{3}{2}}/h^3 \tag{2.11}$$

with m the effective mass, and h Plank's constant. If the populations are really high it becomes very difficult to express n_c and h_v in simple form.

In direct correspondence with (2.1), h_A may be written as

$$h_A=[1/1+\tfrac{1}{2}\exp[-(\epsilon_A-\mu)/kT]]N_A. \tag{2.12}$$

Even though ϵ_D and ϵ_A may be close to ϵ_c and ϵ_v, respectively, the exponentials in (2.1) and (2.12) become small with respect to unity (as $|\mu|>kT$) more rapidly than the corresponding exponentials which appear in the Fermi-Dirac expressions for populations in the valence and conduction bands. This results from the factors of $\frac{1}{2}$ which appear in (2.1) and (2.12). Consequently, it may be possible to use (2.9) and (2.10) as reasonable approximations even in circumstances where the classical approximations to (2.1) and (2.12) are poor.

The weak electrolyte analogy becomes more exact whenever

$$\epsilon_D\approx\epsilon_c\gg\mu+kT, \tag{2.13}$$

$$-\epsilon_A\approx-\epsilon_v=\epsilon_c\gg-\mu+kT, \tag{2.14}$$

so that classical statistics can be applied throughout. For then besides (2.9) and (2.10) the following expressions can be used in place of (2.1) and (2.12)

$$n_D=2N_D\exp[-(\epsilon_c-\mu)/kT], \tag{2.15}$$

$$h_A=2N_A\exp[-(\epsilon_c+\mu)/kT], \tag{2.16}$$

and these lead to the following simple picture.

Let the symbol D_g stand for donor in the gas phase, D_s for undissociated donor in the solid phase, D_s^+ for ionized donor, e^- for electrons, and e^+ for holes. The following *chemical* equilibria may then be assumed to exist in a system in which only donor impurity is present:

$$D_g\rightleftharpoons D_s\rightleftharpoons D_s^++e^-, \tag{2.17}$$

$$e^+e^-\rightleftharpoons e^++e^-. \tag{2.18}$$

[11] See reference 1, p. 238.

The latter refers to the dissociation of the semiconductor lattice itself and may be likened, in effect, to the dissociation of water in an aqueous solution. Corresponding to these equilibria the following mass action expressions can be formulated:

$$p_D = K_D'[D_s], \quad \text{(Henry's law)} \tag{2.19}$$

$$[D_s^+][e^-]/[D_s] = K_+, \tag{2.20}$$

$$[e^+][e^-] = K_0. \tag{2.21}$$

If now we introduce the identifications

$$\begin{aligned} [D_s] &= n_D, \\ [D_s^+] &= N_D - n_D \approx N_D, \\ [e^-] &= n_e, \\ [e^+] &= h_v, \end{aligned} \tag{2.22}$$

we find that [so long as (2.15) and (2.16) are used] K_+ and K_0 are indeed constants having the values

$$K_+ = \Gamma/2, \tag{2.23}$$

$$K_0 = \Gamma^2 \exp(-2\epsilon_c/kT). \tag{2.24}$$

If the system of Eqs. (2.19), (2.20), and (2.21) is solved subject to the restriction of electroneutrality contained in (2.8), one obtains (2.4) with γ_D† expressed in terms of N_D. In effect the mass action approach represents a method for calculating the dependence of μ upon N_D in the special case covered by (2.13) and (2.14).

It is interesting to note that (2.23) and (2.24) are not valid when Fermi-Dirac statistics must be applied, for in that case they contain the additional quantity μ which depends upon N_D. In general the law of mass action fails whenever molecules of the atomic or molecular species involved interact with each other. The failure of mass action in the present instance may also be attributed to interaction, but to a rather unusual kind; the correlation type interaction required by the Pauli exclusion principle[12] which restricts the occupancy of each quantum state to one electron.

Since μ increases with increasing N_D the same is true of γ_D, so that the system should exhibit positive deviations from Henry's law.

If acceptors are added to the system described by (2.17) and (2.18) it becomes necessary to include the additional equilibria

$$A_g \rightleftharpoons A_s \rightleftharpoons A_s^- + e^+ \tag{2.25}$$

and the equations

$$\begin{aligned} p_A &= K_A'[A_s], \\ [A_s^-][e^+]/[A_s] &= K_-, \end{aligned} \tag{2.26}$$

where the symbol A replaces the D of (2.17) and stands for acceptor. The additional identifications

$$\begin{aligned} [A_s] &= h_A, \\ [A_s^-] &= N_A - h_A \approx N_A \end{aligned} \tag{2.27}$$

are required. It turns out that

$$K_- = K_+ = \frac{\Gamma}{2}. \tag{2.28}$$

From the mass action point of view an acceptor should increase the solubility of a donor and vice versa, since the holes it produces through (2.25) can react with electrons through (2.18) and thus shift (2.17) in favor of higher D_s^+. In the same manner a donor should decrease the solubility of another donor. Suppose that a donor is present in low enough concentration so that it has little to do with fixing the Fermi level which is then determined by an excess of some other donor, or by an acceptor. If the vapor pressure, p_D, of the donor is maintained constant, then its concentration N_D will depend upon μ, i.e., upon the concentration of excess donor or acceptor. If N_D^0 represents the concentration when the semiconductor becomes intrinsic, i.e., when there is no excess donor or acceptor, it is an easy matter to show that

$$\frac{N_D}{N_D^0} = \frac{1+\frac{1}{2}\exp[(\epsilon_D-\mu)/kT]}{1+\frac{1}{2}\exp[\epsilon_D/kT]}. \tag{2.29}$$

A similar formula can be derived for acceptors.

These formulas (which in the parlance of the mass action point of view represent the common ion effect[13]) can be used in the manner of (2.5) and (2.7) to gain information on band structure.

In closing this section it is fitting to indicate that the concept of an electron acting as a chemical entity in solution, and thus affecting chemical equilibria through mass action behavior is not new. Wagner[14] recently has explained the solubility of hydrogen in molten binary metallic alloys in terms of a dissociative equilibrium in which hydrogen dissociates into a proton and electron. However, in the present instance the solutions are dilute enough so that we may hope to predict the results of experiments quantitatively.

III. ESTIMATION OF MAGNITUDES OF EFFECTS

In this section the formulas derived in Sec. II will be combined with data on the band structure in germanium to estimate the magnitudes of the effects they predict. Referring to (2.4) we define p_D^0 as the pressure which would result if Henry's law were valid. Thus

$$p_D^0 = K_D N_D$$

and

$$p_D/p_D^0 = \gamma_D = \frac{1+\frac{1}{2}\exp(\epsilon_D/kT)}{1+\frac{1}{2}\exp[(\epsilon_D-\mu)/kT]}. \tag{3.1}$$

† In this case, in view of (2.13), γ_D reduces to $\exp(\mu/kT)$.

[12] R. H. Fowler and E. A. Guggenheim, *Statistical Thermodynamics* (Cambridge University Press, Cambridge, 1939), p. 17.

[13] F. W. Miller, *Elementary Theory of Qualitative Analysis* (D. Appleton Century Company, Inc., New York, 1929), p. 102.

[14] C. Wagner, J. Chem. Phys. 19, 626 (1951).

TABLE I.

N_D (atom/cc)	μ/kT	p_D/p_D^0
0	0	1
5.9×10^{17}	0.2	1.2
1.2×10^{18}	0.4	1.4
2.0×10^{18}	0.6	1.7
2.8×10^{18}	0.8	2.0
3.9×10^{18}	1.0	2.4
$kT=0.1045$ ev		

For

$$\mu \lesssim kT, \tag{3.2}$$

the formula simplifies to

$$p_D/p_D^0=\exp(\mu/kT)$$

or

$$\mu=kT\ln(p_D/p_D^0), \tag{3.3}$$

yielding a rather direct relation between the Fermi level and the activity coefficient.

Within the limit prescribed by (3.2), μ, given by combining (2.1), (2.9), and (2.10) with (2.8), has the form

$$\mu=kT\sinh^{-1}\left[\frac{\exp(\epsilon_c/kT)}{2\Gamma}\right]N_D, \tag{3.4}$$

so that

$$p_D=p_D^0\exp\left[\sinh^{-1}\left(\frac{\exp(\epsilon_c/kT)}{2\Gamma}\right)N_D\right]$$

$$=K_DN_D\exp\left[\sinh^{-1}\left(\frac{\exp(\epsilon_c/kT)}{2\Gamma}\right)N_D\right]. \tag{3.5}$$

This represents a limiting law useful in the extrapolation of data of p_D *versus* N_D to zero N_D, in order to obtain K_D.

For an ordinary impurity quite high temperatures will have to be used before its vapor can be equilibrated adequately with a solid solution, in view of the slow rates of diffusion involved. Unfortunately, at higher temperatures the semiconductor is more intrinsic, and so the anomalous effects expected on the above basis will be smaller. For illustrative purposes the ratio p_D/p_D^0 will be calculated for a typical donor in germanium as a function of N_D, near the melting point of germanium at approximately 1200°K.

The following data will be employed:

$$\epsilon_c=0.31 \text{ ev},$$

$$m=m_0/4,$$

where m the effective mass is taken to be $\frac{1}{4}$ of the normal electron mass m_0. These data represent extrapolations from electrical measurements[15] performed at much lower temperatures (below 800°K) and so may be subject to considerable error. In particular, near the melting point, the crystal begins to fall apart, and the band structure may be severely altered. Furthermore, even if this were not so, the effective mass is a quantity which has a reasonable significance only with respect to the band edges. At high temperatures, with unusual shaped bands, it may become severely formal as electrons and holes penetrate beyond the band edges, and, in fact, may be much larger than at lower temperatures. This would tend to throw the anomalous effects we are seeking to higher values of N_D than it is possible to achieve. Actually, at values of N_D of 10^{19}/cc and greater, Henry's law should begin to fail for reasons other than those based on dissociative phenomena.

It is advisable to base one's experiment on that impurity which can be equilibrated with the semiconductor phase at the lowest temperature.

In Table I we list N_D, μ/kT, and the calculated p_D/p_D^0 at 1200°K, for germanium. It is seen that the effect is quite pronounced even at 1200°K. If the effective mass was m_0 instead of $m_0/4$ all the numbers in the first column would be increased by about a factor of ten.

The ratio, (2.29), describing the common ion effect is merely the reciprocal of p_D/p_D^0 given by (3.1). It is thus evident, numerically, that a donor decreases the solubility of another donor. In investigating the effect of an acceptor on a donor the situation may or may not be complicated by compound formation (in the solid state) between donor and acceptor.[16] Care must always be exercised to insure that this phenomenon is absent.

IV. STATISTICAL CONSIDERATIONS

A covalent crystal is effectively one giant molecule, and it is not clear immediately that the behaviors of valence electrons and atomic kernels can be separated so arbitrarily that they can be treated as independent particles. It is well known, for example, that the total energy ξ_n of the electrons in the nth total quantum state depends upon the relative positions of the nuclei and that, in fact, this dependence upon nuclear position makes it possible to use

$$\xi_n+c \tag{4.1}$$

(where c is a simple term representing the Coulombic repulsion of the nuclei) as a nuclear potential function.[17] The nuclear and electronic energies are inextricably bound to each other.

If ϵ_j is the energy of the jth single electron energy state in the band picture of the crystal, and n_j is the number of electrons occupying this state (in some arbitrary distribution), then

$$\sum_j n_j\epsilon_j \tag{4.2}$$

[15] E. M. Conwell, Bell Laboratories Technical Memorandum 52-110-48 (July, 1952).

[16] C. D. Thurmond, Bell Laboratories, private communication.

[17] Eyring, Walter, and Kimball, *Quantum Chemistry* (John Wiley and Sons, Inc., New York, 1944), p. 190.

is equivalent to some ξ_n+c.[18] If we assume that the electrons are rapidly equilibrated over the band, then, in what follows, n_j stands for the equilibrium distribution, and ξ_n may be denoted by ξ where it is understood that the dropping of the subscript restricts attention to that total electronic quantum state characteristic of equilibrium.

Consider a crystal of N_1 atoms of one component, say component 1. A macroscopic energy level of this crystal may be represented by

$$E_i'=E_i+(\xi^0+c^0). \tag{4.3}$$

Here E_i' stands for the energy level referred to the state of infinite dispersion of electrons and nuclei as standard. ξ^0+c^0 represents $\xi+c$ for the undeformed crystal, so that E_i represents the macroscopic energy level referred to the undeformed crystal as standard, provided that $\xi+c$ is referred to infinite dispersion.

Relative to the state of infinite dispersion the partition function[19] of the crystal can now be written as

$$\begin{aligned} Q&=\exp[-(\xi^0+c^0)/kT]\sum_i \exp(-E_i/kT) \\ &=\exp[-(\xi^0+c^0)/kT]K. \end{aligned} \tag{4.4}$$

In this expression we tacitly assume that the electronic equilibrium state is the state of lowest energy and is nondegenerate, i.e., that the crystal is *normal*. Otherwise each quantum state reflected in (4.4) would receive a weight equal to the electronic degeneracy and the partition function would have to be multiplied by this factor. Furthermore, we note that ξ^0+c^0 is the heat of formation of the undeformed crystal, while K is the partition function for vibrations about equilibrium.

If N_2 atoms of a second component, component 2, are added so as to form a *dilute* solution, the partition function becomes

$$Q=\frac{(N_1+N_2)!}{N_1!N_2!}\exp[-(\xi^0+c^0+\delta_0(N_2))/kT]Kq^{N_2}. \tag{4.5}$$

Each atom of species 2, being sufficiently distant (in the majority of configurations) from a similar atom, perturbs the vibrational partition function K by the same factor, q. This factor represents a splitting of the original energy levels under the impetus of the perturbation. Since the cluster of levels which arises from an original level resembles the level diagram of an individual atomic oscillator, q may be appropriately referred to as the vibrational partition function of an atom of species 2.

In (4.5) $\delta_0(N_2)$ simply represents the increment in the heat of formation of the undeformed crystal which attends the addition of N_2 atoms, while the combinatorial factor which precedes the exponential measures the configurational degeneracy obtainable by permuting N_1 atoms of species 1 and N_2 of species 2, randomly over N_1+N_2 lattice sites.

If species 2 is a donor atom, then, we are no longer justified in assuming that the electrons at equilibrium are restricted to their lowest state. The crystal is no longer *normal*, but *excited*. It therefore becomes necessary to multiply Q by a suitable factor to account for the electronic degeneracy which is now possible. This degeneracy results from the possibility of permuting "holes" and electrons in each of the energy levels of the band scheme. We denote this factor by ψ and write

$$Q=\psi\frac{(N_1+N_2)!}{N_1!N_2!}\exp[-(\xi^0+c^0+\delta_0(N_2))/kT]Kq^{N_2}. \tag{4.6}$$

Our assumption that the electron distribution is always equilibrated implies that the normal vibrations of the crystal are not adiabatic[20] in the quantum-mechanical sense. If, therefore, during the course of vibration the bands undergo violent changes in width, the factor ψ becomes very difficult to compute, since it must then be evaluated with respect to some distribution averaged over the various possible band structures. Since the band widths depend mainly on density, and the normal modes represent distortions rather than large scale changes in density over macroscopic regions, we may assume that the band widths remain essentially fixed so that ψ may be evaluated with respect to the distribution for the undistorted crystal. We shall follow this practice.

The Helmholtz free energy of the crystal may now be derived simply. It is[21]

$$\begin{aligned} A&=-kT\ln Q \\ &=[(\xi^0+c^0+\delta^0(N_2))-Tk\ln\psi]+N_1kT\ln\frac{N_1}{N_1+N_2} \\ &\quad+N_2kT\ln\frac{N_2}{N_1+N_2}-N_2kT\ln q-kT\ln K. \end{aligned} \tag{4.7}$$

The quantity in square brackets is just the electronic free energy A_e, in the undeformed crystal for $(\xi^0+c^0+\delta^0(N_2))$ is the electronic internal energy U_e and $k\ln\psi$, the electronic entropy, S_e. We may thus write for the chemical potential of species 2 in the crystal

$$\begin{aligned} \mu_2&=\left(\frac{\partial A}{\partial N_2}\right)_{T,V}=\left(\frac{\partial A_e}{\partial N_2}\right)_{T,V} \\ &\quad+kT\ln\frac{N_2}{N_1+N_2}-kT\ln q. \end{aligned} \tag{4.8}$$

[18] N. F. Mott and H. Jones, *Theory of the Properties of Metals and Alloys* (Oxford University Press, London, 1936), p. 137.

[19] J. E. Mayer and M. G. Mayer, *Statistical Mechanics* (John Wiley and Sons, Inc., New York, 1940), p. 222.

[20] Glasstone, Laidler, and Eyring, *The Theory of Rate Processes* (McGraw-Hill Book Company, Inc., New York, 1941), p. 87.

[21] See reference 19, p. 223.

If in dilute solution we introduce the excellent approximation

$$N_1+N_2\approx N_1 \tag{4.9}$$

and write N_D for N_2,‡ (4.8) can be rewritten as

$$\mu_D=kT\ln\left[\exp\left\{\frac{1}{kT}\left(\frac{\partial A_e}{\partial N_D}\right)_{T,V}\right\}N_D\right]+B_D(T,p), \tag{4.10}$$

where

$$B_D(T,p)=-kT\ln N_1 q. \tag{4.11}$$

Furthermore the chemical potential of a component of an ideal gas mixture can be expressed as[22]

$$\mu_D{}^g=kT\ln p_D+B(T). \tag{4.12}$$

Equating μ_D and $\mu_D{}^g$ yields

$$p_D=\{\exp[(B_D(T,p)-B(T))/kT]\}$$
$$\times\left\{\exp\left[\frac{1}{kT}\left(\frac{\partial A_e}{\partial N_D}\right)_{T,V}\right]\right\}N_D=K_D''\gamma_D''N_D, \tag{4.13}$$

a form of Henry's law with γ_D'' proportional to the γ_D employed in previous sections.

The evaluation of γ_D or γ_D'' thus reduces to the evaluation of

$$\left(\frac{\partial A_e}{\partial N_D}\right)_{T,V}=\left(\frac{\partial F_e}{\partial N_D}\right)_{T,p}, \tag{4.14}$$

where F_e represents the Gibbs free energy of the electrons.

V. THE RELATION OF THE FERMI LEVEL TO THE TOTAL FREE ENERGY OF AN ELECTRON ASSEMBLY

There is a delicate point, concerning the Fermi level, which is intimately connected with the task of evaluating $(\partial A_e/\partial N_D)_{T,V}$, and which, as far as the author knows, is not generally appreciated, either by writers of treatises on statistical mechanics, or by those who actively employ the Fermi level in nonchemical investigations. This is the fact that *although the Fermi level always represents the chemical potential of a weakly coupled electron assembly, it is hardly ever the Gibbs free energy per electron*. The lack of recognition of this fact by the groups mentioned above does not reflect on the care which they have applied to problems in electron statistics, but only on the fact that in the simple case which has been given overwhelming attention (the case of the perfect electron gas) the Fermi level *is* or *is almost* the free energy per electron. The apparent anomaly lies in the fact that F_e is not always a homogeneous[23] function of N_e, the total number of electrons.

In view of the importance of this point it seems worth while to discuss it at some length, justifying, at the same time, the statements made above.

There are many schemes for deriving the Fermi-Dirac distribution law.[24] All of them lead to the relation§

$$n_j=\frac{\omega_j}{1+\exp[(\epsilon_j-\mu)/kT]}, \tag{5.1}$$

in which ϵ_j is the energy of the jth level in the band scheme, ω_j is the degeneracy of the jth level, and n_j is the average number of electrons in the jth level when thermal equilibrium has been attained. The Fermi level μ is shown, in all derivations, to represent the chemical potential of the electrons in the assembly, in the sense that the equality of μ in two distinct systems is required before they can be at thermal equilibrium with respect to each other when free transfer of electrons between the two systems is possible. In none of these derivations is it demonstrated, generally, however, that μ is the Gibbs free energy per election, i.e.,

$$\mu=F/N, \tag{5.2}$$

where F is the Gibbs free energy and N is the total number of electrons in the assembly. (In this section we shall, for convenience, drop the subscript e which should modify each of the thermodynamic functions of the electron assembly. In the next section the subscript will once again be used.) One cannot, therefore, always compute F by taking the product $N\mu$.

In order to decide under what conditions

$$F=N\mu \tag{5.2a}$$

it is necessary to employ the Fermi-Dirac distribution law to compute A and F directly, by appealing to the relations

$$A=E-TS, \tag{5.3}$$
$$p=-(\partial A/\partial V)_{T,N}, \tag{5.4}$$
$$F=A+pV. \tag{5.5}$$

Before doing this we list a few useful formulas, obtained by defining

$$h_j=\omega_j-n_j, \tag{5.6}$$

‡ Since N_2 refers to the *total* number of atoms of species 2, and N_D is a density this replacement is not entirely free of error. However, if we choose N_1 to correspond to unit volume of pure crystal of species 1, the value of N_2 which goes with it (even though variable) will differ negligibly from a density because of the high state of dilution of the solutions with which we are concerned.

[22] G. N. Lewis and M. Randall, *Thermodynamics* (McGraw-Hill Book Company, Inc., New York, 1923), p. 191.

[23] F. H. MacDougall, *Thermodynamics and Chemistry* (John Wiley and Sons, Inc., New York, 1939), p. 25.

[24] See reference 12, section 214.

§ Here, we have not considered the factors of 2 and ½ which enter the formula when applied to acceptor and donor states, respectively. If these are accounted for explicitly in all formulas which follow in this section the same results are obtained as when they are not accounted for. In the interest of typographical simplicity, we have therefore omitted them from consideration. If we were to be entirely general, the exponential in the Fermi-Dirac distribution function would always be preceded by a weight factor, measuring the ratio of the number of electron states available in a given energy level after and before it is occupied. In most cases this ratio would, however, be unity.

as the number of "holes" in the jth electronic level, and by algebraic manipulation of (5.1):

$$h_j=\omega_j \exp[(\epsilon_j-\mu)/kT]/1+\exp[(\epsilon_j-\mu)/kT] =\omega_j[1+\exp[-(\epsilon_j-\mu)/kT]]^{-1}, \quad (5.7)$$

$$n_j/h_j=\exp[-(\epsilon_j-\mu)/kT], \quad (5.8)$$

$$\omega_j/h_j=[1+\exp[(\epsilon_j-\mu)/kT]]/\exp[(\epsilon_j-\mu)/kT] =1+\exp[-(\epsilon_j-\mu)/kT]. \quad (5.9)$$

In standard texts on statistical mechanics the entropy of a Fermi-Dirac assembly is shown to be[25]

$$S=k\sum_j \omega_j \ln\frac{\omega_j}{\omega_j-n_j}-n_j\ln\frac{n_j}{\omega_j-n_j}. \quad (5.10)$$

Insertion of (5.6) and (5.8) into (5.10) yields

$$S=k\sum_j\left(\omega_j\ln\frac{\omega_j}{h_j}+n_j\frac{(\epsilon_j-\mu)}{kT}\right). \quad (5.11)$$

Since

$$\sum_j n_j=N, \quad (5.12)$$

$$\sum_j n_j\epsilon_j=U, \quad (5.13)$$

one obtains from (5.11)

$$-TS=-U+N\mu-kT\sum_j \omega_j\ln\frac{\omega_j}{h_j}. \quad (5.14)$$

Thus, applying (5.3),

$$A=N\mu-kT\sum_j \omega_j\ln\frac{\omega_j}{h_j}. \quad (5.15)$$

The pressure p can now be computed, using (5.4). At this point it is worth noting that if the proper dependence of ω on V (or alternatively of ϵ on V) is taken into account, in applying (5.4) the pressure derived will not be of the order of hundreds of thousands of atmospheres as is sometimes indicated in treatments of the perfect electron gas, but rather, will be some reasonable value, in the neighborhood of an atmosphere. The spurious large pressure, frequently referred to, represents the *kinetic* contribution to the pressure, obtained by the neglect of interaction terms contained in the dependence of ω or ϵ on volume. This point is discussed at some length by Fowler and Guggenheim.[26]

Some thought will indicate that the most general circumstance can be handled by allowing *either* ω *or* ϵ to depend on temperature and volume while the other remains constant. We shall find it convenient to choose ω as variable. The ϵ are then constant, relative to the state of infinite dispersion of electrons and nuclei.

[25] See reference 19, p. 124.
[26] See reference 12, p. 463.

Then application of (5.4) to (5.15) yields

$$p=\left(\frac{\partial A}{\partial V}\right)_{T,N}=-N\left(\frac{\partial\mu}{\partial V}\right)_{T,N} +kT\sum_j\left(\frac{\partial\omega_j}{\partial V}\right)_{T,N}\ln\frac{\omega_j}{h_j} -\left(\frac{\partial\mu}{\partial V}\right)_{T,N}\sum_j \omega_j/[1+\exp[(\epsilon_j-\mu)/kT]]. \quad (5.16)$$

From (5.1) and (5.12) the sum on the right is N. Thus

$$p=kT\sum_j\left(\frac{\partial\omega_j}{\partial V}\right)_{T,N}\ln\frac{\omega_j}{h_j}. \quad (5.17)$$

Substituting (5.15) and (5.17) into (5.5)

$$F=N\mu+kT\sum_j\left[V\left(\frac{\partial\omega_j}{\partial V}\right)_{T,N}-\omega_j\right]\ln\frac{\omega_j}{h_j}. \quad (5.18)$$

It is apparent from (5.18) that (5.2a) is guaranteed to be fulfilled only when the coefficients in brackets in (5.18) vanish, i.e., when

$$\left(\frac{\partial\ln\omega_j}{\partial\ln V}\right)_{T,N}=1. \quad (5.19)$$

This expression integrates to yield

$$\omega_j=K_j(T,N)V. \quad (5.20)$$

It is worth noting that even in the case of the electron gas in metals ω_j is not strictly given by an equation of the form (5.20), although it is *assumed* to be given by[27]

$$\omega=[8m_0^{\frac{3}{2}}\pi\epsilon^{\frac{1}{2}}d\epsilon/2h^3]V, \quad (5.21)$$

in which m_0 is the electron mass. This formula arises only because the electrons have been treated as free particles in a box. Actually ϵ in (5.21), properly referred to a state of infinite dispersion, would depend upon V in some complicated fashion so that ω in (5.21) does not satisfy the form (5.20). Consequently, even in the case of the electron gas in metals (5.2a) does not really hold.

It becomes seriously invalid when applied to the electron "gas" in a valence crystal constituting a typical semiconductor, where the dependence of ω_j on volume, in the valence band is unknown. In the lower bands (below the valence band), those corresponding to closed shell electrons, the overlap between orbitals on different atoms is so small that ω_j is effectively independent of volume. Suppose that these bands are inhabited by

$$N'=\sum_j{}' n_j \quad (5.22)$$

electrons, where the prime signifies that sum is carried

[27] See reference 12, p. 455.

only over states in the lower bands. Then N in (5.18) may be decomposed as follows:

$$N=(N-N')+N'; \tag{5.23}$$

and since

$$\left(\frac{\partial\omega_j}{\partial V}\right)_{T,N}=0, \tag{5.24}$$

for the lower bands (5.18) may be rewritten as

$$F=\left(N'\mu-kT\sum_j{}'\,\omega_j\ln\frac{\omega_j}{n_j}\right)+(N-N')\mu$$

$$+kT\sum{}''\left[V\left(\frac{\partial\omega_j}{\partial V}\right)_{T,N}-\omega_j\right]\ln\frac{\omega_j}{h_j}. \tag{5.25}$$

In the last term the double prime indicates that the sum is carried over the states in the valence band and higher. The terms in brackets may be simplified by substituting from (5.9) and recognizing that for these low-lying states

$$1+\exp[-(\epsilon_j-\mu)/kT]\approx\exp[-(\epsilon_j-\mu)/kT], \tag{5.26}$$

with very good accuracy. Then the terms in brackets become

$$N'\mu+\sum_j{}'\,\omega_j(\epsilon_j-\mu)=(N'-\sum_j{}'\,\omega_j)\mu+\sum_j{}'\,\omega_j\epsilon_j. \tag{5.27}$$

Since there is only a negligible number of holes in the lower bands,

$$\sum_j{}'\,\omega_j=\sum_j{}'\,n_j=N'. \tag{5.28}$$

Furthermore, because of this

$$\sum_j{}'\,\omega_j\epsilon_j\approx\sum_j n_j\epsilon_j=U'. \tag{5.29}$$

Inserting (5.28) and (5.29) into (5.27) and putting the result back into (5.25) yields

$$F=U'+(N-N')\mu$$

$$+kT\sum_i{}''\left[V\left(\frac{\partial\omega_j}{\partial V}\right)_{T,N}-\omega_j\right]\ln\frac{\omega_j}{h_j}, \tag{5.30}$$

from which it is evident, that the contribution of the lower bands to the Gibbs free energy is nothing more than U', the internal energy due to these bands.

VI. THE EVALUATION OF $(\partial A_e/\partial N_D)_{V,T}$ FOR DILUTE SOLUTIONS OF DONORS AND ACCEPTORS IN SEMICONDUCTORS

Turning to the problem of evaluating $(\partial A_e/\partial N_D)_{T,V}$ or, alternatively, $(\partial F_e/\partial N_D)_{T,p}$ we once again append to the quantities A and F used in Sec. V, the subscript e. Since we shall rely on calculated changes in band structure which result from changes in N_D during which no general compression of the lattice is effected, i.e., changes of N_D at constant pressure, it will be more convenient to use $(\partial F_e/\partial N_D)_{T,p}$ rather than $(\partial A_e/\partial N_D)_{T,V}$. Reference to (5.18) shows, immediately, that difficulty will be encountered because little information is available concerning the derivatives $(\partial\omega_j/\partial V)_{T,N_e}$. On the other hand, since we are dealing with a condensed system and p is of the order of an atmosphere the difference, pV, between A_e and F_e is a negligible quantity of energy compared to other terms in A_e. It is therefore possible to replace F_e with A_e and to evaluate

$$(\partial A_e/\partial N_D)_{T,p} \tag{6.1}$$

as a suitable approximation.

We begin by considering donor solutions. In view of (5.30) it will not be necessary to consider all of the electrons in the crystal but only those in the valence band and above. The contribution to F_e of those in the lower bands is merely U', their internal energy, a quantity whose derivative with respect to N_D is constant, and can thus be incorporated in $B_D(T,p)$ in (4.10). By N_e, therefore, we shall mean the number of electrons in states above the lower bands. With this understanding (5.15) can be written as

$$A_e=N_e\mu-kT\sum_j\omega_j\ln\frac{\omega_j}{h_j}, \tag{6.2}$$

where the sum extends over the valence band and higher. If the semiconductor has s valence electrons per atom, and the donor $y=s+1$ electrons per atom,

$$N_e=sN_1+yN_D=s(N_1+N_D)+N_D. \tag{6.3}$$

Substitution of (6.3) into (6.2) and the latter into (6.1) thus yields

$$\left(\frac{\partial A_e}{\partial N_D}\right)_{T,p}=N_e\left(\frac{\partial\mu}{\partial N_D}\right)_{T,p}+y\mu$$

$$-kT\sum_j\left(\frac{\partial\omega_j}{\partial N_D}\right)_{T,p}\ln\frac{\omega_j}{h_j}$$

$$-kT\sum_j\left(\frac{\partial\omega_j}{\partial N_D}\right)_{T,p}+kT\sum_j\frac{\omega_j}{h_j}\left(\frac{\partial h_j}{\partial N_D}\right)_{T,p}. \tag{6.4}$$

It can be shown, through use of (5.7), that

$$\left(\frac{\partial h_j}{\partial N_D}\right)_{T,p}=\frac{h_j}{\omega_j}\left(\frac{\partial\omega_j}{\partial N_D}\right)_{T,p}-\frac{1}{kT}\left(\frac{\partial\mu}{\partial N_D}\right)_{T,p}\frac{h_jn_j}{\omega_j}. \tag{6.5}$$

Substitution of (6.5) into (6.4) reduces that expression [in view of (5.12)] to

$$\left(\frac{\partial A_e}{\partial N_D}\right)_{T,p}=y\mu-kT\sum_j\left(\frac{\partial\omega_j}{\partial N_D}\right)_{T,p}\ln\frac{\omega_j}{h_j}. \tag{6.6}$$

Now, in the valence band

$$\omega_j=M_j(T,p)N_D \tag{6.7}$$

for donor states, and constant otherwise.‖ For this band, therefore,

$$\left(\frac{\partial\omega_j}{\partial N_D}\right)_{T,\,p}=M_j(T,\,p)=\frac{\omega_j}{N_D}, \tag{6.8}$$

where the subscript j is restricted to donor states in the valence band. The part of the sum in (6.6) referring to the valence band thus becomes

$$-\frac{kT}{N_D}\sum_j{}'\,\omega_j\ln\frac{\omega_j}{h_j}, \tag{6.9}$$

where the prime denotes the restriction to the valence band, and, furthermore, to donor states in the valence band. Since in the valence band

$$-(\epsilon_j-\mu)\gg kT, \tag{6.10}$$

it follows from (5.7) that

$$\frac{\omega_j}{h_j}\approx\exp[-(\epsilon_j-\mu)/kT] \tag{6.11}$$

so that (6.9) becomes

$$\frac{1}{N_D}\sum_j{}'\,\omega_j(\epsilon_j-\mu)=\sum_j{}'\,\omega_j\epsilon_j/N_D-\mu\sum_j{}'\,\omega_j/N_D. \tag{6.12}$$

Now

$$\sum_j{}'\,\omega_j=sN_D, \tag{6.13}$$

and with (6.7)

$$\sum_j{}'\,\omega_j\epsilon_j/N_D=\sum_j{}'\,M_j(T,\,p)\epsilon_j. \tag{6.14}$$

Insertion of (6.13) and (6.14) into (6.12) yields

$$\sum_j{}'\,M_j(T,\,p)\epsilon_j-s\mu. \tag{6.15}$$

The first term in (6.15) is independent of composition and can be incorporated into $B_D(T,\,p)$. The latter term can be used in place of the sum over the valence band in (6.6).

Since instead of adding states to the conduction band, we assume that donor atoms add states to the donor level

$$(\partial\omega_j/\partial N_D)_{T,\,p}$$

is zero in the conduction band while it is unity in the donor level. Using these facts together with the last term of (6.15), (6.6) becomes

$$\left(\frac{\partial A_e}{\partial N_D}\right)_{T,\,p}$$

$$=(\gamma-s)\mu-kT\ln\frac{N_D}{h_D}=\mu-kT\ln\frac{N_D}{h_D}$$

$$=\mu-kT\ln[1+2\exp[-(\epsilon_D-\mu)/kT]]. \tag{6.16}$$

As a result, we derive from (4.13) using (6.16)

$$p_D=K_D''\left\{\frac{\exp(\mu/kT)}{1+2\exp[-(\epsilon_D-\mu)/kT]}\right\}N_D. \tag{6.17}$$

If in this expression we replace K_D'' by

$$K_D''=K_D\{2\exp(-\epsilon_D/kT)+1\}, \tag{6.18}$$

we obtain

$$p_D=K_D\left\{\frac{1+\frac{1}{2}\exp(\epsilon_D/kT)}{1+\frac{1}{2}\exp[(\epsilon_D-\mu)/kT]}\right\}N_D \tag{6.19}$$

in complete agreement with (2.5).

An entirely similar treatment can be given for acceptors which leads to (2.7).

Although the statistical argument presented in these latter sections has made no assumption with respect to the mechanism of transfer of an atom between two phases, it is not entirely without assumptions. These are, however, mild when applied to dilute solutions. In closing it is worth while to list them in summary. It is assumed:

(1) that the solution is sufficiently dilute so that impurity atoms do not interact strongly with each other;

(2) that the entropy of the electron assembly can be calculated in any stage of normal vibration from the band picture for the undeformed crystal;

(3) that F_e can be approximated adequately by A_e;

(4) that the solution is sufficiently dilute so that the main band structure is unaltered by the introduction of impurity atoms, save for the introduction of donor states close to the conduction band and new states in the vicinity of the valence band.

The author wishes to express his appreciation for valuable critical discussions with several of his colleagues at the Bell Telephone Laboratories, among whom are C. D. Thurmond, J. A. Burton, and G. H. Wannier.

‖ We assume here that for sufficiently dilute solutions the addition of the impurity atom merely adds new states close to the valence band leaving the main structure of the valence band unchanged. Similarly, we assume that the main structure of the conduction band remains unchanged.

On the Disorder in Crystalline 2,2-Dinitropropane at Room Temperature*

S. C. ABRAHAMS
Laboratory for Insulation Research, Massachusetts Institute of Technology, Cambridge, Massachusetts
(Received February 19, 1953)

2,2-dinitropropane forms face-centered, cubic crystals at room temperature, with $a_0=8.78\pm0.05$A, and 4 molecules per unit cell. Molecular disorder is necessarily present in the cell, and several models are examined. Excellent agreement is obtained with a model in which the molecule possesses complete orientational disorder. Although the distinction between "rotational" disorder in time and in space is not possible, the following mechanism is suggested: while the disorder is complete at long range, there is a high degree of order at short range.

INTRODUCTION

DIELECTRIC constant and heat capacity studies of several tetra-substituted methanes just below their mp have been taken as indicating rotational freedom in the solid state.[1] A recent study of the dielectric constant and loss of 2,2-dinitropropane[2] shows that the rotator phase has a dielectric relaxation time corresponding to a wavelength close to 3 cm at room temperature. Nuclear magnetic resonance measurements on this crystal indicate that the methyl hydrogens have rotational motion in the plane of the protons at an effective frequency greater than 10^4 cps above *ca* -180°C.[3] No x-ray investigation of this compound, apparently, has previously been undertaken, and the present study is an attempt to describe the nature of the disorder in this crystal at room temperature.

EXPERIMENTAL

With slow sublimation (about 6 months) 2,2-dinitropropane forms well-shaped plates, which plastically deform when handled. A simple technique was devised for preparing single crystals, in which melted 2,2-dinitropropane was admitted into a capillary open at both ends. On cooling, the resulting clear glass-like solid was generally found to be a single crystal. This frequently ruptured later with the formation of bubbles within the crystal. The x-ray data were obtained by means of Laue, rotation and precession photographs, using Mo and Cu radiations. The intensities were estimated visually from a set of multiple exposure precession camera films.

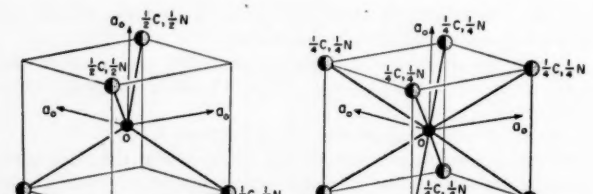

FIG. 1. (a) A tetrahedral distribution of the carbon and nitrogen atoms, with averaged weights, in the noncentrosymmetric, face-centered cubic space groups; (b) An octahedral centrosymmetric distribution. Solid circles represent carbon, and shaded circles nitrogen atoms.

CRYSTAL DATA

2,2-dinitropropane $C_3H_6N_2O_4$ forms colorless, waxy, plastic crystals, which melt at 53°C and undergo a transition at -7°C. The crystal belongs to the cubic system, with $a_0=8.78\pm0.05$A, the only systematic absences being hkl with $h+k=2n+1$, $k+l=2n+1$ and $h+l=2n+1$. Piezoelectric tests are negative. Thus the only possible space groups allowed are $F23$, $F432$, $F\bar{4}3m$, $Fm3$, and $Fm3m$, of which only the last two possess a center of symmetry. The measured density is 1.30, and the calculated, 1.32. There are four molecules per unit cell.

ANALYSIS OF THE DISORDER

The symmetry possessed by each of the five possible space groups requires, in the case of the least amount of disorder, that the methyl and nitro groups occupy identical positions, with the central carbon atom at the origin. Thus the two carbon and the two nitrogen atoms lie either at $x\,x\,x$, $x\,\bar{x}\,\bar{x}$, $\bar{x}\,x\,\bar{x}$, $\bar{x}\,\bar{x}\,x$, if the space group is noncentrosymmetric, or at $x\,x\,x$, $x\,\bar{x}\,\bar{x}$, $\bar{x}\,x\,\bar{x}$, $\bar{x}\,\bar{x}\,x$, $\bar{x}\,\bar{x}\,\bar{x}$, $\bar{x}\,x\,x$, $x\,\bar{x}\,x$, $x\,x\,\bar{x}$, if the space group is centrosymmetric. This, of course, is merely stating that the tetrahedral bond distribution about the central carbon atom is being used by the crystal symmetry (Fig. 1).

The following molecular dimensions are used in all models: C$-$C and C$-$N$=$1.51A, N$-$O$=$1.23A, C$-$H $=$1.09A, O$-\hat{\text{N}}-$O$=$125°, H$-\hat{\text{C}}-$H, C$-\hat{\text{C}}-$C, and N$-\hat{\text{C}}-$N$=$109.5°. In the first four models the hydrogen atoms of the methyl groups are taken as rotating in the plane of the hydrogen triangle.[3] The atomic scattering factors given by James and Brindley[4] were used, with a temperature factor correction of $\exp[-B\{(\sin\theta)/\lambda\}^2]$, where $B=5$A^2.

In the first model considered, the space group was assumed to be centrosymmetric. The oxygen atoms

* Sponsored by the U. S. Office of Naval Research, the Army Signal Corps, and the Air Force under ONR Contracts N5ori-07801 and N5ori-07858.

[1] R. W. Crowe and C. P. Smyth, J. Am. Chem. Soc. **72**, 4009 (1950).

[2] Powles, Williams, and Smyth, J. Chem. Phys. (to be published).

[3] J. G. Powles, private communication.

[4] R. W. James and G. W. Brindley, Z. Krist. **78**, 470 (1931).

were taken as fixed with respect to the rest of the molecule, and each atom must then occupy at least three possible positions. (See the 96-fold position in $Fm3$ and $Fm3m$.) One oxygen atom was placed in the eclipsed position with respect to the three other groups linked to the central carbon atom. The second oxygen atom then necessarily occupied the staggered position. The geometrical structure factor for the carbon and nitrogen atoms is then $8\cos2\pi hx\cos2\pi kx\cos2\pi lx$, and for the oxygen atoms is $8/3[\cos2\pi hx\cos2\pi ky\cos2\pi lx+\cos2\pi hx\cos2\pi kx\cos2\pi ly+\cos2\pi hy\cos2\pi kx\cos2\pi lx]$. For the hydrogen atoms it is $24\cos2\pi hx\cos2\pi kx\times\cos2\pi lxJ_0(t)$, where the center of the hydrogen atom orbit is at $x\,x\,x$, and $J_0(t)$ is the zero-order Bessel function, with $t=2\pi\rho(\sin\alpha)/d$, ρ being the radius of the orbit, α the angle between the planes of the orbit and of the reflection, and d the spacing.[5] The calculated structure factors for this model are listed in Table I under $F1$. The structure factors for the noncentrosymmetric case of this model are found under $|F2|$. The geometrical structure factors for this case are very simply related to those already given. Since it has not been established by other means whether or not the nitro group is also rotating, this possibility was next considered for both centrosymmetric and noncentrosymmetric space groups. The structure factors corresponding to this case are listed, respectively, under $F3$ and $|F4|$.

The maximum molecular disorder which could be present in this crystal gives each atom an equal chance of being at any point on the surface of a sphere, with radius the interatomic distance between that atom and the center of rotation. This would be equivalent to complete rotational disorder, at least, statistically. The geometrical structure factor for a group such as this is $(n_j\sin r_js)/r_js$,[6] where n_j=number of jth atoms, r_j=radius of the jth sphere (the center of the sphere being at the origin of the cell) and $s=(4\pi\sin\theta)/\lambda$. The central carbon atom is almost exactly at the steric center of the molecule, since the C−H distance is 2.32A and the C−O distance is 2.34A. The structure factors for a rotational disorder model with the central carbon atom at the rotation center are given in Table I under $F5$. An alternative center of rotation is the center of inertia,† 0.57A from the central carbon atom. Structure factors for the rotational model with this as center are collected under $F6$.

The agreement between observed and calculated structure factors in Table I is uniformly better for the centrosymmetric case than for the noncentrosymmetric (the rotating models are centrosymmetric). It thus seems likely that the positions $0\,0\,0$, $0\,\frac{1}{2}\,\frac{1}{2}$, $\frac{1}{2}\,0\,\frac{1}{2}$, $\frac{1}{2}\,\frac{1}{2}\,0$ are centers of symmetry.

[5] J. M. Bijvoet and J. A. A. Ketelaar, J. Am. Chem. Soc. **54**, 625 (1932).

[6] R. W. James, *The Optical Principles of the Diffraction of X-rays* (G. Bell and Sons, London, 1948), p. 467.

† The writer is indebted to Dr. W. N. Lipscomb for suggesting this alternative.

TABLE I. Structure factors[a] for the disordered models of 2,2-dinitropropane.

hkl	$F1$	$\|F2\|$	$F3$	$\|F4\|$	$F5$	$F6$	F_{obs}
111	+94	65	+97	65	+125	+113	116
200	+35	20	+29	15	+46	+58	55
220	−3	1	+19	10	−8	−5	6
311	−12	33	−7	20	−8	−10	7
222	+19	50	+8	64	−5	−8	7
400	−25	14	−27	14	+3	−1	5
331	+15	16	+12	14	+4	+3	5

[a] In this table, $\Sigma|F_{hkl}|$ in all columns has arbitrarily been placed equal to 200.

DISCUSSION

In considering a structure model for a crystal such as 2,2-dinitropropane in which some disorder must necessarily be present, the small number of observations imposes a severe limitation. Although very many models may be set up, the usual methods of refinement associated with ordered structures are no longer available, with a consequent loss of detail.[7] Between the four models based on minimum disorder, and the rotational disorder models, an infinity of other models is possible. The agreement of the statistical-rotating model structure factors with the observed values is so good for both centers of rotation, however, that it seems unlikely that the true model would be very different from this. If the molecules may now truly be represented as spheres, with the central carbon atom at the center, the closest approaches between nearest neighbors could be 1.5A. For the center of inertia at the center of the sphere, this approach could be 0.9A. The density is fairly high at 1.32 g cm^{-3}, but there is no apparent reason why any intermolecular contact should be much less than *ca* 2.9A. It thus seems virtually certain that interaction between neighbors must occur. A simple mechanism which would provide for this interaction is that, while the disorder is complete at long range, at short range there is a high degree of order. In this case the closest contacts could be *ca* 2.8A.

It is of interest to note that carbon tetrabromide, in the transition range just below the mp, has been reported as giving good agreement between the observed intensities and those calculated for a rotational disorder model.[8] Similar behavior has also been observed in carbon tetrachloride.[9] However, Marshall, Hart, and Staveley[10] state that their specific heat measurements indicate that the carbon tetrabromide molecules do not freely rotate in the high temperature form.

The writer wishes to thank Dr. J. G. Powles, University of Illinois, for bringing this problem to his attention, and for a gift of 2,2-dinitropropane, and also Professor A. von Hippel for his interest.

[7] See S. C. Abrahams and W. N. Lipscomb, Acta Cryst. **5**, 93 (1952).

[8] C. Finbak, Tidsrkr. Kjemi. Bergvesen **17**, No. 9, 145 (1937).

[9] R. L. Collin, private communication.

[10] Marshall, Hart, and Staveley, Nature **168**, 519 (1951).

On Variational Principles for Irreversible Processes*

PHILIP ROSEN
Applied Physics Laboratory, The Johns Hopkins University, Silver Spring, Maryland
(Received January 26, 1953)

A variational principle is formulated for diffusional processes such as heat and matter diffusion which is a modification of Onsager's principle of minimum dissipation. Also a variational principle is given for the flow of viscous incompressible fluids which has some analogy to Onsager's principle.

I. DIFFUSIONAL PROCESSES

ONSAGER[1] has defined a dissipation function

$$\varphi(J,J)\equiv\frac{1}{2T}\sum_{ik}R_{ik}J_iJ_k \tag{1}$$

which is one-half of the rate of production of irreversible entropy. The currents or fluxes J are related to the generalized forces X by

$$X_i=\sum_k R_{ik}J_k, \tag{2}$$

where R_{ik} is the symmetric generalized resistance tensor.

Onsager has shown that if the integral of the above dissipation function over a volume τ is a minimum, subject to continuity conditions on the currents, the specification of the currents on the boundary and with the forces specified, then Eq. (2) is obtained.

In the case of steady heat flow in an isotropic medium,

$$\varphi=RJ^2/2T,\quad X=-\nabla T/T.$$

In this case Onsager's principle of least dissipation would be

$$\delta\int\left(\frac{RJ^2}{2T}+\lambda\nabla\cdot\mathbf{J}\right)d\tau=0, \tag{3}$$

with the heat current on the boundary J_n fixed and T specified. The Euler LaGrange equation equivalent to Eq. (3) is then

$$R\mathbf{J}/T=\nabla\lambda,$$

where the LaGrange multiplier λ is interpreted as $1/T$.

The purpose of this note is to show that in simple problems of heat flow or matter diffusion, one can define another dissipation function, $\psi=J^2/2\sigma$, where the conductivity σ is the ordinary thermal conductivity for heat flow or the ordinary diffusivity for matter diffusion. The function ψ will lead to simpler variational principles if we assume that σ is only a function of spatial coordinates. We shall consider only the case of nonsteady heat flow in isotropic media here. The case of matter diffusion will follow by analogy.

If the integral $\int(J^2/2\sigma)d\tau$ is stationary, subject to the equation of continuity $\nabla\cdot\mathbf{J}+\rho C_v\partial T/\partial t=0$, with the surface current J_n, T and $\partial T/\partial t$ specified, then

$$\delta\int\left[\frac{J^2}{2\sigma}-\lambda\left(\nabla\cdot\mathbf{J}+\rho C_v\frac{\partial T}{\partial t}\right)\right]d\tau=0 \tag{4}$$

yields

$$\mathbf{J}=-\sigma\nabla\lambda=-\sigma\nabla T, \tag{5}$$

and λ can be interpreted as the temperature T except for a possible additive constant whose effect on the resultant differential equation is nil. Thus far this is analogous to Onsager's principle. However the above variational principle is not as useful as it could be, since the temperature T must be held fixed when the current $\mathbf{J}$ is varied. We wish to vary T alone. We find, by using Eq. (5), that the integral in Eq. (4) becomes

$$I=\int\left[\frac{\sigma(\nabla T)^2}{2}-T\left(\rho C_v\frac{\partial T}{\partial t}-\nabla\cdot\sigma\nabla T\right)\right]d\tau.$$

By virtue of Green's theorem we have

$$\int T\sigma\nabla^2T\,d\tau=-\int\nabla T\cdot\nabla(\sigma T)d\tau+\int T\sigma\frac{\partial T}{\partial n}dS.$$

Thus

$$I=-\int\left[\frac{\sigma}{2}(\nabla T)^2+\rho C_vT\frac{\partial T}{\partial t}\right]d\tau+\int T\sigma\frac{\partial T}{\partial n}dS. \tag{6}$$

If $\delta I=0$ subject to the condition that $\delta J_n=0$ and that $\partial T/\partial t$ is specified, we have

$$\delta I=-\int\left[\rho C_v\frac{\partial T}{\partial t}\delta T+\sigma\nabla T\cdot\nabla\delta T\right]d\tau$$
$$+\int\sigma\frac{\partial T}{\partial n}\delta T\,dS+\int T\sigma\left(\delta\frac{\partial T}{\partial n}\right)dS.$$

Also

$$\int\sigma\nabla T\cdot\nabla\delta T\,d\tau=\int\nabla T\cdot\nabla(\sigma\delta T)d\tau-\int(\nabla T\cdot\nabla\sigma)\delta T\,d\tau$$
$$=-\int(\sigma\nabla^2T+\nabla T\cdot\nabla\sigma)\delta T\,d\tau+\int\sigma\frac{\partial T}{\partial n}\delta T\,dS.$$

* This work was supported by the Bureau of Ordnance, U. S. Navy, under Contract NOrd 7386.
[1] L. Onsager, Phys. Rev. 37, 405 (1931).

Thus

$$\delta I=-\int\left(C_v\rho\frac{\partial T}{\partial t}-\nabla\cdot\sigma\nabla T\right)\delta T d\tau=0,$$

since $\delta J_n=0$. Consequently since δT is arbitrary,

$$C_v\rho\frac{\partial T}{\partial t}=\nabla\cdot\sigma\nabla T. \tag{7}$$

Now the surface integral in Eq. (6) has no effect on the differential equation obtained from the variational principle since it is equivalent to the volume integral of a divergence.[2] The only influence the surface integral has is to change the boundary conditions. If we omit the surface integral, we find that the variation,

$$\delta\int\left[C_v\rho T\frac{\partial T}{\partial t}+\frac{\sigma}{2}(\nabla T)^2\right]d\tau, \tag{8}$$

with $\partial T/\partial t$ fixed and T specified on the boundary leads to Eq. (7).

In using either Eq. (8) or its counterpart containing the surface integral for approximate calculations, one can expand the temperature in the series

$$T=\sum_n a_n(t)\varphi_n(x, y, z),$$

where $\varphi_n(x, y, z)$ is an orthonormal set of functions which can be used to satisfy the boundary conditions. Then we will be able to carry out the above variations with the a_n as variables holding da_n/dt fixed. In the case of convection, the mobile derivative, $DT/Dt=\partial T/\partial t+\mathbf{q}\cdot\nabla T$ replaces $\partial T/\partial t$ and is held fixed in carrying out any of the above variations. Here $\mathbf{q}$ is the velocity of the medium.

II. INCOMPRESSIBLE VISCOUS FLUID

Millikan[3] attempted to obtain a variational principle for describing the flow of a viscous incompressible fluid and came to the conclusion that for three-dimensional flow, unless the vector product of the vorticity and velocity is zero, such a principle could not be found. He however overlooked the possibility of a restricted variational principle similar to Onsager's in which forces are held fixed.

Let us consider the minimization of the dissipation of energy subject to the condition that energy and mass be conserved, with the acceleration at every point specified and the fluid velocity specified at the boundary. If $\mathbf{q}$ is the velocity and u, v, w are the components, then the conservation of energy yields

$$\int\mathbf{q}\cdot P\cdot\mathbf{n}dS=\int\rho\mathbf{q}\cdot\mathbf{A}d\tau+\int\Phi d\tau, \tag{9}$$

where P is the stress tensor, $\mathbf{n}$ is the unit normal to the surface S, ρ is the fluid density, $\mathbf{A}$ is the local acceleration $=D\mathbf{q}/Dt$, and Φ is the dissipation of energy per unit volume. The function[4] Φ for an incompressible fluid can be expressed as

$$\Phi=\eta\left[2\left(\frac{\partial u}{\partial x}\right)^2+2\left(\frac{\partial v}{\partial y}\right)^2+2\left(\frac{\partial w}{\partial z}\right)^2+\left(\frac{\partial w}{\partial y}+\frac{\partial v}{\partial z}\right)^2+\left(\frac{\partial u}{\partial z}+\frac{\partial w}{\partial x}\right)^2+\left(\frac{\partial v}{\partial x}+\frac{\partial u}{\partial y}\right)^2\right], \tag{10}$$

where η is the viscosity. Since ρ is constant, the conservation of mass is simply $\nabla\cdot\mathbf{q}=0$.

If we omit the surface integral in Eq. (9) (since it only affects boundary conditions), then we can state the variational problem as

$$\delta\int\left(\frac{\Phi}{2}-\lambda\rho\mathbf{q}\cdot\mathbf{A}-\mu(x, y, z)\nabla\cdot\mathbf{q}\right)d\tau=0, \tag{11}$$

$\mathbf{A}$ and $\mathbf{q}$ on boundary fixed.

Here λ is an undetermined LaGrangian multiplier and $\mu(xyz)$ an undetermined function. The Euler LaGrange equivalent to Eq. (11) is then

$$-\lambda\rho\mathbf{A}=-\nabla\mu(x, y, z)+\eta\nabla\cdot\nabla\mathbf{q}.$$

Thus we take $\lambda=-1$ and $\mu=p=$the hydrostatic pressure, and the Navier-Stokes equation is obtained.

The author wishes to express his appreciation to Dr. F. T. McClure of the Applied Physics Laboratory and to Professor S. Corrsin of The Johns Hopkins University for stimulating discussions of the subject matter of this note.

[2] R. Weinstock, *Calculus of Variations* (McGraw-Hill Book Company, Inc., New York, 1952).

[3] C. B. Millikan, Phil. Mag. **7**, 641 (1929).

[4] H. Lamb, *Hydrodynamics* (Dover Publications, New York, 1945).

Theory of the Rotational Spectra of Allene-Type Molecules*

MASATAKA MIZUSHIMA†
Department of Physics, Duke University, Durham, North Carolina
(Received January 22, 1953)

The possibility of observing the rotational spectra of allene-type molecules was suggested by the present author and Venkateswarlu. In this paper the effect of nuclear spin on the statistical weight of each rovibrational levels and the transition probability between them are calculated.

I. INTRODUCTION

THE present author and Venkateswarlu[1] showed that it is possible to observe the rotational spectra of allene ($H_2C_3H_2$) type molecules when it is in a degenerate vibrational state. In this paper some general discussion on these spectra will be made.

II. GROUP THEORETICAL DISCUSSION

Allene-type molecules (X_4Y_3) belong to point group V_d, which has representations A_1, A_2, B_1, B_2, and E. On the other hand, these molecules also belong to permutation groups $\mathfrak{S}_4$ and $\mathfrak{S}_3$, since they have four identical X nuclei and three identical Y nuclei. (See Fig. 1.) These three groups are commutable to each other; thus each representation of point group V_d is reducible in the permutation groups.

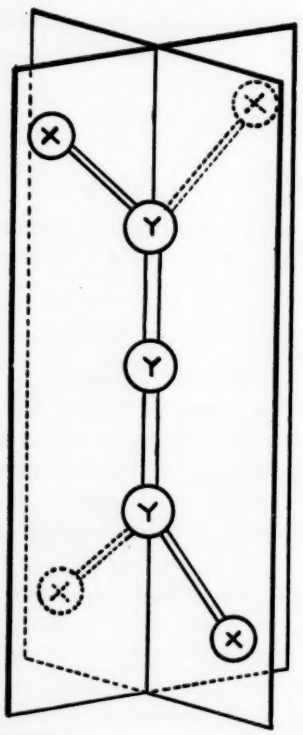

FIG. 1. Allene-type molecule X_4Y_3.

Exchanging X nuclei, we obtain six independent states in A_1 state as shown in Fig. 2, from which we obtain the character in group $\mathfrak{S}_4$ as in Table I. By the usual procedure we find the reduced representation of A_1 as $\chi_0+\chi_1+2\chi_2$, where χ_i are the representations of $\mathfrak{S}_4$, the characters of which are shown in Table II.

If we take molecule in e vibrational state instead of the above nonvibrating one, we obtain the character of E state, by which we can reduce E representation in group $\mathfrak{S}_4$.

When e vibration is excited by two quanta, we obtain A_1, B_2, and B_2 vibrational states as is shown in I. Using the normal coordinates of them, which are obtained in I, we can reduce these representations in group $\mathfrak{S}_4$. The results are summarized in Table III.

If the exchange between three nuclei is taken into account, the number of independent states will be multiplied by three; but one can easily see that none of them remains as it is under any exchange between Y nuclei, that is, the character in group $\mathfrak{S}_3$ is always

TABLE I. Character of A_1 state in group $\mathfrak{S}_4$.

Species	E	(12)	(12)(34)	(123)	(1234)
χ	6	0	6	0	0

expressed as in Table IV. Thus every representation in point group V_d will be reduced as $\chi_0+\chi_1+2\chi_2$ in group $\mathfrak{S}_3$, where χ_0 is the totally symmetric, χ_1 is the antisymmetric, and χ_2 is the two-dimensional representation.

III. REPRESENTATION OF ROTATIONAL AND ROVIBRATIONAL STATES, CONFIGURATION MULTIPLET

The rotational wave function belongs to the rotational subgroup of the point group to which that molecule belongs.[2] The rotational subgroup of point group V_d is V, where representations are related to that of V_d as shown in Table V. (A is the totally symmetric representation, and B_1 is the antisymmetric one with respect to twofold rotations perpendicular to the molecular axis.) The transformation properties of symmetric rotator functions are given by Wilson,[3] from

* The research reported in this paper has been sponsored by the Geophysics Research Directorate of Air Force Cambridge Research Center, Air Research and Development Command.

† On leave from Department of Physics, Faculty of Science, University of Tokyo, Tokyo, Japan.

[1] M. Mizushima and P. Venkateswarlu, J. Chem. Phys. **21**, 705 (1953), hereafter referred to as I.

[2] G. Herzberg, *Infrared and Raman Spectra of Polyatomic Molecules* (D. Van Nostrand Company, Inc., New York, 1945), p. 406.

[3] E. B. Wilson, Jr., J. Chem. Phys. **3**, 276 (1935).

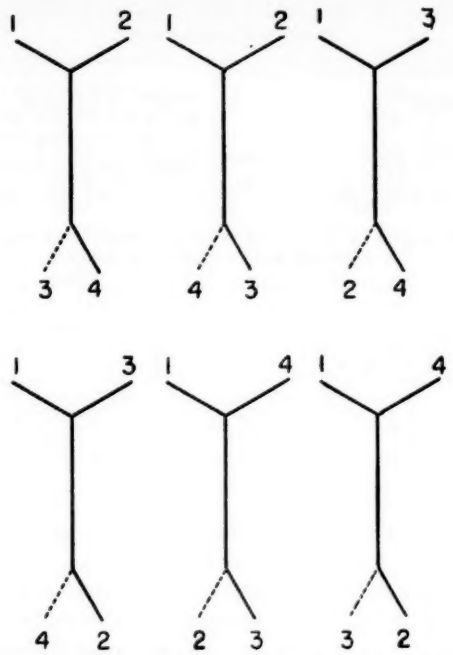

FIG. 2. Six possible configurations of X_4Y_2 molecule obtained by exchanging X nuclei.

which we find the representation to which each function belongs as in Table VI.

When the molecule is in an e vibrational state, each rovibrational state will belong to those representations as are shown in Table VII.

In formulas (7a) and (8a) of I we defined explicitly the wave functions of these rovibrational states. From their transformation properties we obtain the result shown in Table VIII.

From Tables III and V we can easily reduce each representation of group V in group $\mathfrak{S}_4$, the result of which is shown in Table IX. Each rovibrational state will further split corresponding to this reduction. In simpler molecules this splitting will be reduced to inversion doubling, internal rotation, etc., but in our case it is so complicated that it will be better to call it configuration multiplet. The configuration multiplet of each rovibrational state will easily be obtained by Tables VI, VII, and IX. It must be noted that each levels in the multiplet thus obtained will further split into four corresponding to the reduction $\chi_0+\chi_1+2\chi_2$ in group $\mathfrak{S}_3$.

TABLE II. Character of representations of group $\mathfrak{S}_4$.

Species	E	(12)	(12)(34)	(123)	(1234)
χ_0	1	1	1	1	1
χ_1	1	−1	1	1	−1
χ_2	2	0	2	−1	0
χ_3	3	1	−1	0	−1
χ_4	3	−1	−1	0	1

TABLE III. Reduction of representations in group $\mathfrak{S}_4$.

A_1	$\chi_0+\chi_1+2\chi_2$
A_2	$\chi_3+\chi_4$
B_1	$\chi_0+\chi_1+2\chi_2$
B_2	$\chi_3+\chi_4$
E	$2\chi_3+2\chi_4$

TABLE IV. Character of a state in group $\mathfrak{S}_3$ (applicable to all states).

	E	(12)	(123)
χ	n^a	0	0

[a] n is an integer.

IV. STATISTICAL WEIGHT OF ROTATIONAL STATES

The total wave function of a molecule including nuclear spin function must obey Pauli's principle; thus it belongs to χ_0 when I_X is integer, and to χ_1 when I_X is half-integer, where I_X is the spin of X nucleus.

It is not difficult to show that the number of nuclear spin function which belongs to each representation is given as in Table X. From this table we can easily find the statistical weight of each rotational level in nonvibrating molecule; the result is shown in Table XI.

TABLE V. The relation between the representations of V and V_d.

V_d	V
A_1	A
A_2	B_1
B_1	A
B_2	B_1
E	B_2+B_3

When $I_X=\frac{1}{2}$ and 1, it agrees with the results of DeHeer[4] and Lord and Venkateswarlu.[5] Nucleus Y has no effect on the relative weight.

V. FINE STRUCTURE OF ROTATIONAL SPECTRA

It was shown in I that the rotational spectra with selection rule $\Delta J=0, \pm 1$, $\Delta K=0$ can be observed when an allene-type molecule is in e vibrational state.

The rovibrational state will split by means of Coriolis coupling and l-type doubling. The statistical weight of these levels is given in Table XII.

We shall not discuss the magnitude of splitting here, since it is discussed by some other authors.[4,5]

TABLE VI. Representation to which each rotational wave function belongs.

$K=0$ { J odd	B_1
J even	A
$K\neq 0$ { K odd	B_2+B_3
K even	$A+B_1$

[4] J. DeHeer, J. Chem. Phys. **20**, 637 (1952).
[5] R. C. Lord and P. Venkateswarlu, J. Chem. Phys. **20**, 1327 (1952).

TABLE VII. Representation in e vibrating molecule.

$K=0$	B_2+B_3
$K\neq 0$ K odd	$2A+2B_1$
$K\neq 0$ K even	$2B_2+2B_3$

TABLE VIII. Representation to which each wave function defined in formulas (7a) and (8a) of I belongs. (η is the larger one of $|K|$ and $|M|$.)

	$J+\eta+M$ even	$J+\eta+M$ odd
K odd Ψ_+^+, Ψ_+^-	A	B_1
K odd Ψ_-^+, Ψ_-^-	B_1	A
K even Ψ_+^+, Ψ_+^-	B_2	B_3
K even Ψ_-^+, Ψ_-^-	B_3	B_2

The transition probability between these sublevels is calculated in I, but the effect of nuclear spin was not taken into consideration there. The nuclear spin state must remain unchanged under all optical transitions. Since six states illustrated in Fig. 1 are orthogonal to each other, it is equivalent to the selection rule: that "transitions between levels of different over-all species are very strictly forbidden."[3] Applying this rule, we find, from Table VIII, that some Zeeman transitions are forbidden. Thus the over-all transition probability

TABLE IX. Reduction of representation of group V by means of those of group $\mathfrak{S}_4$.

A	$\chi_0+\chi_1+2\chi_2$
B_1	$\chi_3+\chi_4$
B_2	$\chi_3+\chi_4$
B_3	$\chi_3+\chi_4$

TABLE X. Number of nuclear spin function which belongs to each representation of group $\mathfrak{S}_4$.

χ_0	$(1/6)(I_X+1)(I_X+2)(2I_X+1)(2I_X+3)$
χ_1	$(1/6)I_X(I_X-1)(2I_X+1)(2I_X-1)$
χ_2	$(1/3)I_X(I_X+1)(2I_X+1)^2$
χ_3	$(1/2)I_X(I_X+1)(2I_X+1)(2I_X+3)$
χ_4	$(1/2)I_X(I_X+1)(2I_X+1)(2I_X-1)$

TABLE XI. Statistical weight of rotational levels in vibrational ground state.

$K=0$ J odd	$I_X(I_X+1)(2I_X+1)^2$
$K=0$ J even	$\{I_X^3+(I_X+1)^3\}(2I_X+1)$
$K\neq 0$ K odd	$2I_X(I_X+1)(2I_X+1)^2$
$K\neq 0$ K even	$(2I_X^2+2I_X+1)(2I_X+1)^2$

TABLE XII. Statistical weight of sublevels in each rovibrational state (e vibrational state).

	J even	J odd
K odd Ψ_+^+, Ψ_+^-	a	b
K odd Ψ_-^+, Ψ_-^-	b	a

where
$a=(2I_X+1)\{I_X^3+(I_X+1)^3-(K/(2J+1))(2I_X+1)\}$,
$b=(2I_X+1)\{I_X(I_X+1)(2I_X+1)+(K/(2J+1))(2I_X+1)\}$.
K even $I_X(I_X+1)(2I_X+1)^2$, which is common to all sublevels.

becomes small under this effect which is represented by the factor a, given in Table XIII.

The splitting of configuration multiplet seems to be extremely small in our molecule. Probably the largest splitting will be that due to the internal rotation of CH_2 in allene molecule. In this case the height of the hindering potential is estimated to be about 9000 cm^{-1}.[6] If

TABLE XIII. Effect of nuclear spin on transition probability. (The following factor must be multiplied to the formula which is calculated without taking the above effect into account.)[a]

	$J\to J+1$	$J\to J$
$\Psi_+\leftrightarrow\Psi_+$, $\Psi^-\leftrightarrow\Psi^-$	a	$1-a$
$\Psi_+\leftrightarrow\Psi_-$	$1-a$	a

$a=K\{2(J+1)(J+2)+(1/3)(2K^2+1)\}/(J+1)(2J+1)(2J+3)$

[a] In this table, $\Psi_+\leftrightarrow\Psi_+$, for example, means $\Psi_+^+\leftrightarrow\Psi_+^+$, $\Psi_+^+\leftrightarrow\Psi_+^-$ and $\Psi_+^-\leftrightarrow\Psi_+^-$.

one calculates the energy splitting using this value, one obtains the result of about 10^{-10} cycle, both when the perturbation method and the WKB method are used. If the height were as small as 4000 cm^{-1}, one would obtain 10^{-2} cycle, which is still extremely small to be observed.

[6] J. W. Linnett and W. H. Avery, J. Chem. Phys. **6**, 686 (1938).

Some Thermodynamic Properties of Methane Adsorbed on Rutile Between 80 and 140°K*

E. L. PACE, E. L. HERIC, AND KENT S. DENNIS
Morley Chemical Laboratory, Western Reserve University, Cleveland, Ohio

(Received February 23, 1953)

Heat capacities of methane adsorbed on rutile (titanium dioxide) have been determined from 80 to 140°K for concentrations corresponding to the fractions 0.28, 0.56, 0.84, and 1.11 of the monolayer capacity. Integral heats of adsorption, determined at 110, 120, 130, and 140°K, show correlation with the heat capacities within the experimental error. The thermodynamic functions, ΔH, ΔS, and ΔF of the differential adsorption process, have been calculated from the data. The heat capacities indicate an adsorbate having properties differing from bulk methane and possessing some degree of mobility over the surface. No first-order phase changes were in evidence for the concentrations studied. At low surface coverages, the shape of the differential heat of adsorption curve points to the presence of a heterogeneous adsorbent surface, while at coverages approaching the monolayer, dispersion forces are probably in effect. All the differential thermodynamic quantities approach the values for liquid methane at coverages greater than the monolayer in the temperature range from 110 to 140°K.

INTRODUCTION

THE heat capacity of methane adsorbed on rutile (titanium dioxide) has been reported[1] for monolayer coverages from 55 to 90°K. In the present work, the measurement of this property for the methane-rutile system has been extended to 140°K. In addition, some integral heats of adsorption have been measured and correlated with the heat capacity of the adsorbed methane.

Kington and Aston[2] have pointed out that calorimetrically measured heats of adsorption can be interpreted without ambiguity in terms of the reversible thermodynamic properties of the system. Furthermore, in the present investigation, the internal consistency which has been obtained between the directly measured heat capacities and those derived from the temperature coefficient of the integral heat of adsorption indicates strongly an equilibrium adsorption process. Consequently, the data have been used to calculate the entropy, heat content, and free energy changes in the differential adsorption process.

The effect of the heterogeneity of the surface of the solid adsorbent on the thermodynamic properties of the adsorbate has been considered in several recent papers.[3–6] A direct experimental approach to this effect is the measurement of integral heats of adsorption with some precision at low coverages. This has been accomplished with some success in the present work.

EXPERIMENTAL

The calorimeter used in the experimental measurements has already been described.[1] The adsorbate was research grade methane of 99.5 percent minimum purity obtained from the Phillips Petroleum Company. It was further purified by fractional distillation before storage in glass bulbs prior to use. The adsorbent was essentially pure crystalline rutile (titanium dioxide) furnished by the National Lead Company. The BET method of surface area determination indicated a monolayer capacity of 0.03106 moles† of methane at 89.5°K.

The heat capacity of the adsorbate (c_{N_s}) was calculated using the equation[7]

$$\frac{dQ}{dT}=c_{pG}+c_{\text{pcal}}+c_{N_s}-q_{st}\left(\frac{dN_s}{dT}\right)_{\text{expt}}-V_G\left(\frac{dP}{dT}\right)_{\text{expt}}, \quad (1)$$

in which dQ/dT is the total heat capacity; c_{pG}, the heat capacity of the gas phase in the calorimeter; c_{pcal}, the heat capacity of the calorimeter vessel plus adsorbent; q_{st}, the isosteric heat of adsorption; N_s, moles of adsorbed gas; and P, the equilibrium pressure of the adsorbate. dQ/dT and c_{pcal} were obtained from the experimentally measured average values using the method described by Scott *et al.*[8] The maximum corrective term thus introduced was 0.010 calories for a temperature rise of 6.66 degrees. The last two terms of Eq. (1) represent the desorption and compression correction, respectively. Values of the isosteric heat of adsorption were determined from experimental isotherms by use of the Clausius-Clapeyron equation. The dependence of N_s on temperature was determined from a knowledge of the dead space of the system and the experimentally measured equilibrium pressures. The heat capacity of the gas phase in the calorimeter was found to be negligible, since heat capacities were not determined beyond the point where the desorption

* This work was supported by the U. S. Atomic Energy Commission under Contract No. AT(30-1)-824. Some of the equipment used was loaned by the U. S. Office of Naval Research under Contract No. 182(00).

† This value is somewhat lower than that of previous measurements. (See reference 1.) It is believed that the loss of area resulted from partial sintering of the adsorbent at the high temperatures required for soldering the gas-filling tube which was broken between the previous and present set of measurements.

[1] Pace, Sasmor, and Heric, J. Am. Chem. Soc. **74**, 4413 (1952).
[2] G. L. Kington and J. G. Aston, J. Am. Chem. Soc. **23**, 1929 (1951)
[3] G. Halsey, J. Chem. Phys. **16**, 931 (1948).
[4] F. C. Tompkins, Trans. Faraday Soc. **46**, 569 (1950).
[5] T. L. Hill, J. Chem. Phys. **17**, 762 (1949).
[6] L. E. Drain and J. A. Morrison, Trans. Faraday Soc. **48**, 840 (1952).
[7] Morrison, Los, and Drain, Trans. Faraday Soc. **47**, 1023 (1951).
[8] Scott, Meyers, Rands, Brickwedde, and Bekkedahl, J. Research Natl. Bur. Standards **35**, 39 (1945).

correction amounted to ten percent of the adsorbate heat capacity. The maximum correction for the heat of compression was 0.006 calories.

If the integral heat of adsorption for N_s moles Q_{N_s} is defined such that

$$Q_{N_s} = -\int q_{st} dN_s = N_s(E_G - E_{N_s}) + N_s RT, \quad (2)$$

where E_G is the molar energy of the gaseous state and E_{N_s} is the molar energy of the adsorbed state, the integral heat may be found readily from the experimental data by the use of Eq. (1) integrated between the initial and final states of the system:

$$Q_{N_s} = (c_{pG} + c_{pcal} + c_{N_s})\Delta T - V_G \Delta P - Q, \quad (3)$$

in which Q represents any heat introduced by the calorimeter heater. In a heat of adsorption, the temperature rise (ΔT) was determined by following the calorimeter temperature after admission of the gaseous sample. The maximum and minimum heat effects encountered were 83.45 and 6.83 calories with an indicated precision of ± 0.10 calories. At some of the temperatures, the volume of the initial sample was chosen so that the final equilibrium pressure was at least 5 mm. Otherwise, temperature equilibrium was not reached in less than one hour after the sample was introduced. Heats of desorption were taken by two alternative experimental methods. In one, the gas was allowed to desorb with the simultaneous application of a measured amount of heat from the calorimeter heater (Q) so that a net temperature rise resulted. This technique is obviously parallel to that of a heat capacity determination. In the second method, the gas was merely allowed to desorb into an evacuated bulb without the addition of heat, i.e., Q equal to zero. Since it was not possible to lower the temperature of the adiabatic shields to keep pace with the calorimeter, the adiabatic nature of the system during the heat of desorption was not maintained. It was found that the most acceptable substitute for maintaining adiabatic conditions was to set the shields approximately half-way between the initial and final temperatures. Duplicate determinations using both alternative methods for heats of desorption showed that the uncertainty introduced by nonadiabatic conditions was beyond the precision of the measurements. The maximum and minimum temperature changes were 0.47 and 0.36 degrees. Comparison of data for heats of adsorption and desorption shows a reproducibility of about ± 0.10 calories.

To be of any value, consecutive determinations of the integral heats up to a maximum desired concentration must be taken at the same temperature. Since such a restriction cannot be exactly followed experimentally, alternatives must be chosen. The initial temperature of the calorimeter may be regulated each time, so that the heats are measured at almost the same temperature, or the measurements may be begun below the desired temperature and carried through successively to a higher temperature than that desired. In the former alternative, a corrective term must be applied to compensate for the additional moles adsorbed as the temperature is lowered between determinations. If the latter alternative is followed, the value of the heat of adsorption must be adjusted to the desired temperature by the use of the heat capacity data for the system. On occasion, both of these methods were used.

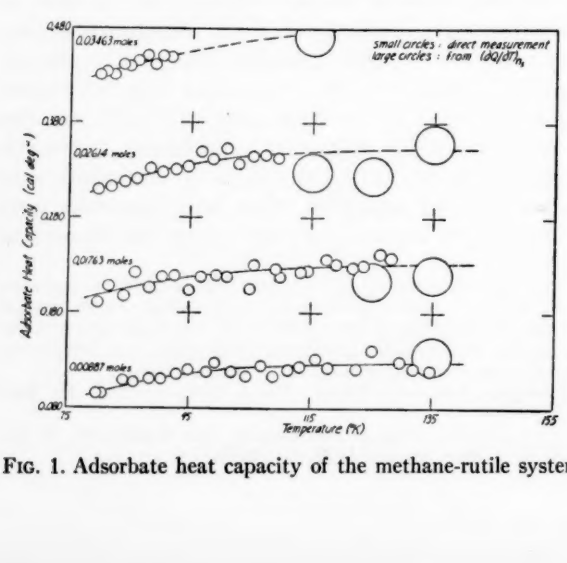

FIG. 1. Adsorbate heat capacity of the methane-rutile system.

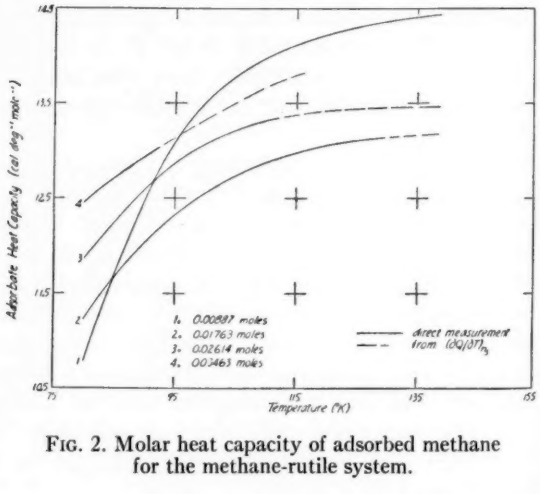

FIG. 2. Molar heat capacity of adsorbed methane for the methane-rutile system.

RESULTS AND DISCUSSION

The heat capacity was determined for 0.00887, 0.01763, 0.02614, and 0.03463 moles of methane adsorbed on rutile. These amounts corresponded to the fractions 0.28, 0.56, 0.84, and 1.11 of the monolayer capacity determined at 89.5°K. The average deviation of the experimental points from the best curves representing the data (Fig. 1) are ± 0.004, ± 0.006, ± 0.003, and ± 0.003 calories, respectively, corresponding to a precision ranging from five to one percent of the value of the adsorbed phase. Figure 1 shows the data for the actual amount of adsorbed phase. Figure 2 shows the

same data on a molar basis. Since the distribution of the points about the curves was random for each run, runs are not differentiated.

From the absence of any discontinuities in the heat capacity *vs* temperature curves, it is concluded that no first-order transitions have been observed in this investigation. The temperature range covered by the data is such that it extends from the region in which the solid is the normal bulk phase to the region in which the normal state is gaseous. The possibility of observing diffuse solid-liquid and liquid-gas phase changes would seemingly be excellent if the adsorbed phase resembled the three-dimensional phase to any marked degree. The absence of any such effect up to the highest concentration studied, 1.1 monolayers, is added argument that the adsorbate, at least in this range of concentration, is distinctly different from the bulk phase.

The molar heat capacity of solid methane at the melting point, 90.6°K, is 10.5 calories degree^{-1} mole^{-1}, and that of the liquid varies from 12.5 at the melting point to 13.0 calories degree^{-1} mole^{-1} at the boiling point, 111.8°K.[9] The molar heat capacity is greater than that of solid methane everywhere in the temperature range observed, so the adsorbate must possess a degree of mobility over the surface, since the adsorbate-adsorbent forces are merely of the van der Waal's type. These results parallel closely the findings of Morrison, Los, and Drain[7] for the system argon-rutile, where the adsorbate heat capacity was greater than that of the bulk phase from liquid hydrogen temperatures to above the argon boiling point.

Also, in the case of the argon-rutile system, Morrison *et al.*[7] have noted a reversal at 20°K in the dependency of the heat capacity of the adsorbed argon on concentration for three concentrations below 0.7 monolayers. Below 20°K, an increase in heat capacity with concentration was observed, whereas above 20°K an increase in concentration resulted in a decrease in the heat capacity. In Fig. 2, a similar reversal in about the same range of concentrations occurs at 80°K for the methane-rutile system. In the argon-rutile system, the behavior below 20°K was attributed to the fact that the adsorbed molecules behaved as localized oscillators whose average frequency was decreasing with increasing coverage because of the heterogeneity of the surface. Above 20°K the higher heat capacity at a lower concentration was attributed to the configurational entropy arising from an energy distribution in which the difference in energy between sites was small compared to the energy of the adsorbed molecules. Considering the facts that the surface areas of the rutile samples are comparable and that the molecular diameters and isosteric heats of argon and methane are of the same order, it is not immediately apparent why the reversals should have occurred at such widely different temperatures for the two systems. Since the reversal

[9] K. Clusius and L. Popp, Z. physik. Chem. **B46**, 63 (1940).

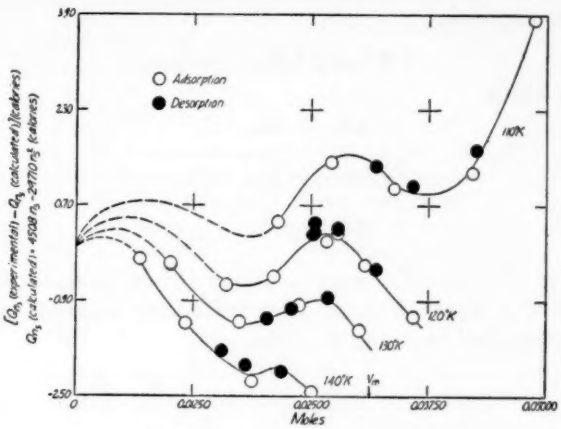

FIG. 3. Integral heat of adsorption of the methane-rutile system.

temperature for the methane-rutile system was 80°K, where the adsorbate was mobile, another explanation is needed for the behavior of methane below 80°K.

The integral heats of adsorption were determined at 110, 120, 130, and 140°K for quantities of adsorbed methane ranging to the monolayer. The experimental values (Q_{N_s}(calc)) are plotted in Fig. 3 as deviations from an arbitrary function,

$$Q_{N_s}(\text{calc}) = 4508N_s - 29710N_s^2, \tag{4}$$

in which N_s is the total number of moles of adsorbed methane. In almost all cases, the methane was added in a cumulative manner. However, in order to test the reversibility of the adsorption, desorptions were carried out. These desorptions are shown as solid circles in Fig. 3.

The temperature coefficient of the integral heat of adsorption is related to the heat capacity of the adsorbed phase by the equation

$$\left(\frac{dQ_{N_s}}{dT}\right)_{N_s} = c_{pG} - c_{N_s}. \tag{5}$$

The values of c_{N_s} obtained in this manner are plotted as the larger circles in Fig. 1. The precision (±0.02 calories) is of the order expected from that of heats of adsorption selected at two temperatures ten degrees apart (±0.2 calories). The reproducibility obtained between (1) heats of adsorption and heats of desorption and (2) heat capacities determined directly and as temperature coefficients of integral heats indicates the reversibility of the adsorption process.

The experimental data have been used to calculate the thermodynamic quantities ΔH, ΔF, and ΔS involved in the isothermal adsorption of one mole of the gas from a state in which it is in equilibrium with the bulk liquid (at pressure p_0) to one in which it is adsorbed on an infinite amount of adsorbent already containing adsorbed gas at equilibrium pressure p. Since the process is differential in nature, there follows

the expression

$$T\Delta S_{\text{diff}}=\Delta H_{\text{diff}}-\Delta F_{\text{diff}}, \tag{6}$$

in which

$$\Delta S_{\text{diff}}=\bar{S}_{N_s}-S_G \tag{7}$$

$$\Delta H_{\text{diff}}=\bar{H}_{N_s}-H_G \tag{8}$$

$$\Delta F_{\text{diff}}=\bar{F}_{N_s}-F_G. \tag{9}$$

$\bar{S}_{N_s}$, $\bar{H}_{N_s}$, and $\bar{F}_{N_s}$ refer to the partial molar quantities for the adsorbed phase. The free energy changes were determined from the equation

$$\Delta F_{\text{diff}}=RT\ln\frac{p}{p_0}, \tag{10}$$

in which the value of p_0 at 110°K was obtained from the data of Stock, Henning, and Kuss,[10] and the adsorbate

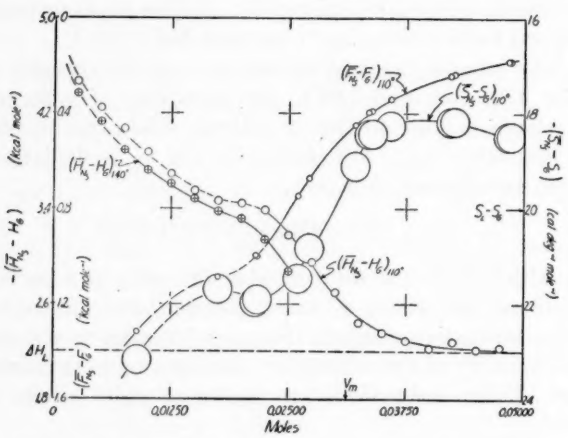

FIG. 4. Differential thermodynamic properties of the methane-rutile system.

equilibrium pressures (p) were calculated by relating the differential heat of adsorption (q_d) to the isosteric heat (q_{st}) by the relation

$$q_{st}=q_d+RT. \tag{11}$$

The results appear in Fig. 4. In Fig. 4, the differential heat (ΔH_{diff}) is shown only for 110° and 140°K to prevent overcrowding. The curves for 120° and 130°K fall between the preceding two and have similar shapes. The circles representing the data signify ±30 calories, ±10 calories and ±0.3 entropy units for the differential heats of adsorption, free energies, and entropies, respectively.

The differential heats of adsorption show an initial high value at low adsorbate concentrations and approach the heat of liquefaction of methane beyond the monolayer. Several investigators[7,11,12] have pointed out that the initial decrease cannot be explained by attractive interaction of the van der Waal's type. Although repulsive interaction is not excluded, present theory and experiments tend to favor an explanation based on a nonuniform surface with a resultant wide distribution of energy at the active sites of the adsorbent. The presence of diffuse maxima in the differential heat curves for the methane-rutile system near 0.0225 moles adsorbed is suggestive of the low maxima observed by Orr[12] for nitrogen and oxygen adsorbed on cesium iodide. The maxima in these cases were related to the appearance of dispersion forces involved in the lateral interaction of adsorbed molecules. It is highly probable that the maxima in the methane-rutile system are caused by a similar interaction. The maxima observed for the methane-rutile system are more diffuse than those observed by Orr. This can be explained by the fact that the rutile used was in a much finer state of subdivision than the ionic crystals used by Orr. This would have the effect of smoothing the maxima because of the increased heterogeneity of the surface. The location of the maxima at a concentration less than a monolayer cannot be related to Orr's maxima at the monolayer in view of the fact that some obscurity exists in the monolayer capacity defined by Orr and that defined by the BET theory.

The entropy curve in Fig. 4 implicity contains differential heat values, so its shape is a consequence of the differential heat curve. While the adsorbate entropy is negative with respect to the gas over the entire range, at concentrations above the monolayer, it is positive with respect to the liquid. Such an effect has been reported by Joyner and Emmett[13] for nitrogen adsorbed on spheron (carbon) which had been sintered to the graphon form. Kington *et al.*[14] have observed a similar situation in the entropy of adsorption of nitrogen on carbon black, but on anatase, another crystalline form of titanium dioxide, the adsorbate entropy is consistently negative to the liquid.

At the highest concentrations observed for the methane-rutile system, the tendency of the entropy curve is to approach that of the bulk liquid. This is a consequence of the fact that the free energy change is simultaneously approaching zero, so that the net entropy change is due merely to the heat of liquefaction of the gas.

[10] Stock, Henning, and Kuss, Ber. deut. chem. Ges. **54**, 1119 (1921).

[11] F. C. Tompkins and D. M. Young, Trans. Faraday Soc., 47 77 (1951).

[12] W. J. C. Orr, Proc. Roy. Soc. (London), **A173**, 349 (1939).

[13] L. G. Joyner and P. H. Emmett, J. Am. Chem. Soc. **70**, 2353 (1948).

[14] Kington, Beebe, Polley, and Smith, J. Am. Chem. Soc. **72**, 1775 (1950).

Theory of Centrifugal Distortion Constants of Polyatomic Rotor Molecules*

DANIEL KIVELSON AND E. BRIGHT WILSON, JR.
Mallinckrodt Chemical Laboratory, Harvard University, Cambridge, Massachusetts

(Received January 26, 1953)

The distortion constants $\tau_{\alpha\beta\gamma\delta}$ are expressed in terms of inverse force constants and of the derivatives of the inertia tensor with respect to interatomic parameters. Harmonic potential functions are assumed. Relations that simplify the procedure for obtaining the required derivatives are obtained. Furthermore, rules are given that enable one to write down directly the derivatives with respect to certain common internal displacement coordinates. Group theoretical considerations are used to obtain some knowledge of the distortion constants.

INTRODUCTION

THE Hamiltonian for the rotational energy of a semi-rigid molecule can be written in the approximate form[1]

$$\mathbf{H}=\tfrac{1}{2}\sum_{\alpha}\sigma_{\alpha\alpha}\mathbf{P}_{\alpha}^{2}+\tfrac{1}{4}\sum_{\alpha,\beta,\gamma,\delta}\tau_{\alpha\beta\gamma\delta}\mathbf{P}_{\alpha}\mathbf{P}_{\beta}\mathbf{P}_{\gamma}\mathbf{P}_{\delta}. \quad (1)$$

The first term is the rigid rotor term, while the second is a correction for the effects of centrifugal distortion. $\mathbf{P}_{\alpha}$ is the operator for the component of the angular momentum along the α axis (α, β, γ, δ are summed over x, y, z); $\sigma_{\alpha\alpha}$ is a constant for a given vibrational state and is related to the $\alpha\alpha$ component of the inverse of the effective principal inertia tensor. The distortion constants $\tau_{\alpha\beta\gamma\delta}$ are independent of the rotational quantum numbers but depend upon the vibrational state under consideration. In the approximation used later, this dependence on vibrational state disappears. These distortion constants are given by the expression

$$\tau_{\alpha\beta\gamma\delta}=\sum_{v'}(v|\mu_{\alpha\beta}|v')(v'|\mu_{\gamma\delta}|v)/h\nu_{vv'}, \quad (2)$$

in which the sum is over the vibrational states v', excluding the state v under consideration. The μ's are components of the inverse instantaneous inertia tensor, and $h\nu_{vv'}$ is the energy difference between the two indicated vibrational states. $(v|\mu_{\alpha\beta}|v')$ is the matrix element of $\mu_{\alpha\beta}$.

In a previous paper[2] a first-order perturbation method of treating Eq. (1) was proposed. The τ's may be determined empirically from the rotational spectrum by this method if sufficient data are available.[3] Then by the use of Eq. (2) some information concerning the vibrational potential constants may be obtained. Conversely, the τ's may be estimated with the aid of known molecular force constants.[4] The purpose of this paper is to reduce Eq. (2), the relation between the τ's and the potential constants, to a more explicit and convenient form.

SIMPLIFICATION OF THE τ's

A simplified expression for the τ's has previously been obtained by expanding μ in terms of normal coordinates and neglecting all terms above those linear in the normal coordinates.[5] This approximation also assumes harmonic forces, which is probably justified since the correction for centrifugal distortion is itself a higher order effect. This procedure will be followed here except that general displacement coordinates rather than normal coordinates will be used, since force constants are available more often than normal coordinates.

Let $\{R_i\}$ be a set of interatomic parameters and let $\{\delta R_i\}$ be the corresponding set of internal displacement coordinates, such as the changes in interatomic distances and angles. If N is the number of atoms in the molecule, $3N-6$ such displacement coordinates are independent. Let $\mu_{\alpha\beta}^{0}$ be the equilibrium value of $\mu_{\alpha\beta}$, that is, the value when all the δR_i's equal zero. Then

$$\mu_{\alpha\beta}=\mu_{\alpha\beta}^{0}+\sum_{i}\mu_{\alpha\beta}^{(i)}\delta R_i+O(\delta R_i^{2}), \quad (3)$$

where

$$\mu_{\alpha\beta}^{(i)}=(\partial\mu_{\alpha\beta}/\partial R_i)_{\delta\mathbf{R}=0}. \quad (4)$$

Since all the quadratic and higher terms in Eq. (3) will be neglected, the basis functions for the matrix elements in Eq. (2) will be orthonormal harmonic-oscillator functions. $\mu_{\alpha\beta}^{0}$ and $\mu_{\alpha\beta}^{(i)}$ are both constants and $v\neq v'$, so the orthogonality property of the basis functions in conjunction with the approximation above leads to

$$(v|\mu_{\alpha\beta}|v')=\sum_{i}\mu_{\alpha\beta}^{(i)}(v|\delta R_i|v'). \quad (5)$$

$\tau_{\alpha\beta\gamma\delta}$ can now be re-expressed as

$$\tau_{\alpha\beta\gamma\delta}=\sum_{v'}\sum_{ij}\mu_{\alpha\beta}^{(i)}\mu_{\gamma\delta}^{(j)}(v|\delta R_i|v')(v'|\delta R_j|v)/h\nu_{vv'}. \quad (6)$$

The coordinates δR_i used here are related to the normal

* The research reported in this paper was made possible by support extended Harvard University by the U. S. Office of Naval Research under ONR Contract N5ori-76, Task Order V.

[1] E. B. Wilson, Jr. and J. B. Howard, J. Chem. Phys. **4**, 260 (1936).

[2] D. Kivelson and E. B. Wilson, Jr., J. Chem. Phys. **20**, 1575 (1952).

[3] R. E. Hilger and M. W. P. Strandberg, Phys. Rev. **83**, 575 (1951).

[4] B. L. Crawford and P. C. Cross, J. Chem. Phys. **5**, 621 (1937); M. H. Sirvetz, J. Chem. Phys. **19**, 938 (1951).

[5] E. B. Wilson, Jr., J. Chem. Phys. **5**, 617 (1937).

coordinates Q_k by a linear transformation; consequently,

$$(v|\delta R_i|v')=(v|\sum_k b_{ik}Q_k|v')=\sum_k b_{ik}(v|Q_k|v'). \quad (7)$$

For the harmonic oscillator, $(v|Q_k|v')$ is nonvanishing only if $v=v'$, except for the single quantum number n_k associated with the normal coordinate Q_k, which must change by ± 1. Consequently,

$$\tau_{\alpha\beta\gamma\delta}=\sum_{ij}\mu_{\alpha\beta}^{(i)}\mu_{\gamma\delta}^{(j)}\sum_k b_{ik}b_{jk}[(n_k|Q_k|n_k+1)\times(n_k+1|Q_k|n_k)/h\nu_{(n_k;\,n_k+1)}+(n_k|Q_k|n_k-1)(n_k-1|Q_k|n_k)/h\nu_{(n_k;\,n_k-1)}]. \quad (8)$$

The factor in brackets can easily be evaluated for the harmonic oscillator,[5] since

$$\begin{aligned}(n_k|Q_k|n_k+1)&=[(n_k+1)h/8\pi^2\nu_k^0]^{\frac{1}{2}},\\ (n_k|Q_k|n_k-1)&=[(n_kh/8\pi^2\nu_k^0]^{\frac{1}{2}},\end{aligned} \quad (9)$$

where $\nu_{vv'}=\mp\nu_k^0$. Use will also be made of the relation

$$(f^{-1})_{ij}=\sum_k b_{ik}b_{jk}/4\pi^2\nu_k^{02}, \quad (10)$$

where f_{ij} is a potential constant which enters into the potential energy, when the latter is expressed in terms of $\delta R_i\delta R_j$ and $(f^{-1})_{ij}$ is an element of the matrix inverse to the $\mathbf{f}$ matrix. Insertion of Eqs. (9) and (10) into Eq. (8) yields

$$\tau_{\alpha\beta\gamma\delta}=-\tfrac{1}{2}\sum_{ij}\mu_{\alpha\beta}^{(i)}\mu_{\gamma\delta}^{(j)}(f^{-1})_{ij}. \quad (11)$$

This relation can also be derived classically following the procedure outlined by Wilson.[6]

It is more convenient to express $\tau_{\alpha\beta\gamma\delta}$ in terms of the inertia tensor rather than in terms of its reciprocal $\boldsymbol{\mu}$. In order to do this the inertia tensor $\mathbf{I}$ is expanded in terms of the coordinates δR_i. Thus,

$$\mathbf{I}=\mathbf{I}^0+\sum_i[\mathbf{J}^{(i)}]_0\delta R_i+\cdots, \quad (12)$$

where $\mathbf{I}^0$ is the equilibrium value,

$$\mathbf{J}^{(i)}=(\partial\mathbf{I}/\partial R_i) \quad (13)$$

and the subscript 0 in Eq. (12) indicates that the derivative is evaluated at $\delta\mathbf{R}=0$. Since $\boldsymbol{\mu}=\mathbf{I}^{-1}$, the following relation may now be formed (in matrix notation):

$$\mathbf{I}\boldsymbol{\mu}=\mathbf{1}=\mathbf{I}^0\boldsymbol{\mu}^0+\mathbf{I}^0\sum_i\boldsymbol{\mu}^{(i)}\delta R_i+\sum_i[\mathbf{J}^{(i)}]_0\delta R_i\boldsymbol{\mu}^0+O(\delta R_i^2). \quad (14)$$

$\boldsymbol{\mu}$ is the inverse of $\mathbf{I}$ for all values of δR_i, and so at equilibrium $\mathbf{I}^0\boldsymbol{\mu}^0=\mathbf{1}$. The situation treated here is one of small oscillations, and so the terms quadratic in the coordinates may be neglected. Since the δR_i's are independent, the result of these considerations is

$$\boldsymbol{\mu}^{(i)}=-\boldsymbol{\mu}^0[\mathbf{J}^{(i)}]_0\boldsymbol{\mu}^0. \quad (15)$$

It is convenient to choose coordinate axes in such a way that $\mathbf{I}^0$ and $\boldsymbol{\mu}^0$ are diagonal matrices, the elements of the latter then being the reciprocals of those of the former. Then

$$\mu_{\alpha\beta}^{(i)}=-[J_{\alpha\beta}^{(i)}]_0/I_{\alpha\alpha}{}^0I_{\beta\beta}{}^0. \quad (16)$$

In practice the equilibrium moment of inertia usually cannot be determined and must be replaced by a moment averaged over the ground vibrational state. These effective moments are calculated from the empirically obtained $\sigma_{\alpha\alpha}$ mentioned above.[7] This procedure is suitable in most cases.

The equilibrium, or averaged, moments are presumed to be known well enough for these calculations. It is convenient at this point to define a new quantity $t_{\alpha\beta\gamma\delta}$ which consists only of terms that have still to be evaluated,

$$\begin{aligned}t_{\alpha\beta\gamma\delta}&=-2(I_{\alpha\alpha}{}^0I_{\beta\beta}{}^0I_{\gamma\gamma}{}^0I_{\delta\delta}{}^0)\tau_{\alpha\beta\gamma\delta}\\&=\sum_{ij}[J_{\alpha\beta}^{(i)}]_0[J_{\gamma\delta}^{(j)}]_0(f^{-1})_{ij}.\end{aligned} \quad (17)$$

EVALUATION OF I AND J

Let $\mathbf{r}=(\boldsymbol{\alpha},\boldsymbol{\beta},\boldsymbol{\gamma})$ be a $3N$-dimensional Cartesian position vector, where $\boldsymbol{\alpha}$, $\boldsymbol{\beta}$, $\boldsymbol{\gamma}$ are N-dimensional subvectors each representing the positions of the N atoms of the molecule along one of the three Cartesian axes. Furthermore, let $\boldsymbol{\alpha}$, $\boldsymbol{\beta}$, $\boldsymbol{\gamma}$ be taken in cyclic order. For example if the ith element of $\boldsymbol{\alpha}$, α_i, stands for the x position of the ith atom, then β_i and γ_i stand for the y and z positions, respectively, of the same atom. The components of the inertia tensor can be written as

$$I_{\alpha\beta}=-\sum m_i\alpha_i\beta_i, \quad (18)$$

$$I_{\alpha\alpha}=\sum m_i(\beta_i^2+\gamma_i^2), \quad (19)$$

where m_i is the mass of the ith atom.

If the molecule is distorted from its equilibrium configuration, the coordinates are altered by increments $\delta\alpha_i$, $\delta\beta_i$, $\delta\gamma_i$. These increments cannot be made arbitrarily but must satisfy the conditions[8]

$$\sum m_i\delta\alpha_i=\sum m_i\delta\beta_i=\sum m_i\delta\gamma_i=0, \quad (20)$$

$$\sum m_i(\alpha_i\delta\beta_i-\beta_i\delta\alpha_i)=0, \text{ etc.} \quad (21)$$

However, it is possible to convert an unallowed set of increments $\delta\alpha_i'$, $\delta\beta_i'$, $\delta\gamma_i'$ into an allowed set by adding appropriate rigid translations and rigid rotations of the whole molecule. Thus

$$\delta\alpha_i=\delta\epsilon_\alpha-\delta\eta_\gamma\cdot\beta_i+\delta\eta_\beta\cdot\gamma_i+\delta\alpha_i', \quad (22)$$

[6] E. B. Wilson, Jr., J. Chem. Phys. 4, 526 (1936).

[7] King, Hainer, and Cross, J. Chem. Phys. 11, 27 (1943).

[8] These restrictions on the distortions may be considered as specifying the coordinate axes. These conditions are implied in the derivation of Eqs. (3)–(17). See reference 1.

in which $\delta\epsilon_\alpha$ is a translation along the α axis, $\delta\eta_\gamma$ is a rotation about the γ axis, etc. Insertion of this in the conditions above shows that, if $\delta\alpha_i$ is to be allowable,

$$\delta\epsilon_\alpha = -\sum m_i\delta\alpha_i'/M, \tag{23}$$

$$\delta\eta_\gamma = -\sum m_i(\alpha_i\delta\beta_i' - \beta_i\delta\alpha_i')/I_{\gamma\gamma}, \tag{24}$$

since the variations are evaluated at equilibrium in the principal axis system and

$$\sum m_i\alpha_i = 0, \quad \sum m_i\alpha_i\beta_i = 0. \tag{25}$$

M is the mass of the molecule. Consequently, we have the results

$$\begin{aligned}\delta I_{\alpha\beta} &= -\sum m_i(\alpha_i\delta\beta_i + \beta_i\delta\alpha_i)\\ &= -\sum m_i(\alpha_i\delta\beta_i' + \beta_i\delta\alpha_i' + \alpha_i^2\delta\eta_\gamma - \beta_i^2\delta\eta_\gamma)\\ &= -2\{\sum m_j\alpha_j^2 \sum m_i\beta_i\delta\alpha_i'\\ &\qquad + \sum m_j\beta_j^2 \sum m_i\alpha_i\delta\beta_i'\}/I_{\gamma\gamma},\end{aligned} \tag{26}$$

$$\begin{aligned}\delta I_{\alpha\alpha} &= 2\sum m_i(\beta_i\delta\beta_i + \gamma_i\delta\gamma_i)\\ &= 2\sum m_i(\beta_i\delta\beta_i' + \gamma_i\delta\gamma_i'),\end{aligned} \tag{27}$$

since all other terms vanish. Here the increments $\delta\alpha_i'$, etc. are entirely arbitrary. The coordinates α_i are equilibrium values measured from the center of mass.

To find a derivative $J_{\alpha\beta}^{(k)} = \partial I_{\alpha\beta}/\partial R_k$ it is only necessary to find any set of increments $\delta\alpha_i'$, etc. which produce an increment δR_k to the kth internal coordinate and leave the other internal coordinates with their equilibrium values. These increments do not need to satisfy the conditions (20) and (21). Without these results the required derivatives are often exceedingly difficult to obtain, as one must express the allowed increments $\delta\alpha$ in terms of the internal displacement coordinates, a process that involves the inversion of a $3N\times 3N$ matrix. The results obtained above have been used to derive rules for writing down the derivatives of **I** with respect to some commonly used internal displacement coordinates. These rules should greatly simplify the evaluation of the derivatives.

BOND STRETCHING

The first application of the above results is to valence bond stretching, a commonly used internal displacement coordinate. The principal axis system of the molecule may be translated so that the origin passes through the atom A at one end of r_a, the valence bond to be stretched. See Fig. 1. All interatomic bonds are initially taken to be vectors directed in a path leading away from A. This path is unique provided that there are no rings, and only molecules without rings will be considered here. Later certain vectors will be reversed as shown by dashed arrowheads in Fig. 1.

To evaluate one of the desired derivatives one must consider the effect of a variation in r_a on $\sum m_i\alpha_i^2$, that is, $2\sum m_i\alpha_i\delta\alpha_i'$. By Eq. (27) $\delta\alpha_i'$ may be arbitrarily chosen. In this particular case one allows all atoms to the right of A to move a distance $\cos(r_a\cdot\alpha)\delta r_a$, while all atoms to the left of B are kept in place. All angles are

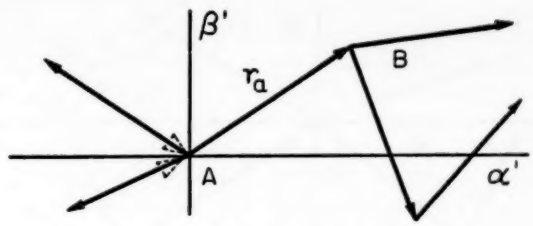

FIG. 1. Bond stretching.

taken between the positive direction of r_i and the positive α axis.

If $\bar\alpha\bar\beta\bar\gamma$ is the position of the center of mass in the displaced coordinate system $\alpha'\beta'\gamma'$, then $\alpha_i = \alpha_i' - \bar\alpha$, where

$$M\bar\alpha = \sum^{A,B} m_i\alpha_i' = \sum^{A,B} M_jr_j\cos(r_j\cdot\alpha). \tag{28}$$

M is the total mass of the molecule, and M_j is the sum of the masses of all atoms "beyond" r_j;[9] $\sum^A$ indicates a sum over all atoms or bonds of the molecule on paths starting at A (including the atom at A) that do not include r_a, and $\sum^B$ is a sum over the rest of the molecule. With the aid of Eq. (28) one obtains

$$\begin{aligned}&2\sum m_i\alpha_i\delta\alpha_i'\\ &= 2\sum^B m_i\alpha_i'\cos(r_a\cdot\alpha)\delta r_a - 2\sum^B m_i\bar\alpha\cos(r_a\cdot\alpha)\delta r_a\\ &= (2/M)\{\sum_i^A m_i\sum_j^B M_jr_j\cos(r_j\cdot\alpha)\cos(r_a\cdot\alpha)\\ &\qquad - \sum_i^B m_i\sum_j^A M_jr_j\cos(r_j\cdot\alpha)\cos(r_a\cdot\alpha)\}\delta r_a.\end{aligned} \tag{29}$$

If the r_j's in $\sum^A$ are now redirected so that they point along paths leading towards A, then $\cos(r_j\cdot\alpha)$ goes to $-\cos(r_j\cdot\alpha)$ in the last term in Eq. (29). Thus,

$$\begin{aligned}&d(\sum m_i\alpha_i^2)/dr_a\\ &\quad = (2/M)\{\sum_j (MM)_{aj}r_j\cos(r_j\cdot\alpha)\cos(r_a\cdot\alpha)\},\end{aligned} \tag{30}$$

where $(MM)_{aj}$ is the product of the sum of all masses "beyond" r_j and "behind" r_a,[10] or vice versa, the choice made in such a way that $(MM)_{aj}$ does not include the masses of any atoms on paths between m_j and m_a. β and γ may be substituted for α in this result.

Equation (26) may be used in a similar fashion with the consequence that

$$\begin{aligned}dI_{\alpha\beta}/dr_a = &-(2/MI_{\gamma\gamma})\\ &\times\{I_\alpha\sum_j(MM)_{aj}r_j\cos(r_j\cdot\beta)\cos(r_a\cdot\alpha)\\ &+ I_\beta\sum_j(MM)_{aj}r_j\cos(r_j\cdot\alpha)\cos(r_a\cdot\beta)\},\end{aligned} \tag{31}$$

[9] "Beyond" r_j refers to all the atoms which are reached (from atom A) by paths which include r_j.

[10] "Behind" r_a refers to all atoms which are not "beyond" r_a.

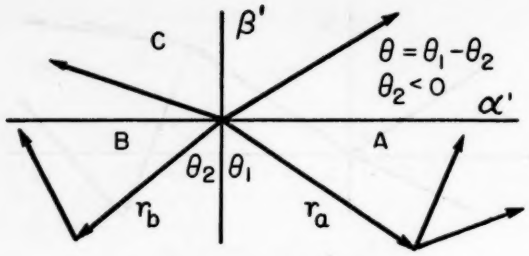

FIG. 2. Valence angle bending.

where the bonds are directed as above and

$$I_\alpha=\sum_i m_i\alpha_i^2$$

$$=(1/M)\sum_{j,k}(MM)_{jk}r_jr_k\cos(r_j\cdot\alpha)\cos(r_k\cdot\alpha). \quad (32)$$

I_β is defined similarly. The derivatives of $I_{\beta\gamma}$ and $I_{\gamma\alpha}$ are obtained by the usual permutations of indices.

VALENCE ANGLE BENDING

The next application of these results is to valence angle bending where the angle lies in a principal plane, for example, the $\alpha\beta$ plane. The principal axis system may be translated so that the origin lies at the apex of the angle under consideration (see Fig. 2). All interatomic bonds are directed along paths leading away from the apex. Since the results above permit one to choose arbitrary displacements, it is convenient in this case to hold side B and the apex part (C) of the molecule rigid while part A of the molecule is moved out rigidly as θ changes. Part A of the molecule is distinguished from Part B by the fact that an increase in θ_1 means a counterclockwise rotation about the positive γ axis, while an increase in θ_2 means a clockwise rotation. The required displacements are

$$\delta\alpha_i'=-\sum_j^i r_j\cos(r_j\cdot\beta)\delta\theta, \quad (33)$$

where the distances and angles refer to part A of the molecule and the sum is over the bonds forming a continuous path from the vertex to atom i. The bonds are ordered along such paths from the vertex to the given atom. No ordering exists for bonds on different branches. All other displacements are set equal to zero. Then

$$2\sum m_i\alpha_i\delta\alpha_i'=-2\sum_i^A m_i\alpha_i'\sum_j^i r_j\cos(r_j\cdot\beta)\delta\theta$$

$$+2\sum_i^A m_i\bar{\alpha}\sum_j^i r_j\cos(r_j\cdot\beta)\delta\theta, \quad (34)$$

where $\sum^A$ is a sum over part A of the molecule. After suitable algebraic manipulations similar to those used in the case above, one has

$$d(\sum m_i\alpha_i^2)/d\theta$$

$$=-(2/M)\{\sum_{i\geqslant j}^{A'} M_iM^{(j)}r_ir_j[\cos(r_i\cdot\alpha)\cos(r_j\cdot\beta)$$

$$+\cos(r_i\cdot\beta)\cos(r_j\cdot\alpha)](1-\delta_{ij}/2)$$

$$-\sum_i^A\sum_j^{B,C,A''} M_iM_jr_ir_j\cos(r_i\cdot\beta)\cos(r_j\cdot\alpha)\}, \quad (35)$$

where $\delta_{ij}=0$, if $i\neq j$, $\delta_{ij}=1$ if $i=j$, and M_i is the sum of masses "beyond" r_i. In the first sum $\sum^{A'}$, $M^{(j)}$ is the sum of all masses "behind" r_j, r_i, and r_j are both in the A part of the molecule, and r_j must be on the path from the vertex to r_i. In the second term $\sum_i^A\sum_j^{A''}$ are sums over the (A) part of the molecule in which r_i and r_j are not on the same path from the vertex.

An equivalent result may be obtained by keeping side A rigid and varying θ_2. The results have the same form

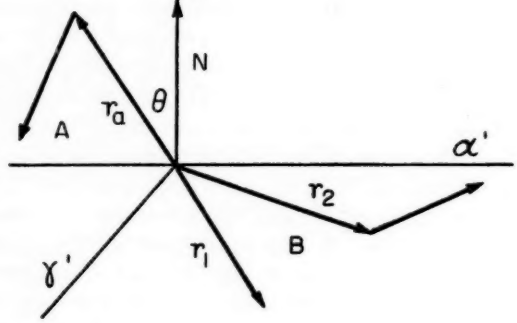

FIG. 3. Plane-bond angle bending.

as those above except that the sums over A are substituted for sums over B, sums over B are substituted for sums over A, and the sign of the entire expression is changed.

$d(\sum m_i\beta_i^2)/d\theta$ is evaluated by the same formula except that α and β are interchanged, and the sign of the expression is changed. These results are valid for any of the principal planes provided that one remembers that $\alpha\beta\gamma$ are in cyclic order.

In a similar manner one may obtain

$$dI_{\alpha\beta}/d\theta=(2/MI_{\gamma\gamma})\{2\sum_{i\geqslant j}^{A'} M_iM^{(j)}r_ir_j$$

$$\times[\cos(r_i\cdot\alpha)\cos(r_j\cdot\alpha)I_\beta$$

$$-\cos(r_j\cdot\beta)\cos(r_i\cdot\beta)I_\alpha](1-\delta_{ij}/2)$$

$$-\sum_i^A\sum_j^{B,C,A''} M_iM_jr_ir_j[\cos(r_i\cdot\alpha)$$

$$\times\cos(r_j\cdot\alpha)I_\beta-\cos(r_i\cdot\beta)\cos(r_j\cdot\beta)I_\alpha]\}. \quad (36)$$

In the case where the valence angle does not lie in a principal plane, valence angle bending is more complicated. In this situation the formulas derived above may be used as expressions for the projections of the molecular motions on the principal planes.

$$d(\sum m_i\alpha_i^2)/d\theta=(d\theta'/d\theta)(dI_\alpha)/d\theta') + (d\theta''/d\theta)(dI_\alpha/d\theta''), \quad (37)$$

where θ' and θ'' are the projections of θ on the $\alpha\beta$ and $\gamma\alpha$ planes, respectively. The quantities evaluated above are really the derivatives with respect to θ'.

By direct but complicated trigonometric and vector manipulations, one obtains the result

$$d\theta'/d\theta=[\sin\theta\sin^2(r_a\cdot\gamma)]^{-1}[\sin^2(r_a\cdot\gamma)\sin^2\theta - \{\cos(r_b\cdot\gamma)-\cos(r_a\cdot\gamma)\cos\theta\}^2]^{\frac{1}{2}}, \quad (38)$$

where θ is the angle between the bonds r_a and r_b; the other angles are taken with respect to the positive γ axis, and r_a and r_b are defined in Fig. 2. Analogous expressions result for projections on the $\beta\gamma$ and $\gamma\alpha$ planes.

PLANE-BOND ANGLE BENDING

Plane-bond bending is the change of angle between the normal (**N**) to a plane formed by two connecting bonds (r_1, r_2) and the bond r_a connected to the vertex of these two bonds where the change takes place in the (r_a, **N**) plane (see Fig. 3). If the angle lies in a principal plane ($\alpha\beta$) the coordinate system may be chosen as in Fig. 3, where the primed axes are parallel to the principal axes. The molecule is divided into (A) and (B) parts as in valence angle bending. It is seen that the results are the same as in Eqs. (35) and (36). For the special case of a planar molecule, the only nonvanishing derivatives are $dI_{\alpha\beta}/d\theta$ and $dI_{\gamma\beta}/d\theta$, where θ is the out-of-plane bending angle.

If the plane in question is not a principal plane the same procedure must be carried out as in Eq. (37). Equation (38) holds here if $\mathbf{r}_b$ is the normal to the plane.

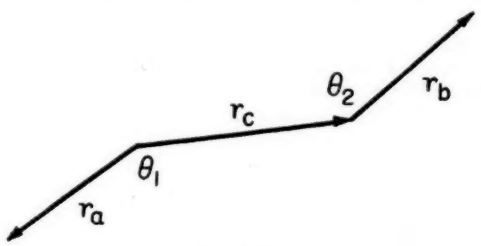

FIG. 4. Torsion.

TORSION

Torsion is the change resulting from rotation about an interatomic bond (r_c) of the angle between the normal of a plane determined by r_c and a connecting bond r_a, and the normal of a plane determined by r_c and a connecting bond at the other end of r_c, i.e., r_b (see Fig. 4). As in the case of valence angle bending, one can consider the projections of the molecule on the various principal planes, see Fig. 5. The r_c bond is the axis of rotation. The part of the molecule designated by B will be kept fixed while the part (A) will rotate about r_c. In the projection in Fig. 5, the "center" of the (A) part is translated to the origin and rotations of the (A) part about the γ' axis are considered. The bonds are directed away from the origin. With (A) and (B) defined in the manner described, the projections of the derivatives with respect to the torsion angle of the inertia tensor takes on the same form as the corresponding projection for angle bending.

However, in this case $d\theta'/d\theta$ is different. One has to consider $\delta\theta$ as the change of the angle between normals; a change in which $\mathbf{r}_a$ changes but $\mathbf{r}_b$, $\mathbf{r}_c$, and θ_1 remain fixed (Fig. 4). The result is

$$\frac{d\theta'}{d\theta}=\frac{n_s'(n_t-n_s\cos\theta)+(1-n_s^2)\sin\theta}{(1-n_s^2)[(1-n_s^2)\sin^2\theta-(n_t-n_s\cos\theta)^2]^{\frac{1}{2}}}, \quad (39)$$

where n_s and n_t are the γ-direction cosines of $\mathbf{r}_c\times\mathbf{r}_a$ and $\mathbf{r}_c\times\mathbf{r}_b$, respectively, θ is the angle between these two vectors, and $n_s'=dn_s/d\theta$. Furthermore,

$$n_s'=\frac{[\cos(r_a\cdot\gamma)-\cos(r_c\cdot\gamma)\cos\theta_1]\sin\theta_2\sin\theta}{\mathbf{C}\cdot(\mathbf{A}\times\mathbf{B})}, \quad (40)$$

where **C**, **A**, **B** are unit vectors in the direction of $\mathbf{r}_c$, $\mathbf{r}_a$, $\mathbf{r}_b$, respectively, and $|\mathbf{C}\times\mathbf{A}|=\sin\theta_1$ and $|\mathbf{C}\times\mathbf{B}|=\sin\theta_2$. These relations may be applied to projections on the $\beta\gamma$ and $\gamma\alpha$ planes by cyclic permutations.

In a symmetric rotor, the rules for torsion give $d\mathbf{I}/d\theta=0$. In a molecule of the type CH_3AB_2, where CAB_2 lies in the $\gamma\alpha$ plane, the rule yields

$$\frac{dI_{\alpha\beta}}{d\theta}=(I_{\alpha\alpha}-I_{\beta\beta})\frac{I_{\gamma\gamma}^{(s)}}{I_{\gamma\gamma}} \quad (41)$$

as the only nonvanishing derivative with respect to the torsion angle where $I_{\gamma\gamma}^{(s)}$ is the $\gamma\gamma$ moment of the CH_3 part of the molecule.

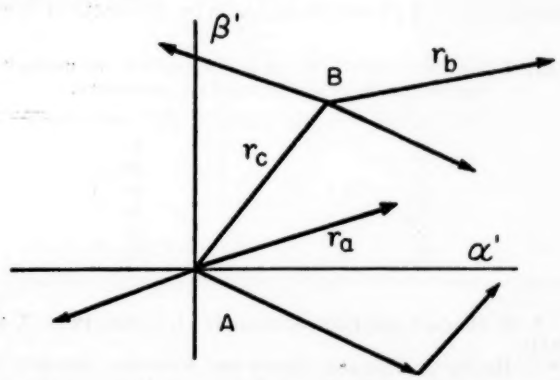

FIG. 5. Torsion. Projection on plane.

SYMMETRY PROPERTIES OF $t_{\alpha\beta\gamma\delta}$

If the molecule has any symmetry, it will usually be convenient to use internal symmetry coordinates.[11] Equation (17) holds if such coordinates are used throughout. The potential constant matrix **f** must be expressed in these internal symmetry coordinates as well. To get $J_{\alpha\beta}{}^{(k)}$, etc., one merely uses increments $\delta\alpha_i'$ etc., which produce an increment to a given internal symmetry coordinate.

The inertia tensor transforms as a tensor of the second rank. It has the same transformation properties as a linear combination of dyads formed from translation vectors. Thus if such a dyad is represented by **P**, which transforms as **rr**, the transformation properties of the inertia tensor may be related to it as follows:

$$I_{\alpha\alpha}\rightarrow P_{\beta\beta}+P_{\gamma\gamma}, \tag{42}$$

$$I_{\alpha\beta}\rightarrow -P_{\alpha\beta}. \tag{43}$$

The transformation properties of **P** under the symmetry operations of the point group to which the molecule belongs may be found in tables,[12] since **P** transforms exactly as the polarizability tensor. The polarizability components, hence also those of **I**, do not always belong uniquely to a given irreducible representation (species), but linear combinations of them do.

If these linear combinations of the moments and products of inertia are expanded in powers of the normal coordinates or of any set of independent symmetry coordinates, each term must have the symmetry just outlined. The linear term will therefore involve only coordinates of this symmetry species. If the problem is set up in terms of internal symmetry coordinates, the coefficients of the linear terms will be the components of $\mathbf{J}^{(k)}$ and these will vanish except for symmetry coordinates of the appropriate species.

If normal coordinates or symmetry coordinates are used, the array of inverse potential constants $(f^{-1})_{ij}$ in Eq. (17) factors into submatrices corresponding to different species of the group. Thus there is no coupling of $[J_{\alpha\beta}{}^{(i)}]_0$ and $[J_{\gamma\delta}{}^{(j)}]_0$ if the ith and jth coordinates belong to different symmetry species. Such terms vanish and do not contribute to $t_{\alpha\beta\gamma\delta}$. The only nonvanishing combinations of t's are those made by products of linear combinations of components of $[\mathbf{J}^{(i)}]_0$ and $[\mathbf{J}^{(j)}]_0$, where the ith and jth coordinates belong to the same symmetry species. Such a product belongs to the completely symmetric species A_1. Since $(f^{-1})_{ij}$ is a constant and unaffected by the group operations on the internal displacement coordinates, it is seen that all nonvanishing linear combinations of t's belong to the A_1 species. This result is very useful in determining which t's vanish and in obtaining relations between the remaining ones. It is thus seen that the symmetry property of a linear combination of t's is determined by the symmetry properties of the product of two linear combinations of components of **I**, hence of **P**. Since $I_{\alpha\alpha}{}^0$ and $I_{\alpha\beta}{}^0$ are constants under the group operations, Eq. (17) can be used to relate the symmetry properties of the t's to those of the τ's.

The use of these results is illustrated below for the case of C_{2v} (asymmetric rotor) and of C_{3v} (symmetric rotor) symmetry.

TABLE I. Symmetry species of the components of the moment of inertia tensor for molecules of C_{2v} symmetry.

I_{xx}	A_1
I_{yy}	A_1
I_{zz}	A_1
I_{xy}	A_2
I_{xz}	B_1
I_{yz}	B_2

MOLECULES OF C_{2v} SYMMETRY

The species of the components of the polarizability may be obtained directly from tables.[12] Noting Eqs. (42) and (43), the relation between the transformation properties of **I** and **P** under the group operations, one obtains the results of Table I for a molecule of C_{2v} symmetry in which a right-handed coordinate system has been used and the z axis has been chosen as the axis of twofold symmetry. It should be remembered that **I** is a symmetrical tensor. By the arguments of the preceding section it is seen that the only t's that do not vanish are those corresponding to a product of components of **I** which belongs to species A_1. Thus each component of the product must belong to the same species as the other. Once the symmetry properties of the t's have been determined it is easy to get those of the τ's. The result of this analysis is to give the following nonvanishing τ's: τ_{xxxx}, τ_{yyyy}, τ_{zzzz}, $\tau_{xxyy}=\tau_{yyxx}$, $\tau_{xxzz}=\tau_{zzxx}$, $\tau_{yyzz}=\tau_{zzyy}$, $\tau_{xyxy}=\tau_{xyyx}=\tau_{yxxy}=\tau_{yxyx}$, $\tau_{yzyz}=\tau_{zyyz}=\tau_{yzzy}=\tau_{zyzy}$, $\tau_{xzxz}=\tau_{xzzx}=\tau_{zxxz}=\tau_{zxzx}$.

TABLE II. Symmetry species of linear combinations of the components of **P** for molecules of C_{3v} symmetry. The y axis is taken in a plane of symmetry.

$(P_{xx}+P_{yy})/\sqrt{2}=P_a$	A_1
$P_{zz}=P_b$	A_1
$(P_{xy}+P_{yx})/\sqrt{2}=P_c$	$E(x)$
$(P_{xx}-P_{yy})/\sqrt{2}=P_d$	$E(y)$
$(P_{xz}+P_{zx})/\sqrt{2}=P_e$	$E(x)$
$(P_{zy}+P_{yz})/\sqrt{2}=P_f$	$E(y)$

MOLECULES OF C_{3v} SYMMETRY

As a second example of the symmetry arguments above consider a molecule of C_{3v} symmetry. In this case not all the components of **P** belong uniquely to a species, and so linear combinations must be formed. The

[11] J. B. Howard and E. B. Wilson, Jr., J. Chem. Phys. **2**, 620 (1934).

[12] G. Herzberg, *Molecular Spectra and Molecular Structure: II. Infrared and Raman Spectra of Polyatomic Molecules* (D. Van Nostrand Company, Inc., New York, 1949), p. 252.

suitable linear combinations and their proper symmetry species are given in Table II. It is necessary to take linear combinations of the products of the linear combinations given in Table II, if the resulting sum of t's is to belong uniquely to a given species. These new combinations and their respective symmetry species are given in Table III. Remembering to identify the transformation properties of the components of $\mathbf{I}$ with those of $\mathbf{P}$ as shown in Eqs. (42) and (43), one may now form the proper combination of t's. Since only combinations of t's belonging to species A_1 are permissible, the other products must vanish. If the y axis lies in a symmetry plane, one gets the following nonvanishing t's: $t_{xxxx}=t_{yyyy}$, $t_{xxyy}=t_{zzzz}-2t_{xyxy}$, $t_{zzzz}=t_{zzyy}$, t_{zzzz}, $t_{zzzx}=t_{zyzy}$, $-t_{xyzx}=t_{yyyz}=-t_{xxyz}$.[13] In the molecules of C_{3v} symmetry, symmetric rotors, $I_{xx}{}^0=I_{yy}{}^0$. Thus by use of Eq. (17), it is seen that the same results hold for the τ's as for the t's.

RELATIONS BETWEEN τ'S AND FORCE CONSTANTS

The arguments given above should simplify the calculation of the τ's. If the force constants and fairly good structural parameters are known for the molecule, the τ's may be calculated and used in the analysis of the rotational spectrum. However, one usually does not have complete information concerning the force constants from vibrational analysis, and so the τ's cannot be calculated exactly. In such cases the distortion constants must be determined empirically from the rotational spectrum.[14] Methods of doing this have been discussed[2,3,15,16] previously. When this latter procedure can be followed, some knowledge of the force constants may be obtained from the empirically determined distortion constants. This knowledge may be used to supplement or check vibrational data.

TABLE III. Symmetry species of products of linear combinations of the components of $\mathbf{P}$ for molecules of C_{3v} symmetry. The abbreviations of Table II are used. The y axis lies in a plane of symmetry.

A_1	A_2	$E(x)$	$E(y)$
$P_a{}^2$	$(P_dP_e-P_cP_f)/\sqrt{2}$	P_aP_c	P_aP_d
$P_b{}^2$		P_aP_e	P_aP_f
P_aP_b		P_bP_c	P_bP_d
$(P_c{}^2+P_d{}^2)/\sqrt{2}$		P_bP_e	P_bP_f
$(P_e{}^2+P_f{}^2)/\sqrt{2}$		$(P_cP_d+P_dP_c)/\sqrt{2}$	$(P_c{}^2-P_d{}^2)/\sqrt{2}$
$(P_cP_e+P_dP_f)/\sqrt{2}$		$(P_cP_f+P_fP_c)/\sqrt{2}$	$(P_e{}^2-P_f{}^2)/\sqrt{2}$
		$(P_cP_f+P_dP_e)/\sqrt{2}$	$(P_cP_e-P_dP_f)/\sqrt{2}$

[13] It is easily seen that, in general, $t_{\mu\nu\mu\nu}=t_{\mu\nu\nu\mu}=t_{\nu\mu\mu\nu}=t_{\nu\mu\nu\mu}$.

[14] In order to evaluate these constants empirically different kinds of transitions are required. If the transitions are of the same type the resulting equations in the constants may be nearly parallel.

[15] J. W. Simmons and W. E. Anderson, Phys. Rev. **80**, 338 (1950).

[16] R. B. Lawrence and M. W. P. Strandberg, Phys. Rev. **83**, 363 (1951).

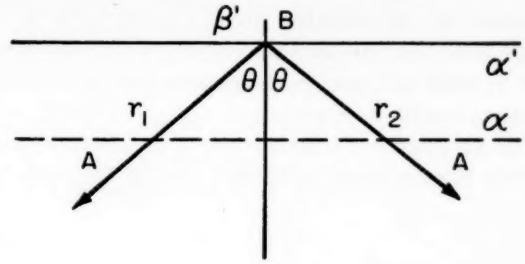

FIG. 6. Nonlinear ABA molecule.

From reference 2 it is seen that only nine independent τ's enter into a first-order treatment of the effect of centrifugal distortion on the rotational energy levels of polyatomic molecules. It is also seen that only six independent linear combinations of these enter into the final expression for the energy. In the case of K doublets in an asymmetric molecule, only five linear combinations can be determined from the rotational spectrum,[2,3] while for a symmetric rotor only three such linear combinations of τ's exist.[17] The force constant information that can be obtained from this analysis of centrifugal distortion is limited by the number of independent combinations of τ's.

A comparison of the distortion constants obtained empirically from rotational spectra with those calculated from the force constants obtained from vibrational spectra has been made for symmetric rotors.[15] The agreement was poor for some still undetermined reason. Such a comparison was also made for an asymmetric rotor (HDS).[3] Only some of the constants could be determined unambiguously from the rotational spectrum, but they were in fairly good agreement with those calculated from vibrational data.

EXAMPLE: NONLINEAR ABA MOLECULE

The principles discussed above can be illustrated most simply in the case of a nonlinear ABA molecule, Fig. 6. In this molecule $r_1=r_2$ at equilibrium. The symmetry properties of such a molecule (C_{2v}) have been discussed above. Three symmetry coordinates that can be used are $S_1=(1/\sqrt{2})(\delta r_1+\delta r_2)$, $S_2=\delta(2\theta)$, $S_3=(1/\sqrt{2})(\delta r_1-\delta r_2)$. They belong to the species A_1, A_1, and B_1, respectively. From Table I one finds that δI_{xx}, δI_{yy}, δI_{zz} are functions of S_1 and S_2, while δI_{xz} is a function of S_3. Application of the rules given above for bond stretching and valence angle bending yields

$$\begin{aligned}
&dI_{xx}/dS_1=2\sqrt{2}m_Ar\sin^2\theta,\\
&dI_{zz}/dS_1=2\sqrt{2}m_Am_Br\cos^2\theta/M,\\
&dI_{xz}/dS_2=2m_Ar^2\sin\theta\cos\theta,\\
&dI_{zz}/dS_2=-2m_Am_Br^2\sin\theta\cos\theta/M,\\
&dI_{xz}/dS_3=(2\sqrt{2}m_Ar\cos\theta\sin\theta)(1+2m_Am_B{}^{-1}\sin^2\theta)^{-1}.
\end{aligned}\tag{44}$$

[17] Z. I. Slawsky and D. M. Dennison, J. Chem. Phys. **7**, 509 (1939).

It must be remembered that $I_{yy}=I_{xx}+I_{zz}$ in this molecule so that the derivatives of I_{yy} with respect to S_1 and S_2 exist and are easily obtainable. All other derivatives vanish as expected.

The symmetry discussion above indicates which t's vanish. Furthermore, it is seen that in this case only four t's are linearly independent, the following relations holding among the seven nonvanishing ones:

$$\begin{aligned} t_{yyyy}&=t_{xxxx}+t_{zzzz}+2t_{xxzz},\\ t_{yyxx}&=t_{xxxx}+t_{xxzz},\\ t_{yyzz}&=t_{zzzz}+t_{xxzz}. \end{aligned} \tag{45}$$

THE JOURNAL OF CHEMICAL PHYSICS VOLUME 21, NUMBER 7 JULY, 1953

An Aid in the Determination of Internal Parameters from Rotational Constants for Polyatomic Molecules*

DANIEL KIVELSON AND E. BRIGHT WILSON, JR.
Mallinckrodt Chemical Laboratory, Harvard University, Cambridge, Massachusetts

(Received January 26, 1953)

The rules given in a previous paper for the derivatives of the principal moments of inertia with respect to internal parameters are shown to be applicable to the problem of obtaining molecular parameters from spectroscopic moments of inertia, even though the conditions on the coordinate axes are different in the two cases.

ROTATIONAL constants, proportional to the reciprocal of the principal moments of the effective inertia tensor, are determined in the analysis of rotational spectra. It is often a difficult process to obtain the molecular bond distances and internal angles from these constants. If fairly good values of these internal parameters are known, they may be improved by solving the relations

$$\delta\sigma_{\alpha\alpha}=\sum_i(d\sigma_{\alpha\alpha}/dr_i)\delta r_i, \tag{1}$$

where r_i is the ith internal parameter, and

$$\sigma_{\alpha\alpha}=\hbar/2\pi I_{\alpha\alpha}, \tag{2}$$

and $I_{\alpha\alpha}$ is the $\alpha\alpha$ principal moment of inertia. Since the variation must be taken in such a way that the molecule remains in the principal axis system, there are three rotation and three translation conditions on the derivatives involved. Thus in a molecule consisting of N atoms, only $3N-6$ internal parameters are considered independent variables, and the derivatives are taken with respect to these, subject to the six imposed conditions.

In a preceding paper[1] it has been shown [Eqs. (22)–(27)] that $I_{\alpha\alpha}$ is not affected by infinitesimal rotations or translations required to insure that the atomic displacements satisfy the requirements on the vibrational coordinate system. In the present problem different rotational conditions are required: namely, that the axes remain principal axes. This condition differs from Eq. (21) of the previous paper only by a change of sign between the two terms, which does not alter the conclusions reached. Consequently, the rules derived for the derivatives $\partial I_{\alpha\alpha}/\partial r_i$ in Eq. (30) and (35) of reference 1 can be used here. With the aid of the relation

$$d\sigma_{\alpha\alpha}/dr_i=-(\hbar/2\pi)I_{\alpha\alpha}^{-2}(dI_{\alpha\alpha}/dr_i), \tag{3}$$

these rules may be used to obtain the derivatives in Eq. (1).

* The research reported in this paper was made possible by support extended Harvard University by the U. S. Office of Naval Research.

[1] D. Kivelson and E. B. Wilson, Jr., J. Chem. Phys. **21**, 1229 (1953), preceding article.

On the Use of a Single Scale Factor in Atomic Wave Functions. I*

CHARLES W. SCHERR
Laboratory of Molecular Structure and Spectra, Department of Physics, The University of Chicago, Chicago 37, Illinois
(Received February 13, 1953)

Single scale factors are determined for converting $1s$, $2s$, and $2p$ self-consistent field orbitals of atoms in the first row of the periodic table into one another. Several simple relationships are found which allow predictions for fluorine and neon.

I. INTRODUCTION

RECENTLY there has been a recognition[1] of a desirability of using SCF (self-consistent field) atomic orbitals rather than the Slater atomic orbitals in problems on molecular structure. Most of the LCAO MO (linear combination of atomic orbitals molecular orbitals) method has been pursued through the use of Slater orbitals; but decidedly different results may be expected from the use of SCF orbitals, as shown, for example, by calculations of overlap integrals.

Any SCF orbital $\chi_{A,S}$ is of the form $R_{A,S}(r)F(\theta,\phi)$, where A and S refer to the atom and the state, respectively. By introducing a scale factor $\lambda_{AB,ST}$ one can expect to predict $\chi_{B,T}$, the SCF orbital of atom B in state T from $\chi_{A,S}$ by an approximation $\chi_{B,T} \approx (\lambda_{AB,ST})^{\frac{1}{2}} R_{A,S}(\lambda_{AB,ST}r)F(\theta,\phi)$. Since the radial part may be approximated[2] by a sum,

$$R_{A,S,n,l} \approx \sum_{k=l}^{n-1} a_k r^k e^{-\zeta_k r}, \tag{1}$$

in which the *last* term is dominant, then

$$\lambda_{AB,ST} \approx \zeta_{n-1,B}/\zeta_{n-1,A}. \tag{2}$$

The a_k's and the ζ_k's (orbital exponents)[3] depend on the particular orbital, atom, and (to a small extent) electronic state.

Some early workers[4] on SCF (self-consistent field) calculations used a scale factor to obtain their first approximations from previously treated atoms, which were nearby in the same row of the periodic table. Brown, Bartlett, and Dunn[5] noted that the reciprocals of the radii at the maxima of the SCF radial wave functions were nearly linear in the atomic number and used the ratios of these reciprocals as scale factors. Hartree[6] has discussed the use of a scale factor, and introduced the idea expressed in Eq. (2).

The present paper is a result of a systematic investigation of the use of a *single* scale factor in the exact *SCF wave functions with exchange* for atoms of the first row of the periodic table. The SCF wave functions are the "best" wave functions arising from the variational method with the use of antisymmetrized spinorbital-product wave functions.

There is a characterizing coefficient used extensively in this paper which it is best to discuss here. $R_{A,S}(r)$ depends on S; but by Slater's theory of complex spectra,[7] $E_S = E_C + \beta_S F^2$, where F^2 is an energy integral and E_C is a configuration energy, hence $R_{A,S}(r) = R_A(r,\beta_S)$ for any given configuration. For example the ^3P ground state of carbon has $\beta = -5/25$, and the ^1D and ^1S states have $\beta = +1/25$ and $+10/25$, respectively.

II. PROCEDURE

We have

$$\int_0^\infty \lambda_{AB,ST} R_{A,S^2}(\lambda_{AB,ST}r) r^2 dr = \int_0^\infty R_{B,T}(r) r^2 dr = 1,$$

where the symbols have all been defined in Sec. I. Further,

$$\lambda_{AC,ST} = \lambda_{AB,SU}\lambda_{BC,UT}, \tag{3}$$

where $\chi_{B,U}$ is any orbital.

Numerically tabulated *SCF with exchange* $rR(r)$ functions from the literature[8–11] for the various s^2p^n states of each of the atoms carbon, nitrogen, oxygen, and neon were approximated by scaling from tabulated *SCF with exchange* $rR(r)$ data for the s^2p^3 states of carbon.[8] Various λ values were tried in each case until that one was found which, for a particular scaling, minimized

$$2\int_0^\infty |(\delta R)R_{B,T}| r^2 dr. \tag{4}$$

* This work was assisted (in part) by the U. S. Office of Naval Research under Task Order IX of Contract N6ori-20 with The University of Chicago.

[1] See for example R. S. Mulliken J. Phys. Chem. **56**, 295 (1952), particularly p. 300.

[2] J. C. Slater, Phys. Rev. **42**, 33 (1932).

[3] This term was introduced by C. C. J. Roothaan and K. Ruedenberg. It is the effective nuclear charge divided by the principal quantum number.

[4] Arnot and McLauchland, Proc. Roy. Soc. (London) **146A**, 662 (1934); Manning and Millman, Phys. Rev. **49**, 848 (1936).

[5] Brown, Bartlett, and Dunn, Phys. Rev. **44**, 296 (1933).

[6] D. R. Hartree, Repts. Progr. Phys. 113 (1946–1947).

[7] J. C. Slater, Phys. Rev. **34**, 1293 (1929).

[8] A. Jucys, Proc. Roy. Soc. (London) **173A**, 59 (1939); also see J. Phys. U.S.S.R. 49 (1947).

[9] Hartree and Hartree, Proc. Roy. Soc. (London) **193A**, 299 (1948).

[10] Hartree, Hartree, and Swirles, Trans. Roy. Soc. (London) **238A**, 229 (1939).

[11] D. R. Hartree, private communication of tentative results (first iteration) by Miss B. H. Worsley for the $2p$ neon orbitals, and of estimations by Hartree for the $1s$ and $2s$ neon orbitals.

TABLE I. The $2p$ scale factors for scaling from carbon[a] SCF orbitals.

From $2p$ in:	To $2p$ in:		Carbon s^2p^2			Nitrogen s^2p^3			Oxygen s^2p^4			Neon s^2p^6
		^1S	^1D	^3P	^2P	^2D	^4S	^1S	^1D	^3P	^1S
	25β:	10	1	−5	0	−6	−15	0	−9	−15	−30
carbon s^2p^2	^1S	1	(1.041)[b]	1.062_5	(1.257)	1.277	(1.301)	1.474	1.495	(1.506)	···
carbon s^2p^2	^1D	0.962_5	1	1.021_5	1.207_5	1.224	1.249	1.416	1.433_5	1.446	1.87
carbon s^2p^2	^3P	(0.938)	0.977	1	(1.180)	(1.196)	1.218	1.384	(1.400)	1.414	···
	Corresponding "criterion errors"										
carbon s^2p^2	^1S	0	(0.038)	0.0567	(0.020)	0.029	(0.048)	0.0066	0.0143	(0.029)	···
carbon s^2p^2	^1D	0.0386	0	0.0204	0.0188	0.0080	0.0101	0.0350	0.0232	0.0162	0.0193
carbon s^2p^2	^3P	(0.058)	0.0233	0	(0.041)	(0.030)	0.0115	∼0.058	(0.049)	0.0389	···

[a] Also ^2P nitrogen scaled to ^3P oxygen, $\lambda = 1.195$, *criterion error*, −0.0037; ^1D oxygen scaled to ^3P oxygen, $\lambda = 1.008_8$, *criterion error*, −0.0064.
[b] The values in parentheses are the mean values of estimates made by one or more methods, for example, by the use of Eq. (3).

This procedure may be compared with the usual[12] least squares treatment of problems of similar type, namely, the minimization of

$$2\int_0^\infty (\delta R) R_{B,T} r^2 dr. \qquad (4a)$$

In integrals (4) and (4a), $R_{B,T}$ is the correct numerical SCF function for the radial part of the orbital that is being approximated. δR is defined as the difference between the correct tabular value of $R_{B,T}$ and the approximtion. The integrals were evaluated by numerical integration.

III. RESULTS

The best values of the scale factors, determined by the above procedure, are tabulated in Tables I, II, and III. The "*criterion error*" reported is the magnitude of the minimized integral (4). These *criterion errors* can be used as measures of the relative errors involved, for

TABLE II. The $2s$ scale factors for scaling from carbon SCF orbitals.

From $2p$ in:	To $2p$ in:	Beryllium s^2		Carbon s^2p^2			Nitrogen s^2p^3			Oxygen s^2p^4		Neon s^2p^6
		^1S	^1S	^1D	^3P	^2P	^2D	^4S	^1S	^1D	^3P	^1S
	25β:	0	10	1	−5	0	−6	−15	0	−9	−15	−30
carbon s^2p^2	^1S	···	1	(0.994)[a]	0.990	1.185_5	(1.181)	1.176_5	1.377_5	(1.374)	1.371_5	···
carbon s^2p^2	^1D	0.594	1.006	1	0.996	1.194	1.189	1.183	1.385_5	1.382	1.378	1.766
carbon s^2p^2	^3P	···	(1.010)	(1.004_5)	1	1.199_5	(1.193)	1.187_5	1.393_5	(1.388)	1.383_5	···
	Corresponding "criterion errors"											
carbon s^2p^2	^1S	···	0	(0.0026)	0.0067	0.0075	(0.0090)	0.0102	0.0095	···[b]	∼0.0112	···
carbon s^2p^2	^1D	0.0176	0.0026	0	0.0028	0.0060	0.0070	0.0099	0.0100	∼0.0094	0.0095	0.0144
carbon s^2p^2	^3P	···	0.0060	(0.0028)	0	0.0079	(0.0040)	0.0065	0.0102	···[b]	0.0094	···

[a] The values in parentheses are the mean values of estimates made by one or more methods, for example, by the use of Eq. (3).
[b] The whole spread of *criterion error* here is too small to make estimates meaningful.

[12] The original purpose of the work was the estimation of two-center overlap integrals, and integral (4) seems better for this purpose than integral (4a). The two minimizations give scale factors that agree in the second decimal.

different atoms and states, in the best computed orbitals of any one kind obtained by scaling with a single scale factor from an initial SCF tabulation. The published SCF data are accurate to ± 0.002 unit. This degree of unreliability would correspond to a *criterion error* of about 0.0035 to 0.0040 for the $2s$ and $2p$ orbitals.

IV. DISCUSSION

For $2s$ or $2p$ scaling from carbon to either oxygen or nitrogen, the scale factors are nearly linear in β. For carbon scaled to carbon the linearity is slightly less good. In Jucy's SCF calculations of carbon, the tabulated values of $rR(r)$ for the $2s$ and $2p$ orbitals in the ^1D state were found to be in agreement, to the accuracy of the calculation, with the results of an interpolation linear in β, at any given r value, between the tabulated values for the ^3P and ^1S states. Hartree and the others in subsequent SCF calculations on nitrogen and oxygen assumed the validity of corresponding relations for these atoms; the wave function of the ^2D state of nitrogen was assumed to be linearly spaced with respect to β between those of the ^2P and ^4S states; likewise the ^1D state of oxygen between the ^1S and ^3P states, and consequently only the last pairs in each case were calculated by them.

TABLE III. The $1s$ scale factors for scaling from carbon SCF orbitals.

To	Beryllium	Carbon	Nitrogen	Oxygen	Neon
From carbon	0.645_5	1	1.172	1.349	1.697_5
Corresponding "criterion errors"					
From carbon	0.0082	0	0.0023	0.0048	0.0003_3

Surprisingly enough, the *criterion error* does not increase as the scaling goes to atoms more remote in the periodic table from carbon. This result may allow one to make safely "long distance" scalings for use as first approximations in SCF calculations. Regularities in the behavior of the *criterion error* indicate that a scaling to the ^2P state of fluorine from the ^1D of carbon should have a *criterion error* of about 0.018, but that scaling to the ^2P state of boron should have a large *criterion error*.

An interesting characteristic of the λ-values, evident if one compares Figs. 1 and 2, is that $\partial\lambda/\partial\beta$ has opposite signs for the $2p$ and $2s$ orbitals. This may be the result of the influence of the inner loop of the $2s$ orbital which, relatively speaking, requires a much smaller λ than the outer loop, as can be seen from Table IV.

The considerable success of a single scale factor in estimating one SCF orbital from another must reflect a close mathematical similarity between the SCF wave functions of the various atoms. The accuracy of such estimates could be increased several fold by using two or more scale factors; for example, in a $2p$ or $1s$ orbital these could be one scale factor for a radius less than, and another for a radius greater than the radius at the maximum of $rR(r)$, and in a $2s$ orbital, one scale factor for each loop.

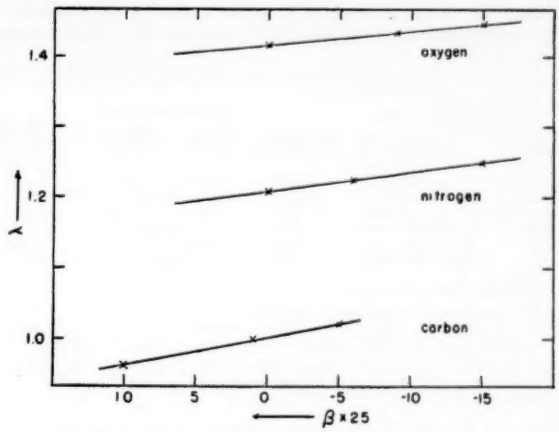

FIG. 1. The $2p$ scale factors as functions of β.

In several of the investigated cases any λ value within an appreciable range gave a satisfactory scaling; that is, the minima of integral (4) were broad. Almost all of these broad minima occurred in scalings with large *criterion errors*.

V. GENERAL FORMULAS

The near linearity of the scale factors with respect to β allows simple formulas to be written for the scale factors of the first row atoms. We use the symbol $\lambda(N, \beta{:}6, 1)$ to mean the scale factor for scaling from $s^2p^2\,{}^1D$ carbon to the s^2p^{N-4} state, characterized by β, for the atom of atomic number N. The formulas[13] are

$$\lambda_{2p}(N, \beta{:}6, 1) = 1.002 + 0.207(N-6) - 0.0983(0.707)^{N-6}\beta, \quad (5)$$

$$\lambda_{2s}(N, \beta{:}6, 1) = 0.999 + 0.194(N-6) + 0.0025(13-N)\beta, \quad (6)$$

$$\lambda_{1s}(N{:}6) = 1 + 0.174(N-6). \quad (7)$$

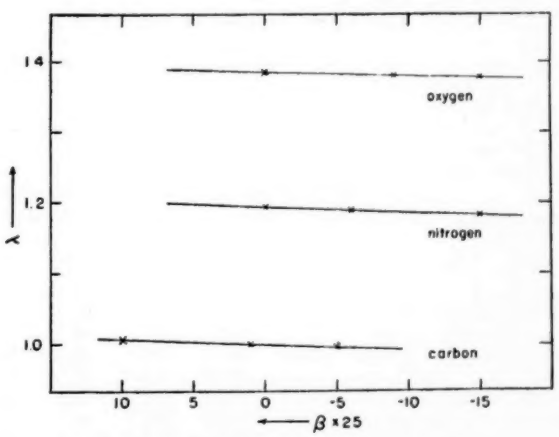

FIG. 2. The $2s$ scale factors as functions of β.

[13] Because of the tentative nature of the neon data, and of the probability that Hartree estimated the $1s$ and $2s$ neon orbitals on a basis similar to ours, these formulas were not adjusted to fit the neon data. The fact that the neon data does fit, however, lends evidence to this supposition.

TABLE IV. A comparison of λ with the use of the ratio of the reciprocals of the radii at maxima in the wave function for scale factors.

Carbon scaled to	Method	λ for the 1s orbitals	λ for the 2s orbitals: Inner max[a]	λ for the 2s orbitals: Outer max[a]	λ for the 2p orbitals
nitrogen	by reciprocals	1.183	1.148	1.184	1.230
nitrogen	calculated here	1.172	1.176–99[b]		1.180–1.301
oxygen	by reciprocals	1.356	1.308	1.414	1.482
oxygen	calculated here	1.349	1.371–93		1.384–1.506
neon	by reciprocals	1.680	1.661	1.768	1.963
neon	calculated here	1.697[5]	1.766		1.87

[a] This refers only to the reciprocal method.
[b] The numbers in this and the next column, under the row heading "calculated here," are the complete spread of scale factors found for each atom as calculated here. Since the maxima of the *SCF* functions of the same orbital for the various states of the same atom coincide, there are no "spreads" for the "reciprocal" rows.

Scale factors for scalings from other than ^1D carbon, can be obtained by the use of Eq. (3). The scale factors calculated from these formulas, for scaling from the ^1D state of carbon to certain states of boron, fluorine, and neon atoms, are presented in Table V.

VI. A COMPARISON OF SCALE FACTORS FROM VARIOUS SOURCES

Slater[14] has given a recipe for orbital exponents[3] to be used in conjunction with his well-known and very useful orbitals. This recipe may be compared directly with our scale factors by means of Eq. (2). It requires for the coefficient of $(N-6)$ in Eq. (5) and Eq. (6), the value 0.2 and in Eq. (7), the value 0.1754. The results of the present and the following paper of this series indicate that these rather arbitrary choices of Slater were remarkably good. This, of course, is no new conclusion.

Duncanson and Coulson[15] have calculated orbital exponents for approximate SCF wave functions. As might be expected (see Table VI), our results are in good agreement with the scale factors constructed from their data.

TABLE V. Some calculated scale factors for scaling from the ^1D state of carbon.

Atom Orbital	Boron s^2p ^2P	Fluorine s^2p^5 ^2P	Neon s^2p^6 ^1S
2p	···	1.651	1.860
2s	···	1.573	1.766
1s	0.826	1.522	1.696

TABLE VI. A comparison of λ with the scale factors constructed from the calculations of Duncanson and Coulson (reference 15).

Atom	State	Scale factor for scaling from s^2p^2 ^3P carbon for the: 1s orbital, Reference 15	1s orbital, λ	2s orbital, Reference 15	2s orbital, λ	2p orbital, Reference 15	2p orbital, λ
Li	^2S	0.473	(0.478)[a]	0.398	(0.419)	···	···
Be	^1S	0.648	0.646	0.593	(0.597)	···	···
B	^2P	0.824	(0.826)	0.800	(0.809)	0.769	(0.777)
N	^4S	1.174	1.172	1.192	1.188	1.224	1.218
O	^3P	1.350	1.349	1.385	1.384	1.423	1.414
F	^2P	1.524	(1.522)	1.580	1.580	1.634	1.613
Ne	^1S	1.700	1.698	1.776	(1.774)	1.846	(1.827)

[a] The values in parentheses have been estimated either by the use of Tables I, II, or by the use of Eqs. (5), (6), (7) in conjunction with Eq. (2).

A comparison of our scale factors with those constructed from the ratios of the reciprocals of the radii at maxima in the wave functions is given in Table IV, where the method can be seen to give fairly good scale factors.

VII. ACKNOWLEDGMENT

I wish to express my indebtedness to Professor R. S. Mulliken for suggesting this investigation and for many helpful discussions; and also Professor C. C. J. Roothaan for some valuable constructive criticism.

[14] J. C. Slater, Phys. Rev. **36**, 57 (1930) and C. Zener, Phys. Rev. **36**, 51 (1930).

[15] Duncanson and Coulson, Proc. Roy. Soc. (Edinburgh) **62A**, 37 (1944).

On the Use of a Single Scale Factor in Atomic Wave Functions. II. Application to Overlap Integrals*

CHARLES W. SCHERR
Laboratory of Molecular Structure and Spectra, Department of Physics, The University of Chicago, Chicago 37, Illinois

(Received February 13, 1953)

A method of estimation of two-center homopolar overlap integrals between SCF atomic orbitals, due to Mulliken, has been tested and verified.

THE calculation of two-center overlap integrals from numerically tabulated SCF (self-consistent field) functions is somewhat laborious, and even with the use of analytical fits to the SCF functions, when available, the calculation is still rather lengthy. It is the purpose of this paper to demonstrate the applicability of a simple method of making estimates of homopolar two-center SCF overlap integrals. This method is applicable to the various atom pairs which can be constructed from any particular row of the periodic table, when exact calculations are available for the SCF overlap integrals of one of those pairs.

The method of estimation used in the present paper has been proposed[1] and used[2] by Mulliken. The idea of the method is that two-center overlap integrals are about the same for all the homopolar atom pairs of the same row of the periodic table, for the same orbitals, for any particular ρ-value, where $\rho=\zeta R$ and ζ is the Slater orbital exponent[3] of the atom, and R is the internuclear distance in atomic units.[4]

Analytical fits using three to five term linear combinations of Slater type orbitals to the "SCF with exchange" numerically tabulated functions for the $rR(r)$ (radial part of the wave function) of the $1s$, $2s$, and $2p$ orbitals of the various states of each of the atoms of carbon, nitrogen, and oxygen, among others, were determined by Dr. P.-O. Löwdin.[5] On the basis of the criterion of accuracy used in the first paper of the present series, these fits give a *criterion error* of less than 0.0050.[6] As a test of Mulliken's method of estimation of SCF overlap integrals, the present author computed the exact SCF overlap integrals for the nitrogen and oxygen molecules at their equilibrium internuclear distances, from Löwdin's fits for nitrogen and oxygen atoms, and compared them with the same integrals which were computed from the ^1D carbon fit at a ρ-value corresponding to that of the exact calculations on the nitrogen or oxygen molecules. This ρ-value depends, of course, on the ζ's (orbital exponents)[3] assigned to the atoms. The exact carbon-carbon bond calculations are tabulated in Table I. Table II presents a comparison of the exact calculations on the nitrogen and oxygen molecules along with estimations of the same integrals (made from interpolations into Table I) based on ζ-values (1) from the Slater recipe[7] and (2) from the formulas of the first paper of the present series. Both estimations are quite satisfactory, and there is little to choose between the two recipes for the ζ's on the basis of these calculations. However, the formulas of the first paper of the present series are more versatile in that they can be adapted without any additional trouble to valence states, or indeed any hypothetical states of the atoms; they also take into account the differences in ζ-values of the $2s$ and $2p$ orbitals.

The row of Table II marked "Rieke" presents estimations derived from the tables of carbon-carbon bond SCF overlap integrals given by Mulliken[8] which are

TABLE I. Overlap integrals for the carbon-carbon bond. These overlap integrals were calculated by the author for the carbon-carbon bond using P.-O. Löwdin's analytical fits, using three- to five-term linear combinations of Slater type orbitals, for the $2s$ and $2p$ SCF orbitals as computed for the s^2p^2, ^1D state of carbon. The r values are the internuclear separations in atomic units at which the integrals were calculated, and $\rho^{\text{Slater}}=1.625r$ is the corresponding two-quantum ρ. The S are the overlap integrals, the subscripts referring to the orbitals $1s$, $2s$, $\sigma(2p\sigma)$, and $\pi(2p\pi)$. For brevity $S_{\pi,\pi}$ is written S_π, etc. These values may be compared with the corresponding values in Table VI of reference 8, which were calculated from the Rieke fit.

r au	2-quantum ρ^{Slater}	S_π	S_σ	S_{2s}	$S_{2s,\sigma}$	$S_{1s,\sigma}$	$S_{1s,2s}$
2.07	3.36	...	0.085	...	...	...	...
2.27	3.69	0.425	0.148	0.511	0.504	0.121	0.070
2.29	3.72	...	0.152	...	...	...	...
2.49	4.04	0.373	0.193	0.455	0.485	0.100	0.056
2.70	4.39	0.327	0.225	...	...	...	...
2.91	4.73	0.287	0.247	0.357	0.429	0.069	0.035
3.20	5.20	0.238	0.260	0.292	0.384	0.055	0.026
3.32	5.39_5	0.219	0.264	...	...	...	...

* This work was assisted in part by the U. S. Office of Naval Research under Task Order IX of Contract N6ori-20 with The University of Chicago.

[1] R. S. Mulliken, J. Am. Chem. Soc. **72**, 4493 (1950).

[2] R. S. Mulliken, J. Phys. Chem. **56**, 295 (1952), footnote 42.

[3] See reference 6, footnote 3.

[4] The extension to heteropolar atom pairs should be complicated. If the ratio of the ζ-values were near unity, e.g., in NO, it would seem reasonable to use a mean ρ-value, $\rho=\frac{1}{2}(\zeta_A+\zeta_B)R$, where ζ_A and ζ_B are the orbital exponents on the two atoms.

[5] Private communication to the author, to be published shortly.

[6] C. W. Scherr, J. Chem. Phys. **21**, 1237 (1953). A *criterion error* of 0.0050 is very close to the error of the SCF calcultions themselves. A *criterion error* of 0.0189 implies a reproduction of the SCF functions to about ± 0.010 units.

[7] J. C. Slater, Phys. Rev. **36**, 57 (1930); C. Zener, Phys. Rev. **36**, 51 (1930). The Slater ζ-values are conveniently summarized in Table I of reference 9.

[8] R. S. Mulliken, J. Chem. Phys. **19**, 900 (1951), Tables VI and IX.

TABLE II. Overlap integral calculations for nitrogen and oxygen bonds. The row marked "SCF" gives values of the two-center overlap integrals of nitrogen and oxygen molecules calculated from P.-O. Löwdin's analytical fit for the SCF data of the atoms in the states indicated. The row marked "Slater" gives values of the integrals for the carbon-carbon bond at a ρ-value found from the Slater ζ-values, $\rho=\zeta R_e$. R_e is the experimental equilibrium distance (2.075 a.u. for the nitrogen molecule and 2.29 a.u. for the oxygen molecule). The row marked "λ" is similar to the "Slater" row except that the ζ-values from the first paper of the present series are used. The row marked "Rieke" is a similar type estimation using Slater ζ-values and carbon-carbon bond overlap integral values from the tables of Mulliken (reference 8).

Integral	S_π			S_σ			S_{2s}		$S_{2s,\sigma}$		$S_{1s,\sigma}$		$S_{1s,2s}$	
Molecule	N_2	O_2		N_2	O_2		N_2	O_2	N_2	O_2	N_2	O_2	N_2	O_2
State of the atoms	^2P	^1S	^3P	^2P	^1S	^3P	^2P	^1S	^2P	^1S	^2P	^1S	^2P	^1S
"SCF"	0.372	0.241	0.227	0.185	0.241	0.246	0.463	0.300	0.482	0.388	0.099	0.058	0.056	0.028
"Slater"	0.373	0.238		0.193	0.260		0.455	0.292	0.485	0.384	0.100	0.055	0.056	0.026
"λ"	0.371	0.232	0.220	0.195	0.261	0.263	0.460	0.299	0.486	0.383	0.098	0.054	0.056	0.027
"Rieke"	0.375	0.242		0.185	0.252		0.449	0.282	0.493	0.390	...	...	...	...

based on an analytical fit made by Mrs. Rieke[9] from the carbon SCF data. This fit gives a *criterion error* of 0.0189.[6] The ζ-recipe used is that of Slater. The results so obtained show that, although the fit is not so accurate as Löwdin's, nevertheless good estimations of overlap integrals can be made from those tables, which are therefore very convenient to use for this purpose.

[9] Mulliken, Rieke, Orloff, and Orloff, J. Chem. Phys. **17**, 1248 (1949), Sec. Vb.

THE JOURNAL OF CHEMICAL PHYSICS VOLUME 21, NUMBER 7 JULY, 1953

Bond Energies and Bond Distances of Hydrocarbons

GEORGE GLOCKLER*
Department of Chemistry, Duke University, Durham, North Carolina
(Received January 29, 1953)

The relations between carbon-carbon bond energies [B(CC)] and distances [R(CC)] and carbon-hydrogen bond energies [B(CH)] and distances [R(CH)] are taken to be a parabola and a straight line, respectively,

$$B(\mathrm{CC})=1450.762-1644.151\cdot R(\mathrm{CC})+491.936\cdot R(\mathrm{CC})^2$$

and

$$B(\mathrm{CH})=252.956-141.721\cdot R(\mathrm{CH}),$$

yielding

$$B(\mathrm{CH})=98.104-0.075\cdot B(\mathrm{CC})+[3.196\cdot B(\mathrm{CC})-246.048]^{\frac{1}{2}}$$

and

$$R(\mathrm{CH})=1.396-0.594\cdot R(\mathrm{CC})+0.261\cdot R(\mathrm{CC})^2.$$

This system of equations is based on the assumption that the heat of sublimation of carbon L(C)=169.75 kcal. Similar relations with L(C)=124.3 and 135.8 kcal are also derived.

INTRODUCTION

A SYSTEM of bond energies was described earlier[1] based on a value of the heat of sublimation of carbon L(C)=169.8 kcal.[2,3] In the meantime, Hansen and Dennison[4] have determined the carbon-carbon and carbon-hydrogen distances in ethane to be 1.543 and 1.102A from the infrared and Raman spectra of light and heavy ethane. It is now possible to use this new information and already known distances (Table III)[5–7] and find new numerical relations.

The ordinary heat of formation of gaseous molecules from the elements in their usual standard states (Qf_0^0), the heat of dissociation of hydrogen [$D(H_2)$=103.239 kcal], and the heat of sublimation of carbon [L(C) assumed to be 169.75, 135.8, or 124.3 kcal per mole, respectively] permit the calculation of the heat of atomization (Qa_0^0) of hydrocarbon molecules. All values are taken at 0°K. The ordinary heats of formation are

* Visiting lecturer; on leave of absence from the State University of Iowa

[1] G. Glockler, J. Chem. Phys. **19**, 124 (1951); Disc. Faraday Soc., No. 10, 26 (1951).

[2] Brewer, Gilles, and Jenkins, J. Chem. Phys. **16**, 797 (1948).

[3] A. L. Marshall and F. J. Norton, J. Am. Chem. Soc. **72**, 2166 (1950).

[4] G. E. Hansen and D. M. Dennison, J. Chem. Phys. **20**, 313 (1952).

[5] G. Herzberg, *Infrared and Raman Spectra of Polyatomic Molecules* (D. Van Nostrand Company, Inc., New York, 1945).

[6] G. Herzberg, *Molecular Spectra and Molecular Structure. I. Spectra of Diatomic Molecules* (D. Van Nostrand Company, Inc., New York, 1950).

[7] D. Riley, Nature **153**, 587 (1944).

taken from *Selected Values of Properties of Hydrocarbons*.[8] The following notation is used:

$B(\mathrm{CC}, \mathrm{C}_x\mathrm{H}_y)$ = carbon-carbon bond energy in molecule $\mathrm{C}_x\mathrm{H}_y$ (kcal);

$B(\mathrm{CH}, \mathrm{C}_x\mathrm{H}_y)$ = carbon-hydrogen bond energy in molecule $\mathrm{C}_x\mathrm{H}_y$ (kcal);

$R(\mathrm{CC}, \mathrm{C}_x\mathrm{H}_y)$ = carbon-carbon bond distance in molecule $\mathrm{C}_x\mathrm{H}_y$(A);

$R(\mathrm{CH}, \mathrm{C}_x\mathrm{H}_y)$ = carbon-hydrogen bond distance in molecule $\mathrm{C}_x\mathrm{H}_y$(A);

$L(\mathrm{C})$ = heat of sublimation of carbon (169.75, 135.8, or 124.3 kcal);

$L(\mathrm{C})/2$ = carbon-carbon bond energy in the diamond = B(CC, diamond);

$Qf_0^0(\mathrm{C}_x\mathrm{H}_y)$ = ordinary heat of formation of a hydrocarbon from the elements in their usual standard states (at 0°K; kcal);

$Qa_0^0(\mathrm{C}_x\mathrm{H}_y)$ = heat of atomization of a gaseous hydrocarbon $\mathrm{C}_x\mathrm{H}_y$ (in a specified state) to the $x+y$ gaseous atoms (in specified states) (at 0°K, kcal) = atomic heat of formation;

$D(AB-C)$ = bond dissociation energy of the bond BC in the molecule ABC: $ABC \rightarrow AB + C + D(AB-C)$ kcal;

$D(\mathrm{H}_2)$ = heat of dissociation of hydrogen, (103.239 kcal).

It must be pointed out at once that the bond energies here calculated are considered estimates only. The *first reason* is that the basic B(CC):R(CC) and B(CH):R(CH) curves may not be a parabola and a straight line, respectively, as will be assumed. *Second* the transfer of bond energy values from one molecule to another is very likely not quite valid. However, the same procedure is followed with force constants and works there tolerably well. Here also it seems legitimate to transfer the stronger bonds (i.e., double and triple bonds) from molecule to molecule, provided, of course, that the chemical behavior of the molecule is such as to warrant such transfer. This transfer of bond energies is used to calculate the other bond energies of the molecule under consideration. For example, in the case of butadiene, it is assumed that the two carbon-carbon double bonds and the four attendant carbon-hydrogen bonds are as in ethylene. Since the atomic heat of formation of butadiene (Qa_0^0) can be determined, the sum of $2B(\mathrm{C{=}C}, \mathrm{C_2H_4})$ and $4B(\mathrm{CH}, \mathrm{C_2H_4})$ may be subtracted from $Qa_0^0(\mathrm{C_4H_6})$, and the remainder is divided between B(CC, center, $\mathrm{C_4H_6}$) and two B(CH, center, $\mathrm{C_4H_6}$) by a set of trial calculations using the basic equations. *Third*, the treatment of carbon-hydrogen bonds in molecules, where these bonds are not all alike, is only approximate. The basic equations will be established with molecules, where all the carbon-carbon and carbon-hydrogen bonds are the same. In other cases, where the carbon-carbon single bond may differ in value from the one in ethane, it is still supposed that the basic equation will give an estimate of the bond energy of the carbon-hydrogen bond attached to such a carbon-carbon bond. If a carbon-hydrogen bond emanates from a carbon atom burdened with a double and single bond (=C−), then it is assumed that the bond energy of the carbon-hydrogen bond is the *average* between the values belonging to the carbon-hydrogen bonds attached to the double and single carbon-carbon bond in question.

[8] *Selected Values of Properties of Hydrocarbons*, Circ. C 461, Natl. Bur. Standards (U. S. Government Printing Office, Washington, 1947).

TABLE I. Carbon-carbon bond energies and distances.

	R(CC) A	B(CC) kcal	Qa_0^0 kcal
	L(C) = 169.75 kcal		
$\mathrm{C_2H_2}$	1.207	182.948	388.410
$\mathrm{C_2}$	1.316	139.022	139.022
$\mathrm{C_2H_4}$	1.353	126.769	531.456
$\mathrm{C_6H_6}$	1.387	116.780	1304.213
$\mathrm{C_2H_6}$	1.543	85.063	665.734
Graphite	1.421	107.761	169.970
Graphite	3.354	16.216	169.970
Diamond	1.5445	84.875	169.75
	L(C) = 135.8 kcal		
$\mathrm{C_2H_2}$	1.207	132.12	320.51
$\mathrm{C_2}$	1.316	101.26	101.26
$\mathrm{C_2H_4}$	1.353	92.98	463.58
$\mathrm{C_6H_6}$	1.363	90.97	1100.52
$\mathrm{C_2H_6}$	1.543	67.98	597.84
Graphite	1.421	80.67	135.80
Graphite	3.354	29.60	135.80
Diamond	1.5445	67.90	135.58
	L(C) = 124.3 kcal		
$\mathrm{C_2H_2}$	1.207	114.954	297.510
$\mathrm{C_2}$	1.316	88.500	88.500
$\mathrm{C_2H_4}$	1.353	81.559	440.556
$\mathrm{C_6H_6}$	1.350	82.120	1031.520
$\mathrm{C_2H_6}$	1.543	62.194	574.834
Graphite	1.421	71.500	124.3
Graphite	3.354	34.100	124.3
Diamond	1.5445	62.150	124.08

TABLE II. Carbon-hydrogen bond energies and distances.

	R(CH) A	B(CH) kcal	Qa_0^0 kcal
	L(C) = 169.75 kcal		
$\mathrm{C_2H_2}$	1.060	102.731	388.410
$\mathrm{C_2H_4}$	1.071	101.172	531.456
$\mathrm{C_6H_6}$	1.075	100.598	1304.213
$\mathrm{C_2H_6}$	1.102	96.779	665.734
$\mathrm{CH_4}$	1.093	98.054	392.216
	L(C) = 135.8 kcal		
$\mathrm{C_2H_2}$	1.060	94.16	320.51
$\mathrm{C_2H_4}$	1.071	92.63	463.58
$\mathrm{C_6H_6}$	1.072	92.49	1100.52
$\mathrm{C_2H_6}$	1.102	88.32	597.84
$\mathrm{CH_4}$	1.093	89.57	358.27
	L(C) = 124.3 kcal		
$\mathrm{C_2H_2}$	1.060	91.278	297.510
$\mathrm{C_2H_4}$	1.071	89.749	440.556
$\mathrm{C_6H_6}$	1.071	89.800	1031.520
$\mathrm{C_2H_6}$	1.102	85.440	574.834
$\mathrm{CH_4}$	1.093	86.691	346.764

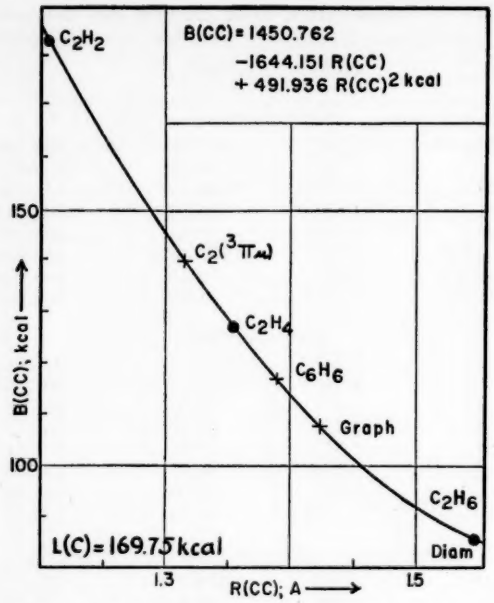

FIG. 1. Relation between carbon-carbon bond energies and distances [Eq. (19)].

It should be noted that the greatest change a carbon-hydrogen bond can suffer is to be attached to a carbon-carbon single bond and then go over to a carbon-carbon triple bond. The difference is 5.932 kcal. This is the largest error than can be made. In the case of butadiene and benzene, the methods outlined above yield very satisfactory results, and the error is estimated to be only about one kilocalorie at the most.

Bond Energies and Distances

In earlier work,[1] the relations between carbon-carbon bond energies $[B(\mathrm{CC})]$ and distances $[R(\mathrm{CC})]$ and carbon-hydrogen bond energies $[B(\mathrm{CH})]$ and distances $[R(\mathrm{CH})]$ were treated graphically. Now, however, sufficient experimental data are at hand to deal with these relations algebraically. It is found possible to write $B(\mathrm{CC})$ as a parabolic function of $R(\mathrm{CC})$ and $B(\mathrm{CH})$ as a straight line in terms of $R(\mathrm{CH})$,

$$B(\mathrm{CC})=a+b\cdot R(\mathrm{CC})+c\cdot R(\mathrm{CC})^2 \qquad (1)$$

and

$$B(\mathrm{CH})=A+B\cdot R(\mathrm{CH}), \qquad (2)$$

where A, B, a, b, and c are constants. The bond energies of the diamond, methane, ethane, ethylene, and acetylene are related to the respective heats of atomization as follows:

$$B(\mathrm{CC},\mathrm{C_2H_2})+2B(\mathrm{CH},\mathrm{C_2H_2})=Qa_0^0(\mathrm{C_2H_2}) \qquad (3)$$

$$B(\mathrm{CC},\mathrm{C_2H_4})+4B(\mathrm{CH},\mathrm{C_2H_4})=Qa_0^0(\mathrm{C_2H_4}) \qquad (4)$$

$$B(\mathrm{CC},\mathrm{C_2H_6})+6B(\mathrm{CH},\mathrm{C_2H_6})=Qa_0^0(\mathrm{C_2H_6}) \qquad (5)$$

$$B(\mathrm{CH},\mathrm{CH_4})=Qa_0^0(\mathrm{CH_4})/4 \qquad (6)$$

$$B(\mathrm{CC},\mathrm{diam})=L(\mathrm{C})/2. \qquad (7)$$

TABLE III. Bond distances in hydrocarbons.

	R(CC) A	R(CH) A	Ref.
C_2H_2	1.207	1.060	5
C_2H_4	1.353	1.071	5
C_2H_6	1.543	1.102	4
CH_4	...	1.093	4, 5
CH	...	1.1305[a]	6
Diamond	1.5445	...	7

[a] Mean value of lowest vibrational state.

When Eqs. (1)–(7) are applied to acetylene, ethylene, ethane, methane, and the diamond, there result eleven equations if $L(\mathrm{C})=169.75$ kcal,

$$B(\mathrm{CC},\mathrm{diam})=a+1.5445\cdot b+2.3855\cdot c$$
$$=84.875 \qquad (8)$$

$$B(\mathrm{CC},\mathrm{C_2H_6})=a+1.5430\cdot b+2.3808\cdot c \qquad (9)$$

$$B(\mathrm{CC},\mathrm{C_2H_4})=a+1.3530\cdot b+1.8307\cdot c \qquad (10)$$

$$B(\mathrm{CC},\mathrm{C_2H_2})=a+1.2070\cdot b+1.4568\cdot c \qquad (11)$$

$$B(\mathrm{CH},\mathrm{CH_4})=A+1.093\cdot B$$
$$=98.054 \qquad (12)$$

$$B(\mathrm{CH},\mathrm{C_2H_6})=A+1.1020\cdot B \qquad (13)$$

$$B(\mathrm{CH},\mathrm{C_2H_4})=A+1.0710\cdot B \qquad (14)$$

$$B(\mathrm{CH},\mathrm{C_2H_2})=A+1.0600\cdot B \qquad (15)$$

$$B(\mathrm{CC},\mathrm{C_2H_6})+6B(\mathrm{CH},\mathrm{C_2H_6})=665.734 \qquad (16)$$

$$B(\mathrm{CC},\mathrm{C_2H_4})+4B(\mathrm{CH},\mathrm{C_2H_4})=531.456 \qquad (17)$$

$$B(\mathrm{CC},\mathrm{C_2H_2})+2B(\mathrm{CH},\mathrm{C_2H_2})=388.410. \qquad (18)$$

Hence, the five constants A, B, a, b, c and the six bond

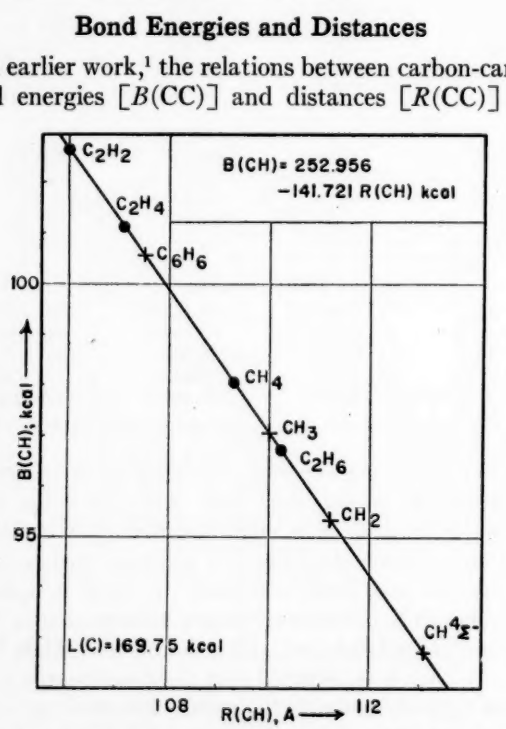

FIG. 2. Relation between carbon-hydrogen bond energies and distances [Eq. (20)].

energies $B(CC, C_2H_6)$, $B(CC, C_2H_4)$, $B(CC, C_2H_2)$, $B(CH, C_2H_6)$, $B(CH, C_2H_4)$, and $B(CH, C_2H_2)$ can be determined.

In earlier investigations as for example by Pauling,[9] it was recognized that carbon-carbon single bonds had a different bond energy from carbon-carbon double bonds and that carbon-carbon triple bonds had a still higher bond energy. However, the bond energies of all carbon hydrogen bonds were taken to be equal. Skinner[10] realized that this assumption was not valid, and he proposed a linear relationship between $B(CH)$ and $R(CH)$. The connection between $B(CC)$ and $R(CC)$ was at that time dealt with graphically. The present attempt to express the dependence of $B(CC)$ on $R(CC)$ in parabolic form is, of course, arbitrary. It gives a relation which yields values of bond energies which differ little from the ones obtained by graphic methods in earlier studies,[1] where it also can be seen that the relation $B(CH):R(CH)$ differed very little from a straight line. The latter assumption is certainly the simplest one to make. At present, it must be made because the number of internuclear distances known accurately at the present time is just sufficient to determine the five constants for a $B(CC):R(CC)$ parbola, and a $B(CH):R(CH)$ straight line *and* six bond energies as indicated in the eleven equations mentioned above.

The solution of these eleven equations leads to Eqs. (19) and (20) if $L(C)=169.75$ kcal. It should be noted that these relations do not tell anything about the nature of the chemical bond, i.e., whether a bond is a single, double, or triple bond. These numerical statements are purely empirical relations. In this sense, single bonds go over to double and triple bonds in continuous fashion. These equations are

$$B(CC)=1450.762-1644.151\cdot R(CC)+491.936\cdot R(CC)^2 \quad (19)$$

and

$$B(CH)=252.956-141.721\cdot R(CH), \quad (20)$$

which together with Eq. 23 yield

$$B(CH)=98.104-0.075\cdot B(CC)+[3.196\cdot B(CC)-246.048]^{\frac{1}{2}}, \quad (21)$$

based on $L(C)=169.75$ kcal. It is claimed that these relations will give estimates of the bond energies of all carbon-carbon and carbon-hydrogen bonds if their distances are known (Tables I and II and Figs. 1, 2, and 3).

Internuclear Distances

The interatomic distances collected in Table III are now known with sufficient accuracy so that they may be used to give a reliable relation between $R(CC)$ and $R(CH)$. It is supposed that $R(CH)$ can be expressed as a parabolic function of $R(CC)$,

$$R(CH)=\alpha+\beta\cdot R(CC)+\gamma\cdot R(CC)^2. \quad (22)$$

Using the molecules acetylene, ethylene, and ethane, it is found that

$$R(CH)=1.396-0.594\cdot R(CC)+0.261\cdot R(CC)^2, \quad (23)$$

and it is claimed that this relation holds generally (Table III, Fig. 4) for carbon-hydrogen distances referred to carbon-hydrogen bonds of a carbon atom to which are attached other identical carbon-hydrogen bonds only.

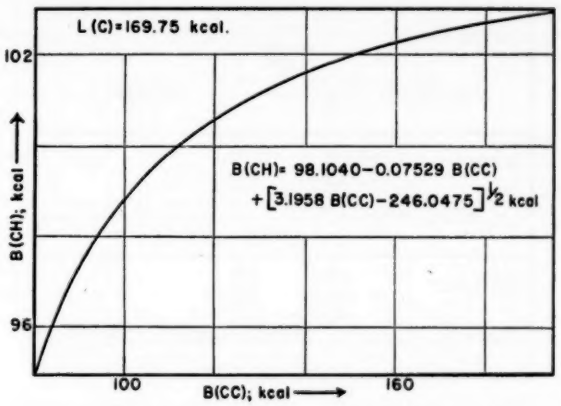

FIG. 3. Relation between carbon-hydrogen and carbon-carbon bond energies [Eq. (21)].

Bond Distribution

Several examples will illustrate how these equations can be used to find a distribution of the atomic heat of

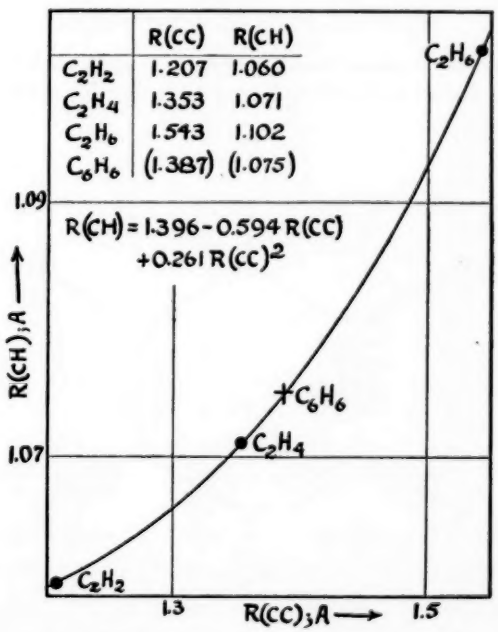

FIG. 4. Relation between carbon-hydrogen and carbon-carbon distances [Eq. (23)].

[9] L. Pauling, *The Nature of the Chemical Bond* (Cornell University Press, Ithaca, 1940).
[10] H. A. Skinner, Trans. Faraday Soc. **41**, 645 (1945).

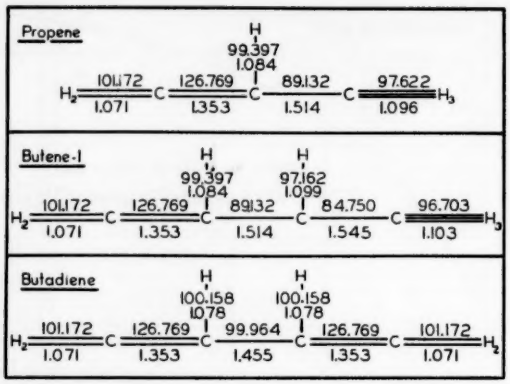

FIG. 5. Bond distribution in propene, butene-1, and butadiene.

formation over the various bonds of a molecule. Double and triple bonds are expected to transfer from the smaller molecules. All olefins are assumed to have ethylene-like double bonds, and the treatment of carbon-hydrogen bond energies has been mentioned in the introduction.

Since Qf_0^0(propene) $= -8.468$ kcal, Qa_0^0(propene) $= 810.499$ kcal (L(C) $= 169.75$ kcal). Labeling double and single bonds in propene I and II, respectively, and assuming that

$$B(\mathrm{C{=}C},\ \mathrm{C_3H_6}) = B(\mathrm{C{=}C},\ \mathrm{C_2H_4})$$

and

$$B(\mathrm{CH},\ \mathrm{I};\ \mathrm{C_3H_6}) = B(\mathrm{CH},\ \mathrm{C_2H_4}),$$

it was found that a good match of Qa_0^0(propene) could be made with

$$B(\mathrm{CC}II,\ \text{propene}) = 89.132 \text{ kcal},$$
$$B(\mathrm{CH}II,\ \text{propene}) = 97.622 \text{ kcal},$$
$$B(\mathrm{CH}\,I\,II,\ \text{propene}) = 99.397 \text{ kcal}.$$

The carbon-carbon bond energy (II) was varied until it was found to be 89.132 kcal, by using Eq. (19) with various assumed R(CCII, propene). R(CHII, propene) was calculated from Eq. (23), and B(CHII, propene) was obtained from Eq. (20). It is assumed that B(CHI II, propene) is the average of B(CH, C_2H_4) and B(CHII, propene). The summation of these bond energies is 810.508 kcal compared with 810.499 kcal (Fig. 5).

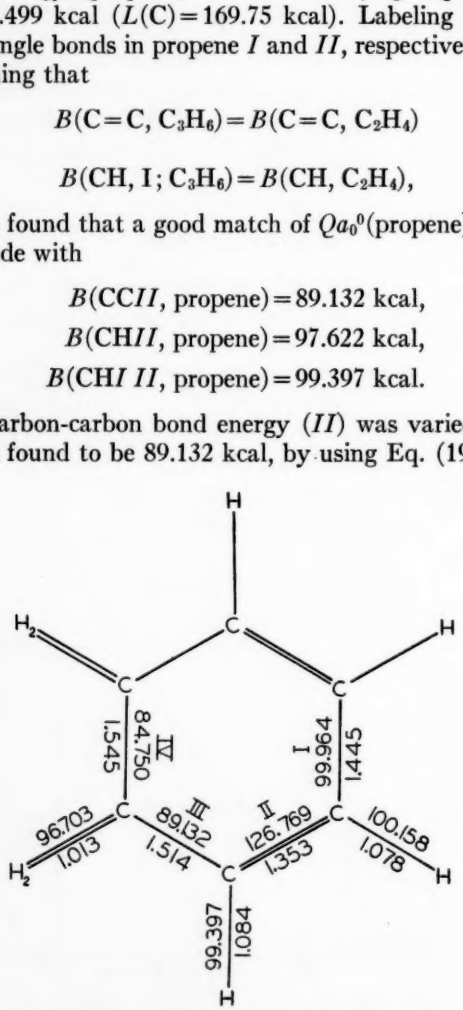

FIG. 6. Bond distribution in 1,3-cyclohexadiene.

The carbon-carbon double bond in butene-1 is labeled (I) and the successive single bonds (II and III), respectively. Carbon-carbon bonds I and II are transferred from propene as well as carbon-hydrogen bonds I and I II. The bonds CCIII, CHII III, and CHIII are adjusted so as to obtain a match with Qa_0^0(butene) $= 1086.793$ kcal [L(C) $= 169.75$ kcal]. The sum of the bond energies given in Fig. 5 is 1086.825 kcal.

The budadiene molecule is dealt with in similar fashion, and the bond structure given in Fig. 5 results.

TABLE IV. Butadiene. Bond energies and bond lengths.

	R A	B kcal	B kcal
	L(C) = 169.75 kcal		
$2B$(C=C, C_2H_4)	1.353	2×126.769	253.538
$4B$(CH, C_2H_4)	1.071	4×101.172	404.688
$1B$(CC, center)	1.455	1× 99.964	99.964
$2B$(CH, center)	1.078	2×100.158	200.317
	Qa_0^0 (actual) = 958.513;[a] Qa_0^0 (calc) = 958.507		
	L(C) = 135.8 kcal		
$2B$(C=C, C_2H_4)	1.353	2× 92.98	185.96
$4B$(CH, C_2H_4)	1.071	4× 92.63	370.52
$1B$(CC, center)	1.4125	1× 82.00	82.00
$2B$(CH, center)	1.075	2× 92.07	184.15
	Qa_0^0 (actual) = 822.72;[a] Qa_0^0 (calc) = 822.63		
	L(C) = 124.3 kcal		
$2B$(C=C, C_2H_4)	1.353	2× 81.56	163.12
$4B$(CH, C_2H_4)	1.071	4× 89.75	359.00
$1B$(CC, center)	1.389	1× 75.80	75.80
$2B$(CH, center)	1.073	2× 89.47	178.94
	Qa_0^0 (actual) = 776.71;[a] Qa_0^0 (calc) = 776.86		

[a] $Qf_0^0(\mathrm{C_4H_6}) = -30.2$ kcal; Aston, Szasz, Wooley, and Brickwedde, J. Chem. Phys. **14**, 67 (1946).

It is seen that the central carbon-carbon bond energy is larger than in ethane.

1,3-cyclohexadiene is an interesting case. Its bond structure can be built up from butadiene and butene-1 as seen in Fig. 6. [Qa_0^0(actual) = 1402.503 and Qa_0^0(matched) = 1402.438 kcal.]

These estimates of bond energies give a more detailed picture of these molecules and the bond distances cannot be obtained by any other method.

Butadiene

In butadiene there exist two carbon-carbon double bonds (positions 1 and 3) and a so-called carbon-carbon single bond in the center of the molecule. These respective bonds have their hydrogen atoms attached to them

with different bond energies. The heat of atomization of butadiene can be calculated from $Qf_0^0(=-30.2$ kcal)[11] and is 958.513 kcal. If it is assumed that the two carbon-carbon double bonds and their four attendant carbon-hydrogen bonds are as in ethylene, then the corresponding bond energies may be subtracted from the total heat of atomization. The remainder can now be divided between one carbon-carbon bond and two carbon-hydrogen bonds. A set of trial calculations using Eqs. (19) and (20) yields R(CC, center) = 1.455A. The fact that the carbon-hydrogen bond is attached to a carbon atom from which originate a carbon-carbon single bond *and* a carbon-carbon double bond was taken into account.

This value of the distance of the central carbon-carbon bond checks the finding of Schomaker and Pauling[12] by electron diffraction (1.46A). The details are shown in the Table IV. In other words a Qa value can be found so as to match the distance of the middle carbon-carbon bond as found by electron diffraction.

Benzene

The heat of atomization of benzene, Qa is 1304.213 kcal, based on L(C) = 169.75 kcal. One-sixth of this amount must be the sum of the bond energies of one carbon-carbon and one carbon-hydrogen bond. A few trial calculations starting with R(CC) = 1.39A indicate that B(CC, C_6H_6) = 116.780 kcal at 1.387A and B(CH, C_6H_6) = 100.598 kcal at 1.075A. The carbon-carbon distance checks the value 1.39A obtained from electron diffraction.[9] The same value is also found in many benzene derivatives. However, the carbon-hydrogen distance has not been determined, and the value just mentioned may serve as an estimate. Its magnitude is reasonable, when compared with R(CH, C_2H_4) = 1.071 and R(CH, C_2H_6) = 1.102A. It is nearer to the former as R(CC, C_6H_6) = 1.387 is closer to R(CC, C_2H_4) = 1.353 than to R(CC, C_2H_6) = 1.543A (Table V). Again, a match of the carbon-carbon distance 1.39 has been found from the B(CC):R(CC) curve.

Methane and Its Radicals

The dissociation energy of methane into a methyl group and one hydrogen atom [$D(CH_3-H)$] is known to be very close to 101 kcal.[13,14] The dissociation energy of ethylene into two methylene radicals [$D(CH_2-CH_2)$] is about 150 kcal.[15,16] The bond energy of the methine radical calculated from Eq. (20) is 92.739 kcal. This value is larger than the commonly accepted figure of 80 kcal.[6] It is of interest in this connection to note that Shida[17] finds by a wave-mechanical calculation that D(CH) ≐ 88 kcal and that very likely a low-lying $^4\Sigma^-$-state exists below the ^2II state. The latter is commonly accepted as the ground state. Gaydon[18] also has mentioned this possibility. The result of these considerations leads to the bond energies and bond dissociation energies of methane and its radicals as shown in Table VI.

TABLE V. Benzene. Bond energies and bond lengths.

	R A	B kcal	B kcal
	L(C) = 169.75 kcal		
$6B$(C≐C, C_6H_6)	1.387	6×116.780	700.680
$6B$(CH, C_6H_6)	1.075	6×100.598	603.588
	Qa_0^0 (actual) = 1304.213;[a] Qa_0^0 (calc) = 1304.268		
	L(C) = 135.8 kcal		
$6B$(C≐C, C_6H_6)	1.363	6× 90.97	545.82
$6B$(CH, C_6H_6)	1.072	6× 92.49	554.94
	Qa_0^0 (actual) = 1100.52;[a] Qa_0^0 (calc) = 1100.76		
	L(C) = 124.3 kcal		
$6B$(C≐C, C_6H_6)	1.35	6× 82.12	492.72
$6B$(CH, C_6H_6)	1.071	6× 89.80	538.80
	Qa_0^0 (actual) = 1031.513;[a] Qa_0^0 (calc) = 1031.52		

[a] $Qf_0^0(C_6H_6) = -24.0$ kcal; reference 8.

L(C) = 135.8 kcal

Since the controversy concerning the correct value of the heat of sublimation of carbon has not yet been

TABLE VI. Methane and its radicals.

	R(CH) A	B(CH) kcal	Qa_0^0 kcal	D(R−H) kcal
	L(C) = 169.75 kcal			
CH_4	1.093	98.054	392.216	101.5
CH_3	1.101	96.905	290.716	100.0
CH_2	1.112	95.364	190.728	98.0
CH	1.1305	92.739	92.739	92.7
	L(C) = 135.8 kcal			
CH_4	1.093	89.568	358.270	101.5
CH_3	1.122	85.590	256.770	100.0
CH_2	1.173	78.395	156.790	72.4
CH	1.1305	84.350	84.350	84.4
	L(C) = 124.3 kcal			
CH_4	1.093	86.691	346.764	101.5
CH_3	1.129	81.755	245.264	100.0
CH_2	1.194	72.639	145.278	63.8
CH	1.1305	81.478	81.478	81.5
L(C)		169.75	135.8	124.3
$C_2H_4 \rightarrow 2C+4H$		−531.456	−463.580	−440.556
$2CH_2 \rightarrow C_2H_4$		150	150	150.
$CH_2 \rightarrow C+2H$		−190.728	−156.790	−145.278

[11] Aston, Szasz, Woolley, and Brickwedde, J. Chem. Phys. **14**, 67 (1946).
[12] V. Schomaker and L. Pauling, J. Am. Chem. Soc. **61**, 1769 (1939).
[13] H. C. Andersen and G. B. Kistiakowsky, J. Chem. Phys. **11**, 6 (1943).
[14] G. B. Kistiakowsky and E. R. Van Artsdalen, J. Chem. Phys. **12**, 469 (1944).
[15] M. Szwarc, Chem. Rev. **47**, 75 (1950).
[16] W. C. Price, Phys. Rev. **45**, 843 (1934); **47**, 444 (1935).
[17] S. Shida, Tokyo Institute of Technology, Tokyo, Japan (private communication).
[18] A. G. Gaydon, Disc. Faraday Soc., No. 10, 108 (1951) and private communication.

resolved,[19] it is necessary to study the same above-mentioned algebraic relations for different values of $L(C)$. Again, eleven equations similar to Eqs. (8) to (18) were derived, yielding

$$B(CC) = 1118.427 - 1307.101 \cdot R(CC) + 405.910 \cdot R(CC)^2 \quad (24)$$

and

$$B(CH) = 241.658 - 139.147 \cdot R(CH). \quad (25)$$

The pertinent data are given in Tables I–III. It is seen that, in the case of benzene, $R(CC, C_6H_6) = 1.363$A. This value does not check electron diffraction results as well as the one based on $L(C) = 169.75$ kcal. The carbon hydrogen distance in benzene is also very close to the one in ethylene, whereas a somewhat greater difference would be expected. In the methylene radical, it is found that the carbon-hydrogen distance is even larger than in the methine radical (1.173 as compared to 1.1305A) and the bond energy is correspondingly less (78.40 and 84.35 kcal). On the supposition that a simple trend might be expected from methane molecule to methine radical, based on the internuclear distances (1.093 and 1.1305A), this finding is unexpected. However, it may be that the change in carbon hybridization leads to such behavior. The heat of dissociation of the methine radical (84.35 kcal) does lie close to the usually accepted value of 80 kcal.[6] On the other hand, $R(CC,$ center) of butadiene is calculated to be 1.413A (Table IV) which does not fit electron diffraction results.[12] The weight of this indirect evidence seems to be in the direction of making the value 135.8 for $L(C)$ less likely than the larger one of 169.75 kcal.

$L(C) = 124.3$ kcal

This value of the heat of sublimation of carbon was used by Pauling,[9] and it is of interest to study this case by the methods outlined above. The eleven Eqs. (8)–(18) yield

$$B(CC) = 1007.354 - 1194.878 \cdot R(CC) + 377.402 \cdot R(CC)^2 \quad (26)$$

and

$$B(CH) = 238.628 - 139.009 \cdot R(CH). \quad (27)$$

The pertinent data are given in Tables I–III. $R(CC, C_6H_6) = 1.35$A as in ethylene and not at all close to the electron diffraction value (1.39A). The carbon-hydrogen distance also is calculated to be the same as in ethylene which is not satisfactory. In the methylene radical, the carbon-hydrogen distance is larger than in the methine radical and the bond energy is less (Table VI). The carbon-carbon distance in the central bond in butadiene is calculated to be 1.389A and hence quite different from the expected value (1.46A) (Table IV). Again, it appears that $L(C) = 124.3$ kcal is less likely than 169.75 kcal.

[19] G. Glockler, Ann. Rev. Phys. Chem. 3, 151 (1952).

Conclusion

The equations derived above are based on the assumption that bond energies are related to bond distances in the manner that force constants depend on these same distances. In general, large force constants go with small interatomic distances. Therefore, curves representing the relations between bond energies and bond distances have a negative slope and are concave upward. At least, they are never expected to be concave downward. In the case of carbon-hydrogen bonds, the bond distance curve is taken to be a straight line, because earlier graphical studies have shown that the concave upward curvature is very small in any event. Furthermore, the two types of curves $B(CC):R(CC)$ and $B(CH):R(CH)$ are connected, and it is not possible to change one of them without affecting the other. For example, the bond energy of the carbon-carbon bond in acetylene cannot be greater than the respective values given in Table I, because, if they were, the carbon-hydrogen bond energies would be smaller than the straight-line values given, and this result would mean that the curve representing carbon-hydrogen bonds would be concave downward. This situation would not be expected on the assumption of similarity of behavior of force constants and bond energies with internuclear distances.

The equations derived above are useful for estimating the bond energies of any carbon-carbon or carbon-hydrogen bond. The procedure is to determine the heat of atomization (Qa_0^0) for the hydrocarbon molecule to be studied from its heat of formation and the heat of sublimation of carbon and the heat of dissociation of hydrogen. The proper number of carbon-carbon bond energies and carbon-hydrogen bond energies are added until their sum equals the heat of atomization.

Resonance Energies of Benzene and Butadiene

GEORGE GLOCKLER*
Department of Chemistry, Duke University, Durham, North Carolina
(Received January 29, 1953)

The resonance energy of benzene based on an ethane-ethylene-like Kekulé structure is 74.86 kcal. The similar quantity for butadiene is 17.28 kcal. These quantities are independent of the value of the heat of sublimation of carbon. They are obtained from the heats of atomization of the appropriate molecules or from the heats of hydrogenation of the pertinent related compounds. Both methods yield the same results if properly applied.

BENZENE: EARLY VALUE

THE resonance energy of benzene referred to a Kekulé structure has been quoted for years at 39 kcal.[1] This early calculation was made by Pauling and was based on the heat of combustion of 789.2 kcal. Using this value, the heat of formation of CO_2 (94.45 kcal) and the heat of formation of water (68.37 kcal) given by Bichowsky and Rossini[2] it is found that the ordinary heat of formation of gaseous benzene (Qf_0^0) is -17.4 kcal. If it is assumed that the heat of sublimation of carbon $L(C)$ is 124.3 kcal and the heat of dissociation of hydrogen ($D(H_2)$) is 103.4 kcal, then the actual heat of atomization of benzene (Qa_0^0, actual) is 1039 kcal. Pauling calculated the heat of atomization of a corresponding Kekulé-like reference structure by using the following bond energies: the carbon-carbon single bond energy is $B(C-C)=58.6$ kcal, the carbon-carbon double bond energy is $B(C=C)=100$ kcal, and the carbon-hydrogen bond energy is $B(CH, CH_4)=87.3$ kcal. It was assumed that all carbon-hydrogen bonds have the same bond energies. The result is $Qa_0^0(\text{Kekulé})=1000$ kcal, whence the resonance energy of benzene is: $Qa_0^0(\text{actual})-Qa_0^0(\text{Kekulé})=39$ kcal.

Another calculation based on the idea that three times the heat of hydrogenation of cyclohexene to cyclohexane minus the heat of hydrogenation of benzene to cyclohexane equals the resonance energy of benzene will be discussed here.

BENZENE: $L(C)=124.3$ KCAL BASIS

Using ordinary heats of formation given by Bichowsky and Rossini[2] with the $L(C)$ and $D(H_2)$ values mentioned above, it is found that $Qa_0^0(CH_4)=349.3$ kcal which leads to $B(CH, CH_4)=87.3$ kcal is used by Pauling. Similarly $Qa_0^0(C_2H_6)=579.8$, $Qa_0^0(C_2H_4)=444.4$ and $Qa_0^0(C_2H_2)=298.1$ kcal. This information leads to the following carbon-carbon bond energies if it is assumed that $B(CH)=87.3$ kcal for all molecules:

$$\begin{aligned} B(CC, C_2H_6)&=579.8-6\times87.3=\ 56.0 \text{ kcal},\\ B(CC, C_2H_4)&=444.4-4\times87.3=\ 95.2 \text{ kcal},\\ B(CC, C_2H_2)&=298.1-2\times87.3=123.5 \text{ kcal},\\ B(CH, \text{general})&=87.3 \text{ kcal}. \end{aligned} \quad (1)$$

These bond energy values differ from the ones used by Pauling: 58.6, 100, and 123 kcal, respectively. They give 977 kcal for the heat of atomization of the Kekulé reference structure: $Qa_0^0(\text{Kekulé})=3\times56+3\times95.2+6\times87.3=977$ kcal. The resonance energy of benzene based on this reference structure is therefore: $Qa_0^0(\text{actual})-Qa_0^0(\text{Kekulé})=1039-977=62$ kcal and not 39 kcal. It is seen that the set of bond energies used by Pauling is not consistent with the basic notion that the summation of the bond energies in a given molecule must equal its heat of atomization. The consistent set of bond energies [Eq. (1)] leads to a much higher value of the resonance energy of benzene. Pauling used the following set of internuclear distances:

$$\begin{aligned} R(CH, CH_4)&=1.09\text{A},\\ R(CC, C_2H_6)&=1.542\text{A},\\ R(CC, C_2H_4)&=1.33\text{A},\\ R(CC, C_2H_2)&=1.204\text{A}. \end{aligned}$$

It may now be assumed that a relation between carbon-carbon bond energies and the corresponding set of internuclear distances exists and that the equation $B(CC)=fR(CC)$ is a parabola. However $B(CH)=\text{const}=87.3$ kcal is still accepted. Then

$$B(CC)=a+b\cdot R(CC)+c\cdot R(CC)^2, \quad (2)$$

or for the specific cases of the diamond, ethane, ethylene, and acetylene [using Eq. (1)]

$$\begin{aligned} B(C-C, \text{diam})&=a+1.545b+2.387c=\ 62.15,\\ B(C-C, C_2H_6)&=a+1.542b+2.378c=\ 56.0,\\ B(C=C, C_2H_4)&=a+1.330b+1.769c=\ 95.2,\\ B(C\equiv C, C_2H_2)&=a+1.204b+1.450c=123.5. \end{aligned} \quad (3)$$

From the last three equations it is found that

$$B(CC)=581.953-522.137\cdot R(CC)+117.412R(CC)^2. \quad (4)$$

* Visiting Lecturer; on leave of absence from the State University of Iowa.

[1] L. Pauling, *The Nature of the Chemical Bond* (Cornell University Press, Ithaca, 1940).

[2] F. R. Bichowsky and F. D. Rossini, *The Thermochemistry of the Chemical Substances* (Reinhold Publishing Corporation, New York, 1936).

TABLE I. Resonance energy of benzene.[a]

$L(C) = 124.3$ kcal	
$3B(CC, C_2H_6) = 3\times 62.194 =$	186.582
$3B(CC, C_2H_4) = 3\times 81.599 =$	244.677
$3B(CH, C_2H_6) = 3\times 85.440 =$	256.320
$3B(CH, C_2H_4) = 3\times 89.749 =$	269.247
Qa_0^0 (actual) = 1031.513; Qa_0^0 (Kekulé) =	956.826
Resonance energy = 74.69 kcal	
$L(C) = 135.8$ kcal	
$3B(CC, C_2H_6) = 3\times 67.98 =$	203.94
$3B(CC, C_2H_4) = 3\times 92.98 =$	278.94
$3B(CH, C_2H_6) = 3\times 88.32 =$	264.96
$3B(CH, C_2H_4) = 3\times 92.63 =$	277.89
Qa_0^0 (actual) = 1100.52; Qa_0^0 (Kekulé) =	1025.73
Resonance energy = 74.79 kcal	
$L(C) = 169.75$ kcal	
$3B(CC, C_2H_6) = 3\times 85.063 =$	255.189
$3B(CC, C_2H_4) = 3\times 126.769 =$	380.307
$3B(CH, C_2H_6) = 3\times 96.779 =$	290.337
$3B(CH, C_2H_4) = 3\times 101.172 =$	303.516
Qa_0^0 (actual) = 1304.213; Qa_0^0 (Kekulé) =	1229.349
Resonance energy = 74.86 kcal	

[a] Reference 3; (Tables I and II).

The bond energy of the diamond is known to be $L(C)/2 = 62.15$ kcal. However Eq. (4) yields 55.5 kcal, showing that the set of Eq. (3) is not consistent.

BENZENE: PRESENT VALUES

It has been shown earlier[3] that a consistent set of equations connecting bond energies and bond distances based on three values of the heat of sublimation of carbon can be derived ($L(C) = 124.3$, 135.8, and 169.75 kcal). This feature is accomplished by replacing the assumption $B(CH) = \text{const} = 87.3$ kcal by the straight-line relation $B(CH) = A + B \cdot R(CH)$, where A and B are constants.[3] The calculations of the resonance energy are shown in Table I. It must be independent of the heat of sublimation of carbon and the heat of dissociation of hydrogen, for

$$Qa_0^0(\text{actual}) = Qf_0^0(\text{actual}) + 6L(C) + 3D(H_2),$$

and

$$Qa_0^0(\text{Kekulé}) = Qf_0^0(\text{Kekulé}) + 6L(C) + 3D(H_2), \quad (5)$$

or

$$\text{res. energy} = Qa_0^0(\text{actual}) - Qa_0^0(\text{Kekulé}) = Qf_0^0(\text{actual}) - Qf_0^0(\text{Kekulé}),$$

where Qf_0^0(Kekulé) is the ordinary heat of formation of the Kekulé reference structure from the elements in their usual standard states

$$6C_s + 3H_2 \rightarrow C_6H_6(\text{Kekulé}); \quad Qf_0^0(\text{Kekulé}) = -98.8 \text{ kcal}. \quad (6)$$

[3] G. Glockler, J. Chem. Phys. **21**, 1242 (1953).

BENZENE: RESONANCE ENERGY

The resonance energy of benzene (74.86 kcal) is called the thermochemical resonance energy by Mulliken and Parr[4] because it is calculated from thermochemical data. The value just cited is referred to an ethylene-ethane basis. Ethylene-ethane-like bonds were chosen because the early calculations were made in this way. The value will of course be different if another molecule is used as the standard. For example, propene might be a better reference substance because it could be argued that benzene resonance should only refer to the extra stability of the six mobile π electrons. They give benzene its aromatic character. The propene molecule may be expected to be nearer to benzene in bond structure as far as bond energy changes attributable to hyperconjugation and similar effects are concerned. Hence these features would be excluded and a benzene resonance energy based on propene would more nearly represent π-electron resonance. The same consideration would lead to butadiene as a possible reference molecule and perhaps to 1,3-cyclohexadiene.

The atomic heat of formation of propene is 810.499 kcal ($L(C) = 169.75$ kcal). If the double bond and the two attendant carbon-hydrogen bonds are as in ethylene, then this value can be matched with the following bond energies by a set of trial calculations:[3]

Propene

$$\begin{aligned} 1B(C{=}C, C_2H_4) &= 1\times 126.769 = 126.769 \text{ kcal},\\ 1B(C{-}C, \text{single}) &= 1\times 89.132 = 89.132 \text{ kcal},\\ 2B(CH, C_2H_4) &= 2\times 101.172 = 202.344 \text{ kcal}, \quad (7)\\ 1B(CH, \text{center}) &= 1\times 99.397 = 99.397 \text{ kcal},\\ 3B(CH, \text{end}) &= 3\times 97.622 = 292.866 \text{ kcal},\\ Qa_0^0(\text{actual}) &= 810.499;\ Qa_0^0(\text{calc}) = 810.508 \text{ kcal}. \end{aligned}$$

If these bond energies are now applied appropriately to benzene, the atomic heat of formation of the propene-like reference structure can be calculated,

Benzene Reference Structure

$$\begin{aligned} 3B(C{=}C, C_2H_4) &= 3\times 126.769 = 380.307 \text{ kcal},\\ 3B(C{-}C, \text{propene}) &= 3\times 89.132 = 267.396 \text{ kcal}, \quad (8)\\ 6B(CH, \text{center}) &= 6\times 99.397 = 596.382 \text{ kcal},\\ Qa_0^0(\text{actual}) &= 1304.213;\ Qa_0^0(\text{calc}) = 1244.085 \text{ kcal}, \end{aligned}$$

and the resonance energy of benzene is 60.128 kcal on a propene basis which is 14.73 kcal less than the value calculated on the Kekulé basis.

In similar fashion a resonance energy for benzene can be obtained on a butadiene standard. The latter molecule has an atomic heat of formation of 958.514 kcal. [$L(C) = 169.75$ kcal].[3] This value can be matched by the following set of bond energies:

[4] R. S. Mulliken and R. G. Parr, J. Chem. Phys. **19**, 1271 (1951).

Butadiene

$$\begin{aligned} 2B(\text{C=C, } C_2H_4) &= 2\times 126.769 = 253.538 \text{ kcal},\\ 1B(\text{C–C, center}) &= 1\times\ 99.964 = \ 99.964 \text{ kcal},\\ 4B(\text{CH, } C_2H_4) &= 4\times 101.172 = 404.688 \text{ kcal},\\ 2B(\text{CH, center}) &= 2\times 100.158 = 200.316 \text{ kcal},\\ Qa_0^0(\text{actual}) &= 958.514;\ Qa_0^0(\text{calc}) = 958.506 \text{ kcal}. \end{aligned} \quad (9)$$

When these bond energies are applied to the case of benzene, the following result is obtained:

Benzene Reference Structure

$$\begin{aligned} 3B(\text{C=C, } C_2H_4) &= 3\times 126.769 = 380.307 \text{ kcal},\\ 3B(\text{C–C, butadiene}) &= 3\times\ 99.964 = 299.892 \text{ kcal},\\ 6B(\text{CH, butadiene}) &= 6\times 100.158 = 600.948 \text{ kcal},\\ Qa_0^0(\text{actual}) &= 1304.213;\ Qa_0^0(\text{calc}) = 1281.147 \text{ kcal}. \end{aligned} \quad (10)$$

Hence the resonance energy of benzene on a butadiene basis is 23.066 kcal. When the same type of calculation is referred to 1,3-cyclohexadiene it is found that the resonance energy of benzene so calculated has the same value as on the butadiene standard. The reason for this finding lies in the fact that the atomic heat of formation of 1,3-cyclohexadiene ($Qa_0^0(C_6H_8) = 1402.503$ kcal) can be matched by bonds transferred from butene-1 and butadiene. The atomic heat of formation of butene-1 ($Qa_0^0(C_4H_8) = 1086.769$ kcal) can be matched as shown below [Eq. (11)]. It is convenient to label the double bond (*I*), the next single bond (*II*), and the third single bond (*III*), and the resonance energy of benzene can be calculated on a butene-1 base,

Butene-1

$$\begin{aligned} B(\text{C=C, } I) &= 1\times 126.769 = 126.769 \text{ kcal},\\ B(\text{C–C, } II) &= 1\times\ 89.132 = \ 89.132 \text{ kcal},\\ B(\text{C–C, } III) &= 1\times\ 84.750 = \ 84.750 \text{ kcal},\\ 2B(\text{CH, } I) &= 2\times 101.172 = 202.344 \text{ kcal},\\ B(\text{CH, } I\ II) &= 1\times\ 99.397 = \ 99.397 \text{ kcal},\\ 2B(\text{CH, } II\ III) &= 2\times\ 97.162 = 194.324 \text{ kcal},\\ 2B(\text{CH, } III) &= 3\times\ 96.703 = 290.109 \text{ kcal},\\ Qa_0^0(\text{actual}) &= 1086.793;\ Qa_0^0(\text{calc}) = 1086.825 \text{ kcal}. \end{aligned} \quad (11)$$

The benzene reference structure based on the butene-1 molecule becomes

Benzene Reference Structure

$$\begin{aligned} 3B(\text{C–C, } C_2H_4) &= 3\times 126.769 = 380.307 \text{ kcal},\\ 3B(\text{C–C, butene-1}) &= 3\times\ 89.132 = 267.396 \text{ kcal},\\ 3B(\text{CH, } C_2H_4) &= 3\times 101.172 = 303.516 \text{ kcal},\\ 3B(\text{CH, butene-1}) &= 3\times\ 99.397 = 298.191 \text{ kcal},\\ Qa_0^0(\text{actual}) &= 1304.213;\ Qa_0^0(\text{calc}) = 1249.410 \text{ kcal}, \end{aligned} \quad (12)$$

and the resonance energy of benzene is 54.80 kcal on a butene-1 basis.

Depending on the reference structure imagined to be appropriate, the following values of the thermochemical resonance energy of benzene result:

Kekulé reference structure: 74.86 kcal,

propene reference structure: 60.13 kcal,

butene reference structure: 54.80 kcal,

butadiene reference structure: 23.07 kcal.

The question obviously arises which standard shall be chosen? It seems best to choose a common standard for hydrocarbons because of the arbitrariness that is involved if any other related structure is taken for reference. The ethane-ethylene base seems as good as any because these molecules are used in the determination of the basic equations. It is true that the whole set of influences such as change in hybridization, near atom effects, near bond effect, hyperconjugation, London forces, and all other interactions between atoms in a molecule will then be involved in the so-called resonance energy. This term seems to be a misnomer anyway because it violates (in the case of benzene glaringly) the fundamental rule of resonance that the nuclear framework should not change when going from the standard molecule to the molecule under consideration. It might be better to call the energy difference so calculated a "stabilization energy" and recognize the fact that molecules may be more or less stable in reference to some preconceived structure, which arbitrarily and naively has been picked as a point of reference. If the Kekulé base is used to derive the ordinary thermochemical resonance energy, the values so calculated can always be broken down into parts as more detailed knowledge of the above-mentioned interactions accumulates.

VERTICAL RESONANCE ENERGY OF BENZENE

The particular resonance energy just discussed is called the thermochemical resonance energy (Th.R.E.) by Mulliken and Parr[4] since it is derived from thermochemical data. In the case of benzene it refers to the process

$$C_6H_6(\text{Kekulé, 1.54, 1.35}) \rightarrow C_6H_6(\text{actual, 1.39});\quad \Delta E = -\text{Th.R.E.} \quad (13)$$

The interatomic distances change during this hypothetical reaction. This behavior is not in conformity with the rules of resonance[5] as Mulliken and Parr[4] point out. Hence they calculate a compression energy (C_K) which refers to the transition

$$C_6H_6(\text{Kekulé, 1.54, 1.35}) \rightarrow C_6H_6(\text{Kekulé, 1.39});\quad \Delta E = C_K, \quad (14)$$

[5] G. W. Wheland, *The Theory of Resonance.* (John Wiley and Sons, Inc., New York, 1944).

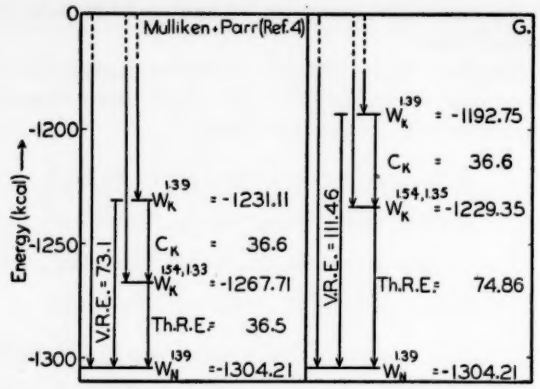

FIG. 1. Energy diagram for benzene, showing relation between resonance energies.

in order to bring the Kekulé molecule into a geometric configuration where the carbon-carbon distances are 1.39A long but still maintain their character as single and double bonds. The change from the Kekulé −1.39 structure to the real molecule releases the vertical resonance energy (V.R.E.),

$$C_6H_6(\text{Kekulé, 1.39}) \rightarrow C_6H_6(\text{actual, 1.39}); \qquad \Delta E = -\text{V.R.E.} \quad (15)$$

These processes are easiest seen on an energy diagram (Fig. 1) from which it is noted that

$$\text{V.R.E.} = C_K + \text{Th.R.E.} \quad (16)$$

Mulliken and Parr's values are: V.R.E. = 73.1, C_K = 36.6, and ThR.E. = 36.5 kcal. Using their value of the compression energy and the present value of Th.R.E. yields 111.5 kcal for the vertical resonance energy rather than 73.1 kcal.

BENZENE HYDROGENATION

Pauling[1] calculated the resonance energy of benzene from the hydrogenation energy of cyclohexene to cyclohexane and of benzene itself to the same end product. The difference of three times the first and the last is said to give the resonance energy of benzene. It has been shown[6] that the resonance energy of benzene is about 80 kcal. With the equations given earlier[3] it has been found that the value of 74.86 kcal is more accurate and that the hydrogenation energies conform to this value if properly considered.

From the work on hydrogenation of benzene, 1,3-cyclohexadiene and cyclohexene of Kistiakowsky *et al.*,[7] the following equations can be written (at 355°K):

$$\begin{aligned} C_6H_6 + H_2 &\rightarrow C_6H_8 - 5.595 \text{ kcal}, \\ C_6H_8 + H_2 &\rightarrow C_6H_{10} + 26.778 \text{ kcal}, \\ C_6H_{10} + H_2 &\rightarrow C_6H_{12} + 28.592 \text{ kcal}, \\ C_6H_6 + 3H_2 &\rightarrow C_6H_{12} + 49.775 \text{ kcal}. \end{aligned} \quad (17)$$

[6] G. Glockler, Disc. Faraday Soc. No. 10, 26 (1951).
[7] Kistiakowsky, Ruhoff, Smith, and Vaughan, J. Am. Chem. Soc. 58, 137 and 146 (1936).

The ordinary heat of formation of benzene and cyclohexane at 355°K were obtained by graphical interpolation[8] and found to be consistent with the hydrogenation energies just cited. The resulting equations refer to 355°K,

$$\begin{aligned} 6C_s + 3H_2 &\rightarrow C_6H_6 - 19.085 \text{ kcal}, \\ 6C_s + 4H_2 &\rightarrow C_6H_8 - 24.680 \text{ kcal}, \\ 6C_s + 5H_2 &\rightarrow C_6H_{10} + 2.098 \text{ kcal}, \\ 6C_s + 6H_2 &\rightarrow C_6H_{12} + 30.690 \text{ kcal}. \end{aligned} \quad (18)$$

The ordinary heats of formation of benzene and cyclohexane at 0°K are known to be −24.00 and 20.01 kcal, respectively.[8] In order to obtain the similar values for 1,3-cyclohexadiene and cyclohexene it was assumed that

$$Qf_0^0(0°\text{K}) = a + b \cdot Qf(355°\text{K}), \quad (19)$$

or

$$Qf_0^0(0°\text{K}) = -7.1254 + 0.8842 Qf(355°\text{K}),$$

yielding at 0°K

$$\begin{aligned} 6C_s + 3H_2 &\rightarrow C_6H_6 - 24.00 \text{ kcal}, \\ 6C_s + 4H_2 &\rightarrow C_6H_8 - 28.948 \text{ kcal}, \\ 6C_s + 5H_2 &\rightarrow C_6H_{10} - 5.270 \text{ kcal}, \\ 6C_s + 6H_2 &\rightarrow C_6H_{12} + 20.01 \text{ kcal}. \end{aligned} \quad (20)$$

The ordinary heats of hydrogenation (at 0°K) are obtained by subtraction,

$$\begin{aligned} C_6H_6 + H_2 &\rightarrow C_6H_8 - 4.948 \text{ kcal}, \\ C_6H_8 + H_2 &\rightarrow C_6H_{10} + 23.678 \text{ kcal}, \\ C_6H_{10} + H_2 &\rightarrow C_6H_{12} + 25.280 \text{ kcal}, \\ C_6H_6 + 3H_2 &\rightarrow C_6H_{12} + 44.010 \text{ kcal}. \end{aligned} \quad (21)$$

Using $L(\text{C}) = 169.75$ and $D(\text{H}_2) = 103.239$ kcal, the atomic heats of formation (at 0°K) are obtained from the ordinary ones,

$$\begin{aligned} 6C + 6H &\rightarrow C_6H_6 + 1304.213 \text{ kcal}, \\ 6C + 8H &\rightarrow C_6H_8 + 1402.503 \text{ kcal}, \\ 6C + 10H &\rightarrow C_6H_{10} + 1529.419 \text{ kcal}, \\ 6C + 12H &\rightarrow C_6H_{12} + 1657.937 \text{ kcal}. \end{aligned} \quad (22)$$

Hence from the rule mentioned at the beginning of the paragraph, the resonance energy of benzene should be

$$\text{Th.R.E.} = 3 \times 25.28 - 44.01 = 31.83 \text{ kcal}, \quad (23)$$

to be compared with 35.97 kcal obtained by Pauling.[1] However in establishing this rule there has been made the implicit assumption that the molecules 1,3-cyclohexadiene, cyclohexene, and cyclohexane are ethane-ethylene-like in their bond energies. This assumption is shown to be invalid by calculating the atomic heats of formation for the four molecules C_6H_{2n} ($n = 3, 4, 5, 6$)

[8] *Selected Values of Properties of Hydrocarbons*, Circ. C461, Natl. Bur. Standards (U. S. Government Printing Office, Washington, 1947).

on a hypothetical Kekulé basis and showing that in all four cases, there exists a difference between the actual heat of atomization and the corresponding Kekulé reference structures. These differences are due to hyperconjugation, near atom effects, change in hybridization etc. (Table II). The rule yields zero resonance for the hypothetical Kekulé reference structures of benzene as can be seen by calculating the ordinary heats of formation of the three Kekulé reference structures from the Qa_0^0(Kekulé) values given in Table II,

$$\begin{aligned} &6C_s+3H_2\rightarrow C_6H_6\ (\text{Kekulé})-98.864\ \text{kcal},\\ &6C_s+4H_2\rightarrow C_6H_8\ (\text{Kekulé})-54.643\ \text{kcal},\\ &6C_s+5H_2\rightarrow C_6H_{10}(\text{Kekulé})-10.421\ \text{kcal},\\ &6C_s+6H_2\rightarrow C_6H_{12}(\text{Kekulé})+33.799\ \text{kcal}, \end{aligned} \tag{24}$$

subtracting these equations in pairs gives the heats of hydrogenation of the Kekulé reference structures,

$$\begin{aligned} &C_6H_6\ (\text{Kekulé})+H_2\rightarrow C_6H_8\ (\text{Kekulé})\ 44.22\ \text{kcal},\\ &C_6H_8\ (\text{Kekulé})+H_2\rightarrow C_6H_{10}(\text{Kekulé})\ 44.22\ \text{kcal},\\ &C_6H_{10}(\text{Kekulé})+H_2\rightarrow C_6H_{12}(\text{Kekulé})\ 44.22\ \text{kcal}. \end{aligned} \tag{25}$$

TABLE II. Atomic heats of formation of Kekulé reference structures of benzene and its reduction products.[a]

Type of bond	Number of bonds C_6H_6 (1)	C_6H_8 (2)	C_6H_{10} (3)	C_6H_{12} (4)
B(C−C, C_2H_6) = 85.063 kcal	3	4	5	6
B(C=C, C_2H_4) = 126.769 kcal	3	2	1	0
B(CH, C_2H_6) = 96.779 kcal	3	6	9	12
B(CH, C_2H_4) = 101.172 kcal	3	2	1	0
Qa_0^0 (actual)	1304.213	1402.503	1529.419	1657.937
Qa_0^0 (Kekulé)	1229.349	1376.808	1524.267	1671.726
Resonance energy, etc.	74.864	25.695	5.152	−13.789

[a] Reference 3; L(C) = 169.75 kcal; Temp. = 0°K.

In every step of hydrogenation of these Kekulé structures one B(C−C, C_2H_6) and three B(CH, C_2H_6) are gained and one B(C=C, C_2H_4) and one B(CH, C_2H_4) are lost (Table II). Since all bonds are assumed to be ethane-ethylene-like, it follows that the three heats of hydrogenation are the same. The difference between successive Qa_0^0(Kekulé) values is 147.459 kcal. Subtracting 103.239 kcal ($D(H_2)$) yields 44.22 kcal. Obviously three times the last step of hydrogenation equal the total hydrogenation of the hypothetical Kekulé benzene structure. This difference is however zero as is to be expected since all bonds are assumed to be as in ethane and/or ethylene.

If the atomic heats of formation of the four Kekulé molecules C_6H_6, C_6H_8, C_6H_{10}, and C_6H_{12} are designated Q_{0i} (i=1, 2, 3, 4) then the above result can be written

$$Q_{04}-Q_{03}=Q_{03}-Q_{02}=Q_{02}-Q_{01}=147.459\ \text{kcal}. \tag{26}$$

For the real molecules, the heats of atom formation are labelled Q_i and their resonance or hyperconjugation energies are designated by R.E.$_i$. Then

$$Q_i=Q_{0i}+\text{R.E.}_i. \tag{27}$$

Substituting this expression into the above equation and rearranging yields

$$3(Q_4-Q_3)-(Q_4-Q_1)=3(\text{R.E.}_4-\text{R.E.}_3)-(\text{R.E.}_4-\text{R.E.}_1). \tag{28}$$

Using the appropriate values from Table II yields 31.83 kcal for either side of this equation. It should be noted that the quantities on the left side of Eq. (28) refer to the hydrogenation of cyclohexene to cyclohexane and of benzene to the same end product by atomic hydrogen

$$\begin{aligned} &C_6H_{10}+2H\rightarrow C_6H_{12}+128.518\ \text{kcal},\\ &C_6H_6+6H\rightarrow C_6H_{12}+353.724\ \text{kcal}. \end{aligned} \tag{29}$$

A similar equation to Eq. (22) can be written for the set C_6H_6, C_6H_8, and C_6H_{10},

$$2(Q_3-Q_2)-(Q_3-Q_1)=2(\text{R.E.}_3-\text{R.E.}_2)-(\text{R.E.}_3-\text{R.E.}_1). \tag{30}$$

Again substituting the appropriate values from Table II yields 28.626 kcal for either side of the equation. From both equations it is seen that R.E.$_1$ cannot be obtained from them unless R.E.$_2$, R.E.$_3$, and R.E.$_4$ are known or are zero. Hence the hydrogenation energies can only yield the complex relation on the right side of Eqs. (28) and (30). It should be noted that Eqs. (26) to (30) can be used if only the Qa_0^0(actual) are known. Some of these latter quantities may be determined from hydrogenation experiments, as was actually done in the present case.

BUTADIENE RESONANCE ENERGY

The value based on a Kekulé base is shown in Table III and is independent of the heat of sublimation of

TABLE III. Resonance energy of butadiene.[a]

L(C) = 124.3 kcal	
$2B$(CC, C_2H_4)	= 2× 81.559 = 163.118
$5B$(CH, C_2H_4)	= 5× 89.749 = 448.745
$1B$(CC, C_2H_6)	= 1× 62.194 = 62.194
$1B$(CH, C_2H_6)	= 1× 85.440 = 85.440
Qa_0^0 (actual) = 776.713; Qa_0^0 (Kekulé) = 759.497	
Resonance energy = 17.22 kcal	
L(C) = 135.8 kcal	
$2B$(CC, C_2H_4)	= 2× 92.98 = 185.96
$5B$(CH, C_2H_4)	= 5× 92.63 = 463.15
$1B$ (CC, C_2H_6)	= 1× 67.98 = 67.98
$1B$(CH, C_2H_6)	= 1× 88.32 = 88.32
Qa_0^0 (actual) = 822.713; Qa_0^0 (Kekulé) = 805.41	
Resonance energy = 17.31 kcal	
L(C) = 169.75 kcal	
$2B$(CC, C_2H_4)	= 2×126.769 = 253.538
$5B$(CH, C_2H_4)	= 5×101.172 = 505.860
$1B$(CC, C_2H_6)	= 1× 85.063 = 85.063
$1B$(CH, C_2H_6)	= 1× 96.779 = 96.779
Qa_0^0 (actual) = 958.514; Qa_0^0 (Kekulé) = 941.240	
Resonance energy = 17.274 kcal	

[a] Reference 3; (Tables I and II).

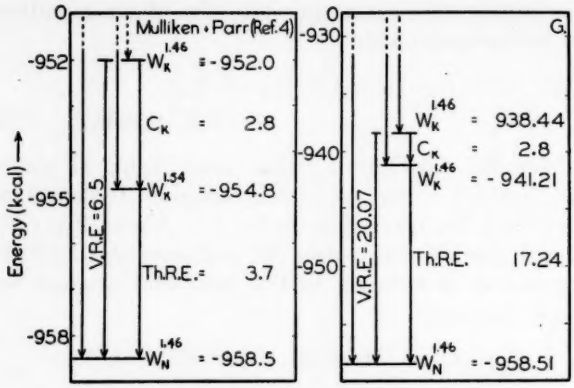

FIG. 2. Energy diagram for butadiene showing relation between resonance energies.

carbon. The thermochemical resonance energy of butadiene is 17.27 kcal. The calculations can be made on a butene-1 base because the atomic heat of formation $Qa_0^0(C_4H_8)$ can be determined to be 1086.793 kcal. The bond energy distribution has been found above [Eq. (11)] leading to a butene-1-like butadiene molecule,

Butadiene Reference Structure

$$\begin{aligned} 2B(\text{C=C, } C_2H_4) &= 2\times 126.769 = 253.538 \text{ kcal},\\ 1B(\text{C—C, center}) &= 1\times\ 89.132 = \ 89.132 \text{ kcal},\\ 4B(\text{CH, } C_2H_4) &= 4\times 101.172 = 404.688 \text{ kcal},\\ 2B(\text{CH, center}) &= 2\times\ 99.397 = 198.794 \text{ kcal},\\ Qa_0^0(\text{actual}) &= 958.514;\ Qa_0^0(\text{calc'd}) = 946.152 \text{ kcal}. \end{aligned} \tag{31}$$

This calculation yields a thermochemical resonance energy of butadiene of 8.36 kcal on a butene-1 base. The two values for the Th.R.E. are then

Kekulé reference structure: 17.27 kcal,

butene-1 reference structure: 8.36 kcal.

The first includes all possible interactions and the last should more nearly represent the stabilization of a conjugated system. In the case of benzene, the value 23.07 kcal indicates the effect of the six nonlocalized electrons. In both cases there may still be involved some hyperconjugation not present in the respective reference molecules. Hence 8.36 and 23.07 kcal are maximum values.

VERTICAL RESONANCE ENERGY OF BUTADIENE

Mulliken and Parr[4] calculated the vertical resonance energy (V.R.E.) to be 6.5 kcal and the compression energy (C_K) to be 2.8 kcal. Their difference is the Th.R.E. and amounts to 3.7 kcal. They mention an experimental value of Th.R.E. of 6.5 kcal. Wheland[5] gives 3.5 kcal for Th.R.E. based on hydrogenation energies. This latter method has been shown to be invalid for benzene. The present value of 17.27 kcal differs radically from the others. Accepting for the moment the compression energy calculated by Mulliken and Parr[4] as 2.8 kcal, then the V.R.E. becomes 20.07 kcal on the present basis [Eq. (16), Fig. 2].

BUTADIENE HYDROGENATION

The two steps of the hydrogenation of butadiene have been determined experimentally by Kistiakowsky *et al.*[7] at 355°K. These values can be obtained from the heats of formation at 0°K from *Selected Values*,[8]

$$C_4H_6 + H_2 \rightarrow C_4H_8 + 25.041 \text{ kcal},$$
$$C_4H_8 + H_2 \rightarrow C_4H_{10} + 28.489 \text{ kcal},$$
$$C_4H_6 + 2H_2 \rightarrow C_4H_{10} + 53.530 \text{ kcal}.$$

If it were true that twice the last step of this set minus the total heat of hydrogenation would give the resonance energy of butadiene, this value would be 3.45 kcal.[5]

TABLE IV. Atomic heat of formation of Kekulé reference structures of butadiene and its reduction products.[a]

Types of bonds	Number of bonds C_4H_6 (1)	C_4H_8 (2)	C_4H_{10} (3)
B(C=C, C_2H_4) = 126.769 kcal	2	1	0
B(CH, C_2H_4) = 101.172 kcal	5	2.5	0
B(C—C, C_2H_6) = 85.063 kcal	1	2	3
B(CH, C_2H_6) = 96.779 kcal	1	5.5	10
Qa_0^0 (actual)	958.514	1086.793	1218.521
Qa_0^0 (Kekulé)	941.240	1082.110	1222.979
Resonance energy, etc.	17.274	4.683	4.458

[a] Reference 3; L(C) = 169.75 kcal; Temp. = 0°K.

In Table IV are given the actual atomic heats of formation of butadiene, butene-1, and butane, as well as the atomic heats of formation of the corresponding Kekulé reference molecules. It is seen that the real molecules have larger atomic heats of formation than the hypothetical ethylene-ethane-like standards. Butene-1 is affected by some extra interaction, such as hyperconjugation when viewed from its imaginary Kekulé counterpart. The resonance energy of butadiene is 17.27 kcal on a Kekulé basis. If both sides of Eq. (30) are applied to the quantities given in Table IV, it is found that

$$2(Q_3 - Q_2) - (Q_3 - Q_1) = 3.45 \text{ kcal},$$

and

$$2(-4.458 - 4.683) - (4.458 - 17.27) = 3.45 \text{ kcal}.$$

The value 17.27 of the resonance energy of butadiene fits into this equation.

Scattering Factors for Certain Polydisperse Systems

MARTIN GOLDSTEIN
Gibbs Memorial Laboratory, Harvard University, Cambridge, Massachusetts
(Received March 4, 1953)

Scattering functions for systems of polydisperse rods are calculated. The reciprocal scattering functions are found to have a greater downward curvature the greater the polydispersity. It is shown that this increased curvature is a property of polydisperse systems under very broad conditions.

ZIMM[1] has shown that the scattering factor for a polydisperse system is given by

$$P_z(\theta)=\frac{\int nf(n)P(\theta)dn}{\int nf(n)dn},$$

where n is the degree of polymerization, $f(n)$ the weight fraction distribution function, and $P(\theta)$ the scattering function for a single molecule of degree of polymerization n. The division by $\int nf(n)dn$ is necessary for normalization.

Assuming distributions of the form $f(n)=(y^{z+1}/z!)\times n^z e^{-yn}$, where z is a parameter having positive integral values, he has calculated scattering functions for distributions of flexible coils. His methods and distributions will be applied here to the case of rigid isotropic rods.[2]

We proceed by assuming a distribution of analogous form

$$f(L)=\frac{y^{z+1}}{z!}L^z e^{-yL},$$

where L is the length of the molecule. Denoting the weight average value of any function $\varphi(L)$ by $\langle\varphi(L)\rangle$, we find $y=z+1/\langle L\rangle$. As Zimm points out, these distributions have a single peak, the width being determined by the parameter z. The lower the value of z, the broader the distribution; a monodisperse system will be denoted by $z=\infty$.

As $P(\theta)$ for the rigid rod contains the function

$$Si(\mu L)=\int_0^{\mu L}\frac{\sin x}{x}dx,$$

μ being the quantity $(4\pi/\lambda)\sin\theta/2$, it is convenient to write $P(\theta)$ in the form

$$\int_0^L 2\frac{L-r}{L^2}\frac{\sin\mu r}{\mu r}dr,$$

r being the distance between scattering elements of the molecule.[3] The scattering function for the polydisperse system is then given by

$$P_z(\theta)=\frac{1}{\langle L\rangle}\int_0^\infty Lf(L)\int_0^L 2\frac{L-r}{L^2}\frac{\sin\mu r}{\mu r}drdL.$$

Thus $P_z(\theta)$ may be expressed in terms of the difference of two integrals; for $z\geqq 1$ both may be readily evaluated using tables of integrals[4] if the order of integration is reversed,

$$\int_0^\infty\int_0^L\cdots drdL=\int_0^\infty\int_r^\infty\cdots dLdr.$$

For the case $z=0$, the second integral is evaluated using the original order.

Letting $x=\mu\langle L\rangle$ we find for $z=0$

$$P_0(\theta)=(2/x)\arctan x-\log(x^2+1).$$

For $z\geqq 1$,

$$P_z(\theta)=(2/x)\arctan\frac{x}{z+1}+\frac{2}{x}\sum_{j=1}^{z-1}\left(\frac{1}{z-j}-\frac{1}{z}\right)\times\frac{\sin\{(z-j)\arctan[x/z(+1)]\}}{\{1+[x^2/(z+1)^2]\}}.$$

The special cases $z=1, 2, 3, 4$ give

$$P_1(\theta)=\frac{2}{x}\arctan\frac{x}{2},$$

$$P_2(\theta)=\frac{2}{x}\arctan\frac{x}{3}+\frac{1}{3[(x^2/9)+1]},$$

$$P_3(\theta)=\frac{2}{x}\arctan\frac{x}{4}+\frac{1}{6[(x^2/16)+1]^2}+\frac{1}{3[(x^2/16)+1]},$$

$$P_4(\theta)=\frac{2}{x}\arctan\frac{x}{5}+\frac{[(3/5)-(x^2/125)]}{6[(x^2/25)+1]^3}+\frac{1}{5[(x^2/25)+1]^2}+\frac{3}{10[(x^2/25)+1]}.$$

[1] B. H. Zimm, J. Chem. Phys. **16**, 1099 (1948).
[2] Isotropic as used here refers to the very special case when the form and intrinsic anisotropies just cancel. The correct scattering functions for the various directions of polarization when this is not so have been calculated by Horn, Benoit, and Oster, J. chim. phys. **48**, 530 (1951).
[3] Zimm, Stein, and Doty, Polymer Bull. **1**, 90 (1945).
[4] D. Bierens de Naan, *Nouvelles Tables D'Integrales Defines* (Stechert, New York, 1939).

In Fig. 1, $P_z^{-1}(\theta)$, the quantity usually obtained from experimental data, has been plotted against $\mu^2\langle L\rangle^2$ (μ^2L^2 for the monodisperse case) for values of $z=1$, 4, and ∞. The figure permits a comparison of three systems having the same weight average molecular weights but different degrees of polydispersity. It can be seen that the more monodisperse the system is, the less the effect of internal interference and hence the greater the turbidity.

In Fig. 2, the same three curves have been replotted using different scales, to bring the initial slopes into coincidence. The downward curvature is seen to be greater, the greater the polydispersity.

The scattering functions calculated by Zimm for polydisperse coils also show these properties; so in addition do scattering functions calculated in this laboratory for certain discrete distributions. It seems plausible that this should be a general property of polydisperse systems: at low angles the larger molecules would be expected to dominate the scattering, and $P^{-1}(\theta)$ would behave initially more like the scattering function of a large molecule. At higher angles the smaller molecules are contributing proportionately more, and $P^{-1}(\theta)$, like $P^{-1}(\theta)$ for a small molecule, will be rising less steeply.

It is of interest to see if a quantitative basis for this behavior may be established.

Debye[5] has shown that, provided the molecule may be regarded as composed of isotropic point scatterers, $P(\theta)$ may be written as a power series in even powers of μ. The terms of the series alternate in sign, and the coefficients are proportional to the even moments of the distance distribution function $g(r)$. We have

$$P(\theta)=1-\frac{\mu^2}{3!}\langle r^2\rangle+\frac{\mu^4}{5!}\langle r^4\rangle-\frac{\mu^6}{7!}\langle r^6\rangle+\cdots,$$

where

$$\langle r^{2n}\rangle=\int r^{2n}g(r)dr.$$

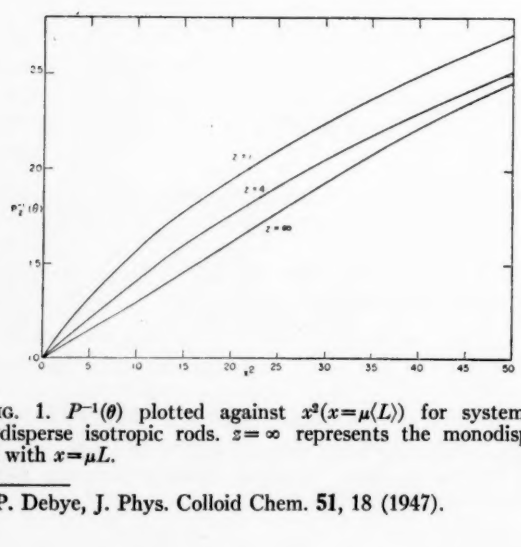

FIG. 1. $P^{-1}(\theta)$ plotted against $x^2(x=\mu\langle L\rangle)$ for systems of polydisperse isotropic rods. $z=\infty$ represents the monodisperse case with $x=\mu L$.

[5] P. Debye, J. Phys. Colloid Chem. **51**, 18 (1947).

On dimensional grounds we know that $P^{-1}(\theta)$ must be a function of μl, where l is a characteristic dimension of the molecule. We may take this dependence into account by measuring r in units of l; we obtain

$$P(\theta)=1-\frac{\mu^2l^2\langle r_0^2\rangle}{3!}+\frac{\mu^4l^4\langle r_0^4\rangle}{5!}-\frac{\mu^6l^6\langle r_0^6\rangle}{7!}+\cdots,$$

where $r_0=r/l$.

The moments $\langle r_0^{2n}\rangle$ are functions of the model but no longer of the size.

Using Zimm's formula for polydisperse systems and assuming that l varies as some positive power α of n, i.e., $l=kn^\alpha$, we obtain

$$P_z(\theta)=1-\frac{\mu^2k^2}{3!}\langle r_0^2\rangle\frac{\langle n^{2\alpha+1}\rangle}{\langle n\rangle}+\frac{\mu^4k^4}{5!}\langle r_0^4\rangle\frac{\langle n^{4\alpha+1}\rangle}{\langle n\rangle}-\frac{\mu^6k^6}{7!}\langle r_0^6\rangle\frac{\langle n^{6\alpha+1}\rangle}{\langle n\rangle}+\cdots.$$

The series reciprocal to this is given by

$$P_z^{-1}(\theta)=1+\frac{\mu^2k^2}{3!}\langle r_0^2\rangle\frac{\langle n^{2\alpha+1}\rangle}{\langle n\rangle}+\left[\left(\frac{1}{3!}\langle r_0^2\rangle\frac{\langle n^{2\alpha+1}\rangle}{\langle n\rangle}\right)^2-\frac{1}{5!}\langle r_0^4\rangle\frac{\langle n^{4\alpha+1}\rangle}{\langle n\rangle}\right]\mu^4k^4+\left[\frac{1}{7!}\langle r_0^6\rangle\frac{\langle n^{6\alpha+1}\rangle}{\langle n\rangle}-\frac{2}{3!5!}\langle r_0^2\rangle\langle r_0^4\rangle\frac{\langle n^{2\alpha+1}\rangle\langle n^{4\alpha+1}\rangle}{\langle n\rangle^2}+\left(\frac{1}{3!}\langle r_0^2\rangle\frac{\langle n^{2\alpha+1}\rangle}{\langle n\rangle}\right)^3\right]\mu^6k^6+\cdots.$$

The series for a monodisperse system is

$$P^{-1}(\theta)=1+\frac{\langle r_0^2\rangle n^{2\alpha}}{3!}\mu^2k^2+\left[\left(\frac{1}{3!}\langle r_0^2\rangle\right)^2-\tfrac{1}{5}\langle r_0^4\rangle\right]n^{4\alpha}\mu^4k^4+\left[\frac{1}{7!}\langle r_0^6\rangle-\frac{2}{3!5!}\langle r_0^2\rangle\langle r_0^4\rangle+\left(\frac{1}{3!}\langle r_0^2\rangle\right)^3\right]n^{6\alpha}\mu^6k^6+\cdots.$$

In a plot of $P^{-1}(\theta)$ against μ^2 (or $\sin^2\theta/2$), the coefficient of the μ^2 term gives the initial slope, and of the μ^4 term the initial curvature. The relations between these coefficients may be explored by means of well-known inequalities; these may all be regarded as special cases of Liapounoff's inequality,[6] and are derived from it in the appendix.

For example, if we are comparing two systems having

[6] J. V. Uspensky, *Introduction to Mathematical Probability* (McGraw-Hill Book Company, Inc., New York, 1937).

the same weight average molecular weight ($\langle n\rangle = n$), the relative values of the initial slopes are determined by the relative values of $\langle n^{2\alpha+1}\rangle/\langle n\rangle$ and $n^{2\alpha} = \langle n\rangle^{2\alpha}$. Inequality 6 shows that $\langle n^{2\alpha+1}\rangle > \langle n\rangle^{2\alpha+1}$; hence in the neighborhood of $\mu = 0$ the polydisperse curve must lie above the monodisperse one. The polydisperse system has more internal interference, hence a lower turbidity.

In testing the fit of the experimental $P(\theta)$ curve to that calculated from a model, it is customary to plot both curves with the same initial slopes and compare the curvatures. Comparing a polydisperse and monodisperse curve in this fashion is equivalent to choosing our systems such that $\langle n^{2\alpha+1}\rangle/\langle n\rangle = n^{2\alpha}$. The curvature at low μ values then depends on the relation between $\langle n^{4\alpha+1}\rangle/\langle n\rangle$ and $(\langle n^{2\alpha+1}\rangle/\langle n\rangle)^2$. From inequality 3 we see that polydispersity causes the curvature to be less, in the algebraic sense, than that for a monodisperse curve with the same initial slope.

Comparing the coefficients of the μ^6 term, we find from inequalities 3 and 5 that

$$\frac{\langle n^{6\alpha+1}\rangle}{\langle n\rangle} > \frac{\langle n^{2\alpha+1}\rangle\langle n^{4\alpha+1}\rangle}{\langle n\rangle^2} > \left(\frac{\langle n^{2\alpha+1}\rangle}{\langle n\rangle}\right)^3$$

and $\langle r_0^6\rangle > \langle r_0^4\rangle\langle r_0^2\rangle > \langle r_0^2\rangle^3$ by 7; however, $1/7! = 1/5040$, $2/3!5! = 1/360$. We conclude that the relative value of this term depends on the model and the distribution of sizes.

The question of whether in any experiment measurements have been made at low enough μ values for the reciprocal scattering curve to be showing its limiting values of slope and curvature has to be raised. This question applies to the determination of the molecular weight by extrapolation of the experimental scattering curve, more stringently to the determination of slope, and even more stringently to the determination of curvature. For the rigid rod, it may be shown that if the scattering function is written as a power series, the third and fourth terms together are equal in value and opposite in sign to the second when $P^{-1}(\theta)$ is about 2.1. The difficulty is even more striking when the scattering function for polydisperse rods of $z = 1$ calculated previously is considered: Here $P^{-1}(\theta)$ fails to converge as a power series at all for $\mu\langle L\rangle > 2$. $P(\theta)$ also fails to converge as a power series at the same point. The scattering function calculated by Zimm[1] for polydisperse coils of $z = 1$, $1/(1+x^2)$, converges as a power series only for $x < 1$, but its reciprocal series converges everywhere. On the other hand, the scattering function of a sphere, $[3/x^3(\sin x - x\cos x)]^2$, converges everywhere; as it possesses zeros on the real axis at the roots of $x = \tan x$, the reciprocal series fails to converge outside of the first such zero.[7] There appears to be no general statement that may be made about the rapidity of convergence of the series for $P^{-1}(\theta)$, and therefore no general answer to the question of how far into the region of large μ the initial curvature makes itself felt.

[7] T. J. I. Bromwich, *An Introduction to the Theory of Infinite Series* (MacMillan and Company, Ltd., London, 1931).

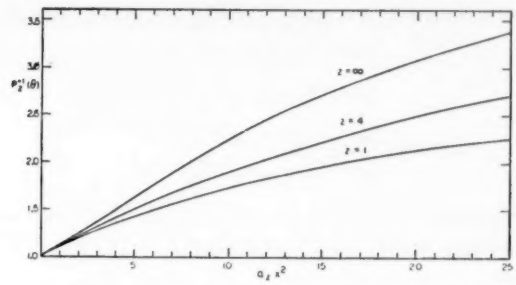

FIG. 2. $P^{-1}(\theta)$ plotted against $a_z x^2$, with a_z the initial slope in the plot of $P^{-1}(\theta)$ *versus* x^2. In this plot all three curves have the same initial slope.

Peterlin[8] has calculated scattering functions for stiff chains; the stiffness is measured by a parameter a, the average projection of an infinite chain on the first segment. The scattering function $P(\theta)$ depends on the ratio of this parameter to the contour length L. For a given stiffness parameter a, short chains are more "rod-like" than long ones, and would hence have a different curvature to the $P^{-1}(\theta)$ plot. In other words, $P(\theta)$ is no longer a function of the single variable μ, and the reasoning of this paper no longer applies.

The effect of stiffening the molecule is to make the curvature of $P^{-1}(\theta)$ more negative; the effect is in the same direction as polydisperity. In systems of unknown polydispersity, we see that the use of Peterlin's theory enables us to place only an upper limit on the stiffness.

Alternatively, if we assumed that the molecule of interest were completely flexible, and attributed any deviation from the theoretical curve for this model to polydispersity, we would obtain a relation between certain moments of the distribution that could be used as a measure of the polydispersity, but this would provide only an upper limit to the polydispersity, the stiffness being unknown.

The author wishes to thank Professor Paul Doty and Dr. Henri Benoit for helpful comments on this paper. The research was carried on with the aid of a grant from the Rockefeller Foundation for the study of protein systems by light scattering in this laboratory.

APPENDIX

Liapounoff's inequality[6] states that if a, b, and c are three real numbers satisfying the inequalities $a \geqq b \geqq c \geqq 0$, and $\langle n^a\rangle$, $\langle n^b\rangle$, and $\langle n^c\rangle$ are absolute moments of order a, b, and c for an arbitrary distribution, then

$$\langle n^b\rangle^{a-c} \leqq \langle n^c\rangle^{a-b}\langle n^a\rangle^{b-c}.$$

In the above expression the inequality sign holds if the distribution is not monodisperse, and if $a > b > c > 0$.

Let $a \geqq b \geqq c \geqq d \geqq 0$, then

$$\langle n^b\rangle^{a-c} \leqq \langle n^c\rangle^{a-b}\langle n^a\rangle^{b-c},$$
$$\langle n^b\rangle^{a-d} \leqq \langle n^d\rangle^{a-b}\langle n^a\rangle^{b-d},$$
$$\langle n^c\rangle^{a-d} \leqq \langle n^d\rangle^{a-c}\langle n^a\rangle^{c-d},$$
$$\langle n^c\rangle^{b-d} \leqq \langle n^d\rangle^{b-c}\langle n^b\rangle^{c-d}.$$

[8] A. Peterlin, J. Polymer Sci. **10**, 425 (1953).

Let $a=6\alpha+1$, $b=4\alpha+1$, $c=2\alpha+1$, $d=1$. We obtain

$$\langle n^{4\alpha+1}\rangle^3 \leqq \langle n\rangle\langle n^{6\alpha+1}\rangle^2, \quad (1)$$

$$\langle n^{2\alpha+1}\rangle^3 \leqq \langle n\rangle^2\langle n^{6\alpha+1}\rangle, \quad (2)$$

$$\langle n^{2\alpha+1}\rangle^2 \leqq \langle n\rangle\langle n^{4\alpha+1}\rangle, \quad (3)$$

$$\langle n^{4\alpha+1}\rangle^2 \leqq \langle n^{2\alpha+1}\rangle\langle n^{6\alpha+1}\rangle. \quad (4)$$

Equations (3) and (4) are also special cases of Schwarz's inequality. If we take the product of (1) and (2), we obtain

$$\langle n^{4\alpha+1}\rangle\langle n^{2\alpha+1}\rangle \leqq \langle n\rangle\langle n^{6\alpha+1}\rangle. \quad (5)$$

If in $\langle n^b\rangle^{a-c} \leqq \langle n^c\rangle^{a-b}\langle n^a\rangle^{b-c}$ we let $c=0$, we obtain

$$\langle n^b\rangle^a \leqq \langle n^a\rangle^b \quad (6a)$$

or

$$\langle n^b\rangle^{1/b} \leqq \langle n^a\rangle^{1/a}. \quad (6b)$$

Similarly

$$\langle n^c\rangle^a \leqq \langle n^a\rangle^c.$$

Multiplying this by (6a) and letting $a=b+c$, we obtain

$$\langle n^a\rangle \geqq \langle n^b\rangle\langle n^c\rangle. \quad (7)$$

Note added in proof.—Benoit[9] has shown that for Gaussian coils the ratio of the asymptotic slope of a $P^{-1}(\theta)$ plot to the initial slope is smaller the greater the polydispersity. An analogous relation holds for rods. From this, and the greater initial downward curvature in polydisperse systems, he was led to the conjecture that polydisperse curves should lie under the monodisperse curve under very broad conditions.

The nature of these conditions may be found as follows: the function $nf(n)/\langle n\rangle$ has the properties of a normalized distribution function. Without loss in generality this function may be expressed in terms of l^2 as a variable, l being the characteristic dimension of the molecule. This new function, $h(l^2)$, has the property that $\langle l^2\rangle$, defined as $\int l^2 h(l^2)d(l^2)$, is the average dimension obtained from the initial slope of a $P^{-1}(\theta)$ plot. Expressing $P(\theta)$ also as a function of l^2, we obtain for polydisperse systems $P_z=\int P(l^2)h(l^2)d(l^2)$. The scattering function for the monodisperse system having the same initial slope is $P(\langle l^2\rangle)$.

The necessary and sufficient condition for the inequality $P(\langle l^2\rangle) \leqq P_z$ is that $P(l^2)$ be a convex function of l^2.[10] From the Debye expression for $P(\theta)$ as a power series, we see that all scattering functions are initially convex. How long they remain convex has to be determined in each case; the rod and Gaussian coil functions are convex everywhere, proving the inequality $P(\langle l^2\rangle) \leqq P_z$ for all polydisperse systems (the equality sign holding only for $\theta=0$). In other words, in a $P^{-1}(\theta)$ plot, the polydisperse curve must always lie below the monodisperse curve for rods and coils.

For molecules such as spheres, whose scattering functions are not convex everywhere, the inequality holds for any distribution in which the largest molecule present is not so large that $P(l^2)$ has ceased to be convex.

[9] H. Benoit, J. Polymer Sci. (to be published).

[10] Hardy, Littlewood, and Polya, *Inequalities* (Cambridge University Press, Cambridge, 1934), Theorem 86.

THE JOURNAL OF CHEMICAL PHYSICS VOLUME 21, NUMBER 7 JULY, 1953

Bromination of Hydrocarbons. VI. Photochemical and Thermal Bromination of Toluene. Bond Dissociation Energies*

HERBERT R. ANDERSON, JR.,† HAROLD A. SCHERAGA, AND ERVIN R. VANARTSDALEN‡
Department of Chemistry, Cornell University, Ithaca, New York

(Received March 9, 1953)

With the aid of a high temperature, high vacuum, corrosion-resistant valve and photometers operating with high sensitivity at low light intensities, it has been possible to study the homogeneous gas-phase kinetics of the photochemical and thermal bromination of toluene. Infrared analyses indicated that the reaction is predominantly a side-chain substitution, the products being benzyl bromide and hydrogen bromide. The photochemical reaction, studied in the temperature range 82° to 132°C, was strongly inhibited by hydrogen bromide. The thermal reaction was studied in the absence of added hydrogen bromide at 166°C. Except for the step involving the dissociation of bromine molecules, both the photochemical and thermal mechanisms involve the same type of atom and radical chain, as found previously for the bromination of simple alkanes. The corrected activation energy of the over-all reaction, as determined from the temperature coefficient of the photochemical reaction, was found to be 7.2 kcal/mole. This value was assigned to the rate determining step Br+RH=R+HBr. From the temperature dependence of the hydrogen bromide inhibition, the activation energy for the reverse of this step was assigned the value 5.0 kcal/mole permitting the C—H bond dissociation energy in the alkyl side chain of toluene to be estimated as 89.5 kcal/mole at room temperature. The discrepancy between this value and Szwarc's value of 77.5 kcal/mole from pyrolysis studies has been pointed out. The efficiency of toluene as a third body in the homogeneous recombination of bromine atoms, and also problems relating to steric effects in atom and radical reactions have been discussed.

INTRODUCTION

PREVIOUS studies of the kinetics of the gas phase bromination of aliphatic hydrocarbons have provided information about the carbon-hydrogen and carbon-carbon bond dissociation energies in these and related compounds.[1–4] It was of interest to consider the effect of the substitution of an aromatic nucleus on the bond dissociation energy in methane, thereby requiring

* In part from the thesis submitted by Herbert R. Anderson, Jr., for the Ph.D. degree at Cornell University, February, 1953.

† U. S. Rubber Company Fellow, 1951–1952.

‡ Present address, Chemistry Division, Oak Ridge National Laboratory, Oak Ridge, Tennessee.

[1] G. B. Kistiakowsky and E. R. VanArtsdalen, J. Chem. Phys. **12**, 469 (1944).

[2] H. C. Andersen and E. R. VanArtsdalen, J. Chem. Phys. **12**, 479 (1944).

[3] E. I. Hormats and E. R. VanArtsdalen, J. Chem. Phys. **19**, 778 (1951).

[4] E. R. VanArtsdalen, J. Chem. Phys. **10**, 653 (1942).

a kinetic study of the bromination of toluene. A preliminary report[5] indicated that the kinetics of this reaction were similar to those found for aliphatic compounds. Also, as might be expected, and as borne out by the results here, the bromination of toluene in the gas phase is a radical reaction involving the alkyl side chain with no attack on the aromatic nucleus.

During the course of this investigation, considerable work by Szwarc has appeared in which bond dissociation energies were determined from pyrolysis studies involving a toluene carrier gas technique.[6] It thus becomes of considerable interest to compare the bond dissociation energies obtained from pyrolysis experiments with those obtained from bromination kinetics.

MATERIALS

In the purification of materials, cognizance was taken of the fact that reactions of this type are extremely sensitive to traces of oxygen and water. All purification operations were carried out in grease-free, high vacuum systems. The toluene used in this investigation was Bureau of Standards sample 211a-8S which had been purified by fractional distillation from petroleum, outgassed under high vacuum, and supplied in ampoules with breakseals. Freezing point measurements made by the Bureau of Standards indicated that the mole percent of impurities was 0.04 ± 0.02. After sealing these ampoules to the high vacuum reaction system, the pressure of noncondensable gases was found to be less than 10^{-6} mm of mercury ("stick" vacuum on a MacLeod gauge). The contents of several ampoules were combined by distillation under high vacuum.

Analytical reagent grade bromine was allowed to stand in vacuum over reagent grade potassium bromide for several weeks to remove traces of chlorine, after which it was distilled in a grease-free high vacuum system through a large tube of phosphorus pentoxide. Several trap-to-trap distillations under conditions of a "stick" vacuum were carried out, followed by fractional distillation, the middle fraction being sealed off in ampoules behind breakseals.

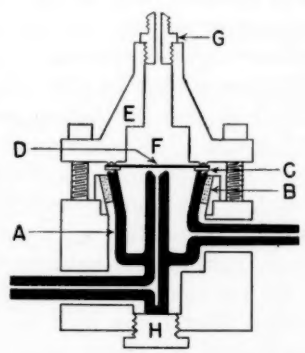

FIG. 1. High temperature, high vacuum, corrosion-resistant valve.

[5] Swegler, Scheraga, and VanArtsdalen, J. Chem. Phys. **19**, 135 (1951).
[6] M. Szwarc, J. Chem. Phys. **16**, 128 (1948), and later papers.

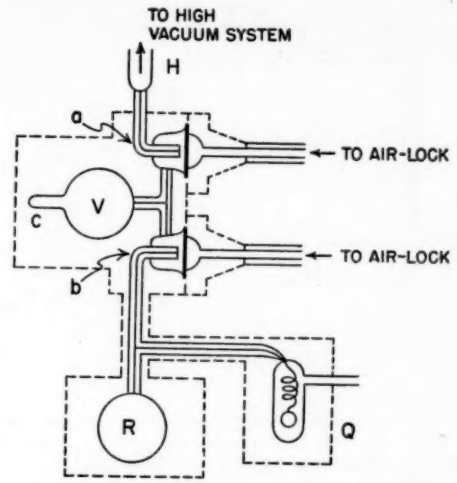

FIG. 2. Thermostatted reaction vessel and related portion of high vacuum system.

Tanked hydrogen bromide (Matheson Company) of a stated purity of 99.5 percent was passed over copper turnings to remove bromine, over phosphorus pentoxide to remove water, then outgassed (stick vacuum) by trap-to-trap distillation under high vacuum, and finally stored as a gas at slightly under 1 atmos pressure in a 1-liter flask behind a breakseal.

Tanked oxygen (Air Reduction Company) of a stated purity of 99.5 percent was introduced into the reaction vessel in several runs to obtain qualitative information about oxygen inhibition.

EXPERIMENTAL

It will be demonstrated below that the gas phase bromination of toluene (herein designated as RH) is a side chain substitution with the production of benzyl bromide (RBr) and hydrogen bromide. Since the products of the reaction are known, the course of the reaction could be studied by observation of the rate of disappearance of bromine. However, the method used in previous investigations of this type[1–3] was not easily applicable to this problem since toluene, unlike the hydrocarbons previously studied, is much higher boiling. Because of this property, consideration had to be given to the problem of avoiding condensation of toluene in the reaction system. This was accomplished by thermostatting the leads and stopcocks of the high vacuum system at a temperature slightly in excess of the normal boiling point of toluene.

Ordinary stopcocks are not suitable at the temperature used here (115°C). Accordingly, the high temperature, high vacuum, corrosion-resistant valve illustrated in Fig. 1 was designed. The glass insert A consists of an envelope, a central capillary tube, and two capillary sidearms. The envelope was constructed from a section of Pyrex pipe which has a conical end designed to withstand large axial stresses. The upper end of the central capillary tube and the rim of the glass envelope

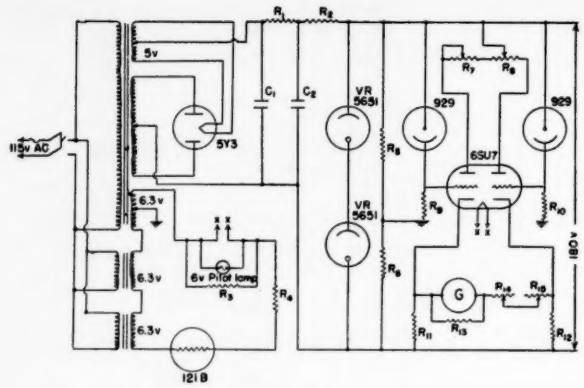

FIG. 3 (a). Photometer circuit used for photochemical runs. C_1, C_2—4 μf; R_1, R_{15}—50kΩ; R_2—25kΩ; R_3—25Ω; R_4—2Ω; R_5—540kΩ; R_6—150kΩ; R_7—20kΩ; R_8—100kΩ; R_9, R_{10}—37 megΩ; R_{11}, R_{12}—240kΩ; R_{13}—15Ω; R_{14}—250kΩ.

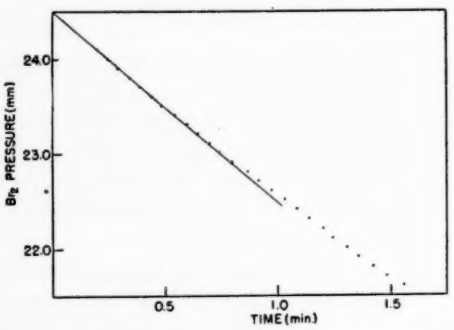

FIG. 3 (b). Typical curve for the rate of disappearance of bromine.

were ground flat so that both surfaces were in the same plane. The rim features a centrally located concentric recess enabling a vacuum-tight seal to be made with the aid of a gasket, C. The lower end of the central capillary tube was ground flat and parallel to the rim of the glass envelope. The glass insert fits into a brass housing and is cushioned from the metal by means of an asbestos insert, B. A ring-type gasket C is placed on the rim of the glass envelope. A thin diaphragm D fits on top of the gasket. Both the gasket and the diaphragm were made from Kel-F, kindly supplied to us by Dr. W. E. Hanford of the M. W. Kellogg Company, New York, New York. The whole assembly is held in place by a brass cover-piece E which is secured to the brass housing by set-screws. The cover-piece features an air-lock F and standard fitting G which can be readily connected to copper tubing. When the assembly has been made vacuum-tight, the set-screw H is adjusted with very slight manual pressure to provide support for the central glass capillary.

In operation, the diaphragm D is forced against the central glass capillary to close the valve by admitting air up to a pressure of one atmos in the air-lock. The valve is opened by evacuating the air-lock. This valve, which was found to be very satisfactory, may be operated in a high vacuum system over a range of temperatures and with a variety of corrosive materials, both liquid and gaseous.

The reaction vessel was made from a 35-mm length of 45-mm i.d. Pyrex tubing whose ends were sealed with parallel, planar windows (Fisher and Porter Company, Hatboro, Pennsylvania). The inlet tube on the cylindrical wall was of 1-mm i.d. capillary tubing to minimize dead space in the 60-cc absorption cell.

A quartz-spiral manometer, attached to the absorption cell by means of a 1-mm i.d. capillary tube, was used as a null instrument against a mercury manometer to measure the gas pressure. In order to prevent condensation of toluene and benzyl bromide in the essential parts of the reaction system (enclosed by the dashed lines in Fig. 2), the high temperature valves a and b, the vaporizing chamber V, and the quartz-spiral manometer Q were maintained at high temperature. The reaction cell R, was also maintained at elevated temperatures by means of an air thermostat (±0.1°C). Temperatures were measured with a 3-junction copper-constantan thermocouple.

The reactants were stored at low temperature (−78°C) behind stopcocks on a high vacuum line leading to the reaction system at H in Fig. 2. These stopcocks were lubricated with perfluorolube oil FCX-334 (we are indebted to Dr. S. W. McCune, III, of the du Pont Company, Wilmington, Delaware for giving us this material).

In filling the reaction cell, bromine was introduced first and its pressure determined by means of the photometer described below. Valve b (Fig. 2) was then closed, and the excess bromine in the high-vacuum line was pumped out. With the aid of a pycnometer attached to the high vacuum line, and a liquid nitrogen bath around the cold finger C, a roughly measured quantity of toluene was distilled into the vaporizing chamber V. Valve a was then closed, the liquid nitrogen bath removed from C, and the cold finger brought to temperature equilibrium with the rest of the reaction system. The vaporized toluene was then introduced into the reaction cell by virtue of the pressure differential existing between V and R when valve b was opened. The total pressure was measured with the quartz-spiral manometer and the toluene pressure was obtained by subtraction of the bromine pressure. In runs involving inhibition studies by HBr, this gas was introduced in a similar manner just before the toluene.

The same light source was used for photoactivation and also for photometric determination of the bromine pressure. The source was a 1000-watt projection lamp, used in conjunction with a suitable optical system to obtain parallel and uniform illumination over the face of the reaction cell, a water filter and a Farrand interference filter being used to obtain light with a peak wavelength of 4890A and half-band width of about 150A. Bromine is the only substance in the reaction mixture which absorbs in this region; it dissociates in the continuum to give one normal and one excited

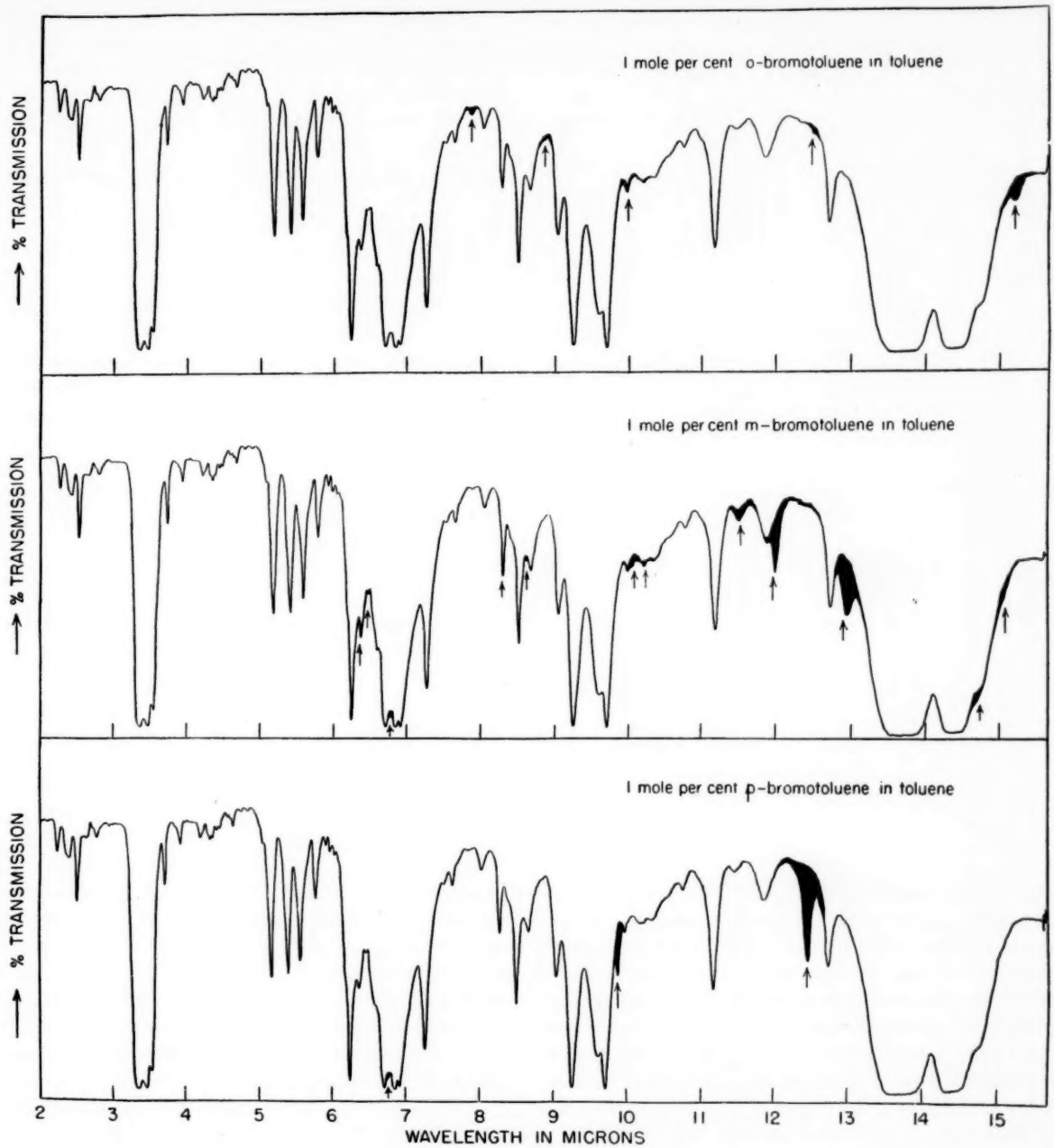
1 mole per cent o-bromotoluene in toluene
1 mole per cent m-bromotoluene in toluene
1 mole per cent p-bromotoluene in toluene
% TRANSMISSION
% TRANSMISSION
% TRANSMISSION
2 3 4 5 6 7 8 9 10 11 12 13 14 15
WAVELENGTH IN MICRONS

FIG. 4. Infrared spectra of bromotoluenes.

atom.[7] The lamp was operated below its rated capacity, and the light intensity was maintained constant by adjustment of the lamp voltage using an *independent* photronic-cell circuit for monitoring purposes. The photronic cell was activated by a by-pass portion of the high light intensity available close to the lamp.

The temperature range in which the photochemical reaction could be studied had to be high enough to volatilize enough toluene but low enough to avoid any thermal bromination. These requirements essentially fixed the allowable temperature range for the photochemical reaction between 80° and 135°C. In order to obtain a conveniently measurable rate of bromination at these temperatures, the light intensity had to be very low so that the usual photronic cell circuits were not sufficiently sensitive. In the photochemical studies, bromine absorption was measured by means of 929 photoelectric cells (with suitable response in the blue region) used in the circuit shown in Fig. 3(a). We are indebted to Mr. Leonard Walker of the Newman Laboratory for Nuclear Studies for the design of this circuit.

[7] W. A. Noyes, Jr., and P. A. Leighton, *Photochemistry of Gases* (Reinhold Publishing Corporation, New York, 1941), p. 133.

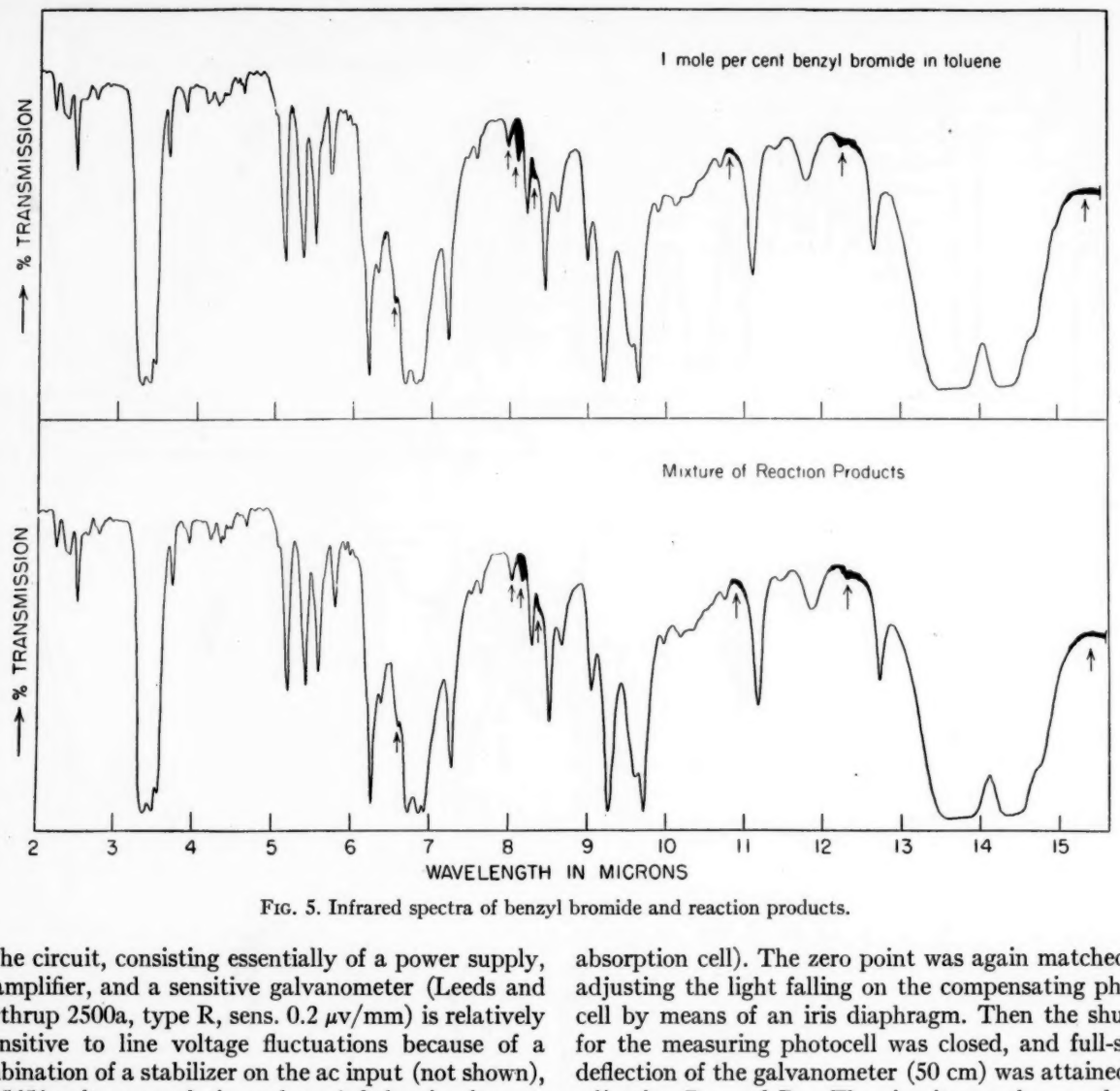
1 mole per cent benzyl bromide in toluene
% TRANSMISSION
Mixture of Reaction Products
% TRANSMISSION
2 3 4 5 6 7 8 9 10 11 12 13 14 15
WAVELENGTH IN MICRONS

FIG. 5. Infrared spectra of benzyl bromide and reaction products.

The circuit, consisting essentially of a power supply, an amplifier, and a sensitive galvanometer (Leeds and Northrup 2500a, type R, sens. 0.2 μv/mm) is relatively insensitive to line voltage fluctuations because of a combination of a stabilizer on the ac input (not shown), the 5651 voltage-regulating tubes, and the circuit symmetry; also, it is capable of a high degree of precision and rapid response. The signal from the two 929 photocells controlled the grids of the 6SU-7 twin triode tube. Any difference in potential existing between the two cathodes of the 6SU-7 gave rise to a flow of current through the galvanometer. One of the 929 tubes was in a path directly behind the reaction cell to detect changes in bromine absorption; the other was in a path illuminated independently by the *same* lamp and served as a compensating tube. Electromagnetically activated shutters were available to cut off either path from the photolamp.

In operation, the galvanometer was removed from the circuit and its zero point determined. It was then reinserted in the circuit and, with no light falling on the 929 tubes, it was reset to this zero point by adjusting the plate potentiometers R_7 and R_8. With the circuit thus balanced, the shutters were opened so that light might fall on both photocells (with no reactants in the absorption cell). The zero point was again matched by adjusting the light falling on the compensating photocell by means of an iris diaphragm. Then the shutter for the measuring photocell was closed, and full-scale deflection of the galvanometer (50 cm) was attained by adjusting R_{14} and R_{15}. The circuit was then ready for measuring the concentration of bromine subsequently placed in the absorption cell.

Reactants were introduced into the absorption cell and the shutter opened to start the reaction. As the latter proceeded, the decrease in bromine concentration caused the galvanometer reading to approach that obtained for the zero point of the galvanometer. The photronic cell monitoring circuit indicated that the light intensity remained constant within 0.2 percent over the period required for a run, usually not more than $\frac{1}{2}$ hr. The galvanometer readings were calibrated against known pressures of bromine in the absorption cell, the pressures having been measured by the quartz-spiral manometer. An exceptionally high degree of precision was achieved using this photometer and circuit as shown by a typical rate curve in Fig. 3b. Particularly noteworthy was the ease with which closely spaced measurements could be made by recording time with a Signal Corps Tape Recorder (BC-1016, Waters

Conley Company, Rochester, Minnesota). This operation merely required one to depress a telegraph key as the galvanometer passed closely spaced, predetermined intervals. In this way a very large number of points was obtained during the critical, initial stages of bromination.

In the thermal runs at a higher temperature (166°C) the light intensity had to be reduced to such a low value to eliminate photochemical reaction that this circuit was no longer sufficiently sensitive without considerable modification. The modifications were not made, however, because of the availability of a photometer normally used in light scattering investigations. This Photovolt Electronic Photometer (Model 512, Photovolt Corporation, New York, New York) provided the required sensitivity for the thermal runs which were followed photometrically at an extremely low level of light intensity.

The thermal reaction is negligible in practically the whole temperature range over which the photochemical reaction was studied. It has a small detectable rate (0.3 percent of the photochemical one) at 133°C, the highest temperature used in the photochemical runs.

Szwarc[6] has shown that none of the reactants or products are pyrolyzed at the temperatures used in the photochemical or thermal runs.

The initial rate of disappearance of bromine was determined from the initial slope of the experimental rate curves. These initial rates were used in all computations of rate constants, inhibition constants, and temperature coefficients in order to minimize the effects of accumulating products of reaction.

The reaction products were analyzed by means of their infrared absorption spectra, obtained with a Perkin-Elmer spectrophotometer, Model 21, using a 0.1-mm sodium chloride absorption cell. The spectra of 1-mole percent solutions of *o*-, *m*-, *p*-bromotoluene, and benzyl bromide in toluene are shown in Figs. 4 and 5. Each diagram represents the absorption spectrum of the given solution superimposed upon that of pure toluene. The shaded areas indicated by arrows represent those peaks not present in toluene but arising only from the respective brominated product. The limit of detectability of these additional peaks was found to correspond to 0.04-mole percent of ring substituted bromotoluenes in the presence of 1-mole percent of benzyl bromide in toluene. This would correspond to 4 percent ring substitution compared to the 96 percent production of benzyl bromide by side chain bromination.

The products obtained from 27 experiments were combined to give a 1-mole percent solution of brominated toluene in toluene as determined from the amount of bromine reacting in each run. The organic material was washed with 10 percent aqueous sodium bisulfite to remove bromine and then with water. It was then dried with anhydrous magnesium sulfate and a portion taken for determination of the infrared absorption spectrum.

TABLE I. Photobromination of toluene at constant light intensity (wavelength 4890A).

	Initial pressures (mm at t°C)		
t°C	Br_2	RH	k(sec^{-1}) ×10^4
	Series A, Light intensity, I_0'		
82.5	10.64	107.1	4.20
	10.90	112.2	3.77
	11.40	112.8	3.86
	19.67	97.4	3.96
	20.40	93.7	3.81
			3.92±0.13
97.1	9.25	113.3	6.95
	9.72	79.1	6.88
	9.95	90.2	6.34
	9.97	67.1	5.70
	10.11	159.3	6.46
	10.33	114.9	5.81
	10.39	192.5	5.93
	10.55	78.2	5.86
	10.66	150.2	6.08
	10.95	192.8	6.09
	11.03	98.7	6.57
	18.93	104.9	5.98
	19.17	102.4	5.53
	24.50	95.1	6.91
	25.06	102.8	6.40
	31.10	108.2	6.61
	32.30	98.8	6.20
			6.25±0.35
132.7	10.35	121.1	15.1
	10.42	186.6	15.4
	10.63	112.0	15.1
	19.80	110.4	17.4
	20.78	107.7	16.7
			15.9 ±0.9
	Series B, Light intensity, I_0		
82.5	10.17	105.8	7.37
	10.70	118.4	6.70
			7.03±0.33
89.8	10.30	118.1	8.55
	10.63	117.6	9.00
	10.67	94.8	8.59
	10.67	117.8	8.27
	11.02	113.4	9.66
			8.81±0.41
115.0	9.15	115.8	17.1
	10.20	119.6	17.5
	10.20	125.4	18.1
	10.44	109.4	17.4
	10.67	114.5	17.3
	10.81	108.8	18.2
	10.89	120.1	18.0
	19.80	113.7	16.4
	20.30	107.8	18.0
			17.6 ±0.4
132.3	9.95	117.9	23.7
	10.20	115.4	25.5
	10.23	118.1	23.2
	10.72	121.5	24.4
			24.2 ±0.8

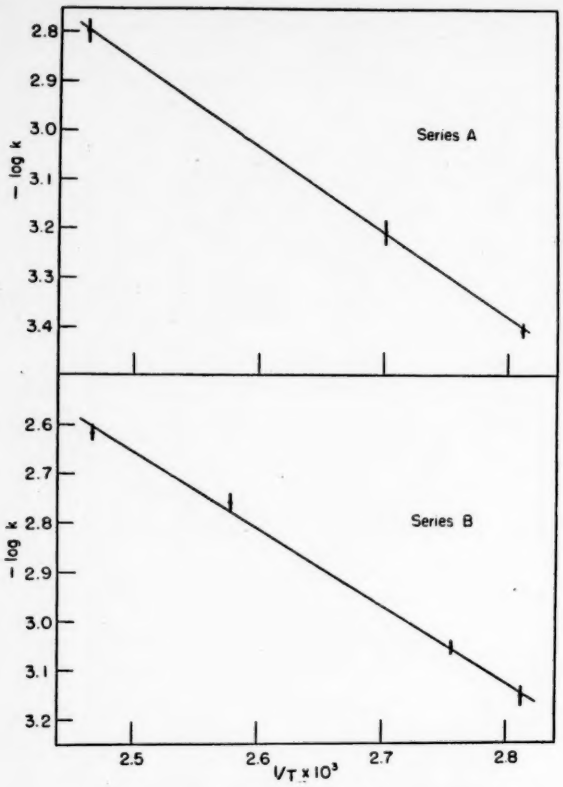

FIG. 6. Temperature dependence of photobromination of toluene for two series of measurements.

The spectrum obtained with these reaction products, bottom of Fig. 5, shows unambiguously that every absorption peak that occurred could be identified with those of toluene or benzyl bromide with no indication of any bromotoluenes. Therefore, it may be concluded that the amount of ring substitution was negligible, and the kinetic study may be based on the correct premise that the reaction is predominantly a side-chain bromination with the formation of benzyl bromide and hydrogen bromide. We are indebted to Professor D. F. DeTar and Mr. T. Wentink for aid with the infrared experiments.

RESULTS

The rate law, which corresponds to the initial rate of disappearance of bromine at constant light intensity, was determined from an extensive series of runs at 97.1°C over approximately a threefold range of pressures of reactants. The specific reaction rate constants k were calculated from the initial rate by means of the expression

$$-d(\mathrm{Br_2})/dt = k(\mathrm{Br_2})^{\frac{1}{2}}(\mathrm{RH})^{\frac{1}{2}}. \qquad \text{(I)}$$

Experimental values of k at several temperatures are given in Table I. It is evident that there are no significant trends in k with changing pressure of either reactant, nor is there any dependence of the reaction rate constant on the sequence in which the runs were carried out. The two series of measurements, A and B, correspond to somewhat different apparatus constants (involving a change in light intensity) which appear in k.

Equation (I) fits the data better than the rate law

$$-d(\mathrm{Br_2})/dt = k'(\mathrm{Br_2})^{\frac{1}{2}}(\mathrm{RH})(1/P)^{\frac{1}{2}}, \qquad \text{(II)}$$

which has been found for the photobromination of methane,[1] where P represents the total pressure. A similar situation was encountered in the photobromination of neopentane.[3] The better precision obtained with Eq. (I) is probably the result of toluene, like neopentane, having an efficiency for aiding in the recombination of bromine atoms very much greater than that of any of the other substances present. It can be seen that Eq. (II) approximates Eq. (I) when the toluene pressure is much greater than the bromine pressure.

TABLE II. Photobromination of toluene at reduced light intensity, $0.511I_0$ (wavelength 4890A).

	Initial pressures (mm at t°C)		
t°C	Br_2	RH	$k(\mathrm{sec^{-1}}) \times 10^4$
115.0	10.91	115.6	12.3
	11.10	110.9	12.4
			12.4±0.1

TABLE III. Photobromination of toluene at constant light intensity, I_0 (wavelength 4890A). Inhibition by HBr.

	Initial pressures (mm at t°C)			
t°C	Br_2	RH	HBr	n
90.0	10.50	130.0	19.2	0.49
	11.70	124.6	18.5	0.71
	19.60	121.5	21.8	0.61
	20.10	115.1	23.6	0.60
	20.30	100.9	20.7	0.57
				0.60±0.05
115.1	10.57	139.6	19.4	0.89
	10.60	130.9	18.7	0.91
	11.60	134.6	16.4	0.96
				0.92±0.03
132.6	9.7	128.9	21.2	1.21
	19.7	124.8	14.9	1.31
	19.8	124.6	16.2	1.43
				1.32±0.08

The effect of change of incident light intensity on the rate of the reaction was investigated by inserting a calibrated screen between the light source and the reaction cell. This screen had a transmission of 51.1 percent. Table II shows the data obtained at 115.0°C at the reduced light intensity ($0.511I_0$). The average value of k is 70.4±1.8 percent of its value at this temperature (Table I, Series B) at the higher light intensity, I_0. If the reaction is one-half order in light intensity, then this screen should reduce the value of k to $(0.511)^{\frac{1}{2}}$ or 71.5 percent of its value without the screen. The ex-

cellent agreement between the calculated reduction and the observed reduction in k supports the view that the rate of reaction is proportional to the square root of the light intensity.

The effect of temperature on the initial rate of photobromination of toluene was investigated over a 50 degree temperature range, and the results are given in Table I and plotted in Fig. 6 for both series of data. While the magnitudes of the specific rate constants in series A and B differ (for the reason stated above), the temperature coefficients for the two series are in reasonable agreement. The best straight lines, obtained by the method of least squares, for each series, are represented by the equations

$$\log k_A = 1.497 - 1742/T \qquad \text{(III)}$$

and

$$\log k_B = 1.270 - 1570/T. \qquad \text{(IV)}$$

Considering that the reaction is half-order in light intensity, it can be shown that the effect of the slight temperature dependence of the absorption coefficient of bromine[8,9] is negligible, and its neglect corresponds to an error no greater than 1.5 percent in the activation energy. It is thus possible to obtain the experimental activation energy from Eqs. (III) and (IV). These are 7.97 kcal/mole for Series A and 7.18 kcal/mole for Series B, the average of the two series being 7.58±0.6 kcal/mole. When corrected for the temperature dependence of the frequency factor in the Arrhenius equation by subtraction of $RT/2$, the activation energy for photobromination becomes 7.2±0.6 kcal.

TABLE IV. Thermal bromination of toluene.

t°C	Initial pressures (mm at t°C) Br_2	RH	k (cc moles^{-1})$^{\frac{1}{2}}$ sec^{-1} ×10^2
166.2	10.75	113.6	9.56
	15.30	107.8	8.51
	19.65	195.6	9.23
	20.80	195.2	9.06
	23.30	127.7	10.03
	27.10	105.4	9.00
			9.23±0.38

Hydrogen bromide, produced during bromination, greatly inhibits this reaction. This inhibition was investigated in the presence of added hydrogen bromide by keeping the hydrogen bromide and toluene pressures approximately constant while the bromine pressure was varied over a twofold range. The complete rate law, taking the inhibition into account, was found to be similar to that obtained in previous bromination studies. Equation (I), therefore, may be modified to

$$-d(Br_2)/dt = \frac{k(Br_2)^{\frac{1}{2}}(RH)^{\frac{1}{2}}}{1+n(HBr)/(Br_2)}, \qquad \text{(V)}$$

since the light intensity was the same as for the data shown in Table I, Series B. Here n is the inhibition constant, k is the value of the rate constant for the uninhibited reaction at the same temperature, and $-d(Br_2)/dt$ is the experimentally observed initial rate of the inhibited reaction in the presence of excess HBr. The values of k used in computing n from experimental rates were calculated from Eq. (IV). It should be pointed out that the value for n is very sensitive to errors in the value of k.

The values of n are quite large compared to those for the bromination of hydrogen[8,10] in the range up to 300°C and methane[1] between 120 and 180°C. They are, however, of similar size to those obtained for neopentane[3] in agreement with the notion that the larger and more complicated the molecule being brominated, the greater appears to be the degree of inhibition by HBr.

The inhibition constant is also temperature dependent, as shown in Table III and Fig. 7. The equation for the best straight line, obtained by the method of least squares, is

$$\log n = 3.007 - 1176/T. \qquad \text{(VI)}$$

From this equation, one can calculate an apparent activation energy of inhibition of 5.38±1.2 kcal/mole. Upon correction for the small temperature dependence of the frequency factor, by subtraction of $RT/2$, the apparent activation energy of inhibition becomes 5.0 ±1.2 kcal/mole.

As with other hydrocarbons, photobromination of toluene is also inhibited by oxygen. It was found that the introduction of 8 mm of oxygen to a mixture containing 20 mm of bromine and 103 mm of toluene caused a fourfold decrease in the normal rate. No extensive study was made of oxygen inhibition.

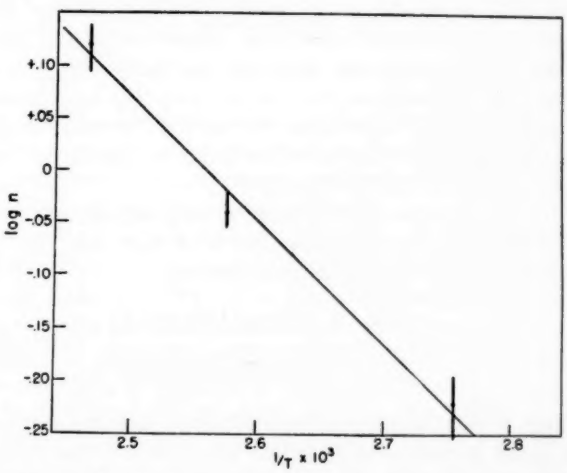

FIG. 7. Temperature dependence of inhibition by hydrogen bromide of photobromination of toluene.

[8] M. Bodenstein and H. Luetkemeyer, Z. physik. Chem. 114, 208 (1924).

[9] Acton, Aickin, and Bayliss, J. Chem. Phys. 4, 474 (1936).

[10] M. Bodenstein and S. C. Lind, Z. physik. Chem. 57, 168 (1906).

It was also desirable to investigate the mechanism of the thermal reaction in order to obtain more detailed information about the rate determining step in the bromination reaction. Since the amount of thermal reaction in the photochemical studies was negligible, it was necessary to raise the temperature to 166.2°C in order to obtain a conveniently measurable rate of reaction between bromine and toluene. Also, in order to follow the reaction photometrically, it was necessary to decrease the incident light intensity to a level which would not produce a photochemical reaction. The data for the thermal runs were calculated from the rate law

$$-d(\mathrm{Br_2})/dt = k(\mathrm{Br_2})^{\frac{1}{2}}(\mathrm{RH}) \qquad \text{(VII)}$$

and are shown in Table IV. Pressures were converted to concentration units by use of the ideal gas law. There is no dependence of the reaction rate constant on the sequence in which the runs were carried out.

DISCUSSION

From a consideration of the observed rate laws for the photochemical and thermal reactions, the inhibition by hydrogen bromide, and the half-order in light intensity, the following mechanism, which was also deduced from similar studies of other hydrocarbons, is postulated:

$$\mathrm{Br_2}+h\nu = 2\ \mathrm{Br} \qquad (1)$$

$$\text{or}\quad \mathrm{Br_2}+M = 2\ \mathrm{Br}+M \qquad (1a)$$

$$\mathrm{Br}+\mathrm{RH} = \mathrm{R}+\mathrm{HBr} \qquad (2)$$

$$\mathrm{R}+\mathrm{Br_2} = \mathrm{RBr}+\mathrm{Br} \qquad (3)$$

$$\mathrm{R}+\mathrm{HBr} = \mathrm{RH}+\mathrm{Br} \qquad (4)$$

$$\mathrm{Br}+\mathrm{Br}+M = \mathrm{Br_2}+M, \qquad (5)$$

where M represents any molecule present. Steps (1) and (1a) represent the photochemical or thermal dissociation of bromine molecules, respectively. The subsequent steps 2–5 are identical for both the photochemical and thermal reactions. Since this mechanism is postulated for the initial part of the bromination reaction only, no consideration need be given to the bromination of benzyl bromide.

By application of steady-state considerations to the postulated mechanism, the following rate law can be derived for the photochemical reaction

$$-\frac{d(\mathrm{Br_2})}{dt} = \frac{k_2(\mathrm{RH})\{\Phi I_a/k_5(M)\}^{\frac{1}{2}}}{1+k_4(\mathrm{HBr})/k_3(\mathrm{Br_2})}, \qquad \text{(VIII)}$$

where Φ represents absorbed effective light quanta and I_a is the intensity of absorbed light. As pointed out in previous papers of this series, $\Phi I_a = k_{\mathrm{app}}\alpha I_0(\mathrm{Br_2})$, where k_{app} is a temperature-independent apparatus constant and α the absorption coefficient of $\mathrm{Br_2}$ for the wavelength of light of incident intensity I_0.

In deriving Eq. (VIII) from the photobromination mechanism it has been assumed that all molecules are equally effective third bodies in the homogeneous recombination of Br atoms. This is not the case, as has been demonstrated for instance by Jost,[11] Rabinowitch,[12] and Kistiakowsky and VanArtsdalen.[1] Actually, the term $k_5(M)$ in Eq. (VIII) should be replaced by a summation of k_5's and (M)'s for each molecular species present. Thus, at the start of the reaction it is possible to write

$$k_5(M) = k_5'(\mathrm{Br_2}) + k_5''(\mathrm{RH}). \qquad \text{(IX)}$$

If $k_5'' \gg k_5'$, i.e., if toluene is a much more effective third body than bromine, and the concentration of toluene is greater than that of bromine, then Eq. (VIII) reduces to the experimentally obtained Eq. (V) at constant incident light intensity I_0, with

$$k = k_2[k_{\mathrm{app}}\alpha I_0/k_5]^{\frac{1}{2}} \quad \text{and} \quad n = k_4/k_3.$$

The rate law for the thermal reaction may be derived in a similar manner, the result being

$$-\frac{d(\mathrm{Br_2})}{dt} = \frac{k_2K^{\frac{1}{2}}(\mathrm{Br_2})^{\frac{1}{2}}(\mathrm{RH})}{1+k_4(\mathrm{HBr})/k_3(\mathrm{Br_2})}, \qquad \text{(X)}$$

where K is the equilibrium constant for the thermal dissociation of bromine and equals k_{1a}/k_5. Relative efficiencies of the various molecules as third bodies are of no consequence since any given molecule must be equally effective in promoting dissociation of bromine molecules and recombination of bromine atoms (principle of microscopic reversibility). If we set the concentration of HBr equal to zero, then a comparison of Eq. (X) with the experimentally obtained rate law for the thermal reaction (Eq. (VII)) indicates that $k = k_2K^{\frac{1}{2}}$.

Reactions involving H atoms have been omitted from consideration on energetic grounds.[1] Other chain termination steps, including heterogeneous reactions at the wall, have been eliminated since they are not consistent with the observed rate law and dependence on light intensity.

The thermal rate law provides data for calculation of k_2 and, thereby, the frequency factor for this rate determining step, since the experimental thermal rate constant is $k_2K^{\frac{1}{2}}$, where K is the equilibrium constant for the reaction: $\mathrm{Br_2}(g) = 2\mathrm{Br}(g)$. The value of $K^{\frac{1}{2}} = 1.06 \times 10^{-11}$ (mole cc^{-1})$^{\frac{1}{2}}$ at 439.4°K was obtained by interpolation of the standard free energy data of Gordon and Barnes.[13] Thus $k_2 = 9.23\times10^{-2}/1.06\times10^{-11} = 8.71 \times 10^9$ (cc mole^{-1} sec^{-1}). Writing the Arrhenius equation as

$$k_2 = s_2Z_2e^{-E_2/RT},$$

where Z_2 is the collision number and s_2 is a steric factor for the reaction $\mathrm{Br}+\mathrm{RH} = \mathrm{R}+\mathrm{HBr}$, the frequency factor is found to be $A_2 = s_2Z_2 = k_2/\exp(-E_2/RT)$

[11] W. Jost, Z. physik. Chem. **B3**, 95 (1929).

[12] E. Rabinowitch and W. C. Wood, Trans. Faraday Soc. **32**, 907 (1936); E. Rabinowitch and H. L. Lehman, Trans. Faraday Soc. **31**, 689 (1935).

[13] A. R. Gordon and C. Barnes, J. Chem. Phys. **1**, 694 (1933).

$=3.3\times10^{13}$ (cc mole^{-1} sec^{-1}), using the value $E_2=7.2$ kcal/mole. The collision number Z_2 was evaluated at 439.4°K using Nasini's value[14] of 5.3A for the diameter of toluene and 3.0A for the diameter of the bromine atom.[3] The value of Z_2 at this temperature is 1.5×10^{14} (cc mole^{-1} sec^{-1}). Thus the value of the steric factor is $s_2=3.3\times10^{13}/1.5\times10^{14}=0.22$. This means that about one-fifth of the collisions, which are energetically adequate for reaction, leads to reaction. The steric factor for the corresponding reaction with methane[1] was of the order of 0.1 to 0.2. Because of inherent imprecision in steric factor calculations, it is not possible to conclude that there is any significant difference between methane and toluene in this respect.

A comparison of steric factors of reactions competing for benzyl radicals may be made with the aid of Eq. (VI) for the temperature coefficient of the inhibition constant n, which is equal to k_4/k_3. Eq. (VI) may be written in the form

$$\log(k_4/k_3)=\log(A_4/A_3)-(E_4-E_3)/2.3RT, \quad \text{(XI)}$$

and by comparison with Eq. (VI) it is seen that $\log(A_4/A_3)=3.01$. Since $A=sZ$ and the collision numbers for the competing reactions are about the same, the steric factor for the reaction

$$\mathrm{R+Br_2=RBr+Br} \qquad (3)$$

is smaller than the steric factor of the reaction

$$\mathrm{R+HBr=RH+Br} \qquad (4)$$

by a factor of approximately 10^3. This difference in steric factors is thought to arise from the ease of approach to within bonding distance of the side-chain carbon of the benzyl radical by the relatively smaller hydrogen end of hydrogen bromide compared to the large bromine atoms in the bromine molecule. This question has been discussed previously in the case of neopentane.[3]

BOND DISSOCIATION ENERGIES

It is possible to determine $\mathrm{D(C_6H_5CH_2-H)}$ for toluene from the experimental activation energies reported here. The bond dissociation energy referred to is the enthalpy change of the reaction $\mathrm{RH=R+H}$ at T°K and a pressure of 1 atmos. The average activation energy, determined from Eqs. (III) and (IV) may be assigned to k_2, because $k_{app}\alpha I_0$ is practically temperature independent, and k_5 would also be temperature independent since the activation energy for the recombination of bromine atoms is considered to be zero. For the reaction

$$\mathrm{Br+RH=R+HBr}, \qquad (2)$$

$E_2=7.2$ kcal/mole. From a comparison of Eqs. (VI) and (XI), $(E_4-E_3)=5.0$ kcal/mole. Since reaction (3) is a quite exothermic radical reaction, we assume that it proceeds with practically zero activation energy. Therefore, $E_4=5.0$ kcal/mole for the reaction

$$\mathrm{R+HBr=RH+Br}. \qquad (4)$$

Clearly, this is a minimum value for E_4, the value being higher if E_3 has a small positive value.

Activation energies of reactions 2 and 4 may be combined to obtain the enthalpy change for the reaction

$$\mathrm{Br+RH=R+HBr}$$

at the mean temperature of the experiments, 381°K. Because there is no volume change in the reaction, we may write

$$\Delta H_{381}=\Delta E_{381}=E_2-E_4=7.2-5.0=2.2 \text{ kcal/mole}$$

with an estimated probable error of ±1.3 kcal. Using the value of the Bureau of Standards[15] for the heat of dissociation of hydrogen bromide, one obtains $\mathrm{D(C_6H_5CH_2-H)}$ in toluene at 381°K in the following manner:

$\mathrm{Br+RH=R+HBr}$	$\Delta H_{381}=2.2$ kcal
$\mathrm{HBr=H+Br}$	$\Delta H_{381}=87.7$ kcal
$\mathrm{RH=R+H}$	$\Delta H_{381}=89.9$ kcal

or $\mathrm{D(C_6H_5CH_2-H)}=89.9$ kcal/mole.

The heat of formation of the benzyl radical may be computed from the value of the C−H bond dissociation energy and the heats of formation of toluene[15] and the hydrogen atom[15] by means of the equation

$$\Delta H_f(\mathrm{R})=\Delta H_f(\mathrm{RH})-\Delta H_f(\mathrm{H})+D(\mathrm{R-H}).$$

The values thus determined are listed in Table V together with the bond dissociation energies at several temperatures, the temperature dependence having been evaluated as was done previously.[1,3]

TABLE V. Heats of formation and dissociation.

T°K	$\Delta H_f(R)$ kcal/mole	$D(R-H)$ kcal/mole
0	53.9±1.4	88.1±1.4
298	49.4±1.4	89.5±1.4
381	48.4±1.4	89.9±1.4

The values of $D(\mathrm{R-H})$ reported here are significantly different from the value 77.5 obtained by Szwarc[6] from pyrolysis studies. This point has been discussed in considerable detail with Szwarc. Thus far it has not been possible to make any unimpeachable criticism of either the reliability of the data or the interpretation of them in both the pyrolytic method and the method of bromination kinetics. It may remain the task of still another independent technique to resolve this discrepancy.

[14] A. G. Nasini, Proc. Roy. Soc. (London) **A123**, 703 (1929).

[15] *Selected Values of Chemical Thermodynamic Properties*, Circ. 500, Natl. Bur. Standards (U. S. Government Printing Office, Washington, 1952).

Radial Distribution Functions and the Equation of State of Monatomic Fluids*†

ROBERT W. ZWANZIG, JOHN G. KIRKWOOD, KENNETH F. STRIPP, AND IRWIN OPPENHEIM
Sterling Chemistry Laboratory, Yale University, New Haven, Connecticut

(Received March 11, 1953)

An approximation is obtained for the radial distribution function in a fluid whose molecules interact with the Lennard-Jones potential. Calculations of the equation of state, the internal energy, and the compressibility are presented and compared with experiment. At temperatures and volumes higher than the critical, agreement with experiment is satisfactory. A systematic method is developed of modifying the theoretical radial distribution function so that calculated thermodynamic quantities agree with their experimental values. In the liquid phase, slight modifications are needed to obtain agreement with experiment.

IN a recent paper,[1] Kirkwood, Lewinson, and Alder reported calculations of thermodynamic properties of argon from an assumed interatomic potential and theoretically determined radial distribution functions. Some of their calculated quantities do not agree well with the known experimental values. Our purpose in this paper is to investigate the effects on thermodynamic properties of changing the interatomic potential and of making slight empirical modifications in the radial distribution functions. The procedure which is followed may be regarded as an experimental determination of the radial distribution function from equation of state data and the use of the theoretical distribution functions $g(x)$ as a first approximation. Thus it is found that a change in scale transforming $g(x)$ into $g(cx)$ brings the calculated and observed thermodynamic functions of argon into agreement, with values of the constant c differing only slightly from unity.

In Sec. II, we obtain the radial distribution function corresponding to an unmodified Lennard-Jones (LJ) potential: the radial distribution function computed by KLA (Kirkwood, Lewinson, and Alder[1]) with a modified (hard core cutoff) LJ potential is theoretically corrected for the change in potential. The equation of state corresponding to the unmodified LJ potential is compared with the results of KLA and with experiment. The new equation of state agrees better with experiment than the KLA equation at temperatures higher than the critical, and densities lower than the critical, and does not differ from it appreciably in the liquid region. In particular, the critical ratio $p_c v_c/RT_c$ agrees almost exactly with its experimental value.

In Sec. III, a systematic method is developed of modifying the theoretical radial distribution function so that calculated thermodynamic properties agree with their experimental values. This is accomplished by putting a parameter into the theoretically determined radial distribution function and empirically adjusting its value for some specified thermodynamic quantity. Values of this parameter, adjusted to give the right pressure, have been obtained along the liquid-vapor line and on the 25°C and 125°C isotherms. Values adjusted to give the correct internal energy have been obtained on the 25°C and 125°C isotherms. The modified radial distribution functions do not differ appreciably from their unmodified forms.

* This work was carried out with support from the U. S. Office of Naval Research under contract with Yale University.
† Contribution No. 1150 from the Sterling Chemistry Laboratory, Yale University.
[1] Kirkwood, Lewinson, and Alder, J. Chem. Phys. **20**, 929 (1952).

I.

In this section we will define some basic quantities and give the expressions which are used to calculate thermodynamic properties. Our notation for the most part follows that of KLA.

We will be concerned only with systems for which the total potential energy may be expressed as a sum of pair potentials. The potential $V(R)$ of a pair of molecules separated by a distance R is more conveniently expressed in reduced or dimensionless units,

$$V(R)=\epsilon\gamma(x), \qquad R=ax, \tag{1}$$

where ϵ is a characteristic energy and a is a characteristic length associated with the potential. The unmodified Lennard-Jones potential is

$$\gamma_L(x)=4\left(\frac{1}{x^{12}}-\frac{1}{x^6}\right); \quad 0<x<\infty, \tag{2}$$

and the modified LJ potential, which was used by KLA, is

$$\gamma_M(x)=\begin{cases}\infty; & 0<x<1\\ \gamma_L(x); & 1\leqslant x<\infty.\end{cases} \tag{3}$$

In the latter case, a hard core has been imposed on the LJ potential, so that the molecules may not approach each other closer than $x=1$ or $R=a$. The values of ϵ and a for argon were determined by Michels,[2] using the second virial coefficient method with the potential $\gamma_L(x)$. These values are

$$\epsilon=1.653\times10^{-14}\text{ erg}, \qquad a=3.405\times10^{-8}\text{ cm}.$$

The radial distribution function $g_0^{(2)}(R)$ is defined as the correlation function for the relative distance of a

[2] Michels, Wijker, and Wijker, Physica **15**, 627 (1949).

pair of particles when the fluid is in thermodynamic equilibrium; $Ng_0^{(2)}(R)/v$ is the average number of molecules per unit volume at a distance R from a given molecule, when the density of the fluid is N/v. We will use the symbol $g_0^{(2)}(R)$ for the true radial distribution function, the one which actually applies in the fluid. The function evaluated by KLA, by solving the Born-Green integral equation with the potential $\gamma_M(x)$ will be called $g_M(x)$. The one which we will use in Sec. II, corresponding to the potential $\gamma_L(x)$, will be called $g_L(x)$.

The radial distribution function depends on the density and temperature of the fluid. It is convenient to express these and other thermodynamic variables in reduced or dimensionless units,

$$\begin{aligned} v^* &= (1/Na^3)v, \\ p^* &= (a^3/\epsilon)p, \\ T^* &= (k/\epsilon)T = 1/\beta\epsilon, \end{aligned} \tag{4}$$

where v is the molar volume of the fluid, N is Avogadro's number, k is the Boltzmann constant, and p and T are pressure and temperature. If we express ϵ in ergs, then p has the units dynes/cm^2. The expressions for pressure and excess internal energy ($E^e = E - \frac{3}{2}NkT$), in terms of $g_0^{(2)}(x)$ and $\gamma(x)$, are

$$\Phi = \frac{pv}{RT} = \frac{p^*v^*}{T^*} = 1 - \frac{2\pi}{3v^*T^*}\int_0^\infty x^3\gamma'(x)g_0^{(2)}(x)dx, \tag{5}$$

$$E^e/N\epsilon = \frac{2\pi}{v^*}\int_0^\infty x^2\gamma(x)g_0^{(2)}(x)dx. \tag{6}$$

In actual calculations one would of course get different results with different potentials and radial distribution functions. We will call these Φ_L and $E_L{}^e$ when g_L and γ_L are used, and Φ_M and $E_M{}^e$ when g_M and γ_M are used.

Another thermodynamic quantity that can be calculated directly from the radial distribution function is the isothermal compressibility K,

$$\begin{aligned} K &= \frac{-1}{v}\left(\frac{\partial v}{\partial p}\right)_T \\ &= \frac{a^3v^*}{\epsilon T^*}\left\{1 + \frac{4\pi}{v^*}\int_0^\infty x^2[g_0^{(2)}(x) - 1]dx\right\}. \end{aligned} \tag{7}$$

This expression, which is derived by considering the fluctuations in density of a fluid, is of some interest because it is not necessary to know the potential explicitly in order to calculate the compressibility.

II.

The radial distribution functions $g_M(x)$ obtained by KLA lead to thermodynamic properties Φ_M and $E_M{}^e$ which do not agree well with their experimental values at all temperatures and densities. These functions were calculated by solving the Born-Green integral equation with the potential γ_M. The hard core cutoff leads to considerable simplification in the method of solution of the integral equation, but on the other hand, it causes complications in the use of the resulting radial distribution functions in calculating transport properties. Also, a potential with a hard core cutoff probably leads to too strong a repulsion. For these reasons, we have devised radial distribution functions to be used with the potential $\gamma_L(x)$:

TABLE I. Equation of state.

v^*	T^*	0.833	1.000	1.250	1.667	2.500	5.000
1.223	Φ_M	−0.594	−0.156	0.263	0.670	1.064	1.457
	Φ_L	−0.626	−0.196	0.213	0.603	0.972	1.308
1.484	Φ_M	−1.445	−0.734	−0.037	0.649	1.326	1.999
	Φ_L	−1.492	−0.796	−0.120	0.534	1.158	1.715
2.261	Φ_M	−2.433	−1.268	−0.116	1.018	2.138	3.244
	Φ_L	−2.506	−1.369	−0.259	0.810	1.822	2.693
3.633	Φ_M	−2.830	−1.382	0.052	1.468	2.855	4.223
	Φ_L	−2.923	−1.515	−0.137	1.188	2.430	3.480

$$g_L(x) = \begin{cases} g_M(1)\exp[-\beta\epsilon\gamma_L(x)]; & 0 < x \leqslant 1 \\ g_M(x); & 1 \leqslant x < \infty. \end{cases} \tag{8}$$

The core part of this $g_L(x)$ is chosen to fit smoothly onto the outer part. Its dependence on the potential is reasonable, since one might expect that at small separations, the repulsive force dominates the effect of the surrounding molecules. Also, there is some mathematical justification for using this core approximation. The Born-Green integral equation, in reduced units, is

$$\ln g(x) = -\beta\epsilon\gamma(x) + \frac{\pi}{v^*x}\int_{-\infty}^\infty K(x-s)s[g(s)-1]ds, \tag{9}$$

where the kernel $K(t)$ is

$$K(t) = \beta\epsilon\int_{|t|}^\infty (s^2 - t^2)\gamma'(s)g(s)ds. \tag{10}$$

Previous experience in solving this equation with the potential $\gamma_M(x)$ showed that the solution is not very sensitive to the exact form of the kernel. That is, if one solves this equation by an iteration process, several iterations may be made with the same kernel before the kernel has to be recalculated. Therefore, in solving this equation with the potential $\gamma_L(x)$, we used the kernel associated with γ_M and g_M.‡ The calculation was performed only at the highest fluid density for which $g_M(x)$ is known, $v^* = 1.223$. The result obtained is $g_L(x)$, Eq. (8). One should not be unduly concerned that $g_L(x)$ was not obtained by solving completely the Born-Green equation with the potential $\gamma_L(x)$ and its associated kernel, because the superposition principle used in deriving the Born-Green equation is probably least satisfactory when the molecules are close together, so

‡ Actually, the calculations were performed with the series expansion of x ln$g$ used by KLA. The quantities $\psi_0(x)$, $\psi_1(x)$, and $\psi_2(x)$ were calculated with the corresponding γ_M, g_M kernels.

that the result would be inaccurate for small separations anyway.

Table I contains the thermodynamic quantities Φ_L and Φ_M as functions of reduced density and temperature. The values of Φ_M are copied over from KLA for the sake of comparison. The values of Φ_L were calculated using Eq. (5), the potential $\gamma_L(x)$, and the radial distribution function $g_L(x)$. For any given temperature and density, the effect of changing from γ_M to γ_L is that the pressure is lowered. Intuitively, one might expect this, since there is less repulsion between the molecules

TABLE II. Critical constants.

	New (g_L)	Old (g_M)	Exptl.
p_c^*	0.147	0.199	0.116
v_c^*	2.89	2.59	3.17
T_c^*	1.48	1.43	1.25
Φ_c	0.287	0.358	0.294

when γ_L is used. The pressures at low temperatures and high densities were negative when γ_M was used and are slightly more negative here. This may be the result of several factors: the failure of the superposition principle, the poor convergence of the expansion method used by KLA to get $g_M(x)$, or the great sensitivity of Φ to small changes in $g(x)$. The latter possibility will be discussed further in Sec. III.

Using the information in Table I, the critical constants p_c^*, v_c^*, T_c^* were evaluated for the Φ_L equation of state. A combination of graphical and numerical methods was used to find the point of horizontal inflection on the critical $p-v$ isotherm. The results are

TABLE III. Equation of state of the gas.

Density (Amagat units)	Φ(exptl)	Φ_M	Φ_L	c
	25°C isotherm			
259	0.983	1.036	0.964	1.001
417	1.212	1.274	1.143	1.002
635	2.247	2.074	1.794	1.008
	150°C isotherm			
259	1.135	1.205	1.154	0.999
417	1.447	1.567	1.430	1.001
635	2.515	2.587	2.246	1.005

presented in Table II, and compared with the constants obtained by KLA for the potential $\gamma_M(x)$ and with experiment.[3] The critical temperature is increased by 4 percent when the potential is changed but the critical pressure and volume are considerably better. The critical ratio Φ_c is independent of the values chosen for a and ϵ and may be used as an absolute check. The critical ratio obtained with $\gamma_L(x)$ and $g_L(x)$ is quite close to its experimental value, differing from it by about 3 percent.

In Tables III and IV we compare the quantities Φ_L and Φ_M with their experimental[2,3] values on the 25°C and 125°C isotherms and along the liquid-vapor equilibrium line from the normal boiling point to the critical point. (In these calculations, Michel's values of a and ϵ were used to convert the experimental densities and temperatures to their reduced values, and the Φ's corresponding to these v^*'s and T^*'s were interpolated from Table I.) In the gas phase Φ_L is slightly further than Φ_M from experiment at high densities, and closer at low densities. Along the liquid-vapor line, both deviate considerably from experiment.

Table V contains a comparison of calculated compressibilities with experiment.[4] The calculations were performed using Eq. (7) for liquid argon at its boiling point under one atmosphere pressure.

Table VI contains a comparison of the computed excess internal energies $E^e{}_M$ and $E^e{}_L$ on the 25°C and 125°C isotherms.[5] At every point use of $g_L(x)$ has brought about better agreement with experiment.

TABLE IV. Equation of state on liquid-vapor line.

T°K	v^*	Φ(exptl)	Φ_M	Φ_L	c
89.9	1.223	0.004	−3.867	−3.941	1.026
97.7	1.268	0.011	−3.000	−3.056	1.023
111.9	1.372	0.026	−1.820	−1.923	1.018
122.3	1.475	0.048	−1.194	−1.303	1.014
137.6	1.725	0.106	−0.510	−0.604	1.011
147.9	2.173	0.181	−0.113	−0.200	1.007
150.7	3.165	0.292	0.175	0.099	1.006

III.

In Sec. II we pointed out that the radial distribution functions $g_M(x)$ and $g_L(x)$ are not identical with the true one, $g_0^{(2)}(x)$. This resulted in imperfect agreement between calculated and experimental pressures, internal energies, and compressibilities. The radial distribution functions are needed, in some cases with considerable accuracy, in the calculation of transport properties of liquids. A natural question is, how may we use the available experimental information about equilibrium properties to convert $g_M(x)$ or $g_L(x)$ into better approximations to $g_0^{(2)}(x)$? In the absence of a satisfactory theoretical method of accomplishing this, we wish to propose an empirical procedure.

Since the potential $\gamma_L(x)$ is more convenient than $\gamma_M(x)$ in the calculation of transport properties, and also probably a better approximation to the true potential, we will consider only systems in which the potential of interaction is $\gamma_L(x)$. The radial distribution function $g_L(x)$ is replaced by $g_L(cx)$, where c is a parameter, close to unity, and a function of temperature and density. Thermodynamic properties are calculated with

[3] *International Critical Tables* (McGraw-Hill Book Company, Inc., New York, 1928), Vol. 3, p. 203.

[4] Reference 3, page 20.

[5] Michels, Lunbeck, and Wolkers, Physica **15**, 689 (1949).

$g_L(cx)$ and the value of c is chosen so that the resulting quantities $\Phi_L(c)$, $K_L(c)$, or $E_L{}^e(c)$ agree with experiment. Kirkwood and Buff used a procedure like this in their calculations of the surface tension[6] and viscosity[7] of liquid argon. They used a "peak" approximation to $g_0{}^{(2)}(x)$, containing two parameters, and adjusted these to give the correct pressure and internal energy. Their results indicate that this procedure is fairly successful. In this article, we use a better starting approximation to $g_0{}^{(2)}(x)$ and only one adjustable parameter. We chose the dependence of $g_L(x)$ on c to be $g_L(cx)$ for two reasons: calculations of the dependence of thermodynamic properties on c are particularly simple in this form, and the general shape of $g_L(x)$ is maintained. Although the distance between the nodes of $g_L(x)-1$ for large x is changed, there is only a slight change in the first peak, which is the significant one for most calculations.

The equations for $\Phi_L(c)$, $E_L{}^e(c)$, and $K_L(c)$ are obtained easily by substitution of $g_L(cx)$ for $g_L(x)$ in Eqs. (5), (6), and (7) and transforming the variable of integration. They are

$$\Phi_L(c)=1-\frac{2\pi}{3v^*T^*}\left\{c^3\int_0^\infty x^3\gamma_L'(x)g_L(x)dx - 48c^3(c^6-1)\int_0^\infty x^{-10}g_L(x)dx\right\}, \quad (11)$$

$$E_L{}^e(c)=\frac{2\pi}{v^*}\left\{c^3\int_0^\infty x^2\gamma_L(x)g_L(x)dx + 4c^3(c^6-1)\int_0^\infty x^{-10}g_L(x)dx\right\}, \quad (12)$$

$$K_L(c)=\frac{a^3v^*}{\epsilon T^*}\left\{1+\frac{4\pi}{v^*c^3}\int_0^\infty x^2[g_L(x)-1]dx\right\}, \quad (13)$$

where all the integrals are now evaluated with the original $g_L(x)$.

TABLE V. Compressibility.

K_{exptl}	4.65×10^{-3}
K_M	6.76×10^{-3}
K_L	7.67×10^{-3}
$K_L(c=1.026)$	7.40×10^{-3}
$c_{\text{exptl}}=1.76$	

Values of c are given in Tables III, IV, V, and VI. They are always close to unity, indicating that only very small changes in $g_L(x)$ are needed in order to get agreement with experiment, except in the case of the compressibility at the normal boiling point, where a value $c=1.76$ is needed.

In Table VII we compare the values of c required to fit the experimental pressure with values of c to fit the internal energy, along the 25°C and 125°C isotherms. It is clearly impossible to fit both properties with the same value of c. Although Φ_L is negative along the liquid-vapor line (Table IV), the values of c needed to obtain agreement with experiment are small, varying between 1.006 and 1.026. If Φ_L is computed at v^* and T^* corresponding to the experimental critical volume and temperature, $c=1.006$ is needed to fit the critical pressure. At the density and temperature corresponding to the normal boiling point, $c=1.026$ is required. This modification in the shape of the radial distribution function, a displacement of the first peak by several percent, changes the pressure by a factor of 10^3.

TABLE VI. Excess internal energy of the gas.

Density (Amagat units)	$-E^e$(exptl)	$-E^e{}_M$	$-E^e{}_L$	c
		25°C isotherm		
259	390	442	411	1.016
417	611	726	670	1.021
635	893	1160	1057	1.028
		125°C isotherm		
259	362	433	389	1.015
417	567	718	644	1.022
635	805	1154	1015	1.028

TABLE VII.

Density (Amagat units)	25°C		125°C	
	$c(\Phi)$	$c(E^e)$	$c(\Phi)$	$c(E^e)$
259	1.001	1.016	0.999	1.015
417	1.002	1.021	1.001	1.022
635	1.008	1.028	1.005	1.028

In future work on the calculation of equilibrium and transport properties of liquids, we suggest that, until better radial distribution functions become available, the function $g_L(cx)$ be used. The values of c should be determined by fitting some appropriate thermodynamic property, for example, the pressure.

[6] J. G. Kirkwood and F. P. Buff, J. Chem. Phys. **17**, 338 (1949).
[7] Kirkwood, Buff, and Green, J. Chem. Phys. **17**, 988 (1949).

A Theory of the Linear Viscoelastic Properties of Dilute Solutions of Coiling Polymers

PRINCE E. ROUSE, JR.
The Franklin Institute, Laboratories for Research and Development, Philadelphia, Pennsylvania
(Received January 27, 1953)

The necessary coordination of the motions of different parts of a polymer molecule is made the basis of a theory of the linear viscoelastic properties of dilute solutions of coiling polymers. This is accomplished by use of the concept of the submolecule, a portion of polymer chain long enough for the separation of its ends to approximate a Gaussian probability distribution. The configuration of a submolecule is specified in terms of the vector which corresponds to its end-to-end separation. The configuration of a molecule which contains N submolecules is described by the corresponding set of N vectors.

The action of a velocity gradient disturbs the distribution of configurations of the polymer molecules away from its equilibrium form, storing free energy in the system. The coordinated thermal motions of the segments cause the configurations to drift toward their equilibrium distribution. The coordination is taken into account by the mathematical requirement that motions of the atom which joins two submolecules change the configurations of both submolecules. By means of an orthogonal transformation of coordinates, the coordination of all the motions of the parts of a molecule is resolved into a series of modes. Each mode has a characteristic relaxation time. The theory produces equations by means of which the relaxation times, the components of the complex viscosity, and the components of the complex rigidity can be calculated from the steady flow viscosities of the solution and the solvent, the molecular weight and concentration of the polymer, and the absolute temperature.

Limitations of the theory may arise from the exclusion from consideration of (1) very rapid relaxation processes involving segments shorter than the submolecule and (2) the obstruction of the motion of a segment by other segments with which it happens to be in contact. Another possible cause of disagreement between the theory and experimental data is the polydispersity of any actual polymer; this factor is important because the calculated relaxation times increase rapidly with increasing molecular weight.

INTRODUCTION

THE unusual elastic and flow properties of systems containing linear polymeric molecules arise from three factors: (1) the length of the polymer molecules, (2) the flexibility of the molecular chains, and (3) the interactions of the segments of a polymer molecule with other segments of the same and other polymer molecules.[1] For such a threadlike molecule to move through its surroundings it must *coordinate* the thermal motions of relatively short segments of the chain.[2] In diffusion and steady flow experiments, only the resultant of the coordinated segmental motions is measured; theories of such phenomena can be developed without analysis of the motions of the molecule as the sum of the motions of its parts. Certain other properties, such as creep, stress relaxation, and dynamic viscosity and rigidity, are functions of time or frequency.[3] Theories of these phenomena must take into account the necessary coordination of the motions of the segments of the polymer molecules.

The physical concept which is the basis of the theory presented here is that a velocity gradient in a solution of a linear polymer continuously alters the distribution of configurations of the polymer molecules. The coordinated thermal motions of the segments of the polymer molecules cause the configurations to drift continuously toward their most probable distribution. The calculation resolves the coordination of the motions of the parts of a polymer molecule into a series of modes; each mode has a characteristic relaxation time. Direct contacts of a segment with segments of other molecules and with remotely connected segments of the same molecule are considered as contributing to the viscous forces which oppose the thermal motions. In its present form the theory does not take into account the obstruction of the motions of a segment by other segments with which it happens to be in contact. Consequently, the agreement between the present theory and experimental data may be expected to be reasonably satisfactory only for dilute solutions of polymers in which intermolecular contacts are relatively infrequent. Modification of the theory to take better account of the effects of interactions should improve the agreement for dilute solutions and make possible the application of the results to the properties of concentrated solutions and of undiluted polymer.

MOTION OF THE LIQUID

It will be assumed that the shearing stress is applied to the liquid by a plane surface lying in the plane $z=0$ of a right-handed system of Cartesian coordinates. The surface executes simple harmonic motions in the x direction with an angular frequency ω and a maximum

[1] Relaxation processes arising from chemical scission of the polymer chains at elevated temperatures [see e.g., A. V. Tobolsky and R. D. Andrews, J. Chem. Phys. **13**, 3 (1945)] are not considered in this calculation.

[2] W. Kauzmann and H. Eyring, J. Am. Chem. Soc. **62**, 3113 (1940).

[3] See e.g., W. Philippoff, Physik. Z. **35**, 884, 900 (1934); A. P. Aleksandrov and Y. S. Lazurkin, J. Tech. Phys. (USSR) **9**, 1249, 1261, 1267 (1939); Gehman, Woodford, and Stambaugh, Ind. Eng. Chem. **33**, 1032 (1941); H. Leaderman, *Elastic and Creep Properties of Filamentous Materials and Other High Polymers* (Textile Foundation, Washington, 1943); Andrews, Hofman-Bang, and Tobolsky, J. Polymer Sci. **3**, 669 (1948); Mason, Baker, McSkimin, and Heiss, Phys. Rev. **73**, 1074, 1873 (1948); *ibid.* **75**, 936 (1949); Marvin, Fitzgerald, and J. Ferry, J. Appl. Phys. **21**, 197 (1950); A. W. Nolle, J. Polymer Sci. **5**, 1 (1950); Ferry, Fitzgerald, Johnson, and Grandine, J. Appl. Phys. **22**, 717 (1951); H. Lederman and R. G. Smith, Phys. Rev. **81**, 303 (1951); R. S. Marvin, Ind. Eng. Chem. **44**, 696 (1952); Ferry, Fitzgerald, Grandine, and Williams, Ind. Eng. Chem. **44**, 703 (1952); R. D. Andrews, Ind. Eng. Chem. **44**, 707 (1952).

velocity v_0. The liquid is assumed to extend to infinity in the direction of z positive. Under these conditions the motion of the liquid[4] can be represented by

$$\dot{x}=v_0\epsilon^{-\Gamma z}e^{i\omega t},\quad \dot{y}=0,\quad \dot{z}=0,\quad \Gamma=(i\omega\rho_l/\eta)^{\frac{1}{2}}. \quad (1)$$

In these equations i is $(-1)^{\frac{1}{2}}$, ρ_l is the density of the liquid and η is its viscosity. For polymer solutions it is necessary to replace η by the complex viscosity,[5] $\eta^*=\eta_1-i\eta_2$. The concept of a complex viscosity has meaning only when steady-state conditions have been established under the influence of a sinusoidally varying shearing stress. The real and imaginary parts of the complex viscosity correspond to the components of the shearing stress which are, respectively, in phase and out of phase with the resultant gradient of velocity.

The waves represented by Eq. (1) are strongly damped. For toluene at 30°C, the viscosity is 0.606 centipoise and the density is 0.856 g/ml; according to Eq. (1) the distance in which the amplitude of the velocity is reduced by a factor e^{-1} is 0.0034 cm if the applied frequency is 200 cycles per sec. At a frequency of 60 kc this distance is only 0.00019 cm. The very rapid attenuation of these waves prevents reflected waves of appreciable amplitude even in relatively thin layers of liquid. Accordingly, only the outgoing wave need be considered and Eq. (1) applies.

The gradient of velocity varies rapidly with z, the distance from the oscillating surface. For mathematical reasons it is necessary to assume in this calculation that, at any instant, the velocity gradient, $\alpha=\partial\dot{x}/\partial z$, has a single value over the entire volume pervaded by a polymer molecule. The variation of α with z is expressed in terms of ϵ, the distance from the arbitrary plane $z=z_0$, by the equation

$$\alpha_{z=z_0+\epsilon}=-v_0\Gamma e^{-\Gamma z_0}e^{i\omega t}[1-\Gamma\epsilon+\Gamma^2\epsilon^2/2\cdots]. \quad (2)$$

The value of $|\alpha|$ will vary less than five percent from its value at $z=z_0$ in the range for which $|\Gamma\epsilon|<0.05$. The range to which ϵ is restricted by this condition decreases with increasing frequency. For a very dilute solution in toluene, the condition restricts $|\epsilon|$ to values below 700A at an applied frequency of 60 kc. The assumption would be reasonably satisfactory under these conditions for molecular configurations whose extension did not exceed 1400A. The root-mean-square separation of the ends of the polystyrene molecules in a toluene solution of a polymer with a molecular weight of 1.61×10^6 was found by Outer, Carr, and Zimm[6] to be about 1300A. The imperfection of the assumption at high frequencies for solutions of very long molecules in solvents of low viscosity is apparent. Data available at present[7] indicate that this does not produce large discrepancies between theory and observation.

MODEL OF POLYMER MOLECULE

The kinetic theory of the equilibrium elastic modulus of rubber[8] is based upon finding an approximate value of the probability $p(x, y, z)dxdydz$ that one end of a molecule will be in the volume element $dxdydz$ in the neighborhood of (x, y, z) when the other end is fixed at the origin of coordinates. For a chain of n freely jointed links, each of length l, the result is

$$p(x, y, z)dxdydz=(b^3/\pi^{\frac{1}{2}})\exp[-b^2(x^2+y^2+z^2)]dxdydz,$$

where b^2 has the value $3/(2nl^2)$. In obtaining this result it is assumed that this probability is proportional to the number of configurations available to the molecule when its ends are in the specified positions. This assumption is satisfactory if the group of molecules corresponding to each value of the end-to-end vector is randomly distributed over the set of available configurations. This condition is attained at equilibrium, i.e., at very long times. It is not attained when a rubber or a solution of a linear polymer is subjected to a force or a deformation which changes with time. Under such conditions the configurations of the molecules are continuously altered in a systematic way. As a result the configurations of the group of molecules which have any particular end-to-end vector are not randomly distributed over all possible configurations consistent with the length of the end-to-end vector. This makes it necessary to specify the configurations of the molecules in more detail than is required in the equilibrium theory, in which the end-to-end vector suffices.

A complete description of the configuration of each molecule requires the specification of the orientation of each chemical bond in the molecular chain. Such a description was used by Kirkwood[9] in a completely general theory of the viscoelastic properties of solutions of linear polymers. The results of the calculation are in a form which cannot readily be used for calculation or comparison with experimental data.

In the calculation presented here mathematical simplicity is achieved with some loss in generality by use of a less detailed description of the configuration of a molecule. The molecule is divided up into N equal submolecules. Each submolecule is a portion of polymer chain just long enough so that, at equilibrium, the separation of its ends obeys, to a first approximation, a Gaussian probability function; i.e., if one end of a submolecule is located at the origin of a system of Cartesian coordinates, the probability $\psi(x, y, z)dxdydz$ that the other end will be in the volume element $dxdydz$ lying between x and $x+dx$, y and $y+dy$, z and $z+dz$ is

[4] H. Lamb, *Hydrodynamics* (Dover Publications, New York, 1945), p. 619.
[5] A. Gemant, Trans. Faraday Soc. **31**, 1582 (1935).
[6] Outer, Carr, and Zimm, J. Chem. Phys. **18**, 830 (1950).
[7] P. E. Rouse, Jr., and K. Sittel, J. Appl. Phys. (to be published).
[8] L. R. G. Treloar, *Physics of Rubber Elasticity* (Oxford University Press, London, 1949).
[9] J. G. Kirkwood, Rec. Trav. Chim. Pays-Bas **68**, 649 (1949).

given approximately by

$$\psi(x, y, z)dxdydz = (\beta/\pi)^{\frac{3}{2}} \times \exp[-\beta(x^2+y^2+z^2)]dxdydz. \quad (3)$$

In this expression $\beta=3/(2\sigma^2)$, where σ^2 is the mean-square separation of the ends of a submolecule.

In this calculation each submolecule has its own private system of Cartesian coordinates. The origin of the system of the jth submolecule is located at the atom which joins the $(j-1)$th and the jth submolecules; the axes are oriented parallel to the corresponding axes of the system used to describe the motion of the liquid. The coordinates x_j, y_j, z_j give the location in this private system of the atom which connects the jth and $(j+1)$th submolecules. The configuration of a molecule composed of a series of N submolecules is described by specifying the components of each of the set of N vectors which give the position of the end of each submolecule with respect to the end of the preceding submolecule. This is equivalent to representing the configuration by a point in a "phase space" of $3N$ dimensions.

It is assumed that the probability, $\Psi_i d\phi_i$, of a molecule having a configuration corresponding to a point in the volume element $d\phi_i$ lying between x_1 and x_1+dx_1, y_1 and y_1+dy_1, z_1 and z_1+dz_1, x_2 and $x_2+dx_2, \cdots$, z_N and z_N+dz_N is proportional to the number of configurations of the molecule which are represented by points in that element of volume. This number of configurations is the product of the numbers of configurations of each of the submolecules having the requisite end-to-end separations; it follows that

$$\Psi_i d\phi_i = \prod_{j=1}^{N} \psi(x_j, y_j, z_j)dx_j dy_j dz_j = (\beta/\pi)^{3N/2} \exp\left[-\beta \sum_{j=1}^{N} (x_j^2+y_j^2+z_j^2)\right] \times dx_1 dy_1 dz_1 dx_2 \cdots dz_N. \quad (4)$$

This assumption is equivalent to the assumption that the configurations of the group of submolecules which, at any instant, have a particular end-to-end separation are randomly distributed over all available configurations consistent with that end-to-end separation. The significance of this assumption for a dynamic measurement made at the angular frequency ω can be seen by considering a group of submolecules each of whose ends are fixed at points the separation of which is small compared to the length of a fully extended submolecule. A small, rapid increase in the separation of the fixed ends of each submolecule will result in the submolecules having configurations which are not randomly distributed over the available configurations. After a time the thermal motions will re-establish a random distribution. If this time is small compared to ω^{-1} the assumption will be valid.

MOTION OF THE POLYMER MOLECULES

A velocity gradient in a solution of a linear polymer produces motions of the polymer molecules which are resolved in this calculation into two components; (1) a motion of the atom at each junction between two submolecules with a velocity equal to that of the surrounding liquid, and (2) the coordinated Brownian motions of the segments of each polymer molecule by which the configurations drift toward their equilibrium distribution. The justification of this procedure rests on the flexibility of the polymer molecules. For each part of a molecule to move with the velocity of the surrounding liquid the configuration of the molecule must be able to change as rapidly as required by the gradient of velocity of the liquid. If the polymer molecule were not sufficiently flexible to allow this rapid change of configuration, the presence of a gradient of velocity in the solution would always entail motion of the solvent relative to the atomic groups of the polymer chain. The relative motions would cause dissipation of energy and the contribution of the polymer to the real part of the complex viscosity would remain large at all frequencies. Actually, the experimental data[7,10,11] indicate that at high frequencies the viscous losses caused by the polymer molecules approach zero. For example, Mason[10] reports measurements made on a solution in cyclohexane of a polyisobutylene with a molecular weight of 3.93×10^6; the solution contained one gram of polymer per 100 ml and had a relative viscosity in steady flow of 30. At 14 megacycles, "the indicated viscosity is only about 10 percent higher than that for the pure solvent alone."[10]

These data strongly support the validity of the assumption that the *primary* effect of the velocity gradient is to carry each segment of each polymer molecule along with the liquid, at least for velocity gradients of the magnitudes encountered in these measurements.

In the calculation the motions of the polymer molecules are expressed in terms of the motions of their representative points in the configuration space. The value of $(\dot{x}_j)_\alpha$, the component in the x_j direction of the velocity of a point caused directly by the velocity gradient α of the liquid, is equal to the difference between the x components of the velocity of the liquid at the two ends of the jth submolecule. Thus

$$(\dot{x}_j)_\alpha = z_j \partial\dot{x}/\partial z = \alpha z_j. \quad (5)$$

Since the velocity of the liquid has a nonvanishing component only in the x direction, the components $(\dot{y}_j)_\alpha$ and $(\dot{z}_j)_\alpha$ are zero.

The calculation of the second component of the motions of the polymer molecules—the diffusional motion by which their distribution of configurations moves toward its equilibrium form—is the central

[10] W. P. Mason, *Piezoelectric Crystals and Their Applications to Ultrasonics* (D. Van Nostrand Company, Inc., New York, 1950), p. 351.

[11] Baker, Mason, and Heiss, J. Polymer Sci. 8, 129 (1952).

part of the theory. This calculation requires first the evaluation of the effect of the perturbation of the distribution of configurations of the polymer molecules upon the thermodynamic potentials of the molecules. This is accomplished by calculating the effect of the velocity gradient α upon the entropy of the ν polymer molecules contained in a volume V of solution. The procedure is a generalization of the one used by Wall[12] in his calculation of the entropy changes produced by elongation of a piece of rubber. The average number of molecules whose representative points lie in the volume element $d\phi_i$ at equilibrium is $n_i=\nu\Psi_i d\phi_i$. If the number of representative points in $d\phi_i$ under the influence of the perturbing velocity gradient is s_i, the change in entropy of the volume V of solution is given by Wall's equation[12]

$$\Delta S=k\sum_i s_i\ln(n_i/s_i). \tag{6}$$

The increase in the Helmholtz free energy is $\Delta A=-T\Delta S$, since it is assumed that all configurations have the same internal energy.

The change in the free energy of the system caused by entrance of a molecule into $d\phi_i$ is

$$\mu_i=\partial(\Delta A)/\partial s_i=kT[1+\ln(s_i/n_i)]. \tag{7}$$

The quantity μ_i is the thermodynamic potential of the polymer molecules in the volume element $d\phi_i$.

The tendency of the free energy of the system to seek a minimum value provides the directing force which impels the configurations of the molecules toward their most probable distribution. The thermal motions of the submolecules produce a flow along each of the coordinates used in describing the configurations. The velocity of the flow along a particular coordinate is taken as the product of the mobility of the end of a submolecule and the negative of the total change in thermodynamic potential of the molecule resulting from a displacement along that coordinate. The validity of this procedure relies upon the legitimacy of the use of thermodynamic functions outside of equilibrium conditions. The conditions under which procedures of this kind are permissible have been discussed by several authors.[13] Comparison of their conclusions with the present calculation suggests that the procedure will give a valid result if the perturbation of the distribution of configurations is small. This condition can be stated quantitatively in terms of an expansion of s_i as a power series in α,

$$s_i=n_i(1+\alpha f+\alpha^2 g+\alpha^3 h+\cdots).$$

The perturbation is sufficiently small if all terms of the expansion which contain powers of α higher than the first can be neglected. The potential μ of a molecule can then be written

$$\mu=kT[1+\ln(1+\alpha f)], \tag{8}$$

where μ and f are functions of the $3N$ coordinates. If α is a sinusoidal function of time, $\alpha=\alpha_0 e^{i\omega t}$, μ and f will be complex, while if α is a constant (steady flow), μ and f will be real.

The calculation of the rate of the configurational diffusion of the polymer molecules is based on consideration of the s_i molecules whose configurations at the time t correspond to points in the volume element $d\phi_i$; although $d\phi_i$ is infinitesimal in volume, the number s_i can be made large enough for statistical treatment by letting the volume V of solution be very large. Motion of the point representing one of these molecules along the x_j coordinate can take place by the displacement in the x direction of the end either of the $(j-1)$th submolecule or of the jth submolecule. Motion of the end of the $(j-1)$th submolecule, with the ends of all other submolecules held fast, changes the values of x_{j-1} and x_j by amounts which are equal in magnitude and opposite in sign. The average velocity of the representative points along the x_j coordinate resulting from thermal motions of the end of the $(j-1)$th submolecule of each of the s_i molecules is

$$(\dot{x}_j)_{j-1}=-B\left[\frac{\partial\mu}{\partial x_j}-\frac{\partial\mu}{\partial x_{j-1}}\right].$$

The symbol B represents the mobility of the end of a submolecule; it will be discussed in the following paragraph. In addition to $(\dot{x}_j)_{j-1}$, an average velocity of the representative points along the x_j coordinate results from thermal motions of the end of the jth submolecule of each of the s_i molecules. It is

$$(\dot{x}_j)_j=-B\left[\frac{\partial\mu}{\partial x_j}-\frac{\partial\mu}{\partial x_{j+1}}\right].$$

The sum of these velocities is the total velocity of diffusion of the points in $d\phi_i$ along the x_j coordinate.

$$(\dot{x}_j)_D=-B\left[-\frac{\partial\mu}{\partial x_{j-1}}+2\frac{\partial\mu}{\partial x_j}-\frac{\partial\mu}{\partial x_{j+1}}\right]. \tag{9}$$

Similar equations will hold for $(\dot{y}_j)_D$ and $(\dot{z}_j)_D$.

The meaning of the mobility B can be made clear by consideration of a large number of polymer chains each equal in length to two submolecules. Choose a distance, a, which is small compared to the length of two fully extended submolecules. Fix one end of each chain at the origin of a private system of Cartesian coordinates; fix the other end at the point $(a, 0, 0)$ of the local coordinate system. The central atom of each chain marks the end of a submolecule. At equilibrium the central atoms have coordinates which are distributed approximately in accordance with the probability density

$$p(x, y, z)=(2\beta/\pi)^{\frac{3}{2}}\exp\{-2\beta[(x-a/2)^2+y^2+z^2]\},$$

[12] F. T. Wall, J. Chem. Phys. **10**, 132, 485 (1942).

[13] S. R. de Groot, *Thermodynamics of Irreversible Processes* (North-Holland Publishing Company, Amsterdam, 1951), pp. 11, 221.

and the average velocity of central atoms located in the neighborhood of (x, y, z) of their respective coordinate systems is zero. If the central atom of each chain is now subjected to a small steady force δF, these atoms will have a small average velocity δv in the direction of the force. It is required that δF be so small that the configurations of the submolecules will always be randomly distributed over the available configurations. The value of δv will change as the distribution of the central atoms becomes significantly different from the equilibrium distribution. The initial value of the ratio of the velocity to the force $(\delta v/\delta F)_0$, is the mobility B of the end of a submolecule. It is clear that B depends upon the viscous forces exerted by the medium along the entire length of chain between the two fixed ends. If the length of chain included in a submolecule were increased above the minimum length which will obey Eq. (3), the viscous forces acting along the chain would be proportionately increased. Thus the mobility B would be inversely proportional to the length of chain included in the submolecule.

The viscous reaction of the medium to motions of the polymer segments depends, of course, on the local concentration of polymer segments. Since this must fluctuate with time and, further, must depend somewhat on the position of the submolecule along the chain, the value of B in Eq. (9) is an average over all the submolecules in the solution.

The set of N partial differential equations which give the components of the motion of the polymer molecules in the various x directions can be summarized in the form of a matrix[14] equation.

$$\mathbf{x}_t = \alpha\mathbf{z} - B\mathbf{A}\{\nabla_x\mu\}. \tag{10a}$$

In this equation $\mathbf{x}_t$, $\mathbf{z}$, and $\{\nabla_x\mu\}$ are column vectors with the forms

$$\mathbf{x}_t = \{\dot{x}_1, \dot{x}_2, \dot{x}_3, \cdots, \dot{x}_N\},$$
$$\mathbf{z} = \{z_1, z_2, z_3, \cdots, z_N\},$$
$$\{\nabla_x\mu\} = \{\partial\mu/\partial x_1, \partial\mu/\partial x_2, \partial\mu/\partial x_3, \cdots, \partial\mu/\partial x_N\}.$$

and $\mathbf{A}$ is the square matrix of order N

$$\mathbf{A} = \begin{bmatrix} 2 & -1 & 0 & 0 & 0 & \cdots & 0 & 0 & 0 \\ -1 & 2 & -1 & 0 & 0 & \cdots & 0 & 0 & 0 \\ 0 & -1 & 2 & -1 & 0 & \cdots & 0 & 0 & 0 \\ 0 & 0 & -1 & 2 & -1 & \cdots & 0 & 0 & 0 \\ 0 & 0 & 0 & -1 & 2 & \cdots & 0 & 0 & 0 \\ \cdot & \cdot & \cdot & \cdot & \cdot & \cdots & \cdot & \cdot & \cdot \\ \cdot & \cdot & \cdot & \cdot & \cdot & \cdots & \cdot & \cdot & \cdot \\ \cdot & \cdot & \cdot & \cdot & \cdot & \cdots & \cdot & \cdot & \cdot \\ 0 & 0 & 0 & 0 & 0 & \cdots & 2 & -1 & 0 \\ 0 & 0 & 0 & 0 & 0 & \cdots & -1 & 2 & -1 \\ 0 & 0 & 0 & 0 & 0 & \cdots & 0 & -1 & 2 \end{bmatrix}$$

The sets of equations for the motions in the y directions and z directions are written in the analogous forms

$$\mathbf{y}_t = -B\mathbf{A}\{\nabla_y\mu\}, \tag{10b}$$

$$\mathbf{z}_t = -B\mathbf{A}\{\nabla_z\mu\}. \tag{10c}$$

The solution of the problem requires a transformation of the original system of $3N$ coordinates into a system in which the component of the velocity of diffusion along each coordinate is a function of the partial derivative of μ with respect to that coordinate alone. This is performed by determining the orthogonal matrix $\mathbf{R}$ such that

$$\mathbf{R}^{-1}\mathbf{A}\mathbf{R} = \mathbf{\Lambda} = [\lambda_p\delta_{pq}], \tag{11}$$

where λ_p is the pth eigenvalue of the set of N eigenvalues of $\mathbf{A}$ and δ_{pq} is the Kronecker delta.

$$\delta_{pq} = \begin{cases} 0; & p \neq q \\ 1; & p = q. \end{cases}$$

The eigenvalues λ_p of the matrix $\mathbf{A}$ are related to the index p and the number of submolecules N by the equation

$$\lambda_p = 4\sin^2\frac{p\pi}{2(N+1)}. \tag{11a}$$

As the new coordinates we take the system $u_1, v_1, w_1, \cdots, u_p, v_p, w_p, \cdots, u_N, v_N, w_N$, which are related to the original coordinates by the three sets of equations

$$\mathbf{u} = \mathbf{R}^{-1}\mathbf{x}, \tag{12a}$$

$$\mathbf{v} = \mathbf{R}^{-1}\mathbf{y}, \tag{12b}$$

$$\mathbf{w} = \mathbf{R}^{-1}\mathbf{z}. \tag{12c}$$

Multiplying Eq. (10a) by $\mathbf{R}^{-1}$ and making use of the fact that $\mathbf{R}\mathbf{R}^{-1} = \mathbf{E}$, the unit matrix, produces the equation

$$\mathbf{R}^{-1}\mathbf{x}_t = \alpha\mathbf{R}^{-1}\mathbf{z} - B\mathbf{R}^{-1}\mathbf{A}\mathbf{R}\mathbf{R}^{-1}\{\nabla_x\mu\}. \tag{13}$$

From Eq. (12a) it can be shown that

$$\{\nabla_x\mu\} = \tilde{\mathbf{R}}^{-1}\{\nabla_u\mu\}, \tag{14}$$

where

$$\{\nabla_u\mu\} = \{\partial\mu/\partial u_1, \partial\mu/\partial u_2, \partial\mu/\partial u_3, \cdots, \partial\mu/\partial u_N\}.$$

Since $\mathbf{R}$ is orthogonal (14) can be written

$$\mathbf{R}^{-1}\{\nabla_x\mu\} = \{\nabla_u\mu\},$$

and Eq. (13) becomes

$$\mathbf{u}_t = \alpha\mathbf{w} - B\mathbf{\Lambda}\{\nabla_u\mu\}. \tag{15a}$$

Application of the treatment given (10a) to (10b) and (10c) gives the result,

$$\mathbf{v}_t = -B\mathbf{\Lambda}\{\nabla_v\mu\}, \tag{15b}$$

$$\mathbf{w}_t = -B\mathbf{\Lambda}\{\nabla_w\mu\}. \tag{15c}$$

[14] The matrix notation and terminology used here are taken from H. Margenau and G. M. Murphy, *The Mathematics of Physics and Chemistry* (D. Van Nostrand Company, Inc., New York, 1943), Chapter 10.

The effect of the orthogonal transformation on the expression for Ψ, the probability density of configurations, can be seen by noting that the coordinates appear only in the term

$$\sum_{j=1}^{N}(x_j^2+y_j^2+z_j^2).$$

This summation is the square of the length of the vector drawn to the representative point from the origin of configuration space. Since the length of a vector is unchanged by an orthogonal transformation, the expression for Ψ in the new coordinates is

$$\Psi(u_1, v_1, w_1, u_2, \cdots, w_N) = (\beta/\pi)^{3N/2}\exp\left[-\beta\sum_{p=1}^{N}(u_p^2+v_p^2+w_p^2)\right]. \quad (16)$$

The volume element $dx_1dy_1dz_1dx_2\cdots dz_N$ transforms into the volume element $du_1dv_1dw_1du_2\cdots dw_N$. The transformation, therefore, leaves unchanged both the equilibrium density of points in configuration space

$$\rho_0=n_i/d\phi_i=\nu\Psi, \quad (17)$$

and the density at time t

$$\rho=s_i/d\phi_i=n_i(1+\alpha f)/d\phi_i=\nu\Psi(1+\alpha f). \quad (18)$$

The function f can be found by solving the equation of continuity

$$\dot{\rho}=-\operatorname{div}(\rho\mathbf{V}), \quad (19)$$

where $\mathbf{V}$, the vector velocity of the representative points is given by Eqs. (15a), (15b), and (15c). The divergence of the flux density is

$$\operatorname{div}(\rho\mathbf{V})=\sum_{p=1}^{N}\left[\frac{\partial(\rho\dot{u}_p)}{\partial u_p}+\frac{\partial(\rho\dot{v}_p)}{\partial v_p}+\frac{\partial(\rho\dot{w}_p)}{\partial w_p}\right]. \quad (20)$$

We will evaluate first $\partial(\rho\dot{u}_p)/\partial u_p$. From (15a) and (18)

$$\rho\dot{u}_p=\nu\Psi(1+\alpha f)\left[\alpha w_p-B\lambda_p\frac{\partial\mu}{\partial u_p}\right].$$

Since we are interested here only in first-order effects we can disregard terms containing powers of α higher than the first. Then, using (8),

$$\rho\dot{u}_p=\alpha\nu\Psi[w_p-D_p\partial f/\partial u_p], \quad (21)$$

in which the symbol D_p replaces the product $BkT\lambda_p$. Differentiation with respect to u_p gives

$$\frac{\partial(\rho\dot{u}_p)}{\partial u_p}=-\alpha\nu\Psi\left\{D_p\frac{\partial^2 f}{\partial u_p^2}+2\beta u_p\left(w_p-D_p\frac{\partial f}{\partial u_p}\right)\right\}. \quad (22a)$$

Similarly, we find from (15b) and (15c)

$$\frac{\partial(\rho\dot{v}_p)}{\partial v_p}=-\alpha\nu\Psi D_p\left[\frac{\partial^2 f}{\partial v_p^2}-2\beta v_p\frac{\partial f}{\partial v_p}\right], \quad (22b)$$

$$\frac{\partial(\rho\dot{w}_p)}{\partial w_p}=-\alpha\nu\Psi D_p\left[\frac{\partial^2 f}{\partial w_p^2}-2\beta w_p\frac{\partial f}{\partial w_p}\right]. \quad (22c)$$

For a sinusoidal oscillation $\alpha=\alpha_0e^{i\omega t}$ the time derivative of the density is

$$\dot{\rho}=i\omega\alpha\nu\Psi f. \quad (23)$$

Substitution of (22a), (22b), (22c), and (23) in (19) and solving for f gives

$$f=\sum_{p=1}^{N}\frac{u_pw_p}{2D_p(1+i\omega\tau_p)}, \quad (24)$$

where

$$\tau_p=(4\beta D_p)^{-1}=\sigma^2(6BkT\lambda_p)^{-1}. \quad (24a)$$

The thermodynamic potential and the velocity of diffusion at any point in configuration space can be evaluated from this expression for the perturbation of the distribution of configurations.

THE VISCOELASTIC PROPERTIES

The shearing stress which will produce a velocity gradient $\alpha=\alpha_0e^{i\omega t}$ in a liquid with a complex viscosity $\eta^*=\eta_1-i\eta_2$ is

$$S=Re\{\eta^*\alpha\}=\alpha_0[\eta_1\cos\omega t+\eta_2\sin\omega t].$$

The rate at which work is done by application of this shearing stress to a unit volume of solution is

$$P=S\alpha_0\cos\omega t = \alpha_0^2[\eta_1\cos^2\omega t+\eta_2\sin\omega t\cos\omega t]. \quad (25)$$

The complex viscosity imparted to a solution by the polymer molecules can be calculated by calculating the rate of input of free energy into the polymer molecules as a result of the motion of each part of each molecule with the velocity of the surrounding liquid. The average rate per molecule of doing work on the molecules whose representative points lie in $d\phi_i$ is given by the scalar product of two vectors, both of which are functions of the $3N$ coordinates of configuration space. The first of these is $\mathbf{V}_l$, the velocity of the liquid, which, in the transformed coordinates, is given by

$$\dot{u}_p=\alpha_0w_p\cos\omega t, \quad \dot{v}_p=0, \quad \dot{w}_p=0. \quad (26)$$

The other vector in the scalar product is $\nabla\mu$, the gradient of the thermodynamic potential. Since the velocity of the liquid has nonvanishing components only in the u-directions, only the components of $\nabla\mu$ in the u-directions will appear in the scalar product. These components are found from (8) and (24) to be

$$\frac{\partial\mu}{\partial u_p}=\frac{\alpha_0kTw_p}{2D_p(1+\omega^2\tau_p^2)}(\cos\omega t+\omega\tau_p\sin\omega t), \quad (27)$$

in which only first-order terms in α have been retained. Combining (26) and (27) we find for the scalar product

$$\mathbf{V}_l\cdot\nabla\mu=\alpha_0^2kT\sum_{p=1}^{N}\frac{w_p^2(\cos^2\omega t+\omega\tau_p\sin\omega t\cos\omega t)}{2D_p(1+\omega^2\tau_p^2)}. \quad (28)$$

The number of molecules per unit volume of solution is $n=\nu/V$; the number of these molecules whose representative points are in the volume element $d\phi_i$ at the time t is $n\Psi(1+\alpha f)d\phi_i$. Multiplying this number by (28) and integrating over configuration space gives the rate at which the shearing stress does work upon the polymer molecules in a unit volume of solution. The result is

$$P_m=\alpha_0^2 nkT\sigma^2\sum_{p=1}^{N}\frac{\cos^2\omega t+\omega\tau_p\sin\omega t\cos\omega t}{6D_p(1+\omega^2\tau_p^2)},$$

in which terms containing powers of α higher than the second have been disregarded. Adding to this expression the energy input into the solvent, $P_s=\eta_s\alpha_0^2\cos^2\omega t$, and comparing the result with (25) shows that

$$\eta_1=\eta_s+\frac{nkT\sigma^2}{6}\sum_{p=1}^{N}\frac{1}{D_p(1+\omega^2\tau_p^2)}, \tag{29a}$$

$$=\eta_s+nkT\sum_{p=1}^{N}\frac{\tau_p}{1+\omega^2\tau_p^2}, \tag{29b}$$

$$\eta_2=\frac{nkT\sigma^2}{6}\sum_{p=1}^{N}\frac{\omega\tau_p}{D_p(1+\omega^2\tau_p^2)}, \tag{29c}$$

$$=nkT\sum_{p=1}^{N}\frac{\omega\tau_p^2}{1+\omega^2\tau_p^2}. \tag{29d}$$

η_s is the viscosity of the solvent.

These results can also be expressed in terms of a complex shear modulus,[15] $G^*=G_1+iG_2=i\omega\eta^*$. The components of G^* are

$$G_1=nkT\sum_{p=1}^{N}\frac{\omega^2\tau_p^2}{1+\omega^2\tau_p^2} \tag{30a}$$

$$G_2=\omega\eta_s+nkT\sum_{p=1}^{N}\frac{\omega\tau_p}{1+\omega^2\tau_p^2}. \tag{30b}$$

The relaxation times, τ_p, in these equations are obtained from (11a) and (24a).

$$\tau_p=\sigma^2\left[24BkT\sin^2\frac{p\pi}{2(N+1)}\right]^{-1}\qquad p=1, 2, \cdots, N. \tag{31}$$

Each relaxation time corresponds to a particular mode of coordination of the motions of the segments of the molecule. The longest relaxation time is that for $p=1$. The ratio between successive relaxation times is large for small values of p, decreases with increasing p, and approaches unity as p approaches N.

In steady flow, $\omega=0$, both components of G^* and the imaginary part of η^* vanish. The real part of η^* becomes the steady-flow viscosity, η_0. From (29b) and (31), we have

$$\eta_0=\eta_s+\frac{n\sigma^2}{24B}\sum_{p=1}^{N}\left[\sin\frac{p\pi}{2(N+1)}\right]^{-2}$$

$$=\eta_s+\frac{n\sigma^2N(N+2)}{36B}. \tag{32}$$

Each relaxation time makes a contribution of $nkT\tau_p$ to η_0. The contribution of τ_1, the longest relaxation time, is

$$n\sigma^2\left[24B\sin^2\frac{\pi}{2(N+1)}\right]^{-1}.$$

The ratio of this contribution to the entire calculated contribution of the polymer is

$$3\left[2N(N+2)\sin^2\frac{\pi}{2(N+1)}\right]^{-1}\cong\frac{6(N+1)^2}{\pi^2N(N+2)}\cong\frac{6}{\pi^2}.$$

This result indicates that the longer relaxation times account for practically all of the viscosity. The short relaxation times, although many in number if N is large, account for only a small part of the total viscosity.

This conclusion is important because the use of the submolecule as the fundamental relaxing unit excludes from consideration any processes involving segments of the chain shorter than the submolecule. Such processes would take place more rapidly than processes requiring the coordination of longer sections of the chain and would, therefore, be expected to give rise to shorter relaxation times. Accordingly, the relative contribution of these processes to the steady-flow viscosity would be expected to be negligible as compared to the contribution of the processes included by the theory.

The shortest relaxation time included by the theory is τ_N; from (31) we have $\tau_N\cong\sigma^2/(24BkT)$ if $N\gg1$. At frequencies for which $\omega\tau_N>0.1$ the excluded processes will be expected to make an appreciable contribution to the real part of the complex shear modulus. The frequency ω_l, at which $\omega_l\tau_N=0.1$, will mark the upper limit of applicability of the theory. Let the relaxation time τ_l be the one for which $\omega_l\tau_l=1$. We then have $\tau_l=10\tau_N$, which leads to

$$\sigma^2\left[24BkT\sin^2\frac{l\pi}{2(N+1)}\right]^{-1}\cong10\sigma^2[24BkT]^{-1},$$

or

$$l\cong N/5.$$

Thus the relaxation times for which $p<N/5$ account for the dispersion of the viscoelastic properties up to frequencies within approximately one decade of the range in which excluded processes should begin to contribute to the real part of the modulus. For the

[15] R. L. Wegel and H. Walther, Physics **6**, 141 (1935).

relaxation times for which $p<N/5$ Eq. (31) simplifies to

$$\tau_p \cong \frac{\sigma^2(N+1)^2}{6\pi^2 p^2 BkT} \cong \frac{\sigma^2 N^2}{6\pi^2 p^2 BkT}. \quad (33)$$

Combining (32) and (33) gives

$$\tau_p = \frac{6(\eta_0-\eta_s)}{\pi^2 p^2 nkT}. \quad (34)$$

Substitution of (34) in (29b) and (30a) gives

$$\eta_1 = \eta_s + \frac{6(\eta_0-\eta_s)}{\pi^2} \sum_{p=1}^{N} \frac{p^2}{p^4+\omega^2\tau_1^2}, \quad \omega\tau_1 < \frac{N^2}{250}, \quad (35)$$

$$G_1 = nkT \sum_{p=1}^{N} \frac{\omega^2\tau_1^2}{p^4+\omega^2\tau_1^2}, \quad \omega\tau_1 < \frac{N^2}{250}. \quad (36)$$

The summations in (35) and (36) have been evaluated (Table I) for ten values of $\omega\tau_1$ between 0.1 and 100. If these summations are replaced by integrals from $p=0.5$ to $p=\infty$ and the results simplified by assuming $\omega\tau_1 \gg 0.5$, we obtain

$$\eta_1 = \eta_s + \frac{3(\eta_0-\eta_s)}{\pi(2\omega\tau_1)^{\frac{1}{2}}}, \quad 2 < \omega\tau_1 < \frac{N^2}{250}, \quad (37)$$

and

$$G_1 = nkT\left[\frac{\pi}{2}\left(\frac{\omega\tau_1}{2}\right)^{\frac{1}{2}} - 0.5\right], \quad 5 < \omega\tau_1 < \frac{N^2}{250}. \quad (38)$$

The lower limits of the indicated ranges of applicability of these equations are based on the requirement that values calculated from these equations agree within approximately 0.1 percent with corresponding values obtained from Eqs. (35) and (36). The upper limit is set by the requirement that no relaxation times for which $p>N/5$ should make an appreciable contribution. The limit of applicability of Eqs. (29) and (30) is one decade higher, i.e., $\omega\tau_1<N^2/25$; it is set by the use of the submolecule as the fundamental relaxing unit.

It is of interest to note the following equation for the imaginary part of the complex viscosity, which was obtained from Eqs. (38) and (34).

$$\eta_2 = \frac{G_1}{\omega} = \frac{3(\eta_0-\eta_s)}{\pi}\left[(2\omega\tau_1)^{-\frac{1}{2}} - (\pi\omega\tau_1)^{-1}\right].$$

This equation, which has necessarily the same range of validity as Eq. (38), shows that at high frequencies the calculated value of η_2 will approach the value of $(\eta_1-\eta_s)$ calculated from Eq. (37).

DISCUSSION OF RESULTS

The result of the calculation, as expressed in Eqs. (29), (30), and (31), predicts that the viscoelastic properties of a polymer solution can be described by a "generalized Maxwell model."[16] Each Maxwell element makes a contribution of nkT to the real part of the complex shear modulus at high frequencies and each of the relaxation times depends in the same way on temperature. Thus the results are consistent with the concept of "reduced variables" introduced by Ferry.[17]

TABLE I. Theoretical values of the real parts of the complex viscosity, Eq. (35), and the complex shear modulus, Eq. (36).

$\omega\tau_1$	$(\eta_1-\eta_s)/(\eta_0-\eta_s)$	$G_1/(nkT)$
0.1	0.9939	0.01072
0.2	0.9762	0.04162
0.5	0.8758	0.2203
1.0	0.6861	0.5785
2.0	0.4776	1.076
5.0	0.3003	1.982
10.0	0.2135	3.012
20.0	0.1511	4.476
50.0	0.0955	7.351
100.0	0.0676	10.60

According to (31) the relaxation times depend upon the temperature through three factors. They are inversely proportional to the absolute temperature and to the mobility of the end of a submolecule, which increases with decreases in the viscous forces exerted by the surrounding medium. And they are directly proportional to σ^2, the mean-square separation of the ends of the submolecule, and consequently to S^2, the mean-square separation of the ends of the molecule;[18] it has been shown by Flory[19] and his collaborators that changes in temperature cause changes in the extension of dissolved polymer molecules which are reflected in the intrinsic viscosity of the solution.

At frequencies below the range in which processes excluded from consideration by use of the concept of the submolecule make an appreciable contribution, the relaxation times predicted by Eq. (33) do not depend upon the number of submolecules into which the chain is divided. This can be seen from the following considerations. The submolecule may be chosen longer than the minimum length which obeys, approximately, the Gaussian law. The viscous forces which reduce the mobility B are directly proportional to the length chosen; accordingly, we may write $B=KN$. Since $\sigma^2 N = S^2$ Eq. (33) becomes

$$\tau_p = S^2/(6K\pi^2 p^2 kT),$$

which contains no factors dependent upon the length of the submolecule.

The contribution of the polymer to the viscosity of

[16] W. Kuhn, Z. physik. Chem. **B42**, 1 (1939); T. Alfrey and P. Doty, J. Appl. Phys. **16**, 700 (1945); R. D. Andrews, Ind. Eng. Chem. **44**, 707 (1952).

[17] J. D. Ferry, J. Am. Chem. Soc. **72**, 3746 (1950).

[18] It is easily shown that $S^2 = N\sigma^2$.

[19] T. G. Fox, Jr., and P. J. Flory, J. Phys. Colloid Chem. **53**, 197 (1949); T. G. Fox, Jr., and P. J. Flory, J. Am. Chem. Soc. **73**, 1909, 1915 (1951); H. L. Wagner and P. J. Flory, ibid. **74**, 195 (1952); L. Mandelkern and P. J. Flory, *ibid.* **74**, 2517 (1952); Flory, Mandelkern, Kinsinger, and Shultz, *ibid.* **74**, 3364 (1952); Krigbaum, Mandelkern, and Flory, J. Polymer Sci. **9**, 381 (1952).

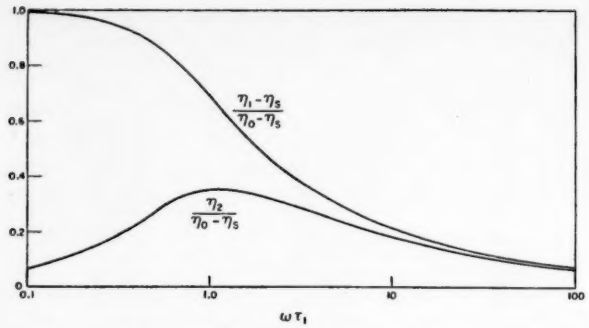

Fig. 1. Contribution of the polymer to the components of the complex viscosity relative to its contribution to the viscosity in steady flow.

the solution in steady flow is given by (32). Since $\sigma^2N=S^2$, this equation can be written

$$\eta_0-\eta_s=nNS^2/(36B),$$

if $N\gg2$. It is interesting to note that this expression has a form similar to that of the expression obtained by Debye[20] in his hydrodynamic calculation of the viscosity of a solution of "free-draining chains." However N is here the number of submolecules rather than the number of atomic groups, and the frictional coefficient of an atomic group is replaced by B^{-1}, the reciprocal of the mobility of the end of a submolecule.

The results are presented in Eqs. (34)–(38) in a form which can be readily used in calculation. The relaxation times as given by (34) can be calculated from the steady-flow viscosities of the solution and solvent, the molecular weight and concentration (in mass per unit volume) of the polymer, and the absolute temperature. The real parts of the complex viscosity and the complex shear modulus at the angular frequency ω can then be calculated. The theoretical curves for the functions $(\eta_1-\eta_s)/(\eta_0-\eta_s)$ and $\eta_2/(\eta_0-\eta_s)$ are shown in Fig. 1. The corresponding curves for $(G_2-\omega\eta_s)/(nkT)$ and $G_1/(nkT)$ are shown in Fig. 2.

Experimental data have recently been obtained[7] which indicate that these curves are at least a good first approximation to the actual viscoelastic behavior of dilute solutions of polystyrene and polyisobutylene. It is hoped that data which will provide a more exacting test will soon be available. Disagreements between theory and experiment are to be expected as the result of the following factors: (1) importance at high frequencies of processes excluded by the calculation, (2) polydispersity of any actual polymer, and (3) effects of intramolecular and intermolecular interferences on the motions of the segments of polymer chains.

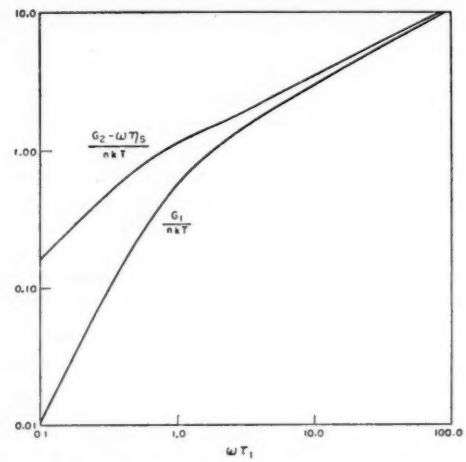

FIG. 2. Contribution of the polymer to the components of the complex rigidity relative to the contribution of a single relaxation mode to the instantaneous rigidity.

ACKNOWLEDGMENT

The author wishes to express his gratitude to Professor P. J. Flory for helpful discussions. Thanks are also due to Miss R. Doering for assistance with the computations.

This work was performed as a part of the research project sponsored by the Reconstruction Finance Corporation, Office of Synthetic Rubber, in connection with the Government Synthetic Rubber Program.

[20] P. Debye, J. Chem. Phys. **14**, 636 (1946).

A Molecular Theory of Stress Relaxation in Polymeric Media

K. W. SCOTT* AND R. S. STEIN†
Frick Chemical Laboratory, Princeton University, Princeton, New Jersey
(Received March 6, 1953)

The application of the kinetic theory of rubber elasticity to the description of the relaxation of crosslinked networks is only permissible in cases where the rate determining process is slow compared to the rate of diffusion of the polymer chains. Relaxation resulting from chemical reactions causing breaking of network crosslinks and formation of new crosslinks is a process of this type.

In this paper, a differential equation is proposed which describes the rate of relaxation in terms of the rates of the molecular processes. A simplified solution of this equation is given, and the consequences of the solution are discussed.

IN attempting to describe the stress relaxation of viscoelastic polymeric materials many phenomenological approaches have been made. Most of these methods have centered around various combinations of the Voigt and Maxwell elements. A Voigt element consists of a spring (representing Hooke's law behavior) and a dashpot (representing Newton's viscosity law behavior) in parallel. For this element the stress f and strain ϵ are related by the equation

$$f=E_v\epsilon+\eta_v(d\epsilon/dt), \tag{1}$$

where E_v is the Voigt elastic modulus and η_v the Newtonian viscosity. The Maxwell element consists of a spring and a dashpot in series. For the Maxwell element the stress-strain-time relationship is given by the differential equation

$$\frac{d\epsilon}{dt}=\frac{1}{E_M}\frac{df}{dt}+\frac{1}{\eta_M}f. \tag{2}$$

For the case of stress relaxation at constant strain these differential equations on integration yield

$$f=E_v\epsilon_0 \quad \text{and} \quad f=f_0\exp(-tE_M/\eta_M). \tag{3}$$

Thus the Voigt element exhibits no stress decay, while the Maxwell element exhibits exponential stress decay. By various combinations of these elements it is possible to set up models with a great range in viscoelastic behavior. This procedure, however, is unsatisfying since one cannot unambiguouly associate certain molecular processes with the mechanical processes of these models.

The kinetic theory of elasticity is a molecular theory concerning the equilibrium elastic properties of polymeric materials.[1] The kinetic theory of elasticity being an equilibrium theory does not permit one to determine the relaxation of stress in a polymeric material.

However, it is possible to apply the methodology of the kinetic theory in certain special cases. In the application of statistical theory to the calculation of the entropy of a molecular network, it is necessary that the network constraints remain constant for a long enough time for the chains to assume all accessible configurations a sufficient number of times so that their average properties approach those which would be statistically calculated. Thus the statistical theory may be applied to a polymer which relaxes by virtue of chemical scission of its crosslinks, provided the average time required for a chemical scission of a given crosslink is large compared with the time required for a transition from one configuration to another. This latter is of the order of magnitude of the time required for Brownian motion or about 10^{-8} second.

In a typical chemical relaxation, in which the stress may decrease to half its value in an hour, the average chain would have a "lifetime" of the order of an hour. The application of statistical theory is certainly justified in these cases. Typical applications are discussed in the papers of Stern and Tobolsky,[2] Tobolsky and Andrews,[3] and Green and Tobolsky.[4]

In these papers, the relaxation of stress is associated with a chemical reaction in which crosslinks are broken and new crosslinks are formed. It is assumed that a chain set free by breaking a crosslink makes no contribution to the stress of the network. It is also assumed that if a new crosslink is formed in a stretched network it is "at equilibrium with the stretched length" and makes no contribution to the stress.

It is one of the purposes of this paper to consider these assumptions from a more fundamental point of view, that is, from the effect of crosslink breaking and crosslink formation on the network distribution functions which are used to calculate the network entropy.

It is believed that the theory which is developed is generally applicable to any relaxation processes involving the formation and loss of crosslinks in a network. These crosslinks need not be restricted to chemical crosslinks but may be of a more transient type such as

* Present address: Kodak Research Laboratories, Eastman Kodak Company, Rochester, New York. This paper represents a portion of a thesis submitted by K. W. Scott to the faculty of Princeton University in partial fulfillment of the requirements of the degree of Doctor of Philosophy, June, 1949.

† Present address: Department of Chemistry, University of Massachusetts, Amherst, Massachusetts.

[1] W. Kuhn, Kolloid Z. 68, 2 (1934).

[2] M. Stern and A. V. Tobolsky, J. Chem. Phys. 14, 93 (1946).

[3] A. V. Tobolsky and R. D. Andrews, J. Chem. Phys. 13, 3 (1945).

[4] M. S. Green and A. V. Tobolsky, J. Chem. Phys. 14, 80 (1946).

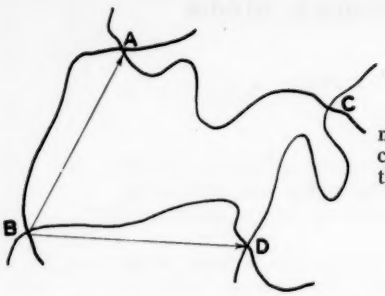

FIG. 1. The displacement vectors and the crosslinkage points in the polymer network.

hydrogen bonds, or even regions of strong dipolar attraction.

THE MODEL

The model assumed here is a three-dimensional network of infinite polymer molecules with a random distribution of crosslinks. The portion of a polymer molecule between nearest crosslinks will be referred to here as a polymer chain. The vector connecting the two crosslinks associated with a polymer chain will be termed the polymer chain's displacement vector.

Figure 1 is a representation of some of the terms used here. A, B, C, and D designate points of crosslinkage. The curved lines represent the polymer molecules. The curved line between A and B is a single network chain and its associated displacement vector is the arrow between A and B. The arrow between B and D is another displacement vector. There is no displacement vector for A and D or B and C since these are not nearest crosslinks in the sense used here. The polymer chain consists of one or more segments. Let us define a chain segment in the Kuhn sense as a number of monomer units such that for all practical purposes adjacent chain segments will not appear to encounter any restricted rotation.

For a given displacement vector and number of segments making up the polymer chain it will be assumed that all configurations are equally probable. This obviously is not exactly true; however, at the present it is a convenient simplification in the statistical approximation here. This assumption implies that certain factors are not considered. The effect of the volume of the polymer on the chain configurations is not considered. Likewise intermolecular and intramolecular interactions, except at points of crosslinkage, are also neglected. It is also assumed that the energy interactions responsible for crosslinking do not influence the configurations of the free portion of the chain between crosslinks.

Let P be the probability that a segment is involved in a crosslinkage. If a chain consists of J segments there will be $J-1$ places where segments are joined and no crosslinkages occur. There will be two places where crosslinkages occur. Hence the probability that a given chain has J segments is $(1-P)^{J-1}P^2$. The number of chains containing J segments is $N_0(1-P)^{J-1}P^2$, where N_0 is the total number of chain segments. $N_0(1-P)^{J-1}P^2$ is, of course, also the number of displacement vectors associated with chains of J segments. For a polymer chain with J segments the probability that the end to end separation lies between r_i, and r_i+dr_i‡ is given by[1,5]

$$\frac{\beta_J^3}{\pi^{\frac{3}{2}}}\exp(-\beta_J^2 r_i^2)d\tau_i, \tag{4}$$

where

$$r_i^2=x_i^2+y_i^2+z_i^2, \quad d\tau_i=dx_i dy_i dz_i,$$

$$\beta_J^2=\frac{3}{2J\sigma^2}\left(\frac{1-\cos\theta}{1+\cos\theta}\right),$$

σ is the length of a chain segment, and θ is the angle between successive bonds. The total number of chains with J segments and an end to end separation between r_i and r_i+dr_i is thus given by

$$N_0(1-P)^{J-1}P^2\frac{\beta_J^3}{\pi^{\frac{3}{2}}}\exp(-\beta_J^2 r_i^2)d\tau_i. \tag{5}$$

On instantaneous deformation of the network, the average position of the points of crosslinking are subject to the same affine transformation as are the macroscopic dimensions of the network. If the polymeric material is stretched by the ratio $\alpha_0=l/l_0$, where l is the stretched length and l_0 is the unstretched length, the total number of chains with J segments and a resulting end to end separation between r_i and r_i+dr_i is given by

$$N_0(1-P)^{J-1}P^2\frac{\beta_J^3}{\pi^{\frac{3}{2}}}$$

$$\times\exp\left[-\beta_J^2\left(\frac{x_i^2}{\alpha_0^2}+\alpha_0 y_i^2+\alpha_0 z_i^2\right)\right]d\tau_i. \tag{6}$$

The distribution of displacement vectors as given by expression (6) is used to determine certain physical properties of the polymeric material. Wall[6] has shown how a distribution function similar to (6) can be used to yield the stress in a strained sample of a polymeric material. This method will be given in detail later in this work. Kuhn and Grun[7] have used a distribution function similar to (6) to determine the birefringence characteristics of a strained polymeric system.

In the unstrained isotropic state the distribution of displacement vectors is spherically symmetrical. Upon straining, this distribution is shifted toward an ellipsoidal shape. Mathematically the relaxation of stress in a polymeric material can be described by the kinetics of the change of the ellipsodial distribution back towards the spherical distribution. The kinetics of this

‡ The contracted form, r_i and r_i+dr_i, used here stands for x_i and x_i+dx_i, y_i and y_i+dy_i, and z_i and z_i+dz_i.

[5] E. Guth and H. Mark, Monatsh. Chem. **65**, 93 (1934).

[6] F. T. Wall, J. Chem. Phys. **10**, 132, 485 (1942); **11**, 527 (1943).

[7] W. Kuhn and F. Grun, Kolloid Z. **101**, 248 (1942).

change will be determined by the kinetics of the molecular processes involved in the stress relaxation.

Let $N(i, J, t)$ be the number of displacement vectors at time t corresponding to chains of J segments whose end to end length, i.e., displacement vector between points of adjacent crosslinking, is between r_i and r_i+dr_i. $N(i, J, t=\infty)$ corresponds to the completely relaxed network and according to the kinetic theory of elasticity is given by

$$N(i, J, t=\infty)=N_0(1-P)^{J-1}P^2(\beta_J{}^3/\pi^{\frac{3}{2}}) \times\exp(-\beta_J{}^2r_i{}^2)d\tau_i. \quad (7)$$

$N(i, J, t=0)$ corresponds to the most highly stressed network due to the initial instantaneous strain. Assuming the volume of the network is unchanged by the strain, the affine transformation yields

$$N(i, J, t=0)=N_0(1-P)^{J-1}P^2(\beta_J{}^3/\pi^{\frac{3}{2}}) \times\exp\left[-\beta_J{}^2\left(\frac{x_i{}^2}{\alpha_0{}^2}+\alpha_0y_i{}^2+\alpha_0z_i{}^2\right)\right]d\tau_i, \quad (8)$$

where α_0 is the ratio of the stretched length l to the unstretched length l_0 of the network.

For this model the number of potential crosslinking points must be much greater than the number crosslinked at any one time. We shall assume here that the number of crosslinks is constant with time, i.e., crosslink forming and crosslink breaking processes occur at the same rate. This implies that the intermittent relaxation curve is a constant. This is not a necessary assumption, and an obvious generalization of this theory is to cases where the breaking and formation processes occur at different rates. The rate determining step for this stress relaxation process involves the breaking and forming of crosslinks. It is assumed that the time required for the network to arrange into a new equilibrium configuration after a crosslink is lost is small compared with the time between the loss of two crosslinks. The crosslinks are assumed to break in a unimolecular process. The fraction of the total number of crosslinks breaking per unit time is defined by the rate constant k', depending only on the temperature and independent of the stress, strain, stage of relaxation, etc. When a crosslink breaks, a chain has time to attain its most probable configuration before recrosslinking, i.e., the rate of segment jumping is greater than the rate of making and breaking crosslinks. The deformation on straining is considered to occur by the displacement of the crosslinks from their positions of greatest probability to positions of lower probability. Subsequently, by virtue of thermal fluctuations a given crosslink will break and on the average another will form somewhere else in the network. When a particular crosslink breaks, the portion of the chain constrained by it can return to a more probable configuration and is subjected only to the constraints of the two neighboring crosslinks.

When a crosslink reforms it will enter in a position of maximum probability with respect to the positions of its two nearest crosslinks. Thus this process of breaking and reforming of a crosslink results in an increase in the probability of the configuration and represents stress relaxation.

THE KINETIC EXPRESSION

There are four ways of changing the distribution of displacement vectors with this model. These are represented diagrammatically in Fig. 2.

In process (1) a crosslink E is broken and the four displacement vectors connecting this crosslink to the four nearest neighbor crosslinks (A, B, C, and D) are lost from the distribution. Simultaneously, two new displacement vectors are formed in this process, for A and B now are nearest neighbor crosslinks as are C and D. The two new displacement vectors, AB and CD, enter the distribution. This is designated as process (2). Processes (4) and (3) are the reverse of these for the formation of a new crosslink (at E), in which case two displacement vectors are lost from the distribution (AB and CD) in process (3), and four new displacement vectors are created (AE, BE, CE, and DE) in process (4).

If it is assumed that the crosslinks break by a first-order reaction and the crosslinks break at random, the rate of loss of a displacement vector of a given type in process (1) will be proportional only to the number of such vectors. Thus the rate of change in the number of displacement vectors because of this process is

$$-\frac{dN(i, J, t)}{dt}=4k'N_c\left(\frac{N(i, J, t)}{2N_c}\right); \quad (9)$$
$$=2k'N(i, J, t)$$

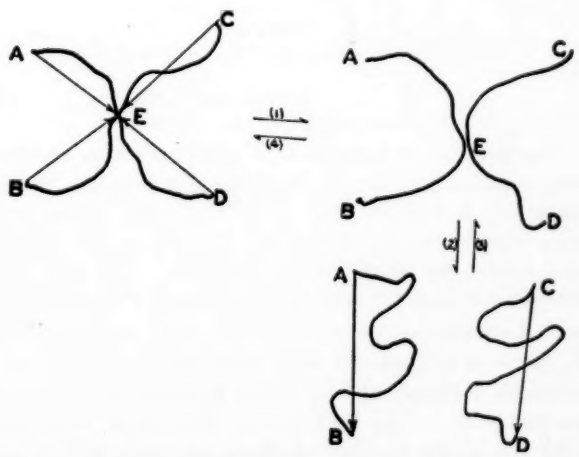

FIG. 2. The processes which are represented by the four terms in the kinetic expression. Process (1) represents the loss of the four displacement vectors AE, BE, CE, and DE, when a crosslink is broken. Process (2) represents the formation of the two new displacement vectors AB and CD when this occurs. Processes (3) and (4) are the reverse of the foregoing processes which occur when a new crosslink forms in the network.

k' is the fraction of the crosslinks broken per second and is assumed to be a constant.§ N_c is the total number of crosslinks of all types. The factor 4 appears here because four displacement vectors are lost every time a crosslink breaks. The term $(N(i, J, t)/2N_c)$ represents the probability that a given displacement vector will be one of type r_{iJ}. ($2N_c$ is the total number of displacement vectors of all types.) It should be noted that the sum of all displacement vectors must be equal to this at any time. Specifically, at $t=\infty$

$$\sum_{J=0}^{\infty}\int_{-\infty}^{\infty} N(i, J, t=\infty)d\tau_i = N_0 P = 2N_c. \quad (10)$$

For a displacement vector r_{iJ} to be formed by the breaking of a crosslink [process (2)], a crosslink must break between the two vectors r_{mn} and $r_{i-m,\,J-n}$. There are two pairs of chains associated with a particular crosslink. The probability that a particular pair of chains will potentially give a r_{iJ} vector is equal to the probability that one chain of the pair has a vector r_{mn}, *viz.*, $N(m, n, t)/2N_c$, times the probability that the other has a vector $r_{i-m,\,J-n}$, *viz.*, $N(i-m, J-n, t)/2N_c$, integrated over all values of r_m and summed over all values of n less than J. The total number of displacement vectors of all types formed per unit time by breaking a crosslink is $2k'N_c$. Hence the number of displacement vectors of the type r_{iJ} formed per unit time by the breaking of crosslinks is

$$\frac{dN(i, J, t)}{dt} = 2k'N_c \sum_{n=}^{J-1}\int_{-\infty}^{\infty}\left(\frac{N(m, n, t)}{2N_c}\right) \times\left(\frac{N(i-m, J-n, t)}{2N_c}\right)d\tau_m$$

$$= \frac{k'}{2N_c}\sum_{n=1}^{J-1}\int_{-\infty}^{\infty} N(m, n, t) \times N(i-m, J-n, t)d\tau_m. \quad (11)$$

The process of formation of crosslinks also involves both a gain and a loss of displacement vectors. In processes (3) and (4) of Fig. 2, if a crosslink forms at E somewhere between A and B, the vector AB will be lost from the distribution; however, the two new vectors AE and BE will be introduced. Corresponding vector changes occur in the other chain which joins at E. Since it is assumed here that the probability of a crosslink forming at any chain element is equal, the vectors will not be lost equally but those associated with the larger number of chain elements will be lost more readily. The probability that a vector r_{iJ} will be lost will be proportional to $(J-1)$ which is the number of places available for crosslinking on a chain of J elements. The number of displacement vectors of type r_{iJ} lost per unit time due to the formation of crosslinks [process (3)] is given by

$$-\frac{dN(i, J, t)}{dt} = 2k'N_c g(J-1)\frac{N(i, J, t)}{2N_c}, \quad (12)$$

where g is the proportionality constant corresponding to the factor $(J-1)$. The proportionality constant g is determined by the condition that

$$\sum_{J=1}^{\infty}\int_{-\infty}^{\infty} g(J-1)\frac{N(i, J, t)}{2N_c}d\tau_i = 1. \quad (13)$$

Equation (13) insures that the total number of displacement vectors of all types lost per unit time due to the formation of crosslinks is $2k'N_c$. Since $N(i, J, t)/2N_c$ is the probability of a vector of type r_{iJ}, it follows immediately from (13) that

$$g(J_{\text{average}}-1) = 1. \quad (14)$$

Since $J_{\text{average}} = 1/P$,

$$g = \frac{1}{(1/P)-1} = \frac{P}{1-P}. \quad (15)$$

Carrying out the integration and summation as indicated in (13) will yield (15). Equation (14) is affirmed since

$$J_{\text{average}} = \frac{\sum_{J=1}^{\infty}\int_{-\infty}^{\infty} JN(i, J, t=\infty)d\tau_i}{\sum_{J=1}^{\infty}\int_{-\infty}^{\infty} N(i, J, t=\infty)d\tau_i} = \frac{N_0}{N_0 P} = \frac{1}{P}. \quad (16)$$

Substituting (15) in (12) yields

$$-\frac{dN(i, J, t)}{dt} = k'(J-1)\frac{P}{1-P}N(i, J, t). \quad (17)$$

In process (4) the number of displacement vectors of type r_{iJ} formed per unit time by crosslinking is given by the product of the total number of vectors of all types formed per unit time by crosslinking and the probability that the Jth chain element of a chain characterized by a vector r_{mn} is at a displacement of r_i from one of the ends integrated over all r_m and summed over all n greater than J. This latter probability is the product of the probability that first the chain to be crosslinked is of type r_{mn}, *viz.*, $N(m, n, t)/2N_c$, and secondly its Jth element is at a distance r_i from one of the ends. Assuming a normal Gaussian distribution this is

$$P\begin{pmatrix} iJ \\ mn \end{pmatrix} \equiv \beta_J^3\beta_{n-J}^3\beta_n^{-3}\pi^{-\frac{3}{2}} \times\exp[-\beta_J^2 r_i^2 - \beta_{n-J}^2(r_m-r_i)^2 + \beta_n^2 r_m^2]. \quad (18)$$

§ This rate constant may actually depend upon temperature, concentration of a reagent which is causing the crosslink to break, and (in the extension of the theory to nonlinear behavior) upon the force on the crosslink.

Hence the number of displacement vectors of type r_{iJ} formed per unit time by crosslinking is

$$\frac{dN(i,J,t)}{dt}=4k'N_c g' \sum_{n=J+1}^{\infty} \times\int_{-\infty}^{\infty}\frac{N(m,n,t)}{2N_c}P\binom{iJ}{mn}d\tau_m, \quad (19)$$

where g' is a proportionality constant and $P\binom{iJ}{mn}$ is defined by (18). The proportionality constant is chosen so that the total number of displacement vectors of all types formed per unit time by crosslinking is $4k'N_c$, i.e.,

$$g'\sum_{J=1}^{\infty}\sum_{n=J+1}^{\infty}\int_{-\infty}^{\infty}\int_{-\infty}^{\infty} \times\frac{N(m,n,t=\infty)}{2N_c}P\binom{iJ}{mn}d\tau_m d\tau_i=1. \quad (20)$$

Integrating yields

$$g'=P/1-P. \quad (21)$$

Hence (19) becomes

$$\frac{dN(i,J,t)}{dt}=2k'\frac{P}{1-P}\sum_{n=J+1}^{\infty}\int_{-\infty}^{\infty} \times N(m,n,t)P\binom{iJ}{mn}d\tau_m. \quad (22)$$

The total change in the number of displacement vectors of type r_{iJ} per unit time is given by the sum of (9), (11), (17), and (22), *viz.*,

$$\frac{dN(i,J,t)}{dt}=-2k'N(i,J,t)+\frac{k'}{2N_c}\sum_{n=1}^{J-1}\int_{-\infty}^{\infty} \times N(m,n,t)N(i-m,J-n,t)d\tau_m -k'\frac{(J-1)P}{1-P}N(i,J,t)+\frac{2k'P}{1-P}\sum_{n=J+1}^{\infty} \times\int_{-\infty}^{\infty}N(m,n,t)P\binom{iJ}{mn}d\tau_m, \quad (23)$$

where $P\binom{iJ}{mn}$ is given by (18).

THE SOLUTION OF THE KINETIC EXPRESSION

The solution of this integro-differential equation (23) subject to the boundary conditions of (7) and (8) is thus the desired result. Substituting (7) in (23) yields $(dN(i,J,t=\infty)/dt)=0$ for all values of r_i and J, i.e., equilibrium has been established. Equation (23) can be used to determine the entropy as a function of time for this model. This procedure will then, of course, indirectly give a solution of (23). The stress relaxation at constant length can then be calculated from the entropy expression. The entropy is given by

$$S=k\ln\prod_{ij}\nu_{iJ}^{N(i,J,t)} \quad (24)$$

where k is the Boltzmann constant and ν_{iJ} is proportional to the number of spatial configurations possible with a r_{iJ} vector, i.e.,

$$\nu_{iJ}=\beta_J^3\pi^{-\frac{3}{2}}\exp(-\beta_J^2 r_i^2). \quad (25)$$

Thus (24) becomes

$$S=k\sum_{J=1}^{\infty}\int_{-\infty}^{\infty}N(i,J,t)\ln\nu_{iJ}$$

$$=k\sum_{J=1}^{\infty}\int_{-\infty}^{\infty}N(i,J,t)\ln\beta_J^3\pi^{-\frac{3}{2}} -k\sum_{J=1}^{\infty}\int_{-\infty}^{\infty}N(i,J,t)\beta_J^2 r_i^2. \quad (26)$$

Since it is permissible to differentiate with respect to time under the integral sign of these definite integrals, one may obtain the time rate of change of the entropy:

$$\frac{dS}{dt}=k\sum_{J=1}^{\infty}\int_{-\infty}^{\infty}\frac{dN(i,J,t)}{dt}\ln\beta_J^3\pi^{-\frac{3}{2}} -k\sum_{J=1}^{\infty}\int_{-\infty}^{\infty}\frac{dN(i,J,t)}{dt}\beta_J^2 r_i^2. \quad (27)$$

Let us assume that the distribution of displacement vectors is given by

$$N(i,J,t)=N_0P^2(1-P)^{J-1}\beta_J^3\pi^{-\frac{3}{2}} \exp\left[-\beta_J^2\left(\frac{x_i^2}{\alpha^2}+\alpha y_i^2+\alpha z_i^2\right)\right]d\tau_i, \quad (28)$$

where α is now a function of time and is of such a nature that it has the value α_0 at time equal to zero and the value 1 after an infinite length of time. Substituting (28) in (23), (27), and (26) and integrating yields

$$\frac{dS}{dt}=kk'N_0P\left(\frac{\alpha^2}{2}+\frac{1}{\alpha}-\frac{3}{2}\right), \quad (29)$$

$$S_e-S=kN_0P\left(\frac{\alpha^2}{2}+\frac{1}{\alpha}-\frac{3}{2}\right), \quad (30)$$

where

$$S_e=-\frac{3}{2}kN_0P^2\sum_{J=1}^{\infty}(1-P)^{J-1}\ln\pi e\beta_J^{-2}.$$

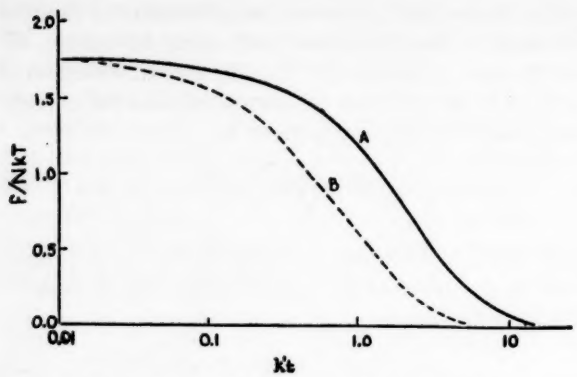

FIG. 3. Curve A—A typical plot of the stress relaxation predicted by this theory (Eq. 38). Curve B—A typical Maxwellian relaxation curve (Eq. 39).

Combining (29) and (30) yields

$$\frac{dS}{dt}=k'(S_e-S). \tag{31}$$

Integrating (31) gives

$$S_e-S=c\exp(-k't). \tag{32}$$

When $t=0$, $\alpha=\alpha_0$ and from (30)

$$S_e-S(t=0)=kN_0P\left(\frac{\alpha_0^2}{2}+\frac{1}{\alpha_0}-\frac{3}{2}\right). \tag{33}$$

Therefore

$$c=kN_0P\left(\frac{\alpha_0^2}{2}+\frac{1}{\alpha_0}-\frac{3}{2}\right),$$

and hence

$$S_e-S=kN_0P\left(\frac{\alpha_0^2}{2}+\frac{1}{\alpha_0}-\frac{3}{2}\right)\exp(-k't). \tag{34}$$

Comparing (34) with (30) shows that $\alpha=\alpha(t)$ is given by

$$\left(\frac{\alpha^2}{2}+\frac{1}{\alpha}-\frac{3}{2}\right)=\left(\frac{\alpha_0^2}{2}+\frac{1}{\alpha_0}-\frac{3}{2}\right)\exp(-k't). \tag{35}$$

Equation (35) satisfies the boundary conditions since here $\alpha(t=0)=\alpha_0$ and $\alpha(t=\infty)=1$.

Assuming that there is no energy contribution to the stress one has

$$f=-\frac{T}{A_0}\left(\frac{dS}{dl}\right)_T, \tag{36}$$

where f is the stress based on original cross section of the sample; T, temperature; A_0, initial area of the rectangular sample; S, entropy; and l is the length of the sample. Since $\alpha=l/l_0$, $l_0d\alpha=dl$, thus the stress is given by

$$f=-\frac{T}{A_0l_0}\left(\frac{dS}{d\alpha}\right)_T. \tag{37}$$

Substituting the entropy as given by (30) in (37), one obtains

$$f=kT\frac{N_0P}{A_0l_0}\left(\alpha-\frac{1}{\alpha^2}\right)=NkT\left(\alpha-\frac{1}{\alpha^2}\right), \tag{38}$$

where $N=(N_0P/A_0l_0)$ is the number of polymer chains per unit volume and $\alpha=\alpha(t)$ is given by (35). Equation (38) is plotted in Fig. 3, where it is compared with the expression

$$f=NkT[\alpha_0-(1/\alpha_0^2)]\exp(-k't). \tag{39}$$

Equations (38) and (35) can be approximated by

$$f=NkT[\alpha_0-(1/\alpha_0^2)]\exp(-\lambda k't). \tag{40}$$

Since the crosslink making and breaking processes are essentially of the first order, one might expect that the stress decay would be nearly a simple Maxwellian exponential decay. Since this method takes into account that crosslinks reform in strain-free positions and later become strained and break, one would expect the Maxwellian relaxation constant to be smaller than k'; the rate constant for the making and breaking of crosslinks. The factor λ shows a slight dependence on α_0. At the limits of very small and very large elongations, λ approaches $\frac{1}{2}$. λ drops rapidly to a value of 0.43 at $\alpha_0=2$ and then decreases gradually to a value of 0.41 at $\alpha_0=7$ before it begins to increase slowly to its limiting value at large elongations. It seems quite reasonable that the stress relaxation time is greater than $1/k'$ by a factor of about 2.

Considering Eq. (40), the stress relaxation behavior is a simple exponential decay with the Maxwellian relaxation constant proportional to the rate constant k'. Thus for the materials to which this model applies, the stress relaxation activation energies experimentally determined by the temperature dependence of the Maxwellian relaxation constant are actually the activation energies for the making and breaking of crosslinks.

Equation (40) is of the same form as that obtained by assuming that as a result of the stress the number of crosslinks decreases via a first order reaction. Thus a continuous Maxwellian type stress relaxation curve in itself cannot be used to distinguish between a conservation or loss of crosslinks with time. Equation (40) is then, of course, of the same form as that obtained by assuming that crosslinks form in stress free positions which remain stress free for all time.

ACKNOWLEDGMENT

The many helpful discussions of the authors with Professor A. V. Tobolsky during the course of this work are greatly appreciated.

The Use of Free Electron Model Wave Functions in the Derivation and Representation of LCAO MO Wave Functions of Conjugated Molecules

H. H. JAFFÉ
Venereal Disease Experimental Laboratory, U. S. Public Health Service, and School of Public Health, University of North Carolina, Chapel Hill, North Carolina

(Received November 24, 1952)

A simple relation between free electron model and LCAO molecular orbital wave functions is derived for linear and cyclic conjugated molecules involving no branching of the π-electron system. On the basis of this relation LCAO MO wave functions and their energies can be calculated without solution of secular equations or extensive numerical computations, and simple analytic expressions for the wave functions and energies can be derived. The method assumes equal resonance and Coulomb integrals in the conjugated system but does not require neglect of overlap integrals. The types of molecules for which the method is most appropriate are discussed. For other molecules the LCAO MO WF's derived from FEM WF's may be improved by perturbation calculations. The relations are also shown to hold for molecules containing heteroatoms and branched π-electron systems if the FEM WF's are replaced by the FEM-like WF's derived. Finally, a simple method of graphic representation of LCAO WF's is proposed and illustrated.

SEVERAL wave mechanical methods for the treatment of conjugated organic molecules are known. One of the most successful and most widely used is the LCAO molecular orbital (MO) method. In this approximation the wave function (WF) of each π-electron is expressed as a linear combination of atomic orbitals of the atoms comprising the conjugated system. For a molecule having n such atoms the LCAO MO WF's ψ are given by[1]

$$\psi_j=\sum_{r=1}^{n} a_{j,r}\varphi_r, \qquad j=1, 2, \cdots n, \quad (1)$$

where the φ_r are the atomic orbitals of the atom r. The n eigenvalues (W_j) of these WF's are the values of the energy for which a set of n linear equations has solutions. The $a_{j,r}$ are obtained by solving these equations for each W_j and normalizing. The evaluation of the W_j and $a_{j,r}$ is frequently a cumbersome process of numerical computation, which must be carried out in detail if certain chemical properties of the molecules are required. In the present paper it will be shown that these numerical calculations can be avoided in certain classes of molecules.

In a recent note from this Laboratory, an empirical relation between LCAO MO and free electron model (FEM) WF's was reported.[2] This relation can be expressed in the following form:

$$a_{j,r}=\psi_j'(r), \qquad \text{for all } j \text{ and } r, \quad (2)$$

where $\psi_j'(r)$ is the amplitude of the FEM WF ψ_j' at the position of the atom r. The FEM is based on the assumption that π-electrons are freely mobile in a one dimensional box of constant potential.[3] The WF's are readily obtained as the solution of the well-known "particle in a box" problem, and have a simple analytic form. The FEM leads to an infinite number of WF's ($j=1, 2\cdots$), while the LCAO MO method leads only to n WF's. However, the FEM WF ψ'_{n+1} has nodes at the positions of all nuclei and hence does not lead to a satisfactory LCAO MO WF by the use of Eq. (2). Furthermore, the FEM WF ψ'_{n+1+j} leads to the same set of $a_{j,r}$ as ψ'_{n+1-j}, so that the LCAO MO WF's derived from FEM WF's with $j>n+1$ are already represented by WF's with $1\leqslant j\leqslant n$.

In the present paper Eq. (2) will be rigorously derived, and simple analytic expressions for the eigenvalues of the LCAO MO WF's will be developed. It will finally be shown that Eq. (2) can also be applied to systems involving heteroatoms and branched π-electron systems.

LINEAR CONJUGATED SYSTEMS

The FEM WF's for a linear conjugated system of n atoms are given by[4]

$$\begin{aligned} &\psi_j'=[2/(n+1)]^{\frac{1}{2}}\sin(b_j x), && 0\leqslant x\leqslant n+1,\\ &\psi_j'=0, && x\leqslant 0;\ x\geqslant n+1, \quad (3)\\ &b_j=j\pi/(n+1), && j=1, 2\cdots. \end{aligned}$$

Here $x=s/a$, with s the distance from one end of the box, and a the distance between any two neighbouring atoms.

The LCAO MO WF's for the same system are given by Eq. (1) where the $a_{j,r}$ are determined by the n identical sets of n equations

$$(a_{j,r-1}+a_{j,r+1})\beta-a_{j,r}W_j=0, \quad j, r=1, 2\cdots n, \quad (4)$$

where $a_{j,0}\equiv a_{j,n+1}\equiv 0$ and β is the resonance integral of two adjacent atoms.[1] Equation (4) is based on the common approximation of neglecting overlap integrals

[1] See, for example, C. A. Coulson and H. C. Longuet-Higgins, Proc. Roy. Soc. (London) **A191**, 39 (1947).
[2] H. H. Jaffé, J. Chem. Phys. **20**, 1646 (1952).
[3] N. S. Bayliss, J. Chem. Phys. **16**, 287 (1948); H. Kuhn, Helv. Chim. Acta **31**, 1441 (1948); Z. Elektrochem. **53**, 165 (1949); S. Nikitine, J. chim. phys. **47**, 614 (1950); and others. The present paper is based primarily on the functions developed by Kuhn.
[4] The length of the box is assumed to extend one bond distance beyond both ends of the conjugated chain. This assumption was first made by Kuhn (see reference 3).

and assuming all Coulomb integrals and all resonance integrals equal.[5]

Substituting Eq. (3) into Eq. (2) the $a_{j,r}$ take the form

$$a_{j,r}=[2/(n+1)]^{\frac{1}{2}}\sin(b_j r). \quad (5)$$

Introducing Eq. (5) into Eq. (4) and rearranging, we obtain

$$W_j/\beta=\{\sin[b_j(r-1)]+\sin[b_j(r+1)]\}/\sin(b_j r)=2\cos b_j. \quad (6)$$

Since $a_{j,0}$ and $a_{j,n+1}$ as evaluated from Eqs. (2) and (3) vanish, their definitions given below Eq. (4) need no special treatment. Since Eq. (6) holds for all j and r, the $a_{j,r}$ in the form (5) satisfy the equations (4). However, only a single set of $a_{j,r}$, except for a normalization factor, can satisfy such a set of equations, and hence Eq. (5) gives the only possible set of relative values of the $a_{j,r}$. Accordingly, the LCAO MO WF's can be written as

$$\psi_j=[2/(n+1)]^{\frac{1}{2}}\sum_{r=1}^{n}\sin(b_j r)\varphi_r. \quad (7)$$

The normalization condition for the LCAO MO WF's is[1]

$$\sum_{r=1}^{n}a_{j,r}^2=1, \qquad \text{for all } j. \quad (8)$$

Hence the WF's of Eq. (7) are normalized if, and only if

$$\sum_{r=1}^{n}\sin^2(b_j r)=(n+1)/2. \quad (9)$$

Equation (9) can be rewritten as

$$\sum_{r=1}^{n}\cos(2b_j r)=-1. \quad (10)$$

The sum in the left-hand side of Eq. (10) can be evaluated as follows:

$$\begin{aligned}&\sum_{r=1}^{n}\cos(2b_j r)\\&=\sin[(2n+1)b_j]/2\sin b_j-\tfrac{1}{2}\\&=[\sin(2nb_j)\cos b_j+\cos(2nb_j)\sin b_j]/2\sin b_j-\tfrac{1}{2}\\&=\sin(nb_j)\cos(nb_j)\cos b_j/\sin b_j-\sin^2(nb_j). \quad (11)\end{aligned}$$

From the definition of b_j in Eq. (3) it follows that $\sin(nb_j)=(-1)^{j+1}\sin b_j$ and $\cos(nb_j)=(-1)^j\cos b_j$. Hence the right-hand side of Eq. (11) equals -1 as required in Eq. (10), the necessary and sufficient condition (9) for normalization is fulfilled, and Eq. (7) is a correct normalized expression for the LCAO MO WF's.

[5] The Coulomb integrals are equated to zero, and thus define the origin of the energy scale. Resonance integrals between unbonded atoms are neglected.

The energies of the WF's (7) are given by Eq. (6), and it follows immediately that $|W_j/\beta|\leqslant 2$ for linear conjugated molecules. It should be noted, however, that these energies are not the same as the eigenvalues of the FEM WF's arising from the "particle in the box" treatment.

This far overlap integrals have been neglected in deriving the LCAO MO formulas. If overlap integrals of bonded atoms are not neglected, but assumed to be all equal,[6] Eq. (4) becomes

$$(a_{j,r-1}+a_{j,r+1})(\beta-SW_j)-a_{j,r}W_j=0. \quad (12)$$

The $a_{j,r}$ given by Eq. (5) satisfy Eq. (12) and hence are the correct values. The expression for the energy eigenvalues becomes

$$W_j/\beta=2\cos b_j/(1+2S\cos b_j). \quad (13)$$

Consequently, the inclusion of overlap integrals poses no problems.

CYCLIC SYSTEMS

For a cyclic conjugated molecule involving no branching of the π-electron system, the FEM method treats the π-electrons as plane rotators. The WF's then have the form

$$\psi_j'=(2\pi)^{-\frac{1}{2}}\exp(ij\theta), \quad j=0,\pm1,\pm2\cdots, \quad (14)$$

where θ is the polar angle. The LCAO MO WF's for a cyclic conjugated molecule of n atoms is[7]

$$\psi_j=(2\pi)^{-\frac{1}{2}}\sum_{r=1}^{n}\varphi_r\exp(2ijr\pi/n)=\sum_{r=1}^{n}a_{j,r}\varphi_r. \quad (15)$$

Hence Eq. (2) holds for cyclic as well as for linear system. The eigenvalues of the energy by the LCAO MO WF's are

$$W_j/\beta=2\cos(2j\pi/n). \quad (16)$$

Equation (16) can also be derived from the FEM WF's in the manner outlined above for the linear systems.

It is customary, for numerical calculation, to replace the WF's (15) by equivalent real WF's. Both FEM and LCAO MO WF's occur in degenerate pairs, except $j=0$ and $j=n/2$. Hence any linear combinations of such degenerate pairs are also satisfactory WF's. The most useful LCAO MO WF's have the form[8]

$$\psi_j=(2/n)^{\frac{1}{2}}\sum_{r=1}^{n}\varphi_r\sin(2jr\pi/n), \quad j=1,2,\cdots(n-2)/2, \quad (17a)$$

$$\psi_j=(2/n)^{\frac{1}{2}}\sum_{r=1}^{n}\varphi_r\cos(2jr\pi/n), \quad j=0,1,\cdots n/2. \quad (17b)$$

[6] This assumption is reasonable as long as the corresponding resonance integrals are assumed equal.

[7] E. Hückel, Z. Physik. **70**, 204 (1930).

[8] Since $\sin(2jr\pi/n)$ for $j=0$ and $j=n/2$ vanishes for all r, Eq. (17a) does not give satisfactory WF for these values of j, and hence Eq. (17b) must be used.

Accordingly, the $a_{j,r}$ corresponding to the WF's in Eq. (17) can be represented by

$$\begin{aligned} a_{j,r}&=i\psi_{-j}'(r)-i\psi_j'(r)=(2/n)^{\frac{1}{2}}\sin(2jr\pi/n),\\ a_{j,r}&=\psi_j'(r)+\psi_{-j}'(r)=(2/n)^{\frac{1}{2}}\cos(2jr\pi/n). \end{aligned} \tag{18}$$

INTRODUCTION OF HETEROATOMS

Kuhn has treated linear conjugated system of an uneven number of atoms with a central heteroatom by introducing a potential well in the center of the FEM "box."[9] This well is of depth V_1 and length a, where a is twice the covalent radius of the heteroatom. The WF's derived for this model contain the FEM energy eigenvalues E_j, for which no analytic expressions can be written.

Kuhn has proposed that the WF's can be approximated by letting a approach zero while holding the product aV_1 constant. For even values of j this treatment leads to the WF's given in Eq. (3). For odd values of j one obtains

$$\begin{aligned} &\psi_j'=A\sin(\rho_j x), && 0\leqslant x\leqslant (n+1)/2,\\ &\psi_j'=A\sin[\rho_j(n+1-x)], && (n+1)/2\leqslant x\leqslant n+1,\\ &\psi_j'=0, && x\leqslant 0;\ x\geqslant n+1,\\ &\rho_j=2\pi a(2mE_j)^{\frac{1}{2}}/h, && j=1,3,5\cdots, \end{aligned} \tag{19}$$

where m is the mass of the electron, and h Planck's constant. For $j=1$, ρ_1 may become imaginary, in which case real WF's are obtained by replacing the sin in Eq. (19) by sinh, and all the trigonometric functions in the following derivations by their hyperbolic equivalents.[10]

The linear equations for the linear conjugated molecules with a central heteroatom of Coulomb integral α are identical to Eq. (4), except for $r=(n+1)/2$. For this case Eq. (4) reads

$$(a_{j,(n-1)/2}+a_{j,(n+3)/2})\beta+a_{j,(n+1)/2}(\alpha-W_j)=0. \tag{20}$$

By combination of Eqs. (2), (19), and (20), the validity of Eq. (2) can be demonstrated in the manner outlined above for the linear molecules. The calculations lead to the following expressions:

$$W_j/\beta=2\cos\rho_j, \tag{21}$$

$$\alpha/\beta=2\sin\rho_j\cot[\rho_j(n+1)/2]. \tag{22}$$

The WF's (19) thus satisfy Eq. (2) if, and only if, Eq. (22) is satisfied. The ρ_j are determined by the FEM in the approximation here considered by the equality

$$\rho_j\cot[\rho_j(n+1)/2]=4\pi^2mV_1a/h^2, \tag{23}$$

which arises out of the conditions that ψ_j' and $d\psi_j'/dx$ be continuous. Equations (22) and (23) do not lead to identical sets of ρ_j. Since we are not interested in the ρ_j for the determination of FEM energies, we will not make use of Eq. (23). Equation (22) permits evaluation of sets of ρ_j which define WF's of the form (19). These WF's satisfy Eq. (2) identically; they will be called FEM-like WF's since they have the same form as the true FEM WF's, but do not involve the same quantization conditions.

Consequently, the LCAO MO WF's for a linear conjugated molecule with a central heteroatom can be expressed in terms of FEM-like WF's. The above developments can easily be extended to molecules having a heteroatom in any position. The WF's are

$$\begin{aligned} &\psi_j'=A\sin(\rho_j x), && 0\leqslant x\leqslant m,\\ &\psi_j'=(-1)^{j+1}B\sin[\rho_j(n+1-x)], && m\leqslant x\leqslant n+1,\\ &\psi_j'=0, && x\leqslant 0;\ x\geqslant n+1,\\ & && j=1,2,3,\cdots, \end{aligned} \tag{24}$$

where the heteroatom is located at $x=m$, and A and B are normalization factors. Further, Eq. (21) remains unchanged, while Eq. (22) is replaced by[11]

$$\alpha/\beta=\sin\rho_j\{\cot(\rho_j m)+\cot[\rho_j(n+1-m)]\}. \tag{25}$$

It should be noted that all values of j are allowed in Eq. (24).

BRANCHED π-ELECTRON SYSTEMS

Kuhn has treated conjugated molecules containing a branched π-electron system by the FEM.[12] His WF's depend on the type of molecule, and we will illustrate the arguments by discussing a compound consisting of a benzene ring with a pair of identical substituents in *para* position. The substituents will be considered to be conjugated with the benzene ring. Since such a compound has a plane of symmetry through the *para* carbon atoms, we will have to deal only with the part of the ring to one side of this plane. All derivations and formulas will hold equally for the other side of the ring. The FEM WF's can be divided into two classes: those symmetric and those antisymmetric with respect to reflection on the lengthwise axis of the compound. The antisymmetric WF's necessarily vanish except in the branched sections of the benzene ring. They have the simple forms given by Kuhn,[12] satisfy Eq. (2), and will not be dealt with further. The symmetric WF's take the form

$$\begin{aligned} &\psi_j'=A\sin(\rho x), && 0\leqslant x\leqslant m_a,\\ & && j \text{ odd}\\ &\psi_j'=B\cos[\rho(n+1-2x)/2], && m_a\leqslant x\leqslant m_b,\\ &\psi_j'=B\sin[\rho(n+1-2x)/2], && j \text{ even}\\ &\psi_j'=(-1)^{j+1}A\sin[\rho(n+1-x)/2], && m_b\leqslant x\leqslant n+1,\\ &\psi_j'=0, && x\leqslant 0;\ x\geqslant n+1, \end{aligned} \tag{26}$$

where $x=m_a$ (and m_b) are the positions of the *para* carbon atoms of the benzene ring, i.e., the points of

[9] H. Kuhn, Helv. Chim. Acta **34**, 2371 (1951).

[10] The range of application of the hyperbolic functions is discussed in the appendix.

[11] Equation (25) is plotted in Fig. 4 in the appendix, for $m=2$, $n=4$.

[12] H. Kuhn, Helv. Chim. Acta **32**, 2247 (1949).

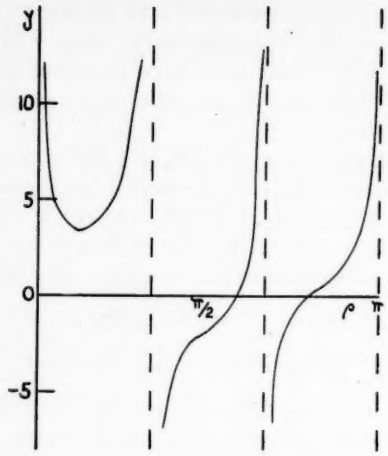

FIG. 1. The function $y(\rho)=\cot\rho_j-\cot(3\rho_j)+2\tan(3\rho_j/2)$ of Eq. (30). The function $y(\rho_j)=\cot\rho_j-\cot(3\rho_j)-2\cot(3\rho_j/2)$ of Eq. (31) is the same as above, with ρ_j replaced by $\pi-\rho_j$, and y by $-y$.

branching of the π-electron system, and n is the number of atoms in the conjugated system, counting only one side of the ring.

The LCAO MO WF's for this system are determined by a set of equations identical to Eqs. (4) except for $r=m_a$ (and m_b), when

$$(a_{j,m_a-1}+2a_{j,m_a+1})\beta-a_{j,m_a}W_j=0. \tag{27}$$

Following the procedure used above, Eqs. (2), (4), and (26) lead to

$$W_j/\beta=2\cos\rho_j, \tag{28}$$

and Eq. (27) leads to the conditions determining the ρ_j:

$$\sin(m_a\rho_j)=0, \tag{29}$$

$$y=\cot\rho_j-\cot(m_a\rho_j)+2\tan[\rho_j(n+1-2m_a)/2]=0, \quad j \text{ odd}, \tag{30}$$

$$y=\cot\rho_j-\cot(m_a\rho_j)-2\cot[\rho_j(n+1-2m_a)/2]=0, \quad j \text{ even}. \tag{31}$$

In Fig. 1 the function y is plotted against ρ for $n=8$, $m_a=3$ (divinylbenzene). Four values of $\rho_j<\pi$ are seen to satisfy either Eq. (30) or (31), and Eq. (29) is satisfied by two further values of ρ_j. However, the LCAO MO treatment leads to eight WF's, for two of which $|W/\beta|>2$. Since Eq. (28) does not permit $|W/\beta|>2$, these latter MO WF's cannot be represented by the FEM-like WF's (26). The lowest energy MO WF for the heteronuclear molecules treated above was found to involve hyperbolic functions. Since the derivations of Eqs. (26) to (31) hold equally for such functions, it appears reasonable to assume a hyperbolic function for the lowest energy MO WF, and it can be shown that this must involve the cosh in the second line of Eq. (26). No simple representations of the highest energy WF has been found. However, this WF is rarely of interest, since it is unoccupied in all molecules. Hence, this point will not be pursued further.

We have thus shown that all but the highest energy WF's of molecules with branched π-electron systems can be expressed in terms of FEM-like WF's, which differ from Kuhn's FEM WF's in the quantization conditions. The arguments were given for a specific type of compound; however, they can readily be applied to other branched π-electron systems.

GRAPHIC REPRESENTATION OF LCAO MO WF'S

LCAO MO theory of conjugated molecules has long suffered from the lack of a simple but adequate graphic representation of its WF's. The only available methods have been (1) construction of π-electron contour diagrams, and (2) plotting the amplitude of ψ_j or the density function ψ_j^2 along some arbitrary line parallel to the main molecular axis. Such diagrams have rarely been computed for conjugated systems, but sometimes schematic diagrams have been given. Equation (2) suggests that the LCAO MO WF's can be represented by the corresponding FEM WF's. An illustration of the WF's of pentadienyl was given in a previous note.[2] It is recognized that such curves are not an accurate picture of the LCAO MO WF's, since they do not take the form of the φ_r into consideration. However, it is believed that they represent a good envelope to the true plot of ψ_j and hence should be useful in attempts to visualize the WF's. The positions of nodal planes, which are often of great importance, can readily be read from such graphs; and comparison of successive curves can give information concerning the changes occurring on excitation. The above discussion of molecules in-

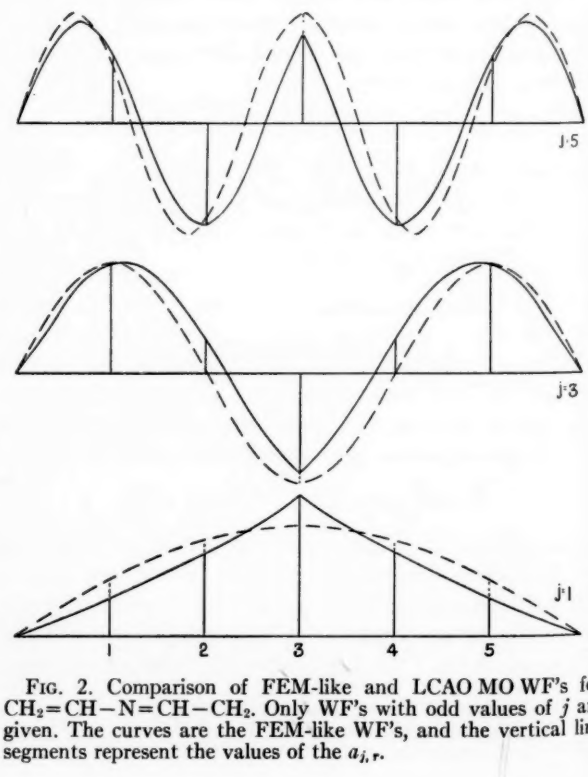

FIG. 2. Comparison of FEM-like and LCAO MO WF's for $CH_2=CH-N=CH-CH_2$. Only WF's with odd values of j are given. The curves are the FEM-like WF's, and the vertical line segments represent the values of the $a_{j,r}$.

volving heteroatoms and branched π-electron systems suggests that the FEM-like WF's derived may be used to represent LCAO MO WF's. Figure 2 gives the FEM-like WF's for the radical or ion $H_2C=CH-N=CH-CH_2$. It was pointed out above that the WF's for even values of j are unaffected by the heteroatom. Consequently, these WF's are omitted from Fig. 2; they have already been given in Fig. 1 of our previous note.[2] The WF's for odd values of j for pentadienyl are included as dashed curves in Fig. 2, which accordingly illustrates the effect of substitution of a nitrogen atom for the central methylene group of pentadienyl. The Coulomb integral (α) of the nitrogen atom was assumed to be 1β.

Figure 3 illustrates some of the WF's of divinylbenzene. The curve represents one side of the ring only, the other side of course being identical. The WF's antisymmetric with respect to reflection on the lengthwise axis of the molecule are not given; they are identical with those given by Kuhn for Wurster's salts.[12]

DISCUSSION

A simple relation between FEM and LCAO MO WF's has been derived for conjugated molecules having a linear or cyclic π-electron system. This relation permits the derivation of the LCAO MO WF's and their energies without extensive numerical calculations, and leads to simple analytic expression of WF's and energies. The method assumes equal resonance integrals involving all bonded atoms, and equal Coulomb integrals for all atoms. These conditions are most nearly fulfilled for even-membered cyclic molecules and for the free radicals or ions derived from odd-membered conjugated linear and cyclic polyenes. If the Coulomb integrals of the nitrogen and the carbon atoms are assumed equal, these conditions are also satisfied for the conjugated chains of the polymethine dyes, for which the FEM theory was developed by Kuhn.[3] The approximations involved in assuming that these conditions are fulfilled in molecules where bonds have different amount of double bond character, as qualitatively seen from valence bond considerations, have been discussed by Kuhn.[3] However, the WF's derived by the method described may well serve as a starting point for perturbation calculations by variation of Coulomb and resonance integrals.[1]

The relations derived for the molecules involving heteroatoms and branched π-electron systems give analytic expressions for the $a_{j,r}$ and W_j in terms of a set of parameters ρ_j. These parameters are defined by transcendental equations like Eq. (25). For some types of molecules the evaluation of the ρ_j is less laborious than the solution of the polynomial equations derived from the secular equation. Furthermore, the solution of the transcendental equations immediately gives the energies and the $a_{j,r}$ of the MO WF's.

The FEM method has been very successful, particularly in the hands of Kuhn,[3,9,12,13] in interpretation of spectra of molecules to which it appears most clearly applicable. The relations derived suggest that this success of FEM WF's may be partially due to their close relation to LCAO MO WF's, which are usually considered a better approximation of the WF's of a molecule than FEM WF's. However, this conclusion must be considered with caution since Kuhn's work is based on FEM energies, which do not agree with the LCAO MO energies derived here.

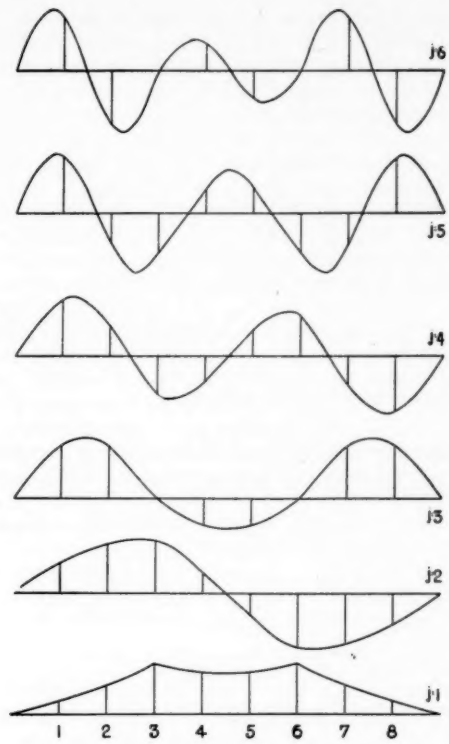

FIG. 3. The WF's of divinylbenzene.

Kuhn's empirical assumption that the "box" containing the π-electrons extends one bond distance beyond the ends of the conjugated chain receives some theoretical basis from the present work, since it is just this dimension of the "box" which leads to the relation of Eq. (2).

ACKNOWLEDGMENT

The author wishes to acknowledge the advice and help of Dr. Alfred T. Brauer of the Department of Mathematics, University of North Carolina.

APPENDIX

The above derivations are based on the secular equations in the form of Eq. (4). This was necessitated by the approach to LCAO MO WF's from FEM WF's through Eq. (2). It will be shown in this appendix that the same results can be derived from the determinantal form of the secular equations.

[13] H. Kuhn, Helv. Chim. Acta 34, 1308 (1951).

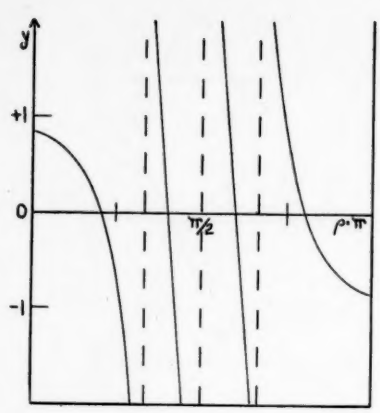

FIG. 4. The function $-y(\rho)=\sin\rho\{\cot(2\rho)+\cot(3\rho)\}$ of Eq. (25′).

The secular determinant for a linear homonuclear conjugated molecule of n atoms can be written as

$$D^{(n)}(-W)=\begin{vmatrix} -W & 1 & 0 & 0 & \cdot & \cdot \\ 1 & -W & 1 & 0 & & \\ 0 & 1 & -W & 1 & & \\ 0 & 0 & 1 & -W & & \\ \cdot & & & \cdot & & \\ \cdot & & & & & \cdot \end{vmatrix}, \tag{32}$$

where $D^{(n)}(-W)$ indicates a determinant, of the form of (32), of rank n in which all diagonal elements are $-W$. The secular equations (4) have solutions for the $a_{j,r}$ only if $D^{(n)}$ vanishes. It can be shown that[14]

$$D^{(n)}(2\cos\rho)=\sin[(n+1)\rho]/\sin\rho. \tag{33}$$

A necessary condition for the vanishing of Eq. (33) is

$$\rho=j\pi/(n+1), \quad j=1, 2, \cdots. \tag{34}$$

This condition is sufficient only if

$$\rho\neq j\pi; j\neq k(n+1), \quad k=1, 2, \cdots. \tag{35}$$

Hence

$$W_j/\beta=2\cos[j\pi/(n+1)], \quad j=1, 2, \cdots, n, \tag{6′}$$

are the eigenvalues. No new values are obtained for $j>n+1$. Since there are just nW_j in Eq. (6′), all the eigenvalues have this form.

In determinantal form, the $a_{j,r}$ are given by

$$a_{j,r}/a_{j,1}=D^{(r-1)}(-W_j)/D^{(0)}(-W_j), \tag{36}$$

with $D^{(0)}(-W_j)=1$. Consequently, from (33) and (36)

$$a_{j,r}/a_{j,1}=\sin r\rho/\sin\rho, \tag{37}$$

in agreement with Eq. (2).

The treatment of a linear molecule with a heteroatom at $r=m$ also follows easily. The secular determinant, $\Delta^{(n)}(-W, \alpha)$, where α is the Coulomb integral of the heteroatom, may be written as

$$\Delta^{(n)}(-W, \alpha)=D^{(n)}(-W)+(\alpha/\beta)D^{(n-m)}(-W)D^{(m-1)}(-W). \tag{38}$$

Again we assume

$$W_j/\beta=2\cos\rho_j, \tag{39}$$

and obtain from (35)

$$\Delta^{(n)}(2\cos\rho, \alpha)=-\frac{\sin[(n+1)\rho]}{\sin\rho}+(\alpha/\beta)\frac{\sin(m\rho)}{\sin\rho}\frac{\sin[(n-m+1)\rho]}{\sin\rho}. \tag{40}$$

Equating (40) to 0, we obtain the following equation as the condition for the vanishing of the determinant (38):

$$\alpha/\beta=-\sin\rho\sin[(n+1)\rho]/\sin(m\rho)\sin[(n-m+1)\rho] =-\sin\rho\{\cot(m\rho)+\cot[(n-m+1)\rho]\}. \tag{25′}$$

Hence the eigenvalues are given by (39), with the ρ_j given by Eq. (25′). If all the W_j are to have this form, Eq. (25′) must be satisfied by n values of $\rho_j<\pi$. Figure 4 is a graph of the right-hand side of Eq. (25′) for the case $n=4$, $m=2$. For $|\alpha/\beta|\leqslant 0.83$ there exist four solutions ρ_j, and hence all W_j have the form of Eq. (39). For $|\alpha/\beta|>0.83$, Eq. (25′) has only three solutions; thus we encounter the case mentioned above where the trignometric functions must be replaced by their hyperbolic equivalents. It can be shown that the critical value of $|\alpha/\beta|$ is in general

$$|\alpha/\beta|=\lim_{\rho\to 0}\{\sin\rho[\cot(m\rho)+\cot(n-m+1)\rho]\} =1/m+1/(n-m+1). \tag{41}$$

A somewhat special case is $m=(n+1)/2$. The critical value of $|\alpha/\beta|$ becomes $4/(n+1)$. However, the graph corresponding to Fig. 4 gives only $(n+1)/2$ solutions for ρ_j. The remaining $(n-1)/2$ solutions were lost in the derivation of (25′) from (40) when it was assumed that

$$\sin^2[(n+1)\rho/2]\neq 0. \tag{42}$$

Equating the left-hand side of (42) to 0, we obtain

$$\rho_k=2k\pi/(n+1), \quad k=1, 2, \cdots(n-1)/2. \tag{43}$$

These ρ_k lead to the wave functions ψ_j' for even j, which were given special treatment in the discussion of the symmetrical heteroatomic linear molecules. It is seen from Eq. (43) that these ρ_k are independent of α.

[14] E. Pascal, *Die Determinanten* (B. G. Teubner, Leipzig, 1900), p. 156.

Letters to the Editor

THIS section will accept reports of new work, provided these are terse and contain few figures, and especially few half-tone cuts. The Editorial Board will not hold itself responsible for opinions expressed by the correspondents. Contributions to this section should not exceed 600 words in length and must reach the office of the Editor not later than the 15th of the second month preceding that of the issue in which the Letter is to appear. No proof will be sent to the authors. A publication charge of $15.00 per Letter is made which, when honored, will entitle the Institution to 100 free reprints.

Centrifugal Distortion Effects in Methyl Chloride

TSU-SHEN CHANG AND DAVID M. DENNISON
Randall Laboratory, University of Michigan, Ann Arbor, Michigan
(Received April 20, 1953)

THE centrifugal distortion constants of the methyl halides were calculated some time ago by Slawsky and Dennison.[1] Using the values of the potential constants which were available at that time they obtained for CH_3Cl the following figures for the coefficients, respectively, of the $-(J^2+J)^2$ and $-(J^2+J)K^2$ terms: $D_{JJ}=+3$ kc/sec and $D_{JK}=-293$ kc/sec. More recently[2] these constants have been determined experimentally from the microwave spectrum of methyl chloride and have been found to be $D_{JJ}=+26.4$ kc/sec, $D_{JK}=+189$ kc/sec for CH_3Cl^{35} and $D_{JJ}=+27.0$ kc/sec, $D_{JK}=+184$ kc/sec for CH_3Cl^{37}. The agreement between theory and experiment is obviously very poor.

Since the work of Slawsky and Dennison, new experimental data have been found which make possible a much more accurate evaluation of the molecular potential constants, and consequently a recalculation of the centrifugal constants has been undertaken. The data now comprise the following items: (1) the six fundamental frequencies[3] of CH_3Cl, (2) the six fundamental frequencies[3] of CD_3Cl, (3) the three ζ of the perpendicular[4] bands of CH_3Cl, and (4) two of the ζ of the perpendicular bands of CD_3Cl. Since the parallel and perpendicular bands of the light and heavy methyl chloride are related through the product rule and since the sum of the ζ is a function only of the moments of inertia, the above items constitute 14 independent data which are available for the calculation of the 12 general potential constants describing the molecule.

The following procedure was employed. The product rules were used to estimate the normal frequencies of both CH_3Cl and CD_3Cl using the methods developed by Hansen and Dennison.[5] It is believed that the normal frequencies so determined are probably accurate to around 0.5 percent. A set of 12 potential constants were found which (1) reproduced the 12 normal frequencies of the light and heavy methyl chloride within 0.5 percent, (2) reproduced the 5 experimental spacings of the fine structure of the perpendicular bands (dependent upon the ζ-values) with an accuracy of better than 8 percent (average error = 4 percent), and (3) described a potential which is essentially of the valence type. This last property means that if the potential is expressed by means of valence coordinates, (i.e., the CCl and CH distances and the H−C−Cl and H−C−H angles) the coefficients of the cross-product terms are small in comparison with those of the diagonal terms. It may be remarked that the most significant cross-product term was found to be the one connecting the CCl distance and the H−C−Cl angles.

Using the new potential constants the centrifugal distortion was calculated and led to the values $D_{JJ}=+18.4$ kc/sec, $D_{JK}=+189$ kc/sec for CH_3Cl^{35} and $D_{JJ}=+17.8$ kc/sec, $D_{JK}=+186$ kc/sec for CH_3Cl^{37}. It will be noted that D_{JK} agrees very well indeed with the corresponding experimental values, but that D_{JJ} differs by a factor of about 1.5.

The discrepancy between the theoretical and observed values of D_{JJ} was examined carefully. Theoretically, the situation appears to be very straightforward. This particular term in the energy arises from the centrifugal distortion of the molecule when it rotates end over end (i.e., when $K=0$). The distortion is caused in large measure by the change in length of CCl distance, and hence it depends directly upon the lowest parallel vibration frequency which lies at 732 cm^{-1}. Indeed a simple calculation in which the methyl chloride molecule is represented as a diatomic molecule with atoms of mass 35 and 15 and with the single frequency 732 cm^{-1} yields the result $D_{JJ}=+19$ kc/sec. It therefore appears that no reasonable change in the potential constants can resolve the discrepancy.

On the side of experiment, however, the evidence is much less conclusive. The determination of D_{JK} depends upon differences in frequency between adjacent microwave lines and an examination of the self-consistency of these lines leads to the estimate that D_{JK} is probably correct to around 1 percent. D_{JJ}, on the other hand, is found by combining lines in quite different regions of the microwave spectrum, e.g., the lines at 26585.77 and 79754.85 mc/sec for CH_3Cl^{35}. If the first of these should be decreased by 0.17 and the second increased by 0.17 mc/sec, the resulting experimental D_{JJ} would equal +18.4 kc/sec in exact agreement with the theoretical value.

The details of the calculation together with the values of the potential constants of methyl chloride will be published shortly.

[1] Z. I. Slawsky and D. M. Dennison, J. Chem. Phys. **7**, 509 (1939).
[2] J. W. Simmons and W. E. Anderson, Phys. Rev. **80**, 338 (1950).
[3] G. Herzberg, *Infra-Red and Raman Spectra of Polyatomic Molecules* (D. Van Nostrand Company, Inc., New York, 1945), p. 315.
[4] See reference 3, p. 438.
[5] G. E. Hansen and D. M. Dennison, J. Chem. Phys. **20**, 313 (1952).

Solutions of Fluorocarbons and Hydrocarbons; the Energy of Mixing

ROBERT DUNLAP
Department of Chemistry, University of Maine, Orono, Maine
(Received May 11, 1953)

RECENT articles on solutions of fluorocarbons and hydrocarbons[1-3] show that large discrepancies exist between the energies of mixing and those calculated from the approximate equation:

$$\bar{E}_1-E_1^0=\left(\frac{X_2V_2}{X_1V_1+X_2V_2}\right)^2V_1\left[\left(\frac{\Delta E_1}{V_1}\right)^{\frac{1}{2}}-\left(\frac{\Delta E_2}{V_2}\right)^{\frac{1}{2}}\right]^2 \quad (1)$$

developed by Hildebrand and Wood[4] and by Scatchard.[5] Simons and Dunlap[1] using the procedure of Hildebrand and Wood, but using $V=X_1\bar{V}_1+X_2\bar{V}_2$ instead of $V=X_1V_1+X_2V_2$, derived the following equation:

$$\bar{E}_1-\frac{V_1}{\bar{V}_1}E_1^0=\left(\frac{X_2\bar{V}_2}{X_1\bar{V}_1+X_2\bar{V}_2}\right)^2\bar{V}_1\left[\left(\frac{V_1\Delta E_1}{\bar{V}_1^2}\right)^{\frac{1}{2}}-\left(\frac{V_2\Delta E_2}{\bar{V}_2^2}\right)^{\frac{1}{2}}\right]^2 \quad (2)$$

from which $\bar{E}_1-\bar{E}_0$ can be calculated. This gives a considerable increase in the energy of mixing, which is primarily due to expansion (about 3 percent in these mixtures), but it was pointed out that this alone was not enough to account for the large energy attending the mixing of *n*-pentane with *n*-pentoforane. The discrepancy was ascribed to properties of the hydrocarbon, and the concept of interpenetration was invented as an adjustment to the existing theory. Simons and Mausteller studied the system *n*-butane–*n*-butforane[2] and found the same discrepancy from the simple theory as was found with the five carbon system. Hildebrand discussed discrepancies from the simple theory[6] in the case of hydrocarbons and designated their behavior as "anamalous." For practical purposes he adjusted the solubility parameter $(\Delta E/V)^{\frac{1}{2}}$ of the hydrocarbons by calculating an empirical value for this quantity from the solubility data.

In the articles[1,2] the partial molal heats and free energies of mixing calculated from liquid vapor equilibrium data are plotted

TABLE I. System n-C_5H_{12}–n-C_5F_{12}.

Mole fraction of n-C_5F_{12}	Partial molal heats and energies for C_5F_{12}: $\bar{E}_1-E_1^0$ Eq. (1) (calc)	$\bar{E}_1-E_1^0$ Eq. (3) (calc)	$\bar{H}_1-\bar{H}_1^i$ exp. (calc)	Mole fraction of n-C_5H_{12}	Partial molal heats and energies for C_5H_{12}: $\bar{E}_2-E_2^0$ Eq. (1) (calc)	$\bar{E}_2-E_2^0$ Eq. (3) (calc)	$\bar{H}_2-\bar{H}_2^i$ exp. (calc)
0.0		1798		0.0		1168	
0.1	220	1428	1425	0.1	170	989	985
0.2	155	1019	925	0.2	145	824	870
0.3	110	711	655	0.3	120	672	735
0.4	80	476	490	0.4	95	536	535
0.5	45	296	320	0.5	75	410	415
0.6	30	158	250	0.6	50	297	355
0.7	15	56	150	0.7	30	196	275
0.8	6	1	0	0.8	15	111	205
0.9	1	0	0	0.9	4	50	140
1.0		0	0	1.0		0	0

against the quantity $(X_2V_2/X_1V_1+X_2V_2)^2V_1$. The free energy plot is essentially a straight line, while the points for the heats of mixing fall on a sinuous curve which is characteristic of both the four and five carbon systems. Neither the concept of interpenetration as it is presently used, nor an adjustment to the solubility parameters will give a wavy line. One might argue that the geometric mean assumption might not hold in these systems. The energy of mixing calculated from simple theory can be increased to the desired magnitude in these systems by assuming the geometric mean to be off by 5 percent. However, this spreads the curves for the two components farther apart on the volume-fraction plot and does not impart the characteristic wavy behavior.

Implicit in the derivations of Eqs. (1) and (2) is the concept that the product of energy and volume for each component is a constant and remains so during the mixing process. Thus Eq. (2) gives the partial molal energy of mixing for component 1 when both liquids are expanded to their partial molal volumes. The quantities $[(V_1/\bar{V}_1^2)E_1]^{\frac{1}{2}}$ and $[(V_2/\bar{V}_2^2)E_2]^{\frac{1}{2}}$ are the solubility parameters for each of the components at their partial molal volumes, and $(V_1/\bar{V}_1)E_1^0$ is the point on the energy curve to which component 1 must be changed before it is mixed. If we designate this point as E_1', we see that $V_1E_1^0=\bar{V}_1E_1'$.

An equation similar to (2) can be derived using the more general energy-volume relationship $E=k/V^n$. We now have $V_1^nE_1^0=\bar{V}_1^nE_1'$, and $V_2^mE_2^0=\bar{V}_2^mE_2'$, and the equation for the partial molal energy of mixing after rearranging and setting $E_1^0=-\Delta E$ is:

$$\bar{E}_1-E_1^0=\left(\frac{X_2\bar{V}_2}{X_1\bar{V}_1+X_2\bar{V}_2}\right)\bar{V}_1\left[\left(\frac{V_1^n\Delta E_1}{\bar{V}_1^{n+1}}\right)^{\frac{1}{2}}-\left(\frac{V_2^m\Delta E_2}{\bar{V}_2^{m+1}}\right)^{\frac{1}{2}}\right]^2-\left(\frac{V_1^n-\bar{V}_1^n}{\bar{V}_1^n}\right)\Delta E_1. \quad (3)$$

This equation reduces to Eq. (1) when there is no volume change on mixing. The first term gives the partial molal energy of mixing at $\bar{V}_1$ and $\bar{V}_2$, and the second term is the energy required to change component 1 from V_1 to $\bar{V}_1$.

In applying this equation to the n-pentane–n-pentforane system and to the n-butane–n-butforane system, let subscript 1 designate the fluorocarbon. The exponent n for the fluorocarbon can be evaluated from the experimental data when $V_2=\bar{V}_2$, that is, at a high concentration of hydrocarbon. The exponent m for the hydrocarbon can be evaluated at $V_1=\bar{V}_1$ or at a high fluorocarbon concentration.

TABLE II. System n-C_4H_{10}–n-C_4F_{10}.

Mole fraction of n-C_4F_{10}	Partial molal heats and energies for nC_4F_{10}: $\bar{E}_1-E_1^0$ Eq. (1) (calc)	$\bar{E}_1-E_1^0$ Eq. (3) (calc)	$\bar{H}_1-\bar{H}_1^i$ exp. (calc)	Mole fraction of n-C_4H_{10}	Partial molal heats and energies for nC_4H_{10}: $\bar{E}_2-E_2^0$ Eq. (1) (calc)	$\bar{E}_2-E_2^0$ Eq. (3) (calc)	$\bar{H}_2-\bar{H}_2^i$ exp. (calc)
0.0				0.0			
0.1	171	1444	1455	0.1	133	845	1185
0.2	123	999	1062	0.2	114	746	992
0.3	86	689	786	0.3	94	692	696
0.4	57	359	638	0.4	75	639	574
0.5	37	265	513	0.5	56	477	495
0.6	21	115	386	0.6	39	367	403
0.7	11	42	138	0.7	24	225	222
0.8	5	40	0	0.8	12	144	69
0.9	1	0	0	0.9	3	58	49
1.0				1.0			

For n-pentane m was found to be 1.28 and for n-pentforane n was found to be 1.85. These exponents were used to calculate the partial molal energy of mixing at each composition for the five carbon and four carbon systems, and these values are compared with the partial molal heats of mixing in Tables I and II. The shape of the energy-volume fraction curves are reproduced rather well. A small discrepancy in the volume change attending mixing would result in a large error in the calculated energy. Calculations of this type certainly show the need for careful measurements on the volume change attending mixing, and may provide a method for determining energy-volume relationships for the expansion of liquids at constant temperature.

This study is supported by the U. S. Office of Ordnance Research, Department of the Army.

[1] J. H. Simons and R. D. Dunlap, J. Chem. Phys. **18**, 335 (1950).
[2] J. H. Simons and J. W. Mausteller, J. Chem. Phys. **20**, 1516 (1952).
[3] Hildebrand, Fisher, and Benesi, J. Am. Chem. Soc., **82**, 4348 (1950).
[4] J. H. Hildebrand and S. E. Wood, J. Chem. Phys. **1**, 817 (1933).
[5] G. Scatchard, Chem. Revs. **8**, 321 (1931).
[6] J. H. Hildebrand, J. Chem. Phys. **18**, 1337 (1950).

Linear Film Growth in Tarnishing Reactions

R. C. WILLIAMS* AND P. R. WALLACE
McGill University, Montreal, Quebec, Canada
(Received May 1, 1953)

ACCORDING to the Cabrera-Mott theory of tarnishing reactions,[1] in the early stages of film growth electrons pass through the tarnishing film either by tunnel effect or thermionic emission to form negative ions at the outer surface. The field of these ions, which is inversely proportional to film thickness, then pulls positive metal ions through the film. This should give rise to an initial logarithmic growth rate, followed by a parabolic one.

Experiments of Perry and Winkler of this University,[2] indicate for growth of AgCl on silver in triphenylmethyl chloride (at temperatures slightly above the critical temperature for film growth), a transition from an initial logarithmic rate of growth to a *linear* one at greater thickness. In attempting to interpret these results, we were led to investigate critically the mechanism proposed by Cabrera and Mott.

Using a one-dimensional square-well model for crystalline AgCl, and adjusting the constants in such a way as to have the top of the valence band at -7.5 ev and the bottom of the conduction band at -3.4 ev[3] as given by L. P. Smith, we first calculated the probability of quantum-mechanical tunnelling of electrons through the film as a function of thickness assuming certainty of capture in ionic levels at the outer film surface. We found that the supply of electrons for forming Cl^- was adequate for sustaining the Mott-Cabrera mechanism up to a film thickness of about 80A, which coincides approximately with the point at which the logarithmic growth law goes over (a) at 65.4°C, to a parabolic one, and (b) at 44.9°C to a linear one. It was thus evident that some other process had to supply the electrons past this point.

We then calculated the flow of electrons due to thermionic emission from the Fermi surface of the metal into the conduction band of AgCl. At all temperatures used in the Perry-Winkler experiments, it was found that the number of electrons getting through the film by this process was inadequate to sustain the reaction, by a large factor. This was due to the large work function (1.3 ev).

Since the existence of a linear growth law clearly suggests that the rate-controlling mechanism does not depend on the thickness of the film, it would seem that in such a case this limiting mechanism is *not* the diffusion of Ag^+ ions, as assumed by Mott and Cabrera, but the formation of Cl^- ions at the film-reagent inter-

face. Also, since the linear growth rate persists even at high triphenylmethyl chloride concentrations, it is reasonable to suppose that the rate-controlling factor is actually the electron supply. Furthermore, the existence of a solvent effect (in toluene, there is linear growth at 44.9°C and not at 65.4°C; in acetonitrile, there is linear growth at 3.5°C and not at 29.5°C) indicates that the limiting mechanism takes place at the outer film surface.

We therefore investigated the rate of formation of ions due to excitation of electrons from the valence band of AgCl into Cl^- levels localized at the surface. For the case in which toluene was the solvent, we found that the rate of film growth at 44.9°C could be explained if the activation energy for this process were slightly less than 0.9 ev. On the other hand, the electron supply at 65.4°C comes out to be nearly ten times as large, so that it is no longer the limiting factor at this temperature, and the Mott-Cabrera theory holds.

In the case in which acetonitrile was the solvent, the activation energy calculated in the same way was found to be 0.78 ev. At 29.5°C and 44.9°C, at which parabolic growth was observed, the electron supply was found to be about 10 and 50 times as large, respectively, and therefore, again, would not be the limiting factor.

* Now at RCA Victor Company, Montreal.
[1] Cabrera and Mott, Repts. Progr. Phys. **12**, 163 (1949).
[2] E. J. Perry and C. A. Winkler, Can. J. Chem. **30**, 235 (1952).
[3] D. K. Henisch, *Semi-Conducting Materials* (Butterworth Scientific Publications, London, 1951), p. 115.

Dielectric Dispersion of Water Vapor Adsorbed on Silica Gel

KAN-ICHI KAMIYOSHI AND TAKESHI ODAKE
Research Institute for Scientific Measurements, Tôhoku University, Sendai, Japan
(Received May 8, 1953)

RECENTLY several investigators[1–5] have observed the low-frequency dielectric dispersion of water vapor adsorbed on silica gel. According to these observations, the resonance frequency increases with the increase in adsorbed amount or with the fall in temperature, but the results are considerably divergent with different investigators. The present writers have also observed this low-frequency dispersion at various temperatures and adsorbed amounts and found a linear relation as shown in Fig. 1. Another linear relation was also obtained between $\log f$ and $1/T$, where f and T are resonance frequency and absolute temperature, respectively. These results are summarized by the equation

$$f = a \exp\left(-\frac{E}{kT} + b\bar{W}\right), \tag{1}$$

where W is adsorbed amount (*wt* percent) and a, b, and E are constants, which, by substituting the experimental values, are $a = 3.6\times10^7$ (c/sec), $b = 0.78$ (per *wt* percent) and $E = 8000$ (cal/mole). The results obtained by Rolland and Bernard[1] were also found to fit to Eq. (1), but the numerical values of the constants are considerably different: $a = 7.2\times10^7$, $b = 0.52$, and $E = 10\,000$. Linear relation between $\log f$ and $1/T$ was also observed by Freymann and Freymann.[2]

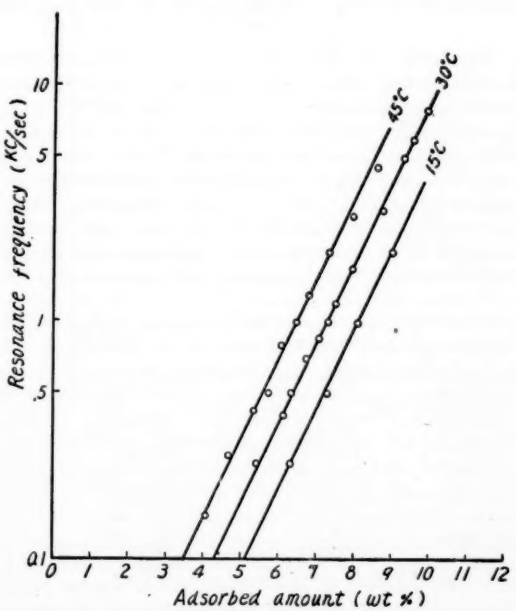

FIG. 1. Relation between resonance frequency and adsorbed amount.

There are two types of model for dispersion phenomena, namely, Debye type and Wagner type, but the experimental distinction is not so clear in most cases. According to Morgan,[6] the maximum of the dispersion curve decreases with rising temperature in Debye type, but it increases in Wagner type. Figure 2 shows the resonance curves at various temperatures. Peak heights increase with rising temperature, suggesting Wagner type. In this figure only dispersion part is shown, subtracting the logarithmic increasing part caused by conductivity on which dispersion curve is superimposed. Resonance curves obtained by Rolland and Bernard[1] show the same conclusion.

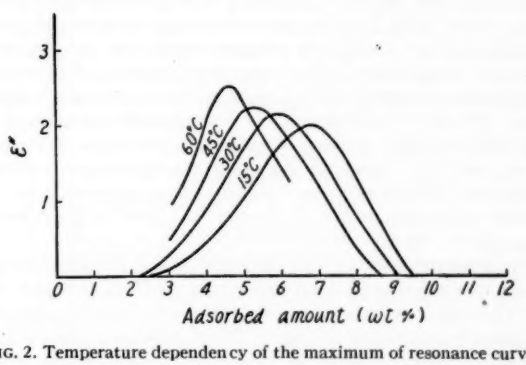

FIG. 2. Temperature dependency of the maximum of resonance curve.

According to Koops' double-layer model[7] which is the modification of Wagner type and which takes into consideration the two relaxation times, the frequency at which ϵ'' becomes maximum is lower than the frequency at which $\epsilon' = (\epsilon_0+\epsilon_\infty)/2$, but these two become nearly equal when the ratio of static to high-frequency resistivity is large.[8] In Debye type these two frequencies coincide in all cases. In the results obtained by Kurosaki[5] who observed the same kind of dispersion, two frequencies are not equal. But in the present experiment no decision could be given because the above ratio is large.

Ice, as is well known, has low-frequency dispersion of probably Debye type, and if the adsorbed water molecule is in the same state as ice, it will have the dispersion of Debye type. But Freymann and Freymann[9] reported that the adsorbed water vapor was probably in liquid state and that the freezing point of it was considerably lower than 0°C. One of the present writers[10] also showed that the adsorbed water molecule at room temperature is in the intermediate state between gas and liquid and gradually tends to liquid state with the increase in adsorbed amount.

Therefore, the low-frequency dispersion of adsorbed water molecule seems to be of Wagner type. According to this dispersion equation,[6]

$$\tau = \frac{2\epsilon_1' + \epsilon_2'}{4\pi(2G_1 + G_2)}, \tag{2}$$

where ϵ_1', ϵ_2', G_1, and G_2 are dielectric constants and conductivities of adsorbed film (1) and silica gel or air or both (2). If one can assume $G_1 \gg G_2$ and $G_1 = a\cdot\exp(b\bar{W})\cdot\exp(-E/kT)$, where E is the activation energy for the migration of ion on the surface of ad-

sorbent, then, as $2\pi f\tau=1$ for resonance frequency, the equation of the same form as Eq. (1) can be obtained.

[1] M-T. Rolland and R. Bernard, Compt. rend. **232**, 1098 (1951).
[2] M. Freymann and R. Freymann, J. Chem. Phys. **20**, 1970 (1952).
[3] J. Le Bot and S. Le Montagner, Compt. rend. **233**, 862 (1951).
[4] M. G. Carpéni, Compt. rend. **233**, 158 (1951).
[5] S. Kurosaki, J. Chem. Soc. (Japan) **73**, 606 (1952).
[6] S. O. Morgan, J. Electrochem. Soc. **65**, 109 (1934).
[7] C. G. Koops, Phys. Rev. **83**, 121 (1951).
[8] K. Kamiyoshi, Sci. Repts. Research Inst. Tôhoku Univ. **3**, 716 (1951).
[9] M. Freymann and R. Freymann, Compt. rend. **232**, 401, 1096 (1951).
[10] K. Kamiyoshi, Sci. Repts. Research Inst. Tôhoku Univ. **3**, 513 (1951).

The Decomposition of Methanol-C^{14} under the Influence of its Own Radiation*

W. J. Skraba,† J. G. Burr, Jr.,‡ and D. N. Hess
Chemistry Division, Oak Ridge National Laboratory, Oak Ridge, Tennessee
(Received April 14, 1953)

THE decomposition of organic compounds labeled with carbon-14 under the influence of their own radiation (beta-particles of average energy 0.049 Mev[1]) must always be a problem when such compounds are stored for long periods of time. There have been no reported observations of such decomposition; and probably it is under most circumstances of minor concern.[2]

We have had occasion, however, to observe the occurrence of such a process on a rather extensive scale; and have been able through the use of isotopic dilution techniques to characterize several of the products. The decomposition occurred in a number of ampoules of methanol-C^{14}; each of these ampoules contained about 100 mC of methanol-C^{14} with a specific activity of 8–10 mC/mM. Recently we had occasion to open some of these ampoules, and then observed that they now contained several atmospheres pressure of a gas which was noncondensable at liquid nitrogen temperature (although they had been sealed initially in vacuum).

The gas from one of these ampoules (No. 2, Table I) was analyzed in the infrared spectrophotometer (Perkin-Elmer Model 21). The only constituent present (except hydrogen) appeared to be about 2 percent of methane. There was no evidence for the presence of carbon monoxide. Mass spectrometer examination of the gas confirmed these observations. The total yield of gas from each ampoule as shown in Table I averaged 5.4 ± 0.3 molecules of gas per 100 ev. The corresponding value found by McDonell[3] for the irradiation of methanol with 28-Mev helium ions was 4.73 ± 0.26.

The recovery of methanol from these ampoules averaged about 81 percent. In transferring this methanol on the vacuum line, the presence of a much less volatile material was observed. After a number of such ampoules had been opened and the volatile contents removed, the pooled less volatile fraction was removed from the line with some difficulty, and about 41 mg of a highly radioactive oil so obtained. The infrared spectrum of this oil (as a film) resembled very closely that of ethylene glycol and contained no evidence for the presence of formaldehyde, a major product reported by McDonell.[3] The remaining oil was then mixed with 15 g of ethylene glycol and 10 g of glycerol, and this mixture fractionated under reduced pressure. A portion of the ethylene glycol fraction was then converted to the dibenzoate (mp 72°).

Table I.

Ampoule No.	mC of Methanol-C^{14} initially	m moles gas produced	G (molecules/100 ev)
1	122	1.12	5.60
2	127.8	1.10	5.24
3	102	1.01	6.04
4	90.7	0.79	5.31
5	73	0.63	5.26
6	95.4	0.75	4.80

After crystallization to constant specific activity (from two solvents) this material then contained 22.25 μC of carbon-14/mM. This represents a total content of 5.38 mC of ethylene glycol in the radiolysis product. The tribenzoate (mp 72–73°) prepared from the glycerol fraction was similarly crystallized to constant specific activity and then contained 0.54 μC of carbon-14/mM. This represents the presence of 0.0587 mC of glycerol in the radiolysis product. The residue from the above distillation was mixed with 2.00 g of *i*-erythritol. After two crystallizations from ethanol, this erythritol had an activity of 0.240 μC of carbon-14/mM. Conversion of this to the dibenzilidine derivative, mp 199°, did not substantially change the molar activity This corresponds to 0.00395 mC of erythritol in the radiolysis product.

Thus the ratio of ethylene glycol to glycerol to erythritol was 1360/14.9/1.00.

These results are in agreement with the observations of McDonell, except for the absence of formaldehyde among the products observed here. In addition, the hydrogen/methane ratio we observe differs from that of McDonell. This may be an effect of the difference in particle velocity, such as observed by Sworski and Burton.[4]

* This document is based upon work performed under Contract Number W-7405-eng-26 for the U. S. Atomic Energy Commission at the Oak Ridge National Laboratory. After the completion of this work and submission of this letter, the recent article by B. M. Tolbert, *et al.*, J. Am. Chem. Soc. **75**, 1867 (1953), appeared describing the radiation decomposition of C^{14}-labeled valine, norvaline, norleucine, choline chloride, calcium glycolate, and cholesterol.

† Present address: Carbide and Carbon Chemicals Division, Union Carbide and Carbon Corporation, South Charleston, West Viriginia.
‡ Requests for reprints should be addressed to this author.

[1] Glenn Jenks, Oak Ridge National Laboratory, private communication.
[2] After the completion of this work, our attention was directed to a forthcoming article in the Journal of the American Chemical Society by Richard M. Lemmon and co-workers upon the radiative self-decomposition of several C^{14}-labeled amino acids.
[3] W. R. McDonel, U. S. Atomic Energy Commission Report, UCRL-1378 (July 6, 1951).
[4] T. J. Sworski and M. Burton, J. Chem. Phys. **73**, 3890 (1951).

Even-Odd Character of the 2900–3200A Absorption Transition in Naphthalene

Harden McConnell
Shell Development Company, Emeryville, California
and
Donald S. McClure
Department of Chemistry, University of California, Berkeley, California
(Received April 20, 1953)

A NUMBER of attempts have been made to determine whether the 2900–3200A absorption transition in naphthalene is an *even→even* ($g\rightarrow g$) or an *even→odd* ($g\rightarrow u$) singlet-singlet electronic transition. These attempts have been reviewed and discussed by Sponer and Nordheim.[1] The present note cites new evidence that this transition is *even→odd*. Table I gives the absorption frequencies (cm^{-1}) and peak intensities (liters/mole-cm) of naphthalene, 2-methylnaphthalene, and 2,6-dimethylnaphthalene as obtained in 3-methylpentane rigid glass solvent at −196°C with a Cary recording spectrophotometer. Absorp-

Table I. Absorption frequencies and intensities of methylnaphthalenes.

Naphthalene cm^{-1} ($\nu-31\,726$)	2-Methyl cm^{-1} ($\nu-31\,412$)	2,6-Dimethyl cm^{-1} ($\nu-30\,950$)	Assignment
0[35.6][a]	0[1235]	0[2520]	(0, 0)
428[455]	425[224]	~485[~290][b]	ν_1
710 [72]	711[505]	706[920]	ν_2
911[246]	956[294]	~902[~350]	ν_2
1131[303]	1135[266]	~1189[~420]	$\nu_1+\nu_2$
1420[405]	1413[822]	1418[1350]	$\nu_4(2\nu_2)$
1607[334]	...	~1626[~460]	$\nu_2+\nu_3$
1899[462]	1860[325]	~1907[~360]	$\nu_1+2\nu_2$
2126[282]	2150[480]	2135[620]	$3\nu_2$
...	...	2856[820]	$2\nu_4$

[a] Numbers in brackets [ ] are peak intensities in 1/mole-cm.
[b] The approximation signs ~ are used when only inflections are seen in absorption.

tivities are accurate to within a 5 percent error and frequencies are accurate to ± 20 cm^{-1}.

The assignment of the 0—0 band of naphthalene in Table I (31 726 cm^{-1}) is in accordance with the absorption and fluorescence measurements of Kasha and Nauman.[2] The close agreements between the vibrational intervals of naphthalene, 2-methylnaphthalene, and 2,6-dimethylnaphthalene are strong evidence that the 31 412 cm^{-1} band of 2-methylnaphthalene and the 30 950 cm^{-1} band of 2,6-dimethylnaphthalene are also 0—0 bands. The fluorescence spectrum of 2,6-dimethylnaphthalene (rigid glass) was determined and found to show a short wavelength (intense) band at 30 800 cm^{-1} on which are superimposed vibrations of frequencies 470 ± 40 730 ± 50 895 ± 35, and 1360 ± 30 cm^{-1} together with some seven combinations of these frequencies. This evidence further supports the 0—0 assignment for 2,6-dimethylnaphthalene.

The evidence that the 2900–3100A absorption in naphthalene arises from a *single* $g\rightarrow u$ transition is as follows:

(1) From Table I it is seen that on introducing one methyl group in naphthalene *all* the bands move 314 cm^{-1} to the red, and introducing the second methyl group moves *all* the bands 462 cm^{-1} further to the red. Thus the bands in Table I could hardly arise from two separate electronic transitions since the energies separating the 0—0 bands of *different* electronic transitions are invariably changed on alkyl substitution.

(2) 2,6-Dimethylnaphthalene shows all the characteristics of an allowed singlet-singlet absorption transition; e.g., a strong 0—0 band in absorption and fluorescence frequencies (see above) compatible with the known totally symmetric Raman frequencies of naphthalene, 512, 764, 1025, and 1380 cm^{-1}. 2,6-Dimethylnaphthalene has almost perfect central symmetry, so the absorption transition, being allowed, is $g\rightarrow u$. If the transition is $g\rightarrow u$ in 2,6-dimethylnaphthalene, it is also $g\rightarrow u$ in naphthalene.

The relative intensities of the 0—0 bands in Table I are in qualitative agreement with the spectroscopic moment theory of Platt if the transition is $g\rightarrow u$.[3] (The moment theory is, incidentally, more strictly applicable to 0—0 intensities than it is to integrated intensities over all bands of an electronic transition.)

(3) From naphthalene vapor absorption[1] and fluorescence,[4] the separation of the 1—0 (1 in ground state, 0 in excited state) and 0—1 bands is 942 ± 5 cm^{-1}. If the transition is $g\rightarrow u$ then the separation of the 0—0 and 0—1 bands must be $942-512=430$ cm^{-1} where 512 cm^{-1} is the totally symmetric Raman frequency of the ground state. This frequency, 430 cm^{-1}, is in satisfactory agreement with the separation of the 0—0 and 0—1 bands of naphthalene and 2-methylnaphthalene given in Table I, 428 and 425 cm^{-1}.

In the fluorescence spectra of naphthalene in both vapor[4] and rigid glass,[2] the 1380 mode appears several times with great intensity. In both cases, however, it does not add onto the 0—0 band but only to the first strong band, 512—0 in the present interpretation. The two totally symmetric frequencies 747, 764 are also prominent in these spectra but their 1—0 bands are very weak. In the absorption in solid solution the 0—1 bands of the 710 mode (assumed to correspond to 747 or 764 or both) is very weak, but gains considerable intensity in combination with 428. It is not so easy to identify the 1380 analog in absorption from the solution spectra, but the crystal spectrum[5] indicates this to be 1190 cm^{-1}. This does not appear as a 0—1 band in absorption, but may be combined with 428 as the band 1607 cm^{-1} from the origin. This behavior of the two modes of only appearing strongly when combined with the 512 (428) mode makes the spectra appear to be electronically forbidden-vibrationally allowed, and accounts for some of the difficulties with the interpretation. The same does not seem to be true of the substituted naphthalenes. In the fluorescence, 1360 and 730 intervals from the 0—0 band appear with great intensity. In absorption $\nu_2(710)$ is many times stronger in the derivatives, although it is not clear whether or not the analog of 1360 appears. It is quite possible that the 512 (428) a_{1g} mode in naphthalene effects the intensification by bringing about vibrational electronic interaction with an electronic state having the same symmetry as the upper state of this transition. It is to be noted from the data in Table I that the electrical effects of substitution in substituted naphthalenes are much stronger than the vibrational electronic interaction effects.

Details of the low-temperature absorption spectra will be given later by one of us (H. Mc.) and an interpretation of the crystal and vapor spectrum of naphthalene in terms of a $g\rightarrow u$ transition will be given by the other (D. Mc.) in collaboration with O. Schnepp.

[1] H. Sponer and G. P. Nordheim, Disc. Faraday Soc. No. 9, 19 (1950).
[2] M. Kasha and R. V. Nauman, J. Chem. Phys. 17, 516 (1949).
[3] J. R. Platt, J. Chem. Phys. 19, 263 (1951); 19, 1418 (1951).
[4] O. Schnepp and D. McClure, J. Chem. Phys. 20, 1375 (1952).
[5] O. Schnepp and D. McClure (unpublished work).

The Vapor Pressures of the Deuteromethanes

GEORGE T. ARMSTRONG, F. G. BRICKWEDDE, AND R. B. SCOTT
National Bureau of Standards, Washington 25, D. C.
(Received April 17, 1953)

ASIDE from an estimate of the boiling point of CH_3D by Stedman[1] and a number of determinations of the triple point temperatures and pressures of CH_3D and CD_4 in Clusius' laboratory,[2–6] the only reported measurements of the vapor pressures of the deuteromethanes are values for CH_3D taken at 99.5°K by Frank and Clusius[4] in connection with the determination of the latent heat of vaporization. Because of the paucity of the data on the deuteromethanes we feel that a preliminary report of the results of a recent recalculation of measurements made at the National Bureau of Standards some years ago would be of general interest. A final, more detailed account of the experiments will be published in the near future.

The measurements were made on samples of the four deuteromethanes prepared by the following reactions:

1. $CH_3MgI+D_2O\rightarrow CH_3D+DOMgI$
2. $CH_2I_2+2C_2H_5OD+2Zn\rightarrow CH_2D_2+2C_2H_5OZnI$
3. $CHCl_3+3C_2H_5OD+3Zn\rightarrow CHD_3+3C_2H_5OZnCl$
4. $CCl_4+4C_2H_5OD+4Zn\rightarrow CD_4+4C_2H_5OZnCl$
5. $2CO+2D_2\rightarrow CD_4+CO_2$.

Nonmethane impurities were removed by fractional distillation. The methanes prepared by reactions 2, 3, and 4 were each found by mass spectrometer analysis to contain relatively large amounts of the other deuteromethanes. Reaction 5 yielded much purer CD_4 than did reaction 4. No impurities were found in the CH_3D. The vapor pressures of the pure compounds were calculated from the observed pressures assuming the mixtures to behave as ideal solutions. Good agreement between the calculated values for CD_4 from reaction 4 and from reaction 5 appears to justify this assumption.

The samples were condensed in cavities in a copper block, and in a separate cavity of this block was placed a sample of carefully purified CH_4 whose vapor pressure had previously been determined. With this block kept at constant temperature the differences in the vapor pressure of CH_4 and the deuteromethanes were measured by differential oil manometers, and the absolute vapor pressure of the CH_4 was measured at the same time by a mercury manometer. The temperature range covered was approximately from 70° to 112°K.

TABLE I.[a]

	Solid range		Liquid range		Triple point		Triple point[b]	
	A	*B*	*A*	*B*	*T*°K	*P*(mm Hg)	*T*°K	*P*(mm Hg)
CH_4	...	...	...	...	90.660	87.60	90.67	87.4
CH_3D	1.259	110.2	1.328	129.5	90.406	84.52	90.42	84.4
CH_2D_2	2.390	195.7	2.742	253.5	90.151	81.80		
CHD_3	4.576	361.7	4.101	355	89.949	80.12		
CD_4	4.915	355.3	5.138	419	89.796	79.13	89.78	78.9

[a] The interval between 90.660° and the triple point of the deuteromethane is not covered by the equations for either the solid or the liquid range.
[b] Values taken from Clusius and Wiegand, reference 5.

It was found to be possible to represent the data for each of the pure deuteromethanes by a relation of the form $T \log P_D/P_H = A - B/T$ where P_D represents the vapor pressure of the deuterium compound and P_H that of CH_4. The values of A and B are listed in Table I. The most uncertain constants are those for CH_2D_2 and CHD_3 because of the difficulty in determining the compositions of the samples accurately. Values for the triple point temperature and pressure observed for each sample were adjusted for composition, and are listed in Table I together with those of CH_4. The most recent values reported from Clusius' laboratory are also listed for comparison.

An approximation that has been used in estimating the vapor pressure of members of a series of isotopically substituted compounds, as, for example, the waters[7] and the ammonias[8] is the assumption that the vapor pressure of an intermediate compound is a geometric mean of the vapor pressures of the extreme members of the series. For the methanes this would suggest that P_D/P_H should form a geometric progression as the number of substituted hydrogen atoms increases. This would be strictly true if A and B increased linearly; however, a noticeable deviation from linearity occurs, especially in the case of CHD_3. Deviation from a geometric progression of P_D/P_H ratios is also evident in the fact that the temperature for which P_D/P_H becomes 1 is not the same for all the deuteromethanes.

The crossing of the vapor pressure curves of CH_4 and the deuteromethanes within the range of the observed data is not unexpected in the light of the discussions of Urey and Teal[9] and of Clusius.[10] The substitution of a deuterium atom for protium on a carbon atom causes a slight increase in the vapor pressure in the region of the normal boiling point in the case of methane as in other compounds that have been studied.

We are indebted to Professor H. S. Taylor and Dr. Kiyoshi Morikawa for the preparation of samples 1–4; and to Professor H. C. Urey and Dr. Marvin Fox for sample 5 and for some early mass spectrometer analyses of the samples.

[1] D. F. Stedman, Can. J. Research **13B**, 114 (1935).
[2] Kruis, Popp, and Clusius, Z. Elektrochem. **43**, 664 (1937).
[3] Clusius, Popp, and Frank, Physica **4**, 1105 (1937).
[4] A. Frank and K. Clusius, Z. physik. Chem. **B42**, 395 (1939).
[5] K. Clusius and K. Wiegand, Z. physik. Chem. **B46**, 1 (1940).
[6] K. Clusius and L. Popp, Z. physik. Chem. **B46**, 63 (1940).
[7] I. Kirshenbaum, *Physical Properties and Analysis of Heavy Water*, (McGraw-Hill Book Company, Inc., New York, 1951).
[8] I. Kirshenbaum and H. C. Urey, J. Chem. Phys. **10**, 706 (1942).
[9] H. C. Urey and G. K. Teal, Revs. Modern Phys. **7**, 34 (1935).
[10] K. Clusius, Z. Elektrochem. **44**, 21 (1938).

Charge-Transfer No-Bond Adsorption of Inert Atoms or Molecules on Metals

J. C. P. MIGNOLET
Service de Chimie Générale, Institut W. Spring, Université de Liége, Belgium
(Received April 27, 1953)

IT was found a few years ago[1] that xenon atoms and some inert molecules adsorbed on bare nickel are strongly polarized with the positive charge outwards. Since then evidence has accumulated, showing that this effect is fairly general (see Table I).

The effect was originally attributed to an "induced polarization." It is believed now that it is just another example of donor-acceptor interaction. Particularly convincing in this respect are the results of Fairbrother[2] who found a notable electric moment for the complex $C_6H_6 \cdot I_2$ composed of nonpolar molecules. Actually, Mulliken[3] in his second article has foreseen the importance of charge-transfer forces in adsorption. According to Mulliken's and other authors' views, the complex $M \cdot X$ resulting from the adsorption of an inert atom or molecule X on a metal surface M may be described as essentially no-bond with a small contribution from the structure $M^- - X^+$. The atom is held by van der Waals' and charge-transfer forces.

TABLE I. Surface potentials (volt).

K·X:	0[a]	Se·X:	+0.096
Ca·X:	0[a]	W·X:	+1.14
Ti·X:	+0.84	Hg·X:	+0.23
Cr·X:	+0.9	Hg·C_3H_8:	+0.23
Fe·X:	+0.66	Hg·C_2H_4:	+0.27
Ni·X:	+0.85	Hg·C_2H_2:	+0.21
Zn·X:	+0.21	Hg·CH_4:	$\gtrsim$ +0.16

[a] Under vapor pressure of xenon at −196°C; adsorption not measured.

Why then is the adsorbed particle generally the donor? First, we note that very few negative ions exist. In the case of the rare gases and probably of many inert molecules, it appears[4] that there is no stationary state with the extra electron in the lowest empty orbital. Therefore, suitable doubly excited states of high energy have to be resorted to. This must be remembered if we try to compare the work function with the electronegativity[5] $\frac{1}{2}(I+E)$ of the adsorbate. Data are lacking for a general discussion, but we may say that these are not against the positive sign adsorption, except in the case of a very few definitely electronegative molecules (O_2 and the halogens) and possibly of the low work function metals.

While the electronegativity indicates in which direction the electron transfer is the lesser endoenergetic, the choice will be determined mainly by the symmetry properties and values of the integrals[3b] $S = \int \psi_0 \psi_1 d\tau$ and $H_{01} = \int \psi_0 H \psi_1 d\tau$. Here, the negative sign adsorption appears generally to be ruled out except in the case of O_2 and the halogens, because the negative ion uses an orbital of higher quantum number that is more divided into regions of alternate signs. Regions of one sign are relatively less important and there is a greater probability of inner compensation in S and H_{01} when regions of opposite signs overlap with the metallic orbital. Thus, Mulliken's theory provides a satisfactory qualitative justification for the positive sign found empirically. A negative sign may be expected for molecular films of O_2 and the halogens, but these will generally react dissociatively with the metal, thus forming negative atomic films. In this respect, it would be interesting to determine the surface potential of O_2 on Hg.

Mercury and tungsten have nearly equal work functions but W·X is five times greater than Hg·X owing, probably, to a difference in the shape of the surface orbitals of W and Hg (the former alone being strongly directed outwards). This factor affects not only the acceptor ability of the surface but also its chemical reactivity and volatility.

I have great pleasure in expressing my deep gratitude to Professor L. D'Or for help and encouragement. My thanks are due Mr. G. Quoilin for technical assistance.

[1] J. C. P. Mignolet, Disc. Faraday Soc. **8**, 105 (1950); see also A. A. Frost: Trans. Electrochem. Soc. **82**, 259 (1942).
[2] F. Fairbrother, J. Chem. Soc. **1948**, 1051.
[3] (a) R. S. Mulliken, J. Am. Chem. Soc. **72**, 600 (1950); (b) **74**, 811 (1952); (c) J. Phys. Chem. **56**, 801 (1952).
[4] H. S. W. Massey, *Negative Ions* (Cambridge University Press, Cambridge, 1950).
[5] R. S. Mulliken, J. Chem. Phys. **2**, 782 (1934).

A United-Atom Treatment of Conjugated Systems

R. D. BROWN*
Sir William Ramsey and Ralph Foster Laboratories, University College, London, England
AND
F. A. MATSEN
The University of Texas, Austin, Texas
(Received May 8, 1953)

ONE of us has recently shown[1] that a united-atom variation function for the hydrogen molecule ion provides a description of the energy levels comparable to a function employing atomic orbitals centered on the nuclei (LCAO). It is of interest to extend the united atom concept to conjugated systems by taking the molecular orbitals to be linear combinations of united-atom orbitals located in each bond of the system (LCUAO). The precise form of these orbitals need not be specified for our present purpose

since in the familiar linear variation treatment, they occur only in the Coulomb and resonance integrals which are regarded as semiempirical parameters. The united-atom orbitals may be considered a particular form of the equivalent orbitals of Lennard-Jones and Pople.[2] For unsaturated systems they may be visualized as $2p\pi$ orbitals.

By analogy to the LCAO approach, one writes for the LCUAO MOs

$$\psi_i = \sum_r C_{ir} u_r,$$

where u_r is a united-atom orbital located on the rth bond of the system. The bond order is then given directly as a sum over probability amplitude

$$p_r = \sum_i V_i C_{ir}^2,$$

where V_i is the occupation number for the ith molecular orbital. This contrasts to the LCAO MO method in which the sum is over

TABLE I.

Bond		LCUAO	LCAO	Bond		LCUAO	LCAO
Ethylene		1	1	Benzene		0.5	0.667
Butadiene	1:2	0.75	0.894	Naphthalene	1:2	0.505	0.725
	2:3	0.5	0.447		2:3	0.452	0.603
Hexatriene	1:2	0.667	0.871		1:9	0.422	0.555
	2:3	0.5	0.483		9:10	0.388	0.518
	3:4	0.667	0.784				

the product of the molecular orbital coefficients on either end of the bond.[3] In Table I are given bond orders calculated by both methods. The results for polyenes are derived from some general results of Longuet-Higgins.[4] From these results, it follows that all odd-numbered bonds have order $\frac{1}{2}$ and all even-numbered bonds have order $P=(n+2)/2n$, where n = the number of bonds. As n approaches infinity, the bond order of all bonds approaches $\frac{1}{2}$.

It is interesting to note that the bond order in the LCAUO scheme resembles the charge density in the LCAO scheme for a molecule with one less carbon atom. Further, the charge density for the atom between the r and $r+1$ bonds in the LCAUO system may be defined as

$$\rho_{r,r+1} = \sum_i V_i C_{ir} C_{i,r+1},$$

which resembles the bond order in the LCAO scheme.

* Present address. Department of Chemistry, University of Melbourne, Melbourne, Australia.

[1] F. A. Matsen, J. Chem. Phys. (to be published).
[2] J. E. Lennard-Jones and J. A. Pople, Disc. Faraday Soc. **10**, 5 (1950).
[3] C. A. Coulson and H. C. Longuet-Higgins, Proc. Roy. Soc. (London).
[4] H. C. Longuet-Higgins, J. Chem. Phys. **18**, 265 (1950).

The Use of Radioactive Alpha-Recoil in the Study of Soluble Ionized Surface Layers

GUNNAR ANIANSSON AND NAFTALI H. STEIGER
Division of Physical Chemistry, Royal Institute of Technology, Stockholm 70, Sweden

(Received April 17, 1953)

As proposed by Aniansson and Lamm,[1,2] the recoil phenomenon in radioactive alpha-decay is well suited for the study of adsorption in liquid- (and solid-) gas interfaces. In the radioactive alpha-decay of bismuth-212, the resulting thallium-208 is given a translational energy of about 117 kev. This recoil atom travels in an essentially straight path a total distance in air of about 0.1 mm. The corresponding range in water is about 1000A. The thallium-208 atom is radioactively unstable and decays with the emission of a beta-particle and some gamma-quanta to the stable lead-208. After the stopping process the thallium-208 atoms are practically all positively charged and can thus be collected on a negative electrode and their amount measured radioactively.

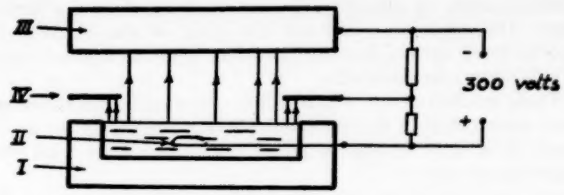

FIG. 1. Schematic figure of the experimental arrangement.

This phenomenon has been applied to the study of the adsorption of bismuth ions in the liquid air interface of soap solutions in the following way (Fig. 1): bismuth-212 ions are dissolved in an acid solution of sodium dodecyl sulfate placed in a cuve (I). Through a platinum wire (II) the solution is connected to the positive pole of a voltage supply. In the air space over the liquid is a brass plate (III) connected to the negative pole of the same voltage supply. In the decay of the bismuth-212 ions that are adsorbed in the liquid air interface, 50 percent of the recoiling thallium-208 atoms are directed upwards. Most of these should be able to penetrate the rest of the surface layer, arrive in the air space, and thus be collected on the negative plate. The negative plate is kept over the solution until the number of thallium-208 atoms has become practically constant. This occurs to within 1 percent after 20 minutes when the number of decaying thallium-208 atoms equals the number of arriving. In order to avoid eventual influences of the edges of the cuve, a brass ring (IV) of a diameter somewhat less than the inner diameter of the cuve is placed between the negative plate and the surface of the solution. With a proper choice of the potential of this circular ring the lines of force will go normal to the liquid surface and the negative plate, and only those recoil atoms will be collected on the negative plate that leave the solution within the projection of the brass ring. (The range of the recoil atoms in air will have no influence since it is only 0.1 mm.)

Because of the very small range, 1000A, of the recoil atoms in water this method will measure almost exclusively the bismuth ions that are in an extremely thin layer under the surface. The thickness of the surface layer of soap and gegenions is of relatively little influence as long as it is small compared to the total range of the recoil atoms. If this thickness for example is less than about 100A, the maximum influence on the amount of thallium-208 atoms will be 10 percent.

Figure 2 gives the radioactivity in the moment when the plate was removed from the liquid and measured under a GM tube, obtained for sodium dodecyl sulfate solutions in 10^{-3} $CHNO_3$ containing a constant amount of bismuth-212 ions (25 microcuries per milliliter). The experiments were performed in a gloved box thermostated at a constant temperature of 24 ± 0.5°C. If the thickness of the surface layer is about 100A or thinner, the measured activity as was discussed above very nearly gives a propor-

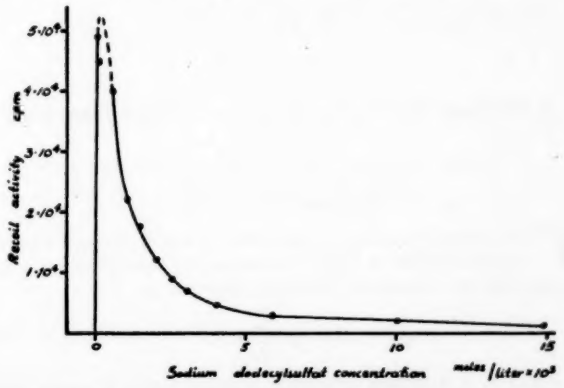

FIG. 2. The recoil activity of sodium dodecyl sulfate in 10^{-3} $CHNO_3$ and 25 microcuries Bi-212 per ml.

tional measure of bismuth-212 ions co-adsorbed in the surface layer. The appearance is much the same as was obtained for calcium ions,[2] but the decrease in surface adsorbed amount begins at still lower concentrations.

These measurements, which will be reported in full elsewhere, were undertaken in order to find optimal conditions for an attempt to a more detailed study of the surface layer with collimated recoil atoms.

[1] G. Aniansson and O. Lamm, Nature **165**, 357 (1950).
[2] G. Aniansson, J. Phys. Colloid and Chem. **55**, 1286 (1951).

Chlorine Pure Quadrupole Resonances*

D. W. McCall† and H. S. Gutowsky
Noyes Chemical Laboratory, University of Illinois, Urbana, Illinois
(Received April 28, 1953)

CHLORINE nuclear quadrupole resonances have been detected in several solids. The compounds and their Cl^{35} resonance frequencies are listed in Table I. Measurements were

TABLE I. Cl^{35} quadrupole resonance frequencies at −196°C.

Compound	Frequency (Mc)	Compound	Frequency (Mc)
C_6H_5COCl	29.93	$C_6H_5CCl_3$	38.898
$(CH_3)_2NCOCl$	31.8		38.824
			38.786
$(C_2H_5)_2NCOCl$	31.877		38.713
$C_6H_5SO_2Cl$	32.44		38.702
			38.288
p-$CH_3C_6H_4SO_2Cl$	32.460	p-$FC_6H_4CCl_3$	39.056
			38.772
PCl_5	32.63	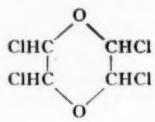	36.968
	32.384		34.824
	32.282		
$SbCl_5$	30.4[a]	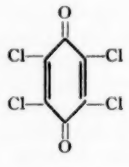	
	28.3		
	27.88[b]		38.50
$CHCl_2CONH_2$	37.750		
	37.238		

[a] Partially resolved double line.
[b] Partially resolved triple line.

made at liquid nitrogen temperature with a superregenerative spectrometer of a type described by Dean.[1] Experiments on the temperature dependence of the chlorine quadrupole resonance frequencies are also in progress in this laboratory.

* Supported in part by the U. S. Office of Naval Research.
† National Science Foundation Predoctoral Fellow.
[1] C. Dean, thesis, Harvard University (1952).

A Method for Computing Zero-Point Energies

P. W. Higgs
Wheatstone Physics Laboratory, King's College, Strand, London, W.C. 2, England
(Received April 14, 1953)

THE zero-point energy of vibration of a polyatomic molecule, the force-field of which is adequately described for small amplitudes by a quadratic potential function, is

$$E_0=\tfrac{1}{2}h\sum_{i=1}^{N}\nu_i, \tag{1}$$

in which ν_i is a typical vibration frequency and N is the total number of normal modes. To calculate E_0 for a molecule of given geometry and force-constants, one usually solves the secular equation for the frequencies in the form,

$$|\mathbf{GF}-\lambda\mathbf{I}|=0,$$

in which $\mathbf{F}$ and $\mathbf{G}$ are the potential and inverse kinetic-energy matrices defined by Wilson,[1] $\mathbf{I}$ is the unit matrix, and $\lambda=4\pi^2\nu^2$. In terms of the diagonal matrix, $\mathbf{\Lambda}=\text{diag}\,(\lambda_i)$, Eq. (1) may be rewritten as

$$E_0=\tfrac{1}{2}h\,\text{trace}\,\mathbf{\Lambda}^{\frac{1}{2}}, \tag{2}$$

where $\mathbf{\Lambda}^{\frac{1}{2}}$ is the positive square root of $\mathbf{\Lambda}$.

Now the equation which determines the amplitudes of the internal coordinates $\mathbf{y}$ in the ith normal mode is

$$\mathbf{GF}\mathbf{y}_i=\lambda_i\mathbf{y}_i;$$

the set of these equations may be written in terms of the matrix $\mathbf{Y}$ which has $\mathbf{y}_i$ for its ith column as

$$\mathbf{\Lambda}=\mathbf{Y}^{-1}\mathbf{GFY}. \tag{3}$$

By using the invariance of the trace of a matrix under a similarity transformation such as (3), Eq. (2) may be transformed into

$$E_0=\tfrac{1}{2}h\,\text{trace}\,(\mathbf{GF})^{\frac{1}{2}}, \tag{4}$$

in which $(\mathbf{GF})^{\frac{1}{2}}$ is the positive square root of $\mathbf{GF}$, i.e., matrix $\mathbf{X}$ which satisfies the equation, $\mathbf{X}^2=\mathbf{GF}$, and has only positive eigenvalues. In principle, Eq. (4) provides a means of calculating E_0 directly from the geometry and force-constants. All that is required is a method for computing the positive square root of a matrix $\mathbf{M}$ which has only positive eigenvalues: such a method is provided by the following iterative process.

Let $\mathbf{X}_n$ be any $N\times N$ matrix which commutes with $\mathbf{M}$ and has only positive eigenvalues. Compute $\mathbf{X}_{n+1}$, defined by the equation,

$$\mathbf{X}_{n+1}=\tfrac{1}{2}(\mathbf{X}_n+\mathbf{X}_n^{-1}\mathbf{M}). \tag{5}$$

Then the sequence of matrices $\mathbf{X}_n$ converges as $n\to\infty$ to the positive square root $\mathbf{M}^{\frac{1}{2}}$. This is easily seen to be so if one applies to Eq. (5) the similarity transformation which diagonalizes $\mathbf{M}$. Since every matrix in (5) commutes with $\mathbf{M}$, the whole equation is diagonalized simultaneously and one obtains for each diagonal element the well-known sequence,

$$x_{n+1}=\tfrac{1}{2}(x_n+x_n^{-1}m),$$

which converges rapidly to $m^{\frac{1}{2}}$ when x_n is positive. A suitable starting value for the iteration is $\mathbf{X}_0=x_0\mathbf{I}$, where x_0 is any positive number.

I would like to thank Professor H. C. Longuet-Higgins for drawing my attention to this problem.

[1] E. B. Wilson, Jr., J. Chem. Phys. **7**, 1047 (1939); **9**, 76 (1941).

The Photosensitized Oxidation of Paraffins

J. A. Gray
Imperial Chemical Industries Research Department, Alkali Division, Northwich, Cheshire, England
(Received February 3, 1953)

IN a recent Letter to the Editor, on the mercury photosensitized oxidation of paraffins, Darwent[1] showed that, in my experiments,[2] quenching by oxygen was far greater than by hydrocarbon. The mechanism of quenching by O_2 is not well established, the possibilities being either the production of O or O_2^*, and my results provide some evidence which is presented in this communication.

It was shown[2] that the reaction between $Hg(^3P_1)$ and a mixture of ethane and oxygen in a flow system yielded a condensable product which, as far as could be ascertained, was mainly ethyl hydroperoxide. If the primary process were (1) it would be expected that the oxygen atoms produced by it would react with the substrate to give the following sequence of reactions:

$$(2)\quad O+RH=OH+R$$
$$(3)\quad OH+RH=H_2O+R.$$

That reaction (2) followed by (3) does not predominate is suggested by the failure to detect water in the condensate. The objection to this is that the nature of the product was such that it was not possible to estimate an upper limit for this impurity; the alternative, i.e., removal of O to give O_3 has not been found to lead to the formation of peroxide. Thus all $Hg(^3P_1)$ which is quenched by oxygen to give O or O_3 is "lost." Although ozone was detected in 50:50 ethane:oxygen mixtures the observation that "little or no ozone" was detected at low oxygen concentrations is not of great importance; this may have been due merely to dilution with ethane. As explained in the original paper, attention was focused only on the products condensable at approximately $-80°$. A further nonproductive reaction which might be suggested is the removal of O by mercury to give HgO.

There is, however, the further possibility that excited oxygen may be the initiating agent in the system. The reasons for rejecting this possibility were not previously dealt with, but it may be convenient to present them here. Reaction might be expected to proceed as follows:

$$(4)\ Hg^*+O_2 = Hg+O_2^*$$
$$(5)\ RH + O_2^* = R+HO_2$$
$$(6)\ R + O_2 = RO_2$$
$$(7)\ RO_2+HO_2\ (\text{or } RH) \rightarrow ROOH+O_2\ (\text{or } R).$$

The arguments against the possibility of reaction (4), followed by (5), being important are drawn from the mercury photosensitized hydrogen-oxygen reaction, which subject has been reviewed by von Elbe and Lewis[3] and by Noyes and Leighton.[4] In more recent work Volman[5] decided that Hg^*+O_2 gave $Hg+O_2$. This explanation is similar to that of Bates,[6] who formulated a rate equation which accounted for the experimental data more satisfactorily than any other then proposed. He concluded, like Kistiakowsky,[7] that O_2^* was incapable of reacting with molecular hydrogen. If methane and ethane may be regarded as behaving in a role similar to that of hydrogen, although less efficient than hydrogen in quenching Hg^*, then the reaction (8) $Hg^*+RH \rightarrow Hg+R+H$ would be preferred as a source of alkyl radicals instead of reaction (5).

There is probably insufficient experimental evidence to enable us with any degree of confidence to favor either one of (8) or (5) rather than the other, but additional weight is lent to the former by a suggestion of Noyes and Leighton[4] that the quenching of mercury by oxygen gives an intermediate HgO_2 which reacts further with oxygen to give $HgO+O_3$.

Whatever the process by which oxygen quenches $Hg(^3P_1)$ it does seem at present that, at least in the ethane/oxygen system, it does not yield a condensable product. Reaction (1) is, in the light of our present knowledge of the subject, a reaction which one would expect to take place and—as Darwent has pointed out—from the data on quenching cross sections it ought to predominate over $Hg(^3P_1)+C_2H_6=Hg(^1S_0)+C_2H_5+H$. That the experimental evidence does not confirm this expectation suggests that either (a) oxygen atoms are removed from the system without reacting with the hydrocarbon (by recombination, formation of ozone, reaction with mercury or some unspecified process) or (b) oxygen atoms are not the initial product of quenching by oxygen. To settle the matter a more detailed investigation would be required on the reaction under discussion and it is suggested also that the mechanism of the quenching of excited mercury by oxygen alone would bear further examination.

I thank Dr. E. W. R. Steacie[8] and Dr. D. E. Hoare[9] for private communications on the same subject.

[1] B. DeB. Darwent, J. Chem. Phys. **20**, 1979 (1952).
[2] J. A. Gray, J. Chem. Soc. **1952**, 3150.
[3] G. von Elbe and B. Lewis, J. Chem. Phys. **7**, 710 (1939).
[4] W. A. Noyes and P. A. Leighton, *The Photochemistry of Gases* (Reinhold Publishing Corporation, New York, 1941).
[5] D. H. Volman, J. Chem. Phys. **14**, 707 (1946).
[6] J. R. Bates, J. Chem. Phys. **1**, 457 (1933).
[7] G. B. Kistiakowsky, J. Am. Chem. Soc. **52**, 1868 (1930).
[8] President, National Research Council of Canada, Ottawa.
[9] University College of Swansea, Swansea, Wales.

The Vibration-Rotation Spectrum of D_2O†

W. S. Benedict
The Johns Hopkins University
and
Norman Gailar* and Earle K. Plyler
National Bureau of Standards, Washington, D. C.
(Received April 20, 1953)

ALTHOUGH several bands of D_2O have been previously observed and analyzed,[1–5] the data have not been sufficient to yield values for the molecular constants of a degree of completeness comparable to those for H_2O. We have accordingly restudied the spectrum in the region 1.25 to 4.2μ (2400 to 8000 cm^{-1}). The analysis of the 3 known bands in this region has been improved and extended to higher rotational levels, and five new bands have been observed. Complete details of our work on D_2O and HDO are being prepared for publication. We wish to report briefly on the most important results at this time.

Two grating spectrometers were used; one with 15 000 lines/in. and a lead sulfide photoconductive detector for the region 1.25 to 2.7μ, and one with 7200 lines/in. and a cooled lead telluride detector for the region 3 to 4.2μ. In the former region a quartz multiple-path absorption cell was used; the path length was 6 meters, and the cell could be heated to 50°C in order to increase the vapor pressure. In the latter region the path length was 1.1 meters. D_2O of >99.5 percent purity was used. Even with extreme precaution, some contamination of the spectra with HDO resulted. It was possible, however, to distinguish among lines of D_2O, HDO, and H_2O by progressively varying the concentration. The HDO spectra are discussed in the following note.[6]

Approximately 1500 lines of D_2O have been measured and over 90 percent of these, including all the stronger ones, have been analyzed. The results of the analysis are summarized in Table I. The most significant new result is the finding of the type *B* fundamental, the symmetrical stretching vibration ν_1, at 2671.79 cm^{-1} and its overtone at 5291.55 cm^{-1}. These bands are approximately $\frac{1}{5}$ to $\frac{1}{3}$ as intense as the type *A* bands in the same region. (In H_2O the corresponding type *B* bands are somewhat weaker relative to the type *A* bands).

The *P* branch of ν_1 falls in a region which is quite free from overlapping by ν_3; the spectrum from 2600 to 2400 cm^{-1} is illustrated in Fig. 1. The strongest observed lines are accounted for by assigned lines of the correct relative intensity; the assignment is confirmed by the appearance in other branches of lines with the same upper state whose frequencies yield ground-state combination differences agreeing to within 0.1 cm^{-1} with those obtained from other bands and from the pure rotation spectrum.[1] The ν_1 lines also fall in regular series, except for $J_\tau'-7_6$ and 8_8. These levels fall very close to the ν_3 levels 7_5 and 8_5 and hence are shifted due to Coriolis resonance perturbation. The other member of the resonance pair also appears in the spectrum as the line marked 7_6*; this might alternatively be identified as the ν_3 transition 7_5-8_8.

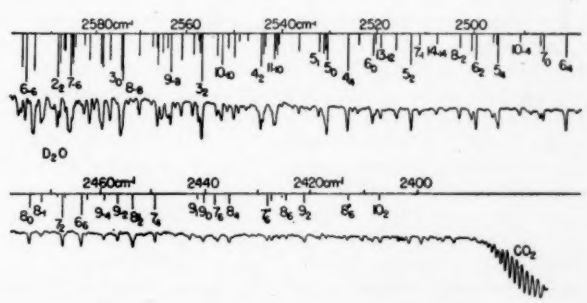

FIG. 1. D_2O absorption, 2600 to 2400 cm^{-1}. Identified lines, nearly all of which belong to *P* branches of the ν_1 band, are marked with lines whose height is proportional to (intensity)$^{\frac{1}{2}}$. J_τ' values are given for the more prominent lines.

TABLE I. Vibration-rotation bands of D_2O.

v_1	v_2	v_3	ν_0 cm^{-1}	Type	Rel. int.	No. ident. lev.	A cm^{-1}	B cm^{-1}	C cm^{-1}	I_a	I_b	I_c	Δ
										10^{-40} g cm^2			
0	0	0	0.00	B		150	15.393	7.263	4.852	1.818	3.853	5.767	0.096
0	1	0[a]	1178.33	B	1000	30	16.58	7.32	4.81	1.688	3.823	5.818	0.307
1	0	0	2671.69	B	200	90	15.16	7.17	4.772	1.846	3.903	5.863	0.114
0	0	1	2788.02	A	1000	120	14.85	7.25	4.795	1.884	3.860	5.836	0.092
0	1	1	3956.18	A	200	90	15.92	7.30	4.755	1.758	3.833	5.885	0.294
0	2	1	5105.44	A	30	45	17.28	7.33	4.69	1.619	3.818	5.966	0.529
2	0	0	5291.55	B	75	50	14.92	7.14	4.701	1.876	3.919	5.953	0.158
1	0	1	5373.98	A	250	80	14.605	7.18	4.713	1.916	3.937	5.937	0.124
2	1	0[b]	6452.0	B	···	2	···	···	···	···	···	···	···
1	1	1	6533.37	A	50	50	15.77	7.19	4.678	1.744	3.892	5.982	0.316
3	0	0[b]	7853.0	B	···	3	···	···	···	···	···	···	···
2	0	1	7899.70	A	20	30	14.46	7.12	4.68	1.935	3.930	5.979	0.114

[a] This band was not studied in the present work. Constants are rederived from data of reference 2.
[b] These bands are not strong enough to be observed, except for the few levels that are in close resonance with the neighboring type A band.

Similar perturbations have been identified in other bands throughout the spectrum. The bands 210 and 300 appear only through these interactions. Only a few lines of each band are affected in this way, inasmuch as the interaction parameter is weak and close resonance of the unshifted levels to within ($\sim\pm 2$ cm^{-1}) is required for an appreciable shift to be observed.

The effective rotational constants and moments of inertia are listed in Table I. Those for the ground state are by far the most accurate both because the levels are free from perturbation and because they are derived from many more observations. The observed moments are in good agreement with those derived from the H_2O spectrum and the usual isotopic relations. A set of harmonic and anharmonic vibrational constants may be fitted to the band origins listed in Table 1.[7] Inasmuch as no bands have as yet been observed in which v_3 is greater than 1, the constant x_{33} must be estimated from isotope relations.

* Present address, Naval Research Laboratory, Washington 25, D. C.
† Work supported by the U. S. Office of Naval Research and the U. S. Atomic Energy Commission.

[1] Fuson, Randall, and Dennison, Phys. Rev. **56**, 982 (1939).
[2] E. P. Dickey and H. H. Nielsen, Phys. Rev. **73**, 1164 (1948).
[3] G. W. King, J. Chem. Phys. **15**, 85 (1947).
[4] Innes, Cross, and Giguere, J. Chem. Phys. **19**, 1086 (1951).
[5] Dickey, Guderjahn, and Palik, J. Chem. Phys. **20**, 375 (1952).
[6] Benedict, Gailar, and Plyler, J. Chem. Phys. **21**, 1302 (1953).
[7] W. S. Benedict, J. Chem. Phys. (to be published).

The Vibration–Rotation Spectrum of HDO†

W. S. BENEDICT
The Johns Hopkins University, Baltimore, Maryland
AND
NORMAN GAILAR* AND EARLE K. PLYLER
National Bureau of Standards, Washington 25, D. C.
(Received April 20, 1953)

THE spectrum of HDO has been very incompletely studied. There exist only low-resolution measurements of the two fundamentals ν_2 and ν_1,[1] the latter of which has been observed with better resolution in the solar spectrum[2,3] and one weak band in the photographic infrared.[4] As discussed in the previous note,[5] we have now obtained the spectrum of HDO with good resolution from 1.5 to 4.2μ (2400 to 6800 cm^{-1}).‡ Approximately 2000 lines due to HDO have been measured. Over 90 percent of these have been analyzed into 9 bands.

The principal results are summarized in Table I. This table lists for each observed vibrational transition ($v_1v_2v_3$–000) the band origin ν_0, the approximate relative intensity of type A and type B rotational transitions, the approximate number of identified rotational levels, the effective rotational constants, and the corresponding effective moments of inertia.

Two features of the spectrum deserve particular comment. The first is the appearance of both type A and type B rotational transitions in a single vibrational transition. Such "hybrid" structure is permitted when, as in HDO, there is no molecular symmetry axis with which the inertial axes may coincide. The relative intensity $A/B=\tan^2\alpha$, where α is the angle between the direction of the effective transition dipole and the intermediate axis of inertia

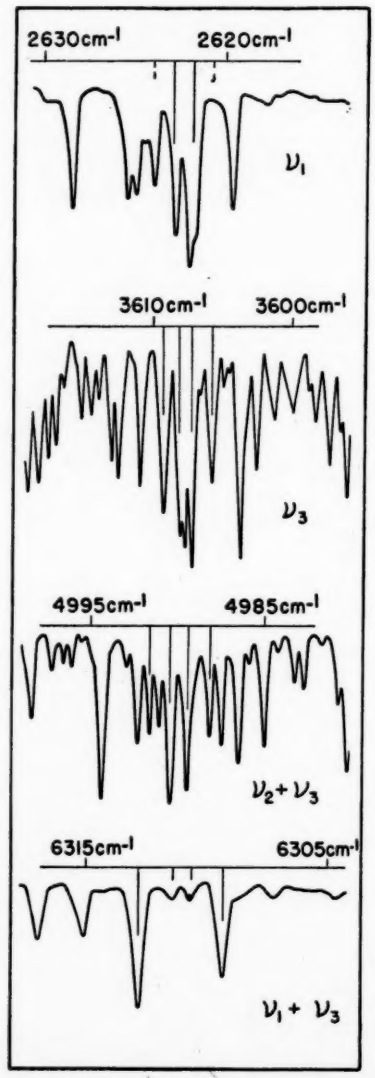

FIG. 1. Corresponding region in P branches of four bands of HDO. The four lines marked on each band are $6_{-5}-7_{-7}$, $6_{-5}-7_{-6}$, $6_{-6}-7_{-7}$, $6_{-6}-7_{-6}$; ν_1 is a pure type A band; ν_3 and $\nu_2+\nu_3$ are hybrids with type A somewhat stronger; $\nu_1+\nu_3$ is predominately type B.

TABLE I. Vibration-rotation bands of HDO.

ν_1	ν_2	ν_3	ν_0 cm^{-1}	Intensity A	Intensity B	No. identified levels	Rotational const, cm^{-1} A	B	C	Moments, 10^{40} g cm^2 I_A	I_B	I_C	Δ
0	0	0	0.00			110	23.400	9.096	6.418	1.196	3.076	4.360	0.088
0	1	0[a]	(1403.3)	(100	500)	10							
(1	0	0	2723.66	1000	<10	110	23.37	8.928	6.315	1.197	3.134	4.431	0.100
⋮													
(0	2	0	2782.16	30	20	15	27.94	9.415	6.215	1.016	2.972	4.502	0.514
0	0	1	3707.47	700	300	90	22.35	9.076	6.330	1.252	3.083	4.421	0.086
(1	1	0	4100.05	50	<2	60	28.45	9.23	6.17	0.984	3.032	4.535	0.519
⋮													
(0	3	0	4145.59	45	<2	40	28.67	9.28	6.20	0.976	3.015	4.513	0.522
0	1	1	5089.59	65	35	90	24.254	9.213	6.258	1.154	3.037	4.472	0.281
2	0	0	5363.59	75	<5	60	22.92	8.752	6.198	1.221	3.197	4.515	0.097
(1	0	1	6415.64	2	20	60	22.795	8.974	6.215	1.228	3.118	4.503	0.167
⋮													
(0	2	1	6452.05	5	<1	35	26.045	9.284	6.158	1.074	3.014	4.544	0.456
0	1	2[a]	(8611.22)	(10	<1)	30	23.12	9.215	6.18	1.210	3.037	4.528	0.281

[a] Not observed in the present work. Constants derived from earlier measurements (references 1 and 4).

(for pure rotation, $\alpha = 21°7'$). Of the observed bands, five are pure type A (type B transitions are too weak to be observed), three are hybrids with nearly equal intensity, and only the 101 band is predominantly type B. The variation of the rotational structure is illustrated by Fig. 1, which shows a segment of about 20 cm^{-1} of the P branches of four bands of different α. Each segment, which is of somewhat different dispersion since the figure was prepared by direct tracing from the records, is centered about the corresponding transitions $6_{-6,-5} - 7_{-7,-6}$. These close pairs of levels give rise to two type A lines of equal intensity, whose spacing is $\Delta E' - \Delta E''$, and two type B lines of equal intensity, whose spacing is $\Delta E' + \Delta E''$. The spacing of the two outer lines in all the bands is $\Delta E'' = 1.29$ cm^{-1}. While the adventitious occurrence of other rotational transitions complicates the appearance of the spectra, especially in the hybrids of nearly equal intensity, it can be seen how the existence of hybrid bands, when well resolved as in our tracings, facilitates the rotational analysis and provides many more ground-state combination differences from which accurate rotational constants may be derived. The resulting ground-state energy levels are in good agreement with the lines that have been observed in the microwave region[6-8] and also permit identification of nearly all of the unidentified lines in the pure rotation spectrum.[9]

The second interesting feature of the HDO spectrum results from the circumstances that $\nu_1 \cong 2\nu_2$. Fermi resonance shifts the positions and mixes the properties (intensity of transition to ground level, rotational constants, etc.) of such close pairs. The magnitude of the effect is, however, much less than predicted[10] from the Darling-Dennison[11] anharmonic potential function. The resonance is almost exact for the levels $\binom{110}{030}$ whose origins are separated by 45.54 cm^{-1}, as is shown by the fact that the lines of 030 are almost as intense as those of 110, for low K_α. In the case of 100 and 020, however, the resonance is not nearly so close and the A component of 020 is very weak. An intermediate degree of resonance is observed for $\binom{101}{021}$. Moreover, with increasing K_α the lines of 030 become weaker relative to 110, and the separation becomes greater than 46 cm^{-1}. This is because the rotational constant A is much greater for unperturbed 030 than for 110, and hence the levels of higher K_α are in less close resonance. From an analysis of such findings we can conclude that the interaction parameter $\alpha_{21} = 26.20$ cm^{-1}, as compared with Libby's value, 88.2 cm^{-1}. A similar discrepancy with the Darling-Dennison potential occurs in the higher vibrational levels of H_2O.

Making use of all the levels listed in Table I and correcting for the effects of Fermi resonance, it is possible to obtain a complete set of vibrational and vibration-rotational interaction constants for HDO. These will be given and discussed in a separate paper.

* Present address, U. S. Naval Research Laboratory, Washington, 25, D. C.

† Work supported by the U. S. Office of Naval Research and the U. S. Atomic Energy Commission.

‡ Measurements between 3400 and 4000 cm^{-1}, where atmospheric absorption due to H_2O is very strong, were also obtained with the 7200-line/in. vacuum grating spectrometer of The Johns Hopkins University Applied Physics Laboratory. We are greatly indebted to Dr. Shirleigh Silverman for securing these spectra.

[1] E. F. Barker and W. W. Sleator, J. Chem. Phys. **3**, 660 (1935).
[2] Shaw, Chapman, Howard, and Oxholm, Astrophys. J. **113**, 268 (1951).
[3] Benesch, Shaw, and Benedict, "The Solar Spectrum from 3.3–4μ," The Johns Hopkins University and U. S. Office of Naval Research Reports, August 1950.
[4] L. Herzberg, Z. Physik **107**, 549 (1937).
[5] Benedict, Gailar, and Plyler, J. Chem. Phys. **21**, 1301 (1953).
[6] M. W. P. Strandberg, J. Chem. Phys. **17**, 901 (1949).
[7] Jen, Bianco, and Massey, J. Chem. Phys. (to be published).
[8] Weisbaum, Beers, and Herrmann, Phys. Rev. **90**, 338 (1953).
[9] Fuson, Randall, and Dennison, Phys. Rev. **56**, 982 (1939).
[10] W. F. Libby, J. Chem. Phys. **11**, 101 (1943).
[11] B. T. Darling and D. M. Dennison, Phys. Rev. **57**, 128 (1940).

Studies on the Gamma-Radiation-Induced Polymerization of Acrylonitrile

IRVING A. BERSTEIN, EARLE C. FARMER, WALTER G. ROTHSCHILD, AND FLORENCE F. SPALDING

Departments of Chemistry and Physics, Tracerlab, Inc., Boston, Massachusetts

(Received February 17, 1953)

THE effects of cobalt-60 gamma-radiation on the polymerization of acrylonitrile monomer have been investigated in order to determine the feasibility of utilizing the pure monomer as a visual-indicating chemical dosimeter. Acrylonitrile monomer was chosen for study for the following reasons: (1) Vinyl compounds polymerized by a chain reaction mechanism involving very long chain lengths. (2) Polyacrylonitrile is insoluble in its own monomer and thus any radiopolymer could be visually detected. (3) The pure monomer is quite stable to heat.

Studies were made on the effect of both varying dose rate and varying total dose on the percent conversion of monomer to polymer over the dose range of 10 r/hr to 9400 r/hr under cobalt-60 gamma-radiation.

The acrylonitrile was exposed to the radiation in black Pyrex tubes which had been sealed under high vacuum. The monomer was deaerated by repeated freezing with liquid nitrogen, evacuated to 0.1 micron, and thawed. It was deaerated further and purified by fractional distillation into a storage bulb on a high-vacuum line. The glass exposure tubes were fitted onto the vacuum

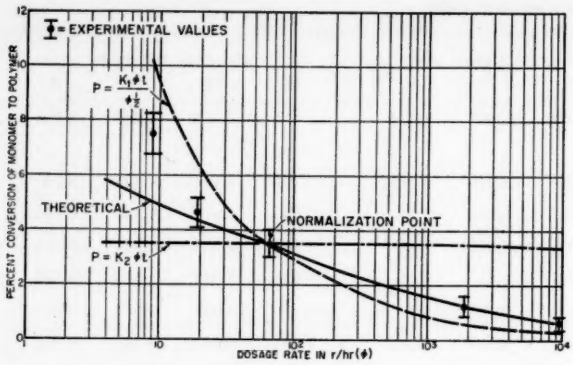

FIG. 1. Percent polymerization of acrylonitrile monomer *vs* dose rate of cobalt-60 gamma-radiation.

line, evacuated to 0.1 micron, heated and sparked with a Tesla coil to remove occluded oxygen and water vapor. The acrylonitrile was introduced into the exposure tubes by distillation from the storage bulb. The tubes were sealed with the monomer frozen with liquid nitrogen. It was necessary to prepare a system as free of oxygen as possible since traces of oxygen greatly desensitize polymerization of acrylonitrile. To avoid any light-induced polymerization, the tubes were wrapped in black friction tape. Acrylonitrile tubes prepared in the above fashion were found to be quite stable to heat, giving no visual indication of polymerization after heating at 61°C for several days.

The various dose rates were obtained using an 87-mc and a 20-c cobalt-60 gamma-source and were calibrated using standard Victoreen ionization chambers.

Experiments were carried out to determine the visual threshold sensitivity as a function of the intensity of incident radiation. At low dose rates of 10–100 r/hr, the samples gave a clearly visible turbidity after exposure to about 20–25 r. At an intensity of 9400 r/hr, exposure to a total dose of about 200 r was required for a comparable change. A careful investigation was then undertaken to determine the percent conversion of monomer to polymer as a function of dose rate. The amount of radiopolymer formed was determined by filtering the contents of the irradiated tubes through a sintered glass funnel, washing the polymer thoroughly with methanol, drying in vacuum and weighing.

Figure 1 is a plot of percent conversion of monomer to polymer as a function of dose rate for a total dose of 2680 r. Figure 2 is a graph of the polymerization rate as a function of dose rate for total dose of 2680 r. Included also in both figures are several theoretical curves for comparison with the experimental results.

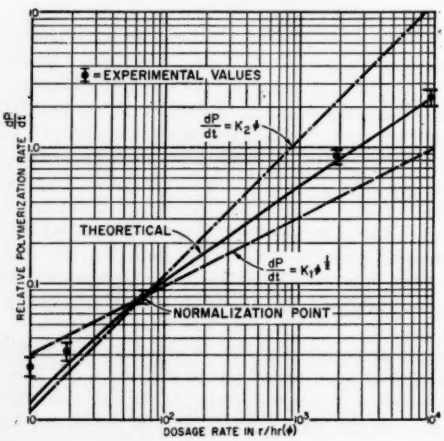

FIG. 2. Relative polymerization rate of acrylonitrile monomer *vs* dose rate of cobalt-60 gamma-radiation.

From a theory assuming a radical mechanism of polymerization and only bimolecular termination of radicals, it is found that the rate of polymerization is proportional to the square root of the dose rate.[1,2] Other theoretical expressions have been proposed,[3] among them expressions which yield a dependence directly proportional to the dose rate.[4,5]

From inspection of both figures, it is seen that our experimental results for percent polymerization and the polymerization rate do not agree with either a simple linear or square root dependence on the dose rate.

Assuming a combination of unimolecular and bimolecular terminations, an expression can be derived which is in much better agreement with the experimental results over most of the intensity range studied.

This expression has the following form:

$$\frac{-d(m_1)}{dt} = \frac{dP}{dt} = \frac{kp(m_1)}{2}\left\{\left[\left(\frac{kt_1}{kt_2}\right)^2 + 4\frac{k_i}{kt_2}(m_1)\phi\right]^{\frac{1}{2}} - \frac{kt_1}{kt_2}\right\}$$

where

$[d(m_1)/dt]$ = rate of change in concentration of monomer,
dP/dt = rate of polymerization,
ϕ = dose rate,
k_i = initiation rate constant,
k_p = propagation rate constant,
kt_1 = unimolecular termination rate constant,
kt_2 = bimolecular termination rate constant.

However, it is noted that where the percent conversion of monomer is high for total dose of 2680 r, the theoretical expression deviates from the experimental results.

A more complete treatment of the data is in progress.

We are pleased to acknowledge the valuable technical assistance of Elizabeth A. McElhill.

[1] A. Chapiro, Compt. rend. **228**, 1490 (1949); **229**, 827 (1949).
[2] Chapiro, Cousin, Landler, and Magat, Rec. trav. chim. **68**, 1037 (1949).
[3] E. Collinson and F. S. Dainton, Disc. Faraday Soc. (April, 1952).
[4] F. S. Dainton, Nature **160**, 268 (1949); J. Phys. & Colloid Chem. **52**, 490 (1948).
[5] B. Manowitz, *et al.*, Progress Report on Fission Products Utilization, Brookhaven National Laboratory, Dec. 1951.

Rayleigh's Ratio (Absolute Turbidity Levels) for Benzene, Carbon Tetrachloride, and Toluene

ROBERT F. STAMM AND PETER A. BUTTON
Stamford Research Laboratories, American Cyanamid Company, Stamford, Connecticut

(Received April 14, 1953)

IN these laboratories we have used benzene as a turbidity standard[1] in calibrating our light scattering apparatus[2] which is employed for evaluating molecular weights by the turbidimetric method of Debye.[3] The value for Rayleigh's ratio for benzene measured by Cabannes and Daure[4] which we had used (after making corrections for wavelength and temperature) was challenged in 1950 by newer values measured in this country.[5–7] At that time we arbitrarily adopted the new values (average of results published in references 5 to 7). Later, while making certain measurements on our ratio instrument involving the polystyrene turbidity standard distributed by Cornell University, it became apparent that certain discrepancies existed in the case of these newer values. As a consequence, a program (lasting more than a year) was started in order to obtain absolute values of the scattering powers of several pure dust-free liquids and also of the polystyrene standard.

It was not until this work was completed that we belatedly came upon the exhaustive researches of the astrophysicist de Vaucouleurs[8] on the same subject. Certain circumstances have conspired to prevent the presentation of the complete details of our own investigation until a later date. However, the disagreement (amounting to nearly 50 percent) between the low results and the high results has been brought out in the open quite re-

TABLE I. Experimental values for Rayleigh's ratio, 25.0(±0.5)°C.

Substance	$R_u \times 10^6$ (cm^{-1})		$R_v \times 10^6$ (cm^{-1})		$R_v \times 10^6$ (cm^{-1}) (calc)[a]	
	4365.7A[e]	5460.7A	4365.7A[e]	5460.7A	4365.7A[e]	5460.7A
CCl_4	9.55[b] ±0.33	3.93[b] ±0.15	18.21[b] ± 0.64	7.37[b] ±0.14	17.46 ±0.48	7.22 ±0.27
C_6H_6	27.59 ±0.83	10.37 ±0.27	38.70 ± 1.13	14.75 ±0.16	38.40 ±0.95	14.56 ±0.42
$C_6H_5CH_3$	32.21 ±1.01	11.83 ±0.49	43.77[b] ± 1.41 48.95[e] ± 1.70	16.38[b] ±0.26 17.32[e] ±0.32	43.24 ±1.69	15.96 ±0.60
"Styron" standard[d]	154.3 ±4.1	57.25 ±1.35	272.8[b] ±10.1 288.0[e] ± 9.5	108.6[b] ±2.7 111.4[e] ±2.6	281.5 ±6.9	106.0 ±2.6

[a] Evaluated by means of the expression $-R_v = R_u[2/(1+\rho_u)]$.
[b] Measured on ratio instrument (see reference 2) relative to benzene.
[c] Measured on absolute instrument but only with beam weakener (b) and with a faulty mounting for the lens used in reference beam. These values were not remeasured after this defect was corrected.
[d] Solution in toluene (0.5 gram in 100 ml of solvent). The values given are those for the solution.
[e] Effective wavelength evaluated from the expression $\lambda_e^4 = [\int i_\lambda \cdot d\lambda]/[\int i_\lambda \lambda^{-4} \cdot d\lambda]$ according to Scott Ewing, J. Opt. Soc. Am. **12**, 15 (1926).
R_u, Rayleigh's ratio at 90°; unpolarized incident light. R_v, Rayleigh's ratio at 90°; vertically polarized incident light. ρ_u, depolarization ratio of light scattered at 90°; unpolarized incident light.

cently by two publications.[9,10] Consequently, we wish to present a synopsis of our results at this time.

These absolute measurements consisted of comparisons of the flux scattered by a given liquid (contained in a sealed cell immersed in water) at an angle of 90° to the incident beam with that reflected to the side by a precision glass beam weakener also immersed in water. The comparisons of radiant energy were all made by means of an R.C.A. type 1P21 photomultiplier which was shifted from one port hole to the other to measure first the scattered radiation and then radiation from the beam weakener. The amplifier, power supply, and recorder have been described in detail.[11]

Three types of beam weakeners (see Fig. 1) were employed. The three-sided hollow cell is of the type originally employed by Debye for photographic measurements of absolute turbidities. We were not able to obtain satisfactory measurements with such an attenuator because of the multiplicity of the images and because of the poor optical quality of the surfaces. The other two beam weakeners were made up for us on special order (and to rigid specifications) by the Perkin-Elmer Corporation.

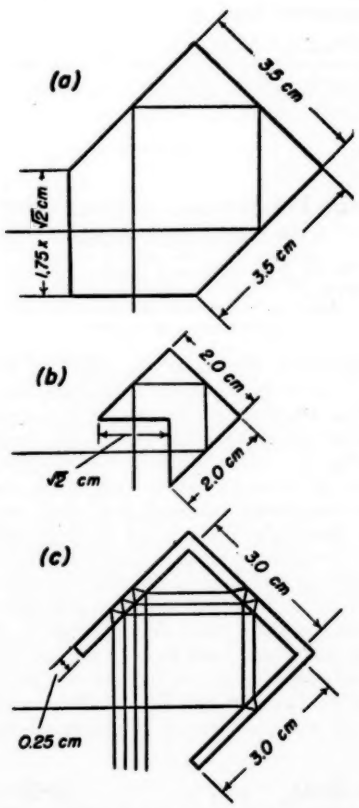

FIG. 1. The three types of beam weakeners employed. The degree of attenuation of intensity provided by these beam weakeners when immersed in water is of the order of 10^{-6} for unpolarized light. The results given were obtained by using types (a) and (b); type (c) was not satisfactory.

The results are presented in Table I. A comparison of these data with those provided in reference 9 will indicate that we belong to the school favoring the low-turbidity values. It seems appropriate to point out that the results obtained indirectly by Hadow, Sheffer, and Hyde[12] also favor the lower region somewhat.

Complete details of these experiments containing the intensity contributions provided by the *integrated* intensities of the Raman lines for these three pure compounds will be submitted for publication as soon as possible.

[1] Stamm, Mariner, and Dixon, J. Chem. Phys. **16**, 423 (1948).
[2] T. Mariner and R. F. Stamm, Rev. Sci. Instr. **22**, 61 (1951).
[3] P. Debye, J. Phys. Colloid Chem. **51**, 18 (1947).
[4] J. Cabannes and P. Daure, Compt. rend. **184**, 520 (1927).
[5] P. Doty and R. F. Steiner, J. Chem. Phys. **18**, 1211 (1950).
[6] Brice, Halwer, and Speiser, J. Opt. Soc. Am. **40**, 768 (1950).
[7] C. I. Carr, Jr., and B. H. Zimm, J. Chem. Phys. **18**, 1616 (1950).
[8] G. de Vaucouleurs, Compt. rend. **228**, 914 (1949); **229**, 35 (1949); Ann. phys. [XII] **5**, 213 (1950).
[9] A. Rousset and R. Lochet, J. Polymer Sci. **10**, 319 (1953).
[10] Bruno H. Zimm, J. Polymer Sci. **10**, 351 (1953).
[11] Stamm, Salzman, and Mariner, J. Opt. Soc. Am. **43**, 119 (1953); R. F. Stamm and C. F. Salzman, Jr., J. Opt. Soc. Am. **43**, 126 (1953).
[12] Hadow, Sheffer, and Hyde, Can. J. Research **B27**, 791 (1949).

Microwave Investigation of Pyridine

BØRGE BAK AND JOHN RASTRUP-ANDERSEN
Chemical Laboratory, University of Copenhagen, Copenhagen, Denmark
(Received May 11, 1953)

DETERMINATION of the distance between adjacent carbon atoms in an aromatic ring is one of the most attractive problems yet to be solved by spectroscopy. Since the prototype molecule benzene has no dipole moment, microwave technique is inapplicable in this case, but it is to be expected that the C—C distance (d_{CC}) in pyridine (which has a dipole moment) does not deviate much from d_{CC} in benzene. In fact, the electron-diffraction patterns[1] and the infrared absorption spectra[2] of the two compounds are very similar. A microwave investigation of pyridine was therefore undertaken.

The sample applied was purified by careful fractional distillation, repeated recrystallizations of the pyridine-$ZnCl_2$ complex from alcohol (8 times), liberation of pyridine by means of KOH and subsequent fractionation. The sample so obtained was still contaminated with sufficient NH_3 to give strong microwave lines from this impurity. It was found that the trace of NH_3 could be almost completely removed by adding water to the purified pyridine and removing the constant-boiling mixture of water and pyridine (in which NH_3 concentrates) by careful fractionation.

The microwave spectrum was studied at room temperature in the frequency interval 18 700–25 800 Mhz and was found by us to consist of 130–140 lines. As far as could be seen the Stark effect

was everywhere quadratic. Fairly high field intensities are therefore necessary to resolve the Stark components. With our present equipment we have so far only succeeded in identifying one line by means of its Stark pattern. Based on this and the remaining data of unidentified lines we can contribute to the knowledge of the configuration of pyridine by the following argument.

From the electron-diffraction pattern[1] it was calculated that $d_{CC}=1.39\pm0.02$ and $d_{CN}=1.37\pm0.03$A .Let $1.05\text{A}<d_{CH}<1.11\text{A}$. Twenty-seven different pyridine models were now constructed by forming all possible combinations of the geometrical parameters: $d_{CC}=1.37, 1.39, 1.41$; $d_{CN}=1.34, 1.37, 1.40$; $d_{CH}=1.05, 1.08, 1.11$ and letting the H−C−C and the C−C−C angles be 120°. For each of the models the asymmetry parameter, κ, $(A+C/2)$, and $(A-C)/2$ were calculated, A being the largest, C the smallest rotational constant. It was found that $0.655\leqslant\kappa\leqslant1.000$.

Inspection of the tables computed by King, Hainer, and Cross[3] shows that within the limits imposed on the value of κ and the rotational constants by the electron-diffraction result, the microwave spectrum of pyridine will be characterized by a group of strong, closely spaced lines, approximately covering a 100-Mhz interval in the 19 000–22 000-Mhz region. The corresponding transitions are of the general type $J_x\rightarrow J_{x+2}$.

The microwave spectrum of pyridine confirmed this fully. From 20 623 to 20 728 Mhz, a group of 12 strong lines was observed. No similar accumulation of lines was found anywhere else in the interval scanned. Independent of the magnitude of κ, the $7_0\rightarrow7_2$ line belongs to this group. For each of the 27 models the position of this line was calculated. It was found that there are only 7 combinations of the geometrical parameters (not all of them being one of the models, but "intermediates") which will give a correct position of the $7_0\rightarrow7_2$ line. Three of the combinations have κ close to 0.85; three others have κ close to 0.70. For the seventh, $\kappa=0.99$, but this possibility can be excluded at once because of the complexity of the spectrum.

In order to find whether κ is 0.70 or 0.85 the line at 20 211.25 Mhz is considered. Whether observed at 2200 or 3200 v per cm it has 6 Stark components. Since all the components are on the high-frequency side of the undisplaced line and since the frequency differences between successive components are increasing with increasing frequency both A' and B' in the expression $\Delta\nu_M=(A'+B'M^2)E^2$ for the Stark displacements of the lines of an asymmetric rotor[4] must be positive. Furthermore the intensity of the Stark components is definitely increasing with increasing frequency, so that the transition must be of the $\Delta J=0$ type.[4]

Frequency measurements of the Stark components[4] confirmed the view that the line at 20 211.25 Mhz is one of the permitted $6_x\rightarrow6_y$ transitions. Of these, the $6_{-1}\rightarrow6_1$ and the $6_{-2}\rightarrow6_0$ lines are the only ones of suitable position. If however, κ is close to 0.85, both lines will belong to the group of strong lines. However, the line at 20 211 Mhz is more than 400 Mhz removed from the group. If we assume that $\kappa\sim0.70$, the line $6_{-2}\rightarrow6_0$ is separated from the group by 300–400 Mhz. Hence we conclude that the line at 20 211 Mhz corresponds to a $6_{-2}\rightarrow6_0$ transition. The models compatible with this fact have $d_{CC}=1.39$–1.40; $d_{CN}=1.34$; $d_{CH}=1.05$–1.11A.

Since we know now that $\kappa\sim0.70$ it is easy to see from the K−H−C-tables that the $7_0\rightarrow7_2$ line will be among the high-frequency lines in the "group." κ is adjusted so that this line falls close to 20 700 Mhz while a value near 20 211 Mhz is calculated for the $6_{-2}\rightarrow6_0$ transition. It is found that κ must be 0.6875 while $(A-C)/2=1611$ Mhz to achieve this.

This value of $(A-C)/2$ is just barely compatible with the electron-diffraction result which permits values of $(A-C/2)$ between 1468 and 1608 Mhz. A model corresponding to $(A-C)/2=1606$ has $d_{CC}=1.39$; $d_{CN}=1.34$ and $d_{CH}=1.05$A. A model with $(A-C)/2=1608$ has $d_{CC}=1.41$; $d_{CN}=1.34$ and $d_{CH}=1.05$A. These models have, respectively, $(A+C)/2=4595$ and 4546 Mhz.

We shall compute the lines for which $J\leqslant10$ to be expected in the microwave spectrum in the 18 700–25 800-Mhz interval and compared with what one finds. At this calculation we use $\kappa=0.6875$ and $(A-C/2)=1611$ Mhz. Since the molecule is planar, $C^{-1}=B^{-}+A^{-1}$ and $(1+\kappa/2)=[C/(A-C)]^2$. The value of $(A+C)/2$ corresponding to $\kappa=0.6875$ and $(A-C)/2=1611$ is 4571 Mhz to be used at the calculation of the spectrum. It is to be noted that this is exactly the mean value of $(A+C)/2$ for the two models considered above.

TABLE I. Calculated and some of the observed microwave lines of pyridine.

Transition	Calc. (Mhz)	Strong lines	Medium lines
$8_0\rightarrow8_2$	19 030	19 098	
$7_{-1}\rightarrow7_1$	19 770	19 809	
$6_3\rightarrow7_{-3}$	19 983		19 932
$3_2\rightarrow4_{-1}$	20 242	20 242	
$6_{-2}\rightarrow6_0$	20 250	20 211	
$5_{-2}\rightarrow5^{-1}$	20 520	20 623	
$6_{-1}\rightarrow6_1$	20 649	20 667	
$4_{-4}\rightarrow4_{-2}$	20 653	20 674	
$2_{-1}\rightarrow3_{-2}$	20 687	20 678	
$4_{-3}\rightarrow4_{-1}$	20 690	20 691	
$7_0\rightarrow7_2$	20 690	20 710	
$2_{-2}\rightarrow3_{-2}$	20 757	20 727	
$8_1\rightarrow8_3$	20 828	20 840	
$9_3\rightarrow9_4$	21 115	21 175	
$9_2\rightarrow10_{-4}$	21 357		21 350
$1_1\rightarrow2_1$	21 506	21 400	
$10_3\rightarrow10_5$	21 603		21 640
$9_1\rightarrow10_{-3}$	21 768		21 770
$5_4\rightarrow6_{-2}$	22 024		22 030
$6_2\rightarrow7_{-2}$	23 512	23 500	
$2_1\rightarrow3_{-1}$	25 601	25 610	

It is seen that the microwave spectrum is consistent with the values of the geometrical parameters assumed ($d_{CC}=1.40$; $d_{CN}=1.34$; $d_{CH}=1.05$A). In order to be able to clarify the constitution unambiguously we are engaged in further studies of the Stark effect and in efforts to prepare 4-deutero pyridine (by decarboxylation of *d*-isonicotinic acid and by treatment of 4-iodopyridine with *DJ*) which is the only deuterated derivative that has a larger κ than pyridine itself.

[1] V. Schomaker, and L. Pauling, J. Am. Chem. Soc. **61**, 1769 (1939).
[2] C. H. Kline, and J. Turkevich, J. Chem. Phys. **12**, 300 (1944).
[3] King, Hainer, and Cross, J. Chem. Phys. **11**, 27 (1943).
[4] S. Golden and E. Bright Wilson, J. Chem. Phys. **16**, 667 (1948).

Dielectric Polarization and Self-Ionization in Carboxylic Acids

FRANK E. HARRIS* AND BERNI J. ALDER
Department of Chemistry and Chemical Engineering, University of California, Berkeley, California
(Received April 14, 1953)

EXPERIMENTAL studies of the dielectric polarization of carboxylic acids in the liquid state show that in some instances the dielectric constants increase with increasing temperature and that they are always larger than would be predicted from a nonpolar structure. Since density,[1] electron diffraction,[2] and infrared studies[3] of the vapor indicate that in the liquid range the acid is almost completely associated into dimer units, it is improbable that there exist in the liquid the large number of polar monomer units required to explain the polarization. However, the phenomenon may be explained by the tendency of these molecules toward self-ionization. Such self-ionization could also be the basis of the broadening of the infrared lines observed in these acids.[4]

A carboxylic acid dimer could form an ion pair by transfer of a proton from one monomer unit to the other in a manner similar to that suggested by Latimer[5] (see Fig. 1). This transfer would be accompanied by a rearrangement of charge on both monomer

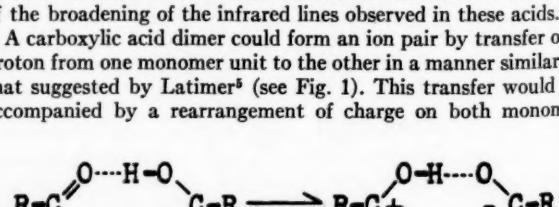

FIG. 1. Equilibrium between the dimer and the ion pair.

TABLE I. Thermodynamic functions for associated ion-pair formation.

	Acetic acid (see reference 7)						
Temp °C	10	20	30	40	50	60	70
$\Delta F°$ (kcal/mole)	3.1	3.2	3.2	3.3	3.3	3.4	3.4
$\Delta H°$ (kcal/mole)	1.1	1.2	1.3	1.4	1.5	1.6	1.7
$\Delta S°$ (eu)	−7	−7	−6	−6	−6	−5	−5
	Butyric acid (see reference 8)						
Temp °C	10			40			70
$\Delta F°$ (kcal/mole)	3.6			3.8			4.0
$\Delta H°$ (kcal/mole)	1.4			1.6			1.7
$\Delta S°$ (eu)	−8			−7			−7
	Trifluoracetic acid (see reference 8)						
Temp °C	−10	0	10	20	30	40	50
$\Delta F°$ (kcal/mole)	2.4	2.5	2.5	2.6	2.7	2.8	2.9
$\Delta H°$ (kcal/mole)	0.4	0.4	0.4	0.4	0.4	0.4	0.4
$\Delta S°$ (eu)	−8	−8	−8	−8	−8	−8	−8

units so that the average charge separation would be about 3.5 to 4 angstroms. This distance corresponds to the location of the center of charge near the middle of the O−C−O group.

The number of ion pairs per unit volume, N_2, can be calculated using the authors' equations for the dielectric polarization of mixtures.[6]

$$\frac{M}{d}\left(\frac{\epsilon-1}{\epsilon+2}\right)=\frac{M}{d}\left(\frac{n^2-1}{n^2+2}\right)+\frac{4\pi}{3}\left(\frac{N_2}{N}\right)\frac{9\epsilon}{(2\epsilon+1)(\epsilon+2)}\frac{N_0\mu_2^2}{3kT}, \quad (1)$$

where M is the molecular weight of the dimer, ϵ and n^2 the dielectric constant and index of refraction of the acid, respectively, d the density, μ_2 the ion-pair dipole moment, N the total number of dimers per unit volume, and N_0 Avogadro's number. It has been assumed that the dimer molecules can be treated as a dielectric continuum with the ion pairs sufficiently separated so that mutual interaction can be neglected. The approximation of a dielectric continuum implies the absence of specific interaction between an ion pair and the surrounding dimers. However, even considerable interaction of this type would not affect the conclusions here obtained.

The dielectric constants of acetic and butyric acids obtained by Smyth and Rogers,[7] and of trifluoroacetic acid obtained by Dannhauser and Cole were used.[8] The effective dipole moment of the ion pairs in the medium was calculated using a charge separation of 3.75A and the Onsager reaction field.[9] From the values of N_2, the equilibrium constants and the thermodynamic functions for the ionization process were calculated. N_2, which ranged from 0.1 to 1 mole percent, was low enough to justify the approximation that the various ion pairs do not interact. It is found (see Table I) that the values of the thermodynamic functions show a slight trend toward increasing $\Delta H°$ and $\Delta F°$ as one proceeds from trifluoroacetic through acetic to butyric acid. The nature of the calculation is too crude to indicate whether or not this difference is significant, although it is consistent with the trend in ionization constants of these acids in aqueous solution. The values of $\Delta H°$, $\Delta F°$, and $\Delta S°$ are quite different from those reported by Jolly[10] since his figures refer to the dissociation into free ions. The discrepancy in $\Delta H°$ is due to the difference in the energy required to pull the ion pair apart and that recovered by solvation energy. The entropy would be expected to decrease markedly upon separation because of the increase in bound solvent. Thus, the work necessary to separate a bound ion pair is large, which results in a small concentration of free ions as is evident, for example, from the low electrical conductivity of these acids.[11]

While this effect adequately explains the polarization of the carboxylic acids, it is found not to be an important factor in water. First, the number of associated ion pairs would be expected to be less, since it would be more difficult for the water to stabilize the charge on a single oxygen than for carboxylic acid on an O−C−O system. Secondly, a maximum change of a few dielectric constant units possible through this mechanism is far too small to explain the large polarization in water.

We acknowledge the interesting discussions with Dr. E. Haycock and Dr. E. Scott.

* Predoctoral Fellow, National Science Foundation.

[1] E. W. Johnson and L. K. Nash, J. Am. Chem. Soc. **72**, 547 (1950); Lundin, Harris, and Nash, J. Am. Chem. Soc. **74**, 743, 4654 (1952).
[2] L. Pauling and L. O. Brockway, Proc. Nat'l. Acad. Sci. U. S. **20**, 336 (1934).
[3] R. Hofstadter, J. Chem. Phys. **6**, 534 (1938); R. C. Herman and R. Hofstadter, J. Chem. Phys. **7**, 460 (1939).
[4] Fuson, Josien, Jones, and Lawson, J. Chem. Phys. **20**, 1627 (1952).
[5] W. Latimer, Chem. Revs. **44**, 59 (1949).
[6] F. E. Harris and B. J. Alder (to be published).
[7] C. P. Smyth and H. E. Rogers, J. Am. Chem. Soc. **52**, 1824 (1930).
[8] W. Dannhauser and R. H. Cole, J. Am. Chem. Soc. **74**, 6105 (1952).
[9] L. Onsager, J. Am. Chem. Soc. **58**, 1486 (1936).
[10] W. L. Jolly, J. Am. Chem. Soc. **74**, 6199 (1952).
[11] I. M. Kolthoff and A. Willman, J. Am. Chem. Soc. **56**, 1007 (1934).

The Vibrational Spectra and Structure of Ferrocene and Ruthenocene*

ELLIS R. LIPPINCOTT AND RICHARD D. NELSON
Department of Chemistry, Kansas State College, Manhattan, Kansas
(Received May 7, 1953)

THE chemical and physical properties of iron biscyclopentadienyl[1,2] have led Wilkinson,[3,4] Rosenblum, Whiting, and Woodward to propose a highly symmetric "sandwich" model for its structure having D_{5d} or D_{5h} symmetry. A number of analogous biscyclopentadienyl compounds of other transition elements have been prepared by Wilkinson and others for which similar models have been proposed.[5] X-ray diffraction studies on ferrocene by a number of investigators have verified the structure with D_{5d} symmetry.[6]

As evidence of a different kind for the unusual structure of these compounds we wish to give a preliminary report on the vibrational spectra of ferrocene, $Fe(C_5H_5)_2$ and ruthenocene, $Ru(C_5H_5)_2$. The samples used were prepared in this laboratory and purified by repeated recrystalization followed by sublimation. The ferrocene and ruthenocene used had melting points of 173–4°C and 196°C, respectively. Infrared spectra in CCl_4, CS_2, and Nujol solutions were obtained in the region from 2 to 25μ with a Perkin-Elmer model 12C spectrometer. Raman spectra in CS_2, CCl_4, $CHCl_3$ and benzene solutions were obtained using a Hilger 612 spectrograph. Spectra on ruthenocene were obtained with both Hg 4358A and Hg 5461A excitation using in each case the appropriate filters. Because ferrocene absorbs throughout much of the visible region, excitation was accomplished with the Hg 5770-5790A doublet as well as the Hg 5461A line using the appropriate filters. It was found that the intensity of the Raman scattering for ferrocene was rather sharply dependent on the concentration and that for a given wavelength there existed an optimum concentra-

TABLE I. The Raman and infrared spectra of ferrocene and ruthenacene (cm^{-1}).

Ferrocene				Ruthenocene			
Raman		Infrared		Raman		Infrared	
303	*m*			330	*s*		
388	*w*			402	*m*		
		478	*s*			446	*s*
		492	*s*			528	*w*
		782	*w*			763	*w*
		811	*s*	804	*w*	806	*s*
		834	*w*				
*ca*1010	*w*	1002	*s*	996	*m*	1002	*s*
1050	*w*	1051	*w*	1056	*m*	1050	*w*
1105	*s*	1108	*s*	1104	*s*	1103	*s*
1178	*m*	1188	*w*	1193	*w*		
1356	*w*			1360	*w*		
1408	*m*	1411	*s*	1412	*m*	1413	*m*
		1620				1622	
		1650				1651	
		1684	*m*			1684	*m*
		1720				1727	
		1758				1774	
3085	*m*			3089	*m*		
3099	*s*	3085	*s*	3104	*s*	3100	*m*

tion for maximum intensity of scattering which was considerably less than that of a saturated solution. This effect was caused by the partial absorption of the exciting radiation before scattering followed by the partial absorption of the Raman radiation after scattering. A detailed description of this with methods of obtaining Raman spectra of absorbing substances will be given in a later publication.

The vibrational spectra given in the table show a number of features consistent with the highly symmetrical "sandwich" model for these compounds. The number of observed Raman lines and infrared absorption peaks is rather small for molecules having 57 vibrational degrees of freedom thus suggesting structures whose symmetry implies rather stringent selection rules. Consistent with this is the appearance of only one type of CH frequency for both compounds in either the infrared or Raman spectra. Evidence for equivalent multiple bonds resulting from delocalization of the π-electrons of the cyclopentadienyl rings is the appearance of multiple bond frequencies near 1410 cm^{-1}. An examination of the selection rules for a D_{5d} model predicts the appearance of 15 Raman ($4A_{1g}$, $5E_{1g}$, and $6E_{2g}$) and 10 infrared ($4A_{2u}$ and $6E_{1u}$) fundamentals. These numbers are in reasonable agreement with those observed in the vibrational spectra.

The vibrational spectra of ferrocene and ruthenocene have some unusual features. An examination of the table shows that most infrared absorption peaks are coincidences or near coincidences. For example in ferrocene the 1406 cm^{-1} Raman multiple bond frequency and the intense 1105 cm^{-1} Raman frequency corresponding to the symmetric ring breathing mode are coincidences. Since the rule of mutual exclusion should hold for the D_{5d} model (D_{5h} model also), the appearance of these coincidences requires explanation. We interpret this to mean that there is little interaction between the symmetric and antisymmetric modes of vibration which involve displacements associated primarily with the cyclopentadienyl rings. This could result if the delocalization of the π-electrons in one ring was essentially independent of the delocalization in the other ring.

Another unusual feature is the appearance of slightly converging band systems near 1700 cm^{-1} in the infrared spectrum of both compounds. These are not readily interpreted in terms of fundamental modes of vibration for two reasons. First, there should be similar fundamental frequencies appearing in the Raman spectra. Second, there is no structural feature of these compounds which would lead us to expect the observation of fundamentals in this region. We feel that this band system is best explained as a difference band system involving the restricted rotation of the cyclopentadienyl rings with respect to one another.

A comparison of the spectrum of ferrocene with that of ruthenocene shows many similarities. Frequencies corresponding to motion within the cyclopentadienyl rings occur at essentially the same cm^{-1} values. Frequencies associated with modes of vibration involving the motion of the rings with respect to the central atom occur at different positions. In particular, the ring-Ru-ring symmetric stretching frequency at 332 cm^{-1} is at a higher value than the corresponding frequency in ferrocene (303 cm^{-1}). We interpret this to mean that the rings are bound more tightly to the metal atom in ruthenocene than in ferrocene.

A detailed assignment of frequencies and calculation of thermodynamic functions will be given in a subsequent publication.

The authors wish to express their gratitude to the Research Corporation of America for a grant-in-aid and to Ernest A. Ikenberry for help in the preparation of ferrocene.

[1] Miller, Tebboths, and Tremaine, J. Chem. Soc. 1952, 632.
[2] T. J. Kealy and P. L. Pauson, Nature, 168, 1039 (1951).
[3] Wilkinson, Rosenblum, Whiting, and Woodward, J. Am. Chem. Soc. 74, 2125 (1952).
[4] Woodward, Rosenblum, and Whiting, J. Am. Chem. Soc. 74, 3458 (1952).
[5] G. Wilkinson, J. Am. Chem. Soc. 74, 6146, 6148 (1952); Wilkinson, Pauson, Birmingham, and Cotton, J. Am. Chem. Soc. 75, 1011 (1953).
[6] P. F. Eiland and R. Pepinsky, J. Am. Chem. Soc. 74, 4971 (1952); J. D. Dunitz and L. E. Orgel, Nature, 171, 121 (1953); E. O. Fischer and W. Pfab, Z. Naturforsch, 7b, 377 (1952).
* Presented in part at the 123rd national meeting of the American Chemical Society at Los Angeles, California (March 1953).

On the Solubility of Hydrogen in Certain Liquid Metals*

Y. L. YAO
Physical Metallurgy Division, Mines Branch, Department of Mines and Technical Surveys, Ottawa, Canada
(Received May 8, 1953)

As far as the behavior with hydrogen is concerned, metals may be classified into three groups: (*A*) those which form saline compounds with stoichiometric ratio, (*B*) those which occlude more hydrogen as the temperature is decreased in the solid state, and (*C*) those which occlude more hydrogen as the temperature is increased in the solid state. The classification is not sharp but useful.

Empirically it is suggested that two conditions are necessary for group *C* metals. One condition is that one of the crystalline forms is face-centered cubic. The other one is that the first molar enthalpy at 25°C is greater than 170 kcal. Thus Pb, Ag, Ni, Cu, Fe, Co, Pd, and Pt are included in this group while Al (139.5 kcal, fcc), Cr (156.9, bcc and cph), Mo (171.7, bcc) and Mn (172.5, complex cubic and tetragonal) are excluded. Experimentally Pd is known to belong to group *B*, Al seems to belong to group *C* and Cr, Mo, and Mn seem to belong to group *B* or *C* according to temperature ranges. Only Al and Pd are exceptions to the above statements.

The reason for enthalpy of ionization being a parameter is obvious. In a sense for the hydrides of groups *A*, the ionization of metal is complete, for the hydrides of group *B* the ionization is partial but appreciable and for the mixtures of group *C* the ionization is negligible.

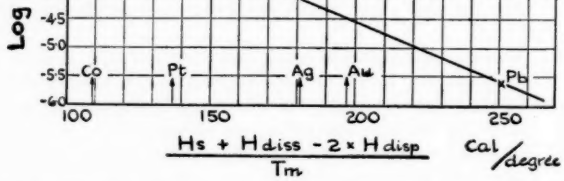

FIG. 1. H_s, H_{diss} and H_{disp} for Ni^{++}, Fe^{+++}, Cu^{++}, Pb^{++}, Ag^{+}, and Co^{++} is taken from "Selected Values of Chemical and Thermodynamical Properties," U. S. Government Printing Office, 1952. H_{disp} for Pt^{++} and Au^{+} is taken from estimations of standard potentials by W. M. Latimer in *The Oxidation States of the Elements and their Potentials in Aqueous Solutions*, (Prentice-Hall, Inc., New York, 1938). No attempt is made to change free energies into enthalpies. Log$x$ at Tm for Ni, Cu, and Fe is taken from D. P. Smith, *Hydrogen in Metals* (University of Chicago Press, Chicago, 1949). Log$x$ for Pb is taken from W. R. Opie and N. J. Grant, Trans. Am. Inst. Mining Met. Engrs. 191, 244 (1951).

Empirically it is also suggested that, for metals fulfilling the above conditions, there is a correlation between log$x$ and $(H_s+H_{diss}-2XH_{disp})/Tm$, where x is the solubility of hydrogen in atomic ratio at one atmospheric pressure and at absolute melting point Tm of the metal. H_s is the molar enthalpy of sublimation of metal at 25°C, H_{diss} is the molar enthalpy of dissociation of hydrogen at 25°C and H_{disp} is the equivalent enthalpy of the following reaction at 25°C:

$$\tfrac{1}{2}H_2+\frac{1}{n}M^{n+}(aq,\ m=1)\rightarrow\frac{1}{n}M+H^{+}(aq,\ m=1).$$

Figure 1 indicates that this expectation holds, and an attempt is made to explain this correlation.

The close neighbor hypothesis could be extended to liquid solutions of hydrogen:

$$\Delta H=(1-x)^2W\doteq W,$$

where ΔH is the partial molar enthalpy of solutions of hydrogen and W is the interchange energy. The interchange energy is defined as equal to bond energy of metal E_{MM}, +bond energy of hydrogen E_{HH}, and $-2X$ bond energy of hydrogen and metal E_{HM}.

In liquid solutions of hydrogen there is no evidence to show that the concentration of hydrogen is not uniform. Thus ΔH has a physical meaning, in contrast with solid solutions. Also strain energy ceases to be important, as is true in any liquid solutions.

Obviously E_{MM} is related to H_s and E_{HH} is related to H_{diss}. Since H_{disp} represents

(enthalpy of dissociation of hydrogen − enthalpy of sublimation of metal) + (enthalpy of ionization of hydrogen − enthalpy of ionization of metal) + (enthalpy of hydration of hydrogen ion − enthalpy of hydration of metallic ion);

on the equivalent basis, E_{MH} is related to H_{disp} if the difference in enthalpy of hydration between hydrogen ion and metallic ion is equal to the difference in enthalpy of solvation (with excess metal as the solvent) between hydrogen ion and metallic ion. In other words, we imagine that hydrogen and metal form an ionic crystal and water or excess metal breaks this ionic crystal and brings out the solution in the same way. Then ΔH is related to $H_s+H_{diss}-2XH_{disp}$.

No activity data of hydrogen in liquid solutions are available. However, if there is a common relation between activity and concentration and if there is a common deviation of entropy from ideal behavior, there will be a correlation between $R\ln x$ and $(H_s+H_{diss}-2XH_{disp})/T$. For comparison purposes T is chosen at Tm.

From Fig. 1 we estimate that $\log x$ at Tm:

Co−2.6, Pt−3.2, Ag−4.2, Au−4.5.

In conclusion, certain trends are shown in the known solubilities of hydrogen at melting points of certain metals. Rough estimations are also possible for unknown solubilities.

* Published by permission of the Director-General of Scientific Services, Department of Mines and Technical Surveys, Ottawa, Canada.

The Optical Properties of Natural and Synthetic Hackmanite

DAVID B. MEDVED*
Research Division, Philco Corporation, Philadelphia 34, Pennsylvania
(Received May 4, 1953)

WHEN rocks containing the mineral hackmanite (evanescent pink sodalite $-Na_6Al_6Si_6O_{24}\cdot 2NaCl$) are broken in the field, they are suffused with a deep magenta coloration which fades upon exposure to visible light. The color returns if the specimens are kept in the dark. Lee[1] showed that strong magenta coloration, accompanied by a bright salmon-orange fluorescence, could be induced by irradiating the bleached mineral with ultraviolet light. Heat or bright radiation bleaches the specimen.

Figure 1 shows the absorption spectrum of hackmanite before and after exposure to 2537A ultraviolet, obtained at room temperature with a Beckman DU Spectrophotometer.† The induced absorption band is shown in Fig. 2. The maximum occurs at 5300±50A. The saturation number N_0 of color centers (as calculated by the Smakula relation)[2] was $N_0=10^{17}/cm^3$. The absorption band produced in hackmanite, protected from external radiation, is of the same general form with its peak at 5300A. There are irregularities in it which do not occur in the bands produced by ultraviolet and these are not always reproducible.

The reversible discoloration and bleaching can be described by a color center model wherein the ultraviolet absorption arises from appropriate ultraviolet "donor" levels in the forbidden band. Excitation under ultraviolet promotes electrons into F levels forming F centers, and the crystal is thus colored. Absorption in the F band subsequently empties the F center and the specimen is bleached. If the ultraviolet levels are identified with the U centers of Hilsch and Pohl,[3] a low thermal activation energy would facilitate discoloration at room temperature since direct transitions from U centers to F center are permissible.

We have prepared a series of synthetic substances whose properties lead us to believe that the above model is essentially correct. Pure sodalite is synthesized by heating a stoichiometric mixture of Al_2O_3, NaCl, SiO_2, and NaOH in a platinum crucible at 1060°C.[4,5] This sodalite is insensitive to ultraviolet but darkens under x-ray irradiation to give the characteristic magenta coloration. The induced absorption band peaks at 5300A. The traps responsible for the F band in hackmanite are therefore unique to the sodalite lattice.

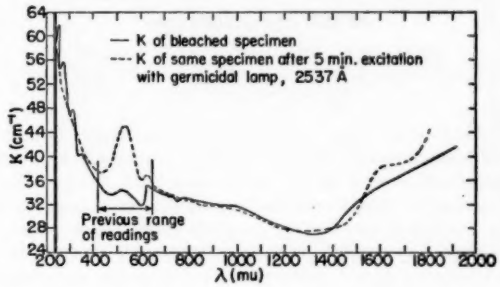
— K of bleached specimen
--- K of same specimen after 5 min. excitation with germicidal lamp, 2537 Å
Previous range of readings
K (cm⁻¹)
λ (mu)

FIG. 1. Absorption coefficient (K) of hackmanite before and after excitation with ultraviolet.

Attempts to introduce ultraviolet donor levels by addition of activating elements to sodalite were unsuccessful. However, if the sodalite is fixed at 1060°C in a reducing atmosphere of hydrogen or in a carbon crucible with limited access to air, it becomes strongly sensitive to 2537A ultraviolet. The induced absorption band has its maximum at 5300A. The sensitivity to 3600A ultraviolet and the orange fluorescence are much weaker than in the natural hackmanite.

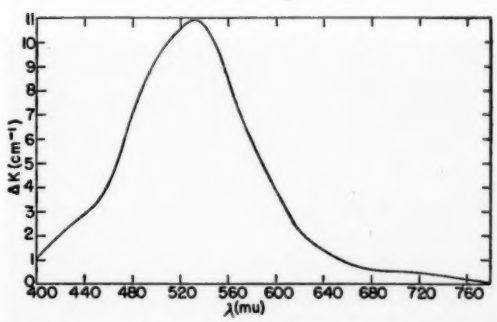

FIG. 2. ΔK *vs* λ for hackmanite which has been exposed for 5 min to radiation from a 15-watt germicidal lamp (1.05 watt-sec/cm²).

In the hydrogen process, the exhaust gases produce turbidity in an $AgNO_3$ solution, signifying that some chlorine is being removed from the sodalite lattice. Our synthetic hackmanite has then the tentative composition $Na_6Al_6Si_6O_{24}$. [(2−X)NaCl, XNaH] in analogy to the replacement of some KBr by KH in the Hilsch-Pohl process.

If the formation of a carbide U center (which should have different absorption from the hydride U center) is possible through replacement of Cl^- by C^- in the sodalite lattice, then we might expect an analogous replacement in the simple halides. Use of a carbide ion, with a larger ionic radius and mass than hydrogen, as a U center, offers a fundamental check on the Mott-Gurney mechanism[6] for the U center transformation, a mechanism which requires atomic diffusion through the lattice. Experimentation in this direction is contemplated.

I wish to thank Mr. W. E. Bradley, Director of Research, Philco Corporation, for his help and encouragement in this work.

* Present address: Physics Department, University of Pennsylvania, Philadelphia 4, Pennsylvania.
† We are indebted to Professor P. H. Miller, Jr. (University of Pennsylvania) for the use of this instrument.
[1] O. Ivan Lee, Am. Mineralogist **26**, 437 (1936).
[2] A. Smakula, Z. Physik **59**, 603 (1930).
[3] R. Hilsch and R. W. Pohl, Trans. Faraday Soc. **34**, 883 (1938).
[4] Polytechnic Institute of Brooklyn, Second Progress Report for Contract No-sbr 39045 (1947).
[5] D. B. Medved, Am. Mineralogist (to be published).
[6] Mott and Gurney, *Electronic Processes in Ionic Crystals*, p. 149.

Kinetic Studies with a Fast-Scanning Mass Spectroscope

EDOUARD G. LÉGER AND CYRIAS OUELLET
Department of Chemistry, Laval University, Quebec, Canada
(Received April 14, 1953)

FOR the study of rapid reactions in the gas phase, a panoramic mass spectroscope has been designed and built, in which the mass spectrum is seen on the screen of a cathode-ray tube and photographed by means of a movie camera. Mass analyses of the reacting gases are obtained at repeated intervals of a few milliseconds, and it is possible to follow the fate of several chemical species during rapid reactions, such as cool flames, occurring in a static system.

In this instrument, molecules leave the heated quartz reaction chamber through a hole 20 microns in diameter sparked through a thin quartz membrane at the apex of a re-entrant cone[1] and travel 2 cm as a molecular stream to a Nier ion source[2] provided with a tantalum filament. The excess gas is exhausted by a large diffusion pump. The ions are accelerated through slits by a saw-tooth wave voltage, superimposed on a dc voltage, so that the focused beam sweeps past a slit in front of the detector, a copper-beryllium ion-electron multiplier kindly supplied by Dr. Hin Lew.[3] The results

FIG. 1. Two strips of film photographed at low speed (16 images per second) showing inrush of ether-oxygen mixtures. Mass-ranges: 25–35 and 20–100.

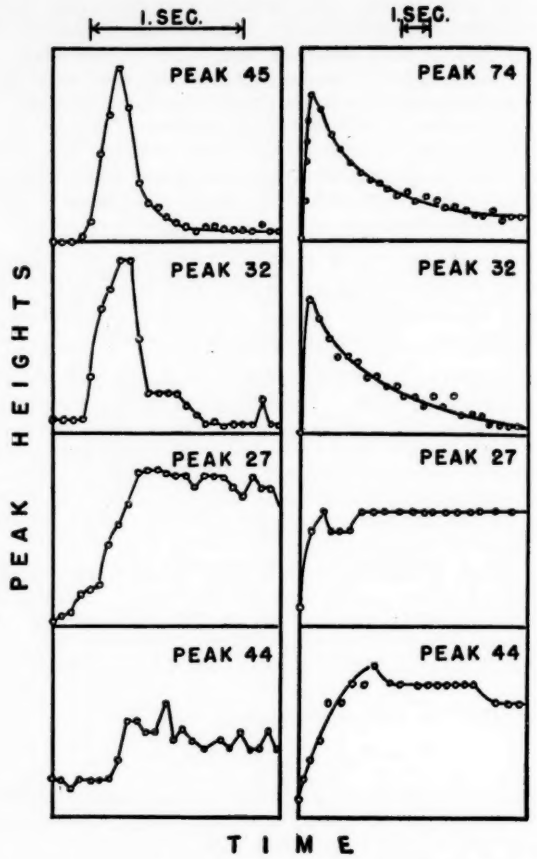

FIG. 2. Variations in peak heights during two reactions (left and right). Ordinates on arbitrary scales.

are panoramically inscribed on a Tektronix 512 oscilloscope by placing the acceleration wave form on the horizontal axis and the output of the multiplier on the vertical axis.[4] A permanent magnet (Alnico-5) provides a constant magnetic field. Inflexion focusing is used.[5] A 40-peak spectrum can be scanned in 5 milliseconds. A description of this instrument will be published elsewhere.

Photographs of two differently expanded mass spectra, showing the rising peaks as an ether-oxygen mixture is rushed into the evacuated reaction vessel, are seen in Fig. 1. Each vertical row in Fig. 2 shows the variations in time of some of the peak heights during a cool flame in an equimolecular mixture of diethylether and oxygen at about 50 mm Hg and 200°C. Ether has been used in these preliminary experiments because it gives cool flames at relatively low temperatures and pressures. As the mixture is rushed into the hot, evacuated vessel, the peaks belonging to the reactants (32 for O_2, 74 and 45 for Et_2O) show a sharp rise soon followed by a decline due to the reaction. Following 74 and 45 very closely are other peaks (not shown) also belonging to Et_2O, such as 31 (CH_3O) and 29 (CHO or C_2H_5). Peaks presumably belonging to the products rise later to a more or less constant value. Of these, 44 is tentatively asigned to CH_3CHO and CO_2, 28 to CO and C_2H_4, 27 mostly to C_2H_3 as a fragment of C_2H_4. The data shown here have been obtained at 25 volts ionizing voltage. Using lower voltages and high sensitivities, it should be possible to single out peaks due to free radicals,[1,6] but their concentrations in cool flames must be very low. We plan to combine these mass spectrometric analyses with photoelectric measurements of the luminescence which accompanies reactions of this type.[7]

We are indebted to the Defence Research Board of Canada for a grant (DRB-129) and for a research associateship to one of us (E.G.L.), also to the National Research Council for scholarships to E.G.L. We thank Mr. L.-P. Blanchard and Mr. J. Lefebvre for

assistance in phases of this work, and also Dr. Kerwin, Dr. Lew, and Dr. Lossing for their interest and advice.

[1] F. P. Lossing and A. W. Tickner, J. Chem. Phys. **20**, 907 (1952).
[2] A. O. C. Nier, Rev. Sci. Instr. **18**, 398 (1947).
[3] H. Lew, Phys. Rev. **76**, 1087 (1949).
[4] W. Siri, Rev. Sci. Instr. **18**, 540 (1947).
[5] L. Kerwin, Rev. Sci. Instr. **20**, 36 (1949).
[6] G. C. Eltenton, J. Chem. Phys. **15**, 455 (1947).
[7] L. Ouellet, E. Léger and C. Ouellet, J. Chem. Phys. **18**, 383 (1950).

The Structure and Residual Entropy of Ice*

R. E. RUNDLE
Department of Chemistry and Institute for Atomic Research, Iowa State College, Ames, Iowa
(Received May 4, 1953)

EVIDENCE that ice forms polar crystals, probably of C_{6V} symmetry, is strong,[1] and arguments of Bjerrum indicate that preferred dipole orientations are most likely.[2] It therefore seems probable that Pauling's disordered structure,[3] which explains the residual entropy[4] and neutron diffraction data,[5] is incorrect.

If we assume that (1) water dipoles interact to maintain, at low temperatures, the maximum net dipole along one direction of the hexagonal axis; (2) that $\measuredangle HOH \cong 104\frac{1}{2}°$ in ice as in the vapor;[6]† and (3) that one OH bond lies directly along one O—O ligand, but that otherwise Pauling's type of disorder prevails, one gets a disordered, polar structure with space group $C_{6V}{}^4-C6mc$, and positions as given in Table I. The number of configurations is as follows: The hydrogen in bonds along the c axis are fixed, say, closer to the oxygens (Table I) at 1/16 and 9/16. Three-fourths of the hydrogens (3/2 mole per mole of water) have two positions (ignoring point 3). But if one requires H_2O molecules, only 3/8 of the configurations about each oxygen are acceptable, so that the number of configurations is $2^{\frac{1}{2}N}(3/8)^N$. Points 1 and 2 require that water molecules with no bond along the c axis have two equally likely configurations for every one previously counted, while those with a bond along with c axis have only one (Fig. 1). There are equal numbers of the two types of water molecules so that the total number of equally probable configurations is $2^{\frac{1}{2}N}(3/8)^N 2^{N/2} = (3/2)^N$, or the number of configurations is exactly that required to explain the residual entropy!

Neutron diffraction intensities for this polar disordered structure are almost identical with those calculated for Pauling's structure except for (10.3) where $P_{obs}=95$ *vs* 70 calculated for Pauling's structure and 130 for the polar structure. Complete ordering along the c axis was assumed in the latter calculation, while complete disordering would lead to the Pauling value. Hence, at an intermediate temperature an intermediate intensity is expected. The neutron data were obtained at −90°C; both lower and higher temperature data would be most pertinent.

The polar structure has better hydrogen bonding along c than otherwise, and the c/a ratio is expected to be less than ideal $2\sqrt{2}/\sqrt{3}=1.6330$ in agreement with Megaw's data,[7] who found that $c/a=1.6289$ at 0° and decreases with temperature.

The polar structure has bent and normal O—H··O hydrogen bonds, and two neighboring O—H stretching frequencies are expected. Sutherland has found two in ice at 3090 and 3135 cm^{-1}.[8]

TABLE I. Polar, disordered ice structure.[a]

Point positions are those of space group $C_{6V}{}^4-C6mc$, as listed in *International Tables for the Determination of Crystal Structures.*

$2O_I$ in 2(*b*)	1/3, 2/3 z,	2/3, 1/3, 1/2+z	$z_I=1/16$
$2O_{II}$ in 2(*b*)	$z_{II}=7/16$		
$2H_a$ in 2(*b*)	$z_a=0.199$		
$6H_{b/3}$ in 6*c*	$x_b=0.457$,	$z_b=0.0272$	
$6H_{c/3}$ in 6*c*	$x_c=0.546$,	$z_c=0.983$	
$12H_{d/6}$ in 12*d*	$x_d=0.467$,	$y_d=0.563$,	$z_d=0.488$

[a] Assume O—H=1A, $\measuredangle HOH = 104\frac{1}{2}°$.

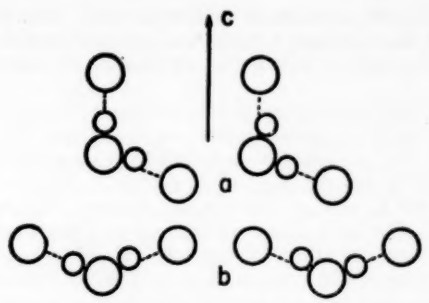

FIG. 1. In *a*, the two orientations for water have different moments along *c*, and only the one on the right is allowed. In *b*, the two orientations for water have equal moments along *c*, and both are counted.

Giauque and Stout[4] note that thermal equilibrium is reached slowly in the region from 80—100°K, as though a new degree of freedom were being excited. It is difficult to judge the potential barrier for the H_2O "wagging" of Fig. 1, but it must be quite low and may result in an anomaly at this low temperature.

A critical point in the entropy argument is the counting of two configurations which differ by only 5°. Since little zero-point energy will be associated with the wagging motion, it does not seem unreasonable to expect two distinguishable arrangements at very low temperatures.

* Contribution No. 221 from the Institute for Atomic Research and Department of Chemistry, Iowa State College, Ames, Iowa. Work was performed in the Ames Laboratory of the U. S. Atomic Energy Commission.
† This is readily justified, since it requires about 0.5 kcal/mole to open the angle to 109°28′, and a negligible amount is regained by better hydrogen bonding.

[1] See E. S. Campbell, J. Chem. Phys. **20**, 1411 (1952) for a review of this point, with references.
[2] N. Bjerrum, Science **115**, 385 (1952).
[3] L. Pauling, J. Am. Chem. Soc. **57**, 2680 (1935).
[4] W. F. Giauque and J. W. Stout, J. Am. Chem. Soc. **58**, 1144 (1936).
[5] Wollan, Davidson, and Shull, Phys. Rev. **75**, 1348 (1949).
[6] G. Herzberg, *Infrared and Raman Spectra* (D. Van Nostrand Company, Inc., New York).
[7] H. D. Megaw, Nature **194**, 900 (1934).
[8] G. B. B. M. Sutherland, Proc. Roy. Soc. (London) **141**, 544 (1933).

The Nature of the Gradual Transition in Sodium Borohydride

W. H. STOCKMAYER AND C. C. STEPHENSON
Department of Chemistry, Massachusetts Institute of Technology, Cambridge, Massachusetts
(Received May 4, 1953)

A GRADUAL transition (λ-point) in solid sodium borohydride, $NaBH_4$, at 190°K has recently been reported by Johnston and Hallett.[1] For the following reasons we conclude that this λ-point is an order-disorder transition involving the orientations of the borohydride ions, similar to the order-disorder transitions involving the orientations of the ammonium ions in the ammonium halides.

(1) The ions BH_4^- and NH_4^+ are isoelectronic. The crystal structure,[2] infrared spectrum,[3] and other properties of sodium borohydride show it to be an essentially ionic crystal composed of Na^+ and tetrahedral BH_4^- ions.

(2) The reported excess entropy of the transition in $NaBH_4$ is 1.2 cal deg^{-1} mole^{-1}; the corresponding values for the ammonium and deutero-ammonium halides[4,5] lie between 1.0 and 1.5 cal deg^{-1} mole^{-1}. All of these figures approximate the theoretical value of R ln2 for a simple order-disorder transition involving two alternate orientations of the tetrahedral ions. This interpretation of the λ-points in the ammonium halides is unequivocally indicated by their infrared spectra[6] and by their structures at temperatures below and above the transitions as revealed by neutron diffraction.[7,8]

(3) The continuity of the "normal" heat capacity curve through the transition in $NaBH_4$ precludes the possibility that complete or

partial rotational freedom of the borohydride ions has been attained at the transition; a significant increase in rotational freedom would require a substantial decrease in the normal heat capacity.[5]

(4) The heat capacity of $NaBH_4$ below the transition is incompatible with rotational freedom of the borohydride ions in this region. The data[1] in fact may be approximated in the range 15° to 100°K by the sum of a six-degree Debye function with $\Theta=268$°K and a three-degree Einstein function with $\Theta=500$°K. The latter figure corresponds to a frequency of torsional oscillation of about 350 cm^{-1} for the BH_4^- ion, which is similar in order of magnitude to those obtained for the ammonium halides from their infrared spectra[6] and from similar analyses of their heat capacities.[4,5] No combination band involving this frequency can be found in the published spectrum,[3] but comparison with the ammonium salts[6] suggests that a low-temperature infrared study would be worth while.

Although the above evidence is convincing, there is an important difference between $NaBH_4$ and the ammonium halides that merits further discussion. The borohydride has a face-centered cubic structure in the temperature range above the gradual transition, while the ammonium salts below and above their order-disorder transitions exist in the body-centered (tetragonal or cubic) form, changing by first-order transitions to face-centered cubic lattices only at higher temperatures. The $NaBH_4$ structure is of course a consequence of the large disparity in the ionic radii ($Na^+\sim 1$A, $BH_4^-\sim 2$A).

From the electronegativities[9] (B, 2.0 decreased by a formal negative charge in BH_4^-; H, 2.1) we should expect a small but definite B—H bond moment, the hydrogen being more negative. Accordingly, the lowest electrostatic energy would probably[10] be achieved by a borohydride ion if one of its B—H bonds were directed at one of the nearest-neighbor sodium ions; spectroscopic[10] and neutron-diffraction[8] studies indicate this to be the probable configuration of the ammonium ions in the face-centered phases of NH_4Br and NH_4I. However, we have seen that the heat capacity of $NaBH_4$ is incompatible with the rotational freedom (in at least one dimension) demanded by this structure. Furthermore, there is no possibility in this arrangement of an order-disorder transition involving just two equivalent orientations. Hence, the hydrogen atoms must be on the cube diagonals, the decrease in overlap energy thus attained apparently outweighing the increase in electrostatic energy. With the known nearest-neighbor Na—B distance[2] of 3.07A and the estimated[3] B—H bond length of 1.26A, each hydrogen atom lies at a distance of 2.56A from three nearest-neighbor sodium ions and 3.39A from three second-neighbor borons.

In the disordered phase the BH_4^- tetrahedra are distributed at random between the two alternative orientations, and the average unit cell of four $NaBH_4$ molecules therefore contains 12 pairs of hydrogens (the two members of a pair being in different ions) at a mean separation of 2.29A and 12 pairs at a mean separation of 2.72A. In the low-temperature ordered phase, if all the tetrahedra had the same orientation (as seems to be the case with NH_4Cl) each unit cell would contain 24 pairs of hydrogens at the smaller separation of 2.3A and none at 2.7A, thus giving a higher repulsive energy (whether due to electrostatic or overlap effects or both) than that of the disordered structure. However, if the ordered structure were built of alternate positively and negatively oriented planes of borohydride ions, there would be only 8 pairs of hydrogens separated by 2.3A and 16 pairs at 2.7A. This tetragonal structure would therefore have a lower energy than the disordered phase, and this might be lowered further by a change from cubic cell shape. Differences in van der Waals or polarization energies between the several structures considered must be truly negligible. We therefore believe the last structure above to be the correct description of the ordered phase. Neutron-diffraction study of $NaBD_4$ both below and above the λ-point would obviously be desirable to establish the correct structure.

Lithium borohydride exists in an orthorhombic structure of lower coordination number[11] and would therefore not be expected to exhibit a λ-point, in agreement with observation.[12] We have found no reports of properties of the higher alkali borohydrides, although KBH_4 has been prepared.[13] It seems likely that $CsBH_4$ (and possibly $RbBH_4$) would have the body-centered cubic structure at ordinary temperatures. If this is so, we may expect (in view of the low polarizability of the alkali ion) a transition completely analogous to that of NH_4Cl: i.e., a cubic ordered phase with all tetrahedra oriented alike.

[1] H. L. Johnston and N. C. Hallett, J. Am. Chem. Soc. **75**, 1467 (1953). Apparently the transition had been earlier discovered by Boodman, Stegeman, and Mason.
[2] A. M. Soldate, J. Am. Chem. Soc. **69**, 987 (1947).
[3] W. C. Price, J. Chem. Phys. **17**, 1044 (1949).
[4] Stephenson, Blue, and Stout, J. Chem. Phys. **20**, 1046 (1952).
[5] Stephenson, Landers, and Cole, J. Chem. Phys. **20**, 1044 (1952); also unpublished data.
[6] E. L. Wagner and D. F. Hornig, J. Chem. Phys. **18**, 296, 305 (1950).
[7] H. A. Levy and S. W. Peterson, Phys. Rev. **86**, 766 (1952).
[8] H. A. Levy and S. W. Peterson, J. Am. C .em. Soc. **75**, 1536 (1953)
[9] L. Pauling *The Nature of the Chemical Bond* (Cornell University Press, Ithaca, New York, 1940), second edition, p. 64.
[10] R. C. Plumb and D. F. Hornig, J. Chem. Phys. **21**, 366 (1953).
[11] P. M. Harris and E. P. Meibohm, J. Am. Chem. Soc. **69**, 1231 (1947).
[12] N. C. Hallett and H. L. Johnston, J. Am. Chem. Soc. **75**, 1496 (1953).
[13] Schlesinger, Brown, Hoekstra, and Rapp, J. Am. Chem. Soc. **75**, 199 (1953).

Errata: The Statistical Mechanical Theory of Irreversible Condensation. I

[J. Chem. Phys. **20**, 1216 (1952)]

HOWARD REISS
Bell Telephone Laboratories, Murray Hill, New Jersey

IN the paper of this title the definition of $\langle u(x)\rangle_{Av}$ contained in Eq. (2.14) is incorrect, for $\langle u(x)\rangle_{Av}$ is temperature dependent. As a result differentiation of both sides of (2.13) with respect to temperature leads, in place of (2.14), to

$$\langle u(x)\rangle_{Av}=\frac{\int\int\cdots\int_{v^v} u(x)e^{-u(x)/kT}(d\omega)^x}{\int\int\cdots\int_{v^v} e^{-u(x)/kT}(d\omega)^x}+T\frac{\partial\langle u(x)\rangle_{Av}}{\partial T}.$$

This differs from (2.14) in that the last term on the right appears. It is quite clear that this term is of the form $-TS(x)$, where $S(x)$ is an entropy, and that $\langle u(x)\rangle_{Av}$ is a free energy. The same is true of $\langle W(\alpha)\rangle_{Av}$ which appears in Eq. (2.36) and $\langle\omega(x)\rangle$ in (2.44). The analysis of the paper remains entirely correct despite the omission of this term provided the quantities mentioned above are redefined to include the omitted term, for the separation in (2.36) can still be performed.

There is an additional point which has been revealed by recent additional work which, although not in the nature of an error, represents an approximation which may not be accurate. Thus in the analysis leading from (2.44) to the end of Sec. II it has been assumed that g when determined by the various conditions would be large enough, and thus the minimum in x^* deep enough so that satisfying (2.21) with a finite series would imply that (2.22) would be very nearly satisfied. Thus only (2.21) was used in the determination of h by (2.55). Careful numerical analysis based on a reliable model now shows this may not be the case. This point will be amplified in the second paper of the series.

Erratum: Emission Spectrum of Undecomposed N Methylpyrrole

[J. Chem. Phys. **21**, 163–164 (1953)]

GIULIO MILAZZO
Instituto Superiore di Sanità, Rome, Italy

AN error occurred in the figure for the intensity of the strongest absorption bands of *n* methylpyrrole. The given value 40 has to be corrected to 700.

Molecular Species Evaporating from a Carbon Surface*

WILLIAM A. CHUPKA
Harvard University, Cambridge, Massachusetts and Argonne National Laboratory, Lemont, Illinois
AND
MARK G. INGHRAM
University of Chicago, Chicago, Illinois and Argonne National Laboratory, Lemont, Illinois
(Received May 8, 1953)

THE previously reported study[1] of the atomic and molecular species evaporating from a hot carbon surface has been extended using the same techniques. The method employs mass analysis of the ions produced by electron bombardment of the vapor. The ionizing electrons are of such low energies that ions are generally produced only from the corresponding neutral species. The disadvantage of low-ion intensities is overcome by the use of an electron multiplier for ion detection.

The ratio of C^+ to C_2^+ ions produced by bombardment of the carbon vapor has been measured more accurately. The ions are produced by 17-volt electrons and it has been shown that at this low energy the C_2^+ ions are produced entirely from molecular species evaporating from the carbon surface and probably mostly from the C_2 molecule. In a series of runs the C^+/C_2^+ ratio was reproducible at a particular temperature and remained constant even when C_2H_2 gas was introduced as long as the energy of the ionizing electrons was kept below about 19 volts. In previous runs using 20-volt electrons, the C^+/C_2^+ ratio did not remain strictly constant even without the introduction of C_2H_2, evidently due to production of some C_2^+ from hydrocarbons, traces of which remained in the mass spectrometer.

The presence of the previously reported C_3 molecule has been confirmed.[2] Some trouble was caused by an HCl peak of the same mass, but this was minimized and a correction was made when necessary. A search for molecules of higher molecular weight indicated they were in negligible quantities compared to C.

The relative intensities of C^+, C_2^+, and C_3^+ were measured using both a carbon filament and a filament machined from spectroscopic graphite rod. The results from both were essentially the same. The relative intensities of C^+, C_2^+, and C_3^+ from the graphite filament at 2450°K using 17-volt electrons were approximately 1.0, 0.5, and 1.6, respectively. These values should be regarded as only a rough measure of the relative abundances of C, C_2, and C_3 in the neutral vapor since ionization cross sections are unknown and the ions are produced in the sharply rising region of the ionization cross-section curve. However, the appearance potentials of all three species appear to be roughly equal, thus reducing the error due to the latter factor.

Measurements of the temperature dependence of the C^+ ion intensity using 17-volt electrons have been repeated six times using both carbon and graphite filaments and a random sequence of temperatures over ranges up to 400°. The values of the apparent ΔH (2000°K) of sublimation all fell within the range 170–182 kcal/mole and gave an average value of 177±6 kcal/mole and a ΔH (1°K) of 176±6 kcal/mole.

In order to eliminate the possibility that an appreciable number of the C^+ ions were formed from C_2 or C_3 by the 17-volt electrons, measurements were carried out using 14-volt electrons. Within experimental error the same temperature dependence was obtained. The ionization efficiency curve for C^+ also shows no detectable break from the appearance potential up to about 21 volts where a sharp break indicates formation of C^+ from another process, possibly from residual gases such as CO. The C^+ from higher energy processes made it difficult if not impractical to obtain good results with electrons of higher energy with our apparatus.

The temperature dependence of both C_2^+ and C_3^+ have been measured and indicate values of ΔH (2500°K) of sublimation of 200±10 kcal/mole for both C_2 and C_3. ΔH (0°K) for C_2 would then be about 211 kcal/mole. The value of ΔH (0°K) for C_2 calculated by the absolute pressure method, assuming that about 15 percent of the carbon evaporated in the usual rate of evaporation experiments[3,4] comes off as C_2, is about 208 kcal/mole. Since both of these methods give upper limits for ΔH, the present data indicate that the value of Brewer, Gilles, and Jenkins[5] ΔH (0°K) = 233.1±7.0 kcal/mole is too high by about 23 kcal/mole or more. Brewer[6] has recently stated that the value measured by Brewer, Gilles, and Jenkins may be too high and that the $^3\pi_\mu$ lower state of the Swan bands used in their measurements may not be the ground state of the C_2 molecule as indicated by the work of Norrish, Porter, and Thrush.[7]

The fact that C_2^+ and C_3^+ intensities have approximately equal temperature dependence suggests the possibility that a large part of the C_2^+ may be formed from C_3. This seems improbable since the appearance potential of C_2^+ agrees with the ionization potential of C_2 as measured by Kallmann and Rosen[8] and no detectable break in the ionization curve has been observed below 19 volts. However, a more careful study of the ionization curve should be made before definitely excluding this possibility.

The concentration of C_3 in carbon vapor and its heat of sublimation are of interest since Herzberg has recently tentatively assigned the so-called 4050A bands to C_3. These bands have recently been observed in absorption in acetylene-oxygen explosions in the region of strong carbon deposition.[8] The large amount of C_3 is also of interest since it probably formed a major part of the carbon vapor collected in the usual rate of evaporation experiments[3,4] and together with C_2 may account for the temperature dependences observed in these experiments which indicate an activation energy for evaporation in the range 177–200 kcal/mole.

Since C atoms are probably a minor constituent of the vapor, the experiments of Simpson, Thorn, and Winslow[3] on the accommodation coefficient of carbon must be regarded as inconclusive. A complete understanding of the evaporation process requires further knowledge especially concerning the accommodation coefficients of the various species. This could probably be done best by use of a Knudsen cell as in previous experiments[4,5] but accompanied by mass analysis of the effusing vapor.

A parallel study by R. E. Honig[9] corroborates much of the above work with the exception of ΔH of evaporation of C_3.

* This work was supported in part by a grant from the National Science Foundation.
[1] W. Chupka and M. Inghram, J. Chem. Phys. **21**, 371 (1953).
The graph of Fig. 1 contains a drafting error. The scale of the abscissa should extend rom 0.40 to 0.49 instead of from 0.40 to 0.50.
[2] W. Chupka and M. Inghram, Argonne National Laboratory Rep.-4993, 14 (Feb. 28, 1953).
[3] A. Marshall and F. Norton, J. Am. Chem. Soc. **72**, 2166 (1950); Simpson, Thorn and Winslow, U. S. Atomic Energy Commission Document, 2680 (1949); Farber and Darnell, J. Am. Chem. Soc. **74**, 3941 (1952).
[4] Doehard, Goldfinger, and Waelbroeck, J. Chem. Phys. **20**, 757 (1952).
[5] Brewer, Gilles, and Jenkins, J. Chem. Phys. **16**, 797 (1948).
[6] Private communication.
[7] Norrish, Porter, and Thrush, Nature **169**, 582 (1952).
[8] Kallmann and Rosen, Z. Physik. **61**, 332 (1930).
[9] R. Honig, Program of the 1952 Washington meeting of the American Physical Society, Abstact L8; also private communication.

Transition Layers on Glass Surfaces and Their Relation to Alkali Content

PAUL PORTER SUTTON
Department of Chemistry, North Carolina State College, Rayleigh, North Carolina
AND
A. D. INDYK AND W. W. KRIEGEL
Department of Ceramic Engineering, North Carolina State College, Raleigh, North Carolina
(Received May 8, 1953)

ALTHOUGH there is an extensive literature dealing with the transition layer which is presumed invariably to form at a glass-vapor interface,[1] there is still a lack of precision measurements which would evaluate the effect of individual factors in fixing the depth of this film. The role played here by the alkali

TABLE I. Compositions and optical constants of glasses: calculated depths of transition layers.

Sample nos.	Moles alkali	Moles CaO	Moles SiO_2	Moles Al_2O_3	Mole fraction alkali	Refractive index	$\rho \times 10^2$		L_{min}, A	
19*a*, 19*b*	40 Na_2O	15	100	0.4	0.257	1.5291	4.4	4.7	179	192
20*a*, 20*b*	50 Na_2O	15	100	0.4	0.302	1.5330 *f*	4.9	5.0	198	202
21*a*, 21*b*	60 Na_2O	15	100	0.4	0.342	1.5345	5.7	5.9	230	238
22*a*, 22*b*	40 K_2O	15	100	0.4	0.257	1.5267	4.7	4.9	193	201
23*a*, 23*b*	50 K_2O	15	100	0.4	0.302	1.5027	5.7	5.9	245	254
24*a*, 24*b*	60 K_2O	15	100	0.4	0.342	1.4966	6.9	...	300	...
7*c*	45 Na_2O	8	100	0	0.294	1.5214	4.6		190	
10*c*	45 K_2O	8	100	0	0.294	1.4900	6.4		283	

content of the glass is disclosed in part by experiments on optical polarization recently performed in these laboratories. (See Fig. 1.)

There was followed in this work a modification of the technique devised earlier by Silverman,[2] whereby an intense beam of monochromatic light ($\lambda = 4900$A) was reflected at the polarizing angle from the surface whose transition film was under study. Passing through a Wollaston prism, this reflected beam was split into components vibrating perpendicularly to one another, and these in turn transmitted onto photomultiplier tubes (RCA 941-A, 1000 volts). The photocurrents delivered by these cells were fed into, and compared by, a bridge circuit in which a galvanometer of high sensitivity served as null indicator. Measurement involved rotation of the prism about the reflected beam until the ratio of balancing bridge resistances was minimized, the square root of this ratio furnishing the (mean) ellipticity ρ of the reflected light. An estimate of L_{min}, the minimal thickness of transition layer consistent with this ρ, was then obtained through

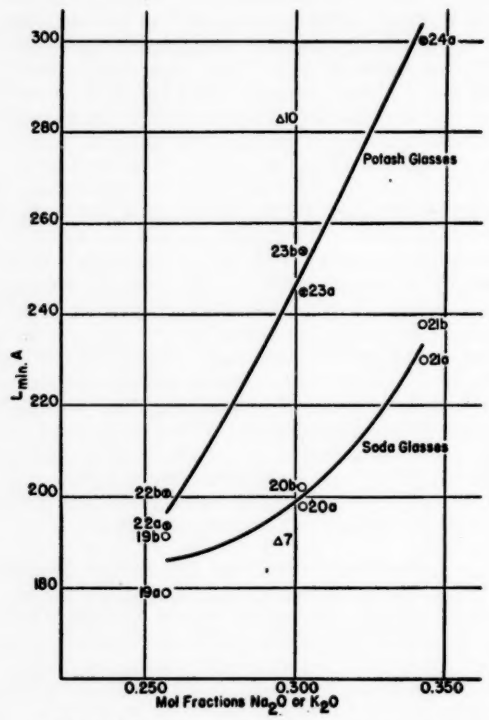

FIG. 1. Effect of alkali on thickness of adsorbed film.

$$L_{min} = \frac{\rho\lambda}{\pi} \frac{1}{\langle 1+n^2 \rangle_{Av}} \frac{n+1}{n-1} \quad (n = \text{index of refraction of glass}) \quad (1)$$

an equation derived by Drude[3] and shown to be valid when applied to films which are thin relative to λ.[4]

Table I indicates the compositions of the glasses examined, all of which were made up from cp chemicals in platinum crucibles with special pains to assure a homogeneous final product free of mechanical strains. The surfaces investigated were ground to optical smoothness by rouge and alcohol (series *a* and *b*) or water (series *c*), washed with soap and water, thoroughly rinsed, dried, and the sample then desiccated until mounted for measurement. In any one series (*a*, *b*, or *c*) all samples were identically and simultaneously treated.

The calculated values of L_{min}, presented also in this Table I, are not now claimed to possess absolute significance. As measures of relative film thickness, however, they show clearly that this latter is increased by replacement of Na_2O with K_2O, the increase being greater at higher concentrations. The consistently larger values found for the samples of series *b* in comparison with those of series *a* are particularly interesting, since differences between the two sets were confined to supposedly minor variations in grinding and cutting. Similar considerations may be important to an understanding of the results obtained on samples 7*c* and 10*c*, for these not only lacked Al_2O_3 in their makeup but were, as well, fired and polished differently from the *a* and *b* glasses.

[1] W. Eitel, *Physikalishe Chemie der Silikate* (Barth, Leipzig, 1941), pp. 444, 586.
[2] S. Silverman, Phys. Rev. **36**, 311 (1930).
[3] P. Drude, *Theory of Optics* (Longmans Green and Company, New York, 1901), p. 287.
[4] See, for example, A. Rothen and M. Hanson, Rev. Sci. Instr. **20**, 66 (1949).